Bacteria-based cancer immunotherapy: A re-emerging strategy with contemporary implications



Australian National University

Andrew A. Almonte

Research School of Biology

Australian National University

A thesis submitted for the degree of

Doctor of Philosophy

October 2023

For Tessa Pollack, may you rest in peace.

During my PhD candidature my research has contributed to nine manuscripts:

Published

1. **Almonte, A. A.** and J. O. Borevitz. 2018. "Adaptation genomics: The angel is in the details." *Plant Cell Environ.* 41: 2244–2246.
2. **Almonte, A. A.***, T. Rungrat*, R. Cheng, P. J. Gollan, T. Stuart, E. M. Aro, J. O. Borevitz, B. Pogson, and P. B. Wilson. 2019. A Genome-Wide Association Study of Non-Photochemical Quenching in response to local seasonal climates in Arabidopsis thaliana. Plant Direct 3: e00138. (*co-first authors)
3. **Almonte, A. A.**, Rangarajan, H., Yip, D., and Fahrer, A. M. (2020). How does the gut microbiome influence immune checkpoint blockade therapy? *Immunol. Cell Biol.* 99: 361-372
4. Carroll, C.S.E., E.R. Andrew, L. Malik, K.F. Elliott, M. Brennan, J. Meyer, A. Hintze, **A. A. Almonte**, C. Lappin, P. MacPherson, K.-M. Schulte, J.E. Dahlstrom, R. Tamhane, T. Neeman, E.W. Herbert, M. Orange, D. Yip, R. Allavena, and A.M. Fahrer. 2021. Simple and effective bacterial-based intratumoral cancer immunotherapy. *J. Immunother. Cancer* 9: e002688.
5. **Almonte, A. A.**, Cavic, G., Neeman, T., Enders, A., and Fahrer, A.M. 2022. Gut microbiome-depleting antibiotic regimens are not tolerated by all mouse strains: learn from (our) bitter experience. *J. Immunother. Cancer* 10: e005575.
6. Kanjanapan, Y., G. Cavic, **A. Almonte**, S. M. Hicks, T. Neeman, J. W. Wang, S. Brew, I. Cockburn, E. Gardiner, A. M. Fahrer, and D. Yip. 2022. Covid-19 Vaccine Response in Patients on Cancer Therapy - Evidence from Australian Data. *Intern. Med. J.* 52: 14–15.

Submitted

1. **Almonte, A. A.**, Cavic, G., Carroll, C. S. E, Neeman, T., and Fahrer, A. M. Early T cell infiltration correlates with anti-CTLA4 treatment response in murine cancer models. *J. Immunol.* (Accepted)
2. **Almonte, A. A.***, G. Cavic*, S. Hicks*, T. Neeman, D. Wang, S. Brew, P. Choi, I. Cockburn, E. Gardiner, D. Yip, A. M. Fahrer, and Y. Kanjanapan. "Response to COVID-19 vaccination in patients on cancer therapy: analysis in a SARS-CoV-2-naïve population." *Asia Pac. J. Clin. Oncol.* (Re-Submitted, *co-first authors)

In Preparation

R. A. Purcell, P. Chiou, P. Parajuli, **A. A. Almonte**, G. J. Mann, P. Collignon, K. Glass, D. Sarrs, D. Gray, R. Hayashi, D. Spensberger, A. Enders, A. M. Fahrer, and A.Lal."A cost-effective detection method for SARS-CoV-2 and other RNA viruses in wastewater."

Posters

Almonte, A. A., Cavic, G., Neeman, T., Fahrer, A. M., (2023, May 13). Early T cell infiltration correlates with anti-CTLA4 treatment response in the P815 mastocytoma model [Poster Abstract]. 2023 American Association of Immunologists: IMMUNOLOGY2023^{TM}, Washington, DC, United States.

Acknowledgements

Completing a PhD project is an immense undertaking that would not have been possible without the invaluable mentorship, guidance, and support of numerous individuals in my professional and private life.

First and foremost, I extend my deepest gratitude to my supervisor, mentor, and friend, Prof Aude M. Fahrer. She imparted upon me the knowledge and skills necessary to become an effective scientist and it was her guidance that enabled me to accomplish this endeavour. Her resilience in the face of adversity is a trait that is to be admired. Moreover, she opened doors to opportunities I never thought possible. I will forever remain grateful.

I also want to thank my friend and colleague, fellow PhD student Mr George Cavic. His invaluable assistance in conducting several of the experiments described in this dissertation is deeply appreciated, and I wish him every success in his own PhD project. I am also indebted to two lab alumni, Dr Erin Andrew and Dr Christina Carroll. Dr Andrew taught me the fine-needle aspirate sampling protocol, which is prominently employed throughout this work. Dr Carroll's assistance in revising the manuscript presented in Chapter 3 for publication is also greatly appreciated.

Special thanks are owed to Dr Teresa Neeman for her help with the statistical analyses of the data presented in this work. Furthermore, thanks to the R programming skills she taught me, I successfully wrote and rendered this entire dissertation – including text, tables, and data figures – using R Markdown.

I am grateful to all the members of my PhD supervisory panel, both past and present. Prof Anne Bruestle, Prof Desmond Yip, Prof Si Ming Mann, and Prof Di Yu, I sincerely appreciate the time, expertise, and guidance you have provided, all of which have contributed significantly to the success of this project.

Profuse thanks go to Prof Yueh-Hsiu Chien and Prof Mark M. Davis from the Stanford University School of Medicine. I am immensely grateful for their generous hospitality, which provided me with the opportunity to conduct my research in their laboratories and utilise their resources. Additionally, my gratitude extends to Dr Qian Yin (who at the time was a member of Prof Davis' laboratory) for allowing me to work with her and use her laboratory resources for my research.

Many others have contributed to this project in various ways, and I would like to express my appreciation to each of them. Prof Rachel Allavena from the University of

Queensland, your invaluable help in examining lung histological sections is genuinely appreciated and acknowledged with immense gratitude. Prof Anselm Enders, I am immensely grateful for your assistance with the antibiotics taste-testing experiments. Fellow PhD student, Ms Rebecca Buckland, your assistance with the neutrophil and complete Freund's adjuvant experiments is deeply appreciated. Prof Naresh Verma, thank you for your guidance in the bacteria-counting experiments. Prof Justin Borevitz, your support and guidance have been instrumental. Dr Farid Rahimi, your work in laboratory services is invaluable. I would also like to extend my thanks to members of the EVEREST team who have not yet been mentioned – Ms Sarah Hicks, Dr Jo-Wai Wang, Ms Sue Brew, Dr Philip Choi, Prof Ian Cockburn, Prof Elizabeth Gardiner, and Dr Yada Kanjanapan. I also thank Dr Kanjanapan for her invaluable assistance in reviewing Table 1 of the published literature review in Chapter 1 of this dissertation.

The Australian Government Research Training Program, the John James Foundation, the Australian National University's Research School of Biology seed funding scheme, the Lea Chapuis Memorial Fund, and the generosity of Tim and Margaret Bourke provided financial support for this work. Additional funding sources are acknowledged in the respective studies included in this dissertation.

I must express my love and deepest gratitude to my parents, Joe and Dora Almonte. Your unwavering encouragement, lessons in hard work, and enduring support have been the bedrock of my journey.

Lastly, I want to express my deepest gratitude to my lifelong partner and devoted husband, Mr. Thomas J. N. Pollack. Your love, patience, guidance, and support have all played a critical role in the realisation of this achievement. I remain forever and profoundly grateful for the countless ways in which you have enriched my life. Thank you for everything. I love you beyond words.

Andrew A. Almonte
Research School of Boiology
The Australian National University
13 June 2023

Abstract

Immunotherapy is a re-emerging alternative to other invasive and debilitating cancer treatments. Monoclonal antibodies that disrupt immune checkpoint molecules, such as programmed cell death protein 1 (PD1) or cytotoxic T-lymphocyte-associated protein 4 (CTLA4), have been paradigm-shifting advances in medical oncology. However, therapy response rates need improvement, and important questions remain regarding the mechanisms by which checkpoint therapies promote their therapeutic effects. One intriguing factor is how the presence and composition of the gut microbiome influence treatment outcomes. I hypothesised that checkpoint therapies allow gut bacteria to colonise extraintestinal tumours, and this theory relates to our laboratory's intratumoural Complete Freund's Adjuvant (CFA) therapy. CFA is a water-in-oil emulsion containing heat-killed mycobacteria, has successfully improved survival in several animal cancer models, and is well tolerated by cancer patients. Thus, the primary aims of this project were to explore the impact of the gut microbiome on checkpoint therapies and enhance the efficacy of our laboratory's CFA therapy.

The research was conducted at the Australian National University (ANU) and the Stanford University School of Medicine. I used six mouse cancer models across three mouse strains and a tumour sampling method developed by our laboratory called fine-needle aspirate (FNA) sampling. FNA sampling with flow cytometry enables the longitudinal comparison of tumour-infiltrating leukocytes (TILs) among animals with disparate treatment outcomes without sacrificing them for data acquisition. This method was also used to investigate how depleting the gut microbiome with antibiotics would impact intratumoural immune reactions following treatment. Lastly, two methods of improving CFA therapeutic efficacy were investigated: (1) combining the treatment with checkpoint therapies and (2) increasing the concentration of heat-killed mycobacteria in the emulsion ten-fold (10x CFA).

Despite the challenges posed by external factors, including the global coronavirus disease 2019 (COVID-19) pandemic, I successfully progressed towards both aims. Preliminary experiments highlighted critical unanswered questions regarding the consequences of combining CFA with checkpoint therapies on the metastatic disease progression of the 4T1 mammary adenocarcinoma model. I also found that 10x CFA significantly increased immune infiltration (primarily neutrophils) into the CT26 colorectal cancer model, an

effect not observed with standard 1 x CFA therapy that may have critical implications on therapeutic efficacy.

While examining checkpoint therapies, I found that the P815 mastocytoma and CT26 cancer models responded well to anti-CTLA4 but not anti-PD1. P815-challenged mice responsive to anti-CTLA4 showed significant increases in tumour-infiltrating $CD8^+$ T cells by days 3, 5, and 7 post-treatment and $CD4^+$ T cells by days 5 and 7. CT26-challenged animals responsive to anti-CTLA4 had significantly more tumour-infiltrating $CD8^+$ T cells by day 11 post-treatment. While investigating how gut microbial depletion affects treatment outcomes in CT26-challenged animals, I found that BALB/c (and DBA/2) mice do not tolerate the taste of a common antibiotic cocktail used in several high-impact publications. Regardless, depletion was successfully achieved, and while anti-CTLA4 therapy was not impacted, I did find evidence of an altered immune state among antibiotic-fed animals.

Collectively, these findings highlight ongoing challenges and unanswered questions in the field of immunotherapy and lay the groundwork for future investigations into these exciting topics.

Contents

List of Figures xv

List of Tables xix

List of Abbreviations xxi

1 Introduction 1

1.1 Early Attempts at Immunotherapy 2

1.2 Back on the Map - Immune Checkpoint Therapies 3

1.3 Our Laboratory's Novel Treatment – Intratumoural Complete Freund's Adjuvant 22

1.4 Bringing it All Together – The Structure and Layout of this Dissertation 31

2 Materials and Methods 33

2.1 Introduction 34

2.2 Animals 34

2.3 Tissue Culture 35

2.4 Tumour Challenge 36

2.5 Tumour Measurement 37

2.6 Cancer Treatment 38

2.7 Examining Lung Metastases 40

2.8 Flow Cytometry 41

2.9 Antibiotic Feeding 45

2.10 Determining Antibiotic Efficiency 46

2.11 Statistical Analysis 48

3 Early T cell Infiltration Correlates with Anti-CTLA4 Treatment Response in the P815 Mastocytoma Model 53

4 Identifying a Useful Tumour Model for Future Cancer Immunotherapy Experiments **93**
4.1 Introduction . . . 93
4.2 MCA-205 Fibrosarcoma Model . . . 96
4.3 B16.F10 Melanoma Model . . . 97
4.4 MC38 Colon Adenocarcinoma . . . 101
4.5 4T1 Mammary Carcinoma . . . 107
4.6 CT26.WT Colon Carcinoma . . . 112
4.7 Discussion . . . 119

5 Gut Microbiome-Depleting Antibiotic Regimens are not Tolerated by All Mouse Strains: Learn from (Our) Bitter Experience **125**
5.1 Introduction . . . 125
5.2 Results . . . 127
5.3 Discussion and Publication . . . 131

6 Investigating Methods to Improve CFA Effectiveness **139**
6.1 Introduction . . . 140
6.2 Combining CFA with Immune Checkpoint Therapies . . . 140
6.3 Increasing the Concentration of *Mycobacterium butyricum* in CFA . . . 148
6.4 Discussion . . . 161

7 General Discussion **169**
7.1 Introduction . . . 169
7.2 Improving our Laboratory's CFA Therapy . . . 172
7.3 Finding an Appropriate Tumour Model . . . 181
7.4 Our First Antibiotics Experiment . . . 189
7.5 Challenges to Progress . . . 193
7.6 Support for Our Hypothesis! . . . 194
7.7 Conclusion . . . 196

Appendices

A Supplementary Figures **201**

B Supplementary Tables **221**

C Simple and effective bacterial-based intratumoral cancer immunotherapy **227**

D Response to COVID-19 vaccination in patients on cancer therapy: analysis in a SARS-CoV-2-naïve population **253**

E A cost-effective detection method for SARS-CoV-2 and other RNA viruses in wastewater **277**

References **301**

List of Figures

1.1 **Three observations have been made that could help explain the mechanism of action for complete Freund's adjuvant** 25

2.1 **Fine-needle aspirate sampling for flow cytometry** 42
2.2 **Determining the efficacy of antibiotics at depleting the gut microbiome** 47

3.1 **Quality control to assess which FNA samples from the P815 model were included in the final analysis.** 83
3.2 **Anti-CTLA4 significantly impacts the growth of the P815 mastocytoma tumour model and improves survival.** 84
3.3 **Survival and tumour growth data from all six experiments analysed in the P815 study.** 85
3.4 **Hazard ratios of each covariate in the Cox proportional hazards analysis that determined checkpoint therapy impact on the P815 model.** 86
3.5 **All treatment antibodies bind with Fcγ receptors (FcγR) on the surface of P815 mastocytoma cells.** 87
3.6 **Gating strategy for characterising tumour-infiltrating leukocyte (TIL) populations.** 88
3.7 **FNA sampling shows no significant differences in TIL profiles among treatment groups.** 89
3.8 **FNA data from all P815-challenged mice treated with immune checkpoint therapy.** 90
3.9 **CD4$^+$ T cell, CD8$^+$ T cell, and Macrophage/Monocyte proportions in anti-CTLA4–treated mice are different between responder and non-responder mice.** 91

4.1 **Euthanising due to ulceration severely limited the data that could be obtained from the MCA-205 Fibrosarcoma model.** 98
4.2 **Checkpoint therapies had no impact on the B16.F10 melanoma model.** 100
4.3 **The gating strategy used to analyse TILs from the B16.F10 model with flow cytometry.** 102

4.4 **Only FNA samples from the B16.F10 model that passed a quality control test were included in the final analysis.** 103
4.5 **FNA sampling from the B16.F10 model showed little variation among the nine cell types identified with flow cytometry.** 104
4.6 **Anti-CTLA4 antibody had surprisingly limited effect on mice challenged with MC38 tumours.** 106
4.7 **Checkpoint therapy and FNA sampling did not impact survival in the 4T1 tumour model** 109
4.8 **The gating strategy used to analyse FNA samples from the 4T1 model with flow cytometry.** 110
4.9 **Quality control to assess which FNA samples from the 4T1 model were included in the final analysis.** 111
4.10 **All mice challenged with the 4T1 model exhibited paraneoplastic syndrome** 112
4.11 **The CT26 tumour model responds well to anti-CTLA4 but not anti-PD1.** 115
4.12 **The gating strategy used to analyse FNA samples from the CT26 model with flow cytometry.** 116
4.13 **Quality control to assess which FNA samples from the CT26 model are to be included in the final analysis.** 117
4.14 **Checkpoint therapies increase the macrophage/monocyte population by the eleventh day following treatment.** 118
4.15 **Average $CD8^+$ T cell, Macrophage/Monocyte, and Neutrophils proportions in anti-CTLA4–treated mice differ between responders and non-responders.** 119

5.1 **BALB/c mice were resistant to drinking the antibiotic solution.** . . . 127
5.2 **Despite dehydration, mice were still consuming antibiotics.** 128
5.3 **Dysbiosis did not affect anti-CTLA4 therapy in the CT26 tumour model.** 130
5.4 **Quality control was performed to determine which FNA samples from C26-challenged mice in the antibiotics experiment was retained for analysis.** 131
5.5 **Tumour-infiltrating leukocyte populations were impacted by antibiotics in the CT26 model.** 132
5.6 **FNA data from antibiotic- and water-fed mice that regressed following anti-CTLA4 treatment.** 133

6.1 **Combining CFA with immune checkpoint therapies in the CT26 model.** 143
6.2 **The 4T1 model did not respond to intratumoural CFA treatment at Stanford University.** . . . 145
6.3 **4T1-challenged mice treated with concomitant CFA and immune checkpoint therapies appeared to develop more lung metastases.** . . . 147
6.4 **H&E-stained lung sections from mice that received CFA and immune checkpoint therapy** . . . 149
6.5 **Complete regression of a CT26 tumour was observed after treatment with 10x CFA** . . . 150
6.6 **First gating strategy used to examine TILs in 10x CFA experiments** 153
6.7 **Second gating strategy used to examine TILs in 10x CFA experiments** 154
6.8 **10x CFA significantly increased the proportion of tumour-infiltrating neutrophils by days 3 and 4** . . . 155
6.9 **The longest-lived CFA- and 10x CFA-treated mice had large proportions of tumour-infiltrating neutrophils** . . . 156
6.10 **10x CFA-treated mice had significantly more neutrophils and significantly fewer CD25$^+$ CD4$^+$ T cells by day 4 post-treatment by proportion** 158
6.11 **10x CFA therapy promotes more immune cell infiltrates** . . . 160
6.12 **10x CFA-treated mice had numerically higher proportions of neutrophils in bone marrow, spleen, TdLN, and tumour** . . . 162

A.1 **The performance of the model used to analyse the MCA-205 tumour growth data presented in Figure** 4.1B . . . 202
A.2 **The performance of the model used to analyse the MCA-205 tumour growth data presented in Figure** 4.1B . . . 203
A.3 **Performances of linear mix-effects regression models of each TIL population identified in the B16.F10 model analysed for Figure** 4.5 . . . 204
A.4 **The estimated marginal means among the different treatment groups for each cell type identified in the B16.F10 model in Figure** 4.5 . . . 205
A.5 **The performance of the model used to analyse the MC38 tumour growth data presented in Figure** 4.6B . . . 206
A.6 **The performance of the model used to analyse the 4T1 tumour growth data presented in Figure** 4.7B . . . 207
A.7 **Performances of linear mix-effects regression models of each TIL population identified in the 4T1 model analysed for Figure** 4.10 . . . 208
A.8 **The estimated marginal means among the different treatment groups for each cell type identified in the 4T1 model in Figure** 4.10 . . . 209

A.9 **The performance of the model used to analyse the CT26 tumour growth data presented in Figure** 4.11B 210
A.10 **Performances of linear mix-effects regression models of each TIL population identified in the CT26 model analysed for Figure** 4.14 . . 211
A.11 **Performances of linear mix-effects regression models of each TIL population identified in anti-CTLA4 - treated CT26 tumours analysed for Figure** 4.15 212
A.12 **The performance of the model used to analyse the CT26 tumour growth data presented in Figure** 5.3B 213
A.13 **Performances of linear mix-effects regression models of each TIL population identified in the CT26 model analysed for Figure** 5.5 . . 214
A.14 **The performance of the model used to analyse the 4T1 tumour growth data presented in Figure** 6.2 215
A.15 **The performance of the model used to analyse the 4T1 tumour growth data presented in Figure** 6.5 215
A.16 **Supplemental survival data for Figure** 6.5 216
A.17 **Photos of all lungs evaluated with India ink and Fekete's solution.** . 217
A.18 **Quality control assessment for FNA data presented in Figure** 6.8 . . 218
A.19 **Performances of linear mix-effects regression models of each TIL population identified in the CT26 model analysed for Figure** 6.8 . . 219
A.20 **LMER model performances of the neutrophil and CD4⁺ T cell populations analysed for Figure** 6.10 220

List of Tables

1.1 Summary of alternate aliases, mouse knockout phenotypes, and cell expression of immune checkpoint molecules 6
1.2 PAMPs and PRRs associated with *Mycobacterium tuberculosis* 27
1.3 Examples of pre-clinical studies that investigated treatment outcomes after combining immune checkpoint therapies with Toll-like receptor agonists 30

2.1 Reagents and solutions used in experiments presented in this dissertation 34
2.2 Recipes for tissue cultures used for cell lines in this dissertation. All reagents were supplied from Gibco unless otherwise noted. 36
2.3 Antibodies used for FACS analyses in this dissertation 44

4.1 Tumour models evaluated for use in future gut microbiome experiments 95

B.1 Hazard Ratios of covariates used in Cox-Proportional Hazards Model in Figure 4.1D 222
B.2 Hazard Ratios of covariates used in Cox-Proportional Hazards Model in Figure 4.2C 222
B.3 Hazard Ratios of covariates used in Cox-Proportional Hazards Model in Figure 4.6C 223
B.4 Hazard Ratios of covariates used in Cox-Proportional Hazards Model in Figure 4.7C 223
B.5 Hazard Ratios of covariates used in Cox-Proportional Hazards Model in Figure 4.11C 223
B.6 Hazard Ratios of covariates used in Cox-Proportional Hazards Model in Figure 5.3A 224
B.7 Hazard Ratios of covariates used in Cox-Proportional Hazards Model in Figure 6.1B 224
B.8 Hazard Ratios of covariates used in Cox-Proportional Hazards Model in Figure 6.2A 225
B.9 Hazard Ratios of covariates used in Cox-Proportional Hazards Model in Figure 6.2C 225

B.10 Hazard Ratios of covariates used in Cox-Proportional Hazards Model in Figure 6.5C 226

List of Abbreviations

7-AAD . . . . . 7-Aminoactinomycin D

ACT . . . . . Australian Capital Territory

APC . . . . . Allophycocyanin

APLAC . . . . . Administrative Panel for Laboratory Animal Care

ATC . . . . . Ammonium Tris-chloride

ANOVA . . . . Analysis of Variance

ATAGI . . . . . Australian Technical Advisory Group on Immunisation

ANU . . . . . Australian National University

ATCC . . . . . American Type Culture Collection

BAU . . . . . Binding Antibody Units

CD-x . . . . . Cluster of Differentiation x

CFA . . . . . Complete Freund's Adjuvant

CFU . . . . . Colony Forming Unit

CI . . . . . Confidence Interval

COVID-19 . . . Coronavirus Disease 2019

CpG-ODN . . . CpG Oligodeoxynucleotide

CT26 . . . . . Colon Tumour 26

CTL . . . . . Cytotoxic T Lymphocyte

CTLA-4 . . . . Cytotoxic T Lymphocyte-Associated Protein 4

DMEM . . . . . Dulbecco's Modified Eagle Medium

EAE . . . . . Experimental Autoimmune Encephalomyelitis

EDTA . . . . . Ethylenediaminetetraacetic acid

ELISA . . . . . Enzyme-Linked Immunosorbent Assay

EVEREST . . . Evaluation of COVID-19 Vaccine Efficacy and Rare Events in Solid Tumours

FACS . . . . . Fluorescence-Activated Cell Sorting

Fc . . . . . Fragment crystallisable

FCS . . . . . Feotal Calf Serum

FNA . . . . . Fine-Needle Aspirate

FMO . . . . . Fluorescence Minus One

G-CSF . . . . . Granulocyte Colony-Stimulating Factor

GM-CSF . . . . Granulocyte-Macrophage Colony-Stimulating Factor

H&E stain . . . Hematoxylin and Eosin stain

HEPES . . . . . 4-(2-hydroxyethyl)-1-piperazineethanesulfonic acid

HLA . . . . . Human Leukocyte Antigen

HI-FCS . . . . . Heat-inactivated Feotal Calf Serum

HREC . . . . . Human Research Ethics Committee

IFA . . . . . Incomplete Freund's Adjuvant

IFN . . . . . Interferon

IgG . . . . . Immunoglobulin G

IL-2R . . . . . Interleukin 2 Receptor

IL-x . . . . . Interleukin x

i.p. . . . . . Intraperitoneal

i.t. . . . . . Intratumoural

i.v. . . . . . Intravenous

JAX . . . . . The Jackson Laboratory

LMER . . . . . Linear-Mixed Effects Regression

LNP . . . . . Lipid Nanoparticle

LPS . . . . . Lipopolysaccharide

Mϕ . . . . . Macrophage

MACS . . . . . Magnetic-Activated Cell Sorting

MEM . . . . . Minimal Essential Medium

MHC . . . . . Major Histocompatibility Complex

Mo . . . . . Monocyte

MoAb . . . . . Monoclonal Antibody

NBF . . . . . Neutral Buffered Formalin

NCBI . . . . . National Center for Biotechnology Information

NEAA . . . . . Non-Essential Amino Acids

NIH . . . . . National Institutes of Health

NK cell . . . . . Natural Killer cell

PBS . . . . . Phosphate-Buffered Saline

PCR . . . . . Polymerase Chain Reaction

PD1 . . . . . Programmed Cell Death Protein 1

PD-L1 . . . . . Programmed Cell Death Protein 1 Ligand

PE . . . . . Phycoerythrin

RBC . . . . . Red Blood Cell

RFU . . . . . Relative Fluorescence Units

RPMI . . . . . Roswell Park Memorial Institute

SARS-CoV-2 . . Severe Acute Respiratory Syndrome Coronavirus 2

spp. . . . . . Botanical shorthand for multiple species (e.g., *Mycobacterium* spp.)

S-RBD . . . . . SARS-CoV-2 Spike Receptor Binding Domain

scRNAseq . . . single-cell RNA sequencing

TAA . . . . . Tumour-Associate Antigen

TB . . . . . Tuberculosis

TdLN . . . . . Tumour-draining Lymph Node

TGFβ . . . . . Transforming Growth Factor β

TIL . . . . . Tumour-Infiltrating Leukocyte

Treg . . . . . Regulatory T cell

1 Introduction

Contents

1.1 Early Attempts at Immunotherapy 2
1.2 Back on the Map - Immune Checkpoint Therapies 3
1.2.1 Discovery of CTLA4 and development of anti-CTLA4 therapy 4
1.2.2 Discovery of PD-L/PD1 axis and development of PD1 blockade therapy 7
1.2.3 Unanswered questions and literature review 8
1.3 Our Laboratory's Novel Treatment – Intratumoural Complete Freund's Adjuvant 22
1.3.1 Brief history of CFA 22
1.3.2 How does CFA work biologically? 25
1.3.3 CFA as a cancer immunotherapy 27
1.3.4 Advantages of CFA over other therapies 29
1.4 Bringing it All Together – The Structure and Layout of this Dissertation 31

We begin by delving into the histories of the treatments that are being explored in this work. This chapter also contains a published literature review that focuses on the significance of the gut microbiome in immune checkpoint therapies and proposes a hypothesis that may explain its influence on cancer treatment outcomes. First, we explore the work of Dr William B. Coley, who pioneered cancer immunotherapy as a subject of study and whose work is the inspiration for our laboratory's novel cancer treatment.

1.1 Early Attempts at Immunotherapy

Cancer immunotherapy became a recognised cancer treatment option in the early 2000s (Zhang & Zhang, 2020). Ironically, it was one of the first cancer treatment modalities to be explored after surgery. Dr William B. Coley, the "Father of Immunotherapy", was inspired to use bacterial injections to treat cancer after reading about a clinical case describing a 32-year-old German man diagnosed with round-celled sarcoma of the neck and who spontaneously regressed after developing severe erysipelas – an infection of the dermis layer of the skin (Gunderson & Martinello, 2012; Hoption Cann et al., 2003). The bacterium *Streptococcus pyogenes* had been identified as the cause of erysipelas ten years earlier (Fehleisen, 1882; Gunderson & Martinello, 2012). Hence, Coley endeavoured to replicate the phenomenon and cure his cancer patients by intentionally infecting them with erysipelas.

The results of Coley's first attempts at using *S. pyogenes* as a cancer treatment (which he had acquired from Robert Koch's laboratory) were published as abbreviated case reports in his seminal 1893 paper (Coley, 1991). He and others repeatedly injected cultures of live bacterium directly into the tumours of sarcoma and carcinoma patients, all of whom had inoperable cases and no expectation of survival. In his paper, he examines 38 cases where erysipelas had been purposefully induced by intratumoural inoculation (15 cases) or accidentally acquired (23 cases). Of these, 12 patients (31.6%) were cured outright following infection. Encouraged by these results, Coley continued to develop his therapy and eventually found that combining heat-killed *S. pyogenes* with that of another bacterium, *Serratia marcescens*, produced more predictable responses (Coley, 1909) without risk of lethal infection (indeed, some patients died because of his therapy). This treatment was hence called Coley's Toxin, and he attained impressive cancer treatment response rates, even by contemporary standards (Hoption Cann et al., 2003), after repeated intratumoural injections. However, Coley soon became impatient to prove his therapy promoted systemic anti-cancer effects and started administering his treatment by other routes, i.e., intramuscularly and intravenously (Fahrer, 2012). It was not until

a year or two before he died that he realised this change in treatment protocol was a mistake (Nauts & McLaren, 1990).

Several significant events occurred in the late 1800s that stalled progress in cancer immunotherapy research, despite its promising potential. The most significant was the development of radiotherapy as a cancer treatment strategy ("News of Science," 1957). This option quickly gained favour because they did not induce the same illness often associated with Coley's Toxins and consequently became the novel and exciting cancer treatment modality of the time (though tumours would later become refractory to treatment and resume growth). Several years passed, and nitrogen mustard gas – a chemical weapon used in World War I – was found to be an effective chemotherapeutic agent during World War II (Einhorn, 1985; S. L. Smith, 2017). Interest in immunotherapy had waned, and the focus of the broader research community turned toward developing and improving radiotherapy, chemotherapies, and eventually hormone therapies (Huggins & Hodges, 2002) to treat cancers.

However, Coley's work was not wholly forgotten, primarily because of the vigilance of his daughter, Helen Coley Nauts. She believed strongly in her father's work, and in 1946 (ten years after her father's death), she published a review of his research and any case reports that described using Coley's Toxin as a cancer treatment (Nauts et al., 1946). She compiled reports of 312 inoperable cases and showed 5-year survival in 112 (35.6%) treated patients. Clearly, something fascinating had been happening but was sadly overlooked.

1.2 Back on the Map - Immune Checkpoint Therapies

Despite Coley's attempts to induce an immune reaction against solid tumours, the idea that the immune system has an active role in protecting the body against malignancy is a young one. In fact, Coley incorrectly argued that the success of his treatment was due to the body reacting to an unidentified family of microparasites that initially caused the malignancy (Coley, 1909). The first articulated notion that immune cells have an active role in protecting the body by searching for and killing neoplastic cells – the

Immune Surveillance Hypothesis – came from Sir MacFarlane Burnet and Lewis Thomas in 1957. This theory was not broadly accepted until the 1990s. The reasons for this slow acceptance have already been described in an impressive review article by Dunn *et al.* (2002), which will not be repeated here.

The Immune Surveillance Hypothesis has since been demonstrated time and again, and it is now an established fact that immunotherapies have great promise for cancer treatment. Several immunotherapy strategies have since been developed, including adoptive cell transfer (Yee et al., 2002), dendritic cell vaccines (Draube et al., 2011), and chimeric antigen receptor T cell therapy (Srivastava & Riddell, 2015), all of which aim to reactivate or repurpose leukocytes to better promote the killing of the tumour and any metastases. This dissertation partly focuses on another strategy – immune checkpoint-inhibiting monoclonal antibodies, the development of which led to Professor Allison and Professor Honjo sharing the 2018 Nobel Prize in Medicine and Physiology.

1.2.1 Discovery of CTLA4 and development of anti-CTLA4 therapy

Brunet *et al.* (1987) discovered murine CTLA4 in 1987, and human CTLA4 was identified the next year (Dariavach et al., 1988). The structural similarities between mouse and human CD28 and CTLA4 were then described by Harper *et al.* (1991). Prof Linsley and his colleagues had experience with CD28 as they had already published evidence showing that it interacted with the co-stimulatory molecule B7 (Linsley et al., 1990) and reasoned that the structural similarities implied similar binding targets. To test this hypothesis, Linsley fused the extracellular domains of CD28 and CTLA4 with the constant region of human IgG1 heavy chain (CD28Ig and CTLA4Ig), then analysed their binding avidities to B7 *in vitro* using both flow cytometry and radiolabelled molecules (Linsley et al., 1991). They observed that CTLA4Ig binds with B7 and did so with a much higher binding avidity than CD28Ig, prompting them to suggest that CTLA4Ig could act in an immunosuppressive capacity.

The following year, Linsley et al. confirmed their *in vitro* results by testing the immunosuppressive capacity of their CTLA4Ig molecule *in vivo*. They did this by injecting CTLA4Ig into BALB/c mice intravenously after immunising them with sheep red blood

cells or keyhole limpet hemocyanin, two potent immunogens, and observing substantially reduced B and T cell responses (Linsley, Greene, et al., 1992). That same year, they further investigated the role of CTLA4 in a physiological setting and showed that CTLA4 was expressed on both activated $CD8^+$ and $CD4^+$ T cells (Boussiotis et al., 1993). The following year a second B7 molecule, B7-2, was discovered using CTLA4Ig selection from a human B cell cDNA expression library (Azuma et al., 1993). The structure and expression of B7-2 were then characterised by two independent groups (Freeman et al., 1993; Krummel & Allison, 1995). B7-2 molecules were also found on macrophages and dendritic cells, and later T cells (Krummel & Allison, 1995; Linsley & Ledbetter, 1993). Linsley *et al.* (1994) later elucidated how B7-1 and B7-2 interacted with CTLA4 and CD28 and renamed B7-1 as CD80 and B7-2 as CD86, the convention used herein.

While the immunosuppressive role of CTLA4Ig was well known, the role of natural CTLA4 in a physiological setting was still controversial. Linsley *et al.* (1992) described a synergistic role between CD28 and CTLA4, while Walunas *et al.* (1994) provided evidence for an inhibitory role for CTLA4. The first explicit demonstration of the immunosuppressive nature of CTLA4 was published in 1995 by Dr Krummel and Prof Allison (Krummel & Allison, 1995), which was confirmed by two studies three months later showing the lethality associated with CTLA4 – knockout mice (Table 1.1, Tivol et al., 1995; Waterhouse et al., 1995). Krummel and Allison investigated the physiological role of CTLA4 by adding activating anti-CD28 and inhibitory anti-CTLA4 antibodies, either alone or in combination, to isolated lymph node T cells (Krummel & Allison, 1995). While they confirmed anti-CD28 induced T cell proliferation and anti-CTLA4 had no effect, they also showed that combining the two further enhanced T cell proliferation. This result seemed to contradict the inhibitory nature of CTLA4, and they had two hypotheses for this outcome: (1) anti-CTLA4 enhances the activation signal, or (2) anti-CTLA4 removes an inhibitory signal. Due to the lack of proliferation from anti-CTLA4, they decided to pursue the latter hypothesis. Further experiments conclusively demonstrated that CTLA4 significantly reduced T cell proliferation and IL-2 production. Additionally, Krummel and Allison showed CTLA4 and CD28 act in opposition in a

Table 1.1: Summary of alternate aliases, mouse knockout phenotypes, and cell expression of immune checkpoint molecules

Surface Molecule	Other Aliases	Mouse Knockout Phenotype	Cellular Expression
CTLA4	CD152	Fatal lymphoproliferative disorder (Tivol et al., 1995)	Activated T cells
CD80	B7-1	Moderate decrease in lymphocyte response to antigen (Freeman et al., 1993)	B cells, DC, Mϕ (Linsley & Ledbetter, 1993) T cells (Krummel & Allison, 1995)
PD1	CD279	- Proliferative chronic lupus-like glomerulonephritis - Arthritis (Nishimura et al., 1996)	Activated T cells
PD-L1	CD274, B7-H1	- Increased expansion and survival of antigen-specific T cells - Severe induced clinical experimental autoimmune encephalitis with increased risk of fatality (Latchman et al., 2004)	B cells, Mϕ (Loke & Allison, 2003) Mo (Bianchini et al., 2019), Myeloid cells, Endothelial cells, Non-lymphoid cells
PD-L2	CD273, B7-DC	- Enhanced T cell activation - Increased T cell proliferation (Zhang et al., 2006) - Diminished Th1 and CTL response - Reduced anti-tumour immune response (Shin et al., 2005)	B cells, DC, Mϕ, Activated T cells
CD86	B7-2, B7-0	- Absence of splenic germinal centres - Decreased antibody production - Severely reduced IgG1 and IgG2a isotype levels (Borriello et al., 1997)	Mϕ, Monocytes, DC, T cells (Krummel & Allison, 1995)
CD28		- Reduced overall antibody titre - Altered isotype ratios - Reduced isotype class switching - Significantly reduced T cell response to antigen (Shahinian et al., 1993)	Plasma cells, T cells

Mϕ, Macrophage; DC, Dendritic Cell

quantitative manner – the first inhibitory, the second activating – and T cell activation ultimately depends on an integration of the two signals (Krummel & Allison, 1995).

Five months later, Krummel, Allison, and Dr Leach built upon their initial observation and published their seminal work on using anti-CTLA4 monoclonal antibodies to block inhibitory signals from cancer and enhance T cell proliferation (Leach et al., 1996). They showed that co-injection of blocking anti-CTLA4 antibody with either transgenic B7$^+$ or wild-type 51BLim10 colon carcinoma cells into BALB/c mice significantly

improved survival, verifying the use of anti-CTLA4 as a potential immunotherapeutic option. They then validated this idea by showing that anti-CTLA4 improved the survival of mice with established 51BLim10 colon carcinoma and Sa1N fibrosarcoma tumours.

Several clinical trials followed that showed the above observations were translatable and that anti-CTLA4 significantly improved cancer patient survival (Robert et al., 2011). In 2011 the US Federal Drug Administration (FDA) approved anti-CTLA4, which is now marketed as Yervoy (ipilimumab, Bristol-Myers Squibb, USA) to be used for the treatment of metastatic melanoma (Almonte et al., 2021, Table 1; Koenig & Elicker, 2011). Allison shared the 2018 Nobel Prize for this work.

1.2.2 Discovery of PD-L/PD1 axis and development of PD1 blockade therapy

Murine PD1 was first identified by Prof Tasuku Honjo in 1992 (Y. Ishida et al., 1992), who also identified the human homologue and chromosomal location in 1994 (Shinohara et al., 1994). His laboratory would publish several more papers on PD1 in the coming years. They first found that PD1 mRNA is expressed mainly in the thymus and spleen, then later identified expression in $CD4^+$, $CD8^+$, and double-negative T cells, T cell receptor (TCR)$\alpha\beta^+$ NK cells, and B cells (Agata et al., 1996; Nishimura et al., 1996). PD1 knockout mice were developed in 1998 (Nishimura et al., 1998), and in 1999 Honjo and his colleagues showed that mice deficient in PD1 presented with proliferative chronic lupus-like glomerulonephritis and arthritis, suggesting that PD1 may have a role in maintaining peripheral immune tolerance (Table 1.1, Nishimura et al., 1999). Notably, at that time, the molecular and chemical mechanisms by which this was achieved were not understood, nor had the ligands for PD1 been identified.

The first PD1 ligand was presented in 1999 when Dong *et al.* (1999) characterised and named the surface protein B7-Homolog 1 (B7-H1). However, they found that B7-H1 stimulates, rather than attenuates, T cell proliferation, which is not consistent with what we know today and most likely reflects the methods they used. Like Linsley, Geene, *et al.* (1992), Dong et al. fused the extracellular portion of B7-H1 to the Fc region of an antibody and, by doing so, may have unknowingly blocked the PD1/B7-H1 interaction,

thereby promoting the T cell proliferation they observed. Approximately ten months later, Honjo and his colleagues characterised the function of B7-H1 and renamed it PD-L1 (Freeman et al., 2000). They used wild-type and PD1–deficient T cells to show the effects of PD-L1 – that it inhibited TCR-mediated T cell proliferation and reduced cytokine production. They also showed that PD-L1 was inducible on monocytes and peripheral blood dendritic cells upon stimulation with inflammatory mediators like interferon γ (IFNγ) and lipopolysaccharides (LPS, Freeman et al., 2000).

The second ligand, PD-L2, was identified by two independent groups that found opposing influences on T cell activation. Tseng *et al.* (2001) named the molecule B7-DC and showed it co-stimulated the production of IFNγ. The following year, Honjo and his colleagues identified and characterised PD-L2 and started to unravel the molecular biology of the PD-L/PD1 axis (Y. Latchman et al., 2001). They suggested this interaction results not in cell death but instead in cell cycle arrest through a phosphorylated SHP-2 mechanism. This paper was also the first to suggest that targeting and blocking the PD-L/PD1 axis might be a viable therapeutic strategy to promote anti-cancer immunity. Honjo and colleagues published their seminal study in 2002, which used an anti-PDL1 antibody to treat DBA/2 mice challenged with P815 mastocytomas that were genetically modified to overexpress PD-L1 (Iwai et al., 2002). Honjo shared the 2018 Nobel Prize in Physiology and Medicine with Allison for this work, and because of their research several checkpoint inhibiting antibody treatments have subsequently been developed, and approved to treat a variety of cancers (Almonte et al., 2021, Table 1).

1.2.3 Unanswered questions and literature review

Immune checkpoint therapies have undoubtedly been revolutionary and patients who respond to therapy do so remarkably well. However, only about a third of treated patients respond to these therapies (Almonte et al., 2021). Additionally, there are significant questions regarding how checkpoint inhibitors work in the clinic, with one striking example being direct evidence showing that ipilimumab, a humanised anti-CTLA4 antibody currently used to treat metastatic melanoma, does not work through a blocking mechanism (Du et al., 2018). There is also the question regarding how the gut microbiome

profoundly impacts immune checkpoint therapy success. This question is a major a focus of this dissertation.

These and other points are addressed in the following literature review, which we published in *Immunology and Cell Biology*. It also describes our proposed mechanism for why the gut microbiome profoundly impacts cancer therapy outcomes. Specifically, we propose that immune checkpoint therapies allow gut microbes to translocate out of the gut lumen, colonise distant solid tumours, and provoke an immune reaction akin to the intratumoural bacteria inoculations in Coley's experiments.

Check for updates

Immunology & Cell Biology 2021; **99**: 361–372
www.wileyonlinelibrary.com/journal/icb

REVIEW

How does the gut microbiome influence immune checkpoint blockade therapy?

Andrew A Almonte[1], Hareesha Rangarajan[1], Desmond Yip[2] & Aude M Fahrer[1]

1 Division of Biomedical Science and Biochemistry, Research School of Biology, Australian National University, Acton, ACT, Australia
2 Department of Medical Oncology, The Canberra Hospital and ANU Medical School, Australian National University, Garran, ACT, Australia

Keywords
CTLA-4/PD-1/PD-L1, gut microbiome, immune checkpoint blockade, immunology, immunotherapy, lymphocytes, T cells, tumor immunology

Correspondence
Andrew A Almonte, Research School of Biology, 46 Sullivans Creek Road, The Australian National University, Canberra, ACT 2600 Australia.
E-mail: Andrew.Almonte@anu.edu.au

Received 18 May 2020; Revised 21 August, 20 October and 1 November 2020; Accepted 1 November 2020

doi: 10.1111/imcb.12423

Immunology & Cell Biology 2021; **99**: 361–372

Abstract

Immune checkpoint blockade (ICB) therapies are revolutionary cancer treatments; however, they only benefit about a third of patients. Therefore, extensive research is underway to find methods to improve their therapeutic efficacy. One avenue of study that has recently emerged is to consider the role the gut microbiome plays in therapeutic success. Several high-impact studies have repeatedly shown that the presence, composition and level of diversity of the gut flora directly impact cancer treatment outcome in both mice and patients. These studies have also highlighted the danger of using antibiotics shortly before or during cancer treatments. However, there are still several questions that need to be answered, including which bacteria promote the greatest benefit, the mechanisms by which they act and how we can use this information to influence treatment outcome. In this review, we explain how the gut microbiome was realized to be of such importance and propose hypotheses for why gut flora have such a critical impact on ICB therapeutic success. We also describe a hypothetical mechanism involving bacterial translocation out of the gut and into the tumor, whereby the bacteria act in an adjuvant capacity to facilitate an antitumor response. By highlighting key papers in the field, we hope to hasten research on the subject so as to find a means to improve the therapeutic efficacy of these ground-breaking cancer treatments.

INTRODUCTION

Immune checkpoint blockade (ICB) therapy is a revolutionary option for cancer treatment. Injections of monoclonal antibodies targeting cytotoxic T-lymphocyte-associated protein 4 (CTLA-4), programmed death protein 1 (PD-1) or its ligand, PD-L1 (programmed death-ligand 1), have shown increased patient survival in multiple clinical trials.[1,2] These treatments also have better safety profiles than conventional chemotherapies,[3,4] making them an attractive, viable alternative to conventional treatment options. However, there are significant problems with ICB therapies. First, a majority of patients (approximately 70%) do not respond to treatment.[5] Second, they can be associated with a high financial burden for the patient, with nivolumab (anti-PD-1) costing about $73 000 in the United States for a course of treatment compared with $26 000 for standard chemotherapy options in 2017.[6] Finally, ICB therapies can cause immune-related adverse events that are not always manageable.[7,8] These issues mean it is incumbent on researchers to find methods to improve the response rate to ICB therapies.

Recently, there has been a resurgence of interest in the potential role bacteria play in anticancer therapies, particularly ICB therapies, and their ability to influence treatment outcome. Indeed, it has been shown that coadministration of antibiotics severely impairs the efficacy of cancer therapies in mice,[9] and this has been directly attributed to the depletion of gut bacteria.[10] This has been confirmed in cancer patients through retrospective studies that have shown those who were treated with antibiotics around the time of receiving anti-PD-L1 therapy have a significantly worse clinical outcome

1. Introduction

than those not given antibiotics.[11] In addition, there are reports showing that some bacterial species can improve ICB treatments, whereas others negatively influence treatment efficacy.

In this review, we first highlight key papers that call into question the assumed "blocking" mechanism of action of ICB therapies. Next, we call attention to key papers that show unequivocally the importance of gut microbes for ICB therapeutic success. We then juxtapose these findings and propose hypotheses for how and why gut microbes are so critical for successful ICB therapeutic outcome. Finally, we propose potential strategies for optimizing ICB therapies in both preclinical experiments and clinical trials. By doing so we hope to hasten research in this important topic and bring attention to potential new methods to optimize these revolutionary treatments.

QUESTIONS ABOUT ICB THERAPY

There are currently three major types of ICB therapies in widespread use in the clinic that target CTLA-4, PD-1 and PD-L1. Murine CTLA-4 was first described in 1987[12] and the human variant was identified the next year.[13] Murine and human PD-1 were both characterized by Tasuku Honjo in 1992[14] and 1994,[15] respectively. In the year 2000, Honjo also characterized and named the first PD-1 ligand, PD-L1.[16] He and Allison both recognized the therapeutic potential of targeting these immune checkpoint molecules for cancer treatment, and shared the 2018 Nobel Prize in Physiology and Medicine for their seminal work.[17,18] Several different drugs based on these inhibitors have been developed for the treatment of a variety of cancers (Table 1).

ICB therapies are presumed to simply sterically block the interactions between checkpoints and their ligands to facilitate an antitumor immune response, and there is evidence to support this "blockade hypothesis."[19] However, recent reports have presented convincing evidence that challenges this assumed mechanism of action. The most striking example was by Du *et al.*[20] who showed that ipilimumab, an IgG1 monoclonal antibody targeting human CTLA-4,[21,22] does not block the interaction of CD80/86 with CTLA-4, nor does it significantly block the CTLA-4-mediated transendocytosis of CD80/86. Yet despite this, ipilimumab still conveys a therapeutic benefit.[20] This study provided the most convincing evidence that our current conception of how "blocking" antibodies work in a physiological setting is inherently flawed.

Other inconsistencies have also been highlighted. It is known that the efficacies of anti-CTLA-4 and anti-PD-L1 monoclonal antibodies are influenced by their Fc regions, another observation that does not agree with a simple blocking mechanism. Anti-CTLA-4 requires a competent Fc region in order to provide optimal therapeutic benefit.[23,24] Furthermore, different isotypes of anti-CTLA-4 have different therapeutic efficacies, with IgG2a being the most potent for anticancer therapy.[25] Anti-PD-L1 is also more effective if it is IgG2a. Conversely, anti-PD-1 is the only one of the trio not to show Fc dependence; indeed it is most effective when the Fc region of the antibody is mutated to prevent binding to Fc receptors.[26] This reliance of anti-CTLA-4 and anti-PD-L1 on Fc competence and isotype identity implies a mechanism of action involving Fc receptors (e.g. CD16/32), which are largely found on myeloid cells. The mechanism could either involve (i) antibody crosslinking or (ii) a direct contribution by myeloid cells (e.g. antibody-dependent cellular cytotoxicity), though this is a question that still needs to be investigated *in vivo*.

Evidence for antibody-dependent cellular cytotoxicity is the finding that anti-CTLA-4 specifically influences the number of tumor-infiltrating regulatory T cells (Treg cells). Treg cells constitutively express high levels of CTLA-4 and are attracted to the tumor microenvironment where they help facilitate cancer immune evasion.[27,28] Anti-CTLA-4 antibodies have been shown to decrease both the intratumoural Treg-to-cytotoxic T lymphocyte ratio and the absolute number of tumour-infiltrating Treg cells in mouse models,[20,23,24] thereby promoting effective anticancer immune responses. The reason why tumor-infiltrating Treg cells, as opposed to Treg cells in other sites, are preferentially targeted following anti-CTLA-4 treatment is unclear, but Allison *et al.* recently published a paper showing upregulation of FcγRIV (CD16.2) on macrophages is key to this outcome.[29]

All of these inconsistencies with the "blockade hypothesis" have been well documented and are reproducible, and the evidence outlined above has prompted a call for a re-evaluation of the mechanism of action of ICB therapies, particularly for anti-CTLA-4 therapy.[20] An intriguing avenue of research has very recently emerged that may offer insights into these mechanisms.

DISCOVERY OF THE IMPORTANCE OF THE GUT MICROBIOME

The importance of gut microbes in cancer therapy was first shown by two papers in the November 2013 issue of *Science*. Viaud *et al.*[30] found that cyclophosphamide, a common form of chemotherapy, relies heavily on an intact intestinal microbiome. Mice treated with cyclophosphamide that were either raised in germ-free conditions or whose microbiome was depleted through

Table 1. Currently available ICB therapies and their suppliers, and the cancers for which they are approved for use by the US FDA.

Therapy name	Supplier	Antibody target	US FDA-approved tumor type
Atezolizumab	Genentech, USA	PD-L1	Hepatocellular carcinoma Non-small-cell lung cancer Small-cell lung cancer Triple-negative breast cancer Urothelial carcinoma
Avelumab	EMD Serono, USA	PD-L1	Merkel cell carcinoma Renal cell carcinoma Urothelial carcinoma
Durvalumab	Astra Zeneca, UK	PD-L1	Non-small-cell lung cancer Small-cell lung cancer Urothelial carcinoma
Ipilimumab	Bristol-Myers Squibb, USA	CTLA-4	Pleural mesothelioma Metastatic melanoma Microsatellite instability-high or mismatch repair-deficient colorectal cancer Renal cell carcinoma
Nivolumab	Bristol-Myers Squibb, USA	PD-1	Melanoma Classic Hodgkin's lymphoma Colorectal cancer with high microsatellite instability or mismatch repair deficiency Hepatocellular carcinoma Non-small-cell lung cancer Pleural mesothelioma Renal cell carcinoma Squamous cell carcinoma of the head and neck Squamous cell carcinoma of esophagus Urothelial carcinoma
Pembrolizumab	Merck, USA	PD-1	Classic Hodgkin's lymphoma Gastric cancer Melanoma Non-small-cell lung cancer Small-cell lung cancer Solid tumors with high microsatellite instability or mismatch repair deficiency Squamous cell carcinoma of the head and neck Squamous cell cancer of the esophagus Urothelial carcinoma

CTLA-4, cytotoxic T-lymphocyte-associated protein 4; FDA, Food and Drug Administration; ICB, immune checkpoint blockade; PD-1, programmed death protein 1; PD-L1, programmed death-ligand 1.

antibiotic treatment had a much poorer anticancer response. Closer investigation found cyclophosphamide-treated mice also showed villus shortening and perturbations in the gut lumen—observations consistent with the digestive problems frequently experienced by patients treated with cyclophosphamide and other chemotherapies. Importantly, Viaud *et al.*[30] also showed that cyclophosphamide treatment caused bacteria to translocate out of the intestine and settle in secondary lymphoid organs, particularly in the spleen and mesenteric lymph nodes. Furthermore, reconstituting the gut of antibiotic-treated mice with Gram-positive bacteria rescued the therapeutic benefit of cyclophosphamide therapies, further showing that gut bacteria play a critical role in therapeutic efficacy.

In the same issue of *Science*, Iida *et al.*[31] showed that gut microbes were also critical for another chemotherapy (oxaliplatin) and were also the first to show an effect of the gut microbiome on cancer immunotherapy. Animals injected subcutaneously with EL4 lymphoma, MC38 carcinoma or B16 melanoma cell lines were treated with a combination of anti-IL10 and CpG oligodeoxynucleotides,

1. Introduction

with or without chronic antibiotic treatment. Mice given antibiotics had significantly decreased survival, increased tumor growth rates and reduced numbers of tumor-infiltrating immune cells. Those tumor-infiltrating immune cells that were present also had a reduced inflammatory profile. Interestingly, gavaging mice with lipopolysaccharides, components of the Gram-negative bacterial cell wall and agonists for the innate immune sensor Toll-like receptor 4, partially rescued the therapeutic benefit from the anti-IL-10/CpG treatment. Mice deficient in *Tlr4* had the same treatment outcomes as mice treated with antibiotics. Thus, gut microbes acting through the Toll-like receptor innate immune pathway were shown to be important for therapeutic success in this immunotherapy model.

The first paper to show an explicit link between ICB therapeutic outcome and gut microbial composition (and a testament to good observation in science) was published 2 years later by Sivan *et al.*[32] The authors implanted B16.SIY melanoma into C57BL/6 mice but noticed a difference in their response to anti-PD-1 therapy based on their point of origin—Jackson Laboratories or Taconic Farms (Figure 1a). Mice from Jackson Laboratories had decreased tumor growth rates and were more responsive to anti-PD-L1 treatment. Importantly, cohousing Jackson Laboratories mice with Taconic Farms mice conferred the former cohort's superior treatment response to the latter. Mice are coprophagous animals, which means cohousing results in sharing of gut microbes. Further investigation also found that Jackson Laboratories mice had higher levels of intratumoral MHC-II^{high} dendritic cells. Sivan *et al.*[32] went further, and found that differences in treatment response correlated with the relative abundance of *Bifidobacterium* spp. present in the small intestine and colon. This study was the first to show that the composition of the gut flora can improve ICB treatment outcome.

ANTIBIOTICS INHIBIT ICB THERAPIES

A series of high-profile publications followed which showed that antibiotic treatment was detrimental to anti-CTLA-4 and anti-PD-1 therapies. This was shown both in mice[9,33] and, importantly, in retrospective analyses of human cancer patients treated with PD-1 blockade therapies.[9,11] Routy *et al.*[9] showed that patients treated for non-small-cell lung carcinoma, renal cell carcinoma and urothelial carcinoma that were treated with either anti-PD-1 or anti-PD-L1 had worse clinical outcomes when they received antibiotics. Derosa *et al.*[11] confirmed these results in a retrospective analysis of patients with advanced renal cell carcinoma or non-small-cell lung carcinoma. Those patients were treated with both anti-PD-1 and anti-PD-L1, either alone or in combination with anti-CTLA-4, and had taken antibiotics up to 3 months prior to receiving ICB therapies.[11] Both studies found patients who had taken antibiotics had consistently lower overall and progression-free survival following ICB therapies than those who did not.

In preparing this review, we noticed all key papers used the same antibiotic cocktail to deplete the microbiome of their mouse models and they all use C57BL/6 mice.[9,30,34,35] We have not been able to replicate these experiments in BALB/c mice as they will not drink the published antibiotic cocktail. Our current hypothesis is that BALB/c mice do not tolerate the bitter taste. Studies have shown that different inbred mouse strains have different tolerances for the taste of bitter compounds, with BALB/c mice being more sensitive and less tolerant to bitterness than C57BL/6 mice.[36,37] It is likely that lower concentrations of the antibiotic cocktail may be utilized with BALB/c mice to achieve the same effect (cf. streptomycin concentration used in Tanoue *et al.*[38]). This is an important consideration when planning future experiments. As many cancer models are on a BALB/c background, this technical problem has likely impeded further elucidation of the mechanism by which gut microbes influence ICB therapies.

BACTERIAL SPECIES IMPORTANT FOR ICB THERAPY SUCCESS

As well as the detrimental effects of antibiotics, several studies have investigated which species of bacteria may influence ICB therapeutic outcome. The techniques used in these studies are summarized in Figure 1 and the bacterial species they identified are summarized in Figure 2. Matson *et al.*[33] transferred eight gut microbial species from human anti-PD-1 responders into mice through fecal matter transplant (FMT) and showed that mice which received the FMT responded better to anti-PD-L1 therapy. Gopalakrishnan *et al.*[39] showed that human melanoma patients who responded to anti-PD-1 not only had higher enrichment of certain gut microbial species, but also a more diverse gut microbiome. Mice that received FMT from these patients also benefited more from anti-PD-L1 therapy, accompanied by significant enrichment of innate effector cells within the tumor. However, it should be noted that this finding was based on investigating only three patients (supplementary figure S12 in Gopalakrishnan *et al.*[39]). Routy *et al.*[9] showed that antibiotics, but not proton-pump inhibitors (which also significantly alter the microbiome[40]), limit the effectiveness of cancer immunotherapy and they also showed that the presence of *Akkermansia muciniphila* significantly increased therapeutic ICB efficacy. Finally,

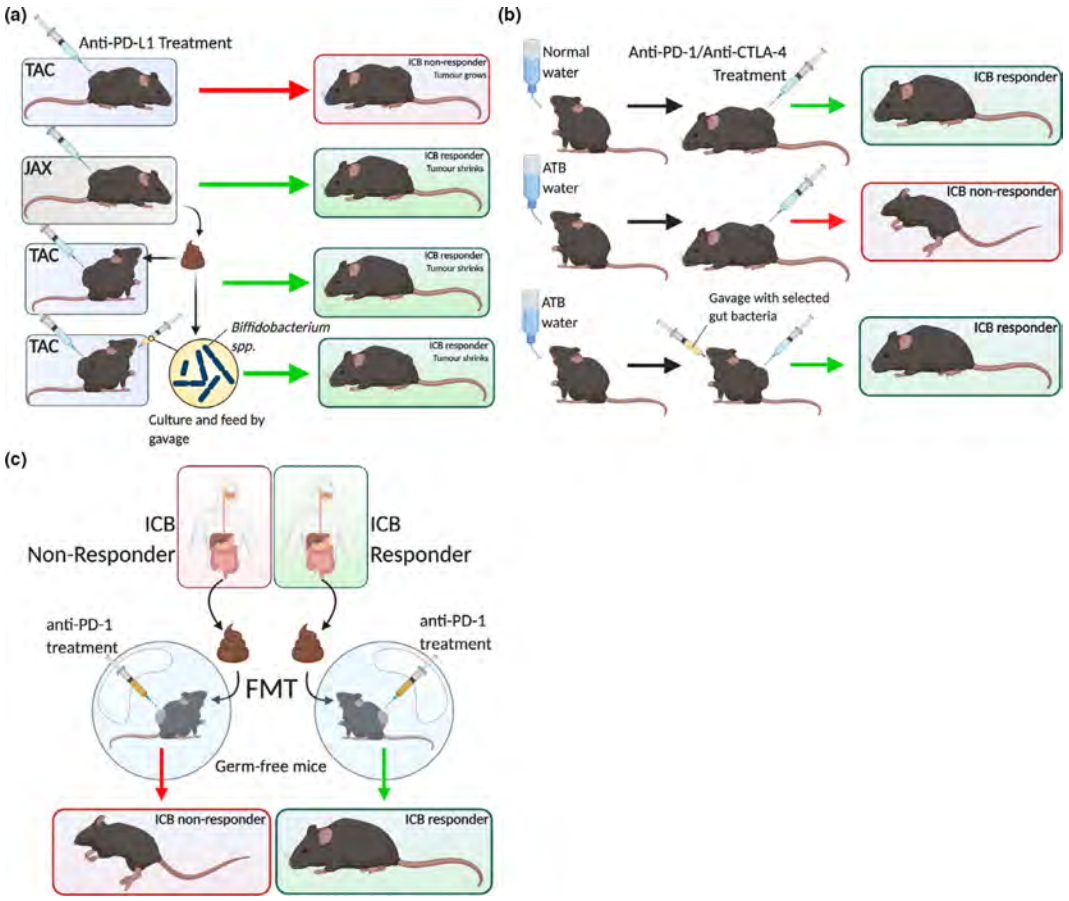
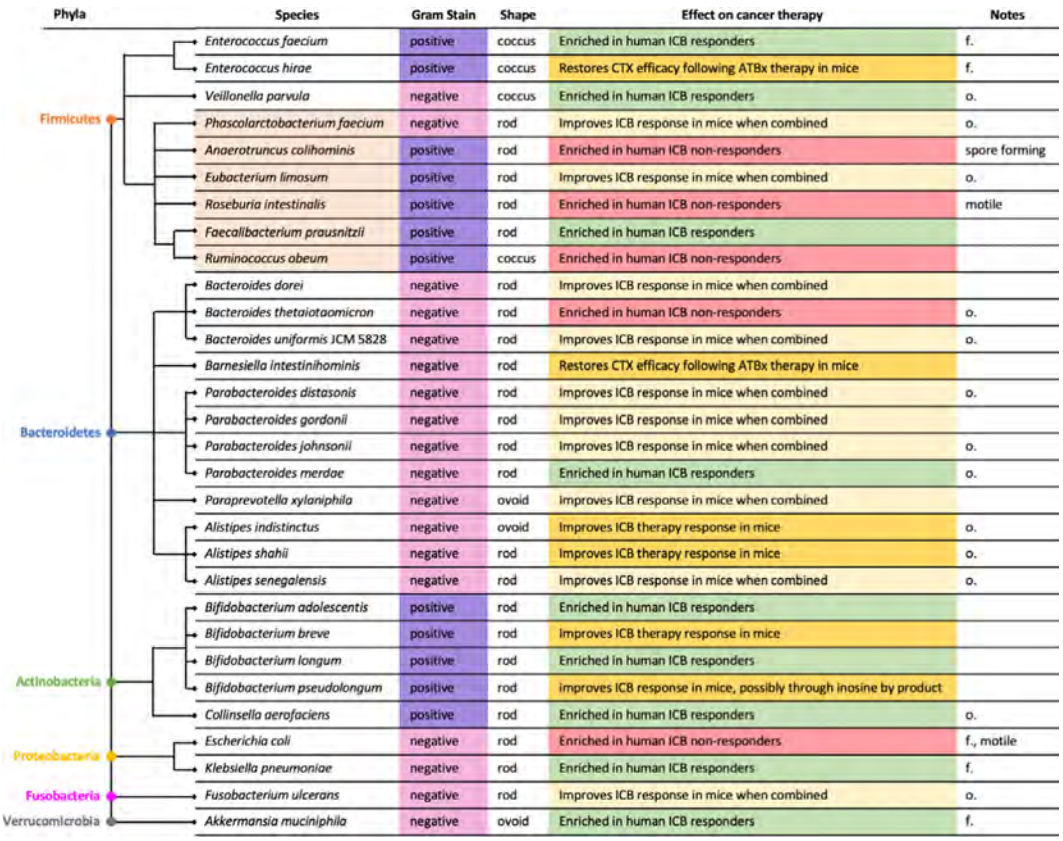


Figure 1. Several experiments have shown that gut microbes are essential for successful immune checkpoint blockade (ICB) therapeutic outcome. **(a)** Sivan *et al.*[32] first published the relationship between gut microbiota and ICB therapies after observing different and consistent responses between mice from Jackson Laboratories (JAX) and Taconic Farms (TAC). Cohousing mice from JAX and TAC improved the latter's response to anti-PD-L1 treatment, and further investigation found *Bifidobacterium* spp. were the main drivers for this increased response. **(b)** Routy *et al.*[9] and Vetizou *et al.*[34] went further by first depleting the gut microbiota with antibiotics (ATBs). Depletion of gut microbiota reduced the treatment efficacy of both anti-PD-1 and anti-CTLA-4, but reconstitution with select bacteria through oral gavage restored the therapeutic effect. **(c)** Other studies transplanted microbiota from human ICB responders and nonresponders into tumor-bearing germ-free mice via fecal matter transplants (FMTs) before administering ICB therapies.[33,34,39] The results in the mice correlated with the results from the human donors, again suggesting that the microbial composition of the ICB therapy recipient is critical for a successful therapeutic response. CTLA-4, cytotoxic T-lymphocyte-associated protein 4; PD-1, programmed death protein 1; PD-L1, programmed death-ligand 1.

Tanoue *et al.*[38] identified a consortium of 11 bacterial species, seven of which were members of the Bacteroidales phylum, that worked in concert to increase the therapeutic efficacy of ICB treatments.

Figure 2 summarizes the bacteria identified in all of these studies and groups them by taxonomy. As can be seen, there is no identifiable pattern among the bacteria found to influence cancer therapies. Both Gram-positive and Gram-negative, both facultative and obligate anaerobes and both coccus and rod-shaped bacteria are found to influence ICB treatment outcome.[9,30,31] Furthermore, the protherapeutic and antitherapeutic nature of gut microbes are not limited to particular phylogenetic classifications as there is variation in



Phyla	Species	Gram Stain	Shape	Effect on cancer therapy	Notes
Firmicutes	*Enterococcus faecium*	positive	coccus	Enriched in human ICB responders	f.
	Enterococcus hirae	positive	coccus	Restores CTX efficacy following ATBx therapy in mice	f.
	Veillonella parvula	negative	coccus	Enriched in human ICB responders	o.
	Phascolarctobacterium faecium	negative	rod	Improves ICB response in mice when combined	o.
	Anaerotruncus colihominis	positive	rod	Enriched in human ICB non-responders	spore forming
	Eubacterium limosum	positive	rod	Improves ICB response in mice when combined	o.
	Roseburia intestinalis	positive	rod	Enriched in human ICB non-responders	motile
	Faecalibacterium prausnitzii	positive	rod	Enriched in human ICB responders	
	Ruminococcus obeum	positive	coccus	Enriched in human ICB non-responders	
Bacteroidetes	*Bacteroides dorei*	negative	rod	Improves ICB response in mice when combined	
	Bacteroides thetaiotaomicron	negative	rod	Enriched in human ICB non-responders	o.
	Bacteroides uniformis JCM 5828	negative	rod	Improves ICB response in mice when combined	o.
	Barnesiella intestinihominis	negative	rod	Restores CTX efficacy following ATBx therapy in mice	
	Parabacteroides distasonis	negative	rod	Improves ICB response in mice when combined	o.
	Parabacteroides gordonii	negative	rod	Improves ICB response in mice when combined	
	Parabacteroides johnsonii	negative	rod	Improves ICB response in mice when combined	o.
	Parabacteroides merdae	negative	rod	Enriched in human ICB responders	o.
	Paraprevotella xylaniphila	negative	ovoid	Improves ICB response in mice when combined	
	Alistipes indistinctus	negative	ovoid	Improves ICB therapy response in mice	o.
	Alistipes shahii	negative	rod	Improves ICB therapy response in mice	o.
	Alistipes senegalensis	negative	rod	Improves ICB response in mice when combined	o.
Actinobacteria	*Bifidobacterium adolescentis*	positive	rod	Enriched in human ICB responders	
	Bifidobacterium breve	positive	rod	Improves ICB therapy response in mice	
	Bifidobacterium longum	positive	rod	Enriched in human ICB responders	
	Bifidobacterium pseudolongum	positive	rod	Improves ICB response in mice, possibly through inosine by product	
	Collinsella aerofaciens	positive	rod	Enriched in human ICB responders	o.
Proteobacteria	*Escherichia coli*	negative	rod	Enriched in human ICB non-responders	f., motile
	Klebsiella pneumoniae	negative	rod	Enriched in human ICB responders	f.
Fusobacteria	*Fusobacterium ulcerans*	negative	rod	Improves ICB response in mice when combined	o.
Verrucomicrobia	*Akkermansia muciniphila*	negative	ovoid	Enriched in human ICB responders	f.

Figure 2. Phylogenetic information of identified bacteria known to influence chemotherapy and immunotherapy. The phyla of the bacterial species are listed on the left in bold text and corresponds to the nodes on the phylogenetic tree. There is no obvious pattern among the phylogeny that correlates with how bacterial species influence cancer therapeutic response. Species highlighted in light orange are members of the Clostridia class and illustrate the variety of influences bacteria within a single taxonomic classification can have on cancer therapies. All species listed are anaerobic and, where known, are further classified as obligate (o) or facultative (f) anaerobes. ATBx, antibiotic treatment; CTX, cyclophosphamide treatment; ICB, immune checkpoint blockade.

treatment outcomes in mice and humans colonized with members of the same class and order. For example, some members of Clostridia were found enriched in human ICB responders,[39] and others were found in nonresponders.[33] It should be remembered that the gut microbiome is a complex and dynamic ecological community, and there is evidence for an as yet uncharacterized interaction among microbial species that either promote or inhibit successful cancer therapeutic responses.[38] Indeed, it has been proposed that researchers pursuing this topic must move past phylogeny and instead focus on the underlying mechanistic properties by which gut bacteria influence ICB therapies.[41]

IMMUNOLOGICAL MECHANISMS

Just as there is no readily apparent pattern among the identified bacteria, the immunological mechanism is equally elusive. Some reports have suggested a $CD4^+$ T-cell-mediated mechanism as a result of increased pathogenic T helper type 17 cell differentiation.[9] These pathogenic T helper type 17 cells may then further enable the differentiation of T helper type 1 cells, which are known to have antitumor effects. A similar mechanism was proposed for the effect of gut microbiome in other cancer therapies.[30,42] Other reports have suggested a $CD8^+$ T-cell-mediated mechanism,[32,33] as the anticancer

effects of positive regulator gut microbes such as *Bifidobacterium* are dependent on $CD8^+$ T-cell priming. Evidence for this mechanism was found when *Bifidobacterium*'s protherapeutic modulatory effects were completely abolished in mice lacking $CD8^+$ T cells, conclusively showing they play an essential role in this microbe's effect on therapy.[32] Tanoue *et al.*[38] found increased $CD8^+$ T-cell levels in the tumor of germ-free mice fed a combination of 11 specified bacterial species and treated with anti-PD-1, and therapeutic efficacy was abolished after $CD8^+$ T-cell depletion.[38] Finally, Iida *et al.*[31] suggested that the adaptive immune system is secondary to the innate immune system, as they found that gut microbes enhance anticancer therapies through tumor necrosis factor and Toll-like receptor 4 signaling (although they were using an immunotherapy different to ICB). Interestingly, they are the only group to propose a non-T-cell-centric mechanism, directly contrasting the previous two theories.

The key questions for future studies include *how* do gut microbes influence cancer immunotherapies? More importantly, is it possible to modulate a patient's gut microbial composition to improve their chances of responding favorably to ICB therapies? In this next section, we present possible answers these questions.

HOW GUT MICROBES MAY INFLUENCE ICB THERAPIES

Bacterial metabolites

One hypothesis proposes it is metabolic and fermentation by-products produced by the gut flora that are the driving factor for increased ICB treatment efficacy.[41] Short-chain fatty acids are the fermented products of undigested carbohydrates, mainly starches and sugars from plant matter.[43] Short-chain fatty acids have been shown to promote $CD8^+$ memory T-cell formation[44] and the differentiation of naïve T cells into T helper type 1 and T helper type 17 phenotypes.[45] Several bacteria shown to positively influence ICB therapeutic efficacy produce short-chain fatty acids and are enriched in high-fiber diets, including members of the Firmicutes and Bacteroidetes phyla, as well as the species *A. muciniphila* (reviewed by Venegas *et al.*[46]). Besides producing short-chain fatty acids, *A. muciniphila* also moderates intestinal inflammation and induces the production of mucus in the colon, resulting in a more robust barrier between the commensals and the intestinal epithelium.[47]

Another recent publication identified a potent immunomodulator that improved murine responses to anti-CTLA-4 therapy.[35] Mager *et al.*[35] found inosine, an adenosine homolog, was produced by *A. muciniphila*[9] and *Bifidobacterium pseudolongum*, two species previously found enriched in ICB responders. Interestingly, mice with subcutaneous MC38 colorectal cancers injected with the sera from mice monocolonized with *B. pseudolongum*, and treated with anti-CTLA-4, were found to develop an improved immune response relative to control animals. Metabolomics analysis of sera from mice colonized with *B. pseudolongum* showed they had significantly higher levels of inosine and inosine degradation products.[35] However, it should be remembered that these animals had an overrepresentation of *B. pseudolongum*, and that normal physiological levels of inosine have been shown to act as an immunosuppressant.[48] Countering this, the authors also note that inosine monophosphate and hypoxanthine (an inosine degradation product) were two of the most elevated bacterial products found in the cecum and sera of mice colonized by the 11 bacteria identified by Tanoue *et al.*[35,38] This excellent study, which also noted that the degree of gut permeabilization following ICB treatments is dependent on the presence of gut microbes, shows it is worth investigating how metabolic by-products influence ICB therapy.

Bacterial translocation into the tumor

An alternative, tantalizing hypothesis is that ICB therapies are allowing bacteria to translocate out of the gut epithelium and into a tumor where they act in an adjuvant-like capacity to facilitate a systemic antitumor immune response (Figure 3). There is evidence to support bacterial translocation. One of the more common immune-related adverse events associated with all three ICB therapies is intestinal inflammation,[8] and a systematic review published in 2018 suggested that patients who experience some grade of intestinal inflammation had a significantly higher chance of responding to ICB treatment.[49] In mouse models, shortening of intestinal villi and perturbations in the gut lining have been observed following anti-CTLA-4 treatment.[34,35] This damage is reminiscent of injury caused by cyclophosphamide treatments, which were shown to allow bacteria to translocate out of the gut into secondary lymphoid organs.[30] It is unclear why ICB therapies cause intestinal pathology, though one intriguing possibility we have considered is that this may be because of the activation of γδ intestinal intraepithelial lymphocytes. These cells express both PD-1 and CTLA-4 and are highly cytotoxic, poised to act and sit between intestinal epithelial cells.[50]

Therefore, it would be reasonable to assume that gut damage caused by both cyclophosphamide and ICB therapies could also allow bacteria to translocate across the gut epithelium and infect distant tissues. Indeed,

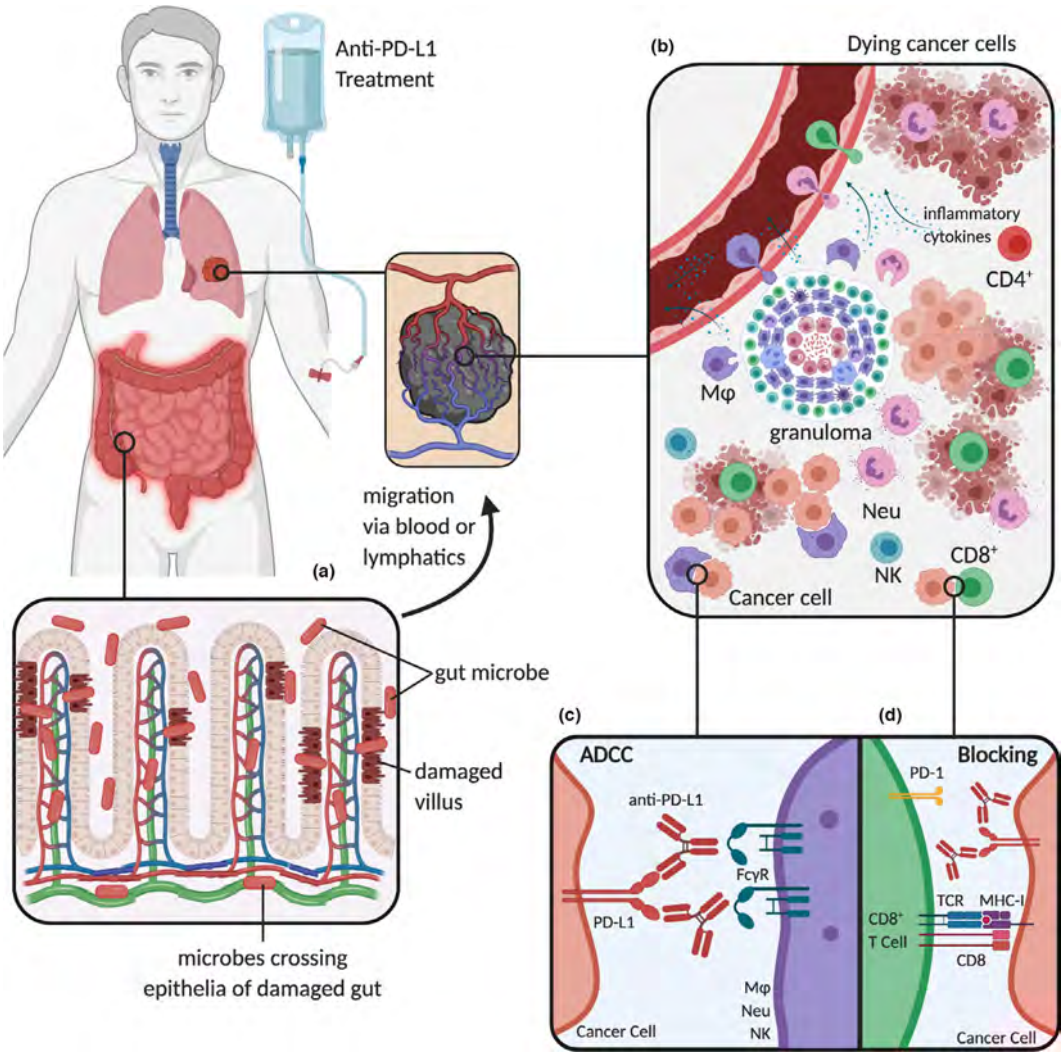


Figure 3. Proposed means by which microbes influence immune checkpoint blockade (ICB) treatment outcome. **(a)** ICB therapies compromise the integrity of the gut lining through a mechanism not completely understood. Microbes can take advantage of this damage to translocate out of the gut and reach distant tissues, including the spleen, mesenteric lymph nodes and solid tumors. **(b)** The physiological, chemical and physical properties of the tumor microenvironment allow accumulation of bacteria. Tumor-infiltrating bacteria activate innate immune pathways and recruit immune cells into the tumor, which initially target the bacteria, but also activate the adaptive immune system and initiate/potentiate an anticancer immune response. **(c)** ICB therapies can mark cells for killing through antibody-dependent cellular cytotoxicity (ADCC). Binding of anti-PD-L1 can result in direct killing of cancer cellswhile binding of anti-CTLA-4 can result in the killing of Treg cells, thus reducing the inhibition of the anticancer immune response. **(d)** ICB therapies can act through traditional blocking mechanisms, thereby increasing the killing of cancer cells by tumor-infiltrating cytotoxic T cells. $CD4^+$, T helper type 1 $CD4^+$ T cell; $CD8^+$, cytotoxic T cell; CTLA-4, cytotoxic T-lymphocyte-associated protein 4; Mφ, macrophage; MHC, major histocompatibility complex; Neu, neutrophil; NK, natural killer (cell); PD-1, programmed death protein 1; PD-L1, programmed death-ligand 1; TCR, T-cell receptor.

because of the leakiness of the tumor vasculature, bacterial colonization of the tumor could be expected. A previous study has shown that intravenously injected particulates approximately the size of bacteria preferentially accumulate within tumor masses.[51] In addition, past reports have already suggested that tumors, which have a hypoxic environment ideal for anaerobic bacterial growth, are viable locations for bacterial colonization.[52–54] Most importantly, direct evidence for bacterial translocation and subsequent colonization of solid tumors has already been shown in at least one mouse model; intratumoral granulomas were found in animals gavaged with *A. muciniphila* and treated with anti-PD-1 (supplementary figure 15 in Routy *et al.*[9]).

After submission of this review, Jennifer Wargo and her colleagues published an impressive study in *Science* using several genetic and visualization techniques to show that tumors collected from patients do contain microbial communities and suggest that different tumors develop distinct "tumor microbiomes."[55] The authors were able to examine over 1000 tumors samples collected from nine independent medical centers and used robust experimental techniques to exclude incidental sample contamination. The bacteria were found present intracellularly within both cancer cells and tumor-infiltrating immune cells. They were also suggested to be metabolically active with gene ontologies showing pathways appropriate and unique to the tumors they colonized. For example, bacteria found in lung cancers caused by smoking expressed enzymes that could metabolize the chemical reagents frequently found in cigarettes, such as toluene and nicotine.[55] Furthermore, though mentioned in passing, Wargo and her colleagues were able to show that bacteria found within melanomas of ICB responders and nonresponders correlated well with bacteria identified in previous studies that improve treatment response when present within the patient's gut microbiome.[9,33,39] Determining if these intratumoral bacteria promote an immune response against the infected tumor and if these bacteria originate from the gut microbiome are critical questions that need to be investigated.

Given the cumulative evidence presented thus far, we propose the following three-point model that could explain how ICB therapies work by either an Fc-dependent or -independent mechanism to promote a successful therapeutic outcome (Figure 3).

First, all three ICB therapies cause gut pathology[8] which would be expected to increase the incidence of bacterial translocation across the gut lumen. As discussed, these bacteria would accumulate in tumors. Their presence will induce an inflammatory milieu within the tumor microenvironment, promoting the recruitment of immune cells and thereby acting as unintentional adjuvants to elicit an antitumor immune response. How ICB therapies cause gut pathology and whether the isotype identity of the monoclonal antibodies plays a role are currently not understood.

Second, the monoclonal antibodies can bind to, and through antibody-dependent cellular cytotoxicity, kill either (i) tumor cells expressing PD-L1[56] or (ii) tumor-infiltrating Treg cells, which constitutively express high levels of CTLA-4.[20,29] In either case, killing would be mediated by cells expressing Fc receptors, including neutrophils, macrophages and natural killer cells. Bacterial infection of the tumor would potentiate this response as they would attract innate immune cells to the tumor. This response would be entirely Fc dependent.

Finally, there is the traditional blocking mechanism which is independent of both bacterial translocation and isotype identity. Nonetheless, even this mechanism could be potentiated by the adjuvant effect of bacteria as this would lead to increased numbers of tumor-infiltrating T cells. Anti-PD-1 and anti-PD-L1 would bind to their ligands on T cells, natural killer cells and cancer cells, blocking the inhibition signals and thus potentiating the killing of cancer cells.[56] Blocking of anti-CTLA-4 is more likely to affect T cells in secondary lymphoid organs during T-cell priming,[57] but as previously discussed, the efficacy of ipilimumab (anti-CTLA-4) has been shown not to rely on a simple blocking mechanism.[20]

Thus, we propose that different ICB therapies work through different combinations of the aforesaid mechanisms. Anti-CTLA-4 would rely on bacterial translocation and the Fc-mediated killing of Treg cells; anti-PD-1 would rely on bacterial translocation and blocking of the interaction between PD-1 and PD-L1 and anti-PD-L1 would rely on all three mechanisms. If accurate, our model would explain why antibiotics—which deplete the gut bacteria and reduce their translocation from the gut into the tumor—substantially decrease the efficacy of ICB therapies. Indeed, given the recent findings of Wargo and colleagues,[55] antibiotics could also potentially deplete bacteria within cancers. However, given the authors found bacteria to be intracellular, this is perhaps unlikely. A nonspecific translocation mechanism as a result of gut damage caused by ICB therapies would also explain why such a large and diverse number of different bacteria can improve treatment efficacy (Figure 2), although why some bacterial species improve therapeutic outcome and others reduce therapeutic benefit is still an open question.

Bacteria and cancer therapies

The concept of using bacteria to influence cancer treatment has a long history. In the late 19th century, Dr

William Coley, the "Father of Immunotherapy," successfully performed intravenous and intratumoral injections with a mixture of *Streptococcus pyogenes* and *Serratia marcescens* to acheive impressive regression rates.[58,59] Intravesical administration of live Bacillus Calmette–Guérin has been one of the most successful immunotherapies against bladder cancer for the past 40 years.[60,61] Our laboratory is currently running a clinical trial investigating the safety of intratumoral injections of complete Freund's adjuvant—a slow release water-in-oil emulsion containing heat-killed Mycobacteria (ACTRN12616001637437)—which will be followed by an approved trial to coadminister this treatment with ICB therapies.[62] Multiple recent studies have been published investigating the potential utility of bacteria in cancer therapies.[63]

POTENTIAL MEANS TO IMPROVE ICB THERAPEUTIC EFFECTIVENESS

Given all the evidence showing the importance of gut microbial presence and composition for ICB therapeutic success, the first, most important, and widely acknowledged method to improve ICB response rates is to avoid prior or coadministration of antibiotics.[64]

Another option may be to optimize the composition of the patient's gut microbiome through FMT. This will only be briefly described as an excellent review on the subject has already been written by McQuade *et al.*[65] The strategy involves transplanting the gut microbiomes of ICB responders into the intestines of either patients just beginning ICB treatment or who show a poor response to ICB therapy. The procedure itself is also relatively simple as it involves either colonic or oral administration through frozen capsules, and it appears to have very few adverse effects. Several clinical trials combining FMT procedures with ICB treatments are already underway (McQuade *et al.*[65]; Table 1). Transplanting entire microbiomes has the advantage of not only establishing beneficial microbiota in the patients' gut, but also redundant and supportive microbes as well.[65]

However, our model for the ICB mechanism of action still relies on some degree of gut pathology to facilitate the translocation of gut microbes. Gastrointestinal pathology is not seen in all patients receiving ICB treatment and, if our hypothesis is correct, would be one reason why not all patients respond to ICB treatment. This could be overcome by injecting selected strains of beneficial bacteria, live or dead, either (i) directly into an accessible tumor or (ii) intravenously at extremely low concentrations. Sepsis can be fatal, so intravenous injections of potentially live bacteria would have to be done carefully to avoid sepsis or septic shock. However, clearly gut bacteria can travel to distant tissues, including the spleen, lymph nodes and cancers without causing sepsis. The optimal timing, route of injection (intravenous *versus* intratumoral) and viability of bacteria relative to ICB injections would need to be determined.

CONCLUSION

ICB therapies are revolutionary treatments for many malignancies and desperately require optimization. It has become apparent that gut bacteria are critical for therapeutic success, but we still do not completely understand which species are important or how they influence therapeutic outcome. Here, we have reviewed the literature that both challenges the conventional blocking hypothesis and implicates the gut microbiome in the success of immune checkpoint "blockade" therapies. We have also proposed a potential mechanism —translocation of bacteria from a damaged gut into the tumor—that explains why antibiotics decrease ICB response rate. Lastly, we have proposed testable hypotheses that may potentiate ICB therapeutic success. Improving the efficacy and success rate of these therapies is the next major challenge and investigating the contribution of the gut microbiome should lead to innovative methods for optimizing ICB treatments in the clinic.

ACKNOWLEDGMENTS

Figures 1 and 3 were created with BioRender. Special thanks go to Dr Yada Kanjanapan for reviewing Table 1.

CONFLICT OF INTEREST

The authors declare there is no conflict of interest to disclose.

AUTHOR CONTRIBUTIONS

Andrew A Almonte: Conceptualization; Investigation; Project administration; Visualization; Writing – original draft; Writing – review and editing. **Hareesha Rangarajan:** Investigation; Resources. **Desmond Yip:** Conceptualization; Supervision; Writing – review and editing. **Aude M Fahrer:** Conceptualization; Supervision; Writing – review and editing.

REFERENCES

1. Hellmann MD, Paz-Ares L, Bernabe Caro R, *et al.* Nivolumab plus Ipilimumab in Advanced Non-Small-Cell Lung Cancer. *N Engl J Med* 2019; **381**: 2020–2031.
2. Larkin J, Chiarion-Sileni V, Gonzalez R, *et al.* Combined Nivolumab and Ipilimumab or monotherapy in untreated melanoma. *N Engl J Med* 2015; **373**: 23–34.

3. Reck M, Rodriguez-Abreu D, Robinson AG, *et al.* Pembrolizumab versus chemotherapy for PD-L1-positive non-small-cell lung cancer. *N Engl J Med* 2016; **375**: 1823–1833.
4. Robert C, Schachter J, Long GV, *et al.* Pembrolizumab versus Ipilimumab in advanced melanoma. *N Engl J Med* 2015; **372**: 2521–2532.
5. Havel JJ, Chowell D, Chan TA. The evolving landscape of biomarkers for checkpoint inhibitor immunotherapy. *Nat Rev Cancer* 2019; **19**: 133–150.
6. Ward MC, Shah C, Adelstein DJ, *et al.* Cost-effectiveness of nivolumab for recurrent or metastatic head and neck cancer. *Oral Oncol* 2017; **74**: 49–55.
7. June CH, Warshauer JT, Bluestone JA. Is autoimmunity the Achilles' heel of cancer immunotherapy? *Nat Med* 2017; **23**: 540–547.
8. Postow MA, Sidlow R, Hellmann MD. Immune-related adverse events associated with immune checkpoint blockade. *N Engl J Med* 2018; **378**: 158–168.
9. Routy B, Le Chatelier E, Derosa L, *et al.* Gut microbiome influences efficacy of PD-1-based immunotherapy against epithelial tumors. *Science* 2018; **359**: 91–97.
10. Viaud S, Daillere R, Boneca IG, *et al.* Gut microbiome and anticancer immune response: really hot Sh*t!. *Cell Death Differ* 2015; **22**: 199–214.
11. Derosa L, Hellmann MD, Spaziano M, *et al.* Negative association of antibiotics on clinical activity of immune checkpoint inhibitors in patients with advanced renal cell and non-small-cell lung cancer. *Ann Oncol* 2018; **29**: 1437–1444.
12. Brunet JF, Denizot F, Luciani MF, *et al.* A new member of the immunoglobulin superfamily–CTLA-4. *Nature* 1987; **328**: 267–270.
13. Dariavach P, Mattei MG, Golstein P, Lefranc MP. Human Ig superfamily CTLA-4 gene: chromosomal localization and identity of protein sequence between murine and human CTLA-4 cytoplasmic domains. *Eur J Immunol* 1988; **18**: 1901–1905.
14. Ishida Y, Agata Y, Shibahara K, Honjo T. Induced expression of PD-1, a novel member of the immunoglobulin gene superfamily, upon programmed cell death. *EMBO J* 1992; **11**: 3887–3895.
15. Shinohara T, Taniwaki M, Ishida Y, Kawaichi M, Honjo T. Structure and chromosomal localization of the human PD-1 gene (PDCD1). *Genomics* 1994; **23**: 704–706.
16. Freeman GJ, Long AJ, Iwai Y, *et al.* Engagement of the PD-1 immunoinhibitory receptor by a novel B7 family member leads to negative regulation of lymphocyte activation. *J Exp Med* 2000; **192**: 1027–1034.
17. Leach DR, Krummel MF, Allison JP. Enhancement of antitumor immunity by CTLA-4 blockade. *Science* 1996; **271**: 1734–1736.
18. Iwai Y, Ishida M, Tanaka Y, Okazaki T, Honjo T, Minato N. Involvement of PD-L1 on tumor cells in the escape from host immune system and tumor immunotherapy by PD-L1 blockade. *Proc Natl Acad Sci USA* 2002; **99**: 12293–12297.
19. Fenwick C, Loredo-Varela JL, Joo V, *et al.* Tumor suppression of novel anti-PD-1 antibodies mediated through CD28 costimulatory pathway. *J Exp Med* 2019; **216**: 1525–1541.
20. Du X, Tang F, Liu M, *et al.* A reappraisal of CTLA-4 checkpoint blockade in cancer immunotherapy. *Cell Res* 2018; **28**: 416–432.
21. Koenig S, Elicker J. FDA Approves YERVOY™ (ipilimumab) for the Treatment of Patients with Newly Diagnosed or Previously-Treated Unresectable or Metastatic Melanoma, the Deadliest Form of Skin Cancer. Bristol-Myers Squibb Company; 2011, March 25. https://news.bms.com/news/r-and-d/2011/FDA-Approves-YERVOY-ipilimumab-for-the-Treatment-of-Patients-with-Newly-Diagnosed-or-Previously-Treated-Unresectable-or-Metastatic-Melanoma-the-Deadliest-Form-of-Skin-Cancer/default.aspx
22. Lipson EJ, Drake CG. Ipilimumab: an anti-CTLA-4 antibody for metastatic melanoma. *Clin Cancer Res* 2011; **17**: 6958–6962.
23. Simpson TR, Li F, Montalvo-Ortiz W, *et al.* Fc-dependent depletion of tumor-infiltrating regulatory T cells co-defines the efficacy of anti-CTLA-4 therapy against melanoma. *J Exp Med* 2013; **210**: 1695–1710.
24. Arce Vargas F, Furness AJS, Litchfield K, *et al.* Fc effector function contributes to the activity of human anti-CTLA-4 antibodies. *Cancer Cell* 2018; **33**: 649–663 e644.
25. Selby MJ, Engelhardt JJ, Quigley M, *et al.* Anti-CTLA-4 antibodies of IgG2a isotype enhance antitumor activity through reduction of intratumoral regulatory T cells. *Cancer Immunol Res* 2013; **1**: 32–42.
26. Dahan R, Sega E, Engelhardt J, Selby M, Korman AJ, Ravetch JV. FcγRs modulate the anti-tumor activity of antibodies targeting the PD-1/PD-L1 axis. *Cancer Cell* 2015; **28**: 285–295.
27. Curiel TJ, Coukos G, Zou L, *et al.* Specific recruitment of regulatory T cells in ovarian carcinoma fosters immune privilege and predicts reduced survival. *Nat Med* 2004; **10**: 942–949.
28. Ohue Y, Nishikawa H. Regulatory T (Treg) cells in cancer: Can Treg cells be a new therapeutic target? *Cancer Sci* 2019; **110**: 2080–2089.
29. Sharma N, Vacher J, Allison JP. TLR1/2 ligand enhances antitumor efficacy of CTLA-4 blockade by increasing intratumoral Treg depletion. *Proc Natl Acad Sci USA* 2019; **116**: 10453–10462.
30. Viaud S, Saccheri F, Mignot G, *et al.* The intestinal microbiota modulates the anticancer immune effects of cyclophosphamide. *Science* 2013; **342**: 971–976.
31. Iida N, Dzutsev A, Stewart CA, *et al.* Commensal bacteria control cancer response to therapy by modulating the tumor microenvironment. *Science* 2013; **342**: 967–970.
32. Sivan A, Corrales L, Hubert N, *et al.* Commensal *Bifidobacterium* promotes antitumor immunity and facilitates anti-PD-L1 efficacy. *Science* 2015; **350**: 1084–1089.
33. Matson V, Fessler J, Bao R, *et al.* The commensal microbiome is associated with anti-PD-1 efficacy in metastatic melanoma patients. *Science* 2018; **359**: 104–108.
34. Vetizou M, Pitt JM, Daillere R, *et al.* Anticancer immunotherapy by CTLA-4 blockade relies on the gut microbiota. *Science* 2015; **350**: 1079–1084.

1. Introduction

35. Mager LF, Burkhard R, Pett N, *et al.* Microbiome-derived inosine modulates response to checkpoint inhibitor immunotherapy. *Science* 2020; **369**: 1481–1489.
36. Boughter JD Jr, Bachmanov AA. Behavioral genetics and taste. *BMC Neurosci* 2007; **8**(Suppl 3): S3.
37. Klein TW, DeFries JC. Similar polymorphism of taste sensitivity to PTC in mice and men. *Nature* 1970; **225**: 555–557.
38. Tanoue T, Morita S, Plichta DR, *et al.* A defined commensal consortium elicits CD8 T cells and anti-cancer immunity. *Nature* 2019; **565**: 600–605.
39. Gopalakrishnan V, Spencer CN, Nezi L, *et al.* Gut microbiome modulates response to anti-PD-1 immunotherapy in melanoma patients. *Science* 2018; **359**: 97–103.
40. Jackson MA, Goodrich JK, Maxan ME, *et al.* Proton pump inhibitors alter the composition of the gut microbiota. *Gut* 2016; **65**: 749–756.
41. Finlay BB, Goldszmid R, Honda K, Trinchieri G, Wargo J, Zitvogel L. Can we harness the microbiota to enhance the efficacy of cancer immunotherapy? *Nat Rev Immunol* 2020; **20**: 522–528.
42. Daillere R, Vetizou M, Waldschmitt N, *et al. Enterococcus hirae* and *Barnesiella intestinihominis* facilitate cyclophosphamide-induced therapeutic immunomodulatory effects. *Immunity* 2016; **45**: 931–943.
43. Macfarlane S, Macfarlane GT. Regulation of short-chain fatty acid production. *Proc Nutr Soc* 2003; **62**: 67–72.
44. Bachem A, Makhlouf C, Binger KJ, *et al.* Microbiota-derived short-chain fatty acids promote the memory potential of antigen-activated $CD8^+$ T cells. *Immunity* 2019; **51**: 285–297.e5.
45. Park J, Kim M, Kang SG, *et al.* Short-chain fatty acids induce both effector and regulatory T cells by suppression of histone deacetylases and regulation of the mTOR-S6K pathway. *Muc Immunol* 2015; **8**: 80–93.
46. Venegas DP, De la Fuente MK, Landskron G, *et al.* Short chain fatty acids (SCFAs)-mediated gut epithelial and immune regulation and its relevance for inflammatory bowel diseases. *Front Immunol* 2019; **10**: 277.
47. Naito Y, Uchiyama K, Takagi T. A next-generation beneficial microbe: *Akkermansia muciniphila*. *J Clin Biochem Nutr* 2018; **63**: 33–35.
48. Hasko G, Kuhel DG, Nemeth ZH, *et al.* Inosine inhibits inflammatory cytokine production by a posttranscriptional mechanism and protects against endotoxin-induced shock. *J Immunol* 2000; **164**: 1013–1019.
49. Soularue E, Lepage P, Colombel JF, *et al.* Enterocolitis due to immune checkpoint inhibitors: a systematic review. *Gut* 2018; **67**: 2056–2067.
50. Fahrer AM, Konigshofer Y, Kerr EM, *et al.* Attributes of γδ intraepithelial lymphocytes as suggested by their transcriptional profile. *Proc Natl Acad Sci USA* 2001; **98**: 10261–10266.
51. Perry JL, Reuter KG, Luft JC, Pecot CV, Zamboni W, DeSimone JM. Mediating passive tumor accumulation through particle size, tumor type, and location. *Nano Lett* 2017; **17**: 2879–2886.
52. Cantwell AR Jr, Kelso DW. Microbial findings in cancers of the breast and in their metastases to the skin. Implications for etiology. *J Dermatol Surg Oncol* 1981; **7**: 483–491.
53. Chanudet E, Adam P, Nicholson AG, *et al. Chlamydiae* and *Mycoplasma* infections in pulmonary MALT lymphoma. *Br J Cancer* 2007; **97**: 949–951.
54. Hooper SJ, Crean SJ, Fardy MJ, *et al.* A molecular analysis of the bacteria present within oral squamous cell carcinoma. *J Med Microbiol* 2007; **56**: 1651–1659.
55. Nejman D, Livyatan I, Fuks G, *et al.* The human tumor microbiome is composed of tumor type-specific intracellular bacteria. *Science* 2020; **368**: 973–980.
56. Park JE, Kim SE, Keam B, *et al.* Anti-tumor effects of NK cells and anti-PD-L1 antibody with antibody-dependent cellular cytotoxicity in PD-L1-positive cancer cell lines. *J Immunother Cancer* 2020; **8**: e000873.
57. Walker LS, Sansom DM. The emerging role of CTLA4 as a cell-extrinsic regulator of T cell responses. *Nat Rev Immunol* 2011; **11**: 852–863.
58. Starnes CO. Coley's toxins in perspective. *Nature* 1992; **357**: 11–12.
59. Coley WB. The treatment of inoperable sarcoma by bacterial toxins (the mixed toxins of the *Streptococcus erysipelas* and the *Bacillus prodigiosus*). *Proc R Soc Med* 1909; **3**: 1–48.
60. Lamm DL, Blumenstein BA, Crawford ED, *et al.* A randomized trial of intravesical doxorubicin and immunotherapy with bacille Calmette-Guérin for transitional-cell carcinoma of the bladder. *N Engl J Med* 1991; **325**: 1205–1209.
61. Larsen ES, Joensen UN, Poulsen AM, Goletti D, Johansen IS. Bacillus Calmette-Guérin immunotherapy for bladder cancer: a review of immunological aspects, clinical effects and BCG infections. *APMIS* 2020; **128**: 92–103.
62. Fahrer AM. A proposal for a simple and inexpensive therapeutic cancer vaccine. *Immunol Cell Biol* 2012; **90**: 310–313.
63. Sedighi M, Zahedi Bialvaei A, Hamblin MR, *et al.* Therapeutic bacteria to combat cancer; current advances, challenges, and opportunities. *Cancer Med* 2019; **8**: 3167–3181.
64. Pinato DJ, Gramenitskaya D, Altmann DM, *et al.* Antibiotic therapy and outcome from immune-checkpoint inhibitors. *J Immunother Cancer* 2019; **7**: 287.
65. McQuade JL, Ologun GO, Arora R, Wargo JA. Gut microbiome modulation via fecal microbiota transplant to augment immunotherapy in patients with melanoma or other cancers. *Curr Oncol Rep* 2020; **22**: 74.

© 2020 Australian and New Zealand Society for Immunology, Inc.

1.3 Our Laboratory's Novel Treatment – Intratumoural Complete Freund's Adjuvant

Complete Freund's adjuvant (CFA) is a water-in-oil emulsion consisting of mineral oil, an emulsifier, and heat-killed and dried mycobacteria, that American immunologist Dr Jules T. Freund developed in the mid-20th century (Freund & McDermott, 1942). He demonstrated that injecting an animal model with an antigen emulsified with CFA can induce a long-lasting and intense humoral immune response against the antigen (Freund & Bonanto, 1944). This response is partially due to the persistence of CFA at the injection site (Allison & Gregoriadis, 1974), which acts as a slow-release depot of antigen and pathogen-associated molecular patterns (PAMPs) derived from mycobacteria (Freund & Lipton, 1955). CFA has been an invaluable tool for basic immunology research, but like Coley and his therapy, our laboratory has found that injecting CFA intratumourally can be an effective (and affordable) immunotherapy option (C. S. E. Carroll et al., 2021; Fahrer, 2012). The second aim of this PhD project is to build upon previous studies conducted by our laboratory and investigate methods that may improve CFA's therapeutic efficacy as a cancer immunotherapy.

1.3.1 Brief history of CFA

Tuberculosis (TB) was a significant public health concern in the 19th and early 20th centuries (Luca & Mihaescu, 2013). Research into methods that promoted protection against the causative pathogen (tubercle bacillus, now known as *Mycobacterium tuberculosis*) brought about vaccines like Bacillus-Calmette Guerin (BCG), which was developed by Albert Calmette and Camille Guerin in 1924 (Luca & Mihaescu, 2013) and uses a live attenuated strain of *M. bovis*. The following year, it was observed that guinea pigs infected with TB and immunised with an antigen were more effective at creating antibodies against the antigen (Dienes & Schoenheit, 1929), thus marking TB as a surprisingly successful adjuvant at the time. Experiments also confirmed that killed TB can produce the same adjuvant effect (Dienes, 1928), thus allowing researchers to study its adjuvanticity without fear of infection.

Freund developed a keen interest in the adjuvant properties of TB and conducted research to identify methods that could enhance it. In 1937, he injected rabbits and guinea pigs with paraffin oil containing heat-killed *M. tuberculosis* and, using a purified protein derivative (PPD) skin test, found that experimental animals successfully developed strong immune reactions against the bacteria (Freund et al., 1937). However, he did not observe the same reaction against antigens like hen egg white that had been injected into lesions produced by injections of the bacteria-oil suspension.

Freund sought to improve the adjuvanticity of his formulation so it could induce immune responses against other antigens. He started by asking if an immune reaction against the antigen was not being produced because the antigen was somehow separating from the oil. He overcame this issue in his landmark paper (Freund & McDermott, 1942), where he emulsified horse serum (the antigen) diluted in saline, paraffin oil, heat-killed *M. tuberculosis*, and an emulsifier – a lanolin-like substance called Aquaphor. When the emulsion was injected intramuscularly into guinea pigs, PPD tests showed the animals developed intense, long-lasting immune reactions against horse serum that lasted up to a year after treatment. Antibody activity could also be observed with a precipitin reaction test one month after the inoculation, and positive results were found in all inoculated animals. This work also demonstrated that the antigen needs to be emulsified with the paraffin oil and an emulsifying agent for a successful immune reaction. The first reported use of CFA, as we know it today, had been published.

Freund continued his research and asked if there was a limit to the type of antigen that could be included in the emulsion and still provoke the intense immune reaction he had observed. To answer this question, he vaccinated guinea pigs and rabbits with CFA emulsified with water-soluble diphtheric toxoid (inactivated diphtheria toxin) or particulates like formalin-killed *Salmonella enterica* serotype typhi. He consequently found significantly increased antibody titres against both antigens, suggesting an immune reaction can develop against any antigen included in the emulsion (Freund & Bonanto, 1944). Freund then tested the vaccination potential of his adjuvant in two small studies involving malaria. He vaccinated ducks against *Plasmodium lophurae* in one study (Freund, Sommer, et al., 1945) and Rhesus monkeys against *P. knowlesi* in another (Freund,

Thomson, et al., 1945). In both studies, the animals were vaccinated with CFA emulsified with formalin-killed parasites, and both studies found that the vaccinated animals had substantial protection against the pathogens.

If CFA has been demonstrated to be an effective vaccination agent against malaria, specifically in non-human primates, why is it not used in the clinic today? The reasons cited have been that the emulsion causes extensive necrosis and unacceptable granuloma formation at the injection site (Allison & Gregoriadis, 1974). Even Freund noted that the adjuvant might be useful for immunising domesticated animals, but not humans, because of the development of increased sensitisation to antigen, nodule formation at the injection site, and possible abscess formation, especially in people allergic to the mycobacteria in the emulsion (Freund & Bonanto, 1944). To overcome this last point, he suggested replacing the inactivated *M. tuberculosis* with inactivated *M. phlei* (Freund & Bonanto, 1944). CFAs containing *M. tuberculosis H37Ra*, an avirulent strain of *M. tuberculosis H37Rv* (Blischak et al., 2015), and *M. butyricum* are now commercially available, but only for research purposes. Both *Mycobacterium* spp. have been used in CFA experiments in this dissertation.

Today, CFA is typically used in animal studies for the initial injection of an immunisation protocol against an antigen, followed by subsequent injections with incomplete Freund's adjuvant (IFA), which lacks the mycobacterial components. However, due to the intense immune reaction that results from CFA inoculation, research regulators like the National Institutes of Health (NIH) insist that alternative adjuvants be used in animal research, if possible, because of the adverse reactions mentioned earlier (*Animal Research Advisory Committee (ARAC) Guidelines | OACU*, 2023). That said, CFA still has an important place in medical research. It is the most successful adjuvant for consistently inducing high-titre antibodies against a variety of antigens and it is also used to induce experimental autoimmune encephalitis (EAE) in mouse models of multiple sclerosis (MS, Freund, 1947; Stromnes & Goverman, 2006b, 2006a).

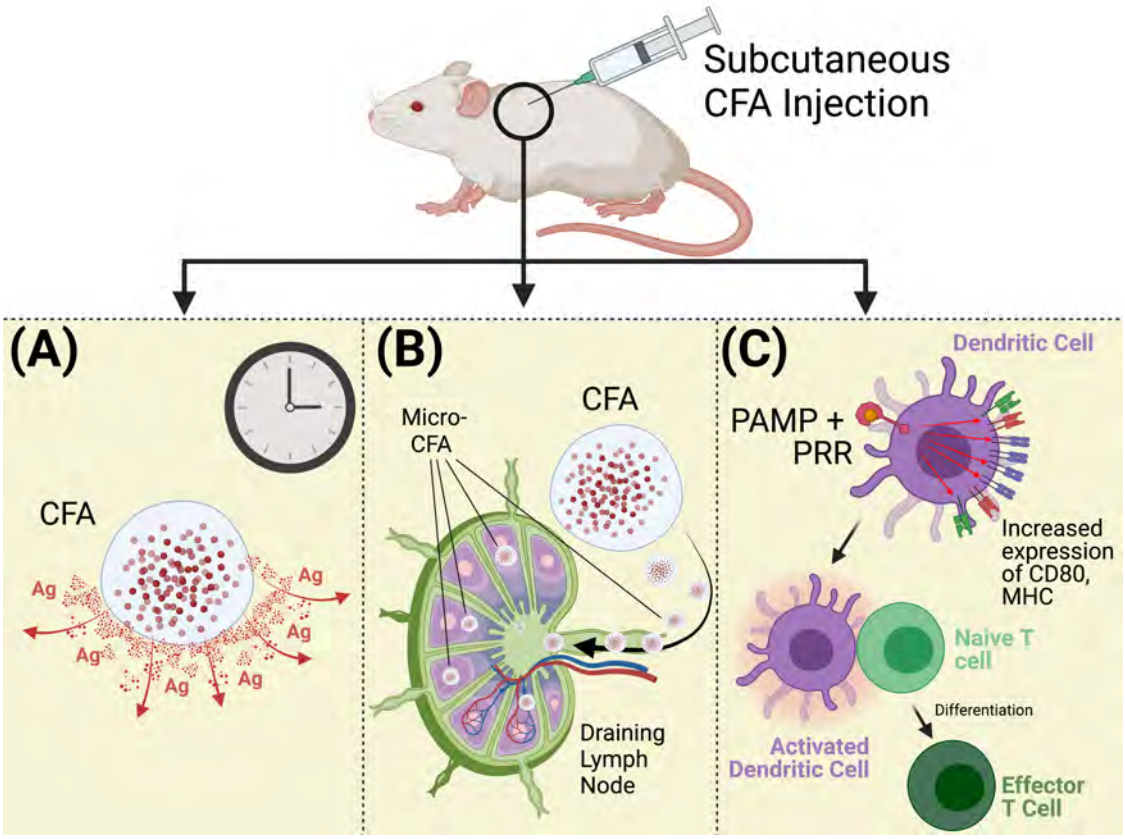


Figure 1.1: Three observations have been made that could help explain the mechanism of action for complete Freund's adjuvant. **(A)** CFA acts as a local depot that slowly releases antigen (Ag) over a long period. **(B)** Oil droplets containing antigen travel through the lymphatic network to draining lymph nodes. These micro-CFAs act as local antigen depots that prolong the immune response, even after the main CFA injection has been excised. **(C)** The mycobacteria-derived pathogen-associated molecular patterns (PAMPs) engage with pattern recognition receptors (PRRs) on antigen-presenting cells (i.e., dendritic cells). The result is increased expression of MHC and co-stimulatory molecules on the APC, which travel to draining lymph nodes and activate an adaptive immune response.

1.3.2 How does CFA work biologically?

Although CFA is the de facto gold standard for adjuvants (Stills, 2005), much about its immunopotentiating effect has yet to be understood. Three observations have been made following CFA inoculation that may offer clues about its mechanism of action *in vivo* (Stills, 2005), and they are summarised in Figure 1.1.

The first is that CFA acts as a depot for the slow release of antigens over time, thus leading to prolonged immune stimulation (Chu et al., 1997; Freund & Lipton, 1955). The mineral oil in the CFA is not metabolisable and does not allow the emulsion to

diffuse from the injection site (Freund, 1956). Indeed, antigen has been found to persist at the injection site up to 22 weeks after subcutaneous inoculation (Halbert et al., 1946; Stills, 2005).

The second observation was that the mineral oil in the emulsion provides a vehicle for transporting antigens and mycobacteria through the lymphatic network. When CFA was emulsified with *S. enterica* in saline and examined under a microscope, Freund noted that the *S. enterica* remained in the water phase of the emulsion while the mycobacteria stayed in the oil phase (Freund & Bonanto, 1944). He also observed that mycobacteria and oil droplets could be found within the lungs, draining lymph nodes, and large, phagocytic, mononuclear cells (most likely macrophages and dendritic cells) following inoculation (Freund et al., 1940; Freund, 1956). Furthermore, surgically removing subcutaneous CFA from rabbits within 30 minutes of injection did not impact the resulting antibody reaction (Freund, 1951; Stills, 2005). An explanation for these observations may be that tiny antigen-adjuvant emulsion droplets travel through the lymphatic circulation and deposit themselves into secondary lymphoid organs (Freund, 1951; Osebold, 1982; Waksman, 1979). There, they can act as localised depots of antigen and mycobacteria to further stimulate the immune response.

Finally, the mycobacteria component, which is indispensable for CFA's successful adjuvanticity (Raffel, 1948), provides an essential source of immune stimulation by supplying a consortium of PAMPs to the local milieu (Table 1.2). These PAMPs then engage with pattern recognition receptors (PRRs) on innate immune cells, most importantly Toll-like receptor 2 (TLR2) and TLR4. Engagement activates antigen-presenting cells (APCs) like macrophages and dendritic cells by upregulating major histocompatibility complex (MHC) molecules and co-stimulatory molecules like CD80 and CD86. Hence, the PAMPs in the CFA contribute to activating an acute inflammatory reaction, leading to a Th1-style immune response (Billiau & Matthys, 2001; Chu et al., 1997; Stamm et al., 2015).

Table 1.2: PAMPs and PRRs associated with *Mycobacterium tuberculosis*

Receptor Class	PRR Cellular Expression[a]	PRR	Identified Mtb PAMP	Citations
Toll-like receptors	Mo, Mϕ, DC, Neu, B cells	TLR1/2	triacylated lipoproteins	Jones et al., 2001
		TLR2	Cpn60.2	Cehovin et al., 2010
			ESAT-6	Chatterjee et al., 2011
			Hsp70	Bulut et al., 2005 Stamm et al., 2015
			Lipomannan	Stamm et al., 2015 Quesniaux et al., 2004
			LpqH	Prados-Rosales et al., 2011
			LprA (Rv1270)	Pecora et al., 2006
			LprG (Rv1411c)	Gehring et al., 2004 Prados-Rosales et al., 2011
			Mannosylated phosphatidylinositol	Gilleron et al., 1997 Jones et al., 2001 Stamm et al., 2015
			PE-PGRS33	Basu et al., 2007
			Rv0577	Stamm et al., 2015
			TB10.4	Liu et al., 2014
	Mo, Mϕ, DC, Neu	TLR2/6	diacylated lipoprotieins	Thoma-Uszynski et al., 2001
		TLR4	50S Ribosomal protein Rv6052	Kim et al., 2012
			Cpn60.1	Cehovin et al., 2010
			Hsp65	Bulut et al., 2005
	Mo, Mϕ, DC, Neu, Lymphocytes	TLR9	CpG DNA	Hemmi et al., 2000
Surface receptors	Mϕ, Neu	CD14	Cpn60.1	Lewthwaite et al., 2001
			Lipoarabinomannan	Pugin et al., 1994
class B scavenger receptor	Mo, Mϕ, DC	CD36	Lipomannan	Stamm et al., 2015
			Mannosylated Lipoarabinomannan	
Type II Transmembrane receptors	Mϕ, DC	DC-SIGN[b]	Lipomannan	Tailleux et al., 2003
		Dectin-1	unknown[c]	Lee et al., 2009
class A scavenger receptor	Mϕ	MARCO	low-density lipoprotein	Kraal et al., 2000
C-type lectin receptor	Mϕ	Mincle	Trehalose-6,6'-dimycolate	Ishikawa et al., 2009
Mannose-receptors	Mϕ	MRC1	Lipomannan	Martinez-Pomares 2012
		MRC2	Mannosylated phosphatidylinositol	

[a] Sourced from Carroll, 2016
[b] Only expressed in humans.
[c] The agonist for Dectin-1 is not currently known, but reports show it is a critical PRR as Dectin-$1^{-/-}$ mice lack sufficient response against Mtb infection.
DC, Dendritic Cell; Hsp, Heat-shock protein; MARCO, Macrophage receptor with collagenous structure; Mo, Monocyte; Mϕ, Macrophage; Mtb, *Mycobacterium tuberculosis*; Neu, Neutrophil; PAMP, Pathogen-associated Molecular Pattern; PRR, Pattern Recognition Receptor

1.3.3 CFA as a cancer immunotherapy

Despite not being approved for clinical use, the resulting immune reaction following inoculation gives CFA great potential for as a cancer immunotherapy option. Aude Fahrer was inspired by Coley's experiments and published an essay arguing for CFA's merits as a cancer treatment (Fahrer, 2012). In brief, CFA emulsified without antigen could be

injected intratumourally to evoke an intense inflammatory reaction within the tumour, which itself is an *in situ* antigen source. The slow-release mechanism described earlier (Figure 1.1A) would induce APCs to recognise the tumour as pathogenic and traffic to the injection site. They will then be activated by the mycobacteria PAMPs (Figure 1.1C and Table 1.2) while collecting tumour-associated antigens (TAAs) to present to naïve T cells in the tumour-draining lymph nodes and other lymphoid organs. Those T cells will consequently recognise and kill the injected tumour and any metastases that express TAAs. Thus, a CFA-injected tumour is repurposed into an *in situ* cancer vaccine. Notably, the same is true for BCG immunotherapy treatment, which contains an attenuated variant of *M. bovis* and (apart from being an effective vaccine against TB) has been the accepted treatment for superficial non-muscle-invasive bladder cancer for decades (Lobo et al., 2021).

Evidence supports using CFA as a cancer therapy (Fahrer, 2012). First, there is the BCG treatment just mentioned, which is the only accepted cancer treatment that contains an attenuated mycobacteria species. Second, several clinical studies have already been published that show CFA has merit as a cancer treatment. Hughes *et al.* (1970) reported injecting 20 cancer patients intramuscularly with CFA emulsified with tumour extract and found improvements in over a third (7/20; 35%) of their patients. Five-year survival rates were significantly improved in two other studies that injected patients with CFA emulsified with TAAs collected from biopsies. One described giving patients intradermal CFA injections (Takita et al., 1991), while the other gave lung cancer patients one subcutaneous injection every three months for three injections (Hollinshead, 1991). Another study demonstrated that lung cancer patients inoculated with intradermal injections of CFA emulsified with TAA successfully overcame the immunosuppressive properties of the chemotherapy methotrexate (Stewart et al., 1976). None of these studies evaluated intratumoural CFA injections like we propose. However, they all demonstrated that CFA has the potential to be a viable cancer immunotherapy, and that it can be combined with other conventional cancer treatments.

Ten years after Fahrer's essay was published, our laboratory published the first report demonstrating the potential of intratumoural CFA injections and showed it is a viable

treatment strategy (C. S. E. Carroll et al., 2021, Appendix C). We evaluated the therapy in three syngeneic murine cancer models and naturally occurring canine and equine cancers; significant increases in survival were observed in two of the mouse models tested (the third nearly reached significance), and tumour regression was observed among all treated animals. Importantly, 12 cancer patients were given 0.5-2 mL intratumoural CFA injections, and all treatments were well tolerated. Furthermore, one 69-year-old man with metastatic renal cancer had a tumour on his neck injected with CFA, and both the injected tumour and distant lung metastases shrank considerably (C. S. E. Carroll et al., 2021).

Using our laboratory's fine-needle aspirate (FNA) sampling protocol in mouse tumour models (C. S. E. Carroll et al., 2015), we found little change in T cell and APC tumour infiltration early after treatment (within seven days). However, we did find a significant increase in tumour-infiltrating neutrophils among mice challenged with the P815 tumour model and inoculated with intratumoural CFA. This tumour model responded most successfully to CFA treatment. Furthermore, neutrophils appeared indispensable for CFA treatment efficacy as eliminating them with systemic anti-GR1 antibody ablated CFA's therapeutic effect (C. S. E. Carroll et al., 2021, fig. 5). This result was a surprising one because tumour-associated neutrophils are generally regarded as immunosuppressive and high numbers within a tumour are found to correlate with a poor prognosis (Shaul & Fridlender, 2019). However, new research continues to challenge our understanding of the neutrophil's role in a cancer context (B. E. Hsu et al., 2019; Mackey et al., 2019; Quail et al., 2022; Sagiv et al., 2015; Zilionis et al., 2019). Therefore, this dissertation provides data from preliminary experiments designed to better understand their role in CFA therapy.

1.3.4 Advantages of CFA over other therapies

Compared to conventional therapies, intratumoural CFA treatment is predicted to have relatively mild side effects that are of little concern to patients, especially those in the terminal phase of their disease (Fahrer, 2012). In one previously cited cancer study, all CFA-treated patients developed ulcers, a fever, and enlarged lymph nodes around the inoculation site (Stewart et al., 1976). The fever was reported to last no longer than 30

hours and responded well to bed rest and aspirin. The ulcers were tolerated by all patients and completely healed within a year, to which the authors noted that "[the] final scar [was] no more unsightly than that of a routine vaccination". Since we propose to inject the CFA intratumourally, ulceration is expected to be of little concern. However, in case of unforeseen or intolerable side effects, the injection can be easily excised (Fahrer, 2012).

CFA treatments would have a minimal financial cost. Each injection can be as little as $10, while other cancer therapies can easily cost thousands (Almonte et al., 2021). This substantial difference in price means CFA could be an accessible alternative cancer treatment for underdeveloped countries and underprivileged communities. This last point relates to an additional advantage: one injection may be sufficient to treat a malignancy because the mineral oil prevents the emulsion from diffusing from the injection site (Allison & Gregoriadis, 1974; Stills, 2005).

Table 1.3: Examples of pre-clinical studies that investigated treatment outcomes after combining immune checkpoint therapies with Toll-like receptor agonists

Toll-like Receptor	Immune Checkpoint Therapy	Agonist	Cancer Models	Result	Citation
TLR1/2	anti-CTLA4	Pam3CSK4	B16.F10	- increased survival - increased intratumoural Treg depletion - decreased tumour growth	N. Sharma et al., 2019
TLR4	anti-PD1	EcML	B16.F10	- increased DC action - decreased tumour growth	Jeong et al., 2020
		anti-TLR4 agonist	EG7 B16.F10-OVA MC38-OVA	- increase antigen-specific T cells - decreased tumour growth	Tsukamoto et al., 2019
	anti-PD1 and anti-PD-L1	BLS	B16	- Increased immune infiltration - Increase survival with anti-PD1, but not BLS alone or anti-PDL1	Farias et al., 2021
TLR7	anti-PDL1	anti-PDL1/ SZU-101 NDC[a]	CT26	- Increased survival - Increased anti-tumour immunity - Decreased tumour growth	Yu et al., 2022
TLR9	anti-PD1 and anti-PD-L1	ODN1585	Hepa1-6	- Increased survival - Decreased tumour growth	Zhou et al., 2020
		SD101	CT26	- Increased tumour-infiltrating $CD8^+$ T cells - Increased survival - Decreased tumour growth	S. Wang et al., 2016
	anti-CTLA4	CpG1826	A20 4T1 2F3	- Increased survival when combined with anti-OX40 agonist - Decreased tumour growth - All treatments injected into tumours	Marabelle et al., 2013
	anti-PDL1	sHDL-CpG	GL261	- Increase antigen-specific $CD8^+$ T cells - Increased anti-tumour immunity - Increased survival - Decreased tumour growth	Scheetz et al., 2020

[a] Yu et al. (2022) fused TLR7-agonist SZU-101 to the Fc portion of anti-PDL1 to form a nano-drug conjugate (NDC)
BLS, Brucella lumazine synthase; Treg, regulatory T cell

Several pre-clinical studies have investigated whether other immunotherapy adjuvants can stimulate an innate immune reaction that would improve the response rate to immune checkpoint therapies. The favoured targets in the literature are mainly TLRs, and some examples of these studies are summarized in Table 1.3. Each study combines one TLR agonist or agonistic antibody with either anti-CTLA4 or PD1 blockade antibodies. However, CFA has a major advantage over the strategies presented by these studies. While they evaluated the engagement of a single TLR at any given time, the *Mycobacterium* spp. in the CFA provides a consortium of PAMPs that will engage multiple PRRs (Table 1.2), thus increasing the magnitude of immune reaction at the injected tumour.

1.4 Bringing it All Together – The Structure and Layout of this Dissertation

Thus far, we have described early attempts by William Coley to treat inoperable sarcomas and carcinomas by injecting bacteria and bacteria filtrates into tumours to provoke an anti-cancer immune reaction; we have argued in a published literature review that a reason for the gut microbiome's importance for immune checkpoint therapies may be that commensal bacteria are escaping the gut lumen and colonising distant solid tumours; finally, our laboratory has shown that CFA – an emulsion containing heat-killed mycobacteria – can be a successful cancer therapy when injected into solid tumours. In each instance, bacteria-derived PAMPs are used to stimulate an immune reaction at the tumour site, thus promoting an anti-tumour immune response. This work aims to build upon this underlying theme, specifically by first attempting to examine the gut microbiome's impact on immune checkpoint therapy and by finding means of improving our intratumoural CFA cancer treatment.

This work consists of four results chapters, one of which is a submitted manuscript, and another contains a published research article. Chapters 3 and 4 explain experiments that were conducted to find an appropriate tumour model that we could use to evaluate our gut translocation hypothesis. Chapter 5 describes our first attempt to manipulate the gut microbiome of tumour-challenged mice with a published antibiotic cocktail and the

consequences this manipulation had on anti-CTLA4 treatment outcomes. It also includes an article we published in *The Journal for ImmunoTherapy of Cancer* that further explains our findings. Chapter 6 presents data from preliminary studies investigating methods for improving our laboratory's CFA immunotherapy.

This dissertation has a sizeable appendix section. Appendix A presents supplementary figures demonstrating the "goodness-of-fit" of the statistical models used in this project, along with other relevant photographs and figures. Supplementary tables are presented in Appendix B. Appendix C contains our laboratory's CFA study published in *The Journal for ImmunoTherapy of Cancer*, to which I contributed by analysing data with R and constructing some key figures. Lastly, due to the significant impact that the COVID-19 pandemic had on my project, I have included additional research that I contributed to, but which is not directly related to the focus of this dissertation. Appendix D presents an unpublished manuscript (of which I am a co-first author) that evaluated the efficacy of COVID-19 vaccines in cancer patients receiving various treatment modalities. Appendix E is a prepared manuscript describing methods for detecting thr SARS-CoV-2 virus in sewage, to which I assisted by analysing data and constructing all the figures in R.

2

Materials and Methods

Contents

2.1 Introduction 34
2.2 Animals 34
2.3 Tissue Culture 35
2.4 Tumour Challenge 36
2.5 Tumour Measurement 37
2.6 Cancer Treatment 38
2.6.1 Immune checkpoint therapies 38
2.6.2 Complete Freund's Adjuvant 39
2.7 Examining Lung Metastases 40
2.7.1 Gross examination 40
2.7.2 Microscopic examination 41
2.8 Flow Cytometry 41
2.8.1 Fine-needle aspirate (FNA) sampling 41
2.8.2 Single-cell suspensions 42
2.8.3 Surface staining 44
2.9 Antibiotic Feeding 45
2.10 Determining Antibiotic Efficiency 46
2.11 Statistical Analysis 48
2.11.1 LMER models 48
2.11.2 Survival 50
2.11.3 Other statistical tests and R packages 50

2.1 Introduction

This dissertation includes several published papers and submitted manuscripts, both within chapters (e.g., Chapters 3, and 4) and in the Appendices (e.g., Appendix C). This chapter explains methods that either are not explained in those manuscripts or require more clarification. The solutions and reagents used in all experiments are shown in Table 2.1.

Table 2.1: Reagents and solutions used in experiments presented in this dissertation

1x Phosphate Buffered Saline (PBS), pH 7.4[a]	
NaCl	136.9 mM
KCl	2.68 mM
Na_2HPO_4	10.2 mM
KH_2PO_4	1.84 mM
Ultra-pure Water	Solvent
FACS Buffer	
Heat-inactivated Foetal Calf Serum[b]	2% (v/v)
EDTA[c]	0.5 mM
1x PBS	Solvent
Digestion Solution	
Collagenase Type 1 Worthington biochemical, NJ, USA	5 mg/mL
Hyaluronidase Type I-S Sigma Aldrich, MO, USA	1.5 mg/mL
DNAse Worthington biochemical, NJ, USA	0.01 mg/mL
Heat-inactivated Foetal Calf Serum[b]	1% (v/v)
RPMI-1640 or DMEM Gibco	Solvent

1x Antibiotics Solution	
Colistin sulphate Sigma-Aldrich, cat. No. PHR1605	1 mg/mL
Ampicillin sodium salt Sigma-Aldrich, cat. No. A9518	1 mg/mL
Streptomycin sulphate salt Sigma-Aldrich, cat. No. S6501	5 mg/mL
Autoclaved tap water	Solvent
India Ink Solution	
India Ink[d]	15% (v/v)
Tap Water	Solvent
Fekete's Solution	
70% Alcohol	100 mL
Formalin	10 mL
Glacial Acetic Acid	5 mL

[a] Experiments at Stanford University used PBS purchased from Gibco.
[b] Prepared by incubating foetal calf serum in a 56^{o}C water bath for 30 minutes.
[c] EDTA was added to FACS buffer in experiments at Stanford University
[d] Kind gift from Dr Ranjani Ramachandra, Stanford University

2.2 Animals

Experiments were performed at the ANU and the Stanford University School of Medicine. Six- to 8-week-old female mice were used in all experiments.

At the ANU, BALB/c and C57BL/6 mice were purchased from Charles River and maintained at the Animal Phenomics Facility (Canberra, Australia). DBA/2 mice were purchased from the Animal Resources Centre (Perth, WA, Australia). Animals were

allowed to acclimate to their new environment for at least seven days before starting any experiments. All studies were approved by the Animal Experimentation Ethics Committee (AEEC) under protocols A2017/46, A2020/45, and A2021/05.

At Stanford University, BALB/c and C57BL/6 mice were purchased from the Jackson Laboratory, and all the animals were cared for in the Stanford Animal Facility under US federal, state, and NIH guidelines. Animals were allowed to acclimate for five days in their new environment before starting any experiments. All experiments were approved by the Stanford University Administrative Panel on Laboratory Animal Care under protocol number 30883.

All animals were humanely euthanised with CO_2 asphyxiation and/or cervical dislocation when they reached an experimental endpoint, became severely ill, lost more than 20% of initial body weight, developed ulcerated tumours, or needed to be sacrificed for experimental protocols.

2.3 Tissue Culture

The P815, CT26.WT (CT26), and 4T1 cell lines were purchased from the American Type Culture Collection (ATCC). The MCA-205 cell line was purchased from Merck. The B16.F10 cell line was kindly gifted by Prof Joseph Altin (ANU, Canberra), and the MC38 cell line was kindly gifted by Dr Jing Li (Stanford University). All cells were incubated at 37°C in a humidified environment with a 5% CO_2 injection. Table 2.2 summarises the culture media used for each cell type.

Table 2.2: Recipes for tissue cultures used for cell lines in this dissertation. All reagents were supplied from Gibco unless otherwise noted.

Syngeneic Strain	**C57BL/6**			**BALB/c**		**DBA/2**
Tumour Cell Line	**B16.F10**	**MC38**	**MCA-205**	**CT26**	**4T1**	**P815**
Base Medium	RPMI-1640	DMEM	RPMI-1640	RPMI-1640	RPMI-1640	DMEM
HI-FCS[a]	10%	10%	10%	10%	10%	10%
GlutaMAX^{TM}	20 mM	20 mM[b]	20 mM	20 mM	20 mM	20 mM
$C_3H_3NaO_3$	10 mM	10 mM	10 mM	10 mM	10 mM	10 mM
HEPES	0.1 M	0.1 M	0.1 M	0.1 M	0.1 M	0.1 M
Penicillin[c]	10 IU/mL	10 IU/mL	10 IU/mL	10 IU/mL	10 IU/mL	10 IU/mL
Streptomycin[c]	10 μg/mL	10 μg/mL	10 μg/mL	10 μg/mL	10 μg/mL	10 μg/mL
NEAA		1x	1x			
β-Mercaptoethanol[d]			0.05mM			
Gentamicin sulphate[e]		50 μg/mL				

[a] Feotal calf serum was supplied by Sigma-Aldrich. Heat-inactivated as described above.
[b] GlutaMAX^{TM} was already included in the base medium.
[c] Penicillin and streptomycin were added to the media in a single commercial product called Penicillin-Streptomycin.
[d] β-Mercaptoethanol was supplied by Sigma-Aldrich, cat No. M6250
[e] Gentamicin sulphate was supplied by Lonza Group, cat No. 17-518Z
HEPES, N-2-hydroxyethylpiperazine-N-2-ethane sulfonic acid; DMEM, Dulbecco's Modified Eagle Medium; HI-FCS, Heat-inactivated foetal calf serum; IU, International units; NEAA, Non-essential amino acids; RPMI, Roswell Park Memorial Institute

2.4 Tumour Challenge

Mice were challenged with tumours syngeneic to their strain. To prepare cell lines for injection, adherent cells were recovered from culture using 0.25% trypsin (Gibco), then washed two to three times with unsupplemented media, spinning at 200–400xg for 5 minutes between each wash. Live cells were then counted with either a hemocytometer using Trypan Blue (Sigma-Aldrich) or an automated cell counter using ReadyCount™ Green/Red Viability Stain (Invitrogen). In all instances, cells were re-suspended in a volume of 50% unsupplemented base medium and 50% autoclaved 1x PBS to attain the required concentration of live cells for injection.

Animals were anesthetised with 3% isoflurane in oxygen flowing at 1 L/min before shaving the injection site with a hair trimmer. All the following cell lines were subcutaneously injected into the left flank in 0.1 mL solution. DBA/2 mice were injected with 0.3 x 10^6 P815 cells (ATCC TIB-64); C57BL/6 mice were injected with either 0.2 x 10^6 B16.F10 cells (gift from Prof Altin, ANU), 0.5 x 10^6 MC38 cells (gift from Dr Li,

Stanford University), or 0.8 x 10^6 MCA-205 cells (Merck, cat no. SCC173); BALB/c mice were injected with 0.5 x 10^6 CT26 cells (ATCC CRL-2638).

Injections of 4T1 cells (ATCC CRL-2539) into BALB/c mice were done using one of two methods, both of which injected 0.1 x 10^6 cells orthotopically into the mammary fat pads. For experiments presented in Section 4.5, mice were first anaesthetised with 3% isoflurane in oxygen flowing at 1 L/min. A lower abdominal mammary fat pad was shaved with a hair trimmer before injecting it with 15 μL of 4T1 cells using 25 μL Hamilton glass syringes fitted with 25G needles. In all 4T1 experiments presented in Chapter 6, mice were not anaesthetised. Instead, the animal's left #3 mammary fat pad (located on the chest) was marked with an indelible marker before the animal was safely restrained. This was done by gently but firmly placing one hand over the shoulders and quickly grasping the scruff of the neck close to the base of the skull with the thumb and forefinger, then restraining the tail with the little finger. The marked site was shaved with a hair trimmer before being subcutaneously injecting with 0.5 x 10^6 4T1 cells in 0.1 mL solution.

2.5 Tumour Measurement

Tumours were monitored frequently after injection and mouse health was assessed according to each university's standing policies. After treatment, tumour size was measured every second or third day with digital callipers. Tumours were measured on two orthogonal axes, with one being the longest, and the average tumour diameter was calculated and used for all statistical analyses. If multiple tumours were present, the average tumour diameter was calculated with the equation:

$$T = \sqrt[3]{\sum_{i=1}^{N} t_i^3}$$

Where T is the average tumour diameter used for further analyses, N is the number of tumours, and t_i is the average diameter of each tumour, measured as described above. At the ANU, mice were euthanised when the average tumour diameter reached 15 mm, or 17 mm, in the case of the P815 model. A different endpoint was used for the P815 tumour model due to (i) absence of illness or distress in the animals, and (ii) necropsies of

animals euthanised when the average diameter reached 15 mm revealed necrotic tumours, meaning that recorded measurements were an underestimate of living tumour tissue.

At Stanford University, tumour volume was calculated using the equation $V = 0.5 * (L * W^2)$, with W being the width and L being the length and longest axis. The volumes of each tumour were added if multiple tumours were present. Mice were euthanised when the total tumour volume reached 2000 mm³. However, average tumour diameters were used in all treatment timing decisions and statistical analyses.

At both institutions, some mice with tumour sizes close to, but less than, the ethical limit on a previous measurement had exceeded this limit by the next. On the advice of collaborating biostatistician Dr Teresa Neeman (ANU, Statistical Consulting Unit), any mouse with an average tumour diameter over 16 mm when it was euthanised had days deducted from its survival. That is, mice with average tumour diameters of 16–17.4 mm had one day deducted, mice with average tumour diameters of 17.5–18.0 mm had two days deducted, and any mouse with an average tumour diameter greater than 18.0 mm had three days deducted. A similar means of correction was used for P815-challenged mice, though tumours rarely exceeded 18 mm. Any mouse found dead was recorded as having survived to the previous day (i.e., had one day deducted).

2.6 Cancer Treatment

Once the average tumour diameter of the experimental cohort reached 4.0–5.0 mm, the mice were distributed into treatment groups so that each group had a similar average and range of tumour sizes. Each cage thus contained mice belonging to multiple treatment groups to avoid confounding effects due to cage or litter differences.

2.6.1 Immune checkpoint therapies

Animals received intraperitoneal or intravenous injections of either anti-PD1 (RMP1-14), anti-CTLA4 (9D9), or anti-PDL1 (10F.9G2), either alone or in combination, in amounts ranging from 0.1 mg to 0.25 mg as specified in the figure captions. Control animals received isotype-matched control antibodies: anti-trinitrophenol (rat IgG2a, clone 2A3)

for anti-PD1, a mouse IgG2b (clone MPC-11) of unknown specificity for anti-CTLA4, or anti-keyhole limpet hemocyanin (rat IgG2b, clone LTF-2) for anti-PD-L1. Control animals received all relevant isotype control antibodies in experiments evaluating differences between two immune checkpoint therapies. For example, if one treatment group received 0.1 mg of anti-CTLA4 and another group received 0.1 mg of anti-PD1, the control-treated animals received 0.1 mg each of MPC-11 and 2A3 (thus receiving 0.2 mg antibody total). All antibodies were purchased from BioXcell (NH, USA).

2.6.2 Complete Freund's Adjuvant

CFA containing 1 mg/mL of heat-killed *Mycobacterium butyricum* (BD Biosciences, NJ, USA) or 1 mg/mL of heat-killed *M. tuberculosis H37ra* (Sigma-Aldrich, MO, USA) was prepared by first vortexing the solution to suspend the mycobacteria thoroughly and evenly in the mineral oil. CFA and PBS were then collected in separate Luer Lock glass syringes in equal volumes before attaching them to either end of a Luer Lock 18 G micro-emulsifying needle (Cadence Science, VA, USA). CFA was emulsified by repeatedly passing the solution between the connected syringes for approximately 10 minutes or until a thick water-in-oil emulsion had formed. The emulsion was tested by adding a drop to cold water and ensuring it remained intact; rapid diffusion of the CFA indicated that phase inversion had occurred, and an oil-in-water emulsion had been produced. Only water-in-oil emulsions were used in all CFA experiments. The viscous CFA emulsion was transferred to 0.3 mL insulin syringes (Terumo), by removing the plunger and injecting the CFA directly into the syringe with a wide-bore needle (typically 18G or lower). The plunger was replaced, and the syringes were stood needle-side up so that any trapped air bubbles would travel towards the needle to be easily expelled before injection. This preparation produced CFA containing 0.5 mg/mL of *Mycobacterium* sp.

10x CFA was prepared by first supplementing 10 mL of fresh CFA containing 1 mg/mL of *M. butyricum* with an additional 90 mg of desiccated heat-killed *M. butyricum* (BD Biosciences, NJ, USA) to achieve a final 10 mg/mL concentration. The CFA emulsion was then prepared as described above, giving the resulting product 5 mg/mL of heat-killed *M. butyricum*.

Animals receiving intratumoural treatments were first anaesthetised with 3% isoflurane in oxygen at 1 L/min. Tumours were injected with either 0.05 mL of CFA, 10x CFA, or autoclaved PBS as controls. This volume was chosen because a spherical tumour of 5 mm in diameter would have a volume of approximately 65.4 mm^3 (or 0.064 mL), and 0.05 mL was the largest volume that could be practically administered to a tumour of this size. Incomplete Freund's adjuvant (IFA), which contains all the components of CFA except the mycobacteria, was not used as a control treatment because no difference in tumour growth or survival was observed between mice given intratumoural IFA or PBS (C. S. E. Carroll et al., 2021, Supplementary Figure 1)

2.7 Examining Lung Metastases

All experiments examining lung metastases in the 4T1 model were performed at the Stanford University School of Medicine.

2.7.1 Gross examination

4T1-challenged and -naïve mice were sacrificed with CO_2 asphyxiation on the 11^{th}, 12^{th}, or 13^{th} day post-treatment before the lungs were processed as previously described (Marabelle et al., 2013). In brief, the euthanised mouse was pinned, and then the skin was opened from the urethral orifice to the neck with scissors and removed. The rib cage was removed to expose the lungs and heart, and the trachea was raised with a 0.2 mL pipette tip. Next, approximately 5.0–10 mL of 15% (v/v) India ink solution was perfused into the lungs through the trachea with a syringe until they were fully inflated. The lungs and heart were then removed from the chest cavity, dipped twice in tap water to wash away excess India ink solution, and then transferred to and fixed in Fekete's solution (Table 2.1), in which they can be stored indefinitely. Metastases on ink-stained lungs fixed in Fekete's solution appeared as opaque white spots, which were counted by eye under a dissecting microscope. Photos of the lungs were taken with a mobile phone.

2.7.2 Microscopic examination

Lung samples that had been stained with India ink in Fekete's solution and samples fixed with 10% neutral buffered formalin (NBF) were sent to Professor Rachel Allavena (University of Queensland, Brisbane, Australia) for examination. For lungs fixed with formalin, the India ink and Fekete's solution in the protocol described in the previous section were replaced with NBF.

The large left lobe of each mouse was sent to Hist-Tec Laboratory Inc. (Hayward, CA, USA) to be prepared and embedded into paraffin blocks. These blocks were sent to Prof Allavena, who stained the samples with haematoxylin and eosin (H&E) and assessed them for metastasis under a microscope. All photos of H&E-stained lung samples were prepared and photographed by Prof Allavena.

2.8 Flow Cytometry

2.8.1 Fine-needle aspirate (FNA) sampling

FNA sampling was performed as previously described (C. S. E. Carroll et al., 2015) and shown in Figure 2.1. In brief, a 1 mL syringe was preloaded with 0.5 mL of unsupplemented media and fitted with a 25G needle. Mice were anaesthetised with 3% isoflurane in oxygen flowing at 1 L/min during the procedure. The syringe was inserted into the tumour, and a small amount of negative pressure was exerted as the needle was gently removed. The tumour was sampled at three different sites to maximise intratumoural cellular representation. Following collection, the aspirate samples were immediately transferred to a 1.5 mL Eppendorf tube and kept on ice until further processing. To obtain single-cell suspensions, each aspirate sample was digested by adding 0.5 mL digestion solution (Table 2.1), incubated for 20 minutes at 37°C. The digestion solution was washed three times with FACS buffer (Table 2.1) before distributing the sample equally between two antibody stain cocktails.

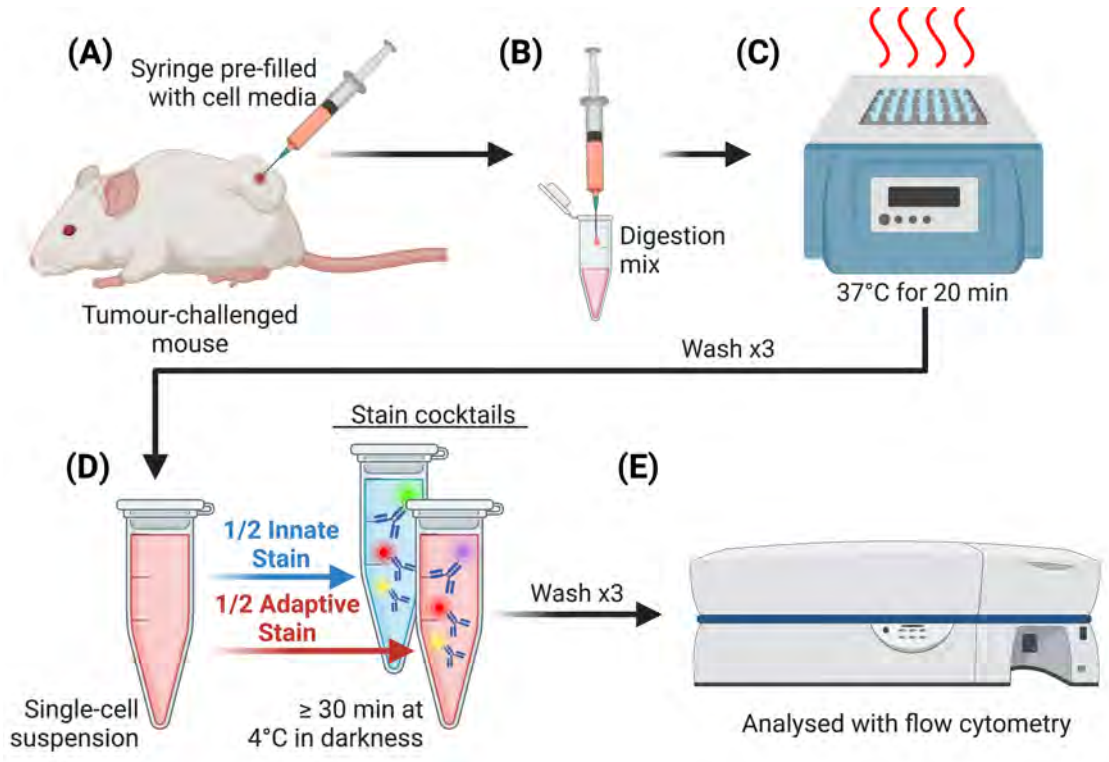


Figure 2.1: Fine-needle aspirate sampling for flow cytometry. **(A)** A syringe pre-loaded with 0.5 mL of unsupplemented cell culture media was used to aspirate cells from a subcutaneous tumour. **(B)** The contents of the aspirate were dispensed into digestion mix solution containing collagenase, hyaluronidase, DNase, and foetal calf serum. **(C)** The sample was then incubated at 37°C for 20 minutes to dissociate the cells into a single cell suspension. **(D)** After washing away the digestion mix, the cells were equally portioned between two cocktails of fluorophore-conjugated antibodies, then incubated in darkness at 4°C for at least 30 minutes. **(E)** After incubation, unbound antibody was washed away three times before cells were analysed with a BD LSR II flow cytometer.

2.8.2 Single-cell suspensions

Lymphoid organs

Spleens, thymi, and lymph nodes collected during necropsies was processed by passing the tissue through a 70 μm cell strainer (BD Biosciences) with the rubber end of a syringe plunger and FACS buffer (Table 2.1) to obtain single-cell suspensions. The samples were spun at 200xg for 5 minutes and decanted, after which the lymph nodes and thymi were resuspended in 0.5 mL and 2 mL of FACS buffer, respectively.

Spleens were further processed by re-suspending in 2 mL of Ammonium Tris-chloride (ATC, Gibco) for 30 seconds at room temperature to lyse red blood cells. FACS buffer was added to bring the volume to 10-15 mL to stop the reaction. The sample was then

spun three times at 200xg for 5 minutes and washed with FACS buffer between each spin before resuspending the cells in 5 mL of FACS buffer.

Bone marrow

The femurs of mice were collected and cleaned of tissue before cutting off the proximal and distal epiphyses with a scalpel. The bone marrow was flushed out of the femur with approximately 5 mL of FACS buffer onto a 70 μm cell strainer (BD Biosciences) with a syringe attached to an 18G needle. Any tissue on the strainer was gently passed through with the rubber end of a syringe plunger. The resulting cell suspension was spun at 200xg for 5 minutes, then resuspended in 0.5 mL of FACS buffer.

Whole-tumour digests (WTD)

Tumours were harvested and finely minced in a petri dish with approximately 2 mL of unsupplemented DMEM or RPMI-1640 (depending on which media was used to culture the cell line) until a slurry had formed. The slurry was then transferred to a Falcon tube, mixed with 2 mL of digestion solution, then incubated for 30 minutes at 37°C with gentle rocking. After incubation, tumours were passed through a 70 μm strainer (BD Biosciences) with FACS buffer and the rubber end of a syringe plunger. The sample was spun three times at 200xg for 5 minutes and washed with FACS buffer between each spin. The cells were counted with a haemocytometer and Trypan Blue, then resuspended to a volume that gave 40 x 10^6 live cells/mL.

Cultured tumour cells

Adherent tumour cells were recovered from culture using 0.25% trypsin (Gibco), then washed two to three times with unsupplemented media and spinning at 200-400xg for 5 minutes. Cells from one T-175 flask that were 80–90% confluent were re-suspended in approximately 5 mL of FACs buffer.

2.8.3 Surface staining

Processed tissue, cultured cells, and FNA samples were stained in a total volume of 50 μL (25 μL cells in 25 μL stain) in 96-well U-bottom plates for $\geq$ 30 minutes at 4°C covered in foil. Appropriate concentrations of antibodies were pre-determined by titration of cells from control tissues and conducted by various members of the laboratory. Control tissues included spleen, thymus, lymph node, bone marrow, and tumour, as these samples contained cells with high concentrations of surface antigens. Single colour controls using control tissue were included for each antibody in each experiment, which are presented in Table 2.3. The chemical compound 7-AAD (0.2 mg/mL; Invitrogen) was used as the live/dead discriminator in all FACS experiments.

Table 2.3: Antibodies used for FACS analyses in this dissertation

Antigen Target	Fluorophore	Clone	Channel	Control Tissue
CD45.2	AF488	104	FITC	Bone Marrow
CD11b	BV510	M1/70	AmCyan	
TER-119	PE	TER-119	PE	
TER-119	PerCP	TER-119	CyChrome	
CD63	PE	NVG-2	PE	Cultured P815
I-A[b]	AF647	KH74	APC	Mix[a]
I-A[d]	AF647	39-10-8	APC	
CD49b	APC	DX5	APC	
$\gamma\delta$TCR	BV421	GL3	Pacific Blue	
Ly6C	BV421	HK1.4	Pacific Blue	
CD25	PE	7D4	PE	
CD11c	PE/Cy7	N418	PE/Cy7	
Ly6G	APC/Cy7	1A8	APC/Cy7	Spleen
CD19	BV510	6D5	AmCyan	
CD101	PE	Moushi101[b]	PE	
CD8α	APC/Cy7	53-6.7	APC/Cy7	Thymus
CD4	PE/Cy7	GK1.5	PE/Cy7	

[a] Mix samples contained cells from bone marrow, thymi, spleens, cultured cancer cells, and lymph nodes.

[b] CD101 (PE) was supplied by ThermoFisher. All other antibodies were supplied by BioLegend.

Following surface staining, samples were spun three times at 200xg for 5 minutes and 4°C and washed in between spins with FACS buffer. After the final spin, stained

cells were resuspended in 100 μL FACS buffer and transferred to cluster tubes (BD Biosciences) for data collection.

Flow cytometry data were collected using a BD LSR II and FACSdiva software (BD Biosciences). Due to the paucity of cells collected from FNA sampling, data for compensation matrices were collected once per experiment using single-cell suspensions from control tissues. All FNA samples within each experiment were analysed with the same compensation matrix, voltage parameters, and the gating strategies indicated. All flow cytometry data were analysed using Flowjo V10 software (BD Biosciences), which was then exported for further analysis using R (R Core Team, 2021).

2.9 Antibiotic Feeding

A 10x solution of colistin sulphate, ampicillin sodium salt, and streptomycin sulphate salt (all purchased from Sigma-Aldrich, Table 2.1) was prepared in autoclaved tap water and frozen at -20°C before the experiment was performed. When required, the solution was thawed and mixed with autoclaved tap water in a mouse sipper bottle wrapped in aluminium foil for a final concentration of 1 mg/mL colistin, 1 mg/mL ampicillin, and 5 mg/mL streptomycin before feeding to the animals. Fresh 1x antibiotics solutions were prepared every three days. Animals fed antibiotics were assessed daily for dehydration by weighing, and by checking skin elasticity ("tent test") and body condition. Any mouse that approached 80% of its initial weight (determined on the first day of antibiotic feeding) was immediately removed to a separate cage and given standard water. Those that lost over 20% of their initial weight were humanely euthanised.

To promote antibiotic consumption and reduce dehydration, food pellets were wetted in a 5 mL petri dish in the middle of the cage with approximately 5–10 mL of antibiotic solution. Attempts to mask the bitter antibiotic flavour and promote drinking were made by including either 1% or 5% (v/v) of Ribena™ (a blackcurrant fruit drink concentrate, Suntory Ltd., Osaka, Japan) in the antibiotic solution.

2.10 Determining Antibiotic Efficiency

Antibiotic efficiency was determined as shown in Figure 2.2. Faecal pellets were collected from all antibiotic-fed mice and several water-fed mice three days before and on the day of tumour challenge to set a baseline. Samples were then collected every five days after tumour challenge to monitor the depletion and reconstitution of the gut flora during and following antibiotic feeding. The pellets were weighed before being suspended in autoclaved 1x PBS that had been passed through a 0.22 μm syringe filter, then homogenised using a TissueLyser (Qiagen) set to 24 Hz for at least 90 seconds. The homogenate was then serially diluted in autoclaved, filtered 1x PBS in ten-fold dilutions before plating in triplicate onto Columbia horse-blood agar plates (Thermo Fisher, cat No. PP2001) in 30 μL drops. Two plates were prepared for each dilution; one plate was incubated at 37°C in aerobic conditions (24 hours) and the other in anaerobic conditions (48 hours), and the resulting colonies were counted at the lowest countable dilution. A value of 0.5 was recorded for drops in the lowest countable dilution that did not grow any colonies. This value was chosen to account for the assumption that no *detectable* colonies were present. For example, if one drop in a dilution had two colonies and the other two drops did not, then the values 2, 0.5, and 0.5 were recorded. If no colonies grew in any dilution, all drops at the lowest plated dilution were assumed to have 0.5 colonies.

To calculate the colony forming units (CFU) per gram of faeces, we first calculated the geometric mean of the number of colonies counted using the equation:

$$A = e^{\frac{1}{3}\sum_{i=1}^{3} ln(c_i)}$$

Where c_i is the counted number of colonies in each drop i. The geometric mean (A) was used in the analysis because of the exponential characteristic of bacterial growth, which could be overestimated if the arithmetic mean was used.

Next, the value A was divided by 30, the volume used to plate each drop, to get the number of colonies per μL.

$$C = \frac{A}{30}$$

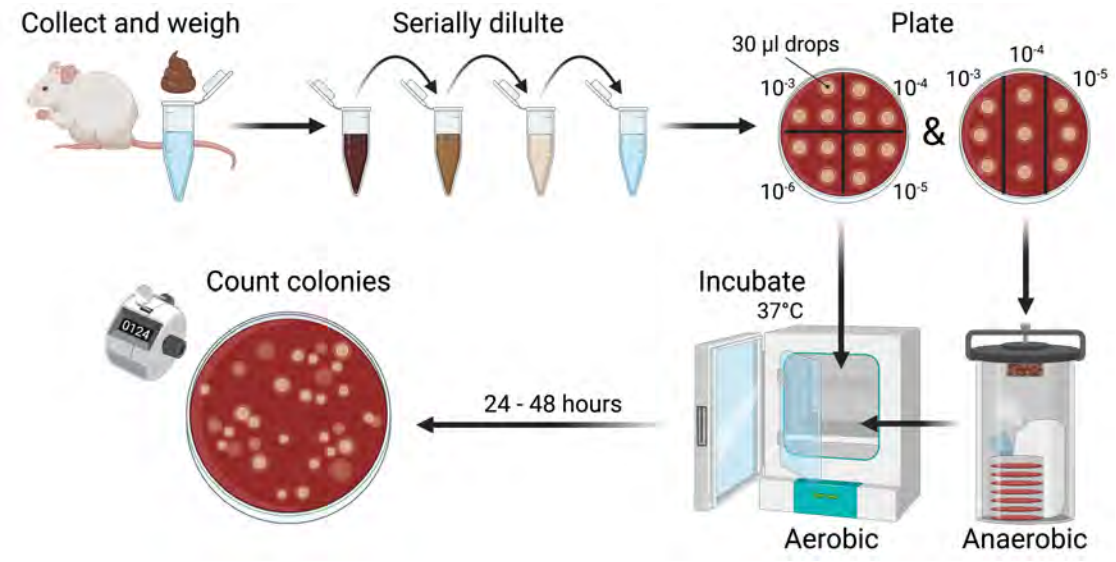


Figure 2.2: Determining the efficacy of antibiotics at depleting the gut microbiome. Faecal pellets were periodically collected from all antibiotic antibiotic-fed mice and several water-fed control mice. The pellets were weighed and homogenised in autoclaved, filtered 1x PBS. The homogenate was serially diluted in ten-fold dilutions before plating each dilution, in three 30 μL volumes per dilution, onto two horse-blood agar plates. The plates were then incubated in both aerobic and anaerobic conditions for 24–48 hours. Any resulting colonies were counted at the lowest countable dilutions, or reported as having a value of 0.5 in the lowest plated dilution if colonies were absent.

This value is then divided by the dilution factor d to obtain the number of colonies forming units per μL in the neat homogenate (H).

$$H = \frac{C}{d}$$

Next, H is multiplied by the volume V (in μL) used to homogenise the faecal pellet, then divided by the mass of the pellet m to obtain the total number of colony-forming units per gram of faeces.

$$CFU/g = \frac{H * V}{m}$$

Thus, the entire equation used to calculate the bacterial load in each faecal sample evaluates to:

$$CFU/g = \frac{1}{m} * \frac{e^{\frac{1}{3}\sum_{i=1}^{3} ln(c_i)} * V}{30 * d}$$

Where m is the mass of the faecal pellet in grams, c_i is the counted number of colonies in each drop i plated at dilution d, and V is the volume of 1x PBS used to homogenise the pellet.

2.11 Statistical Analysis

All statistical analyses were done using RStudio, an integrated development environment for the R programming language (R Core Team, 2021). A p-value ≤ 0.05 was considered significant in all statistical tests.

2.11.1 LMER models

The linear mixed-effects regression (LMER) model was used to analyse the impact of various treatments on tumor growth in all studies. It was also used to determine if treatments impacted the tumour-infiltrating leukocyte (TIL) profiles within FNA samples in experiments where more than two FNA samples were collected.

The LMER model allows for estimating fixed effects to capture population-level relationships and random effects to capture individual deviations from the population mean. It was necessary for our studies because we had multiple observations and measurements from each mouse. We used the lme4 package (Bates et al., 2022) in R to fit our LMER models and evaluated their accuracy by assessing their goodness of fit using residual plots from the ggResidpanel package (Goode & Rey, 2019). These plots can be found in Appendix A.

Tumour growth

The LMER equation that evaluated tumour growth was generally defined as:

$$Y \sim T * x + (x|E/c/m)$$

The fixed effects portion of the model contains the terms Y (tumour growth), T (treatment), and x (days post-treatment). The models only included data from day 0 (time of first treatment injection) to the day one treatment group fell to half its initial number due to mouse attrition (i.e., regression or euthanasia). This restriction was used so the model

did not suffer from attrition bias and skew the results. For the antibiotics experiment, the model was modified to:

$$Y \sim T * x * A + (x|c/m)$$

Where A represents the presence or absence of antibiotics.

The random effects portion of the model contains a nested structure to account for variations among the individual mice (m) housed in their cages (c) within an experimental replicate (E, but only if multiple experiments were performed). The x term is also included to account for the fact that each mouse in every experiment has a unique tumour growth rate at the time it was treated. If the model showed that the tumour growth rate was significantly impacted by treatment (an interaction effect between day [x] and treatment [T]), a pairwise comparison among all the treatment groups was performed using the emmeans package (Lenth, 2023) to determine which treatment groups significantly deviated from each other.

FNA samples

To analyse FNA samples, each cell type was fitted to its own LMER model using the equation:

$$P \sim T * x + (1|E/m)$$

For FNA samples collected from mice fed antibiotics, the equation is modified to:

$$P \sim T * x * A + (1|E/m)$$

Where P represents the proportion (or number, in the case of Figure 6.11) of the immune cell type being evaluated as a percentage of all living CD45.2$^+$ immune cells in the sample. The model of each cell type was then evaluated with an ANOVA using the car package (Fox & Weisberg, 2019) to determine if treatment had a significant effect.

If a significant effect was found and the data included FNA samples from more than two time points, differences in the estimated marginal means of linear trends among the treatment groups were further evaluated with the emtrends function from the emmeans package (Lenth, 2023). This calculation determined if there was a significant change in

cell proportions over time due to treatment. For FNA samples with only two timepoints, significance among differences in estimated marginal means were assessed using the emmeans function.

2.11.2 Survival

Survival between treatments was compared using a Cox-proportional hazards model using the survival package (Terry M. Therneau & Patricia M. Grambsch, 2000; Therneau, 2023). The model was constructed by first performing a univariate analysis of all pertinent factors, including the experimental replicate, the route of treatment injection (intravenous vs intraperitoneal.), the number of injections, the size of the tumour at the time of the first treatment, the cage the animal was treated in, and the treatment itself. In the univariate analysis, any factors with a P-value ≤ 0.1 were included in the model as a covariate with treatment. The model was then assessed for significance with a type II ANOVA with the car package (Fox & Weisberg, 2019). Any mouse euthanised for ulceration was treated like a clinical study would treat patients as "lost to follow-up" and censored from the survival analyses.

2.11.3 Other statistical tests and R packages

Non-parametric testing was performed by Kruskal-Wallis one-way ANOVA on ranks among three or more groups. Pairwise comparisons among treatment groups were then assessed using a Wilcoxon rank sum test.

Other packages that enabled the analyses and data visualisations written and created in R include the following: readxl (Wickham & Bryan, 2023) for data import; tidyverse (Wickham et al., 2019), lubridate (Spinu et al., 2023), and broom (Robinson et al., 2023) for data wrangling; ggplot2 (Wickham et al., 2023), ggpubr (Kassambara, 2023), gridExtra (Auguie, 2017), papaja (Aust & Barth, 2022), patchwork (Pedersen, 2022), and scales (Wickham & Seidel, 2022) to create data visualisations; survminer (Kassambara et al., 2021) was used to create the Kaplan-Meir plots; figpatch (Johnston, 2022) enabled the import of experiment schemas, which were created with BioRender.com; and, the gt

(Iannone et al., 2022) and gtsummary (Sjoberg et al., 2021) packages, which were used to produce tables in Appendix B and Figure 4.11B.

This entire dissertation was compiled in R Markdown using the oxforddown template (Lyngs, 2019).

3

Early T cell Infiltration Correlates with Anti-CTLA4 Treatment Response in the P815 Mastocytoma Model

Title: Early T cell infiltration correlates with anti-CTLA4 treatment response in the P815 mastocytoma model[1]

Authors*:*

Andrew A Almonte[*] (ORCiD: 0000-0002-8131-7805)

George Cavic[*] (ORCiD: 0000-0003-2657-8129)

Teresa Neeman[†] (ORCiD: 0000-0002-7315-3695)

Aude M Fahrer[*] (ORCiD: 0000-0001-8556-0223) [corresponding author]

Affiliations*:*

[*]Division of Biomedical Science and Biochemistry, Research School of Biology, Australian National University. Canberra, ACT, 2601

[†]Biological Data Science Institute**,** The Australian National University. Canberra, ACT, 2601

Corresponding Author: aude.fahrer@anu.edu.au

Conflicts of interest: The authors declare there is no conflict of interest to disclose

Running Title: Immune Checkpoint Blockade and P815

Keywords: Immunotherapy, CTLA-4, PD-1, Fine-needle aspirate

Word Count: 4,585

Reference Count: 42

Abstract (223/250 words):

Immune checkpoint blockade (ICB) antibodies are a revolutionary class of cancer treatment, but only approximately 30% of patients receive a lasting benefit from therapy. Pre-clinical studies using animals from the same genetic backgrounds, challenged with the same cancer models, also show non-uniform responses. Most mouse studies that have evaluated tumour-

[1] This project was funded by the Australian Government Research Training Program, the Lea Chapuis Memorial Fund, The Lionel & Yvonne Spencer and William G Maxwell Trusts administered through Perpetual's IMPACT Philanthropy, and the generosity of Tim and Margaret Bourke.

3. Early T cell Infiltration Correlates with Anti-CTLA4 Treatment Response in the P815 Mastocytoma Model

infiltrating leukocytes (TILs) after ICB therapy cannot directly correlate their findings with treatment outcomes because terminal methods were used to acquire immune infiltrate data. In the present study, we used fine-needle aspiration (a non-terminal sampling method) to collect multiple aspirates over several days from subcutaneously implanted P815 mastocytomas treated with ICB antibodies. These aspirates were then analysed with flow cytometry to directly correlate nine TIL populations from both the innate and adaptive arms of immunity with treatment success. We found that the P815 model responds well to anti-CTLA4 but not anti-PD1. Mice that regressed following anti-CTLA4 therapy showed a significant increase in CD8+ T cells on days 3, 5, and 7 and CD4+ T cells on days 5 and 7, and a simultaneous decrease in macrophages and monocytes on days 3, 5, and 7 post-treatment. Our study is the first to directly correlate early tumour infiltration of T cells with anti-CTLA4 treatment success, thus providing a mechanistic clue toward understanding why alloidentical mice challenged with identical tumours do not respond uniformly to ICB therapies.

Immune Checkpoint Blockade and P815

Introduction (599):

Immune checkpoint blockade (ICB) monoclonal antibodies targeting cytotoxic T lymphocyte-associated protein 4 (CTLA4), programmed death protein 1 (PD1), or its ligand, PD-L1, are a revolutionary class of cancer therapies aimed at restoring the body's anti-cancer immune response. They have increased patient survival in multiple clinical trials (Hellmann et al., 2019; Larkin et al., 2015; Seidel et al., 2018) and have better safety profiles than conventional chemotherapies (Reck et al., 2016; Robert et al., 2015), thus making them attractive treatment options. Their profound impact on oncology is reflected by Professors Allison and Honjo sharing the 2018 Nobel Prize for their work in developing anti-CTLA4 and PD1/PD-L1 blockade as viable cancer therapies (Iwai et al., 2002; Leach et al., 1996).

However, research published in high-impact journals has called into question whether a simple steric interaction is, as has always been assumed, necessarily the primary mode of action for these treatments. For example, recent work has demonstrated that ipilimumab (a fully humanised IgG1 anti-CTLA4 antibody) does not block the interaction between CTLA4 and CD28 yet still provides a therapeutic benefit (Du et al., 2018). Other studies have shown that the identity and competency of the Fc regions of anti-PD1, anti-PD-L1, and anti-CTLA4 antibodies have essential roles in their therapeutic effectiveness (Dahan et al., 2015; Selby et al., 2013; Simpson et al., 2013), a finding inconsistent with a simple blocking model. There is also the curious observation that mice treated with anti-CTLA4 have their tumour-infiltrating $CD4^+$ regulatory T cells depleted, but not those in peripheral lymphoid organs (Simpson et al., 2013; Wei et al., 2017), thus suggesting a model wherein antibody-dependent cellular cytotoxicity plays a substantial role. Finally, recent research has repeatedly and convincingly shown that the gut microbiome plays a significant role in ICB treatment success (Almonte et al., 2020; Routy et al., 2018; Vetizou et al., 2015). Taken together, these findings strongly

suggest that a mechanism reliant on blocking interactions between target and ligand does not wholly explain how ICB therapies confer therapeutic benefit.

Given that only approximately 30% of patients (Havel et al., 2019) and a minority of inbred syngeneic tumour-challenged mice respond to ICB treatments, it is vital we better understand the mechanism of action of these therapies, find means to improve their therapeutic effectiveness, and identify potential biomarkers that can predict therapeutic outcomes. Such an investigation is best achieved by first identifying key differences between ICB responders and non-responders.

In 2015, our laboratory published a novel non-terminal protocol for sampling tumour-infiltrating leukocytes (TILs) from subcutaneous P815 mastocytomas by fine-needle aspiration (FNA) (Carroll et al., 2015). We showed that the representation of TILs identified by flow cytometry from FNA sampling does not significantly deviate from results obtained from whole-tumour digests. Our technique has recently been applied to other murine tumour models (Sitnikova et al., 2021). Unlike a whole-tumour digest – a terminal procedure that provides data for a single timepoint – FNA sampling does not require animals to be euthanised to identify TILs by flow cytometry, and the procedure allows a tumour to be sampled multiple times over several days. Furthermore, FNA sampling was shown not to significantly impact tumour growth trajectories, TIL composition, or survival of mice challenged with the P815, CT26, MCA205, and A20 models (Carroll et al., 2015; Sitnikova et al., 2021). Thus, FNA sampling allows us to determine changes in TIL populations over time following pharmacological intervention. Most importantly, these changes can be used to identify key differences in TIL composition among animals with different treatment outcomes.

Immune Checkpoint Blockade and P815

In this study, we used our FNA sampling protocol to identify TILs in mice challenged with P815 tumours and treated with anti-PD1 or anti-CTLA4 monoclonal antibodies, two ICB therapies commonly used in both mouse studies and the clinic. We used flow cytometry to identify nine different TIL populations across both the innate and adaptive immune system and, through retrospective analysis, found that tumour regression following anti-CTLA4 treatment was associated with an increase in CD8+ and CD4+ T cells and a decrease in macrophages/monocytes during the first seven days post-treatment.

Immune Checkpoint Blockade and P815

Materials and Methods:

Mouse husbandry

Female DBA/2 mice were purchased from the Animal Resources Centre (Perth, WA). They were housed in a dedicated mouse-handling room on a 12-hour day/night cycle in an air handling unit (SmartFLow; Tecniplast) that maintained internal cage temperatures at 21°C. Autoclaved pellets of Gordons Rat & Mouse Premium 23% Protein Diet (Gordons Specialty Feeds, NSW) and autoclaved tap water were made freely available. The animals were allowed to acclimate to their new environment for at least seven days before starting any experiments. All animal experiments were approved by the Australian National University Ethics and Experimentation Committee under protocol A2017/46.

Cell culture

P815 mastocytoma cells (ATCC) were cultured in Dulbecco's Modified Eagle Medium (DMEM; Sigma) containing 4 g/L D-glucose and supplemented with 20 mM Glutamax (Gibco), 10% heat-inactivated foetal calf serum (Sigma), 1 mM sodium pyruvate (Gibco), 0.1 M HEPES (Gibco), 500 IU/mL penicillin, and 500 μg/mL streptomycin (Penicillin-Streptomycin; Gibco). CT26 colorectal cancer cells and 4T1 mammary adenocarcinoma cells were cultured in RPMI-1640 media (Sigma) supplemented with 20 mM Glutamax (Gibco), 10% heat-inactivated foetal calf serum (Sigma), 1 mM sodium pyruvate (Gibco), 0.1 M HEPES (Gibco), 500 IU/mL penicillin, and 500 μg/mL streptomycin (Penicillin-Streptomycin; Gibco). All cells were incubated at 37°C in a humidified environment with a 5% CO_2 injection.

Tumour Challenge and Treatment

Immune Checkpoint Blockade and P815

Six- to eight-week-old female DBA/2 mice were anaesthetised with 3% isoflurane in oxygen flowing at 1 L/min before shaving the left flank with a hair trimmer. They were then injected subcutaneously in the shaved injection site with 0.3 x 10^6 P815 mastocytoma cells suspended in 100 μL of a 1:1 mix of sterile saline and unsupplemented DMEM. Once tumours became palpable, they were measured frequently with digital callipers until they reached a size appropriate for treatment. Tumour size was determined by taking the average diameter of two orthogonal measurements, one being the tumour's longest axis.

Once the average tumour diameter of the experimental cohort reached 4 – 5 mm, the mice were distributed into treatment groups so that each group had a similar average and range of tumour size. Each cage thus contained mice belonging to multiple treatment groups to avoid confounding effects due to any cage or litter differences. Animals received either 0.2 mg of anti-CTLA-4 (9D9), 0.2 mg of anti-PD-1 (RMP1-14), or a control solution containing 0.2 mg each of both rat IgG2A (2A3) and mouse IgG2b (MPC-11) isotype control antibodies (0.4 mg total). In one experiment, control mice were given 0.2 mg each of mouse IgG2b (MPC-11) and rat IgG2b, κ (LTF-2) in combination. All antibodies were purchased from BioXcell. The mice received two to four 100 μL injections of their treatments suspended in sterile saline, given every three days, either intraperitoneally (i.p.) or intravenously (i.v.). Tumour size was measured every second day with digital callipers. In the case that multiple distinct tumours were present, tumour burden was calculated with the following equation:

$$T = \sqrt[3]{\sum_{i=1}^{N} t_i^3}$$

where T is the overall tumour burden, N is the number of tumours, and t_i is the average diameter of each tumour, measured as described above. All animals were humanely culled if they became ill or exceeded the ethical tumour size limit of 17 mm.

Fine-Needle Aspirate (FNA) Sampling

FNA sampling was performed as previously described (Carroll et al., 2015). In brief, a 1 mL syringe was preloaded with 0.5 mL of unsupplemented DMEM and fitted with a 25G needle. Mice were anaesthetised with 3% isoflurane in oxygen flowing at 1 L/min during the procedure. The syringe was inserted into the tumour, and a small amount of negative pressure was exerted as the needle was gently removed. Each tumour was sampled at three different sites to maximise intratumoural cellular representation. Following collection, the aspirate samples were immediately transferred to a 1.5 mL Eppendorf tube and kept on ice until further processing.

Flow Cytometry

To obtain single-cell suspensions, each aspirate sample was digested by adding 0.5 mL of a solution containing 10 mg/mL collagenase type 1 (Worthington Biochemicals, USA), 3 mg/mL hyaluronidase type I-S (Sigma), 0.02 mg/mL DNase (Worthington Biochemicals, USA), and 2% heat-inactivated foetal calf serum (Sigma), all suspended in unsupplemented DMEM (Sigma). The samples were then incubated for 20 min at 37^{o}C. The digestion mix was washed three times with FACS wash (phosphate-buffered saline with 2% (v/v) heat-inactivated foetal calf serum) before distributing the sample equally between two antibody stain cocktails.

Immune Checkpoint Blockade and P815

Single colour controls and cytometer setup were performed once for each experimental mouse cohort using thymus, spleen, and bone marrow samples. The adaptive immune cell stain contained PanNK - APC (DX5), CD8α - APC/Cy7 (53-6.7), CD45.2 - AF488 (104), CD19 - BV510 (6D5), TER119 - PE (TER-119), CD63 - PE (NVG-2), γδTCR - BV421 (GL3), and CD4 - PE/Cy7 (GK1.5). The innate immune cell stain contained I-A^d - AF647 (39-10-8), Ly6G - APC/Cy7 (1A8), CD45.2 - AF488 (104), CD11b - BV510 (M1/70), TER119 - PE (TER-119), CD63 - PE (NVG-2), Ly6C - BV421 (HK1.4), and CD11c - PE/Cy7 (N418). All fluorophore-conjugated antibodies were purchased from BioLegend (San Diego, USA). Both stains included 2 μg/mL of 7-AAD (Invitrogen) as a live/dead discriminator.

Samples were incubated in stain cocktails at 4°C in the dark for at least 30 minutes. Cells were washed three times with FACS wash before data were acquired on a BD LSR II flow cytometer and analysed with FLOWjo V7 software (Becton-Dickinson, New Jersey, USA).

Fluorophore Conjugation and Staining

A PE/R-Phycoerythrin Lightning-Link® amine conjugation kit (ab102918, Abcam, Cambridge, UK) was used to conjugate phycoerythrin (PE) to the treatment and control antibodies by following the manufacturer's instructions. In brief, antibodies were added to the kit's modifying agent at a concentration of 1 μg/μL, then incubated at room temperature for three hours. The kit's quencher reagent was then added, and the antibodies were incubated at room temperature for a further 30 minutes. The PE-conjugated antibodies were then stored in darkness at 4°C until required.

Cultured 4T1, CT26, or P815 cancer cells were stained with 1 μL PE-conjugated antibodies at 10^6 cells per 100 μL FACS wash. Cells treated with Fc block were first incubated with 1 μL anti-

177 CD16/32 (BD Pharmingen, San Diego, USA) in 50 µL for 25 minutes before adding PE-
178 conjugated antibodies.

179

180 **Bioinformatics Analysis**

181 The RNAseq analysis workflow was created and implemented on the Galaxy (v22.05.1) cloud
182 computing platform. The FASTq files SRR15403092, SRR15403093, and SRR15403094 (all from
183 GSE181773) were extracted from the Gene Expression Omnibus (Barrett et al., 2013)
184 maintained by the National Center for Biotechnology Information (NCBI). Sequence reads
185 were aligned with HISAT2. Read counts were generated with featureCounts, from the
186 Subread package, using the mm10 reference genome. The annotateMyIDs tool was used to
187 convert ENTREZID values to GeneID and gene descriptions.

188

189 **Statistical Analysis**

190 All statistical modelling was done using the statistical software package R version 4.1.0 (R Core
191 Team, 2020). Tumour growth by treatment was estimated using a random slopes model that
192 included growth data up to the 17th day following treatment, followed by a Tukey correction
193 to account for multiple comparisons. The 17-day threshold was chosen to minimise any bias
194 that may result in the initial tumour growth estimates in mice who experienced tumour
195 regression.
196 Survival between treatments was compared using a Cox-proportional hazards model that was
197 constructed by first performing a univariate analysis of all pertinent factors, including the
198 experimental replicate, the route of treatment injection (i.v. vs i.p.), the number of injections,
199 the size of the tumour at the time of the first treatment, and the treatment itself. In the

univariate analysis, any factors or covariates found to have a *P*-value ≤ 0.1 were included in the model as a co-variate with treatment. The model was then assessed for significance with a Type II ANOVA.

FNA-derived TIL populations were examined for quality control (Figure 3.1), then compared between treatments using linear mixed-effects models and assessed for significance with a Type II ANOVA. Contrasts were assessed between treatment groups on different days if the overall *P*-value was ≤ 0.05. Only samples with more than 20 events in the "All Immune Cells" gate (Figure 3.1) were analysed to avoid percentage anomalies due to small sample sizes. A *P*-value ≤ 0.05 was considered significant in all statistical tests.

Immune Checkpoint Blockade and P815

Results (1186)

P815 tumour model responds to anti-CTLA4 therapy

To assess the effectiveness of anti-PD1 and anti-CTLA4 therapies, we performed six independent *in vivo* experiments using female DBA/2 mice challenged subcutaneously with 0.3 x 10^6 P815 mastocytoma cells (Figure 3.2A). Once tumours reached an average diameter of 4 – 5 mm, mice received two to four treatments of immune checkpoint blockade (ICB) therapy or control treatment, either intravenously (i.v.) or intraperitoneally (i.p.), with one injection given every three days (Figure 3.2A). Mice receiving anti-CTLA4 and anti-PD1 were given 100 µL injections containing 0.2 mg of antibody, while control mice were given 100 µL injections containing 0.2 mg of each isotype control antibody (0.4 mg total). FNA sampling was performed on days 1, 3, 5, and 7 post-treatment. The animals were monitored until they reached an ethical endpoint, or their tumours regressed. Regressors were monitored for at least 60 days post-treatment to confirm they did not relapse.

While performing these experiments, we observed that some control mice were regressing following treatment (Figure 3.2B and Figure 3.3, first seen in experiment 3). We were curious as to why animals treated with non-specific isotype control antibodies were regressing because, in 156 control-treated mice from previous experiments using intratumoural therapies, we had never observed a control mouse spontaneously regress with this tumour model (Carroll et al., 2015; Carroll et al., 2021). We initially questioned our injection technique and amended our treatment protocol from i.p. injections to i.v. injections because, although unlikely, we reasoned i.p. injections might inadvertently be piercing the gut. Such an injury could allow gut bacteria to infect the host and induce a systemic inflammatory response, potentially improving the anti-cancer immune response (Almonte et al., 2020). However,

Immune Checkpoint Blockade and P815

regressing mice were also seen when injecting isotype control antibodies i.v. (Figure 3.3, experiment 5).

Importantly, statistical analysis showed that neither the injection route ($P = 0.91$) nor number of treatment injections ($P = 0.08$) had a significant impact on treatment outcomes and overall survival (Figure 3.2C). Thus, all six individual experiments were combined for analysis (Figure 3.4).

Individual tumour growth trajectories from all six experiments are shown in Figure 3.2B. Analysis of tumour growth with a random slopes model showed that anti-CTLA4 treatment had a significant impact relative to mice treated with isotype control antibodies. However, this was not the case for mice treated with anti-PD1. Mice treated with anti-CTLA4 also had more regressors (10/42; 23.8%) compared with 5/37 (13.5%) and 4/35 (11.4%) regressors in anti-PD1 and control-treated mice, respectively.

Analysis of survival with a Cox proportional hazards model showed that mice treated with anti-CTLA4 had significantly improved survival outcomes (Figures 3.2C and 3.4), which was consistent with the data acquired from the tumour growth. Anti-PD1 – treated mice had no improved survival benefit above the isotype control-treated mice.

Antibodies bind to Fcγ receptors on the surface of P815 cells

We were curious as to why some mice treated with non-specific isotype control antibodies (rat IgG2a [2A3] and mouse IgG2b [MPC-11]) regressed, having formally eliminated our i.p. injection technique as the cause. As the P815 model is a cancer of mast cells and knowing that mast cells express Fcγ receptors on their surface (Malbec & Daeron, 2007) (along with the better known Fcε receptors), we sought to determine if the treatment antibodies – anti-

Immune Checkpoint Blockade and P815

PD1 (RMP1-14) and anti-CTLA4 (9D9) – and isotype control antibodies were binding to Fcγ receptors on the P815 mast cell line. We also asked if P815 cells expressed either PD1 or CTLA4 and could, therefore, potentially be direct immune cell targets of these therapies. We therefore conjugated phycoerythrin (PE) to our treatment and isotype control antibodies, and measured binding to P815 cells by flow cytometry in the absence or presence of unconjugated anti-CD16/32 antibodies (Fc block).

As shown in Figure 3.5, both the treatment and isotype control antibodies bound to P815 cells. In all cases, Fc block substantially reduced binding, providing clear evidence that all four antibodies bound with P815 cells *in vitro* by engaging with CD16/32. Anti-PD1 was the only antibody that was not wholly inhibited from binding with P815 cells following treatment with Fc block. Further testing is required to determine if there is any residual Fc-independent binding of the anti-PD1 antibody. We tested two other commonly used cancer models – CT26 colorectal carcinoma and 4T1 mammary adenocarcinoma – and did not see any binding to the cancer cells (Figure 3.5C).

To corroborate our results, we examined an RNAseq dataset recently uploaded to the NCBI GEO database, accession GSE181773, that provided RNAseq data for the P815 mastocytoma cell line. As shown in Figure 3.5D, P815 cells have high expression of CD16 and CD32, low expression of PD1, and no detectable expression of CTLA4, which agrees with the results in Figure 3.5B. High expression of CD45 and CD63 (markers used in our flow cytometry panel) as well as FcεRIg and PD-L1 was also noticed. Thus, antibody binding through Fc receptors is a serious consideration in the P815 model and, by extension, should also be considered in other immune cell cancer models. Fortunately, this is not common to all cancer cell lines; and was not detected in the 4T1 breast cancer and CT26 colon cancer cell lines (Figure 3.5C).

Immune Checkpoint Blockade and P815

Tumour-infiltrating immune cell proportions differentiate responders and non-responders in anti-CTLA4 – treated mice

FNA samples were collected on days 1, 3, 5, and 7 after the first treatment injection (Figure 3.2A). Samples were stained and analysed by flow cytometry using the gating strategy shown in Figure 3.6. Nine different tumour-infiltrating leukocyte (TIL) populations were identified, and the results are presented as a percentage of live non-cancerous immune cells (Figure 3.7). We were able to remove cancerous cells from the analysis because P815 cells express the mast cell marker CD63 (Carroll et al., 2015; He et al., 2013, and Figure 2D), which, combined with their relatively large size, allows them to be excluded with our gating strategy (Figure 3.6A).

Figure 3.7A shows the changes in proportions of TIL subsets identified with flow cytometry in P815 tumours on days 1, 3, 5, and 7 following the first treatment. Samples which passed quality control (>20 TILs in the “All Immune Cells” gate, Figure 3.6B) were included in the analysis (Figure 3.1). These same data are summarised in Figure 3.7B as a stacked bar chart, and the individual data for each mouse analysed in this study are presented in Figure 3.8. The only cell type that was significantly impacted by treatment were tumour-infiltrating CD4+ T cells. As seen in Figure 3.7A, Animals treated with anti-PD1 or isotype control antibodies showed a decrease in CD4+ T cell proportions over the first week following treatment, whereas mice treated with anti-CTLA4 presented an increase in CD4+ T cells.

However, the advantage of FNA sampling is that it allows us to retrospectively identify differences in TIL proportions among animals with disparate treatment outcomes. As shown in Figure 3.9, we found that when compared to mice in which anti-CTLA4 therapy was not

3. Early T cell Infiltration Correlates with Anti-CTLA4 Treatment Response in the P815 Mastocytoma Model

301 successful, mice that had regressed following anti-CTLA4 therapy had a statistically
302 significant: increases in tumour infiltrating $CD8^+$ T cells on days 3, 5, and 7; increases in tumour
303 infiltrating $CD4^+$ T cells on days 5 and 7 post-treatment; and decreased CD11b+ Ly6C+ Ly6G-
304 macrophages/monocytes on day 3 post-treatment.

Immune Checkpoint Blockade and P815

Discussion (1438):

ICB therapies are a revolutionary class of cancer treatment, but questions remain regarding why only a minority of recipients – in both mice and humans – are responsive. Here we addressed this question by analysing tumour-infiltrating leukocytes in the first week after treatment. We found key differences only become apparent when comparing mice which respond to therapy to mice which do not. We have also demonstrated that the P815 mastocytoma model responds well to anti-CTLA4 therapy but not to anti-PD1 therapy. Finally, and most importantly, we were able to use the FNA data we acquired to identify key differences in TIL profiles between anti-CTLA4 responders and non-responders. Our analysis showed that mice responsive to anti-CTLA4 treatment had significantly increased proportions of tumour infiltrating $CD4^+$ and $CD8^+$ T cells, and decreased proportions of macrophages/monocytes following treatment.

Our P815-challenged mice did not respond to anti-PD1 treatment, despite Honjo using this model to demonstrate the concept of PD-1/PD-L1 blockade (Iwai et al., 2002). However, there are several major differences between our study and Honjo's seminal paper. First, Honjo used anti-PD-L1 clone 1-111A (Ishida et al., 2002) while we used anti-PD1, clone RMP1-14; second, he started treatment the day following tumour challenge whereas we started treatments once tumours reached 4 – 5 mm, approximately six to 11 days following tumour challenge; lastly, we used the wild-type P815 cell line whereas Honjo used a transgenic cell line that overexpressed PD-L1. However, studies have since shown that relying on PD-L1 expression to predict the success of PD1 blockade treatment in human patients is highly variable (Davis & Patel, 2019; Uruga & Mino-Kenudson, 2021). Indeed, the RNAseq data we examined confirms that wild-type P815 cells do express PD-L1 RNA transcripts. Therefore, the level of PD-L1

328 expression on the wild-type P815 cell line does not wholly explain why we found anti-PD1
329 treatments to be ineffective.

330 Another possible explanation for the lack of a therapeutic anti-PD1 response may be that
331 P815 tumours lack a significant pre-existing T cell infiltrate (Figure 3.7A, Day 1 and isotype
332 controls). Previous studies in humans and mice have found that PD1 blockade primarily
333 targets pre-existing tumour-infiltrating cytotoxic $CD8^+$ T cells (Sade-Feldman et al., 2018; Wei
334 et al., 2017) and that patients whose cancers are highly infiltrated by T cells tend to respond
335 better to treatment (Lei et al., 2020; Tumeh et al., 2014). Tumour-infiltrating cytotoxic $CD8^+$
336 T cells often have increased PD-1 surface expression due to chronic antigenic stimulation,
337 which leads to an anergic "exhausted" state (Wherry & Kurachi, 2015) and provides a
338 therapeutic target for anti-PD1 antibodies. However, whether anti-PD1 works by
339 reinvigorating exhausted $CD8^+$ T cells or by promoting the infiltration of fresh new cytotoxic
340 $CD8^+$ T cells from peripheral lymphoid organs is not entirely understood. Two independent
341 studies evaluating cancers from human patients have shown that exhausted $CD8^+$ T cells were
342 not reinvigorated to an effector phenotype following anti-PD1 therapy. Instead, they were
343 replaced by T cells from a distinct lineage from other peripheral sources (Sade-Feldman et al.,
344 2018; Yost et al., 2019). In contrast, at least one study using a mouse model for chronic
345 lymphocytic choriomeningitis virus – an infectious agent that provides chronic antigenic
346 stimulation – treated with PD1 blockade suggests that exhausted T cells can reacquire some
347 features of effector T cells (Pauken et al., 2016). These studies further highlight critical
348 questions surrounding how PD1/PD-L1 blockade therapies provide therapeutic benefit.

349 The isotype control group's spontaneous regressors were unexpected and emphasised the
350 importance of having such controls in any *in vivo* study. Previous studies by our laboratory

have used the P815 tumour model across many experiments, summing to at least 156 control-treated mice. Those control mice were given intratumoural injections of either incomplete Freund's adjuvant or phosphate-buffered saline (Carroll et al., 2015; Carroll et al., 2021). No tumour-challenged mouse given a control treatment was ever seen to regress. Thus, the regressors described herein, treated intraperitoneally or intravenously with non-specific isotype control antibodies, represent the first instances of regression following control treatment we have observed. We should note that the control-treated mice were given twice the amount of antibody (0.4 mg combined) than the mice treated with either anti-PD1 or anti-CLTA4 (0.2 mg each). As shown in Figure 3.5, control and treatment antibodies can bind Fcγ receptors expressed on the surface of P815 cells. While these data were collected from cultured cells, they provide a likely explanation for the regressor mice in this study: isotype control antibodies binding Fcγ receptors on P815 cells *in vivo*, leading to cell death.

Importantly, anti-CTLA4 treatment gave a clear survival benefit to mice challenged with the P815 tumour model, which gave us the opportunity to evaluate differences in TILs between mice that did and did not respond to treatment (Figures 4A and 5). Our findings agree with previous studies, which observed increased T cell infiltrates following anti-CTLA4 treatment through histological methods (Chen et al., 2016; Motoshima et al., 2015), flow cytometry (Oliver et al., 2019), and mass cytometry (Wei et al., 2019). It is worth noting, however, that most murine studies of the tumour microenvironment require terminal or invasive procedures (Principe et al., 2020; Zemek et al., 2020), making it impossible to directly correlate treatment success with immune infiltrates. An impressive, non-invasive method using heavy-metal-conjugated nanobodies and positron emission tomography has been described (Rashidian et al., 2017), but it does not enumerate the number of tumour-infiltrating T cells. FNA sampling is a non-terminal, relatively non-invasive procedure that uses

accessible equipment and can be performed multiple times on each animal, thus allowing a unique temporal insight into immune infiltration following tumour treatment.

Our data suggest that rapid infiltration of $CD8^+$ and $CD4^+$ T cells (by 3 days and 5 days post-treatment, respectively), and a simultaneous decrease in proportions of tumour-infiltrating macrophages and monocytes, strongly correlates with anti-CTLA4 treatment success (Figure 3.9). From a mechanistic point of view, this rapid increase in T cell infiltration is consistent with our understanding of CTLA4 biology. CTLA4 is a surface molecule expressed by all activated T cells and is constitutively expressed by $CD4^+$ Treg cells. It competes for binding to CD80 and CD86 – essential co-stimulatory molecules required by naïve T cells upon priming and activation. Exactly how CTLA4 regulates CD28 signalling is not entirely understood, and several cell-intrinsic and -extrinsic mechanisms have been proposed (Walker & Sansom, 2011). One of many demonstrated means by which CTLA4 can control CD28 signalling is by the physical removal of CD80/86 from the surface of antigen-presenting cells via transendocytosis (Qureshi et al., 2011). Regardless of the exact mechanism, inhibiting CTLA4:CD80/86 interactions in the secondary lymphoid organs by anti-CTLA4 monoclonal antibodies is expected to lead to increased priming of anti-tumour T cells (Wei et al., 2017). This inhibition could then lead to a rapid increase in tumour-infiltrating T cells, as we found in our study.

Along with questions about the exact biology of CTLA4, there are also questions about the exact mechanisms of action of anti-CTLA4 checkpoint inhibitors, most strikingly shown by a study demonstrating that ipilimumab (human IgG1 anti-CTLA4 treatment) does not work through a blocking mechanism (Du et al., 2018). Indeed, Ingram *et al.* have elegantly shown that merely blocking the interactions of CTLA-4 with CD80/86 using an alpaca heavy-chain

only antibody fragment conveys no therapeutic benefit in a B16 melanoma model; however, therapeutic efficacy was rescued when the fragment was conjugated to a murine IgG2a constant region (Ingram et al., 2018). These, and other questions, are further discussed in our recent review paper (Almonte et al., 2020).

One mouse that showed complete tumour regression in our study did not exhibit increased T cell infiltrates in the tumour but instead showed a very high level of neutrophil infiltrates (Figure 3.9, Mouse 171, Figure 3.8A). We have previously shown that increased neutrophil infiltrates predict which mice achieve complete tumour regressions in the P815 mastocytoma model after intratumoural injection of Complete Freund's Adjuvant (CFA) (Carroll et al., 2021). Although preliminary, Mouse 171 may indicate that there could be more than one immune signature leading to tumour regression.

In conclusion, we have shown that the P815 mastocytoma model responds to anti-CTLA4, but not anti-PD1 checkpoint blockade therapies. We have also shown that P815 mastocytoma can regress following isotype control antibody injection. This appears to be due to binding of antibodies to Fc receptors on the cancer cells, which has significant implications for researchers studying the response of immunological cancers to checkpoint blockade or other antibody-based treatments. On the other hand, this finding could also have positive implications for the treatment of immunological cancers.

Our study directly correlates successful anti-CTLA4 treatment outcome with an increase in tumour-infiltrating T cells and simultaneous decrease in tumour-infiltrating macrophages and monocytes. We also showed this change is most critical to treatment success around days 3, 5, and 7 post-treatment. Therefore, our study provides a mechanistic clue to the critical question of why alloidentical mice injected with identical tumours do not respond identically

421 to treatment. If similar in human cancers, this could ultimately be used to rapidly identify
422 which patients are likely to derive benefit from continued anti-CTLA4 treatment. Thus, further
423 studies correlating early immune infiltrates following ICB treatment in both mice and humans
424 are clearly warranted.

References

Almonte, A. A., Rangarajan, H., Yip, D., & Fahrer, A. M. (2020). How does the gut microbiome influence immune checkpoint blockade therapy? *Immunol. Cell Biol.* https://doi.org/10.1111/imcb.12423

Barrett, T., Wilhite, S. E., Ledoux, P., Evangelista, C., Kim, I. F., Tomashevsky, M., Marshall, K. A., Phillippy, K. H., Sherman, P. M., Holko, M., Yefanov, A., Lee, H., Zhang, N., Robertson, C. L., Serova, N., Davis, S., & Soboleva, A. (2013). NCBI GEO: archive for functional genomics data sets--update. *Nucleic Acids Res*, *41*(Database issue), D991-995. https://www.ncbi.nlm.nih.gov/pubmed/23193258 https://www.ncbi.nlm.nih.gov/pmc/articles/PMC3531084/pdf/gks1193.pdf

Carroll, C. S. E., Altin, J. G., Neeman, T., & Fahrer, A. M. (2015). Repeated fine-needle aspiration of solid tumours in mice allows the identification of multiple infiltrating immune cell types. *J. Immunol. Methods*, *425*, 102-107. https://doi.org/10.1016/j.jim.2015.06.015

Carroll, C. S. E., Andrew, E. R., Malik, L., Elliot, K. F., Brennan, M., Meyer, J., Hintze, A., Almonte, A. A., Lappin, C., MacPherson, P., Schulte, K.-M., Dahlstrom, J. E., Tamhane, R., Neeman, T., Woolsey Herbert, E., Orange, M., Yip, D., Allavena, R., & Fahrer, A. (2021). Simple and effective bacterial-based intratumoral cancer immunotherapy [Research]. *J Immunother Cancer*. https://doi.org/10.1136/jitc-2021-002688

Chen, P. L., Roh, W., Reuben, A., Cooper, Z. A., Spencer, C. N., Prieto, P. A., Miller, J. P., Bassett, R. L., Gopalakrishnan, V., Wani, K., De Macedo, M. P., Austin-Breneman, J. L., Jiang, H., Chang, Q., Reddy, S. M., Chen, W. S., Tetzlaff, M. T., Broaddus, R. J., Davies, M. A., . . . Wargo, J. A. (2016). Analysis of Immune Signatures in Longitudinal Tumor Samples Yields Insight into Biomarkers of Response and Mechanisms of Resistance to Immune Checkpoint Blockade. *Cancer Discov*, *6*(8), 827-837. https://www.ncbi.nlm.nih.gov/pubmed/27301722https://cancerdiscovery.aacrjournals.org/content/candisc/6/8/827.full.pdf https://www.ncbi.nlm.nih.gov/pmc/articles/PMC5082984/pdf/nihms796563.pdf

Dahan, R., Sega, E., Engelhardt, J., Selby, M., Korman, A. J., & Ravetch, J. V. (2015). FcgammaRs Modulate the Anti-tumor Activity of Antibodies Targeting the PD-1/PD-L1 Axis. *Cancer Cell*, *28*(4), 543. https://doi.org/10.1016/j.ccell.2015.09.011

Davis, A. A., & Patel, V. G. (2019). The role of PD-L1 expression as a predictive biomarker: an analysis of all US Food and Drug Administration (FDA) approvals of immune checkpoint inhibitors. *J Immunother Cancer*, *7*(1), 278. https://www.ncbi.nlm.nih.gov/pubmed/31655605https://www.ncbi.nlm.nih.gov/pmc/articles/PMC6815032/pdf/40425_2019_Article_768.pdf https://jitc.bmj.com/content/jitc/7/1/278.full.pdf

Du, X., Tang, F., Liu, M., Su, J., Zhang, Y., Wu, W., Devenport, M., Lazarski, C. A., Zhang, P., Wang, X., Ye, P., Wang, C., Hwang, E., Zhu, T., Xu, T., Zheng, P., & Liu, Y. (2018). A reappraisal of CTLA-4 checkpoint blockade in cancer immunotherapy. *Cell Res*, *28*(4), 416-432.

https://www.ncbi.nlm.nih.gov/pubmed/29472691https://www.ncbi.nlm.nih.gov/pmc/articles/PMC5939050/pdf/41422_2018_Article_11.pdf
https://www.nature.com/articles/s41422-018-0011-0.pdf

Havel, J. J., Chowell, D., & Chan, T. A. (2019). The evolving landscape of biomarkers for checkpoint inhibitor immunotherapy. *Nat Rev Cancer*, *19*(3), 133-150. https://www.ncbi.nlm.nih.gov/pubmed/30755690https://www.nature.com/articles/s41568-019-0116-x.pdf
https://www.ncbi.nlm.nih.gov/pmc/articles/PMC6705396/pdf/nihms-1043064.pdf

He, S. H., Zhang, H. Y., Zeng, X. N., Chen, D., & Yang, P. C. (2013). Mast cells and basophils are essential for allergies: mechanisms of allergic inflammation and a proposed procedure for diagnosis. *Acta Pharmacol. Sin.*, *34*(10), 1270-1283. https://doi.org/10.1038/aps.2013.88

Hellmann, M. D., Paz-Ares, L., Bernabe Caro, R., Zurawski, B., Kim, S. W., Carcereny Costa, E., Park, K., Alexandru, A., Lupinacci, L., de la Mora Jimenez, E., Sakai, H., Albert, I., Vergnenegre, A., Peters, S., Syrigos, K., Barlesi, F., Reck, M., Borghaei, H., Brahmer, J. R., . . . Ramalingam, S. S. (2019). Nivolumab plus Ipilimumab in Advanced Non-Small-Cell Lung Cancer. *N Engl J Med*, *381*(21), 2020-2031. https://www.ncbi.nlm.nih.gov/pubmed/31562796https://www.nejm.org/doi/pdf/10.1056/NEJMoa1910231?articleTools=true
https://www.nejm.org/doi/pdf/10.1056/NEJMoa1910231?articleTools=true

Ingram, J. R., Blomberg, O. S., Rashidian, M., Ali, L., Garforth, S., Fedorov, E., Fedorov, A. A., Bonanno, J. B., Le Gall, C., Crowley, S., Espinosa, C., Biary, T., Keliher, E. J., Weissleder, R., Almo, S. C., Dougan, S. K., Ploegh, H. L., & Dougan, M. (2018). Anti-CTLA-4 therapy requires an Fc domain for efficacy. *Proc Natl Acad Sci U S A*, *115*(15), 3912-3917. https://doi.org/10.1073/pnas.1801524115

Ishida, M., Iwai, Y., Tanaka, Y., Okazaki, T., Freeman, G. J., Minato, N., & Honjo, T. (2002). Differential expression of PD-L1 and PD-L2, ligands for an inhibitory receptor PD-1, in the cells of lymphohematopoietic tissues. *Immunol Lett*, *84*(1), 57-62. https://www.ncbi.nlm.nih.gov/pubmed/12161284https://www.sciencedirect.com/science/article/pii/S0165247802001426?via%3Dihub

Iwai, Y., Ishida, M., Tanaka, Y., Okazaki, T., Honjo, T., & Minato, N. (2002). Involvement of PD-L1 on tumor cells in the escape from host immune system and tumor immunotherapy by PD-L1 blockade. *Proc. Natl. Acad. Sci. U.S.A.*, *99*(19), 12293-12297. https://doi.org/10.1073/pnas.192461099

Larkin, J., Chiarion-Sileni, V., Gonzalez, R., Grob, J. J., Cowey, C. L., Lao, C. D., Schadendorf, D., Dummer, R., Smylie, M., Rutkowski, P., Ferrucci, P. F., Hill, A., Wagstaff, J., Carlino, M. S., Haanen, J. B., Maio, M., Marquez-Rodas, I., McArthur, G. A., Ascierto, P. A., . . . Wolchok, J. D. (2015). Combined Nivolumab and Ipilimumab or Monotherapy in Untreated Melanoma. *N Engl J Med*, *373*(1), 23-34.

https://www.ncbi.nlm.nih.gov/pubmed/26027431https://www.nejm.org/doi/pdf/10.1056/NEJMoa1504030?articleTools=true
https://www.nejm.org/doi/pdf/10.1056/NEJMoa1504030?articleTools=true

Leach, D. R., Krummel, M. F., & Allison, J. P. (1996). Enhancement of antitumor immunity by CTLA-4 blockade. *Science*, *271*(5256), 1734-1736. https://www.ncbi.nlm.nih.gov/pubmed/8596936https://science-sciencemag-org.virtual.anu.edu.au/content/sci/271/5256/1734.full.pdf

Lei, Q., Wang, D., Sun, K., Wang, L., & Zhang, Y. (2020). Resistance Mechanisms of Anti-PD1/PDL1 Therapy in Solid Tumors. *Front Cell Dev Biol*, *8*, 672. https://www.ncbi.nlm.nih.gov/pubmed/32793604https://www.ncbi.nlm.nih.gov/pmc/articles/PMC7385189/pdf/fcell-08-00672.pdf
https://www.ncbi.nlm.nih.gov/pmc/articles/PMC7385189/pdf/fcell-08-00672.pdf

Malbec, O., & Daeron, M. (2007). The mast cell IgG receptors and their roles in tissue inflammation. *Immunol Rev*, *217*, 206-221. https://www.ncbi.nlm.nih.gov/pubmed/17498061https://onlinelibrary-wiley-com.virtual.anu.edu.au/doi/pdfdirect/10.1111/j.1600-065X.2007.00510.x
https://onlinelibrary.wiley.com/doi/10.1111/j.1600-065X.2007.00510.x

Motoshima, T., Komohara, Y., Horlad, H., Takeuchi, A., Maeda, Y., Tanoue, K., Kawano, Y., Harada, M., Takeya, M., & Eto, M. (2015). Sorafenib enhances the antitumor effects of anti-CTLA-4 antibody in a murine cancer model by inhibiting myeloid-derived suppressor cells. *Oncol Rep*, *33*(6), 2947-2953. https://www.ncbi.nlm.nih.gov/pubmed/25845968https://www.spandidos-publications.com/10.3892/or.2015.3893/download
https://www.spandidos-publications.com/10.3892/or.2015.3893/download

Oliver, A. J., Davey, A. S., Keam, S. P., Mardiana, S., Chan, J. D., von Scheidt, B., Beavis, P. A., House, I. G., Van Audernaerde, J. R., Darcy, P. K., Kershaw, M. H., & Slaney, C. Y. (2019). Tissue-specific tumor microenvironments influence responses to immunotherapies. *Clin Transl Immunology*, *8*(11), e1094. https://doi.org/10.1002/cti2.1094

Pauken, K. E., Sammons, M. A., Odorizzi, P. M., Manne, S., Godec, J., Khan, O., Drake, A. M., Chen, Z., Sen, D. R., Kurachi, M., Barnitz, R. A., Bartman, C., Bengsch, B., Huang, A. C., Schenkel, J. M., Vahedi, G., Haining, W. N., Berger, S. L., & Wherry, E. J. (2016). Epigenetic stability of exhausted T cells limits durability of reinvigoration by PD-1 blockade. *Science*, *354*(6316), 1160-1165. https://www.ncbi.nlm.nih.gov/pubmed/27789795https://www.ncbi.nlm.nih.gov/pmc/articles/PMC5484795/pdf/nihms866030.pdf
https://www.ncbi.nlm.nih.gov/pmc/articles/PMC5484795/pdf/nihms866030.pdf

Principe, N., Kidman, J., Goh, S., Tilsed, C. M., Fisher, S. A., Fear, V. S., Forbes, C. A., Zemek, R. M., Chopra, A., Watson, M., Dick, I. M., Boon, L., Holt, R. A., Lake, R. A., Nowak, A. K., Lesterhuis, W. J., McDonnell, A. M., & Chee, J. (2020). Tumor Infiltrating Effector Memory

Antigen-Specific CD8(+) T Cells Predict Response to Immune Checkpoint Therapy. *Front Immunol*, *11*, 584423. https://www.ncbi.nlm.nih.gov/pubmed/33262762https://www.ncbi.nlm.nih.gov/pmc/articles/PMC7688517/pdf/fimmu-11-584423.pdf https://www.ncbi.nlm.nih.gov/pmc/articles/PMC7688517/pdf/fimmu-11-584423.pdf

Qureshi, O. S., Zheng, Y., Nakamura, K., Attridge, K., Manzotti, C., Schmidt, E. M., Baker, J., Jeffery, L. E., Kaur, S., Briggs, Z., Hou, T. Z., Futter, C. E., Anderson, G., Walker, L. S., & Sansom, D. M. (2011). Trans-endocytosis of CD80 and CD86: a molecular basis for the cell-extrinsic function of CTLA-4. *Science*, *332*(6029), 600-603. https://doi.org/10.1126/science.1202947

R Core Team. (2020). *R: A language and environment for statistical computing.* In R Foundation for Statistical Computing. http://www.R-project.org

Rashidian, M., Ingram, J. R., Dougan, M., Dongre, A., Whang, K. A., LeGall, C., Cragnolini, J. J., Bierie, B., Gostissa, M., Gorman, J., Grotenbreg, G. M., Bhan, A., Weinberg, R. A., & Ploegh, H. L. (2017). Predicting the response to CTLA-4 blockade by longitudinal noninvasive monitoring of CD8 T cells. *J Exp Med*, *214*(8), 2243-2255. https://www.ncbi.nlm.nih.gov/pubmed/28666979https://www.ncbi.nlm.nih.gov/pmc/articles/PMC5551571/pdf/JEM_20161950.pdf https://www.ncbi.nlm.nih.gov/pmc/articles/PMC5551571/pdf/JEM_20161950.pdf

Reck, M., Rodriguez-Abreu, D., Robinson, A. G., Hui, R., Csoszi, T., Fulop, A., Gottfried, M., Peled, N., Tafreshi, A., Cuffe, S., O'Brien, M., Rao, S., Hotta, K., Leiby, M. A., Lubiniecki, G. M., Shentu, Y., Rangwala, R., Brahmer, J. R., & Investigators, K.-. (2016). Pembrolizumab versus Chemotherapy for PD-L1-Positive Non-Small-Cell Lung Cancer. *N Engl J Med*, *375*(19), 1823-1833. https://doi.org/10.1056/NEJMoa1606774

Robert, C., Schachter, J., Long, G. V., Arance, A., Grob, J. J., Mortier, L., Daud, A., Carlino, M. S., McNeil, C., Lotem, M., Larkin, J., Lorigan, P., Neyns, B., Blank, C. U., Hamid, O., Mateus, C., Shapira-Frommer, R., Kosh, M., Zhou, H., . . . investigators, K.-. (2015). Pembrolizumab versus Ipilimumab in Advanced Melanoma. *N Engl J Med*, *372*(26), 2521-2532. https://doi.org/10.1056/NEJMoa1503093

Routy, B., Le Chatelier, E., Derosa, L., Duong, C. P. M., Alou, M. T., Daillere, R., Fluckiger, A., Messaoudene, M., Rauber, C., Roberti, M. P., Fidelle, M., Flament, C., Poirier-Colame, V., Opolon, P., Klein, C., Iribarren, K., Mondragon, L., Jacquelot, N., Qu, B., . . . Zitvogel, L. (2018). Gut microbiome influences efficacy of PD-1-based immunotherapy against epithelial tumors. *Science*, *359*(6371), 91-97. https://www.ncbi.nlm.nih.gov/pubmed/29097494https://science.sciencemag.org/content/sci/359/6371/91.full.pdf

Sade-Feldman, M., Yizhak, K., Bjorgaard, S. L., Ray, J. P., de Boer, C. G., Jenkins, R. W., Lieb, D. J., Chen, J. H., Frederick, D. T., Barzily-Rokni, M., Freeman, S. S., Reuben, A., Hoover, P. J., Villani, A. C., Ivanova, E., Portell, A., Lizotte, P. H., Aref, A. R., Eliane, J. P., . . . Hacohen, N. (2018). Defining T Cell States Associated with Response to Checkpoint Immunotherapy in

Melanoma. *Cell*, *175*(4), 998-1013 e1020. https://www.ncbi.nlm.nih.gov/pubmed/30388456https://www.cell.com/cell/pdf/S0092-8674(18)31394-1.pdf https://www.cell.com/cell/pdf/S0092-8674(18)31394-1.pdf

Seidel, J. A., Otsuka, A., & Kabashima, K. (2018). Anti-PD-1 and Anti-CTLA-4 Therapies in Cancer: Mechanisms of Action, Efficacy, and Limitations. *Front Oncol*, *8*, 86. https://www.ncbi.nlm.nih.gov/pubmed/29644214https://www.ncbi.nlm.nih.gov/pmc/articles/PMC5883082/pdf/fonc-08-00086.pdf https://www.ncbi.nlm.nih.gov/pmc/articles/PMC5883082/pdf/fonc-08-00086.pdf

Selby, M. J., Engelhardt, J. J., Quigley, M., Henning, K. A., Chen, T., Srinivasan, M., & Korman, A. J. (2013). Anti-CTLA-4 antibodies of IgG2a isotype enhance antitumor activity through reduction of intratumoral regulatory T cells. *Cancer Immunol Res*, *1*(1), 32-42. https://www.ncbi.nlm.nih.gov/pubmed/24777248https://cancerimmunolres.aacrjournals.org/content/canimm/1/1/32.full.pdf https://watermark.silverchair.com/32.pdf?token=AQECAHi208BE49Ooan9kkhW_Ercy7Dm3ZL_9Cf3qfKAc485ysgAAArgwggK0BgkqhkiG9w0BBwagggKlMIICoQIBADCCApoGCSqGSIb3DQEHATAeBglghkgBZQMEAS4wEQQMFrJSJVyZmEItOEhKAgEQgIICa0wxgUfavfW3EbTV_ox7NV4eYafFgaSxp_LpePWitgp5MEz_AheLQV0I9uvSZsbobSeyl-n1LbF15tEhylu5LiCroy_3zjfONu6nHetl_K9pqyUXakxwzfedAtfiTtssS0Hiif7EXo2fzIIrEIL9DyKqVyiWvkvZTMmmBTUbH_MUoTrCgazihYxwG32sPPM2qzjH1iKGPpb12AzkEH4OQDOUPeDb2zDodeDEDJ2KW1HR2W2m6TSiwRXYXO7XhIkcqwIleMHIinq7DU5P5_tYBhYA7AS2F3DN2QEOyZuXb1yNDSi7GzymcmTv0Za6fJ7KmaoS8d8SQQgZUsC1qPtVImwcO_Llx17Kh5wVklqRJAlh5_ygj8haUAIFXpr095BPjr4Nbx29lWk6mW5KvLpHCv84mMAvO7ZhYmOzbha22Jh2izLIUGgiTOwmGM_QKFVyd10Mv5W806_UKyaeWRndS64_1m7l0lZlqtixshV_RW82pvyN9ApZpBZIxiw7zorC19tDqRhXJ3szMmINMqaHRJLdM4HwYI5biOHkg4vYoWCvgCJ-JMmq7uzgPeRAt3CQ0jGltnRiKag5NgT01lXcILVPz8XN3m4OdqBBJVGhVyuoLeJCL2rE5HYG8VL5CSvKCbpmz7lWnegD20NA_ks4PF3qTbiZVt3aB5O5hVOTo-TD9V-zsVtlQkzx9zfrI9cLbWAUQWk0s5o_gbHqmQb1Nzwr9iC3Bi02sGZ2LM247TwfrVnQKCYIsWcbEtV9urXAWG9MouVeFXrM4pWxeVSvf_xTUsyZAoo675JCv7eqdWp8_BSVTbwIMtZ_y3k

Simpson, T. R., Li, F., Montalvo-Ortiz, W., Sepulveda, M. A., Bergerhoff, K., Arce, F., Roddie, C., Henry, J. Y., Yagita, H., Wolchok, J. D., Peggs, K. S., Ravetch, J. V., Allison, J. P., & Quezada, S. A. (2013). Fc-dependent depletion of tumor-infiltrating regulatory T cells co-defines the efficacy of anti-CTLA-4 therapy against melanoma. *J Exp Med*, *210*(9), 1695-1710. https://www.ncbi.nlm.nih.gov/pubmed/23897981https://www.ncbi.nlm.nih.gov/pmc/articles/PMC3754863/pdf/JEM_20130579.pdf https://www.ncbi.nlm.nih.gov/pmc/articles/PMC3754863/pdf/JEM_20130579.pdf

Sitnikova, S. I., Munnings-Tomes, S., Galvani, E., Kentner, S., Mulgrew, K., Rands, C., Espana Agusti, J., Zhang, T., Ilieva, K. M., Rosignoli, G., Ghadially, H., Robinson, M. J., Slidel, T., Wilkinson, R. W., & Dovedi, S. J. (2021). Novel non-terminal tumor sampling procedure using fine needle aspiration supports immuno-oncology biomarker discovery in preclinical mouse models. *J Immunother Cancer*, *9*(6).

https://www.ncbi.nlm.nih.gov/pubmed/34145033https://www.ncbi.nlm.nih.gov/pmc/articles/PMC8215240/pdf/jitc-2021-002894.pdf

Tumeh, P. C., Harview, C. L., Yearley, J. H., Shintaku, I. P., Taylor, E. J., Robert, L., Chmielowski, B., Spasic, M., Henry, G., Ciobanu, V., West, A. N., Carmona, M., Kivork, C., Seja, E., Cherry, G., Gutierrez, A. J., Grogan, T. R., Mateus, C., Tomasic, G., . . . Ribas, A. (2014). PD-1 blockade induces responses by inhibiting adaptive immune resistance. *Nature*, *515*(7528), 568-571. https://www.ncbi.nlm.nih.gov/pubmed/25428505https://escholarship.org/content/qt7jm3422h/qt7jm3422h.pdf?t=qaeugo
https://www.ncbi.nlm.nih.gov/pmc/articles/PMC4246418/pdf/nihms634668.pdf

Uruga, H., & Mino-Kenudson, M. (2021). Predictive biomarkers for response to immune checkpoint inhibitors in lung cancer: PD-L1 and beyond. *Virchows Arch*, *478*(1), 31-44. https://www.ncbi.nlm.nih.gov/pubmed/33486574https://link.springer.com/content/pdf/10.1007/s00428-021-03030-8.pdf
https://link.springer.com/article/10.1007/s00428-021-03030-8

Vetizou, M., Pitt, J. M., Daillere, R., Lepage, P., Waldschmitt, N., Flament, C., Rusakiewicz, S., Routy, B., Roberti, M. P., Duong, C. P., Poirier-Colame, V., Roux, A., Becharef, S., Formenti, S., Golden, E., Cording, S., Eberl, G., Schlitzer, A., Ginhoux, F., . . . Zitvogel, L. (2015). Anticancer immunotherapy by CTLA-4 blockade relies on the gut microbiota. *Science*, *350*(6264), 1079-1084. https://www.ncbi.nlm.nih.gov/pubmed/26541610
https://www.ncbi.nlm.nih.gov/pmc/articles/PMC4721659/pdf/nihms751616.pdf

Walker, L. S., & Sansom, D. M. (2011). The emerging role of CTLA4 as a cell-extrinsic regulator of T cell responses. *Nat Rev Immunol*, *11*(12), 852-863. https://www.ncbi.nlm.nih.gov/pubmed/22116087https://www.nature.com/articles/nri3108https://www.nature.com/articles/nri3108.pdf
https://www.nature.com/articles/nri3108

Wei, S. C., Anang, N. A. S., Sharma, R., Andrews, M. C., Reuben, A., Levine, J. H., Cogdill, A. P., Mancuso, J. J., Wargo, J. A., Pe'er, D., & Allison, J. P. (2019). Combination anti-CTLA-4 plus anti-PD-1 checkpoint blockade utilizes cellular mechanisms partially distinct from monotherapies. *Proc Natl Acad Sci U S A*, *116*(45), 22699-22709. https://doi.org/10.1073/pnas.1821218116

Wei, S. C., Levine, J. H., Cogdill, A. P., Zhao, Y., Anang, N. A. S., Andrews, M. C., Sharma, P., Wang, J., Wargo, J. A., Pe'er, D., & Allison, J. P. (2017). Distinct Cellular Mechanisms Underlie Anti-CTLA-4 and Anti-PD-1 Checkpoint Blockade. *Cell*, *170*(6), 1120-1133 e1117. https://www.ncbi.nlm.nih.gov/pubmed/28803728https://www.cell.com/cell/pdf/S0092-8674(17)30831-0.pdf
https://www.cell.com/cell/pdf/S0092-8674(17)30831-0.pdf

Wherry, E. J., & Kurachi, M. (2015). Molecular and cellular insights into T cell exhaustion. *Nat Rev Immunol*, *15*(8), 486-499.

https://www.ncbi.nlm.nih.gov/pubmed/26205583https://www.nature.com/articles/nri3862.pdf
https://www.ncbi.nlm.nih.gov/pmc/articles/PMC4889009/pdf/nihms-787381.pdf

Yost, K. E., Satpathy, A. T., Wells, D. K., Qi, Y., Wang, C., Kageyama, R., McNamara, K. L., Granja, J. M., Sarin, K. Y., Brown, R. A., Gupta, R. K., Curtis, C., Bucktrout, S. L., Davis, M. M., Chang, A. L. S., & Chang, H. Y. (2019). Clonal replacement of tumor-specific T cells following PD-1 blockade. *Nat Med*, *25*(8), 1251-1259. https://www.ncbi.nlm.nih.gov/pubmed/31359002https://www.nature.com/articles/s41591-019-0522-3.pdf
https://www.ncbi.nlm.nih.gov/pmc/articles/PMC6689255/pdf/nihms-1531727.pdf

Zemek, R. M., Fear, V. S., Forbes, C., de Jong, E., Casey, T. H., Boon, L., Lassmann, T., Bosco, A., Millward, M. J., Nowak, A. K., Lake, R. A., & Lesterhuis, W. J. (2020). Bilateral murine tumor models for characterizing the response to immune checkpoint blockade. *Nat Protoc*, *15*(5), 1628-1648.
https://www.ncbi.nlm.nih.gov/pubmed/32238953https://www.nature.com/articles/s41596-020-0299-3.pdf
https://www.nature.com/articles/s41596-020-0299-3

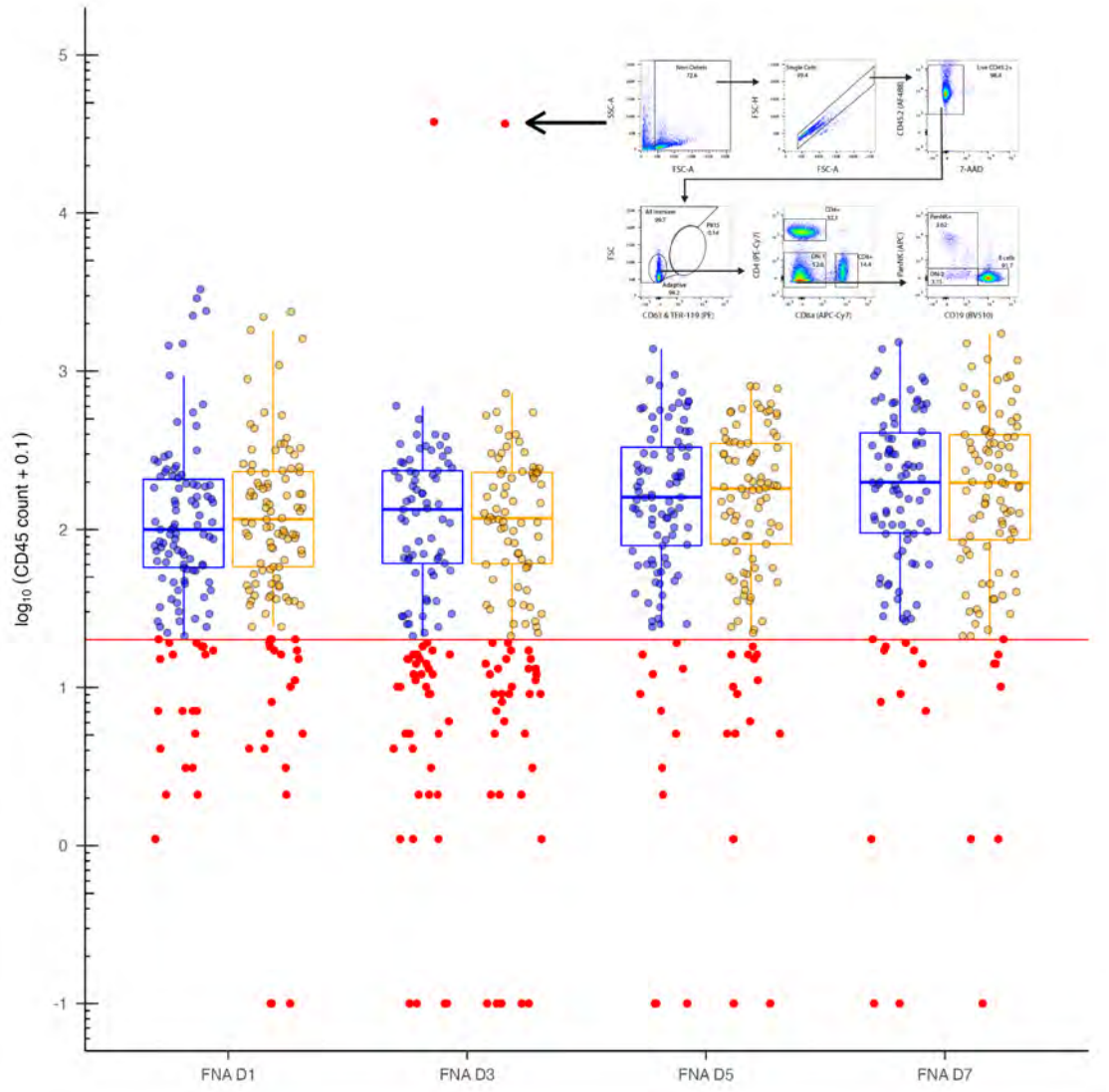


Figure 3.1: Quality control to assess which FNA samples from the P815 model were included in the final analysis. Only FNA samples with greater than 20 events in the "All Immune Cell" gate (Figure 3.6B) were retained to avoid percentage anomalies due to small sample sizes. Above the red threshold line, blue boxplots and dots show sample counts from the Innate Stain while orange boxplots and dots show samples from the adaptive stain. Below the threshold line, all red dots indicate samples that were excluded. One sample collected on FNA D3 presented data consistent with a tumour-draining lymph node and was therefore also removed from the analysis. Thus, a total of 676/839 samples (80.57%) were retained for the final analysis. Each dot indicates the cell count in the relevant stain from an individual FNA sample.

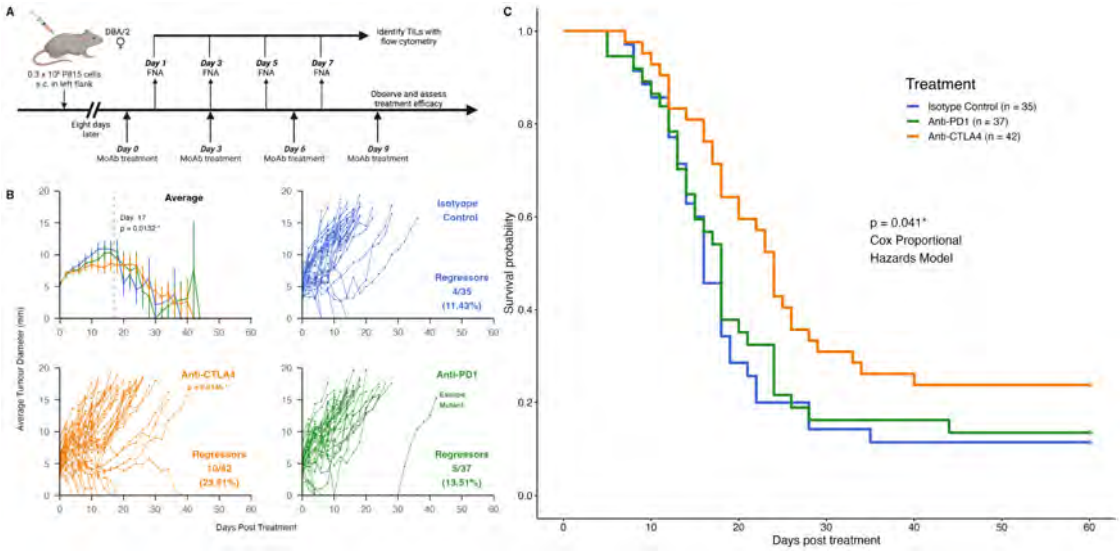


Figure 3.2: Anti-CTLA4 significantly impacts the growth of the P815 mastocytoma tumour model and improves survival. **(A)** The schema used for all experiments is shown. Tumours reached treatable size between six- and 11-days following tumour challenge. Mice were then given two to four injections of 0.2 mg ICB therapy or a cocktail of 0.2 mg each of both relevant isotype control antibodies. FNA samples were collected on days 1, 3, 5, and 7 after the first treatment injection. **(B)** The top left plot compares tumour growth averages between the treatment groups (green – anti-PD1 [n = 37]; orange – anti-CTLA4 [n = 42]; blue – Isotype control [n = 35]). The vertical, dashed red lines indicate treatment days, and the dashed grey line indicates the day to which statistical analysis of tumour growth was assessed. The other plots display the growth curves of individual mice and tumour size averages (black lines and points). Fractions and percentages indicate the number of mice from each treatment group that regressed by 60 days post-treatment. Error bars indicate standard error. **(C)** A Kaplan-Meier curve showing mouse survival. Data combined from six experimental replicates are shown; anti-CTLA4 – treated mice had significantly improved survival compared with the control treatment group. Data for individual experiments are shown in Figure 3.3.

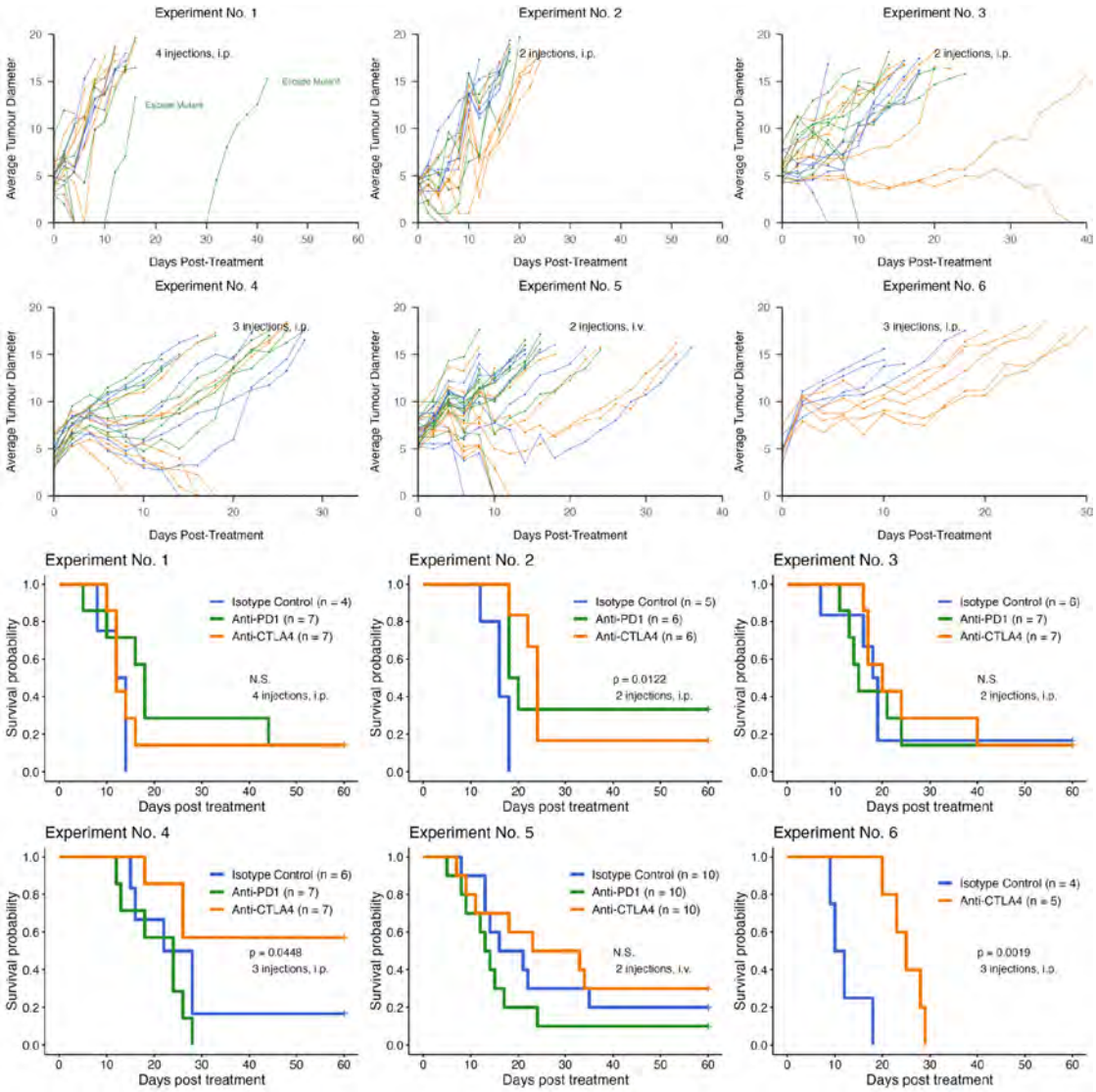


Figure 3.3: Survival and tumour growth data from all six experiments analysed in the P815 study. Experiments 1, 2, and 6 progressed as expected, but experiments 3, 4, and 5 all had spontaneous regressors in mice given isotype control antibodies. To exclude regressors caused by faulty technique, antibodies were administered by i.v. injection (Experiment 5), but regression of two control mice was still observed.

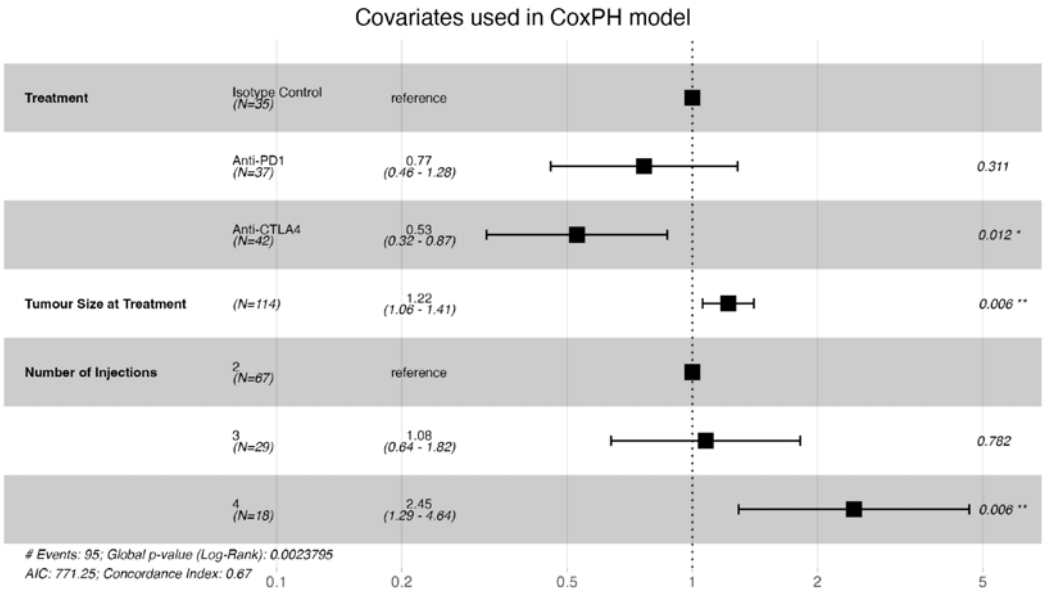


Figure 3.4: Hazard ratios of each covariate in the Cox proportional hazards analysis that determined checkpoint therapy impact on the P815 model. Anti-CTLA4 treatments, tumour size at the time of treatment, and the number of injections had a significant impact on hazard ratios. Anti-CTLA4 therapy improved survival relative to isotype control mice (p = 0.008). Animals with larger tumours tended to have a poorer outcome, though this was to be expected. Mice that received four injections did worse than animals with two or three, though only one experiment of six had animals that received four injections.

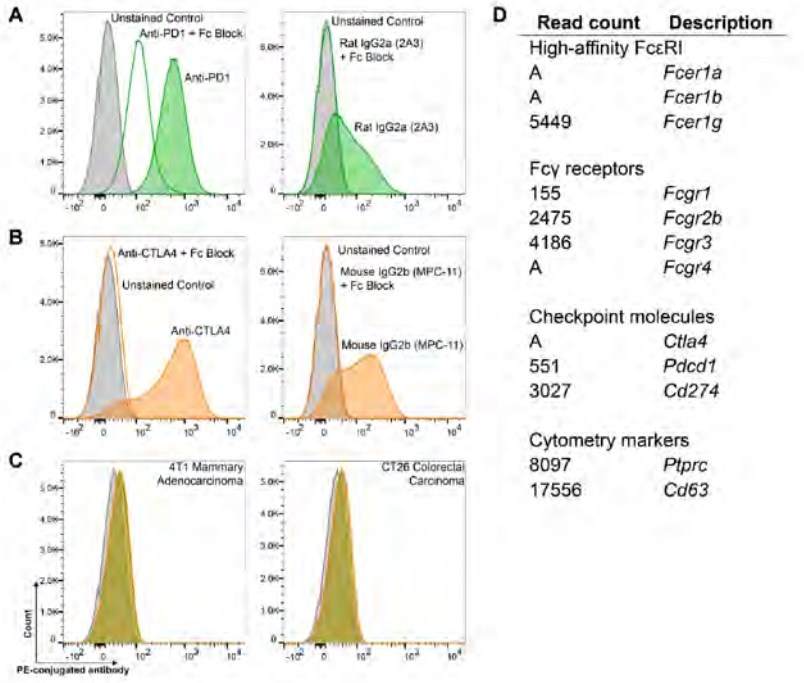


Figure 3.5: All treatment antibodies bind with Fcγ receptors (FcγR) on the surface of P815 mastocytoma cells. Cultured cancer cell lines were stained with treatment or control antibodies conjugated with phycoerythrin (PE), then analysed by flow cytometry. Staining was done with and without Fc-block to determine if Fcγ receptors mediated antibody binding. **(A)** The binding of anti-PD1 (RMP1-14; left) and its relevant isotype control (Rat IgG2a [2A3]; right) to P815 mastocytoma cells is shown, both in the presence (green outline, no fill) and absence (green outline and fill) of Fc-block. **(B)** Similarly, the binding of anti-CTLA4 (9D9; left) and its relevant isotype control (Mouse IgG2b [MPC-11]; right) to P815 mastocytoma cells is shown, both in the presence (orange outline, no fill) and absence (orange outline and fill) of Fc-block. **(C)** Anti-PD1 and anti-CTLA4 antibodies have no binding affinity to cultured 4T1 mammary adenocarcinoma cells (left) or CT26 colorectal carcinoma cells (right). Representative data from 2 replicate experiments are shown. **(D)** RNAseq data was downloaded from the NCBI GEO database and analysed to determine expression levels for high-affinity FcϵRI, Fcγ receptors, checkpoint molecules, and select cytometry markers. A, absent

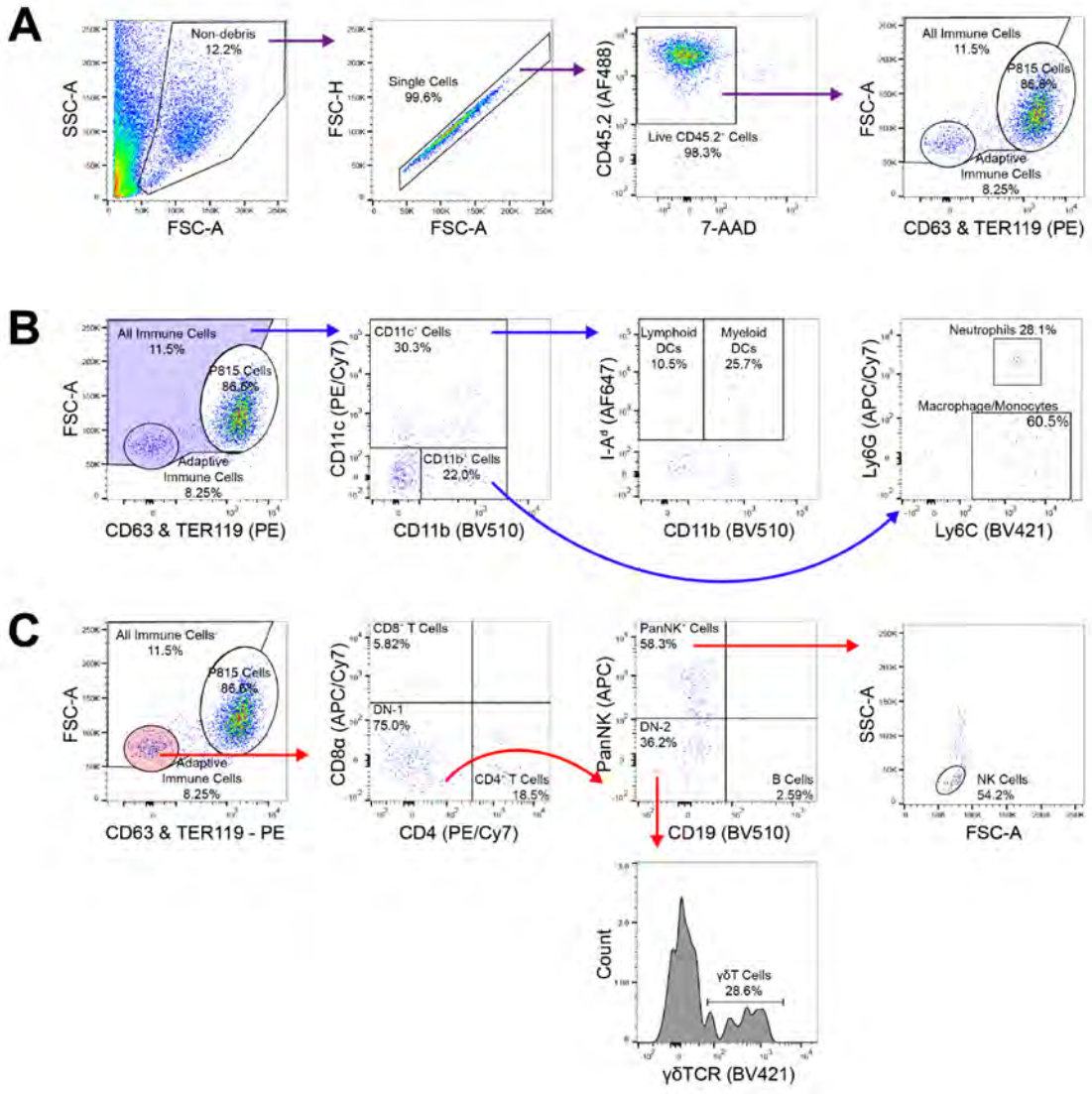


Figure 3.6: Gating strategy for characterising tumour-infiltrating leukocyte (TIL) populations. Digested fine-needle aspirate (FNA) samples were distributed between two staining cocktails, one designed to identify innate immune cells and the other to identify adaptive immune cells, each with its own gating strategies. **(A)** The initial gates are the same for both stains and were designed to isolate single living immune cells and exclude cellular debris, dead cells, P815 tumour cells, and red blood cells. **(B)** The innate stain gating strategy proceeds from a gate surrounding all non-P815 immune cells, which were sorted into either CD11c$^+$ or CD11b$^+$ CD11cgates. Cells in the CD11c$^+$ gate were then further identified as either lymphoid (CD11b$^-$) or myeloid (CD11b$^+$) dendritic cells by the expression of MHC-II (I-A[d]). The cells in the CD11b$^+$ CD11c$^-$ gate were further resolved as either neutrophils (Ly6C$^+$ Ly6G$^+$) or macrophage/monocytes (Ly6C$^+$ Ly6G$^-$). **(C)** The gating strategy used to identify adaptive immune cells started with an explicit adaptive immune cell gate (FSC^{lo} CD63$^-$), made to limit autofluorescence from granular innate immune cells. CD4$^+$ and CD8$^+$ T cells are identified first, with the double negative population then further identified as PanNK$^+$ cells or B cells. NK cells were identified within the PanNK$^+$ gate based on size and granularity to avoid double-counting this population between the adaptive and innate stains. Cells that were negative to the other adaptive markers were gated for $\gamma\delta$ T cells.

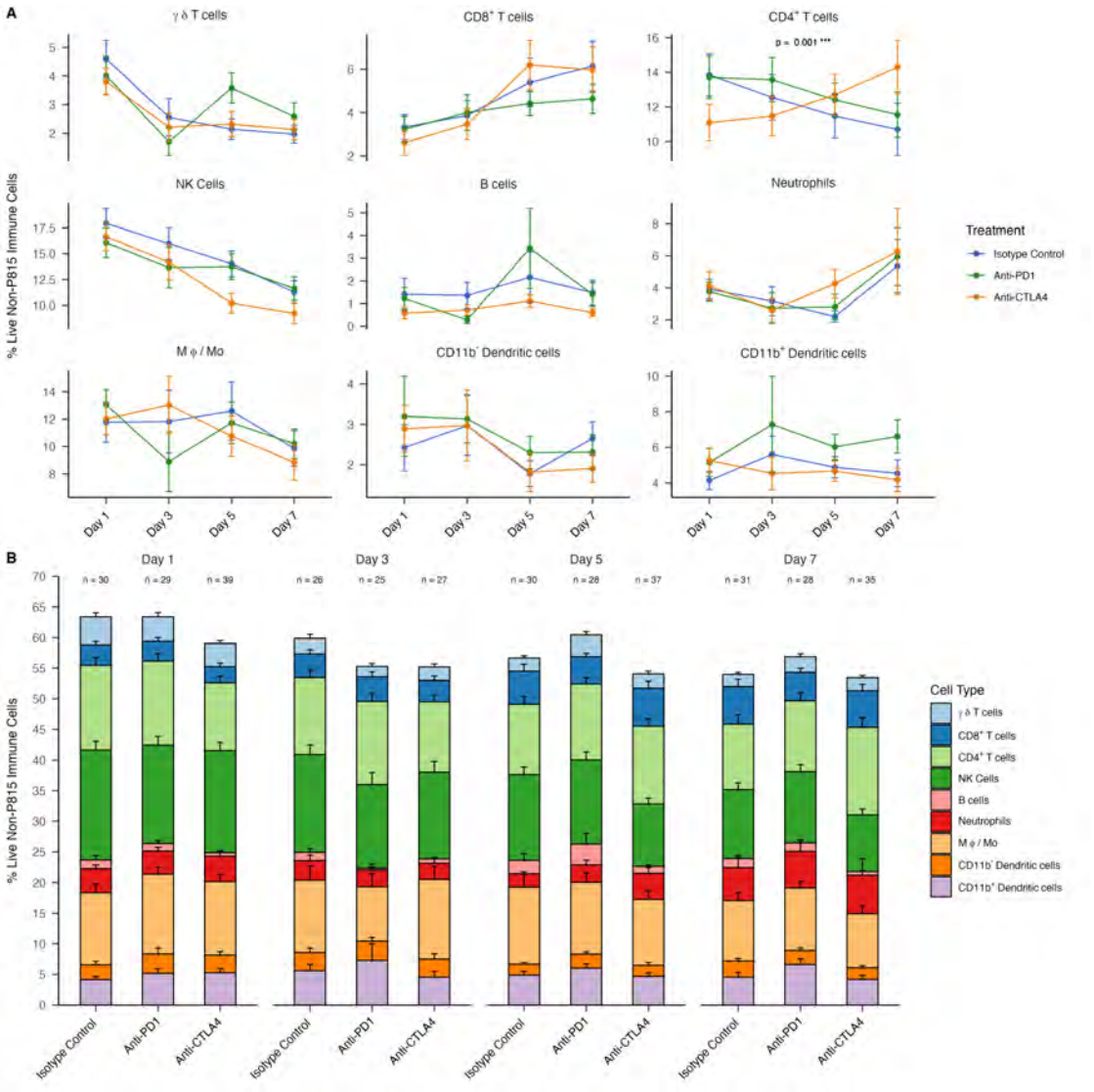


Figure 3.7: FNA sampling shows no significant differences in TIL profiles among treatment groups. **(A)** FNA samples were collected on days 1, 3, 5 and 7 after the first treatment. These samples were analysed by flow cytometry using the gating strategy described in Figure 3.6 to quantify nine different TIL populations across the innate and adaptive arms of immunity. Each cell type was analysed with a linear mixed-effects model and evaluated for significance with a Type II ANOVA. Only CD4+ T Cells were statistically significant, with anti-CTLA4 – treated mice showing increased numbers, while anti-PD1 and control-treated mice showing decreased numbers. **(B)** The summary of the data shown in **(A)** is presented as a stacked bar graph to better display context for TIL proportions. The sample number noted above each bar varies between days due to either tumour regression, mouse attrition, or sample quality control. All error bars indicate standard error. Data from 6 experimental replicates are shown.

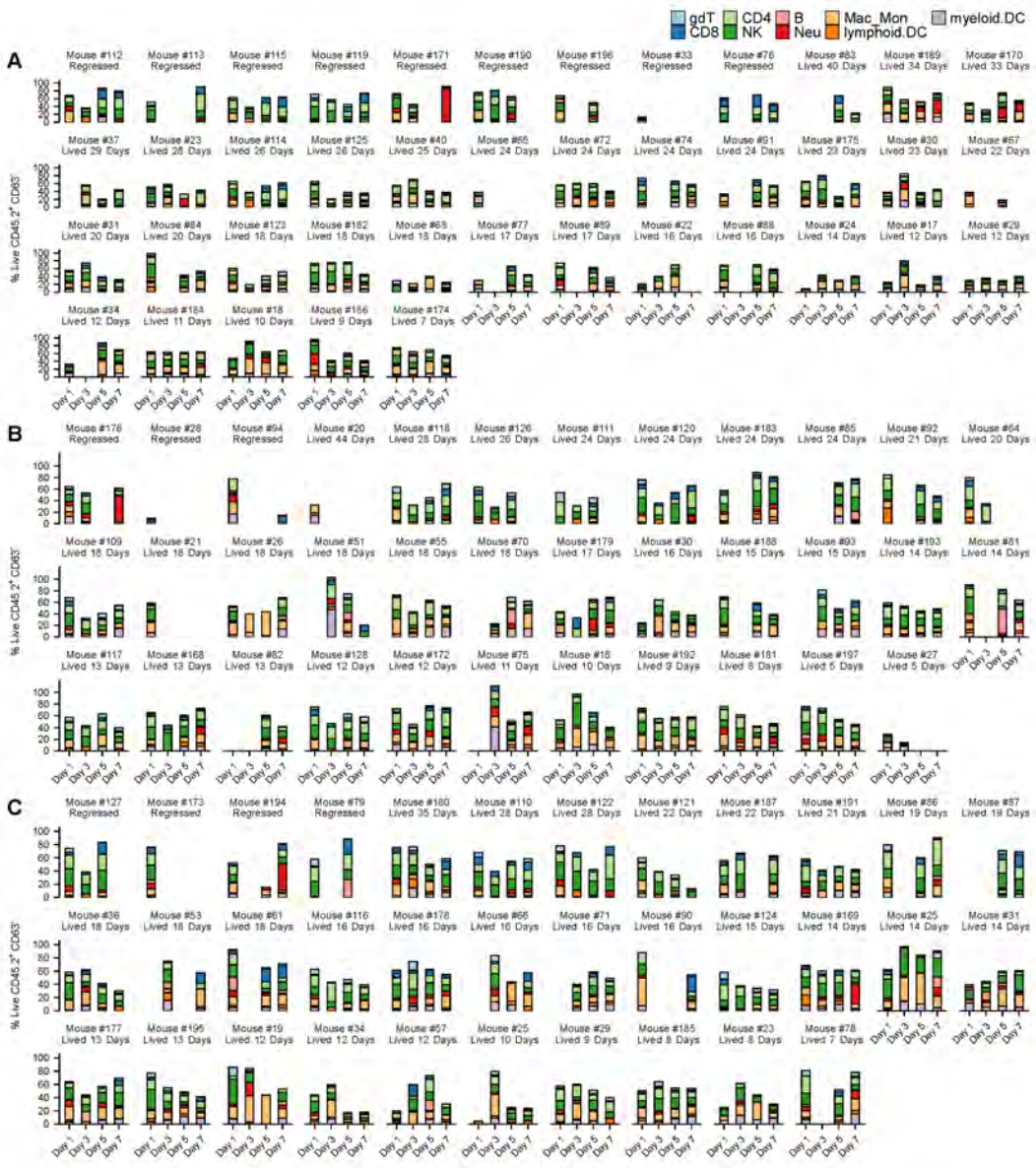


Figure 3.8: FNA data from all P815-challenged mice treated with immune checkpoint therapy. Stacked bar plots are arranged and colour-coded as in Figure 3.7. Mice treated with **(A)** anti-CTLA4, **(B)** anti-PD1, and **(C)** isotype control antibodies are arranged from longest living to shortest living following treatment, indicating either the number of days post-treatment for which they lived or if they completely regressed. Some mice may have whole days of data missing because FNA sampling did not provide the adequate number of cells required for accurate analysis. One regressor mouse (Mouse 171) had near complete neutrophil infiltration on Day 7, is highlighted in the legend of Figure 3.9, and further discussed in the chapter text.

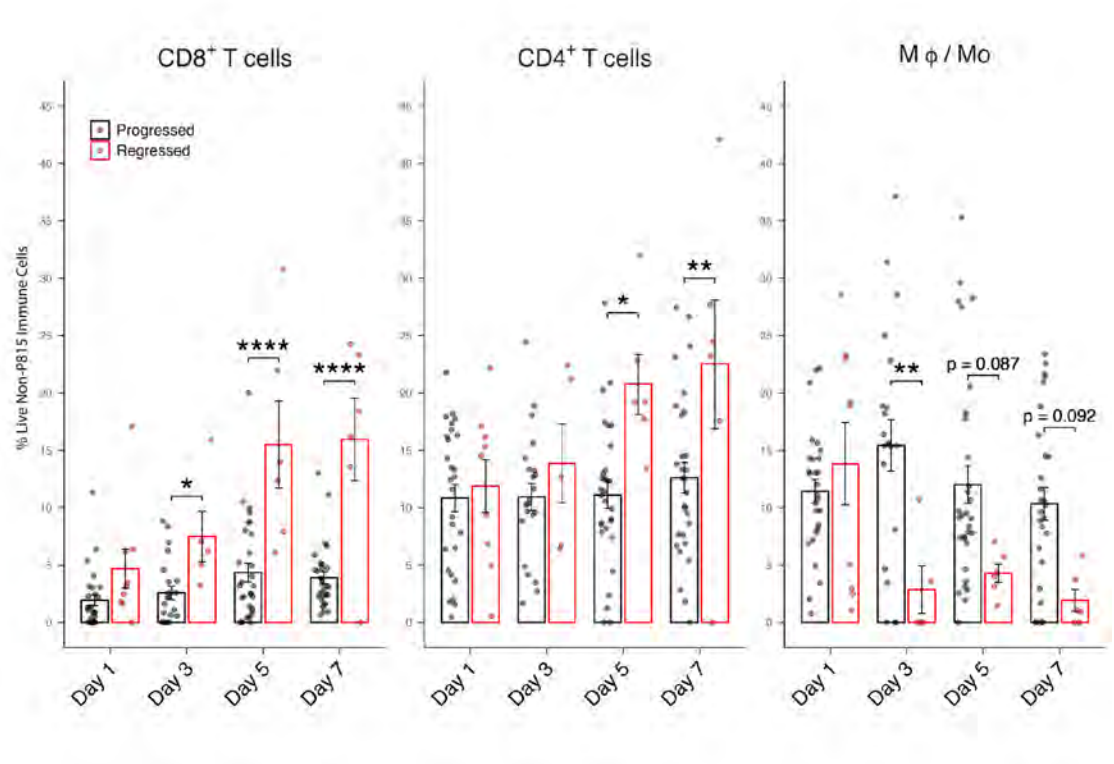


Figure 3.9: CD4+ T cell, CD8+ T cell, and Macrophage/Monocyte proportions in anti-CTLA4–treated mice are different between responder and non-responder mice. FNA sampling allows retrospective analysis and comparison of mice that responded to anti-CTLA4 treatment against those that did not. Responders are characterised by a significantly higher proportion of CD8+ T cells at days 3, 5, and 7, higher CD4+ T cells at days 5 and 7, and lower macrophages/monocytes on day 3 after treatment. The one regressor mouse showing no CD4+ or CD8+ T cell infiltrates at day 7 is mouse 171, which instead showed a high neutrophil infiltrate (Figure 3.8A). Error bars indicate standard error. Data from 6 experimental replicates are shown. Each cell type was analysed with a linear mixed-effects model and evaluated for significance with a Type II ANOVA. *, $p \leq 0.05$; ****, $p \leq 0.0001$

4

Identifying a Useful Tumour Model for Future Cancer Immunotherapy Experiments

Contents

4.1 Introduction 93
4.2 MCA-205 Fibrosarcoma Model 96
4.3 B16.F10 Melanoma Model 97
4.4 MC38 Colon Adenocarcinoma 101
4.5 4T1 Mammary Carcinoma 107
4.6 CT26.WT Colon Carcinoma 112
4.7 Discussion 119

4.1 Introduction

As highlighted in Chapter 1, the presence of a healthy and diverse gut microbiome significantly impacts the effectiveness of immune checkpoint inhibitor therapies in both mice and humans (Davar et al., 2021; Hakozaki et al., 2020; Matson et al., 2018; Rizvi et al., 2021). We have proposed that checkpoint therapy-induced colitis may lead to gut microbial translocation and subsequent colonization of distant solid tumours (Almonte et al., 2021). There, they could enhance the immune response in a manner like our

intratumoral complete Freund's adjuvant (CFA) therapy (C. S. E. Carroll et al., 2021), which will be discussed later in this dissertation.

A suitable mouse tumour model is needed to investigate our gut translocation hypothesis, and it should have three key characteristics:

i) The tumour should not be too aggressive, meaning mice should not die before the treatment can take effect, thus allowing for useful data to be obtained.

ii) The tumour should be responsive to one or more immune checkpoint inhibitor therapies.

iii) The tumour should be suitable for fine-needle aspirate (FNA) sampling, i.e., the procedure should not significantly impact survival outcomes.

Six different tumour models (summarised in Table 4.1) were evaluated throughout my PhD project to determine which would be most suitable for investigating the validity of our hypothesis. The B16.F10 melanoma, MCA-205 fibrosarcoma, and MC38 colorectal cancer models were selected due to their frequent occurrence in published checkpoint inhibitor therapy research (Arce Vargas et al., 2018; Du et al., 2018; Mager et al., 2020; Routy et al., 2018; Sade-Feldman et al., 2018). The CT26 colorectal cancer, 4T1 mammary carcinoma, and P815 mastocytoma models were chosen because our laboratory has extensive experience using these models for CFA and FNA studies (Andrews et al., 2021; C. Carroll, 2016; C. S. E. Carroll et al., 2015, 2021).

Table 4.1: Tumour models evaluated for use in future gut microbiome experiments

Tumour Model	Mouse Strain	Cells Injected (x 10^6)	Site of Injection	Number of Experiments	Checkpoint Therapies[a]	FNAs Collected	Comments
MCA-205 Fibrosarcoma	C57BL/6	0.8	Heterotopic left flank	2	Anti-CTLA4 and anti-PD1 dual therapy[c]	No FNAs	High incidence of ulceration; no regressors
B16.F10 Melanoma	C57BL/6	0.2	Orthotopic left flank	1	Anti-CTLA4 or anti-PD1 monotherapies	Days 1, 3, 5, and 7	No response to therapy
MC38 Colorectal Cancer[d]	C57BL/6	0.5	Heterotopic left flank	1	Anti-CTLA4 monotherapy	No FNAs	One mouse regressed; some ulceration observed
4T1 Mammary Carcinoma	BALB/c	0.5	Orthotopic mammary fat pad	2	Anti-CTLA4 or anti-PD1 monotherapies	Days 1, 2, 3, 4, 5, 6, and 7[e]	No response to therapy; neutrophilia and splenomegaly observed
CT26 Colorectal Cancer	BALB/c	0.5	Heterotopic left flank	2	Anti-CTLA4 or anti-PD1 monotherapies	Days 4 and 11	Responsive to anti-CTLA4, not to anti-PD1; responders had higher $CD8^+$ T cells, lower Mϕ/Mo
P815 Mastocytoma	DBA/2	0.3	Orthotopic left flank	6	Anti-CTLA4 or anti-PD1 monotherapies	Days 1, 3, 5, and 7	Responsive to anti-CTLA4, not to anti-PD1; responders had higher $CD8^+$ and $CD4^+$ T cells, lower Mϕ/Mo; results submitted for publication

[a] Checkpoint therapies were administered as intraperitoneal or intravenous injections, with one injection given every three days. The anti-CTLA4 (9D9), anti-PD1 (RMP1-14), and anti-PDL1 (10F.9G2) were paired with their corresponding isotype control antibodies; mouse IgG2b, κ (MPC-11), anti-trinitrophenol (2A3), and anti-keyhole limpet hemocyanin (LTF-2), respectively. In experiments where monotherapies were given, control-treated mice received all relevant isotype control antibodies. Mice were measured every 2–3 days with digital callipers following treatment.
[b] FNAs were collected on the indicated days post-treatment (i.e., days post-first treatment injection) unless otherwise noted.
[c] Treatments for the MCA-205 model were a combination of 0.1 mg anti-CTLA4 and 0.25 mg anti-PD1.
[d] The experiment evaluating the MC38 model was conducted at the Stanford University School of Medicine. Mice received four injections of 0.1 mg anti-CTLA4.
[e] In experiment 1, FNAs were collected on days 1, 3, 5, and 7 post-treatment, while in experiment 2 they were collected on days 2, 4, and 6 post-treatment
Mϕ, Macrophage; Mo, Monocyte

The literature has consistently demonstrated that the *composition*, and not just the presence, of a healthy gut microbiome significantly impacts the outcome of immune checkpoint therapies. This finding suggests that mice from different institutions, which can be obtained from different suppliers and have different protocols for mouse husbandry (environment, chow, etc.), may have different responses to the same therapy. Indeed, this has already been demonstrated by observing disparate responses to checkpoint therapy among mice from different vendors (Sivan et al., 2015). Therefore, a necessary first step is determining if mice in our laboratory challenged with these tumour models were responsive to immune checkpoint therapies in our hands.

Experiments evaluating the P815 model were presented in the previous chapter. That work was submitted for publication in the *Journal of Immunology* and is currently undergoing revision. This chapter will describe the experiments we conducted to evaluate

the other five tumour models, starting with (for our purposes) what I judged as the least useful model and ending with the most useful one.

4.2 MCA-205 Fibrosarcoma Model

The MCA-205 fibrosarcoma is a weakly immunogenic 3-methylcholanthrene-induced cancer cell line syngeneic to C57BL/6 mice. Steven Rosenberg's laboratory first developed it in the late 1980s by injecting mice with 3-methylcholanthrene (a known carcinogen) mixed with sesame oil (Barth et al., 1990; Spiess et al., 1987). This model has since been used in well over 100 published studies (as of this writing, a PubMed search for "MCA-205" OR "MCA205" produced 127 results).

This dissertation aimed to investigate the gut microbiome's impact on checkpoint therapies, and the literature suggests that the MCA-205 tumour model would be a suitable model for our experiments. For example, Prof Laurence Zitvogel's laboratory has published extensively about the effects of gut bacteria on cancer therapies and used the MCA-205 model in many of their published works (Andrew, 2020; Daillere et al., 2016; Fluckiger et al., 2020; Routy et al., 2018; Vetizou et al., 2015; Viaud et al., 2013). Furthermore, the model is reportedly very responsive to immune checkpoint therapies (Arce Vargas et al., 2018; Redmond et al., 2014; Routy et al., 2018; Vetizou et al., 2015), despite the supplier stating that it is poorly immunogenic.

However, we trialled this model at an unfortunate time. When we began our experiments, the ANU Animal Experimentation Ethics Committee (AEEC) had just decided to institute a new standing policy stating that any mouse with an ulcerated tumour must be euthanised within 48 hours of first finding the ulcer. As will soon be made clear, this policy severely affected the quality of the data we could obtain using the MCA-205 model, along with other tumour models in later experiments.

As shown in Figure 4.1A and described in Table 4.1, we challenged six- and 11-week-old female C57BL/6 mice with MCA-205 cells. Once tumours reached a treatable size of 4-5 mm, the animals were distributed into treatment groups by tumour size. Care was taken to ensure that treatment groups were evenly distributed among the cages to account

for potential cage and litter effects in the analysis. They then received anti-CTLA4 and anti-PD1 dual therapy, while control mice received equal amounts of relevant non-specific isotype control antibodies (mouse IgG2b, κ [MPC-11] and anti-trinitrophenol [2A3]). Ethical endpoints were defined as tumours reaching ethical size limit of 15 mm or if the animals became ill.

As shown in Figure 4.1B, tumour growth was significantly impacted by immune checkpoint therapy, though none of the animals regressed following treatment. However, these results may be a case of the animals not being allowed to live long enough to assess treatment effectiveness adequately. Between the two experiments performed and the 23 mice used, 19 (82.61%) developed an ulcerated tumour (Figure 4.1C). Thus, we were required by the AEEC to euthanise the majority of experimental animals. Any mouse euthanised because they developed an ulcerated tumour needed to be censored from our survival analysis (Figure 4.1D), which had the unfortunate consequence of preventing any meaningful statistical analysis from being performed. As a result, we found the MCA-205 model to have limited use for future experiments.

4.3 B16.F10 Melanoma Model

The B16.F10 melanoma model is a highly metastatic variant of the original B16 melanoma cell line (Winkelhake & Nicolson, 1976) that has been used or mentioned in over 2,000 publications indexed on PubMed. Researchers have had some success treating the B16.F10 model with anti-CTLA4 and anti-PD1 therapies in mice. For example, James P. Allison found significantly increased survival in mice challenged with B16.F10 and treated with anti-CTLA4 (Holmgaard et al., 2013). Matson *et al.* (2018) found significantly impacted tumour growth in mice given four injections of anti-PDL1 (10F.9G2) after being challenged with the B16.F10.SIY model, which are B16.F10 cells engineered to present the H2-K[b] – restricted antigen SIYRYYGL (Kline et al., 2012). Other studies have found significantly improved survival in B16.F10-challenged mice following immune checkpoint therapy treatments, including one that recently investigated the contribution of gut bacteria to treatment efficacy (Griffin et al., 2021; Triplett et al., 2018).

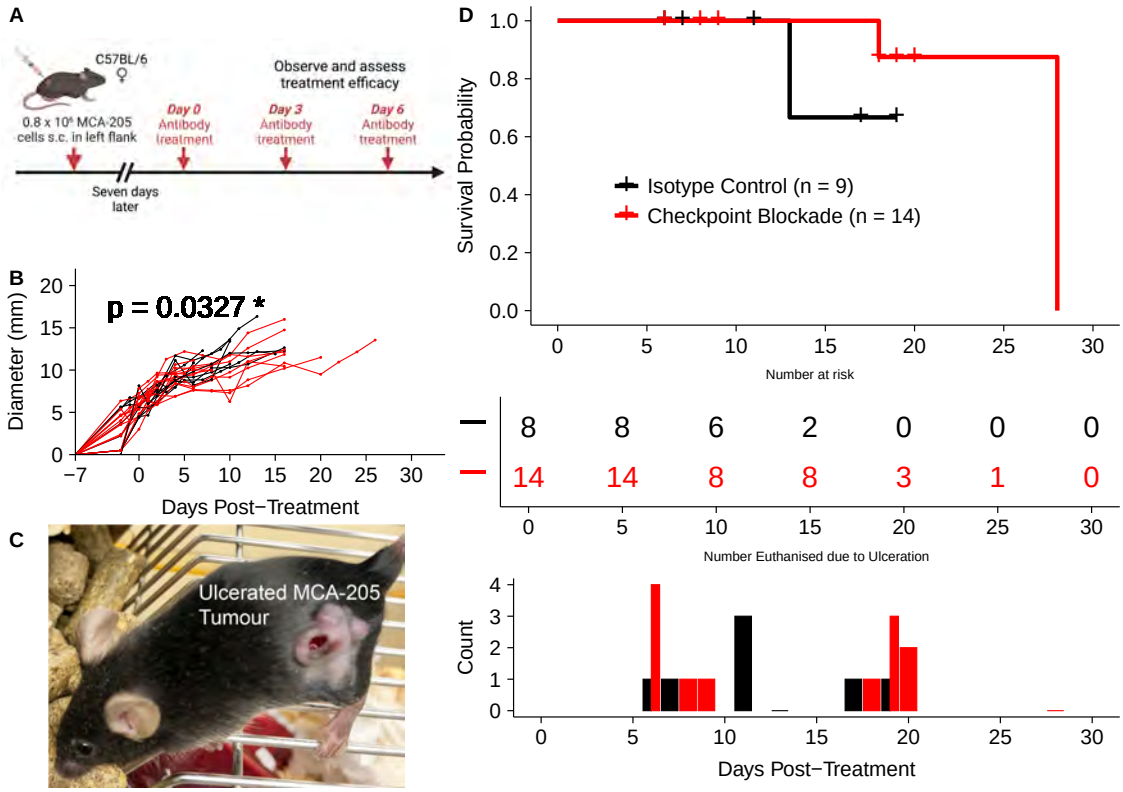


Figure 4.1: Euthanising due to ulceration severely limited the data that could be obtained from the MCA-205 Fibrosarcoma model. **(A)** Mice were challenged with MCA-205 cells in the left flank and treated seven days later with a checkpoint therapy cocktail containing both anti-CTLA4 (9D9) and anti-PD1 (RMP1-14) or an isotype control cocktail containing both mouse IgG2b, κ (MPC-11) or anti-trinitrophenol (2A3). Animals were given three i.p. injections, with one every three days. **(B)** Tumour growth trajectories of each animal evaluated in this experiment. Although combination checkpoint blockade significantly affected MCA-205 growth, no animal experienced complete regression. **(C)** Unfortunately, 82.61% of all MCA-205 – challenged mice developed ulcerated tumours, thus (as required by the AEEC) resulting in their humane euthanising before the planned experimental endpoints. **(D)** The Kaplan-Meier plot is shown, with each vertical dash representing a mouse euthanised because of ulceration. A Cox proportional hazards analysis found no significant difference in survival (p = 1). The risk table indicates the number of animals still being evaluated on each indicated day and the bar plot indicates the number of animals euthanised due to ulceration each indicated day. Data from two independent experiments are presented.

However, not all studies have yielded results showing improved survival when using immune checkpoint therapies in mice challenged with B16 or its variants. For example, van Elsas *et al.* (1999) showed that treating the B16.BL6 model with anti-CTLA4 without GVAX – an irradiated B16 cell line that constitutively secretes GM-CSF (Dranoff et al., 1993) – did not lead to a successful therapeutic response.

Regardless, we reasoned that the B16.F10 model would be a helpful tool to explore our gut translocation hypothesis (Almonte et al., 2021), which fundamentally relies on an accidental bacterial infection originating from the gut. A consequence of bacterial infection is the activation of the innate immune response after sensing pathogen-associated molecular patterns (PAMPs), likely through (but not limited to) the toll-like receptors (TLRs). For instance, Sharma *et al.* (2019) found that co-administration of a TLR1/2 dimer agonist with anti-CTLA4 significantly improved survival in mice challenged with B16.F10 melanoma. Moreover, the authors found that GVAX improves the response to anti-CTLA4 by inducing the recruitment of innate immune cells, most of which are macrophages. Indeed, any survival advantage was lost when the treatments were administered individually or if they were given to mice lacking TLR signalling on macrophages. Thus, TLR activation has been found to be a requirement for a successful immune checkpoint therapy response in the B16 model. Additionally, if our theory is correct, then tumour-colonising bacteria should greatly improve the survival of B16-F10—challenged mice treated with immune checkpoint therapy.

We challenged six-week-old C57BL/6 mice with the B16-F10 cell line in the left flank, then treating 13 days later when the tumours came to size (Table 4.1, Figure 4.2A). The mice were then given three intraperitoneal injections of anti-CTLA4, anti-PD1, or a cocktail containing both mouse IgG2b, κ (MPC-11) and anti-trinitrophenol (2A3). As shown in Figures 4.2 B and 4.2C, neither tumour growth nor survival were affected by either checkpoint therapy in our hands. Curiously, a Cox proportional hazards analysis showed survival nearly approaching significance ($p = 0.0572$). However, a closer look at the contribution of each covariate that was included in the model found significant variations in survival among mice housed in different cages (Figure 4.2D). This result reaffirms the need for even distribution of treatment groups among all cages to account

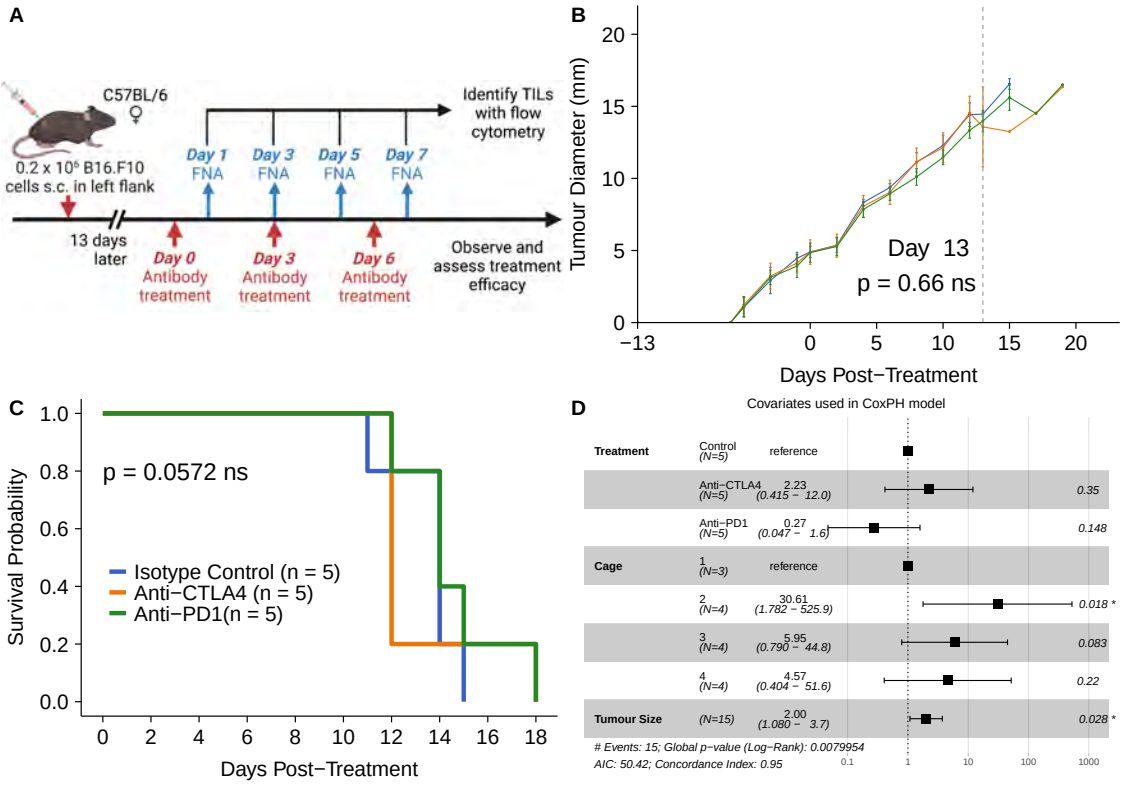


Figure 4.2: Checkpoint therapies had no impact on the B16.F10 melanoma model. (A) Mice were challenged with the B16.F10 melanoma model, then treated 13 days later with either anti-CTLA4 (9D9), anti-PD1 (RMP1-14), or a mixture of MPC-11 or 2A3 (thus, mice given isotype control antibodies received twice the amount of antibodies). Animals were given three intraperitoneal injections, with one every three days. Fine-needle aspirate (FNA) samples were collected on Days 1, 3, 5, and 7 post-treatment, which were digested, stained, and then analysed with flow cytometry. **(B)** Immune checkpoint therapies did not affect the growth trajectories of the B16.F10 tumour model. All animals were euthanised because the tumours reached or exceeded the ethical size limit of 15 mm. Error bars indicate the standard error of the means. **(C)** Kaplan-Meier plot showing the survival probability of mice challenged with the B16.F10 model and given the indicated treatments. **(D)** Forest plot showing the effects of each covariate analysed in the Cox proportional hazards model.

for cage and litter effects. Importantly, the forest plot also confirms that the treatments did not significantly impact survival.

Tumour-infiltrating leukocyte (TILs) were analysed by FNA sampling before the lack of treatment efficacy on the B16.F10 model was known. The procedure was performed as previously described (C. S. E. Carroll et al., 2015), and the gating strategy is shown in Figure 4.3. The tumours bled heavily during sampling (something we did not observed in the other tumour models), but the bleeding stopped soon after pressure was applied. Consequently, all FNA samples from the B16.F10 model had high concentrations of red

blood cells (RBCs). We chose to remove them from the analysis by flow cytometry rather than using a lysis buffer so as not to risk losing any cells from samples that may already have low cell counts.

After first removing poor-quality FNA samples (Figure 4.4), no significant variation in TIL proportions was found among the treatment groups (Figure 4.5). The lymphoid ($CD11b^-$) dendritic cell population was the only one to show a significant change over time between the treatment groups (Figure 4.5A). Further experiments are needed to determine if this is a reproducible result.

Despite being amenable to FNA sampling, the B16.F10 model was too aggressive and, more importantly, not responsive to immune checkpoint therapies. Thus, this model had limited use for future planned experiments.

4.4 MC38 Colon Adenocarcinoma

The MC38 colon adenocarcinoma is an immunogenic cell line used extensively to study immune checkpoint therapies. It was isolated from the colon tumours of C57BL/6 mice that had long-term exposure to the carcinogen 1,2- dimethylhydrazine dihydrochloride (Corbett et al., 1975). Over 900 studies in PubMed since 1986 have used or mentioned this tumour model, including several that have investigated critical unanswered questions regarding immune checkpoint therapies relevant to the aims of this dissertation.

For example, Selby *et al.* (2013) used the model to demonstrate that different isotypes of these checkpoint therapies have different therapeutic efficacies, and that the IgG2a isotype of anti-CTLA4 is most effective as a treatment in mice. Arce Vargas *et al.* (2018) used the MC38 model to demonstrate that Fc effector function is essential for anti-CTLA4 therapy success. Dahan *et al.* (2015) used the model to show that the Fc region also impacted the efficacy of anti-PD1 therapies and that an Fc-null variant of anti-PD1 had increased efficacy in both tumour control and mouse survival. Perhaps most intriguingly, Du *et al.* (2018) used the MC38 model to demonstrate that anti-CTLA4 is therapeutically effective even when its capacity to inhibit CTLA4/B7 interactions is removed, thus questioning our assumptions regarding how immune checkpoint therapies work in the clinic.

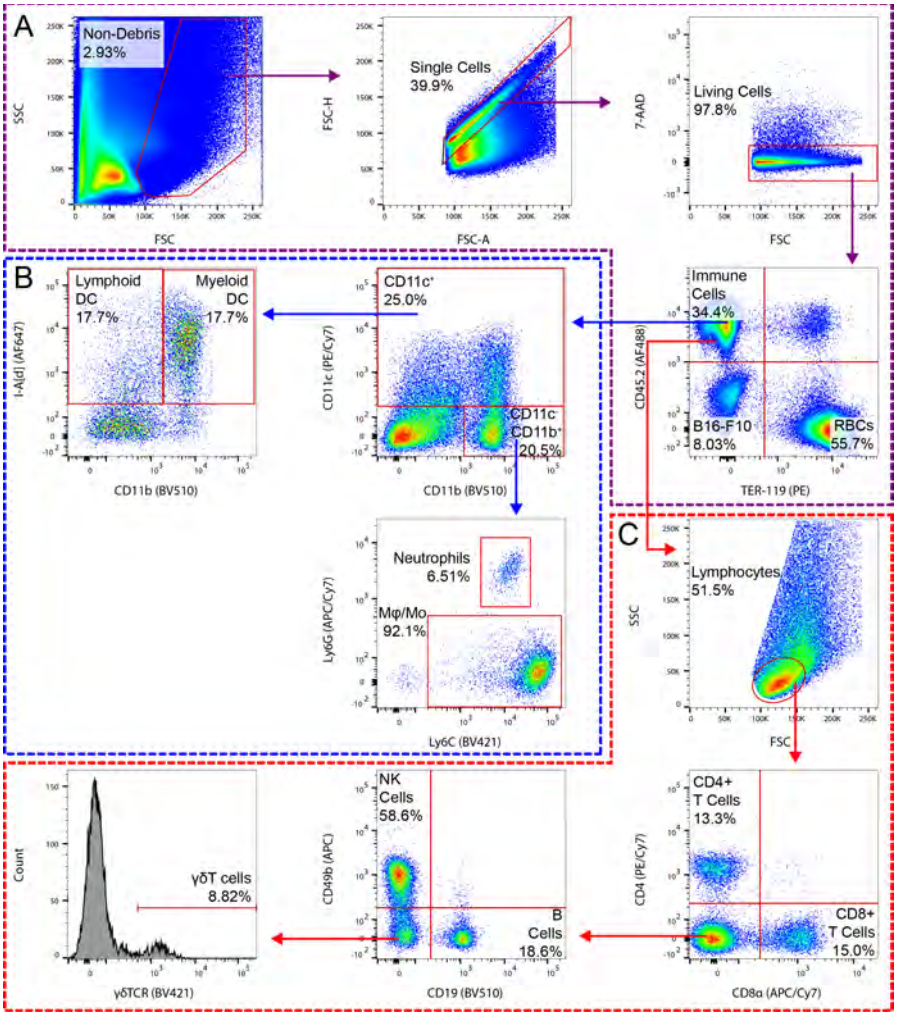


Figure 4.3: The gating strategy used to analyse TILs from the B16.F10 model with flow cytometry. Due to the paucity of cells obtained from each sampling, data from all FNA samples collected in this experiment were concatenated in this plot to facilitate identification of cell populations. Digested FNA samples were distributed between two staining cocktails, one designed to identify innate immune cells and the other to identify adaptive immune cells. **(A)** The initial gates are the same for both stains and were designed to isolate single living immune cells and exclude cellular debris, dead cells, and red blood cells (RBCs). **(B)** The innate stain gating strategy proceeds from living CD45.2$^+$ immune cells sorted into either CD11c$^+$ or CD11b$^+$ CD11c$^-$ gates. Cells in the CD11c$^+$ gate were then further identified as lymphoid (CD11b$^-$) or myeloid (CD11b$^+$) dendritic cells (DC) by expression of MHC-II (I-A[b]). The cells in the CD11b$^+$ CD11c$^-$ gate were further resolved as either neutrophils (Ly6G$^+$ Ly6C$^+$) or macrophages/monocytes (Mϕ/Mo; Ly6G$^-$ Ly6C$^+$). **(C)** The gating strategy used to identify adaptive immune cells started with an explicit lymphocyte gate (FSC^{lo} SSC^{lo}), made to limit autofluorescence from granular innate immune cells. CD4$^+$ and CD8$^+$ T cells were identified first, with the double negative population then further identified as NK cells (CD49b$^+$) or B cells (CD19$^+$). Cells that were negative to the other adaptive markers were gated for $\gamma\delta$ T cells based on $\gamma\delta$TCR expression.

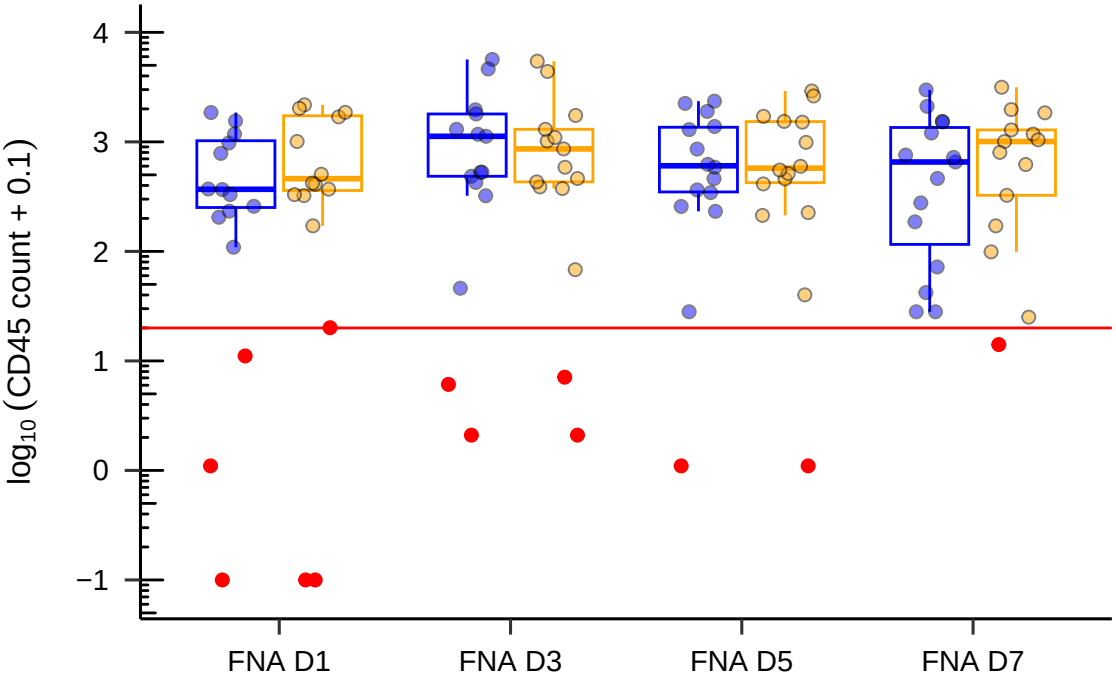


Figure 4.4: Only FNA samples from the B16.F10 model that passed a quality control test were included in the final analysis. Only FNA samples with greater than 20 events in the live CD45.2⁺ gate were retained to minimise potential misrepresentation in the final analysis. Above the horizontal red threshold line, blue box plots and dots show sample counts from the Innate stain, while the orange box plots and dots show sample counts from the Adaptive stain.All red dots below the threshold line indicate FNA samples that were excluded from the analysis. Thus, of the 120 samples collected, 107 (89.17%) were retained for the final analysis. Each dot indicates the cell count in the relevant stain from a unique FNA sample.

The MC38 model has an established place in gut microbiome research as well. Iida *et al.* (2013) used the model to demonstrate that gut microbes modulate the tumour microenvironment following immunotherapy and that depleting the gut with antibiotics severely abrogates immunotherapy efficacy. Tanoue *et al.* (2019) demonstrated that a consortium of gut microbes improved the therapeutic benefit of anti-PD1 and anti-CTLA4 in mice challenged with the MC38 model. Mager *et al.* (2020) observed that animals bearing MC38 tumours had a significantly improved immune response to anti-CTLA4 therapy after being injected with sera from mice that were gavaged with *Bifidobacterium psuedolongum*, and they argue that this result is evidence for the modulation of immune responses with bacterial metabolites. However, the answer to the question of how gut microbes modulate immune responses still needs to be clarified. These studies and others like them (Fenwick et al., 2019; Grasselly et al., 2018; Ngiow et al., 2015; Vetizou

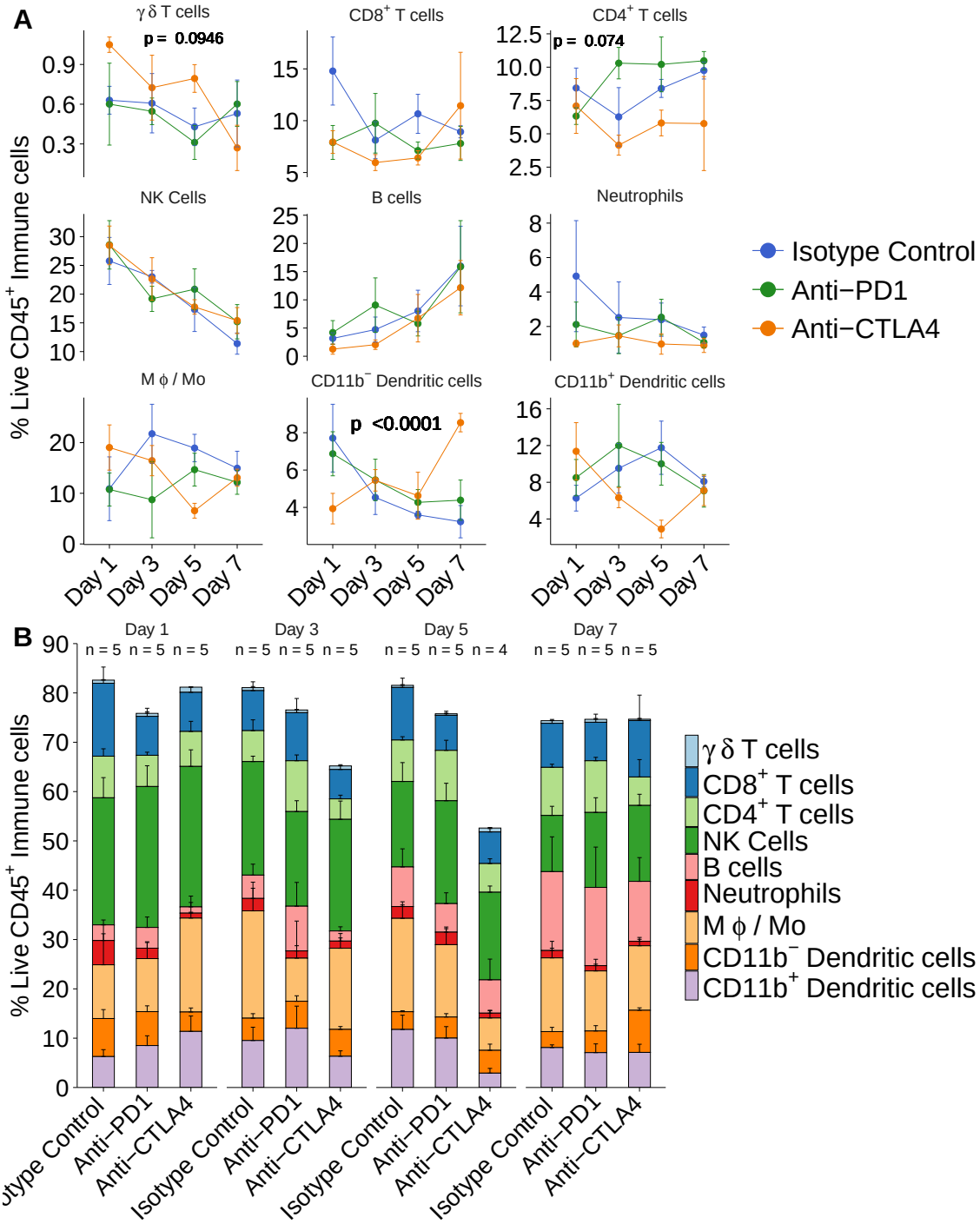


Figure 4.5: FNA sampling from the B16.F10 model showed little variation among the nine cell types identified with flow cytometry. **(A)** Analysis with a liner mixed-effects model found significant changes over time solely in the lymphoid (CD11b^{-}) dendritic cell population. Interestingly, of the tumours analysed with FNA sampling in this dissertation, the B16.F10 model is the only one to show an increase in proportions of tumour-infiltrating B cells. **(B)** The same data shown in A is presented as a stacked bar chart showing each cell types' relative proportion. The numbers above indicate the number of mice sampled on a given day, which may fluctuate due to the exclusion of poor-quality samples (see Figure 4.4). Error bars indicate standard error. Mϕ, Macrophages; Mo, Monocytes

et al., 2015; Zhao et al., 2019) have all successfully used the MC38 model to answer critical questions about immune checkpoint therapies and the gut microbe contribution to treatment efficacy.

To test this model for our purposes, C57BL/6 mice were challenged with MC38 cells (Figure 4.6A, Table 4.1), which reached treatable size 13 days later. They were then given four intraperitoneal injection (one every three days) of anti-CTLA4 or mouse IgG2b, κ as control. Tumours were measured with digital callipers every three days following the first treatment injection. Notably, this experiment was conducted at the Stanford University School of Medicine.

Surprisingly, in our hands neither tumour growth nor survival was significantly impacted by anti-CTLA4 treatment. Only one mouse (1/17, 5.8%) responded to therapy soon after the second treatment injection (Figure 4.6B). Due to ulceration, some animals had to be euthanised by the directive of Stanford University's Administrative Panel for Laboratory Animal Care (APLAC). However, the extent of ulceration was not as problematic as with the MCA-205 model shown in Figure 4.1D. Furthermore, Stanford University's APLAC was far more lenient than the ANU's AEEC regarding what extent of ulceration was deemed ethically acceptable as mice were not required to be euthanised within 48 hours of first noticing an ulcer.

Two main factors could have contributed to the MC38 model's poor response to anti-CTLA4 in this study. As mentioned earlier, mice from different institutions may respond differently to the same therapy because of different protocols regarding mouse husbandry. The mice at Stanford, for example, were fed different chow from the mice at the ANU, thus implying a different gut microbiota composition. Another factor may be that the anti-CTLA4 antibody used in this experiment may have been suboptimal. The 9D9 clone is an IgG2b antibody, whereas it has been established in the literature that the IgG2a isotype is more effective at treating the MC38 model (Selby et al., 2013). All experiments presented in this dissertation used the 9D9 clone (Table 4.1). Thus, the MC38 model may still be useful for future experiments if a different anti-CTLA4 clone were used, but more validation is be required.

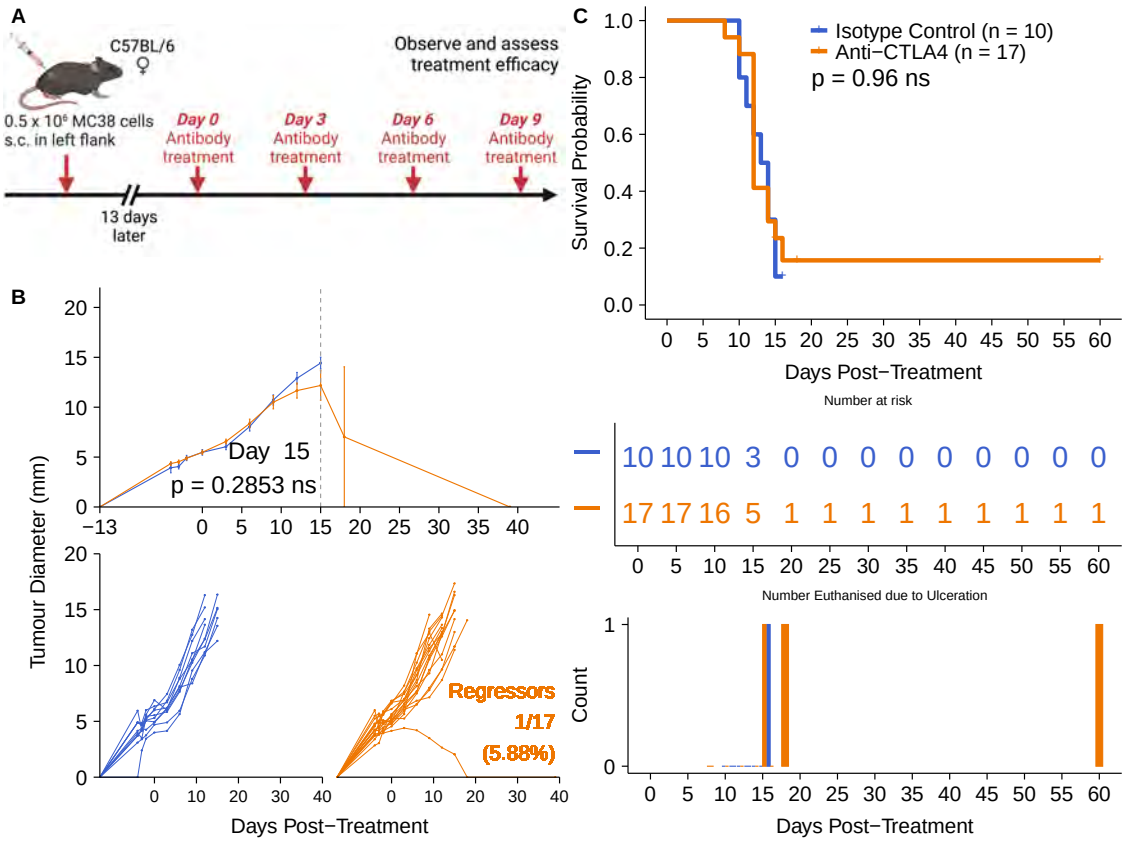


Figure 4.6: Anti-CTLA4 antibody had surprisingly limited effect on mice challenged with MC38 tumours. **(A)** Female C57BL/6 mice were challenged with 0.8 x 10^6 MC38 cells (kindly gifted by Dr Jing Li, Stanford University) in the left flank, then treated 13 days later when they reached 4-5 mm in average diameter. They were given four injections of either 0.1 mg anti-CTLA4 (9D9) or non-specific isotype control antibody (mouse IgG2b [MPC-11]). No FNA sampling was performed in this experiment, which was conducted at the Stanford University School of Medicine. **(B)** The top plot shows the average tumour growth among the treatment groups. Error bars indicate standard error of the means. The bottom plots show the same data for each mouse in this experiment. No significant difference was found between the tumour growth trajectories among the treatment groups. However, one anti-CTLA4–treated mouse did ultimately regress. **(C)** The survival data from the same experiment are shown and is organised in the same fashion as the survival from Figure 4.1D. Three mice (two anti-CTLA4 [11.76%] and one isotype control [10%]) were required to be euthanised due to ulceration. A Cox proportional hazards analysis showed no significant difference between the treatment groups.

4.5 4T1 Mammary Carcinoma

The 4T1 mammary carcinoma model is a metastatic cancer model syngeneic to BALB/c mice. The background, history, and characteristics of this cell line have already been well described by Pulaski and Ostrand-Rosenberg (Pulaski & Ostrand-Rosenberg, 2001). In brief, the model was derived from a spontaneously arising 410.4 tumour in MMTV$^+$ BALB/c mice in the late 1970's (Dexter et al., 1978) and a PubMed search has shown it has been used or mentioned in over 3,600 published studies.

The usefulness of the 4T1 cell line in cancer research lies in the fact that it can be implanted orthotopically into the mammary fat pads and that metastates spontaneously develop, with the progressive spread of disease arising in the lymph nodes, brain, bone, lungs, liver, and blood. Additionally, a clinical situation can be readily simulated by removing the primary tumour and studying the ongoing spread of metastatic disease (Pulaski & Ostrand-Rosenberg, 1998). All of these characteristics make 4T1 a useful representation of stage IV human breast cancer.

The 4T1 model is also associated with a paraneoplastic syndrome in tumour-challenged mice that has been well characterised by the works of Sally DuPre and Kenneth Hunter Jr. (DuPre et al., 2007, 2008; DuPre & Hunter, 2007) and frequently observed in our laboratory's mouse experiments with this model. 4T1 cancer cells constitutively secrete the cytokine granulocyte colony-stimulating factor (G-CSF) *in vivo*, which consequently causes massive granulocytosis, peripheral neutrophilia, bone marrow hyperplasia, and marked splenomegaly, all while leaving lymphocyte counts unchanged (DuPre & Hunter, 2007). Eventually (approximately 17-20 days after tumour challenge), there is an increased expression of PD-L1 within 4T1 tumours due to the presence of an inflammatory reaction and prolonged exposure to IFNγ (DuPre et al., 2008).

There does not appear to be consensus in the literature regarding the effectiveness of immune checkpoint therapies in treating the 4T1 model. Triplett *et al.* (2018) were able to significantly improve the survival of mice that were challenged orthotopically with the 4T1 model and treated with three intraperitoneal injections of anti-CTLA4 (UC10-4F10-11, an Armenian hamster IgG, 10 mg/kg given every three days). In contrast, Demaria *et*

al. (2005) were unable to improve the survival of mice or reduce the number of lung metastases after three intraperitoneal injections of the 9H10 clone of anti-CTLA4 (a Syrian hamster IgG, 0.2 mg given every three days). Kim *et al.* (2014) were able to achieve significantly improved survival, but only after mice were given four injections of anti-CTLA4 (9H10) and anti-PD1 (RMP1-14) dual therapy on days 11, 13, 15, and 17 post-tumour challenge.

Our laboratory has already demonstrated that 4T1-challenged mice treated with an intratumoural injection of CFA therapy have significantly improved survival (C. S. E. Carroll et al., 2021). However, we also found that FNA sampling may significantly decrease the survival probability of 4T1-challenged mice treated with CFA (Andrew, 2020, fig. 3.10, p. 88). Therefore, the impact of FNA sampling on survival needed to be re-evaluated if this model was to be successfully used in experiments designed to achieve the aims of this dissertation.

These experiments had three goals. First, determine if immune checkpoint therapies affected the growth and survival of mice challenged orthotopically with the 4T1 model. Second, determine if FNA sampling impacted the therapeutic outcome of 4T1-challenged mice that have been treated with immune checkpoint therapies. Finally, use FNA sampling to determine if immune checkpoint therapies altered the TIL composition within the tumour microenvironment (TME), which has frequently been observed by our laboratory to be replete with neutrophils.

Six- to seven-week-old mice were challenged orthotopically with 4T1 cells in their mammary fat pads at the ANU (Table 4.1, Figure 4.7A). Tumours reliably reached treatable size eight days later, after which mice were treated with either anti-CTLA4, anti-PDL1, or a combination of mouse IgG2b, κ and anti-keyhole limpet hemocyanin as isotype controls. FNA samples were collected for each day following treatment from half of the mice in each experiment.

Treatment efficacy and any impacts that FNA sampling may have had on treatment outcome were analysed simultaneously. A linear mixed-effects regression (LMER) model assessing tumour growth up to (but not including) day 20 found that treatments had a significant effect on tumour growth trajectories ($p = 0.0474$, Figure 4.7B). The same

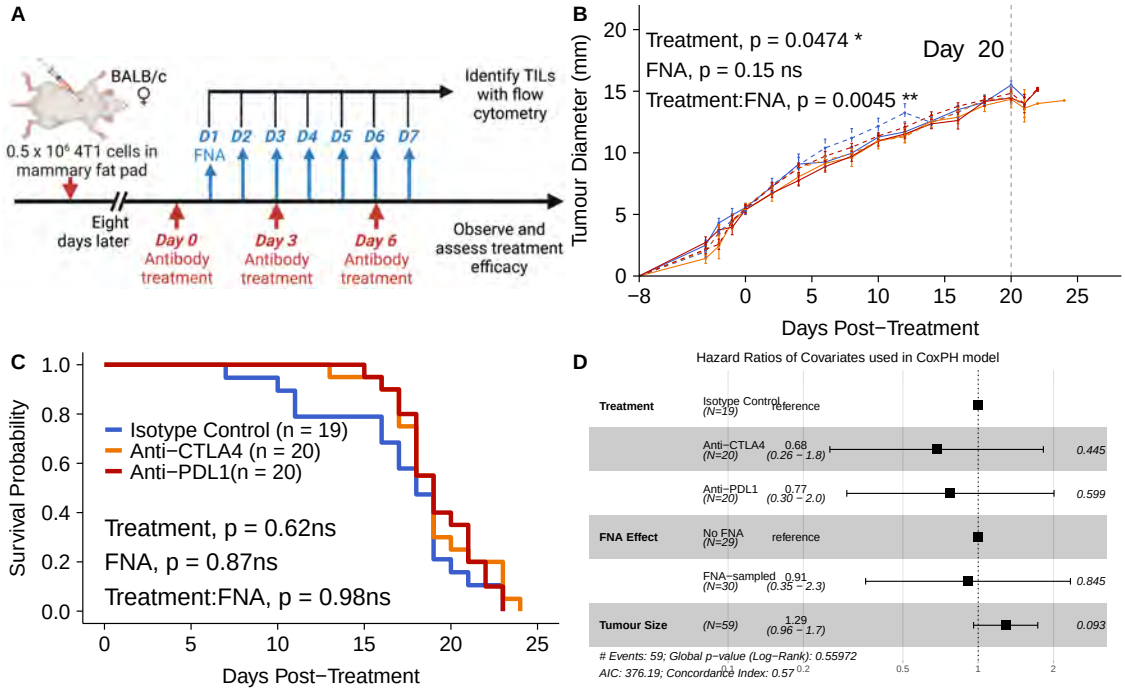


Figure 4.7: Checkpoint therapy and FNA sampling did not impact survival in the 4T1 tumour model. **(A)** Female BALB/c mice were challenged with 4T1 cells in the mammary fat pad, then treated seven days later when they reached 4-5 mm in average diameter. They were given three intraperitoneal injections – one every three days – of either anti-CTLA4 , anti-PDL1, or a combination of mouse IgG2b, κ (MPC-11) and anti-keyhole limpet hemocyanin (LTF-2). FNA samples were collected and assessed with flow cytometry from half the treated mice in the first week following treatment. Mice were assessed for treatment effectiveness and to determine if FNA sampling impacted treatment outcome. **(B)** Tumour treatment, alone and when interacting with FNA sampling, show a significant impact on tumour growth. Dashed lines represent FNA-sampled treatment groups. Error bars represent standard error. **(C)** Kaplan-Meier plot showing the survival probability of mice challenged with the 4T1 model and indicating that neither checkpoint therapies nor FNA sampling impacted survival probability. **(D)** Forest plot showing the effects of the covariates analysed in the Cox proportional hazards model. Importantly, FNA sampling (denoted as the FNA Effect) did not significantly affect survival in the 4T1 model. "Tumour Size" refers to the average diameter of the tumour at the time of treatment. Data from two independent experiments are shown.

statistical model found that, while FNA sampling alone did not impact tumour growth (p = 0.15), there was a highly significant interaction between FNA sampling and treatments received (p = 0.0045). However, as shown in Figures 4.7C and 4.7D, neither treatment, FNA sampling, nor an interaction of the two factors had a significant impact on survival probability.

FNA samples were analysed as described in Section 4.3. The gating strategy is shown in Figure 4.8 and 98.57% of samples passed quality control (Figure 4.9). Immune

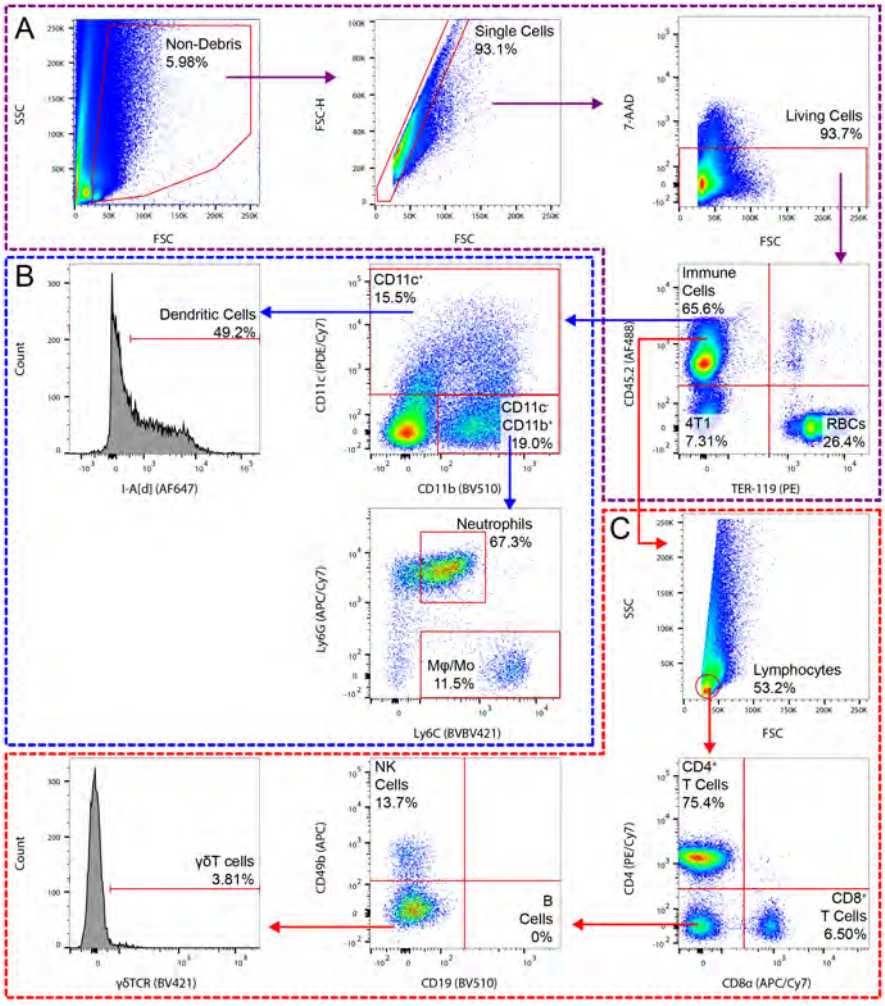


Figure 4.8: The gating strategy used to analyse FNA samples from the 4T1 model with flow cytometry. Due to the paucity of cells obtained from each sampling, data fine-needle aspirate (FNA) samples collected on days 2, 4, and 6 were concatenated in this plot to facilitate identification of cell populations. Digested FNA samples were distributed between two staining cocktails, one designed to identify innate immune cells and the other to identify adaptive immune cells. **(A)** The initial gates are the same for both stains and were designed to isolate single living immune cells and exclude cellular debris, dead cells, and red blood cells (RBCs). **(B)** The innate stain gating strategy proceeds from living CD45.2^{+} immune cells sorted into either CD11c^{+} or CD11b^{+} CD11c^{-} gates. Cells in the CD11c^{+} gate were then further identified as Dendritic Cells by expression of MHC-II (I-A[d]). The cells in the CD11b^{+} CD11c^{-} gate were further resolved as either neutrophils (Ly6G^{+} Ly6C^{+}) or macrophages/monocytes (Mϕ/Mo; Ly6G^{-} Ly6C^{+}). **(C)** The gating strategy used to identify adaptive immune cells started with an explicit lymphocyte gate (FSC^{lo} SSC^{lo}), made to limit autofluorescence from granular innate immune cells. CD4^{+} and CD8^{+} T cells were identified first, with the double negative population then further identified as NK cells (CD49b^{+}) or B cells (CD19^{+}). Cells that were negative to the other adaptive markers were gated for $\gamma\delta$ T cells based on $\gamma\delta$TCR expression.

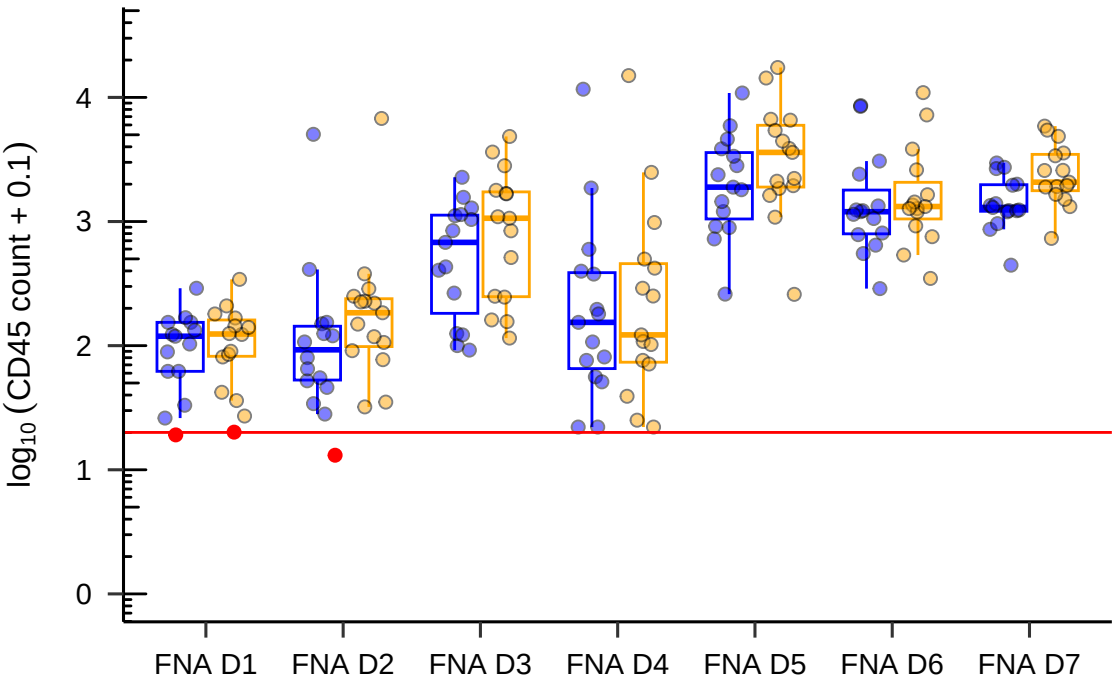


Figure 4.9: Quality control to assess which FNA samples were included in the final analysis. Like with the B16 model, shown in Figure 4.4, only FNA samples with greater than 20 events in the live CD45.2⁺ gate were retained to minimise any potential misrepresentation in the final analysis. Above the horizontal red threshold line, blue boxplots and dots show sample counts from the Innate stain, while the orange boxplots and dots show samples from the adaptive stain. Below the threshold line, all red dots indicate samples that were excluded. Thus, 207/210 samples (98.57%)were retained for the final analysis. Each dot indicates the cell count in the relevant stain from an individual FNA sample.

checkpoint therapies had no impact on the proportions of TILs within the TME (Figure 4.10). We did find the proportion of tumour-infiltrating neutrophils gradually increased in all mice over time, which is consistent with the published literature (DuPre et al., 2007, 2008; DuPre & Hunter, 2007) and our own experience (Andrew, 2020, figs. 3.6, pp.78–79; C. Carroll, 2016, fig. 6.3 and 6.4, pp. 199-202).

These results showed that the 4T1 model was not responsive to intraperitoneal injections of immune checkpoint therapies in our hands, but we have previously reported that it is responsive to intratumoural injections of CFA (C. S. E. Carroll et al., 2021). Furthermore, while tumour growth was impacted by FNA sampling, survival (our main metric for treatment success) was not. Therefore, while it has limited used in gut microbiome studies, this model may still useful for other experiments that fall within the scope of this dissertation.

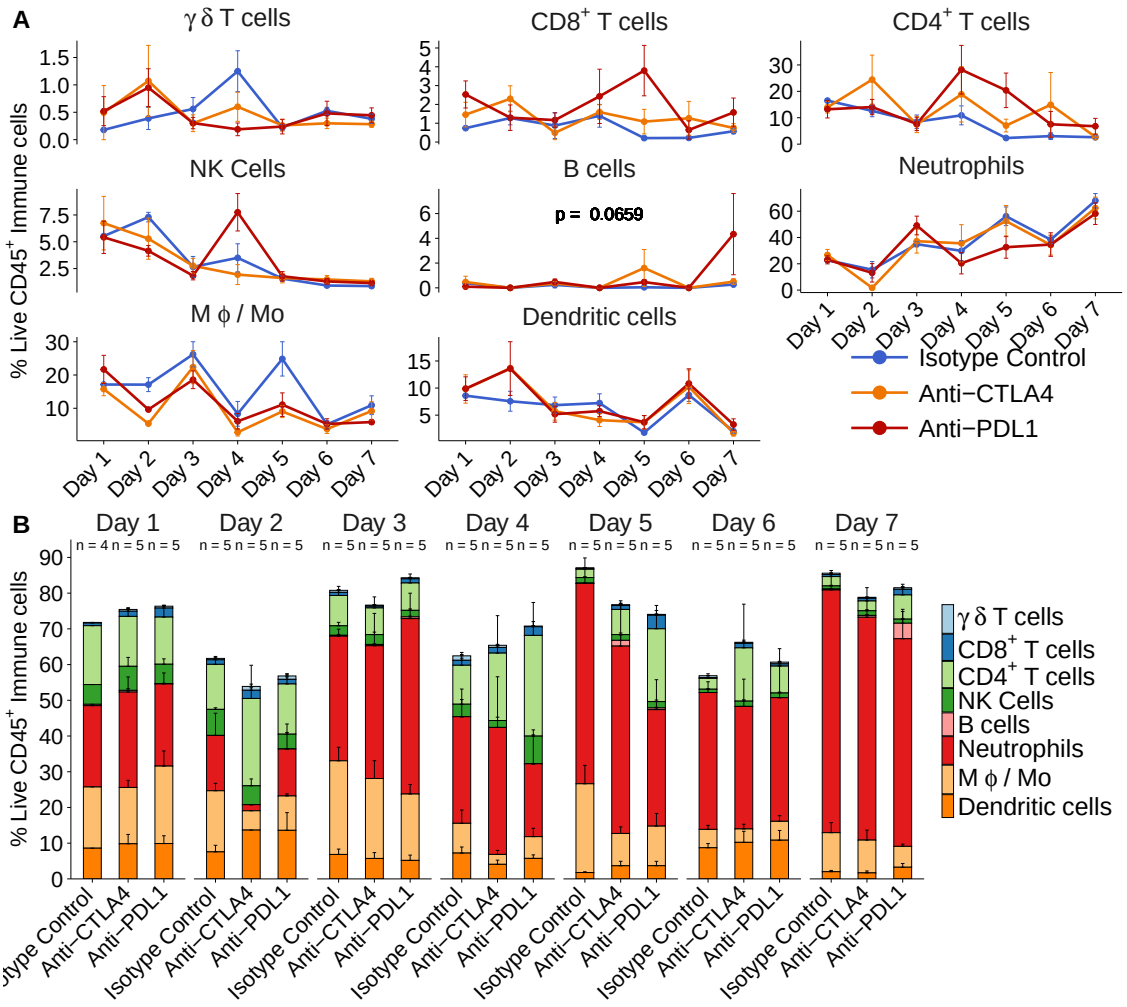


Figure 4.10: All mice challenged with the 4T1 model exhibited paraneoplastic syndrome. **(A)** FNA sampling confirms massive granulocytosis associated with the 4T1 model. Neutrophils (CD45.2+ CD11b+ Ly6C^{int} Ly6G+ cells) continue to increase in proportion throughout the week following treatment among all treatment groups. No cell type shows a significant change in proportion between the treatment groups. The data shown in **(B)** are the same as in (A) but presented as a stacked bar plot, further confirming the large proportion of neutrophils seen in the 4T1 model. Data from two independent experiments are shown. Mϕ, Macrophages; Mo, Monocytes

4.6 CT26.WT Colon Carcinoma

Dr Corbett developed the colon tumour 26 (CT26) model in 1975 by injecting BALB/c mice with N-methyl-N-nitrosourea (Belnap et al., 1979; Corbett et al., 1975). It was later found to be a highly immunogenic model useful for cancer immunology studies (Belnap et al., 1979) that spontaneously metastasises to lymph nodes and lungs (Colmerauer et al., 1980). The original CT26 line was later cloned in a tumour antigen study to

minimise antigenic heterogeneity and was named CT26.WT (M. Wang et al., 1995). This dissertation uses the CT26.WT cell line in all relevant experiments and will herein be referred to as "CT26".

The high immunogenicity of the CT26 model, like the MC38 model, makes it useful for immune checkpoint therapy studies. Again, there appears to be no consensus in the literature about the effectiveness immune checkpoint therapy — specifically PD1 blockade — on this tumour model. For example, both Ngiow *et al.* (2015) and Dyck *et al.* (2016) demonstrated that CT26 was unresponsive to intraperitoneal injections of anti-PD1 therapy. In contrast, Wang *et al.* (2016) showed that five injections of anti-PD1 (0.25 mg per injection) could induce complete or partial regression in 17% of CT26-challenged mice. Hsu *et al.* (2018) found that anti-PD1 significantly improves tumour control and survival in CT26-challenged mice and that the effector function of NK cells plays a critical role in treatment success. All of these studies used the RMP1-14 clone of anti-PD1.

In contrast, other studies have reported that the CT26 tumour model is highly responsive to anti-CTLA4 therapy (Selby et al., 2013; Simpson et al., 2013; Vetizou et al., 2015) and other immunotherapies. For example, Sagiv-Barfi *et al.* (2018) showed that intratumoural injections of both CpG oligodeoxynucleotide and agonistic anti-OX40 antibody effectively treated CT26 tumours and resulted in tumour regression. The specificity of the immune response that develops following administration of this therapy was also demonstrated using the CT26 model; in mice challenged with multiple tumour models, only distal CT26 tumours regressed when the therapy was injected into a subcutaneous CT26 tumour.

Here, BALB/c mice were challenged with C26 cells heterotopically on the left flank (Table 4.1, Figure 4.11A). When the tumours reached 4-5 mm in average diameter, they were treated with either anti-CTLA4, anti-PD1, or a combination of mouse IgG2b, κ and anti-trinitrophenol. We have previously used the CT26 model to evaluate intratumoural CFA therapy effectiveness (C. S. E. Carroll et al., 2021) and demonstrated that FNA sampling does not impact treatment outcomes (Andrew, 2020, fig. 3.10, p. 88). Therefore,

FNA samples were collected from all mice on days 4 and 11 post-treatment to investigate if these therapies have an impact on TIL composition.

As shown in Figure 4.11B and 4.11C, anti-CTLA4 therapy significantly influenced the tumour growth trajectory and survival of CT26-challenged mice. This result agreed well with the published literature (Selby et al., 2013; Vetizou et al., 2015). However, in our hands the CT26 model was not responsive to anti-PD1 therapy. Curiously, one mouse treated with isotype control antibodies spontaneously regressed. This result was also observed when the P815 model was treated with isotype control antibodies and was discussed in more detail in the previous chapter. Despite the animal having regressed, it was found dead approximately 10 weeks later from unknown causes.

The response of CT26-challenged mice to anti-CTLA4 therapy was inconsistent among the treatment group. Two mice showed no response to the therapy and followed a growth pattern similar to the isotype control- and anti-PD1-treated animals. The other mice exhibited initial signs of a response, as their tumours began to shrink, or their tumour growth stalled for some time. Upon completion of the treatment protocol, most tumours relapsed while 3/12 (25%) of the anti-CTLA4-treated mice completely regressed. The Kaplan-Meier plot in Figure 4.11C reflects this observation, showing that the animals had significantly improved survival because they took longer to reach the ethical endpoint of 15 mm average tumour diameter. It is worth noting that all mice challenged with the CT26 model in these experiments were humanely euthanised because they reached this ethical size limit, as none became ill or developed ulcerated tumours.

FNA samples from CT26 tumours were analysed with flow cytometry and TILs were identified using the gating strategy shown in Figure 4.12. Sample quality control found that 97.87% of samples were included in the analysis (Figure 4.13). Eight different TIL populations were identified, and the macrophage/monocyte population was found to be significantly decreased in the isotype control-treated mice relative to the other treatment groups by day 11 post-treatment (Figure 4.14).

However, as explained in the previous chapter, the advantage of the FNA sampling protocol is the ability to compare differences in TIL populations among mice that responded to treatment with those that did not. An adequate number of CT26-challenged

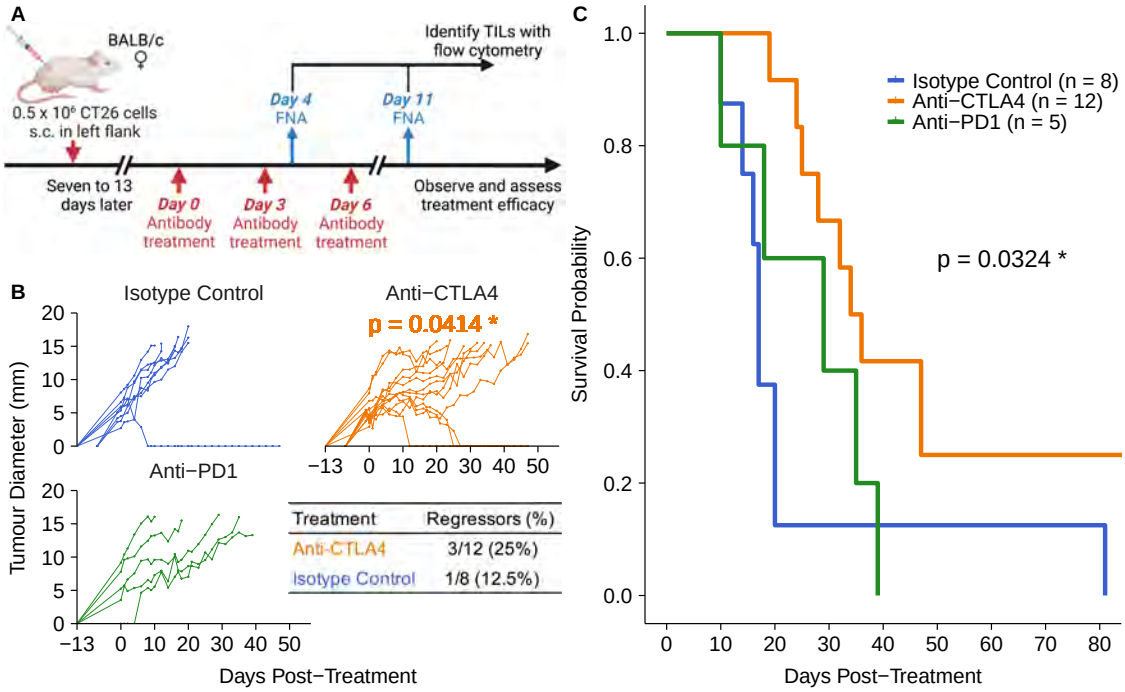


Figure 4.11: The CT26 tumour model responds well to anti-CTLA4 but not anti-PD1. (A) Female BALB/c mice were challenged subcutaneously with 0.5 x 10^6 CT26 cells in the left flank. When the tumours reached 4-5 mm in average diameter, the animals were given three intraperitoneal injections – one every three days – of either anti-CTLA4 (9D9), anti-PD1 (RMP1-14), or a combination of relevant non-specific isotype control antibodies (thus control-treated mice received double the amount of antibody). FNA samples were collected on the 4^{th} and 11^{th} day after treatment, and TILs were identified with flow cytometry. Tumour challenge and treatment, FNA sampling, tumour growth measurements, and gating were all performed by PhD student Mr George Cavic. **(B)** Anti-CTLA4, but not anti-PD1, had a significant effect on the growth trajectory of the CT26 cancer model. Assessing tumour growth with an LMER model from day 0 to day 17 found that anti-CTLA4 promoted tumour regression in 3/12 mice (25%). Interestingly, one isotype control-treated mouse (12.5%) spontaneously regressed. **(C)** Mice treated with anti-CTLA4 had a significant survival advantage. Univariate analyses found treatment to be the only significant factor influencing survival. Further analysis found that anti-CTLA4–treated mice had a significant survival advantage above isotype control-treated mice (p = 0.0249). The isotype control mouse that spontaneously regressed was found dead approximately 10 weeks after treatment.

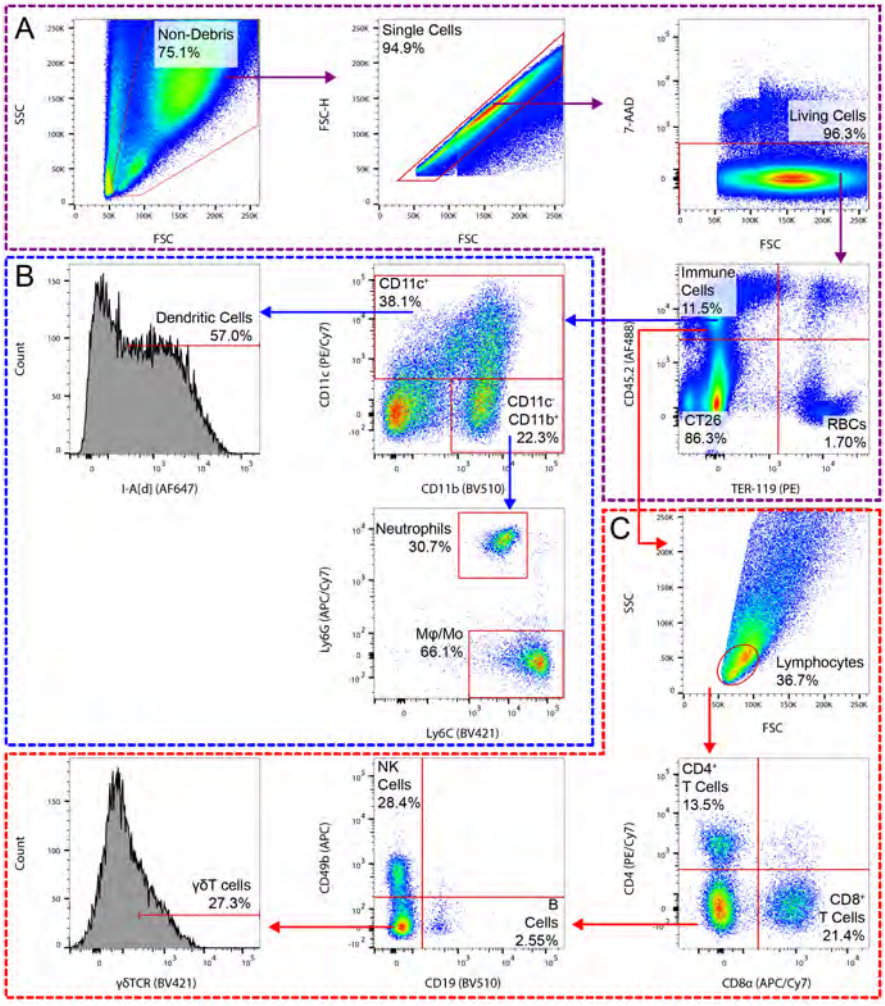


Figure 4.12: The gating strategy used to analyse FNA samples from the CT26 model with flow cytometry. Due to the paucity of cells obtained from each sampling, data fine-needle aspirate (FNA) samples collected from one experiment were concatenated in this plot to facilitate identification of cell populations. Digested FNA samples were distributed between two staining cocktails, one designed to identify innate immune cells and the other to identify adaptive immune cells. **(A)** The initial gates are the same for both stains and were designed to isolate single living immune cells and exclude cellular debris, dead cells, and red blood cells (RBCs). **(B)** The innate stain gating strategy proceeds from living CD45.2$^+$ immune cells sorted into either CD11c$^+$ or CD11b$^+$ CD11c$^-$ gates. Cells in the CD11c$^+$ gate were then further identified as Myeloid (CD11b$^+$) or Lymphoid (CD11b$^-$) Dendritic Cells (DC) by expression of MHC-II (I-A[d]). The cells in the CD11b$^+$ CD11c$^-$ gate were further resolved as either neutrophils (Ly6G$^+$ Ly6C$^+$) or macrophages/monocytes (Mϕ/Mo; Ly6G$^-$ Ly6C$^+$). **(C)** The gating strategy used to identify adaptive immune cells started with an explicit lymphocyte gate (FSC^{lo} SSC^{lo}), made to limit autofluorescence from granular innate immune cells. CD4$^+$ and CD8$^+$ T cells were identified first, with the double negative population then further identified as NK cells (CD49b$^+$) or B cells (CD19$^+$). Cells that were negative to the other adaptive markers were gated for $\gamma\delta$ T cells based on $\gamma\delta$TCR expression.

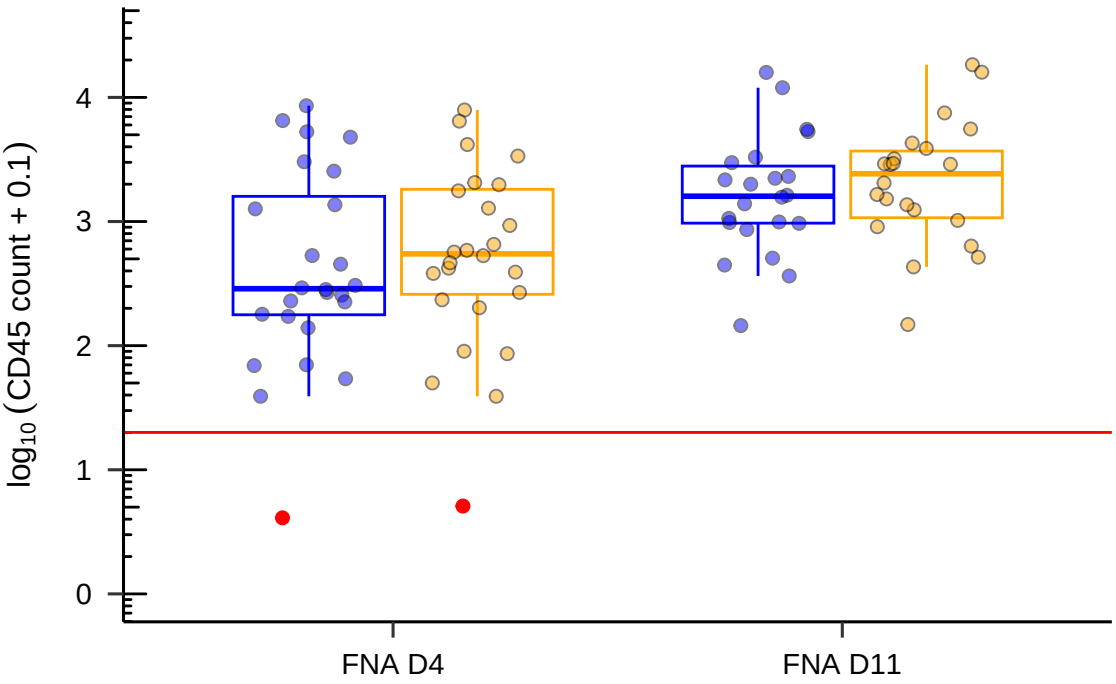


Figure 4.13: Quality control to assess which FNA samples from the CT26 model are to be included in the final analysis. Like the B16 and 4T1 models, shown in Figure 4.4 and Figure 4.9, only FNA samples with greater than 20 events in the live CD45.2⁺ gate were retained to minimise any potential misrepresentation in the final analysis. Above the horizontal red threshold line, blue boxplots and dots show sample counts from the Innate stain, while the orange boxplots and dots show samples from the adaptive stain. Below the threshold line, all red dots indicate samples that were excluded. Thus, 92/ 94 samples (97.87%) were retained for the final analysis. Each dot indicates the cell count in the relevant stain from an individual FNA sample.

mice responded to anti-CTLA4 treatment to allow this analysis, and the results are shown in Figure 4.15. Mice that regressed following anti-CTLA4 therapy developed a significantly higher proportion of tumour-infiltrating CD8⁺ T cells and significantly lower proportions of macrophages/monocytes by the 11ᵗʰ day post-treatment. They also had lower proportions of tumour-associated neutrophils by day 11, though this difference was not significant ($p = 0.09$).

These data show that the CT26 model met all of our prerequisites for a useful tumour model. The tumour did not cause debilitating illness nor was it prone to ulceration — all mice in these experiments were euthanised because the tumours reached the ethical size limit. We also found the CT26 model to be responsive the anti-CTLA4 therapy, but not anti-PD1. Finally, we and others using our methodology (Sitnikova et al., 2021) have established that FNA sampling does not impact survival outcomes following treatment.

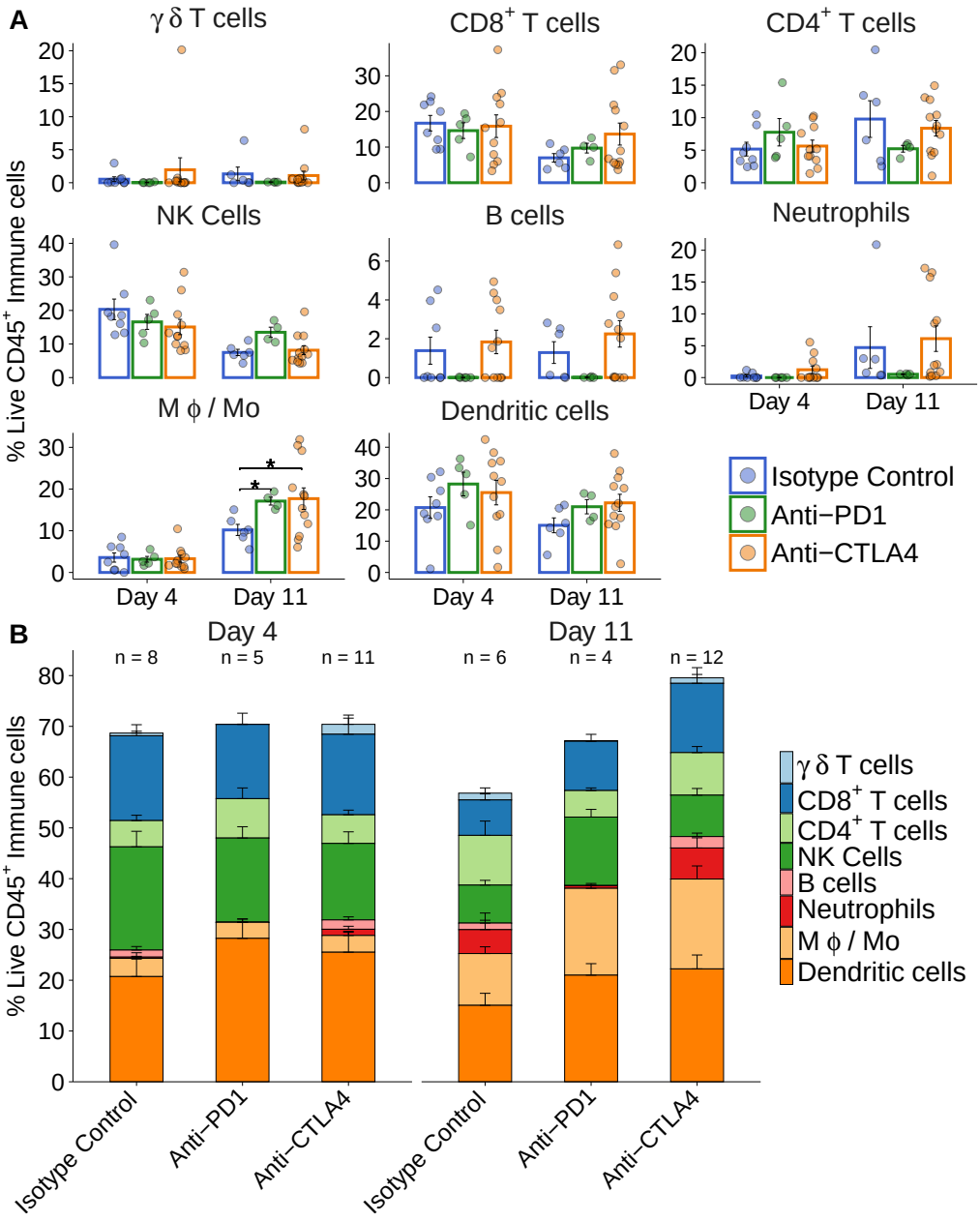


Figure 4.14: Checkpoint therapies increase the macrophage/monocyte population by the eleventh day following treatment. **(A)** FNA samples were collected on days 4 and 11 after the first treatment. These samples were analysed by flow cytometry using the gating strategy described in Figure 4.12 to quantify eight different TIL populations across the innate and adaptive arms of immunity. Each cell type was analysed with a linear mixed-effects model and evaluated for significance with a Type II ANOVA. Only the macrophage/monocyte population was statistically significant, with anti-CTLA4 – and anti-PD1–treated mice showing increased proportions above the control-treated mice by day 11. **(B)** A summary of the same data shown in (A) is presented as a stacked bar graph to display the context for TIL proportions better. The sample number noted above each bar varies between days due to either tumour regression, mouse attrition, or sample quality control. All error bars indicate standard error. Data from 2 experimental replicates are shown. * $p < 0.05$; Mϕ, Macrophages; Mo, Monocytes

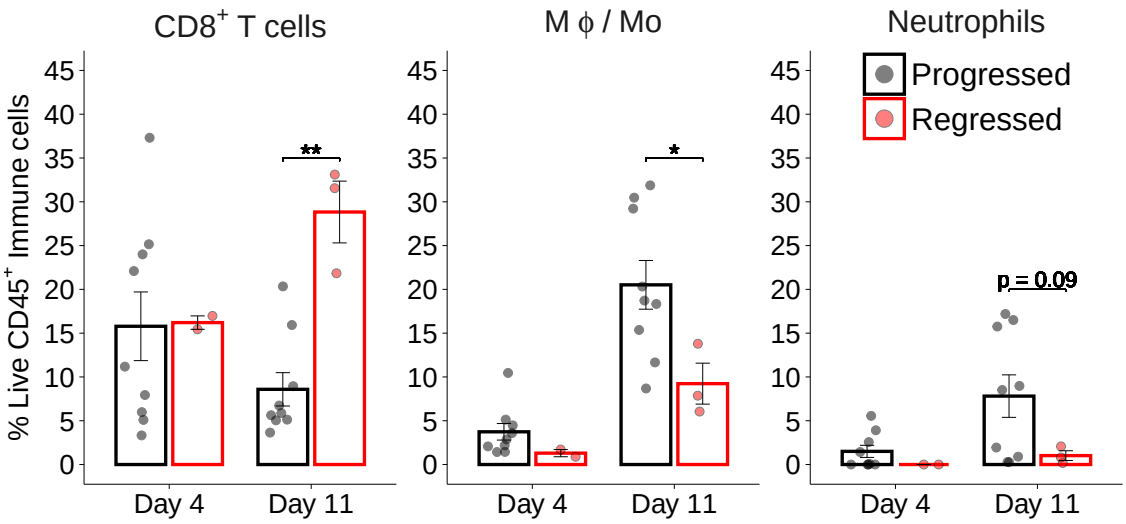


Figure 4.15: Average CD8⁺ T cell, Macrophage/Monocyte, and Neutrophils proportions in anti-CTLA4–treated mice differ between responders and non-responders. FNA sampling allows retrospective analysis and comparison of mice that responded to anti-CTLA4 treatment against those that did not. Responders are characterised by a significantly higher proportion of tumour-infiltrating CD8⁺ T cells at day 11 after treatment. In contrast, non-responding mice had significantly increased numbers of macrophages and monocytes on day 11. Neutrophil proportions were not significantly different but tended to also be higher in non-responding mice by day 11. Error bars indicate standard error. Data from 2 experimental replicates are shown. Each cell type was analysed with a linear mixed-effects model and evaluated for significance with a Type II ANOVA. Mϕ, Macrophages; Mo, Monocytes; *, p <0.05; ** p <0.01

Therefore, the CT26 model is the ideal cell line to use in future gut microbiome studies.

4.7 Discussion

The experiments described in the preceding and current chapters aimed to find a suitable mouse tumour model for investigating our gut translocation hypothesis (Almonte et al., 2021). This work, conducted between two research institutions, aimed to validate six tumour models derived from three different mouse strains. The tumour models, and important details of the experiments used to evaluate them, are summarised in Table 4.1.

The MCA-205 fibrosarcoma model had the potential to be useful for our experiments as tumour growth was significantly impacted by anti-CTLA4 and anti-PD1 dual therapy. However, the experiments that evaluated this model were conducted at an inopportune time. Not long before the studies began, the ANU's AEEC instituted a new standing policy stating that any mouse found with an ulcerated tumour must be humanely eu-

thanised within 48 hours of discovering the ulcer, regardless of its severity. We found the MCA-205 model to be highly prone to ulceration as over 80% of the animals in the study developed ulcerated tumours. These animals were censored from the analysis because they did not die according to our pre-defined parameters (tumour size, moribund, or [in very rare cases] death). Consequently, while tumour growth was significantly impacted, there was no way to determine if the therapy significantly impacted survival (Figure 4.1). Thus, this model was found unsuitable for our purposes.

The lack of a response in the MC38 colorectal cancer model following anti-CTLA4 therapy was surprising given the large number of published studies that successfully used this model (Fenwick et al., 2019; Grasselly et al., 2018; Iida et al., 2013; Mager et al., 2020; Ngiow et al., 2015; Tanoue et al., 2019; Vetizou et al., 2015; Zhao et al., 2019). Though one mouse regressed after treatment, there was no significant impact on tumour growth or survival between the treatment groups after four injections of anti-CTLA4 therapy (Figure 4.6). A possible explanation for this result could be that mice housed at Stanford University have different gut microbial compositions. Studies have repeatedly confirmed that gut microbe composition influences immune checkpoint therapy outcomes (Gopalakrishnan et al., 2018; Tanoue et al., 2019), suggesting that diet and environment have significant roles in treatment success. Indeed, interest in the gut microbiome's role in immune checkpoint therapies began after observing that mice from two different suppliers had disparate treatment outcomes after being treated with the same therapies (Sivan et al., 2015). Regardless, the experiment with the MC38 model needs to be repeated to determine its usefulness for future studies.

Neither the B16.F10 melanoma nor the 4T1 mammary carcinoma models were responsive to immune checkpoint therapies in our hands. This outcome is perhaps not surprising as both models are poorly immunogenic and used to study aggressive, deadly, metastatic cancers. There is no consensus in the literature about the effectiveness of immune checkpoint therapies in these models. For the B16.F10 model, an adjuvant to stimulate innate immune cells, such as GVAX (Curran & Allison, 2009) or FVAX (Curran et al., 2010), appears to be required for immune checkpoint therapeutic success in mice.

The 4T1 tumour model has a unique complication because at least two published studies have found that frequent (three to six) injections of anti-PD1 or anti-PDL1 can cause death in mice due to anaphylactic shock (Arai et al., 2022; Mall et al., 2016). The reason behind this phenomenon is unclear, but peripheral neutrophilia (a consequence of bearing the 4T1 model or a CT26 model transduced to overexpress G-CSF) plays a critical role. That said, we suspect this odd result is not an outcome restricted to PD1 blockade *per se*, but rather a consequence of the immune system reacting to anti-drug antibodies that develop against biological therapies (i.e., not just checkpoint therapies). We also suspect this problem may be unique to mouse tumour models for two reasons. First, antibody treatments used in the clinic, such as nivolumab (anti-PD1) and ipilimumab (anti-CTLA4), are humanised. In contrast, many of the antibodies used to treat mouse tumour models in the laboratory are xenogenic (i.e., derived from hamsters and rats). Second, peripheral neutrophilia, a critical component of this phenomenon, is rarely found in human cancers.

Regardless, the healthy caution that has been developed upon learning of this anaphylactic phenomenon and the 4T1 model's unresponsiveness to immune checkpoint therapies make it inadequate for future gut microbial studies. However, its responsiveness to CFA therapy (C. S. E. Carroll et al., 2021) means it still has a role in the scope of this dissertation.

The DBA/2-derived P815 mastocytoma and BALB/c-derived CT26 colorectal carcinoma models met all the criteria required for a useful murine tumour model for future gut microbiome studies. Neither was so aggressive that mice died or had to be humanely euthanised before the therapies had a chance to take effect. That said, it is important to note that approximately one-third of mice challenged with the P815 model became ill and required humane euthanasia. This illness can (and has, in limited instances) quickly lead to death if not found and addressed quickly. Mice challenged with these models found significantly improved survival following anti-CTLA4 monotherapy, with some resulting in complete regression, though this was not the case with anti-PD1 monotherapy. Furthermore, FNA sampling did not impact treatment efficacy, and TIL profiling with

flow cytometry found differences among animals with disparate treatment outcomes. Therefore, both tumour models can be useful for gut microbiome mouse studies.

Having overcome the scientific and experimental challenges, the next hurdles we faced were logistical and, unfortunately, beyond our control. DBA/2 mice soon became inaccessible to us because of the COVID-19 pandemic. For most of 2020, Canberra (and the ANU) re-opened for business while the rest of Australia was still under lock-down restrictions because the city had a distinct lack of COVID-19 cases. (This situation offered a unique opportunity to assess COVID-19 vaccine efficacy in cancer patients. That study is presented in Appendix D.) During this period of apparent normalcy, flights that delivered DBA/2 mice from the Animal Resources Centre (ARC; their only supplier in Australia) in Perth, Western Australia, could not be flown direct to Canberra but could be flown to Sydney. However, the AEEC would not allow us to use private transportation to collect the animals after they had been delivered to the city. The following year, we received notice that the ARC had to shut down for 12-18 months starting July 2021 as it could not "operate in a financially self-sustaining manner, as required by legislation" (Fahrer, A. M., private correspondence). Consequently, DBA/2 mice and the P815 tumour model were inaccessible for all experiments for at least two years.

Fortunately, the ANU's Animal Phenomics Facility (APF) maintained a colony of BALB/c mice that could be used for our experiments. Thus, our next goal was to replicate previously published studies that treated tumour-challenged mice depleted of gut microbes with checkpoint therapies using the CT26 tumour model. When we planned the experiment, there was no published research on the impact gut microbes had on the effectiveness of anti-CTLA4 treatment in CT26-challenged mice, nor had a study used a method like our FNA sampling protocol to monitor how dysbiosis may affect TIL profiles and treatment outcomes. We spent 18 months getting approval from the AEEC to feed mice antibiotics in drinking water, and only then under strict oversight by the head veterinarian.

As the following chapter will explain, our first experiment involving gut microbial depletion through antibiotics did not go as planned. However, we discovered an important technical aspect regarding such experiments that was not well documented in

the literature. We were eager to publish our findings, provide a more in-depth discussion on the matter, and hopefully save other researchers time and mice when they plan their experiments.

5

Gut Microbiome-Depleting Antibiotic Regimens are not Tolerated by All Mouse Strains: Learn from (Our) Bitter Experience

Contents

5.1 Introduction **125**
5.2 Results **127**
5.3 Discussion and Publication **131**

This chapter includes our published paper (Almonte et al., 2022) as well as the unpublished experiments that lead to its publication.

5.1 Introduction

Studies have repeatedly confirmed that the presence and composition of gut microbes influence the anti-tumour immune response in mice and patients receiving checkpoint inhibitor therapy (Derosa et al., 2018; Gopalakrishnan et al., 2018; Matson et al., 2018; Vetizou et al., 2015). Pre-clinical mouse studies have demonstrated that a diverse gut microbial community (Tanoue et al., 2019; Vetizou et al., 2015) or animals monocolo-

nized with select bacterial species (Mager et al., 2020; Sivan et al., 2015) can improve checkpoint therapy responses. However, the question of how gut microbes significantly impact immune checkpoint therapy outcomes remains unanswered.

Several hypotheses for how gut microbes influence therapeutic outcomes have been proposed in the literature. As explained in Chapter 1 of this dissertation, we hypothesised that gut microbes translocate out of the gut, colonise distant solid tumours, and act in an adjuvant capacity to promote an immune reaction (Almonte et al., 2021). Various studies that support our theory have been published since we published our hypothesis paper. In one recent report, bacteria were found within archived solid tumour samples that were collected from human patients and previously believed to be sterile (Nejman et al., 2020). Additionally, bacterial antigens have been found bound to human leukocyte antigen (HLA) molecules presented on the surfaces of cancer cells in human melanoma patients (Kalaora et al., 2021). Indeed, since the publication of our literature review, a fascinating study has been published in *Science Immunology* presenting data showing both that mice treated with checkpoint therapies have a higher incidence of intratumoural bacteria and that these bacteria are required for treatment success (Choi et al., 2023). This paper is discussed in more detail in Chapter 7, Section 7.6 on page 194 of this dissertation.

Previous experiments described in this dissertation found that the CT26 tumour model responded well to anti-CTLA4 therapy (Figure 4.11). Furthermore, we found that mice responsive to anti-CTLA4 had significantly more tumour-infiltrating $CD8^+$ T cells by day 11 than non-responding mice (Figure 4.15). We therefore sought to use the CT26 tumour model to investigate why gut microbes impact the response to anti-CTLA4 therapy (Mager et al., 2020; Vetizou et al., 2015). We also wanted to use our FNA sampling protocol to determine whether depleting gut microbes would alter the TIL composition in mice following treatment. By identifying how TILs change over time and retrospectively comparing mice with disparate treatment outcomes, we hoped to better understand how gut microbes may impact the effectiveness of anti-CTLA4 treatment. However, we encountered a previously unappreciated challenge in that the BALB/c mice refused to drink published solutions of antibiotics used for gut microbe depletion.

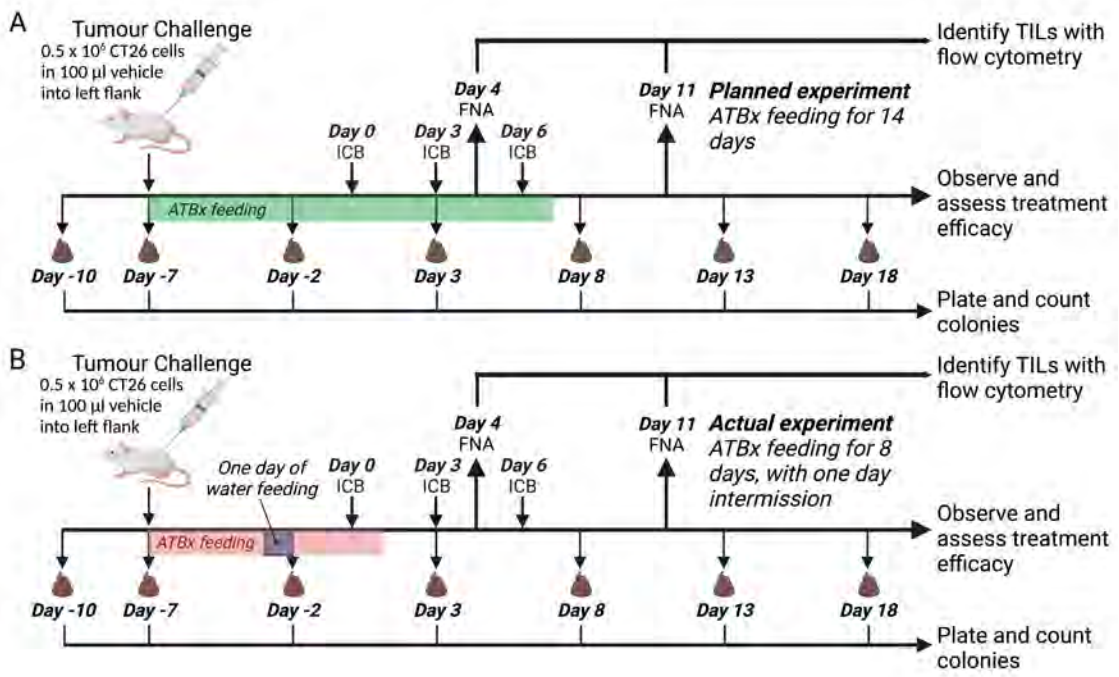


Figure 5.1: BALB/c mice were resistant to drinking the antibiotic solution. (A) A solution of 1 mg/mL colistin, 1 mg/mL ampicillin, and 5 mg/mL streptomycin (broad-spectrum antibiotics; ATBx) was intended to be fed *ad libitum* for 14 days starting from the day of tumour challenge. **(B)** However, we observed that the mice were becoming dehydrated because they were not drinking the antibiotics solution or staying adequately hydrated on wetted food. Thus, the ATBx feeding regimen was shortened from the original 14-day plan to eight days, with a one-day intermission on standard water.

5.2 Results

Our first antibiotic experiment aimed to assess the response of the CT26 tumour model to anti-CTLA4 therapy in the presence or absence of gut microbe-depleting antibiotics. To this end, we employed a broad-spectrum antibiotic cocktail composed of colistin, ampicillin, and streptomycin, as previously described in several papers published in *Science* (Mager et al., 2020; Routy et al., 2018; Viaud et al., 2013). As shown in Figure 5.1A, the antibiotics were intended to be administered *ad libitum* for 14 days, starting from the day the mice were subcutaneously injected with CT26 colon cancer cells.

However, we encountered a challenge in administering the antibiotics to the mice. Despite our efforts to flavour the water with 1% and 5% Ribena (a sweet blackcurrant-based fruit drink concentrate, which even water-fed mice refused to drink at the 5% concentration), the mice were reluctant to drink the antibiotic solution, leading to weight

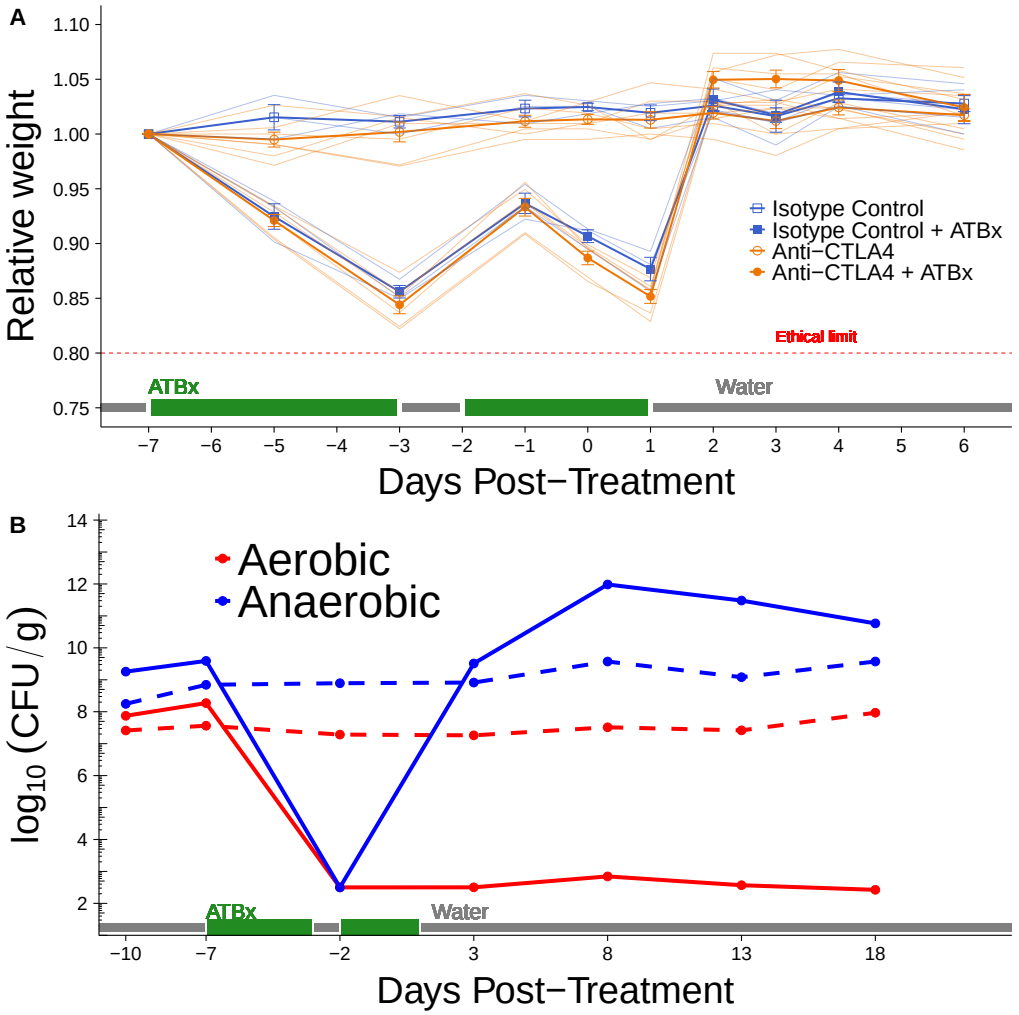


Figure 5.2: Despite dehydration, mice were still consuming antibiotics. **(A)** Mice were routinely weighed to monitor hydration and ensure they did not lose more than 20% of their initial body weight. All weights are relative to the initial weight recorded on the day antibiotic feeding began. **(B)** The calculated numbers of aerobic (red) and anaerobic (blue) colonies were plotted over time, beginning three days before the mice were fed antibiotics. The dashed lines represent samples from water-fed mice. Horizontal green bars indicate times mice were fed antibiotics. Error bars represent standard error. ATBx, antibiotics feeding.

loss and dehydration (Figure 5.2A). Efforts to maintain hydration and simultaneously promote antibiotic consumption by feeding the animals food wetted with the antibiotic-water had limited success. As a result, we were forced to modify our experiment to the schema shown in Figure 5.1B. On days -3 to -2, the mice were allowed access to standard water to recover their lost weight, though they lost weight again once they returned to the antibiotic-water. Ultimately, we had to end the antibiotic-feeding regimen six days earlier than intended.

Despite the altered regimen, we were able to continue the rest of our experimental protocols as planned. With the assistance of fellow PhD student Mr. George Cavic, we confirmed the depletion of gut microbiota in all antibiotic-fed mice through periodic collection, weighing, and plating of feacal pellets on Columbia horse blood agar plates. By counting the colonies that formed after 24-48 hours of incubation, we calculated the colony-forming units (CFU) per gram of faeces (Figure 5.2B). Both aerobic and anaerobic bacteria were successfully depleted during the antibiotic treatment, but the anaerobic bacteria quickly surpassed pre-treatment levels after the mice were returned to standard water.

Despite successfully inducing gut dysbiosis, anti-CTLA4 therapeutic outcomes were not impacted, as indicated by the results of our survival and tumour growth analysis (Figure 5.3). The mice were given three intraperitoneal injections of either 0.1 mg anti-CTLA4 (9D9) or 0.1 mg of isotype control (MPC-11; mouse IgG2b, κ), with one injection given every three days. The Cox proportional hazards model showed that anti-CTLA4 therapy significantly improved survival when analysed alone ($p = 0.0004$), while antibiotics did not impact survival, either when analysed alone or when assessed as an interaction effect with treatment ($p = 0.52$ and $p = 0.85$, respectively). Tumour growth analysis up to day 14 also indicated a significant impact of anti-CTLA4 therapy ($p < 0.0001$) but not of antibiotics ($p = 0.96$) or when assessed in conjunction with therapy ($p = 0.69$). Thus, anti-CTLA4 therapy was successful and not affected by antibiotic-induced gut dysbiosis.

To evaluate whether depleting the gut microbiome had any effect on TIL profiles, FNA samples were collected from all mice on days 4 and 11 post-treatment and analysed using flow cytometry with the gating strategy depicted in Figure 4.12 on page 116. After passing quality control measures (Figure 5.4), we found that mice fed antibiotics had a higher proportion of tumour-infiltrating B cells by day 11 compared to water-fed mice, regardless of the antibody treatment received (Figure 5.5A). On the other hand, mice that received water showed proportionally higher $CD8^+$ T cells on both days 4 and 11 and $CD4^+$ T cells on day 11 (again precluding antibody treatments). Only three anti-CTLA4 —- treated mice fully regressed after treatment (two were given antibiotics), thus

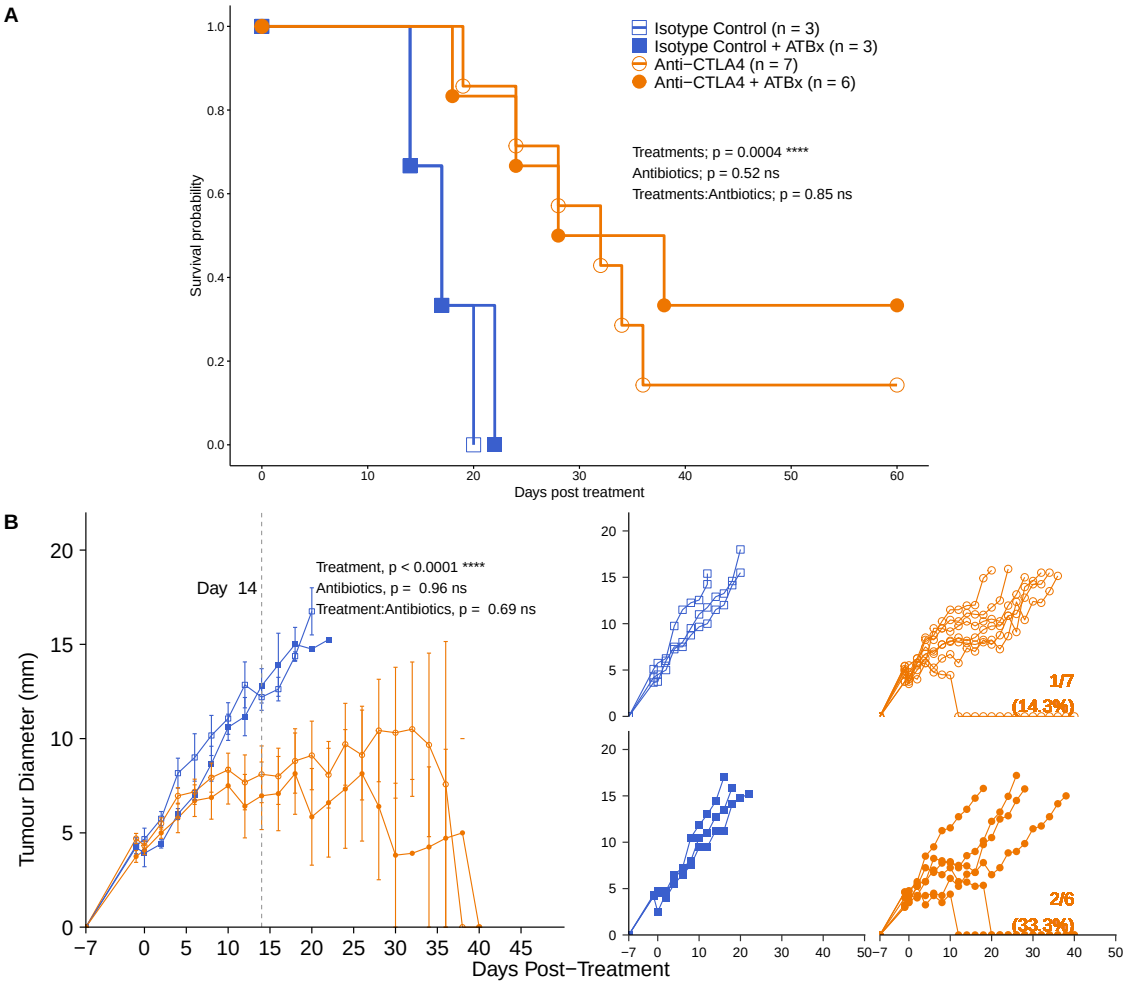


Figure 5.3: Dysbiosis did not affect anti-CTLA4 therapy in the CT26 tumour model. Mice bearing CT26 tumours were fed a solution of 1 mg/mL each of colistin and ampicillin and 5 mg/mL streptomycin for eight days, commencing on the day of tumour challenge. The antibiotics were given both in the drinking water and on wetted food. **(A)** Survival and **(B)** tumour growth were monitored after three i.p. injections with anti-CTLA4 antibody. The antibiotics had no effect on the efficacy of the anti-CTLA4 therapy as determined by statistical analysis. Fractions noted in the tumour growth curves indicate the number and percentage and regressed mice in the respective treatment group. Error bars indicate standard error.

making statistical analysis of TIL profiles between responding and non-responding mice impossible. However, to allow examination of the TIL profiles among regressing animals, the individual FNA results for these mice are shown in Figure 5.6. Mouse 11, which was the only mouse fed standard water, appears to have the highest proportion of $CD8^+$ T cells, but additional samples are required to make any valid conclusions.

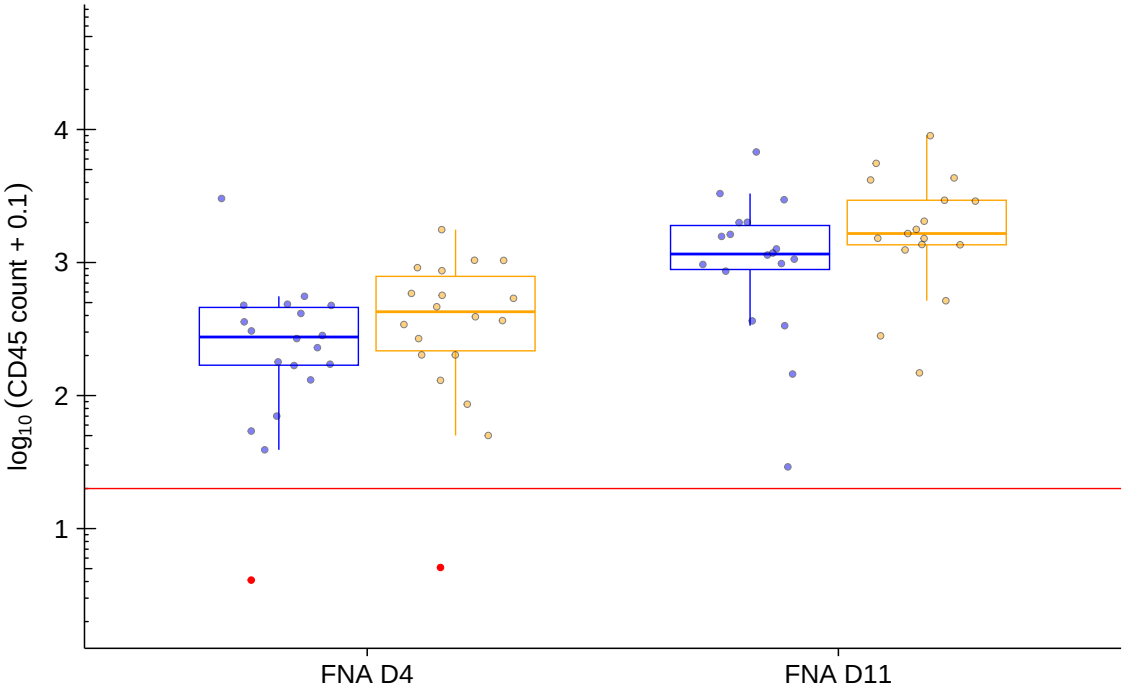


Figure 5.4: Quality control was performed to determine which FNA samples from C26-challenged mice in the antibiotics experiment was retained for analysis. Quality control was performed to determine which FNA samples from the CT26 model would be included in the final analysis. Only samples with more than 20 events in the live CD45.2$^+$ gate were retained to prevent percentage anomalies due to small sample sizes. The box plots and dots above the horizontal red threshold line represent sample counts from the Innate stain (blue) and the Adaptive stain (orange), respectively. The red dots below the threshold line represent samples that were excluded. As a result, 72 out of 74 samples (97.3%) were retained for the final analysis. Each dot represents the cell count in the relevant stain from individual FNA samples.

5.3 Discussion and Publication

We showed earlier in this dissertation that anti-CTLA4 therapy significantly impacted the survival of mice challenged with the CT26 tumour model (Figure 4.11 on page 115). We also showed that mice responsive to therapy had significantly higher numbers of CD8$^+$ T cells and significantly lower numbers of macrophage/monocytes (Figure 4.15 on page 119). In this chapter, we aimed to use the same tumour model to determine whether depleting gut microbes with broad-spectrum antibiotics would impact anti-CTLA4 treatment efficacy. We also sought to use FNA sampling to determine if gut bacteria depletion would alter the TIL composition of antibiotic-fed anti-CTLA4 – treated mice.

However, the study faced unfortunate challenges because the BALB/c mice would not drink the broad-spectrum antibiotic solution when it was fed *ad libitum*. Efforts to

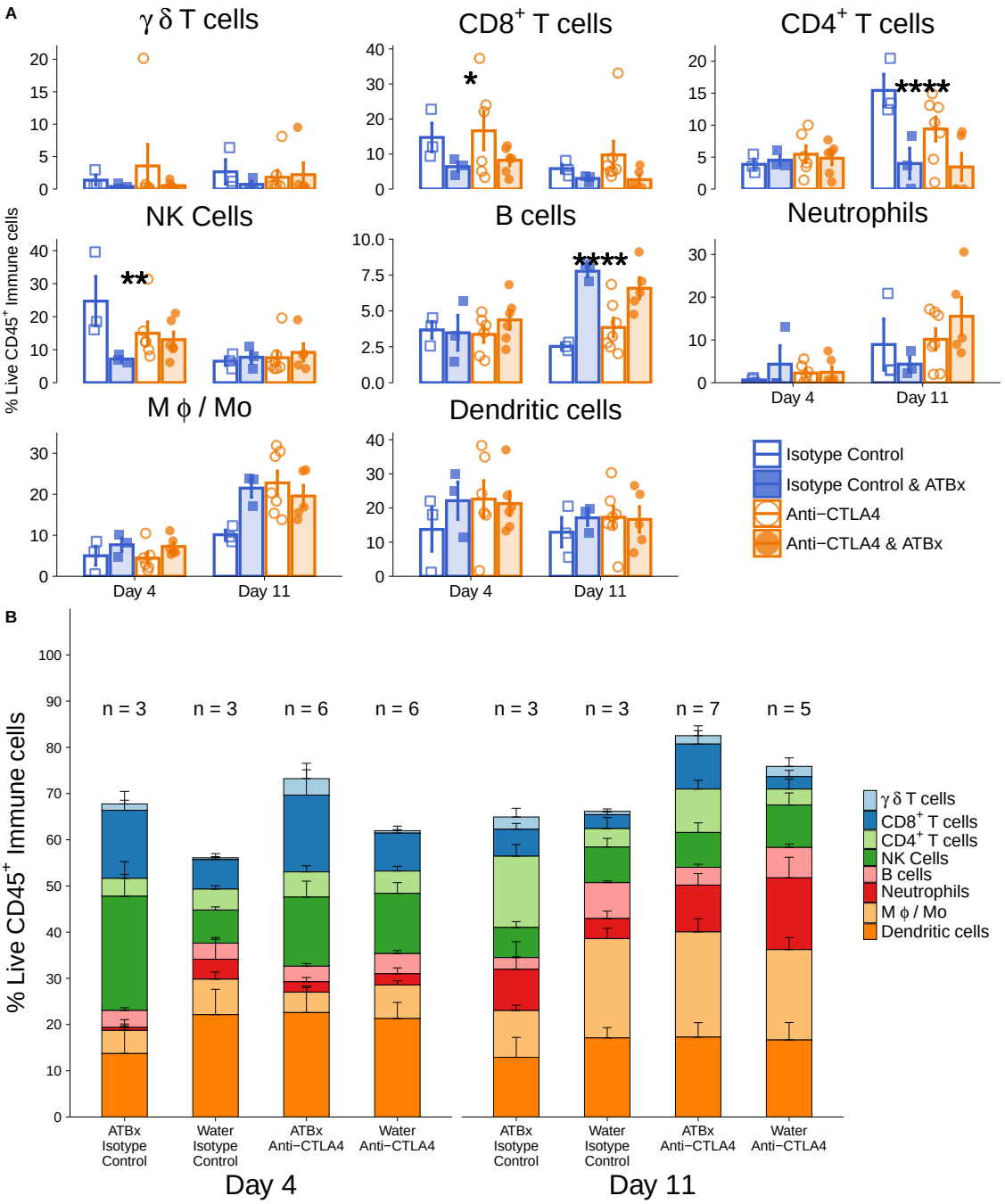


Figure 5.5: Tumour-infiltrating leukocyte populations were impacted by antibiotics in the CT26 model. **(A)** FNA samples were analysed by flow cytometry using the gating strategy outlined in Figure 4.12 to quantify eight different TIL populations across the innate and adaptive arms of immunity. A linear mixed-effects model and a Type II ANOVA were used to evaluate the of differences in proportions of each cell type. Antibiotics alone caused significant differences in the NK cells and CD8+ T cell populations on Day 4, and B cells and CD4+ T cell populations on Day 11. **(B)** A summary of the data shown in (A) is presented as a stacked bar graph to provide a better visual representation of the TIL proportions. The sample numbers noted above each bar may vary between days due to tumour regression, mouse attrition, or sample quality control. Error bars represent standard error. Mϕ, Macrophages; Mo, Monocytes; *, $p < 0.05$; ** $p < 0.01$; **** $p < 0.0001$

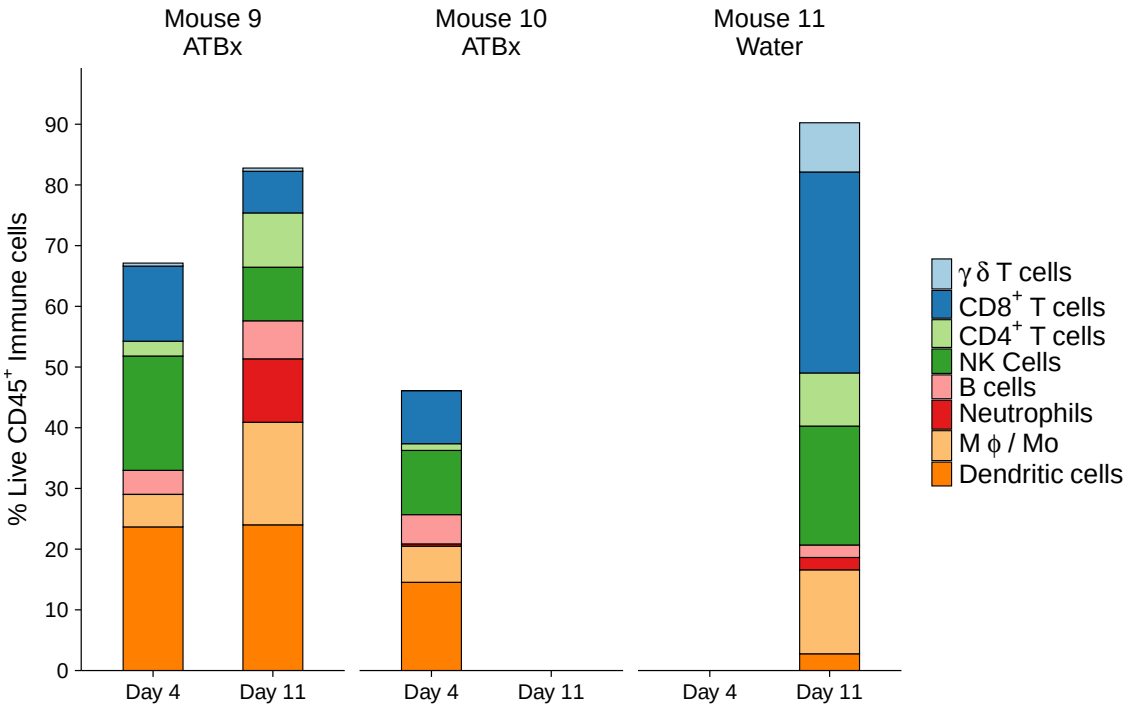


Figure 5.6: FNA data from antibiotic- and water-fed mice that regressed following anti-CTLA4 treatment. Three mice regressed after receiving three intraperitoneal injections of anti-CTLA4. Two mice were fed antibiotics and one was fed standard water. Data from Day 11 for Mouse 10 is absent because the tumour had regressed before it could be sampled. Data from Day 4 for Mouse 11 did not pass quality control.

maintain hydration so the animals would not exceed the ethical weight-loss limit and be euthanised meant that the planned experimental protocol needed to be modified. This resistance to drinking the antibiotic-water was unexpected because many published studies have used this formulation to deplete gut microbes in other mouse experiments, seemingly without any problems (Candon et al., 2015; Lochner et al., 2011; Mager et al., 2020; Routy et al., 2018; Sawa et al., 2011; Vetizou et al., 2015; Viaud et al., 2015). Attempts to seek advice from the authors of one of these studies were unsuccessful.

Regardless, mice fed antibiotics were consuming the solution through the wetted food and the gut microbiota were successfully depleted. However, contrary to findings from other published tumour models (Mager et al., 2020; Vetizou et al., 2015), dysbiosis did not impact the efficacy of anti-CTLA4 treatment in mice challenged with the CT26 model in our experiments (Figure 5.3). This difference in findings may be due to the reduced time that mice were fed antibiotics from the planned 14-day period to only eight days, with a one-day intermission for feeding standard water. For example, Mager *et al.*

(2020) fed tumour-challenged mice antibiotics throughout the entire experiment (which reportedly lasted 32 days). Vetizou *et al.* (2015) fed their animals antibiotics for 2-3 weeks before tumour implantation. It is also possible that the dehydration experienced by the antibiotic-fed mice may have impacted their immune responses and produced unanticipated consequences. However, we cannot make any valid conclusions until the experiment is repeated.

While anti-CTLA4 efficacy in the CT26 model was not impacted by dysbiosis, FNA sampling and TIL profiling via flow cytometry showed significant differences in the tumour-infiltrating B cells (Figure 5.5). Additionally, we found that both $CD4^+$ and $CD8^+$ T cells were proportionally higher in all water-fed mice. Our finding that B cells were statistically higher in antibiotic-fed mice was surprising and may warrant further investigation. While many studies have found a link between gut bacteria and the anti-tumour responses of T lymphocytes (reviewed in Almonte et al., 2021), none have investigated a possible relationship between intratumoural B cells, gut microbes, and immune checkpoint therapies. With evidence suggesting a correlation between the formation of tertiary lymphoid structures and therapeutic success in melanoma patients receiving checkpoint therapies (Cabrita et al., 2020), this interaction may be worthy of further investigation.

The difficulties we encountered in this study led the ANU Animal Experimentation Ethics Committee (AEEC) to decide that all antibiotic-based experiments be discontinued, thus preventing us from repeating the study. A review of the literature revealed that almost all reports that used this ampicillin/colistin/streptomycin combination also used C57BL/6 mice, a strain found to have a higher tolerance for bitter solutions than other strains (Blizard, 2007; Boughter & Bachmanov, 2007). This realisation led us to hypothesise that C57BL/6 mice would be more willing to consume the antibiotics than BALB/c mice, which was tested in collaboration with another research group. We published our findings in a commentary article (Almonte et al., 2022) in the hope that it would aid other researchers in avoiding similar challenges when planning experiments that involve feeding antibiotics to mice. That article is included here as the second half of this chapter.

Open access Commentary

Journal for ImmunoTherapy of Cancer

Gut microbiome-depleting antibiotic regimens are not tolerated by all mouse strains: learn from (our) bitter experience

Andrew A Almonte [1], George Cavic [1], Teresa Neeman [2], Anselm Enders [3], Aude M Fahrer [1]

To cite: Almonte AA, Cavic G, Neeman T, *et al*. Gut microbiome-depleting antibiotic regimens are not tolerated by all mouse strains: learn from (our) bitter experience. *Journal for ImmunoTherapy of Cancer* 2022;**10**:e005575. doi:10.1136/jitc-2022-005575

Accepted 30 September 2022

Check for updates

© Author(s) (or their employer(s)) 2022. Re-use permitted under CC BY-NC. No commercial re-use. See rights and permissions. Published by BMJ.

[1]Research School of Biology, College of Science, Australian National University, Canberra, ACT, Australia
[2]Biological Data Science Institute, College of Science, Australian National University, Canberra, ACT, Australia
[3]John Curtin School of Medical Research, College of Health and Medicine, Australian National University, Canberra, ACT, Australia

Correspondence to
Dr Aude M Fahrer; aude.fahrer@anu.edu.au

ABSTRACT

Why the gut microbiome is critical for the success of checkpoint inhibitor cancer therapy is a question that remains unanswered, but progress has slowed. We argue that this lack of advancement is due to an unappreciated biological detail. Here, we show that the antibiotic cocktail used in seminal publications—all of which have used the C57BL/6 mouse strain—are bitter and not tolerated by other common mouse strains (ie, BALB/c and DBA/2). We write to alert readers of this important biological limitation that must be considered when planning cancer experiments investigating the gut microbiota, to prevent the unnecessary dehydration of experimental animals, and to save our colleagues valuable experimental time and resources.

REPORT

The importance of commensal gut bacteria on the effectiveness of cancer immunotherapies has been well established in both mouse models[1–3] and patients.[2 4] Though these papers have fully established the gut microbiome's importance, none have adequately explained how the gut microbes influence therapeutic outcome. We have proposed a model dependent on bacteria translocating out of the colon and infecting the host, eventually colonizing a solid tumor, and promoting an adjuvant effect.[5] Others have highlighted the role of bacterial by-products, such as inosine and butyrate, which can modulate systemic immunity and improve the anticancer immune response.[6 7] Understanding this mechanism is critical for improving the success rate of checkpoint inhibitor therapy in patients with cancer. A viable mouse model that is amenable to having its gut flora modified is required to investigate these hypotheses and study the complex interactions between commensals, their host, and therapeutic outcome. We have attempted to make such a model but have encountered an unexpected experimental difficulty, and so wanted to publish our experience in this editorial to inform other researchers and encourage further investigation into this fascinating topic.

Broad-spectrum antibiotics are the most accessible tool to modulate gut microbes. Several published papers have used this method, and a common solution has been a mix of 1 mg/mL colistin, 1 mg/mL ampicillin, and 5 mg/mL of streptomycin.[2 7 8] Our attempt to replicate these experiments failed with BALB/c mice because they refused to drink the antibiotic water and became severely dehydrated. We tried to overcome their aversion by flavoring the antibiotic-water but failed. We had some success at preventing dehydration by wetting food pellets with the antibiotic solution. However, we were ultimately obliged to end the experiment early due to ethical concerns for the animals' well-being.

To understand why we were unable to replicate previously published studies, we first questioned the published concentrations of the antibiotics. However, two independent laboratories had successfully used the same antibiotic solution to deplete the gut flora of their mice.[2 7–9] An alternative hypothesis was that different mouse strains may have different tolerances for bitter compounds. This was supported by finding literature describing how C57BL/6 mice had a higher tolerance for bitter compounds than both DBA/2 mice and BALB/c mice[10 11] and that all of the studies we were trying to replicate were indeed feeding their antibiotic solution ad libitum to only C57BL/6 mice. Tasting of the antibiotic water by one of the authors (expendable PhD student; without swallowing) confirmed the antibiotic water was extremely bitter.

To quickly evaluate whether there was a difference in tolerance to the antibiotic solution between C57BL/6 mice and BALB/c mice, we first compared tolerances for the individual antibiotic components at either

J Immunother Cancer: first published as 10.1136/jitc-2022-005575 on 2 November 2022. Downloaded from http://jitc.bmj.com/ on December 8, 2022 at Lane Medical Library, Stanford University Medical Center. Protected by copyright.

Open access

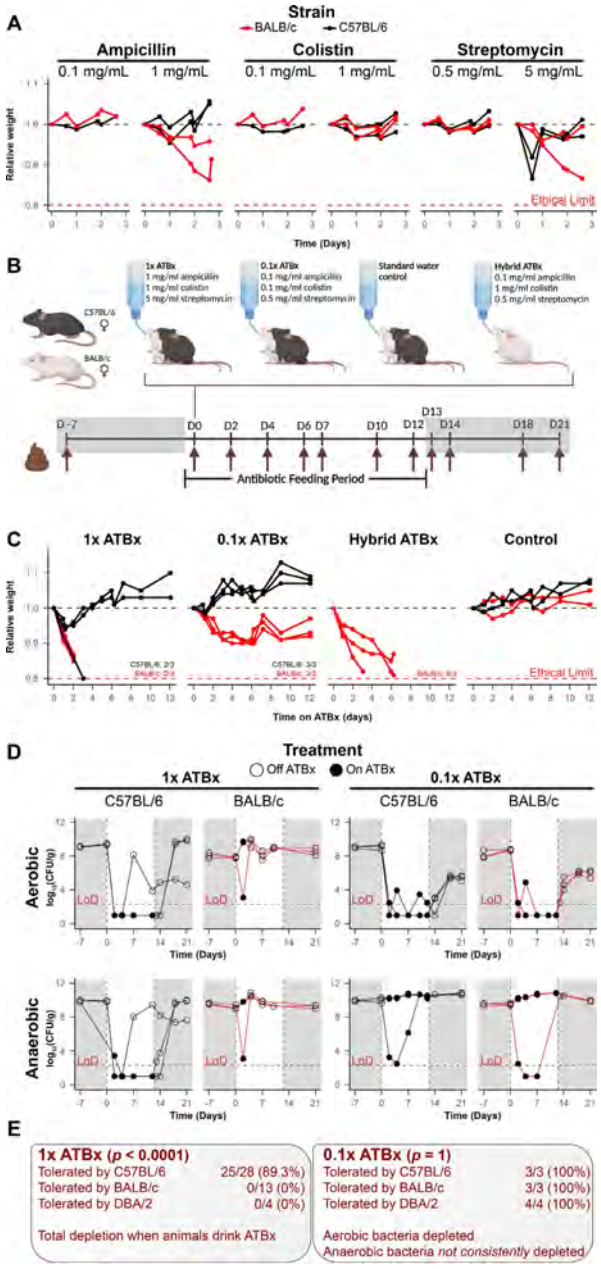


Figure 1 Antibiotic tolerance was tested in both BALB/c and C57BL/6 mice. (A, C) Relative weights of mice (red – BALB/c, black – C57BL/6), as a measure of antibiotic (ATBx) water intake. (A) Animals were fed individual antibiotics ad libitum at both the published and 1/10th of published concentrations. (B) Experimental design for C and D. (C) Effects of different antibiotic formulations fed ad libidum on weights of age-matched and sex-matched BALB/c and C57BL/6 mice (n=3, each group). Results in A and C are from two representative experiments. (D) Aerobic and anaerobic bacterial counts from fecal pellets collected from the same mice shown in C and plated on horse blood agar. Samples were collected when mice were fed standard water (open circles) and ATBx (closed circles). Linear mixed effects models of $\log_{10}$(CFA/g) with strain, day and bacteria type as fixed effects and mouse as random effect were fit for each antibiotic dose (1x and 0.1x). P values: 1x ATBx (p=0.006) and 0.1x ATBx (p=0.95) indicate a statistically significant effect of mouse strain on bacterial depletion only at the higher antibiotic dose. (E) A summary of our experience with feeding antibiotics to several common laboratory mouse strains, summary of five independent experiments. Fisher's exact test was used to compare strains (p<0.0001 and 1 at higher and lower antibiotic concentrations, respectively). Figure 1B was created in BioRender.com. CFU, colony forming unit; LoD; limit of detection,.

J Immunother Cancer: first published as 10.1136/jitc-2022-005575 on 2 November 2022. Downloaded from http://jitc.bmj.com/ on December 8, 2022 at Lane Medical Library, Stanford University Medical Center. Protected by copyright.

the published concentrations or at 1/10th the concentration over a 2.5-day period. We quickly observed that BALB/c mice did not reliably drink the published ampicillin and streptomycin concentrations but could tolerate 1/10th concentrations. Both strains could tolerate the published colistin concentration (figure 1A).

Building on the first experiment, we designed a second experiment with the aim of establishing whether the mice can tolerate all three antibiotics mixed at their individual maximum tolerable doses. Furthermore, we wanted to determine if these solutions were still effective at depleting the gut flora. Age-matched and sex-matched BALB/c and C57BL/6 mice were fed antibiotics over a 12-day period. To estimate the microbial load of each mouse, fecal samples were collected, diluted, and plated onto horse blood agar plates, incubated at 37°C in aerobic and anaerobic conditions, and the resulting colonies counted. These values were used to calculate the colony-forming units per gram of feces. Animals that approached or reached 80% of their initial bodyweight were removed to a separate cage with standard water. These animals regained all their lost weight within 24 hours.

As expected, the BALB/c mice needed to be removed from the published antibiotic concentrations within 48 hours, while two of three C57BL/6 mice reliably drank the solution (figure 1C). All animals tolerated the 1/10th concentration solution, but the colony counts showed the antibiotics were not of sufficient strength to deplete the anaerobic gut flora. A hybrid solution with the full dose of colistin but 1/10th of the published dose for ampicillin and streptomycin was tested on only BALB/c mice, but it was also not tolerated (figure 1C). We also conducted a series of similar experiments with DBA/2 mice and obtained comparable results in tolerances and bactericidal activity as observed in the BALB/c mice (data not shown).

From the experiments described above, it became apparent to us that C57BL/6 mice are best suited for feeding a broad-spectrum antibiotic solution containing 1 mg/mL ampicillin, 1 mg/mL colistin, and 5 mg/mL of streptomycin. Of the concentrations tested, it is the most effective at completely depleting the gut microbiome, but of the three strains we studied, C57BL/6 mice were the only strain tolerant of the bitter-tasting solution. It is worth noting that streptomycin is poorly absorbed by the gastrointestinal tract, thus oral administration is the optimal route for the effective depletion of gut microbes (colistin and ampicillin can be injected to achieve the same effect). Therefore, researchers should consider oral gavage or mixing antibiotics in the food if planning to use this antibiotic cocktail with BALB/c or DBA/2 mice in their gut microbiome studies.

Individual mouse strain differences have also been shown when the aim of antibiotic administration is to modulate rather than deplete intestinal bacteria.[12–14] Depending on the stain of mouse and antibiotics used, the effects on the gut microbiome can be distinct; the same antibiotics alter the gut microbiomes of individual mouse strains differently, with proportions of some bacterial genera increasing in C57BL/6 mice while decreasing or remaining unchanged in BALB/c mice.[12 13] The reason for this is unclear, but may be due to the bias C57BL/6 mice have toward a Th1-type immune response, and BALB/c and DBA/2 mice have toward a Th2-style immune response.[12 15 16]

Elucidating the mechanism by which gut microbes impact cancer immunotherapies (and chemotherapies[9 17]) is critical for the improved treatment of patients with cancer. However, many important murine cancer models are not on the C57BL/6 background. Where the aim is complete depletion of the gut microbiome, C57BL/6 will tolerate the commonly used combination of ampicillin, colistin and streptomycin in their drinking water, while DBA/2 and BALB/c mice will not. We write to alert readers of this important technical limitation, to prevent the unnecessary dehydration of experimental animals, and to save our colleagues valuable experimental time and resources.

Twitter Andrew A Almonte @andrew_almo

Acknowledgements We would like to thank Dr. Naresh Verma for helpful advice.

Contributors AMF, AE, and AAA conceived experiments. AAA and GC conducted experiments. AAA and TN analyzed data. TN provided expert guidance on statistical analyses. AAA and AMF wrote the initial draft. AAA, GC, TN, AE, and AMF reviewed and edited the final manuscript.

Funding Funding for this project was provided by the Australian Government Research Training Program, the Lea Chapuis Memorial Fund, and the generosity of Tim and Margaret Bourke.

Competing interests None declared.

Patient consent for publication Not applicable.

Ethics approval All experiments were approved by the ANU's Animal Experimentation Ethics Committee under protocols A2017/46, A2020/45, and A2021/05.

Provenance and peer review Not commissioned; externally peer reviewed.

Open access This is an open access article distributed in accordance with the Creative Commons Attribution Non Commercial (CC BY-NC 4.0) license, which permits others to distribute, remix, adapt, build upon this work non-commercially, and license their derivative works on different terms, provided the original work is properly cited, appropriate credit is given, any changes made indicated, and the use is non-commercial. See http://creativecommons.org/licenses/by-nc/4.0/.

ORCID iDs
Andrew A Almonte http://orcid.org/0000-0002-8131-7805
George Cavic http://orcid.org/0000-0003-2657-8129
Teresa Neeman http://orcid.org/0000-0002-7315-3695
Anselm Enders http://orcid.org/0000-0001-5933-6463
Aude M Fahrer http://orcid.org/0000-0001-8556-0223

REFERENCES

1 Sivan A, Corrales L, Hubert N, *et al*. Commensal Bifidobacterium promotes antitumor immunity and facilitates anti-PD-L1 efficacy. *Science* 2015;350:1084–9.
2 Routy B, Le Chatelier E, Derosa L, *et al*. Gut microbiome influences efficacy of PD-1-based immunotherapy against epithelial tumors. *Science* 2018;359:91–7.
3 Tanoue T, Morita S, Plichta DR, *et al*. A defined commensal consortium elicits CD8 T cells and anti-cancer immunity. *Nature* 2019;565:600–5.
4 Derosa L, Hellmann MD, Spaziano M, *et al*. Negative association of antibiotics on clinical activity of immune checkpoint inhibitors in

J Immunother Cancer: first published as 10.1136/jitc-2022-005575 on 2 November 2022. Downloaded from http://jitc.bmj.com/ on December 8, 2022 at Lane Medical Library, Stanford University Medical Center. Protected by copyright.

patients with advanced renal cell and non-small-cell lung cancer. *Ann Oncol* 2018;29:1437–44.
5 Almonte AA, Rangarajan H, Yip D, *et al*. How does the gut microbiome influence immune checkpoint blockade therapy? *Immunol Cell Biol* 2021;99:361–72.
6 Bachem A, Makhlouf C, Binger KJ, *et al*. Microbiota-derived short-chain fatty acids promote the memory potential of antigen-activated CD8+ T Cells. *Immunity* 2019;51:e285:285–97.
7 Mager LF, Burkhard R, Pett N, *et al*. Microbiome-derived inosine modulates response to checkpoint inhibitor immunotherapy. *Science* 2020;369:1481–9.
8 Vétizou M, Pitt JM, Daillère R, *et al*. Anticancer immunotherapy by CTLA-4 blockade relies on the gut microbiota. *Science* 2015;350:1079–84.
9 Viaud S, Saccheri F, Mignot G, *et al*. The intestinal microbiota modulates the anticancer immune effects of cyclophosphamide. *Science* 2013;342:971–6.
10 Blizard DA. Sweet and bitter taste of ethanol in C57BL/6J and DBA2/J mouse strains. *Behav Genet* 2007;37:146–59.
11 Boughter JD, Bachmanov AA. Behavioral genetics and taste. *BMC Neurosci* 2007;8 Suppl 3:S3.
12 Ray P, Pandey U, Aich P. Comparative analysis of beneficial effects of vancomycin treatment on Th1- and Th2-biased mice and the role of gut microbiota. *J Appl Microbiol* 2021;130:1337–56.
13 Horne R, St Pierre J, Odeh S, *et al*. Microbe and host interaction in gastrointestinal homeostasis. *Psychopharmacology* 2019;236:1623–40.
14 Fransen F, Zagato E, Mazzini E, *et al*. BALB/C and C57BL/6 mice differ in polyreactive IgA abundance, which impacts the generation of antigen-specific IgA and microbiota diversity. *Immunity* 2015;43:527–40.
15 Watanabe H, Numata K, Ito T, *et al*. Innate immune response in Th1- and Th2-dominant mouse strains. *Shock* 2004;22:460–6.
16 Mills CD, Kincaid K, Alt JM, *et al*. M-1/M-2 macrophages and the Th1/Th2 paradigm. *J Immunol* 2000;164:6166–73.
17 Iida N, Dzutsev A, Stewart CA, *et al*. Commensal bacteria control cancer response to therapy by modulating the tumor microenvironment. *Science* 2013;342:967–70.

J Immunother Cancer: first published as 10.1136/jitc-2022-005575 on 2 November 2022. Downloaded from http://jitc.bmj.com/ on December 8, 2022 at Lane Medical Library, Stanford University Medical Center. Protected by copyright.

6

Investigating Methods to Improve CFA Effectiveness

Contents

6.1 Introduction 140
6.2 Combining CFA with Immune Checkpoint Therapies 140
6.2.1 Exploring synergies between CFA and immune checkpoint therapies amidst the COVID-19 lockdown. 141
6.2.2 The 4T1 tumour model did not respond to CFA treatments at Stanford University. 143
6.2.3 Influence of combined treatments on lung metastasis was inconclusive 146
6.3 Increasing the Concentration of *Mycobacterium butyricum* in CFA 148
6.3.1 First observed regression of a CT26-challenged mouse following CFA monotherapy 148
6.3.2 10x CFA-treated mice had significantly higher proportions of neutrophils 152
6.3.3 All neutrophils increased while regulatory T cells decreased . 157
6.3.4 10x CFA attracts more immune cells into the tumour microenvironment 159
6.4 Discussion 161
6.4.1 Combining with immune checkpoint therapies 163
6.4.2 Increasing the concentration of *M. butyricum* 166
6.4.3 Conclusion 168

6.1 Introduction

The second aim of this PhD project was to investigate methods of improving our intratumoural complete Freund's adjuvant (CFA) therapy. This chapter presents data investigating two strategies and is divided into two parts. The first will explain the experiments conducted at both at the ANU and at Stanford University, which investigated combining intratumoural CFA injections with systemic immune checkpoint therapies in mice challenged with the 4T1 and CT26 cancer models. The second part elaborates on experiments conducted at the ANU, wherein we treated mice challenged with the CT26 cancer model with CFA containing ten-fold (5 mg/mL, 10x CFA) the concentration of heat-killed *Mycobacterium butyricum* used in all our laboratory's previous studies. These preliminary experiments lay the groundwork for future investigations into these questions.

6.2 Combining CFA with Immune Checkpoint Therapies

CFA is a water-in-oil emulsion developed by Dr Jules Freund in the 1940s and 1950s that has since been invaluable for basic immunology research (Billiau & Matthys, 2001; Freund & McDermott, 1942). The reagents in CFA include paraffin oil, an emulsifier, and a heat-killed *Mycobacterium* species. In 2012, Aude Fahrer published an essay explaining the advantages that intratumoural injections of CFA may have as a simple and inexpensive cancer immunotherapy (Fahrer, 2012). When injected into a solid tumour, the emulsion functions as a slow-release depot of pathogen-associated molecular patterns (PAMPs) provided by the *Mycobacterium* sp. and provokes an immune reaction (see Table 1.2 on page 27 and Figure 1.1 on page 25). The treatment aims to activate a robust innate immune response, specifically by activating antigen-presenting cells (APCs), so that they can more efficiently acquire, process, and present tumour-associated antigens (TAAs) as a result of being activated by the PAMPs supplied by the CFA (Billiau & Matthys, 2001; Fahrer, 2012). We have since reported encouraging results using intratumoural CFA as an immunotherapy in multiple syngeneic murine tumour models, naturally occurring canine and equine cancers, and solid tumours in human patients (C. S. E. Carroll et al., 2021).

We hypothesised that intratumoural CFA, which targets innate immunity, would work synergistically with the immune checkpoint therapies that we evaluated in chapters 3-5 and which target adaptive immunity. Other laboratories have used similar approaches to enhance immune checkpoint therapies. For example, GVAX – an irradiated B16 cell line that constitutively secretes granulocyte-macrophage colony-stimulating factor (GM-CSF, Curran & Allison, 2009), thus promoting the development and release of macrophages and neutrophils from the bone marrow – has been used to improve the outcomes of B16-challenged mice treated with anti-CTLA4 (Curran et al., 2010; Quezada & Peggs, 2019). Others have used immune checkpoint therapies combined with toll-like receptor (TLR) agonists to stimulate innate immune responses and strengthen adaptive anti-cancer immune responses (see Table 1.3, Sagiv-Barfi et al., 2018; Sharma et al., 2019; S. Wang et al., 2016). We expect that the *Mycobacterium* spp. in the CFA will provide a large consortium of PAMPs to stimulate a variety of pattern recognition receptors (PRRs, Stamm et al., 2015), provoke a vigorous innate immune response, and consequently improve immunotherapy treatment outcomes.

6.2.1 Exploring synergies between CFA and immune checkpoint therapies amidst the COVID-19 lockdown.

In December 2019, a new strain of coronavirus that caused severe acute respiratory syndrome (SARS-CoV-2), the causative agent of Coronavirus Disease 2019 (COVID-19), emerged from Wuhan, China and spread worldwide. On 20 March 2020, the Australian Government instituted a nationwide lockdown policy to limit the spread of the disease into Australia ("AUSTRALIA IS CLOSED," 2020). This decision led the Animal Experimentation Ethics Committee (AEEC) to prohibit non-COVID-19 related research at the ANU (Animal Ethics, personal communication, 25 March 2020). At the time, we had already injected 30 BALB/c mice with subcutaneous CT26 tumours to repeat the antibiotics experiment presented in Section 5.2 on page 127 with the aim of feeding the animals antibiotics by oral gavage. However, the new lockdown measures meant we could not undertake experiments that required significant veterinary oversight. Believing that euthanising the mice without obtaining scientific data is unethical, and having already

shown that the CT26 cancer model is almost responsive to intratumoural CFA treatment (C. S. E. Carroll et al., 2021, p = 0.07, see Appendix C, Figure 1), we repurposed the animals to examine if potential synergy could exist between intratumoural CFA injections and systemic immune checkpoint therapies.

We distributed the mice among six treatment groups (Figure 6.1A). Two groups received CFA or anti-CTLA4 monotherapies; three groups received dual therapies (CFA with anti-PD1, CFA with anti-CTLA4, or anti-CTLA4 with anti-PD1); and one group received a "tri-therapy", (CFA with both anti-PD1 and anti-CTLA4). CFA injections (0.05 mL containing 0.5 mg/mL heat-killed *M. butyricum*) were given on day 0, and antibody therapies (0.1 mg each) were given as three intraperitoneal injections on days 0, 3, and 6. The 9D9 clone of anti-CTLA4 and RMP1-14 clone of anti-PD1 were used in all treatment groups. Since no animals received isotype control antibodies or intratumoural PBS injections, the dual checkpoint therapy-treated and CFA-treated groups were designated positive and negative controls, respectively.

As shown in Figure 6.1B and 6.1C, neither the mice given CFA monotherapy nor the mice given CFA and anti-PD1 dual therapy responded to treatment; they were euthanised after tumours exceeded the ethical size limit. This lack of response to CFA and responsiveness to anti-CTLA4 are consistent with previously published results (C. S. E. Carroll et al., 2021) and data presented in Section 4.6 of this dissertation. In contrast, one mouse (1/5; 20%) given anti-CTLA4 monotherapy, and 2/5 mice (40%) given anti-PD1 and anti-CTLA4 dual therapy regressed after therapy. Mice in the tri-therapy treatment cohort initially responded well to treatment, with 1/5 mice (20%) regressing and 3/5 mice (60%) having their tumour growth stalled for a time. However, growth resumed 35 days after treatment, and the sole regressor mouse was found dead not long after fully regressing; a necropsy could not determine the cause of death. One mouse (1/5, 20%) from the CFA and anti-CTLA4 dual therapy group regressed after treatment, but we were later required to euthanise it by the AEEC because of a scab remaining at the tumour site.

This experiment was the first in which we had observed the CT26 model regress after intratumoural CFA injections and suggested a likely path forward for improving the efficacy of our treatment. It was also the last conducted by our laboratory immediately before

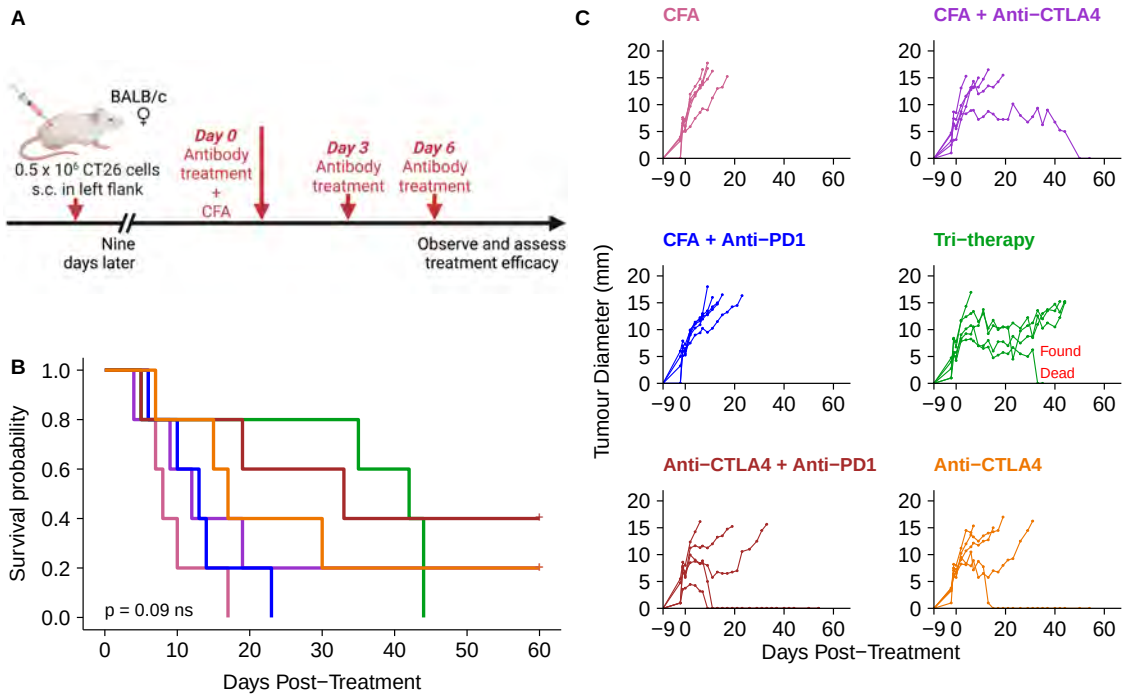


Figure 6.1: Combining CFA with immune checkpoint therapies in the CT26 model. **(A)** The experimental design used to evaluate the combination of CFA and immune checkpoint therapies. Female BALB/c mice were subcutaneously injected with 0.5 x 10^6 CT26 cells. Mice were distributed into treatment groups nine days later, when the average tumour diameters reached 4-5 mm. CFA was injected into the tumour once, while the antibody treatments were injected intraperitoneally once every three days for three injections. **(B)** Survival and **(C)** tumour growth trajectories of mice from each treatment group are shown. The regressor mouse in the tri-therapy treatment group was found deceased due to unknown causes. The Tri-therapy group refers to mice that received CFA, anti-CTLA4, and anti-PD1 treatments. The hazard ratios of each covariate used for the survival analysis in (B) are presented in Table B.7. Each treatment group contained 5 mice.

the nationwide lockdowns caused by the COVID-19 pandemic. When those lockdowns were lifted, the AEEC prevented us from continuing experiments that would have built upon this finding. However, I was given an amazing opportunity to pursue our research in the laboratories of Prof Yueh-Hsiu Chien and Prof Mark Davis at the Stanford University School of Medicine, where the following experiments were conducted.

6.2.2 The 4T1 tumour model did not respond to CFA treatments at Stanford University.

While working at Stanford University, I was required to follow the guidelines specified by the Davis Laboratory's animal ethics protocol. Considering that neither the CT26 nor

P815 tumour models were approved for mouse studies by that protocol, that my time at Stanford was limited, and that proposing an amendment to use those models would have been a time-consuming process, we decided to focus on the 4T1 breast cancer model. This model was already approved for use by the laboratory and we have previously shown that it was responsive to intratumoural CFA therapy (C. S. E. Carroll et al., 2021). Therefore, the 4T1 model was used in all experiments conducted at Stanford University that investigated how intratumoural CFA may influence the treatment outcomes of systemic immune checkpoint therapies.

The first experiment used a schema similar to that presented in Figure 6.1A. Female BALB/c mice were orthotopically injected with 0.5 x 10^6 4T1 cells into the mammary fat pad. Once the average tumour diameters reached 4-5 mm (typically seven days later), the mice were distributed into treatment groups and given one intratumoural injection of 0.05 mL CFA or PBS and three intraperitoneal injections (one given every three days) of both anti-CTLA4 (9D9) and anti-PD1 (RMP1-14) or isotype control antibodies (mouse IgG2b, κ [MPC-11] and anti-trinitrophenol [2A3]). Notably, the CFA used in these experiments contained 0.5 mg/mL of heat-killed *M. tuberculosis H37Ra* – an avirulent mutant of *M. tuberculosis H37Rv* (Blischak et al., 2015) – rather than 0.5 mg/mL of heat-killed *M. butyricum* used in the CFA in our studies conducted at the ANU.

The 4T1 tumour model did not demonstrate a significant improvement in survival or tumour growth control after intratumoural CFA treatment or CFA given in combination with immune checkpoint therapies (Figure 6.2A). As we were not reproducing the survival results we had obtained at the ANU, and knowing that different *Mycobacterium* strains can activate different innate immune pathways (Carmona et al., 2013) and promote different cytokine profiles (Shah et al., 2013), we asked if the *Mycobacterium* sp. in the CFA preparation had impacted its treatment efficacy. Therefore, we treated 4T1-challenged mice with intratumoural injections of CFA containing either heat-killed *M. tuberculosis H37Ra* or heat-killed *M. butyricum* (both at 0.5 mg/mL, Figure 6.2C and 6.2D). However, neither CFA treatment demonstrated a significant improvement in survival or tumour growth control compared with the isotype control group, nor were significant differences in treatment efficacy found between the two CFA preparations.

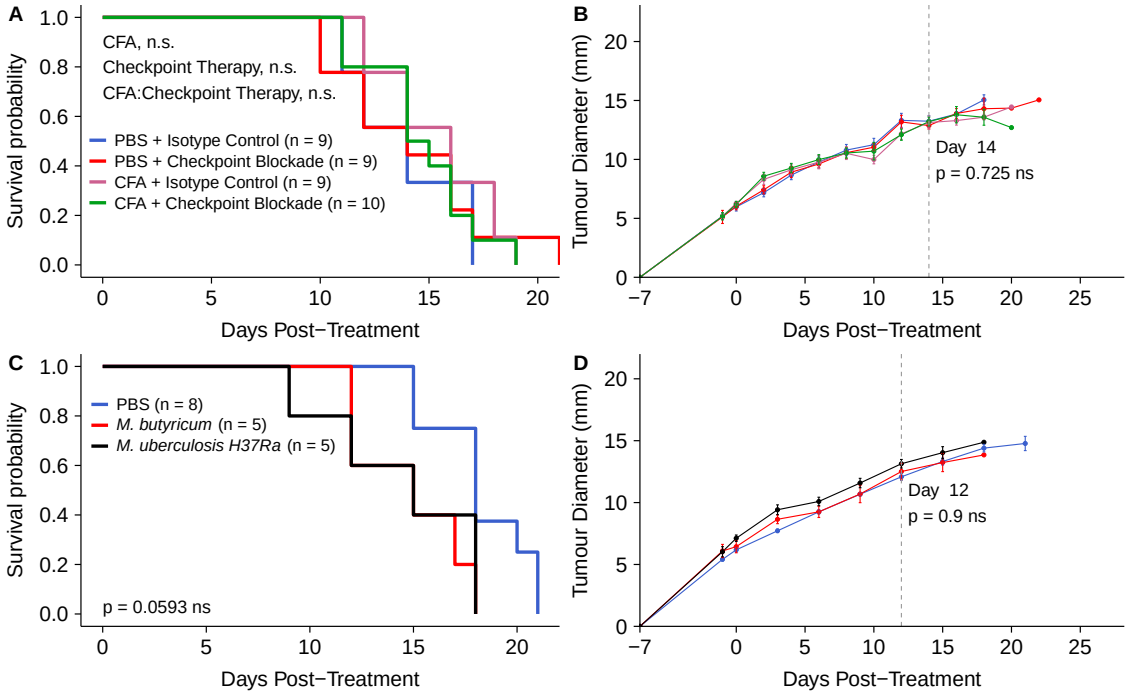


Figure 6.2: The 4T1 model did not respond to intratumoural CFA treatment at Stanford University. **(A)** Neither intratumoural CFA nor systemic immune checkpoint therapies improve the survival of mice challenged with the 4T1 model (p = 0.15 and p = 0.75, respectively). Immune checkpoint therapy also did not improve CFA treatment efficacy (p = 0. 49). **(B)** Tumour growth analysed up to day 14 post-treatment found no significant difference in tumour growth trajectories. **(C)** A Cox proportional hazards model found no difference in treatment outcomes between mice treated with CFA containing 0.5 mg/mL of heat-killed *Mycobacterium tuberculosis H37Ra* or 0.5 mg/mL of heat-killed *M. butyricum*. **(D)** Intratumoural CFA treatments containing the different *Mycobacterium* spp. did not significantly impact tumour growth. Data from two experiments are shown in (A) and (B), and one experiment is shown in (C) and (D). Error bars represent the standard error of the means. The performances of the LMER models used for (B) and (D) is presented in Figure A.14, and the hazard ratios of the covariates used in the survival analyses of (A) and (C) are presented in Tables B.8 and B.9, respectively. n.s., not significant

Importantly, the mice treated with CFA in this second experiment (Figure 6.2C and D) were outliers rejected from another study conducted by the Davis Laboratory because their tumours were either too large or too small for their purposes. This factor likely explains why control-treated animals appeared to have improved survival; hence, this experiment may not accurately represent CFA treatment efficacy.

6.2.3 Influence of combined treatments on lung metastasis was inconclusive

Despite CFA not impacting tumour growth or survival, we suspected that only a few CFA-treated 4T1-challenged mice, at both Stanford University and the ANU, deteriorated in body condition or became ill as almost all CFA-treated 4T1-challenged animals were euthanised because the tumour reached the ethical size limit. In our experience with murine cancer studies, mice become ill primarily due to metastases. While these experiments saw no improvement in survival, we asked if CFA treatments may impact metastatic disease progression in the 4T1 model (C. Carroll, 2016, p. 138). To determine if this was the case, mice were orthotopically challenged with 4T1 cells, treated with CFA and immune checkpoint therapies, and then sacrificed 11 to 13 days post-treatment (Figure 6.3A). The lungs were perfused with a solution of tap water and 15% (v/v) India ink solution through the trachea, excised, and then fixed in Fekete's solution (100 ml 70% alcohol, 10 ml formalin, and 5 ml glacial acetic acid) for 1-3 days at 4°C (Table 2.1, Marabelle et al., 2013; Zimmerman et al., 2010). This fixation protocol highlights metastatic foci as off-white opaque spots against a healthy, pitch black-stained lung (Figure 6.3C) that can easily be counted by eye under a dissecting microscope.

Metastases were found on the lung surfaces of all mice challenged with the 4T1 model, despite the treatments received. However, CFA-treated mice presented the highest number of white spots and thus more metastases (Figure 6.3B and Figure A.17). Indeed, the number of metastases appeared to increase in animals additionally treated with systemic immune checkpoint therapies. Notably, while more numerous, the individual metastases were also typically much smaller, giving the lungs from mice that received both CFA and immune checkpoint therapies a speckled, miliary pattern (Figure A.17). We first suspected this appearance resulted from inflammation-induced fibrotic scarring rather than metastases, possibly due to increased leukocyte activity triggered by a treatment protocol designed to increase immune activation and remove natural immune checkpoints simultaneously.

To confirm that what we observed were true metastases, the left lobe from each mouse was sent to a collaborator and expert veterinary pathologist, Prof Rachel Allavena

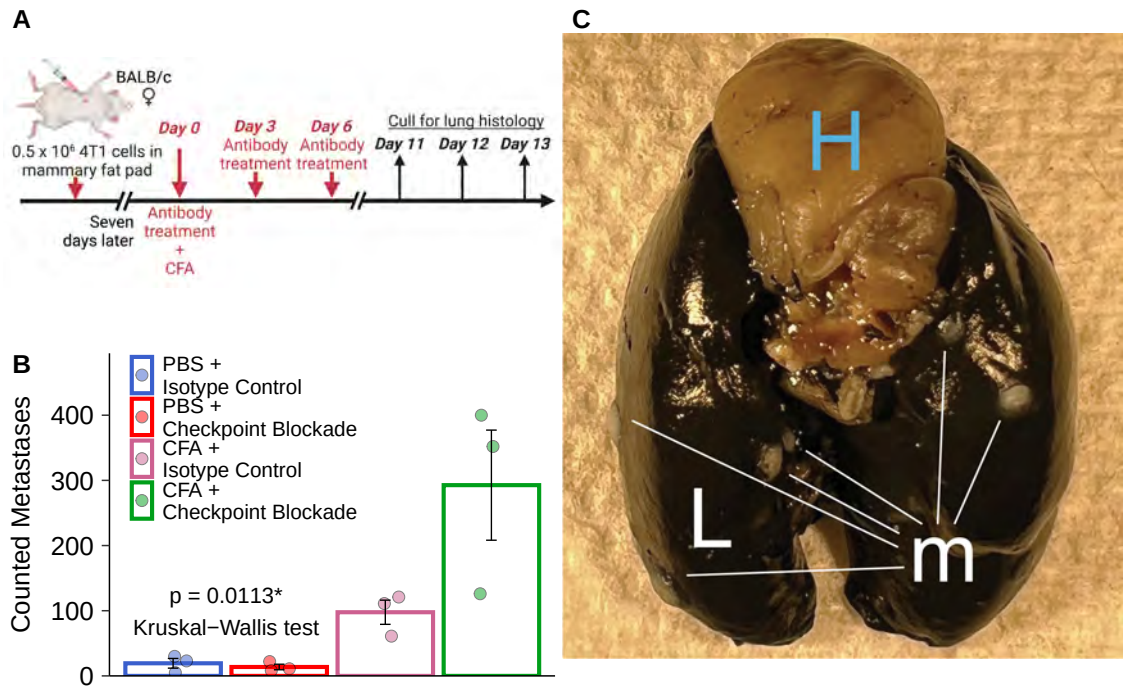


Figure 6.3: 4T1-challenged mice treated with concomitant CFA and immune checkpoint therapies appeared to develop more lung metastases. (A) Female BALB/c mice were injected orthotopically with 0.5 x 10^6 4T1 cells into the mammary fat pad. They were treated seven days later with intratumoural injections of CFA or PBS and intraperitoneal injections of both anti-CTLA4 (0.1 mg, 9D9) and anti-PD1 (0.2 mg, RMP1-14), or relevant isotype control antibodies. The intratumoural injections were administered once, while antibody injections were given every three days for three injections. The mice were sacrificed on Days 11, 12, and 13, and their lungs were collected and examined for metastasis. **(B)** A Kruskal-Wallis test found a significant difference in the average number of metastases among the treatment groups. Each dot represents a count from a single mouse. n = 3 mice per treatment group. **(C)** Example of a pair of mouse lungs perfused with India ink and fixed in Fekete's solution. Metastatic foci appeared as off-white spots, which were counted by eye and recorded. All of the lung photos taken in this experiment are presented in the Appendix in Figure A.17. L, lung; H, heart; m, metastasis

(University of Queensland, Australia), for examination. Extensive osmotic damage was observed because the India ink was diluted in tap water (compare Figures 6.4A and 6.4B). However, Prof Allavena was able to confirm that all the small white spots we observed on the lung surface were indeed cancer and that the number of lung metastases was higher in all mice treated with both CFA and immune checkpoint therapies (Figure 6.4C and Figure A.17). The experiment was repeated without the India ink solution to validate these findings. Instead, the lungs were perfused with and fixed in 10% neutral buffered formalin (NBF) before being embedded in paraffin and sent to Prof Allavena for examination. However, the second experiment found that the mice across all treatment groups had few

metastases (Figure 6.4E). Therefore, how CFA impacts metastatic disease progression is a question that remains unresolved and requires a more appropriate metastatic tumour model to investigate.

6.3 Increasing the Concentration of *Mycobacterium butyricum* in CFA

CFA is used to induce experimental autoimmune encephalomyelitis (EAE) in mouse models of multiple sclerosis (Billiau & Matthys, 2001; Stromnes & Goverman, 2006b, 2006a). We learned that laboratories using this protocol often supplement or prepare CFA emulsions with heat-killed *Mycobacterium* species to final concentrations ranging from 1 to 5 mg/mL (Rebecca Buckland, fellow PhD student, personal communication, 26 June 2019). The variable mycobacteria concentrations used in CFA as an EAE-stimulant led us to ask if the effectiveness of CFA as an immunotherapy could be improved if the heat-killed *M. butyricum* concentration was increased.

We used the CT26 tumour model to investigate this question, primarily because DBA/2 mice (and thus, the CFA-responsive P815 model) were not accessible to us when the experiments were planned and carried out. We had previously reported that intratumoural CFA's effect on the survival of CT26-challenged mice approached significance (C. S. E. Carroll et al., 2021, $p = 0.07$). Thus, we aimed to determine if CFA that was supplemented with desiccated heat-killed *M. butyricum* (purchased from Becton, Dickinson, and Co [BD]) to a ten-fold concentration (5 mg/mL, 10x CFA) would significantly improve survival in a tumour model that nearly attained significance with 1x CFA therapy. We also used FNA sampling to compare the influence that 1x and 10x CFA therapies had on TIL compositions of treated tumours.

6.3.1 First observed regression of a CT26-challenged mouse following CFA monotherapy

We first conducted a treatment efficacy study to determine if 10x CFA would be effective as a cancer immunotherapy. Female BALB/c mice were challenged with subcutaneous CT26 tumours on the left flank, then given intratumoural injections seven days later with

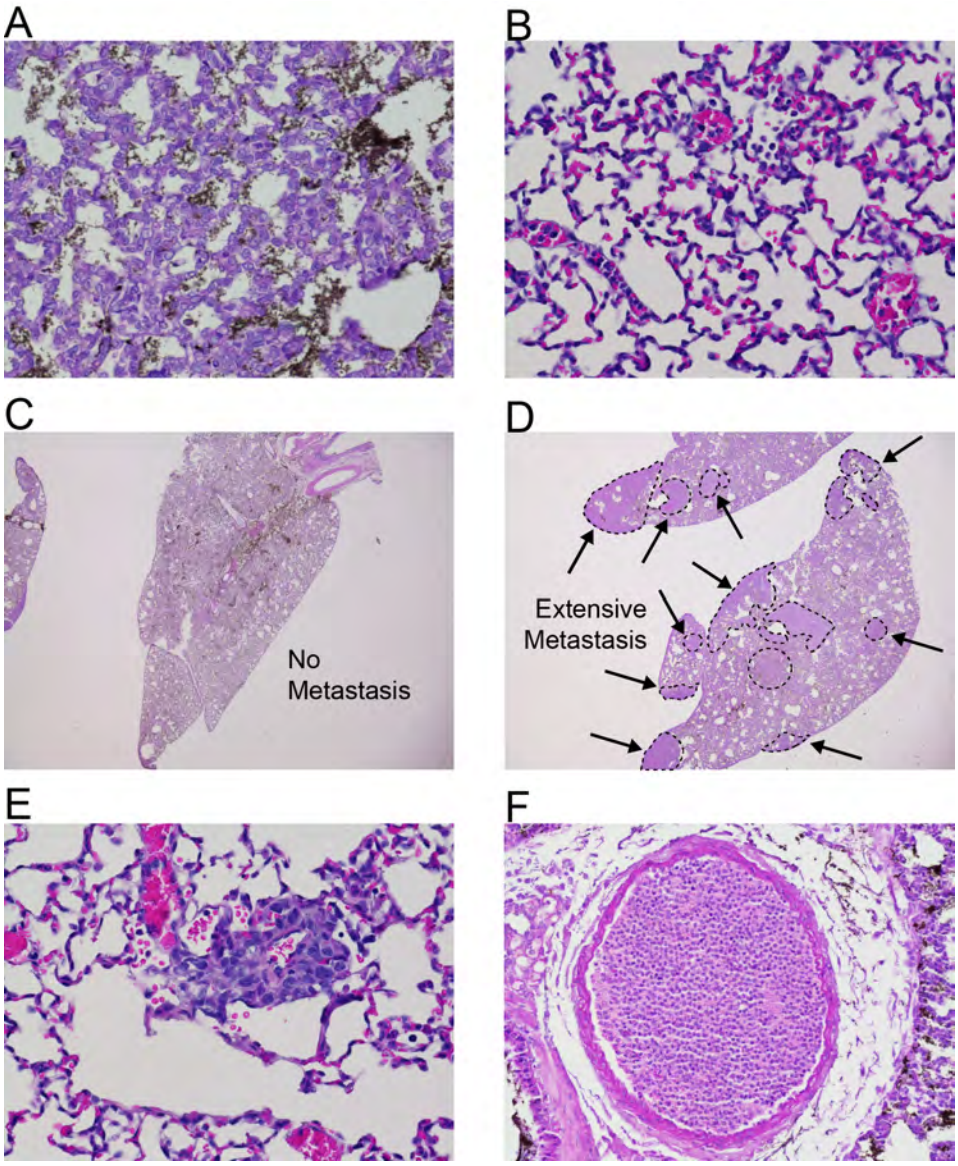


Figure 6.4: H&E-stained lung sections from mice that received CFA and immune checkpoint therapy. The lungs of mice were embedded in paraffin blocks and sent to pathology expert, Prof Rachel Allavena (University of Queensland), for staining and microscopic analysis. **(A)** Lung perfused with India ink in tap water and fixed in Fekete's solution (400x, FS). **(B)** Lung perfused with and fixed in 10% neutral buffered formalin (400x, NBF). **(C)** Lung from a mouse treated with intratumoural PBS and systemic immune checkpoint therapy (50x, FS). **(D)** Lung from a mouse given intratumoural CFA and systemic immune checkpoint therapy. Metastases are demarcated with dotted black lines and arrows (50x, FS). **(E)** Lung from a mouse treated with intratumoural CFA and systemic isotype control antibodies presenting a small interstitial metastasis (400x, NBF). **(F)** Bronchial artery from a mouse treated with PBS and immune checkpoint therapy full of neutrophils (200x, FS). H&E staining and photography done by Prof Allavena (University of Queensland). FS, Fixed with Fekete's Solution after perfusing with India ink in tap water; NBF, perfused with and fixed in 10% neutral-buffered formalin.

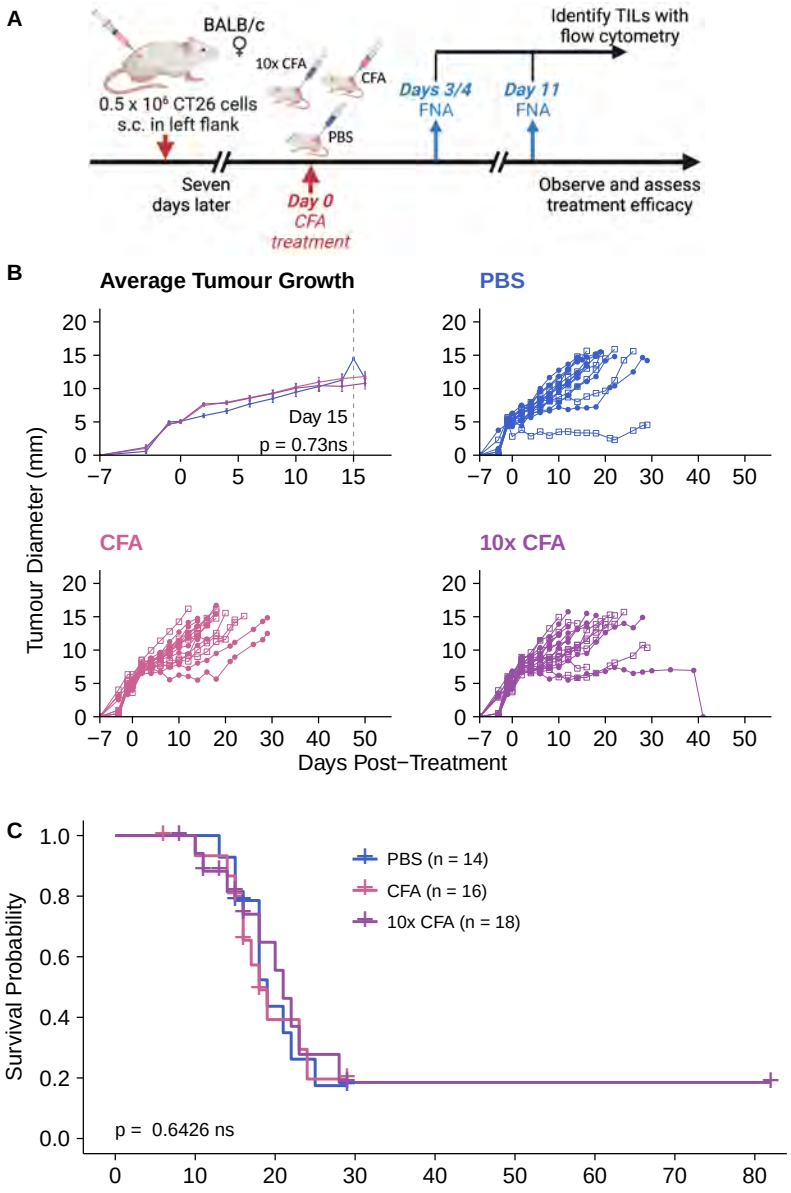


Figure 6.5: Complete regression of a CT26 tumour was observed after treatment with 10x CFA. (A) Female BALB/C mice were challenged with CT26 cancer cells, then treated seven days later with intratumoural injections of PBS, CFA (0.5 mg/mL heat-killed *Mycobacterium butyricum*), or 10x CFA (5 mg/mL heat-killed *M. butyricum*). FNA samples were collected from half the mice in each treatment group on either day 3 or 4 and on day 11 post-treatment for analysis with flow cytometry. **(B)** Analysis up to day 15 found that CFA treatments did not affect tumour growth. Data from individual mice that were FNA-sampled (closed circles) and non-FNA-sampled (open squares) mice are also shown. Error bars indicate standard error. **(C)** One 10x CFA-treated mouse fully regressed, marking the first instance observed by our laboratory of a CT26 tumour regression following intratumoural CFA monotherapy. Survival was not observed to be affected by treatment. However, this may have been due to the number of animals that were prematurely euthanised due to ulceration (including the regressor) and censored from the analysis. The performance of the linear mixed-effects regression (LMER) model used in (B) is presented in Figure A.15 and the hazard ratios for the survival analysis are in Table B.10. A more detailed presentation of the survival data is also included in Figure A.16. Combined data from two experiments are shown.

0.05 mL of PBS, CFA (0.5 mg/mL heat-killed *M. butyricum*), or 10x CFA (5 mg/mL heat-killed *M. butyricum*; Figure 6.5A). This experiment was repeated twice, and FNA samples were collected from half the mice in both experiments (to confirm that the sampling procedure did not affect treatment outcomes). In the first experiment, FNAs were collected on days 3 and 11, while mice in the second experiment were sampled on days 4 and 11. Animals were euthanised when the tumours reached 15 mm in average tumour diameter or (as dictated by the AEEC in the second experiment only) if the animals developed ulcerated tumours.

As shown in Figure 6.5B, analysis of the combined tumour growth from both experiments in the first 15 days following treatment with a linear mixed-effects regression (LMER) model found no significant effect of therapy. This result was obtained despite the observation that injection of CFA into tumours produced an immediate transient increase in size due to the emulsion's thick, viscous consistency (compare the blue line with the red and purple lines in Figure 6.5B). That said, all the animals tolerated the CFA treatments well. Since half the animals were FNA sampled, we could confirm with statistical testing that the procedure did not influence the tumour growth trajectories ($p = 0.295$).

While tumour growth was not impacted, we observed one mouse regress following treatment with 10x CFA – the first instance observed by our laboratory of a CT26-challenged mouse regress following CFA *monotherapy* (Figure 6.5C). Unfortunately, the AEEC heavily influenced this study's outcome, especially the data collected from the second experiment. They directed us to euthanise 25% (12/48) of all mice, including the regressor mouse, across the two experiments because the animals developed ulcerated tumours or had a scab at the site of tumour regression. These animals were consequently censored from the survival analysis. Thus, while overall survival was not observed to be impacted by treatment, this may have resulted from the number of mice we were required to pre-maturely euthanise, thus making the true impact of these treatments on survival impossible to determine.

Regardless, we were encouraged to have observed our laboratory's first CFA-treated CT26-challenged regressor mouse from these experiments, and we believe that further investigation of this modification to the CFA therapy is warranted.

6.3.2 10x CFA-treated mice had significantly higher proportions of neutrophils

As explained in the previous section, FNA samples were collected from half the mice in both experiments. These samples were analysed with flow cytometry using two similar gating strategies. In the first experiment, FNA samples were assessed using the strategy shown in Figure 6.6, identifying eight immune cell subsets across the innate and adaptive arms of immunity. The stain for the second experiment was slightly modified by combining the live/dead discriminator (7-AAD) and red blood cell marker (TER-119) into a single dump channel (Figure 6.7, Table 2.3 on page 44). This change allowed us to include anti-CD101-PE and anti-CD25-PE antibodies in the innate and adaptive stains, respectively. Other than this modification, the gating strategy used to identify the eight immune cell subsets shown in Figure 6.6 was similar across both experiments. Thus, the data were combined for analysis.

When the TILs were surveyed and statistically analysed (all FNA samples passed quality control, Figure A.18), we found that 10x CFA-treated mice had highly significant increases in proportions of neutrophils on days 3 and 4 relative to the other treatment groups (Figure 6.8A). The therapy also significantly decreased the proportions of macrophages and monocytes relative to the CFA-treated mice. That said, the decreases in cell types other than neutrophils on days 3 and 4 in the 10x CFA-treated mice (significant for the macrophages and monocyte populations but indicating a smaller trend for all others) may be due to the large influx of neutrophils into the tumour.

Our previously published work showed that at least one tumour model treated with CFA appears to benefit from a high early neutrophil infiltrate (P815, C. S. E. Carroll et al., 2021). To determine if a similar trend was apparent in this study, the FNA profiles of all sampled mice were individually collated and arranged by the number of days post-treatment the animals survived. These data are presented in Figure 6.9. Unfortunately, 12 of the 25 mice (48%) presented in this figure were prematurely euthanised because of ulcerated tumours, thus making it impossible to conclude whether those animals with high neutrophil infiltrates would have responded to treatment (e.g., see Mice 142, 127, 154, and 168 in the bottom row). However, finding that three of the five longest-living

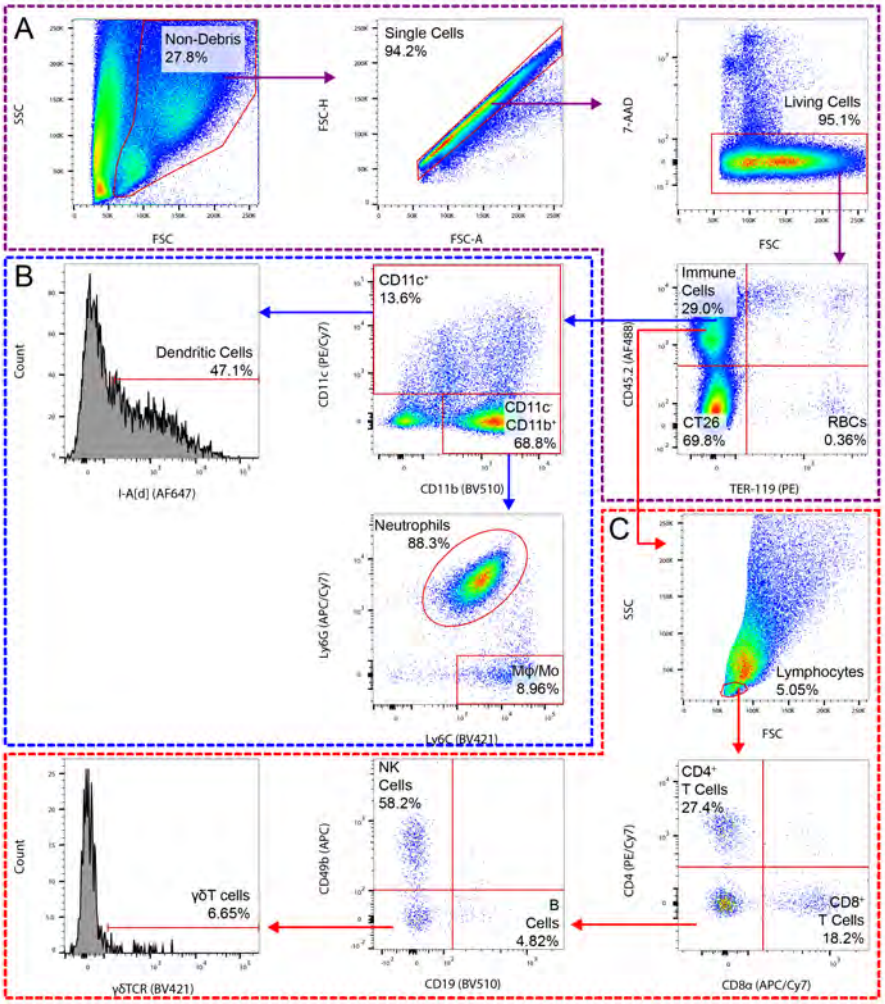


Figure 6.6: First gating strategy used to examine TILs in 10x CFA experiments. Data from all FNA samples collected in the first experiment were concatenated in this plot to facilitate identification of cell populations. FNA samples were distributed between two staining cocktails, one designed to identify innate immune cells and the other to identify adaptive immune cells. **(A)** The initial gates are the same for both stains and were designed to isolate single living immune cells and exclude cellular debris, dead cells, and red blood cells (RBCs). **(B)** The innate immune cell gating strategy proceeds from living CD45.2$^+$ immune cells sorted into either CD11c$^+$ or CD11b$^+$ CD11c$^-$ gates. Cells in the CD11c$^+$ gate were then further identified as dendritic cells by expression of MHC-II (I-A[d]). The cells in the CD11b$^+$ CD11c$^-$ gate were further resolved as either neutrophils (Ly6G$^+$ Ly6C$^+$) or macrophages/monocytes (Mϕ/Mo; Ly6G$^-$ Ly6C$^+$). **(C)** The gating strategy used to identify adaptive immune cells started with an explicit lymphocyte gate (FSC^{lo} SSC^{lo}), made to limit autofluorescence from granular innate immune cells. CD4$^+$ and CD8$^+$ T cells were identified first, with the double negative population then further identified as NK cells (CD49b$^+$) or B cells (CD19$^+$). Cells negative for the other adaptive markers were gated for $\gamma\delta$ T cells based on $\gamma\delta$TCR expression.

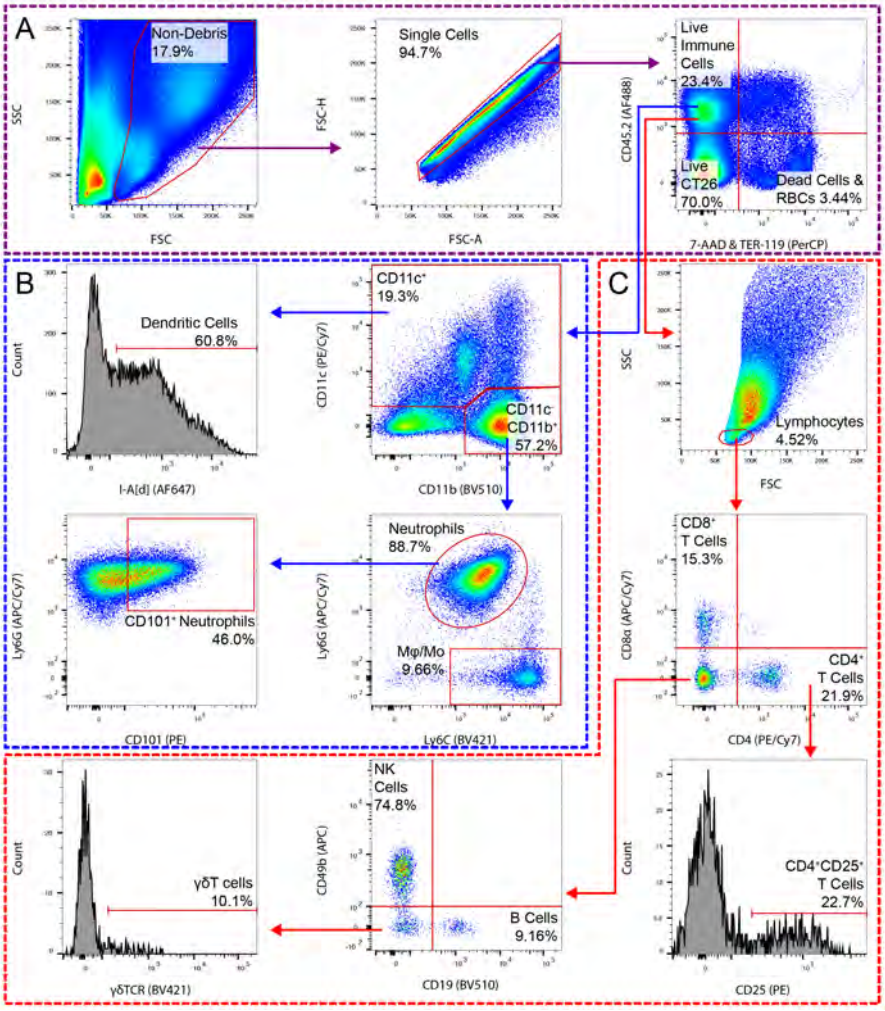


Figure 6.7: Second gating strategy used to examine TILs in 10x CFA experiments. This gating strategy is identical to that shown in Figure 6.6, but was modified to identify CD101⁺ neutrophils and CD25⁺ CD4⁺ T cells. **(A)** The initial gates are the same for both the innate and adaptive stains and were designed to isolate single living immune cells. Here, the dead 7-AAD⁺ and TER-119⁺ RBCs were combined in a single dump channel when gating for live immune cells. **(B)** The innate immune cell gating strategy proceeds similarly to that shown in Figure 6.6B. Here, mature neutrophils were identified among the neutrophil population based on the surface expression of CD101. **(C)** The gating strategy used to identify adaptive immune cells is identical to that shown in Figure 6.6C. Here, activated CD4⁺ T cells were identified based on CD25 expression. CD25⁺ CD4⁺ T cells can be regulatory T cells or activated T cells. Mϕ, Macrophages; Mo, Monocytes.

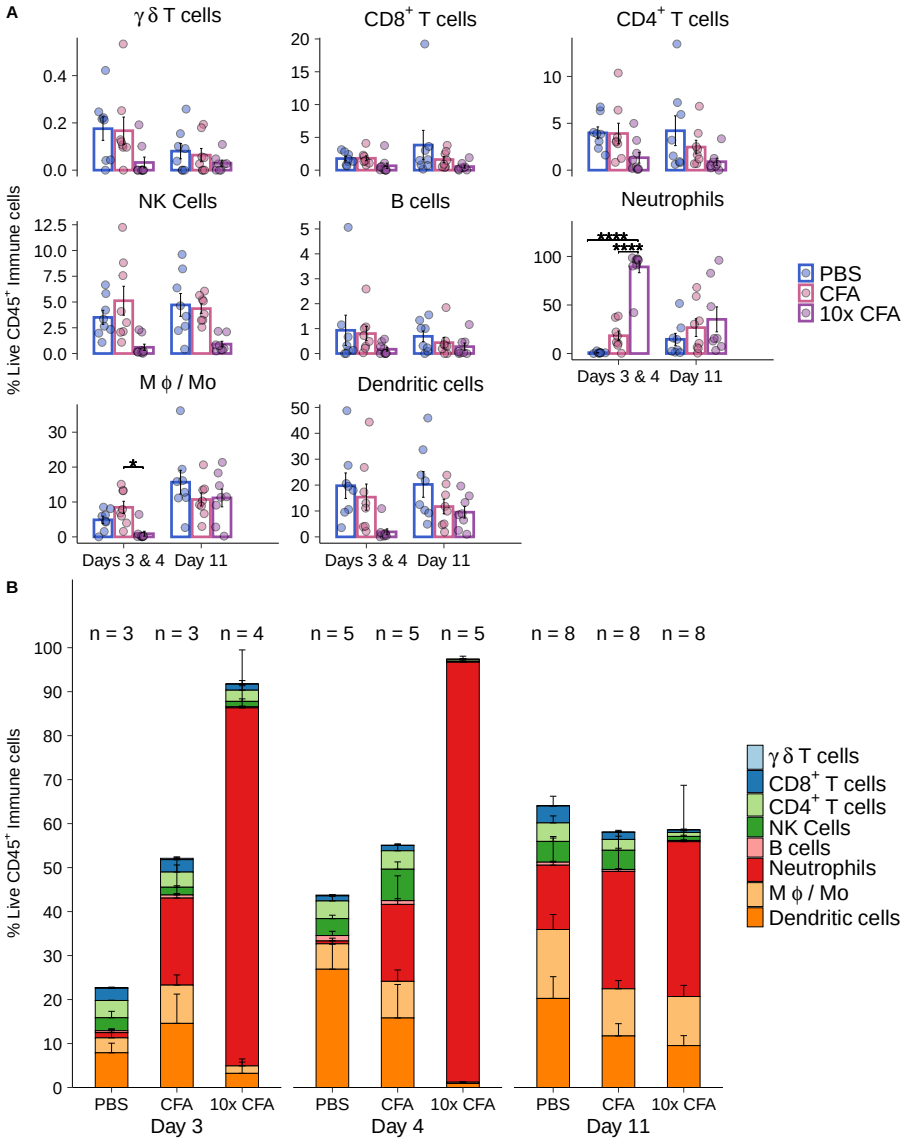


Figure 6.8: 10x CFA significantly increased the proportion of tumour-infiltrating neutrophils by days 3 and 4. **(A)** Eight different immune cells were assessed with the gating strategies presented in Figures 6.6 and 6.7. Mice treated with 10x CFA had significantly higher proportions of tumour infiltrating neutrophils by days three and four relative to the other treatment groups. They also had significantly lower proportions of macrophages and monocytes relative to CFA-treated mice. Each dot represents a sample from a single mouse. Samples collected on days three and four were combined in the statistical analysis. **(B)** The data presented in (A) are shown as a stacked bar graph, with data from days 3 and 4 separated, to give context for tumour infiltrating leukocyte proportions. The numbers of mice sampled on each day in each treatment group are listed above the plots. The performance of each cell population's LMER model is presented in Figure A.19. Data from two experiments are shown. Error bars represent standard error. ****, $p < 0.0001$; *, $p < 0.05$, Mϕ, Macrophages; Mo, Monocytes.

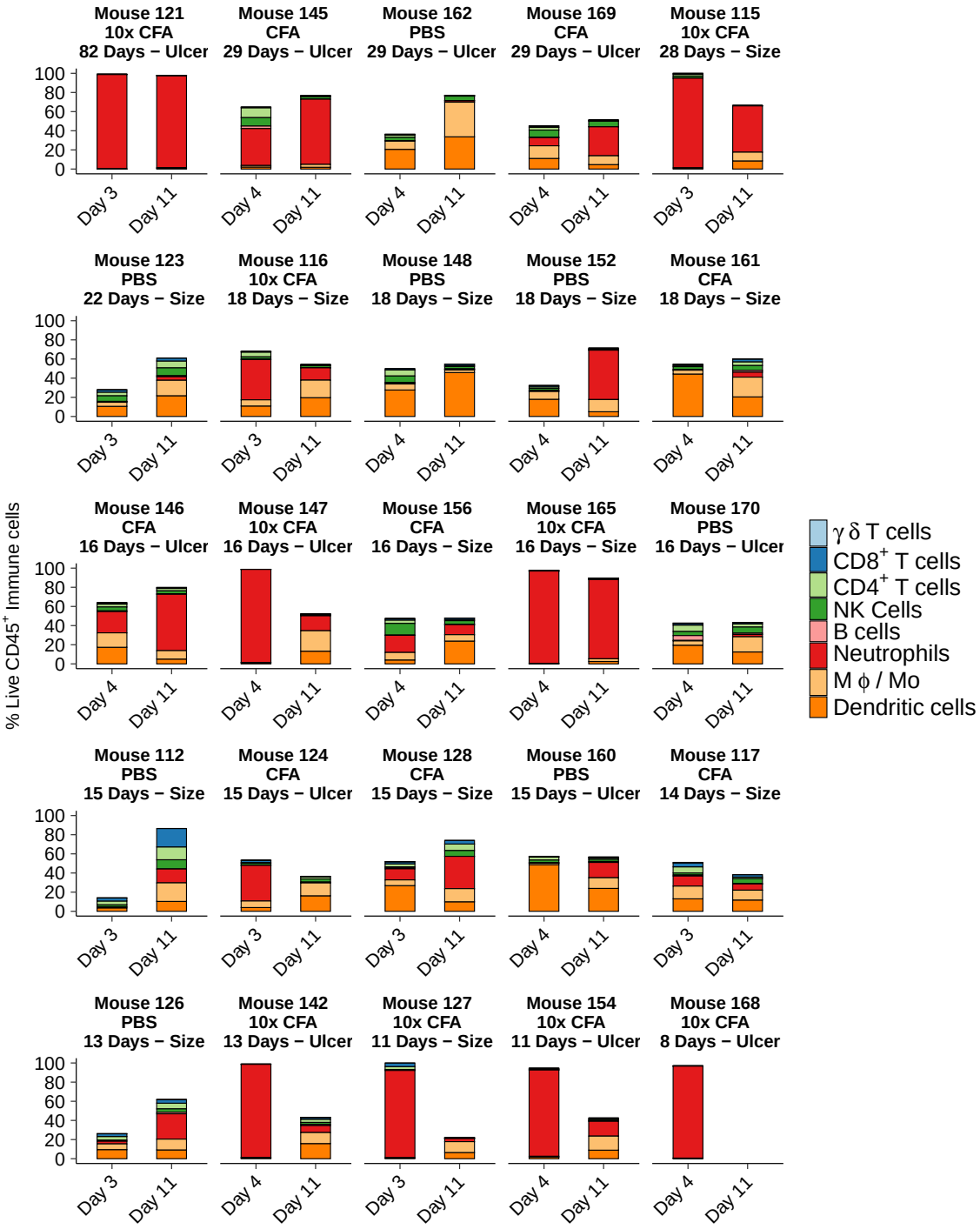


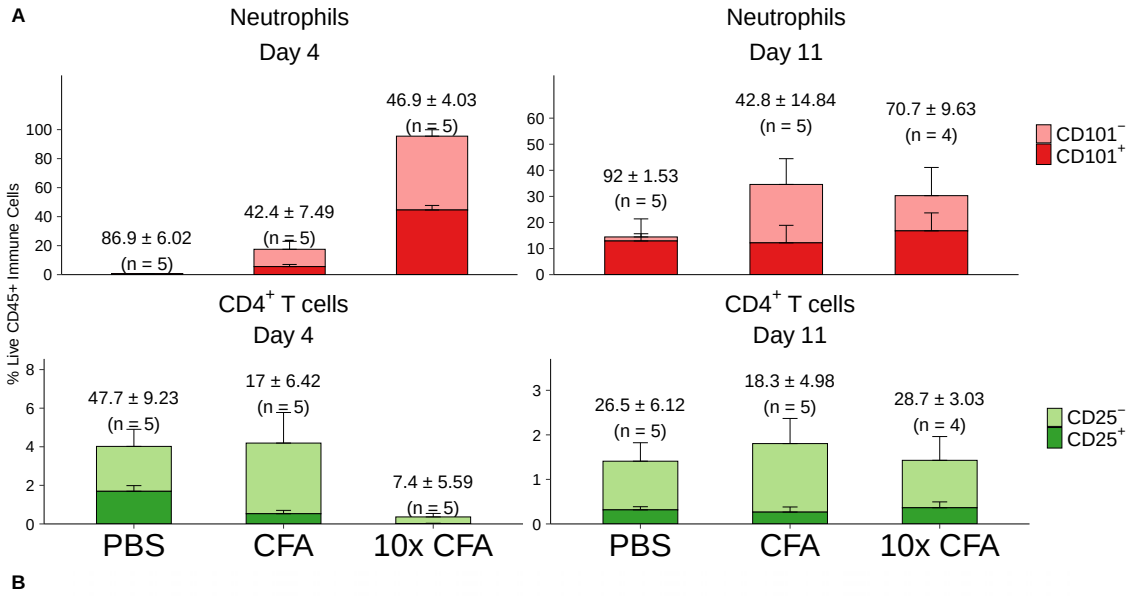
Figure 6.9: The longest-lived CFA- and 10x CFA-treated mice had large proportions of tumour-infiltrating neutrophils. The proportions of TILs for each FNA sampled mouse across two experiments are shown. The mouse identification number, treatment received, number of days post-treatment lived, and the reason the mouse was euthanised is noted above each plot. Size indicates mice were euthanised because the average tumour diameter reached 15 mm. The mice are ordered by the days they lived post-treatment, with the longest living in the top left and the shortest living in the bottom right. Three of the five longest-living mice had high neutrophil proportions on both days sampled. The TILs in the mouse that fully regressed (Mouse 121) were almost exclusively neutrophils on both days.

mice had high proportions of neutrophil infiltrate is encouraging. Indeed, the sole regressor mouse, Mouse 121, was found to have had almost exclusively neutrophils infiltrating the tumour on both days sampled.

6.3.3 All neutrophils increased while regulatory T cells decreased

Given the high proportions of neutrophils induced by our CFA treatments and the controversial role these cells play in cancer immunotherapies, we asked what kind of neutrophils our CFA therapies were attracting into the tumour. We hypothesised that the neutrophils we were finding adopted an immunostimulatory (or at least, non-immunosuppressive) phenotype. A literature review found that immature neutrophils are more immunosuppressive in a cancer context (Evrard et al., 2018; B. E. Hsu et al., 2019; Mackey et al., 2019; Rice et al., 2018; Sagiv et al., 2015) and that the surface marker CD101 was recently identified as a marker for neutrophil maturity (Evrard et al., 2018). Hence, we modified the staining panel and gating strategy for the second experiment to that shown in Figure 6.7 to distinguish mature $CD101^+$ neutrophils from immature $CD101^-$ neutrophils. We also wanted to determine if any differences in proportions of $CD25^+$ $CD4^+$ T cells, a typical regulatory T cell phenotype (Spolski et al., 2018), could be found in the tumour following treatment. These analyses are shown in Figure 6.10.

We had shown that there was a significant increase in neutrophils by day 4 in the 10x CFA-treated mice (Figure 6.8A). However, the results presented in Figure 6.10 show that this influx of neutrophils into the tumor include equal proportions of both $CD101^-$ and $CD101^+$ neutrophils, thus indicating that CFA and 10x CFA did not favour the influx of either phenotype. For example, we discovered that although tumour-infiltrating neutrophils were present in low numbers among the PBS-treated control mice, the majority of these neutrophils were $CD101^+$ on both days (day 4: 86.9%, day 11: 92.0%). However, in CFA- and 10x CFA-treated mice on day 4, the proportion of mature $CD101^+$ cells among the neutrophil population decreased to less than half of all tumour-infiltrating neutrophils (42.4% and 46.9%, respectively). These findings were unexpected because we had assumed the large influx of neutrophils would be composed of mostly mature or immature neutrophils rather than equal proportions of both. This trend continued to day



B

Cell Type	Day	Treatment	Proportion (%)	P-value
$CD25^+$ $CD4^+$ T cells	Day 4	PBS	47.7 ± 9.23	–
		CFA	**17.0 ± 6.42**	**p < 0.0001**
		10x CFA	**7.40 ± 5.59**	**p < 0.0001**
	Day 11	PBS	26.5 ± 6.12	–
		CFA	18.3 ± 4.98	ns
		10x CFA	28.7 ± 3.03	ns
$CD101^+$ Neutrophils	Day 4	PBS	86.9 ± 6.02	–
		CFA	**42.4 ± 7.49**	**p < 0.0001**
		10x CFA	**46.9 ± 4.03**	**p < 0.0001**
	Day 11	PBS	92.0 ± 1.53	–
		CFA	42.8 ± 14.8	ns
		10x CFA	70.7 ± 9.63	ns

Figure 6.10: 10x CFA-treated mice had significantly more neutrophils and significantly fewer $CD25^+$ $CD4^+$ T cells by day 4 post-treatment by proportion. **(A)** FNA samples from days 4 and 11 were assessed for $CD101^+$ neutrophils and $CD25^+$ $CD4^+$ T cells according to the gating strategy presented in Figure 6.7. The numbers above each bar indicate the average proportion of neutrophils or T cells that were $CD101^+$ or $CD25^+$, respectively. They also show the standard error of those proportions and the number of mice sampled. Error bars represent the standard error. **(B)** The statistical analysis results of the data presented in (A) comparing the proportions of neutrophils and $CD4^+$ T cell populations between each treatment group on both days. No corrections were made for multiple comparisons. The performance of each cell population's LMER model is presented in Figure A.20. Data from one experiment are shown.

11 in the CFA-treated mice, whose proportions of mature neutrophils remained stable at 42.8%. On the other hand, these neutrophils increased from 46.9% on day 4 to 70.7% on day 11 among the 10x CFA-treated mice. It is unclear whether this result indicates neutrophils are maturing *in situ* or if additional mature neutrophils are infiltrating the tumour at later time points and replacing the immature CD101$^-$ neutrophils. This is a question that requires further investigation.

By day 4, all neutrophils were increased in 10x CFA-treated mice, whereas CD4$^+$ T cells exhibited a different pattern and decreased proportionally in these mice but remained unchanged in PBS- and CFA-treated mice. However, the proportion of CD25$^+$ CD4$^+$ T cells was significantly lower in the 10x CFA-treated mice than in the PBS-treated control mice, and the difference approached significance among CFA-treated mice ($p = 0.08$, see Figure 6.10B). This result could be interpreted as 10x CFA therapy decreasing the intratumoural Treg cell population, which constitutively express CD25 (Spolski et al., 2018). However, to confirm this, intracellular FoxP3 staining is required to conclusively identify these cells as CD4$^+$ Treg cells.

This experiment must be repeated to validate these findings. If reproducible, these results suggest that the TME of 10x CFA-treated mice may be an overall less immunosuppressive environment early after treatment, which could facilitate immune rejection of the treated tumour.

6.3.4 10x CFA attracts more immune cells into the tumour microenvironment

We have previously seen that 10x CFA treatment significantly increases the proportion of neutrophils and decreases the proportion of macrophages and monocytes within four days following treatment in our FNA samples (Figure 6.8). However, as we alluded to in section 6.3.2, is this the result of more immune cells infiltrating the tumour or are neutrophils so numerous that they are proportionally dominating the other immune cell types? To try to answer this question, we changed the analysis from measuring proportions of live CD45.2$^+$ immune cells to examining the raw cell counts of the eight identified immune cells in our FNA samples (Figure 6.11). From these data, it is immediately

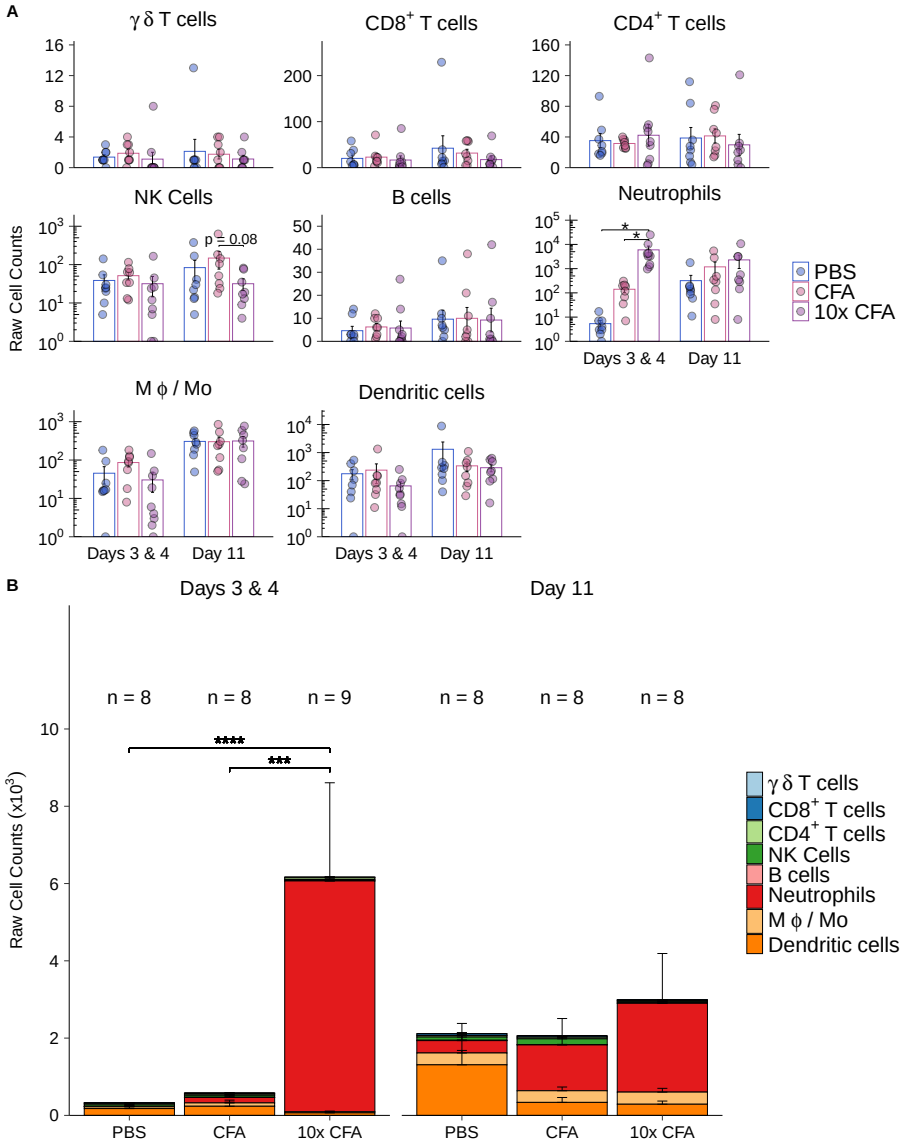


Figure 6.11: 10x CFA therapy promotes more immune cell infiltrates. We investigated if neutrophils were proportionally dominating other tumour-infiltrating immune cells in our FNA samples by re-analysing the data presented in Figure 6.8 and comparing differences in raw cell counts. **(A)** The results showed that 10x CFA-treated mice had a significantly higher number (rather than proportion) of neutrophils than both the CFA- and PBS control-treated mice by days 3 and 4. The y-axes for the NK cells, Neutrophils, Mϕ/Mo, and Dendritic cell plots are presented on a $\log_{10}$ scale to better visualize the numeric differences between the treatment groups. Each dot represents data from a single mouse. **(B)** By days 3 and 4, there was a significant increase in the total number of TILs found within a treated tumor in 10x CFA-treated animals, but not in mice receiving 1x CFA. This increase was driven exclusively by neutrophils. Significance stars indicate statistical differences between log-transformed immune cell numbers among the treatment groups. Error bars in both plots represent the standard error. *** $p < 0.001$; **** $p < 0.0001$, Mϕ, Macrophages; Mo, Monocytes.

apparent that 10x CFA-treated mice had overwhelmingly more immune cells by days 3 and 4, that the majority of these infiltrates are primarily neutrophils, and that there is little change in numbers among the other identified immune cell types. Notably, the difference was significant among the 10x CFA-treated tumours, but not those treated with 1x CFA. Regrettably, the consequences of this difference on treatment outcome could not be determined.

Given these results, we also asked if the CFA treatments caused a systemic immune reaction and tried to answer this question by examining immune cells in other lymphoid organs. We collected and stained single-cell suspensions from bone marrow, spleen, and tumour-draining lymph nodes (TdLNs) and cells prepared from whole-tumour digests and examined them with flow cytometry (Figure 6.12). These tissue samples were collected on day 3 post-treatment and analysed with the gating strategy shown in Figure 6.7. Only three mice were included in this pilot experiment, thus limiting the statistical power of the analysis. However, 10x CFA-treated mice had higher proportions of neutrophils in the spleen and TdLN, and (in agreement with data presented thus far) a Kruskal-Wallis analysis confirmed a statistically higher proportion of neutrophils in the tumour. These data may suggest a systemic effect caused by the 10x CFA treatment, but more validation and larger sample numbers are required to confirm this conclusion.

We have shown that 10x CFA treatments induce more immune cells to infiltrate the tumour within three to four days following treatment, and the immune cell infiltrates are primarily neutrophils as few others are attracted to the tumour early after treatment. Mice treated with 1x CFA also have significantly higher numbers of neutrophils, but they do not reach the numbers found in 10x CFA-treated animals. There is also a hint of a systemic immune reaction which, if true, may have important implications on our CFA therapy's mechanism of action.

6.4 Discussion

This chapter presented data from experiments investigating methods that may improve the effectiveness of intratumoural complete Freund's adjuvant (CFA) therapy. First, we

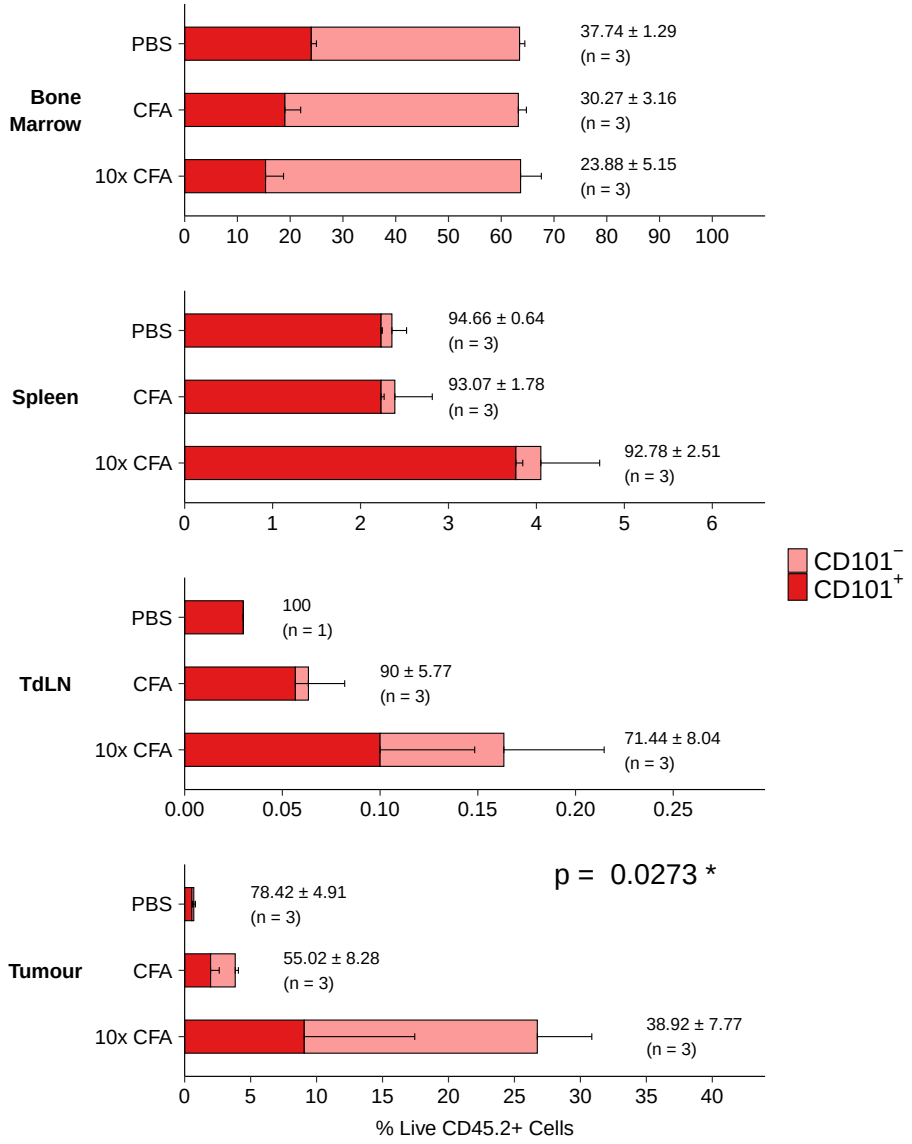


Figure 6.12: 10x CFA-treated mice had numerically higher proportions of neutrophils in bone marrow, spleen, TdLN, and tumour. Single-cell suspensions from bone marrow, spleen, tumour-draining lymph node (TdLN), and tumour were prepared three days after mice were given intratumoural injections of PBS, CFA, or 10x CFA. The cells were stained and analysed for neutrophil populations according to the gating strategy shown in Figure 6.7B. Mice had significantly higher proportions of neutrophils within the tumour and numerically higher proportions in the TdLN and Spleen (though they did approach significance; $p = 0.0608$). Data from one experiment are shown. P-values indicate results of a Kruskal-Wallis statistical test examining total neutrophil proportions. No correction was made for multiple comparisons. The numbers to the right of each bar indicate the average proportion of neutrophils that were CD101$^+$, the standard error of those proportions, and the number of mice sampled. Sample numbers varied since only those containing more than 20 living CD45.2$^+$ cells were analysed. Error bars indicate standard error.

examined if CFA and immune checkpoint therapy could be combined to produce a synergistic effect in the CT26 and 4T1 cancer models. Second, we increased the concentration of heat-killed *M. butyricum* in the CFA preparation by ten-fold, then examined treatment efficacy and systematic effects using the CT26 model. The experiments presented in this chapter are preliminary, but they produced intriguing data and highlighted critical questions regarding the mechanism of action of intratumoural CFA therapy.

6.4.1 Combining with immune checkpoint therapies

Immediately prior to the COVID-19 pandemic, we conducted an experiment wherein we combined intratumoural CFA treatment with systemic immune checkpoint therapies in the CT26 tumour model. Of 96 CT26-challenged mice across nine experiments treated with CFA, this is the first time we observed this tumour model regress following a CFA treatment protocol. Regrettably, the pandemic and the AEEC prevented us from pursuing this finding at the ANU. However, we were extremely fortunate to be allowed to continue our research at the Stanford University School of Medicine. Stanford's animal ethics protocol required that we use the 4T1 tumour model in our experiments, though we found the model was not responsive to intratumoural CFA injections. Furthermore, gross pathology and microscopy assessment found contrasting results between two independent experiments that investigated the impact that CFA and immune checkpoint dual therapy may have on metastatic disease progression.

Several factors may have contributed to CFA's apparent ineffectiveness in the 4T1 tumour model in these experiments:

i) First, we may need to use more mice to see an effect. Figure 1 of Carroll *et al.* (2021) shows that the median survival times for CFA- and PBS-treated mice are 20- and 17.5-days post-treatment, respectively. As the survival of four treatment groups was being compared, many more mice may be required to attain sufficient statistical power to observe an effect.
ii) Second, mice housed at Stanford University will invariably have a different gut microbial composition from mice housed at the ANU because they were kept in

a completely different environment and fed a different diet. Intra-institutional differences have been a well-documented source of experimental variation among mouse cancer studies (Ivanov et al., 2009; Rasmussen et al., 2019; Sivan et al., 2015), and diet influences gut microbial compositions (Hills et al., 2019) that in turn affect cancer therapy outcomes (Gopalakrishnan et al., 2018; Tanoue et al., 2019).

iii) Third, the animals at Stanford were sourced from Jackson Laboratory. In contrast, mice at the ANU were sourced from the Australian Phenomics Facility (APF), and they were initially supplied by Charles River Laboratories International Inc. Thus, variations among the animals used at the two research institutions are compounded by differences in host genetics that may influence the immune response to CFA and checkpoint therapies (Sivan et al., 2015).

iv) Finally, CFA is a complex biological reagent, thus subjecting it to possible batch inconsistency. The CFA containing *M. tuberculosis H37Ra* was supplied by ThermoFisher Scientific Inc., while the CFA containing *M. butyricum* and used in the study by Carroll *et al.* (2021, and all mouse studies by our laboratory at the ANU) was supplied by BD. While differences in *Mycobacterium* spp. within the CFA injections appeared unlikely as causes for therapeutic differences (Figure 6.2C); variations among the other reagents in CFA from different vendors could not be discounted.

Despite not improving survival, we suspected that few 4T1-challenged mice given CFA therapy were becoming sick (an observation also made at the ANU), as most were being euthanised due to tumour size. This led us to question whether CFA impacted the metastatic disease progression. As reported by DuPre and others (DuPre et al., 2007, 2008; DuPre & Hunter, 2007; Pulaski & Ostrand-Rosenberg, 2001) and described in Section 4.5, the 4T1 model spontaneously metastasises to various organs, including the lungs. Since 4T1 cells are resistant to 6-thioguanine, a standard method for identifying the extent of metastatic burden is to dissociate the lungs into a single-cell suspension, expose them to 6-thioguanine on a plate, and count any cells that remain (Pulaski &

Ostrand-Rosenberg, 2001). However, previous attempts to carry out this protocol by our laboratory found it unreliable (C. Carroll, 2016, pp. 138–139). A more straightforward protocol was used after consulting with the Levy Laboratory at Stanford University (Aurelian J. A. Marabelle, private correspondence, 11 June 2022), wherein lungs are perfused with an India ink solution through the trachea and fixed in Fekete's solution (Marabelle et al., 2013; Zimmerman et al., 2010). The result is that all metastases are highlighted as opaque white spots against a pitch-black lung that can be easily counted under a dissecting microscope.

With the help of expert veterinary pathologist Prof Allavena, the metastatic burden of 4T1-challenged mice was examined in two independent experiments, but each yielded very different results. In the first experiment, the India ink method showed high numbers of metastases in mice treated with CFA, and the number of metastases was increased in mice treated with both CFA and immune checkpoint therapies. This second point was a discouraging finding, but the odd miliary pattern the metastases presented (Figure A.17) led us to question whether what we observed were true metastases or fibrotic scarring. We repeated the experiment without the India ink – only NBF was used to fix the lungs – but oddly, the results showed little metastatic disease progression across all four treatment groups. We reasoned that these contradictory results might be due to genetic variations in the cell line acquired from frequent sub-culturing (Ben-David et al., 2018; Cao et al., 2021) or spontaneous mutations that may have arisen in the mouse strain (Chebib et al., 2021). Both theories underly the importance of multiple replicates in mouse tumour experiments.

Understanding the effect of CFA and immune checkpoint therapy combinations on tumour metastasis is critical, but a more appropriate tumour model other than 4T1 is required to answer the question for several reasons. First, the experiments we just presented show that the 4T1 model is not reliably responsive to CFA therapy (Figure 6.2), nor is it responsive to immune checkpoint therapies (Figure 4.7). Second, CFA therapy relies on neutrophils for its therapeutic actions, at least in the P815 tumour model (C. S. E. Carroll et al., 2021). However, 4T1-challenged mice present with severe neutrophilia (Figure 4.10) and how this impacts the CFA mechanism of action is still being determined.

Finally, published research has shown that mice challenged with the 4T1 model and subsequently treated with multiple systemic injections of PD1 blockade antibodies (anti-PD1 [RMP1-14] or anti-PDL1 [10F.9G2]) develop rapid and fatal hypersensitivity and bronchiolitis pneumonia reactions characterised by the interstitial and alveolar neutrophilic accumulation in the lungs (Arai et al., 2022; Mall et al., 2016). While, fortunately, we never observed this reaction in our experiments (most likely due to never giving more than three injections of immune checkpoint therapies), we potentially observed evidence of this neutrophilic accumulation in the lungs when they were microscopically examined for metastases (Figure 6.4F).

Given these points, experiments investigating metastatic formation following CFA therapy require a metastatic disease model responsive to CFA and immune checkpoint therapies and does not induce severe peripheral neutrophilia. The P815 mastocytoma model is an obvious candidate; it is responsive to both CFA (C. S. E. Carroll et al., 2021) and immune checkpoint therapies (Chapter 3, submitted) and spontaneously metastasises to various organs, most prominently the spleen and liver (T. B. Dunn & Potter, 1957). The B16.F10 model may be another, as innate immune-activating adjuvants are required for this tumour model to respond successfully to immune checkpoint therapies (Curran & Allison, 2009; Quezada et al., 2006).

6.4.2 Increasing the concentration of *M. butyricum*

We investigated two ideas for improving CFA, with the second being to increase the concentration of heat-killed M. butyricum in the emulsion from 0.5 mg/mL to 5 mg/mL (10x CFA). Doing so produced our laboratory's first observed CT26 tumour regression following CFA monotherapy, though the treatment's effects on overall survival could not be determined because of the interference of the AEEC. When we examined data from FNA samples and whole-tumour digests, we found that 10x CFA induces a more potent immune reaction, evidenced by significant increases in tumour-infiltrating neutrophils (regardless of maturity status) and decreases in $CD25^+$ $CD4^+$ T cells, a well characterised Treg cell phenotype (Spolski et al., 2018). This effect was much smaller in tumours given

1x CFA injections. Additionally, a systemic effect may have been observed following 10x CFA treatment that was not seen with 1x CFA-treated animals.

That we observed our first CT26 regression following CFA monotherapy was exciting. However, attempts to validate this finding were stymied by the interference of the AEEC, who demanded that we euthanise 1/4 of all animals because of ulceration or scab formation. These premature euthanisations destroyed any attempts at repeating the treatment efficacy study, which was more unfortunate given that our FNA data showed high neutrophil infiltrates in many 10x CFA-treated mice. Our previous work suggests that higher proportions of tumour-infiltrating neutrophils soon after CFA injection correlate well with treatment success in the P815 model (C. S. E. Carroll et al., 2021), which would have been important to determine if the same was true in the CT26 model. Indeed, the sole regressor mouse from these 10x CFA studies had almost exclusively neutrophil infiltrates on both days the tumour was examined with FNA sampling. As the other mice were prematurely euthanised, we will never know if the 10x CFA-treated animals that showed high neutrophil infiltration into the treated tumours would have successfully responded to therapy.

New research continues to challenge our understanding of the neutrophil's role in a cancer context. Renewed interest developed when Fridlender *et al.* (2009) proposed the N1 anti-tumour/N2 pro-tumour dichotomy and showed that the TME largely polarises neutrophils into an N2 phenotype. Over the past several years, research has found that the immunobiology behind this question is far more complex. It is reviewed in detail in an excellent consensus statement after a meeting of several experts at the Banbury Centre at the Cold Spring Harbour Laboratory (Quail et al., 2022). In it, they describe how recent evidence shows that the N1 anti-tumour/N2 pro-tumour dichotomy, though appropriate at the time it was proposed, is now too simplistic. For instance, Zilionis *et al.* (2019) used single-cell RNA sequencing to identify five distinct neutrophil populations associated with human lung tumours. Three of these populations are conserved in mice, and one is uniquely associated with tumours. Neutrophil maturity has also been found to correlate with pro- or anti-tumour characteristics, with immature neutrophils frequently (but not

exclusively) found to be more immunosuppressive (B. E. Hsu et al., 2019; Mackey et al., 2019; Sagiv et al., 2015).

Hence, we wanted to examine more closely what kind of neutrophils our CFA treatments attracted into the TME. Using CD101 as a marker for neutrophil maturity, we found the proportions of all neutrophils – both mature $CD101^{+}$ and immature $CD101^{-}$ – infiltrating the tumour were increasing following 10x CFA treatment. Furthermore, they were approximately equally distributed between mature $CD101^{+}$ and immature $CD101^{-}$ phenotypes. This result was in contrast with what was found in FNA results from PBS-treated control mice, whose few neutrophils present within the tumour were mostly mature $CD101^{+}$ neutrophils. The implications of this finding on treatment efficacy still need to be understood, and more experimentation is required before any conclusions can be made.

6.4.3 Conclusion

This chapter provided preliminary data from studies investigating two ways to improve CFA's therapeutic efficacy. The first, co-treating with systemic immune checkpoint therapies, highlighted the importance of selecting appropriate tumour models and maintaining consistency among animals, tools, reagents, and vendors. The second found that increasing the concentration of *M. butyricum* in the emulsion by ten-fold significantly increased immune filtration into the tumour, and this influx was composed of approximately equal ratios of mature and immature neutrophils. Both studies are preliminary, but they lay the groundwork for future investigations to answer these questions.

7 General Discussion

Contents

7.1 Introduction 169
7.2 Improving our Laboratory's CFA Therapy 172
7.2.1 Combining with immune checkpoint therapies 173
7.2.2 Increasing concentration of *Mycobacterium butyricum* 177
7.3 Finding an Appropriate Tumour Model 181
7.3.1 The MCA-205 and MC38 models 182
7.3.2 The B16.F10 and 4T1 models 184
7.3.3 The CT26 and P815 models 186
7.4 Our First Antibiotics Experiment 189
7.5 Challenges to Progress 193
7.6 Support for Our Hypothesis! 194
7.7 Conclusion 196

7.1 Introduction

This PhD project had two aims: the first was to determine how the gut microbiome impacts immune checkpoint therapy, and the second was to determine if we could improve our novel intratumoural Complete Freund's Adjuvant (CFA) therapy.

To accomplish the first aim, we evaluated six murine tumour models across three strains of inbred mice and found that the CT26 colon cancer (syngeneic to BALB/c) and P815 mastocytoma (syngeneic to DBA/2) models are responsive to anti-CTLA4 therapy;

they were not overly aggressive, meaning the meaningful data could be acquired before the animals were euthanised, and our fine-needle aspirate (FNA) sampling protocol did not impact tumour growth trajectories or treatment outcomes. Our work with the P815 model has since been submitted to *The Journal of Immunology* and is currently undergoing revision for publication.

We later tried to deplete the gut microbiota of CT26-challenged BALB/c mice with a broad-spectrum antibiotic cocktail used in multiple studies published in high-impact journals containing colistin, ampicillin, and streptomycin in their drinking water (Mager et al., 2020; Routy et al., 2018; Viaud et al., 2013). However, BALB/c (and DBA/2) mice would not willingly drink the solution and consequently became severely dehydrated, thus obliging us to modify our antibiotic feeding schedule. A literature search revealed that (a) most published studies that fed mice antibiotics to deplete their gut microbiota used the C57BL/6 strain in their experiments and (b) that this mouse strain is more tolerant of the solution's bitter taste. We confirmed the latter point by performing taste-test experiments among the C57BL/6, BALB/c, and DBA/2 mouse strains with different combinations and concentrations of the antibiotics. The results of those experiments are published in *The Journal for ImmunoTherapy of Cancer* to highlight this technical issue and hopefully encourage more research into how gut microbes influence immune checkpoint therapies in tumour models not syngeneic to C57BL/6 mice (Almonte et al., 2022).

Regardless of the animals' willingness to drink water spiked with antibiotics, bacterial cultures from faecal pellets confirmed that the mice were consuming the drugs on food pellets wetted with the antibiotic solution. This method was successful in staving off dehydration and depleting the gut microbiomes in CT26-challenged BALB/c mice. Contrary to what has been reported in the literature, gut dysbiosis did not decrease the survival of mice treated with anti-CTLA4 therapy in this tumour model. However, examination of tumour-infiltrating leukocyte (TIL) compositions with FNA sampling and flow cytometry suggested that antibiotics consumption may cause differences in TIL profiles; mice fed antibiotics had significantly lower $CD4^+$ and $CD8^+$ T cells than those fed normal tap water. Hence, while anti-CTLA4 treatment outcomes in the CT26 model were not negatively impacted by gut microbiome depletion, there was still evidence of

an altered immune state. Repeat experiments are required to examine the implications and validate these findings.

The second aim of this project was to determine if we could improve our intratumoural CFA therapy, which was shown effective in syngeneic murine models, naturally occurring canine and equine cancers, and is well tolerated by human patients (C. S. E. Carroll et al., 2021). Both options were examined with preliminary studies

The first idea was to determine if co-injection of intratumoural CFA with systemic immune checkpoint therapy improves the therapeutic response over either treatment given alone. A pre-COVID-19 preliminary experiment performed at the ANU immediately before nationwide lockdowns suggested that CT26, which does not respond to CFA monotherapy, responded to a treatment protocol involving co-injection of intratumoural CFA with systemic anti-CTLA4 therapy. We continued this investigation in the laboratories of Prof Mark Davis and Prof Yueh-Hsiu Chien at the Stanford University School of Medicine. There, we used the 4T1 breast cancer model in our experiments because their animal ethics protocol did not permit the use of the CT26 model, and we had previously demonstrated that the 4T1 model is responsive to intratumoural CFA therapy. However, experiments conducted at Stanford University did not show improved survival among CFA-treated 4T1-challenged mice. Despite a lack of response to treatment, we observed fewer mice among the treated cohort becoming sick, leading us to investigate what impact CFA and immune checkpoint therapy combination treatments may have had on metastatic disease progression. However, two independent experiments examining this question delivered conflicting results. Collectively, these studies led us to conclude that experimentation with a different tumour model is required to sufficiently investigate both how CFA combination therapies impact treatment outcomes and how CFA impacts metastatic disease progression.

The second option we examined was increasing the concentration of the heat-killed *Mycobacterium butyricum* in the CFA emulsion from 0.5 mg/mL to 5 mg/mL (a ten-fold increase in concentration, 10x CFA). We observed our laboratory's first CT26-challenged regressor mouse following treatment with a CFA monotherapy (treated with 10x CFA).

Furthermore, 10x CFA induces a significantly increased number of immune cells infiltrating the tumour, which is primarily composed of neutrophils. These data suggest that increasing the concentration of innate immune-stimulating pathogen-associated molecular patterns (PAMPs) within the tumour microenvironment (TME) may stimulate a stronger innate immune response. Previous research from our lab shows this may produce a more favourable immunotherapeutic effect against solid, treatable tumours (C. S. E. Carroll et al., 2021).

All the experiments presented in this dissertation rely on a fundamental premise: intratumoural bacteria, whether sourced from the gut or intentionally injected, can initiate a robust immune response against the malignancy. Unfortunately, the aims of this PhD project were only partially achieved, primarily due to an unreasonable and dilatory Animal Experimentation Ethics Committee (AEEC) and delays caused by the global COVID-19 pandemic. Despite these barriers to progress, this project lays the groundwork for future investigations into bacteria's important role in our most advanced cancer therapies and suggests methods that may improve our laboratory's novel bacteria-based cancer immunotherapy.

7.2 Improving our Laboratory's CFA Therapy

One aim of this project was to investigate methods of potentially improving our intratumoural CFA therapy. To briefly recount the history of this idea, Aude Fahrer wrote an essay explaining the merits of CFA as a cancer therapy in 2012 (Fahrer, 2012). We published results supporting the claim ten years later in *The Journal for ImmunoTherapy of Cancer* that presents data showing the efficacy and safety of the treatment in three syngeneic mouse tumour models, horse melanomas and dog mastocytomas, and 12 cancer patients (C. S. E. Carroll et al., 2021). The therapy significantly improved the survival in mice challenged with P815 and 4T1 tumour models, and complete tumour regressions were observed in all three non-human species following the treatment. Upon further investigation of the mechanism, we found that CFA therapy appears to rely on a strong initial innate immune response that involves primarily neutrophils, which precedes

an anticancer adaptive immune response. We also found that human cancer patients tolerated multiple intratumoural CFA injections (up to 2 mL intratumoural injections at 6-week intervals) and an abscopal anti-tumour effect was observed in one treated patient.

Given these findings and considering that CFA therapy has the potential to be an affordable and accessible cancer immunotherapy option, we wanted to find ways to improve its efficacy. We considered two strategies. The first was to combine intratumoural CFA with systemic immune checkpoint therapies, thus merging two therapies that each targets either the innate or adaptive arms of immunity. The second was to increase the concentration of the *Mycobacterium* sp. in the emulsion, thus supplying more PAMPs and enhancing the therapy's potential for stimulating an intense anti-tumour immune reaction.

7.2.1 Combining with immune checkpoint therapies

The first method we investigated to improve CFA efficacy was to combine it with systemic immune checkpoint therapies. Several studies have leveraged the idea of improving immune checkpoint treatment outcomes using reagents that activate innate immune cells via surface PRRs (e.g., toll-like receptors [TLRs], Table 1.3 on page 30) on myeloid cells. For example, we have previously shown that the CT26 model is resistant to anti-PD1 therapy (Figure 4.11), but Wang *et al.* (2016) have demonstrated that CT26 can be responsive to systemic anti-PD1 therapy when combined with intratumoural injections of CpG oligodeoxynucleotide (CpG ODN; a TLR9 agonist). Tsukamoto *et al.* (2019) injected mice with an agonistic anti-TLR4 antibody to improve immunotherapy efficacies in EG7-OVA, EL4, and B16.F10 mouse models, and responses to anti-PD1 in MC38-challenged mice. Jeong *et al.* (2020) systemically injected lipid nanoparticles (LNPs) composed of *E. coli*-derived lipids as TLR4 agonists that boost dendritic cell maturation and enhance anti-PD1 efficacy in B16.F10-challenged mice. Finally, Sagiv-Barfi *et al.* (2018) combined agonist anti-OX40 with CpG ODN to promote impressive therapeutic responses against cancer with vaccine-like effects.

Unlike these studies, which investigated individual PRR agonists, CFA has the advantage of supplying a consortium of PAMPs to engage numerous PRRs, all supplied by the heat-killed *M. butyricum* included in the emulsion (Table 1.2 and references therein,

page 27, Billiau & Matthys, 2001). Thus, we hypothesised that mice receiving both systemic injections of immune checkpoint therapies and intratumoural CFA injections would have improved therapeutic outcomes resulting from direct engagement with innate and adaptive immunity.

In a preliminary experiment conducted immediately before the Australian Government imposed nationwide lockdowns in response to the COVID-19 pandemic, we found that the CT26 model responded to CFA therapy when combined with systemic anti-CTLA4 antibody. Unfortunately, no FNA samples could be collected in this experiment due to COVID-19 restrictions, so we are uncertain how TIL profiles may have differed between responding and non-responding mice. However, using data extrapolated from other experiments and presented in Figures 6.8, 6.9, and 6.11, we can speculate that CFA monotherapy's ineffectiveness in this model may be due to limited neutrophil infiltration into the TME following treatment (Andrew, 2020; C. Carroll, 2016; C. S. E. Carroll et al., 2021). Combining intratumoural CFA with systemic anti-PD1 and anti-CTLA4 dual therapy (tri-therapy) initially showed promise, as 3/5 mice had their tumour growth stall and one completely regressed. Unfortunately, the only mouse that regressed was later found dead. Like the CT26 mouse that regressed after being given isotype control therapy in Figure 4.11, we do not have an explanation for its sudden demise as a necropsy could not determine a cause of death. Importantly, our laboratory has since repeated the experiment (underway as of this writing). The preliminary data is encouraging as mice given tri-therapy have lived much longer than the pilot experiment presented in this dissertation.

The findings from the pre-COVID-19 preliminary experiment were encouraging. However, given the challenges associated with the ANU AEEC and obtaining the required reagents, we found it best to pursue the question elsewhere. Fortunately, I had the incredible opportunity of pursuing the research in the laboratories of Prof Yueh-Hsiu Chien and Prof Mark Davis at the Stanford University School of Medicine. There, we re-attempted the experiment using the 4T1 breast cancer model in BALB/c mice, which we previously found responsive to CFA monotherapy (C. S. E. Carroll et al., 2021).

Unfortunately, the experiment at Stanford University did not present the same improvements in survival with CFA monotherapies among 4T1-challenged mice that we observed at the ANU. Several explanations may contribute to these differences in treatment outcomes and were discussed in Section 6.4.1. First, we may not have used enough animals to observe an effect as the median survival times for CFA- and PBS-treated 4T1-challenged mice are 20- and 17.5-days post-treatment, respectively (C. S. E. Carroll et al., 2021). As we were comparing the survival among four treatment groups, more animals would have been required to achieve sufficient statistical power to observe an effect.

Second, CFA is a complex biological reagent, thus making it sensitive to possible batch effects. The CFA used at Stanford University was sourced from ThermoFisher Scientific Inc. (ThermoFisher), while the CFA used by Carroll *et al.* (2021) was supplied by Becton, Dickinson, and Co. (BD). We did not initially source the treatment from BD at Stanford University because the lead time was unacceptably long, and we only had six months to perform our experiments. Notably, the CFA from ThermoFisher also contained *M. tuberculosis H37Ra* while the CFA from BD contained *M. butyricum*. While different strains of *Mycobacterium* spp. can have different effects on immune responses (Carmona et al., 2013; Shah et al., 2013), the results of the small pilot experiment presented in Figure 6.2 suggests that the different *Mycobacterium* spp. in the CFA preparations was not the cause for the disparate treatment outcomes found in experiments between the two institutions.

A third explanation may be the genetic and gut microbial heterogeneity that is an inevitable consequence of sourcing mice from different suppliers. The ANU sources all BALB/c mice from Charles River Laboratories International Inc. (Charles River) and maintains an in-house colony at the Animal Phenomics Facility (APF, Canberra, Australia) for institutional mouse research. All the mice used in our studies at Stanford were supplied and delivered directly from the Jackson Laboratory (JAX). Intra-vendor variation has been a well-known cause of complications in the reproducibility of animal research and cancer treatment responses (Ivanov et al., 2009; Rasmussen et al., 2019; Sivan et al., 2015). Furthermore, mice sourced from different vendors have unique gut microbiomes (Ivanov et al., 2009; Sivan et al., 2015); both the environment they are

housed in and the diet they are fed have profound impacts on gut microbial composition (Hills et al., 2019; Hufeldt et al., 2010), which in turn can impact on cancer immunotherapy outcomes (Gopalakrishnan et al., 2018; Tanoue et al., 2019).

Despite the lack of a therapeutic response to CFA among 4T1-challenged mice at Stanford University, we continued to observe that fewer CFA-treated animals were becoming sick. Indeed, this is an observation made among all 4T1-challenged mice treated with CFA, both at the ANU and at Stanford University, though at this stage, any correlation with treatment is speculative. Illness in tumour-challenged mice indicates metastatic disease progression, which is the primary cause of death among human cancer patients. At the ANU, we had speculated that CFA was improving survival in 4T1-challenged mice by promoting a systemic effect and reducing metastatic burden (C. Carroll, 2016, pp. 138–139). Indeed, we observed that CFA injections reduced the metastatic burden in P815-challenged DBA/2 mice as fewer liver metastases were found at necropsy (Andrew, 2020, p. 90).

To examine if our CFA treatments were impacting metastatic disease progression, we needed to accurately quantify the number of metastases. The 4T1 model is resistant to the carcinogen 6-thioguanine, hence providing a method for counting micro-metastases in distant organs much like one would use antibiotics to select for antibiotic-resistant bacteria (Pulaski & Ostrand-Rosenberg, 2001); single-cell suspensions of the tissue of interest would be prepared, plated, and exposed to 6-thioguanine for a time, then any remaining colonies (the 4T1 metastases) would be counted. Our laboratory had previously attempted this protocol without success, but an alternative method (Zimmerman et al., 2010) was identified after consulting with other laboratories at Stanford University (Aurelian J. A. Marabelle, personal correspondence, 11 June 2022). Lung metastases can be counted by eye with gross histology after lungs are perfused with an India ink and fixed in Fekete's solution, which causes metastases to appear as opaque white spots against "healthy" black lungs (Marabelle et al., 2013; Zimmerman et al., 2010). Using this method, it became immediately apparent that all 4T1-challenged mice became afflicted with lung metastases 11 to 13 days after tumour challenge, regardless of which treatment the animals received.

We further examined the lung samples with the help of Prof Rachel Allavena (University of Queensland), an expert veterinary pathologist, to better determine what impact CFA and immune checkpoint therapies may have had on metastatic disease progression. Prof Allavena examined them more closely with H&E staining and microscopy, and she was able to confirm both that what we observed were true metastases and that at least one 4T1-challenged mouse had large accumulations of neutrophils within the bronchial vasculature (Figure 6.4F). These observations are consistent with both published literature (DuPre et al., 2007, 2008; DuPre & Hunter, 2007) and our own experience using this model.

However, two independent experiments examining our treatment's effects on lung metastasis formation produced contradictory results. The first experiment found increased metastatic numbers in the lungs of CFA-treated mice, which was magnified when the mice were also given immune checkpoint therapies. Notably, in mice receiving both CFA and immune checkpoint therapies, the metastases were both more numerous and much smaller. In contrast, the second experiment, which did not use the India ink method but instead fixed the lungs with 10% neutral buffered formalin, found low but consistent metastatic numbers across all treatment groups. We do not know the cause for these contradictory experimental outcomes, but it is apparent from these experiments that a more appropriate tumour model may be required. An obvious candidate is the P815 model as it is responsive to intratumoural CFA and systemic anti-CTLA4 therapies, and has a metastatic disease progression that can be examined after treatment (T. B. Dunn & Potter, 1957). The B16.F10 model, which we alluded to in Section 4.3, may also be useful model to investigate this question.

7.2.2 Increasing concentration of *Mycobacterium butyricum*

Increasing the concentration of *M. butyricum* by ten-fold from 0.5 mg/mL to 5 mg/mL (10x CFA) is a relatively simple modification to the therapy design. This idea came after hearing and reading about CFA being used to induce experimental autoimmune encephalitis (EAE) in mouse models of multiple sclerosis (MS) and that laboratories using

this protocol prepared CFA with concentrations of Mycobacterium spp. ranging from 1 mg/mL to 5 mg/mL (Contarini et al., 2018; Stromnes & Goverman, 2006b, 2006a).

We used CT26-challenged BALB/c mice to investigate the efficacy of 10x CFA because DBA/2 mice (required for the CFA-responsive P815 tumour model) were inaccessible at the time the experiments were performed. This study produced the first complete regression of a CT26 tumour in our laboratory following treatment with a CFA monotherapy. Through FNA sampling, we observed that mice given intratumoural 10x CFA treatments had far higher numbers of tumour-infiltrating neutrophils (Figure 6.11), thus showing that antigen concentration has a significant role in CFA's potential for stimulating an immune reaction. We additionally found that several of the longest-lived animals and the sole regressor mouse had the highest proportions of tumour-infiltrating neutrophils (Figure 6.9). These findings are consistent with our previously published report showing that P815 tumours treated with CFA therapy rely on a large early neutrophil infiltrate for treatment success (C. S. E. Carroll et al., 2021). Unfortunately, we cannot make any conclusions about the effect of this therapy on overall survival or if neutrophil infiltration is essential for therapeutic outcomes in the CT26 model because the AEEC directly interfered with the progress and results of this study.

Research into the neutrophil's role in cancer is ongoing. Transforming growth factor β (TGFβ) within the TME is thought to polarise tumour-infiltrating neutrophils to a pro-tumour phenotype. This finding led to the N1 anti-tumour/ N2 pro-tumour dichotomy inspired by the M1/M2 model for macrophages (Fridlender et al., 2009). Later research found that Type 1 interferons (i.e., IFNα and IFNβ) within a tumour correlate with anti-tumour neutrophils (Andzinski et al., 2016), seemingly confirming the N1/N2 model. However, new methods such as single-cell RNA sequencing (scRNAseq) and dimensional reduction models have since identified up to 19 distinct neutrophil subtypes (Ustyanovska Avtenyuk et al., 2020), many of which are associated exclusively with murine and human tumours (Zilionis et al., 2019).

To investigate what kinds of neutrophils our CFA treatment attracted into the treated tumour, we used neutrophil maturity status as a proxy for pro- and anti-tumour phenotypes. Immature neutrophils are generally considered 'pro-tumour' and can facilitate

metastatic disease progression (B. E. Hsu et al., 2019; Mackey et al., 2019), and the CD101 glycoprotein was recently identified as a convenient surface marker to distinguish immature and mature neutrophils (Evrard et al., 2018). Thus, we revised our antibody panel to include CD101 (and CD25 for T cells) to better investigate potential changes in neutrophil phenotypes that may have resulted from treatment.

With this revised panel, we found that approximately half of all tumour-infiltrating neutrophils in 1x CFA- and 10x CFA-treated mice presented the immature pro-tumour $CD101^-$ phenotype by day 4 post-treatment (Figure 6.10), demonstrating that CFA attracts both mature and immature neutrophils rather than favouring either phenotype. This surge in neutrophil infiltrate could be a consequence of emergency granulopoiesis, i.e., the systemic expelling of large quantities of neutrophils from the bone marrow to overcome an infection when the immune system becomes maximally challenged (Manz & Boettcher, 2014). Indeed, data from the spleens of 10x CFA-treated animals show higher proportions of neutrophils than the 1x CFA- or PBS control-treated mice (Figure 6.12). This experiment will need to be repeated with a greater number of animals to confirm if the results attain significance.

Intriguingly, while the ratio of immature-to-mature neutrophils is approximately equivalent early after treatment in all CFA-treated mice, it shifted in only 10x CFA-treated mice by day 11, such that mature neutrophils held the majority (Figure 6.10A). Neutrophils are a dynamic cell type, and the state of the TME impacts their pro- and anti-tumour polarisation, especially in the later stages of the disease (Fridlender et al., 2009; Sagiv et al., 2015; Zilionis et al., 2019). Furthermore, whether neutrophils can be reverted or changed into an immunostimulatory anticancer phenotype *in situ* is not clear. Thus, it would be of great interest to further investigate whether intratumoural CFA injection can change neutrophils into an anti-cancer phenotype.

Along with CD101, we also included CD25 in our revised cytometry panel to determine how the numbers of $CD25^+$ $CD4^+$ T cells change following 10x CFA treatment. The interleukin-2 receptor (IL-2R) can take three forms, all with differing affinities for IL-2 (Spolski et al., 2018; Takeshita et al., 1992; X. Wang et al., 2009):

i) The α chain (CD25) can exist as a monomer with low affinity.

ii) A dimer composed of the IL-2Rβ and IL-2Rγ chains has intermediate affinity.

iii) A trimer composed of the IL-2Rα, IL-2Rβ, and IL-2Rγ chains has the highest affinity.

All T cells transiently express the high-affinity trimeric form upon initial activation, which quickly subsides after approximately 8 hours (Leonard et al., 1985). The intermediate dimeric form of IL-2R is constitutively expressed by resting T cells, NK cells, and CD8$^+$ T cells, while the high-affinity trimeric IL-2R (which includes CD25) is constitutively expressed by regulatory T (Treg) cells and group 2 innate lymphoid cells (Monticelli et al., 2011; Sakaguchi et al., 1995). Thus, while not definitive without intracellular Foxp3 staining, there is a high likelihood that intratumoural CD25$^+$ CD4$^+$ T cells are natural Treg cells.

When we examined the CD25$^+$ CD4$^+$ T cells following CFA treatment, we were intrigued to find this cell population significantly decreased in the CFA- and 10x CFA-treated mice (Figure 6.10). This result suggests that intratumoural 10x CFA treatments reduce the number of intratumoural Treg cells. With increased immune cell numbers, 10x CFA therapy may lead to a less immunosuppressive TME and facilitate tumour rejection. Experiments that allow us to keep animals alive to better determine treatment outcomes are required to validate this theory.

Lastly, the effect of 10x CFA on the presentation of TAAs by professional APCs needs to be better understood. To address this question, an investigation can be conducted using H-2[d] tetramers loaded with a P1A peptide to track the CD8$^+$ cytotoxic T lymphocyte (CTL) response against CFA-treated P815 tumours. P1A is a surface protein primarily expressed in the placenta and male germline cells while silent in other tissues (Amar-Costesec et al., 1994). Consequently, presenting a P1A epitope bound to an MHC-I molecule is regarded as *abnormal* and leads to cell destruction (precluding the presence of any immunosuppressive mechanisms). Therefore, utilising tetramers conjugated to a P1A epitope (Amar-Costesec et al., 1994) can quantify tumour-specific CTLs through

flow cytometry and provide valuable insights into the mechanistic changes in adaptive immune reactions following CFA or 10x CFA treatments.

These CFA experiments represent preliminary studies that investigated intratumoral bacterial injections as cancer immunotherapies. They could have direct implications for the mechanism by which the gut microbiome impacts immune checkpoint therapy outcomes.

7.3 Finding an Appropriate Tumour Model

A critical unanswered question in immunotherapy research is how the gut microbiome impacts immune checkpoint therapy outcomes in mice and human patients. As the literature review included in Chapter 1 explained (Almonte et al., 2021), we proposed the gut translocation hypothesis. In brief, colitis is a frequent immune-related adverse event caused by immune checkpoint therapies (Postow et al., 2018), and patients who experience colitis appear to have an improved response to treatment (Soularue et al., 2018; Ye et al., 2021). We suspect that colitis-induced injuries may offer a means for commensal gut bacteria to translocate out of the gut and migrate to and colonise distant solid tumours. Indeed, if commensals disseminate systemically from the gut lumen, they may preferentially accumulate within solid tumours via a haematological route through physical processes alone (J. L. Perry et al., 2017). Since the publication of our literature review, several papers have found evidence of bacteria in human tumours previously thought to be sterile, either through genetic sequencing of archived tumour samples (Nejman et al., 2020), bacterial epitopes presented on the major histocompatibility complex (MHC) molecules on the surfaces of human melanoma cells (Kalaora et al., 2021), or gut bacterial DNA found within soft-tissue sarcomas in human patients (L. M. Perry et al., 2023). After colonising the tumour, bacteria may act as adjuvants that improve immune checkpoint therapies (which primarily act on adaptive immune cells) by providing stimuli (e.g., PAMPs) that activate the innate immune response. These stimuli improve cytokine signalling, antigen presentation, and effector immune responses, all synergising to promote an effective Th1-style anticancer immune reaction. Our intratumoural CFA

therapy promotes immune responses by taking advantage of this process; CFA supplies *M. butyricum*-derived PAMPs to activate innate immunity through pattern recognition receptors (PRRs, Table 1.2 on page 27).

However, before further investigating our hypothesis, we needed an appropriate mouse tumour model that was not overly aggressive, responded to one or more immune checkpoint therapies and was not impacted by our FNA sampling protocol. We evaluated six tumour models (Table 4.1 on page 95) to determine the most appropriate model for future studies.

7.3.1 The MCA-205 and MC38 models

We were surprised that the MCA-205 fibrosarcoma and MC38 colon cancer models were not more useful for our purposes. Both have been used extensively in immune checkpoint research and were shown to be responsive to therapy (Arce Vargas et al., 2018; Dahan et al., 2015; Du et al., 2018; Fenwick et al., 2019; Hannani et al., 2015; Iida et al., 2013; Lei et al., 2020; Mager et al., 2020; Redmond et al., 2014; Routy et al., 2018; Selby et al., 2013; Vetizou et al., 2015; Wei et al., 2017, 2019), yet our evaluations found that each had unique challenges.

First, animals challenged subcutaneously with the MCA-205 tumour failed to regress after treatment, though we did find significant differences in tumour growth trajectories among mice treated with immune checkpoint therapies (Figure 4.1). But most worryingly, of the six cell lines we evaluated, animals challenged with this model were the most at risk of ulceration. Unfortunately, this high incidence of ulceration meant that we were required by the new rules imposed by the ANU's AEEC to euthanise the animals within 48 hours of noticing an ulcer, regardless of size, severity, or its effect on the animal's wellbeing (most of the ulcers found in our studies appeared benign as they had no effect on animal behaviour). Hence, the MCA-205 cell line had little application for our purposes.

Ulceration did not appear to be an issue with the other published studies. For example, Redmond *et al.* (2014) found that MCA-205 was not responsive to anti-CTLA4 but could keep challenged mice alive longer than we could in our experiments. Arce Vargas *et al.* (2018) found that anti-CTLA4 improved the survival of MCA-205–challenged mice,

which lived up to 80 days post-tumour-challenge. Hannani *et al.* (2015) did not examine impacts on survival but did find improved tumour control following anti-CTLA4 therapy. They also presented data showing mice lived up to 16 days post-treatment, while we had to euthanise many mice within ten days post-treatment in our studies. Lastly, Vetizou *et al.* (2015) used the MCA-205 line to show it was less responsive to anti-CTLA4 when implanted in germ-free mice as opposed to specific pathogen-free (SPF) mice, also seemingly without needing to euthanise animals due to ulceration.

In accordance with the ethics protocols that allowed the studies presented in this dissertation (Section 2.2), we have defined endpoints as specific indicators of animal welfare. These endpoints included tumour size (see Section 2.5 on page 37), or illness (hunched back, ruffled fur, orbital tightening, etc.), which, in our experience, signals metastatic disease progression. Therefore, in all studies presented in this dissertation, we accounted for any mouse euthanised for ulceration like a clinical study would treat patients as "lost to follow-up" and censored them from our survival analyses. Hence, we could not obtain valid survival data (our primary metric for treatment success) from mice challenged with the MCA-205 model.

While we could not use the MCA-205 model due to technical complications, we found the MC38 tumour model unresponsive to anti-CTLA4 therapy in our hands. This finding contradicts other studies showing the tumour model is responsive to immune checkpoint therapies (Hannani et al., 2015; Mager et al., 2020; Vetizou et al., 2015). We have thought of a few possible reasons for why we obtained this outcome. One reason is differences in gut microbial composition – a critical unanswered question in the field and a subject of this dissertation. Institutions and vendors handle their animals differently, invariably promoting the development of unique gut microbiomes (Sivan et al., 2015), which may lead to different immune checkpoint therapy outcomes (Gopalakrishnan et al., 2018; Tanoue et al., 2019). Another reason could be differences in treatment protocols between our experiments and various published studies. We injected mice four times, once every three days, with anti-CTLA4 (9D9) given at 0.1 mg per intraperitoneal injection. Other groups gave their mice up to five injections (Hannani et al., 2015; Vetizou et al., 2015) or doubled the concentration to 0.2 mg (Mager et al., 2020). At least one group used a

mixed approach, i.e., an initial injection was given at 0.2 mg with subsequent injections at 0.1 mg (Wei et al., 2019). Finally, genetic heterogeneity among the MC38 cell lines may exist between different institutions and laboratories (Schrors et al., 2023). The cell line we used was a gift from Dr Jing Li of the Stanford University School of Medicine and the cell line used by Mager *et al.* (2020) was gifted to the authors by Dr Charles Drake (unknown affiliation). Though we (and presumably Mager *et al.* (2020)) are immensely grateful for the gifted cell lines, the fact remains that we cannot discount the possibility that mutations spontaneously accumulated through prior sub-culturing may have influenced therapeutic outcomes (Ben-David et al., 2018). Despite these points, the experiment performed to evaluate the MC38 cell line was only conducted once, making repeating this experiment a required step to further validate its usefulness for future studies.

7.3.2 The B16.F10 and 4T1 models

The 4T1 breast cancer and B16.F10 melanoma models were completely unresponsive to immune checkpoint therapies, making them of limited use for our gut microbiome and immune checkpoint therapy studies. That said, both tumour models are poorly immunogenic, perhaps making the lack of response to immune checkpoint therapy (without an adjuvant) unsurprising.

Immune checkpoint therapies used to treat B16-challenged mice in the published literature are often accompanied by a concomitant vaccination with GVAX – an irradiated B16 cell line engineered to constitutively secrete GM-CSF (Dranoff et al., 1993; Quezada et al., 2006), or FVAX – an irradiated B16 cell line engineered to express the Flt3-ligand (Curran & Allison, 2009), which supports the survival, proliferation, and differentiation of hematopoietic progenitors (Shurin et al., 1998). They are typically given in three doses, each containing 10^6 cells, injected into the contralateral flank from the primary tumour. The first dose is given early (i.e., the third day after tumour challenge), and subsequent injections are given every three days (Curran et al., 2010; Curran & Allison, 2009; Quezada et al., 2006). Both vaccines are designed to improve activation and antigen presentation by myeloid cells and thus stimulate a more effective anticancer adaptive immune response.

Thus, this could offer a rationale for combining immune checkpoint therapies with our laboratory's intratumoural CFA therapy to treat the B16.F10 model.

FNA sampling is a powerful method that helps us identify different immune responses affecting animal survival without sacrificing mice to collect the data (C. S. E. Carroll et al., 2015). Our laboratory had already established that FNA sampling did not affect treatment outcomes in the CT26 and P815 models (C. S. E. Carroll et al., 2015), which an independent laboratory also confirmed for the CT26 model (Sitnikova et al., 2021). When our laboratory developed this method, we compared the proportions of immune cells observed from an FNA sample and a paired whole-tumour digest in the P815 model. In the P815 model (C. S. E. Carroll et al., 2015), and an independent evaluation of the CT26 model (Sitnikova et al., 2021), there was no significant differences in TIL proportions between the two methods. Therefore, we can sample tumours at different times to conduct a longitudinal analysis and identify potential differences in TIL profiles among treatment groups and (importantly) mice with varying treatment responses.

We applied our FNA sampling protocol to immune checkpoint-treated B16.F10-challenged mice. While we found a steady rise in CD11b^{-} lymphoid dendritic cells in animals treated with anti-CTLA4, there was no other difference in immune cell proportions. The practical implication of this finding needs to be clarified, as neither anti-CTLA4 nor anti-PD1 therapies improved survival in these mice.

Similarly, the 4T1 model was found unresponsive to anti-CTLA4 (both as a monotherapy and dual therapy with anti-PD1) and anti-PDL1. In conjunction with its unresponsiveness to immune checkpoint therapies, recent studies have shown that 4T1-challenged mice given multiple (three to six) injections of either anti-PD1 or anti-PDL1 antibodies can suffer from fatal anaphylaxis (Arai et al., 2022; Mall et al., 2016), thus implying the 4T1 cell line may have limited use for future studies involving PD1 blockade. The reasons for this phenomenon are unclear, but Arai *et al.* (2022) used the 4T1 and CT26 cell lines to show that neutrophilia is a critical factor in these reactions. Mice challenged with the 4T1 model are known to present with paraneoplastic effects, specifically marked splenomegaly and peripheral neutrophilia (DuPre et al., 2007, 2008; DuPre & Hunter,

2007; Pulaski & Ostrand-Rosenberg, 2001). Experiments presented in this dissertation have repeatedly confirmed these observations.

Notably, Arai *et al.* (2022) also observes increased neutrophilia and significant splenomegaly among CT26-challenged mice, as well as fatal anaphylaxis in animals thar received multiple treatments with PD1 blockade antibodies. These reactions were not observed in our experiments. Indeed, the data presented in this dissertation does not corroborate their observations (Figure 4.14). Therefore, we suspect Arai *et al.* (2022) may have used a genetically modified CT26 cell line in their study, and we are in the process of writing a piece to the *Journal for ImmunoTherapy of Cancer* highlighting this point.

Thankfully, the reported hypersensitivity reactions reported by Arai *et al.* (2022) and Mall *et al.* (2016) in the 4T1-challenged were not observed in our experiments, possibly because we never gave our animals more than three injections. Furthermore, this reaction is not likely to be a problem in the clinic. Mouse immune checkpoint antibodies are xenogenic and mainly derived from rats or hamsters. In contrast, human therapies such as nivolumab (anti-PD1) and avelumab (anti-PDL1) are humanised antibodies (IgG4 and IgG1, respectively). While there have been some reported cases of hypersensitivity in the clinic (Pirlog et al., 2022), immune checkpoint therapies continue to be well tolerated by the majority of patients and are far less likely to induce the alloreactivity reactions reported in mice upon repeated treatment with PD1 blockade antibodies.

7.3.3 The CT26 and P815 models

The BALB/c-derived CT26 colon cancer and DBA/2-derived P815 mastocytoma models were found most appropriate for our studies investigating our gut translocation hypothesis. Both tumour models were not so overly aggressive that mice needed to be humanely euthanised before the treatments could take effect; they both had significantly improved survival following systemic anti-CTLA4 therapy; and, they were both amenable to FNA sampling.

Firstly, neither the CT26 nor the P815 tumours grew or caused illness to the extent that humane euthanasia was required before the treatments had sufficient time to take effect. Illness, caused by widespread metastasis in mice and the primary cause of death,

was observed in some P815-challenged mice. Death was never used as an endpoint in any of our murine studies. However, we have observed mice challenged with P815 tumours go from fully active to moribund in less than 12 hours, and a minority were found dead in our experiments (6.6%). For this reason, we implemented euthanasia at the lowest illness score specifically for this model. In contrast, all the CT26-challenged animals were euthanised because their tumours reached the ethical size limit; no mouse challenged subcutaneously with the CT26 model required euthanasia due to illness.

Remarkably, we observed few differences in TIL profiles among the various treatment groups in both tumour models using our FNA protocol. In the P815 model, anti-CTLA4–treated mice showed a steady increase in tumour-infiltrating $CD4^+$ T cells during the first week after treatment (Chapter 3, Figure 4). In the CT26 model, the only difference we observed was a slight but significant decrease in the macrophage/monocyte populations by Day 11 post-treatment (Figure 4.14). We were initially surprised not to observe a more considerable difference in TIL profiles between control-treated and immune checkpoint-treated mice, as immune checkpoint therapies are designed to promote consequential changes in the adaptive immune response. Such a difference would have presumably been accomplished by either "blocking" the activity of CTLA4 and thus promoting T cell activation (Leach et al., 1996; Seidel et al., 2018) or "blocking" the interaction between PD1 and PD-L1, thus preventing T cell exhaustion and promoting effector functions (Iwai et al., 2002). Consequently, giving mice either treatment was expected to increase the presence of tumour-infiltrating T cells (Curran et al., 2010), yet this is not what we observed.

The primary advantage of our FNA protocol is the capability of comparing TIL profiles among animals with disparate treatment outcomes. We found that both CT26- and P815-challenged mice responsive to anti-CTLA4 therapy presented higher proportions of intratumoural T cells and lower macrophage/monocyte proportions. In the P815 model, we observed that anti-CTLA4–responders had higher $CD8^+$ T cells as soon as day 3 post-treatment and $CD4^+$ T cells by day 5 (Chapter 3, Figure 5). Increases in intratumoural $CD8^+$ T cells among CT26-challenged mice responsive to anti-CTLA4 were found by day 11 post-treatment (Figure 4.15). The increase in T cell populations among responding

mice is consistent with the published literature (Agdashian et al., 2019; Sharma et al., 2019; Wei et al., 2017). However, unlike those previous studies, we were able to show a *direct* correlation between TIL compositions among animals responsive to treatments, which would not have been possible had we sacrificed the animals to collect tumour samples for analysis.

The CT26 tumour is a highly immunogenic model, making it surprising that it was not more responsive to anti-PD1 therapy. There are two possible explanations for why this was the case (and which may also apply to the P815 model). First, anti-PD1 is most effective against tumours with a large pre-existing T cell infiltrate prior to therapy (Lei et al., 2020; Tumeh et al., 2014). By examining FNA samples from isotype control-treated mice and comparing them with anti-PD1–treated animals, we observe that neither tumour had a large T cell infiltrate when the animals were given their first treatments. These observations are corroborated by other studies showing few T cells in untreated CT26 and P815 tumours (C. S. E. Carroll et al., 2021; Lechner et al., 2013). Second, anti-PD1 antibodies may not be penetrating the TME at sufficient concentrations to convey a therapeutic benefit. Unlike anti-CTLA4, which is thought to function in the T cell priming stage in peripheral lymphoid organs, anti-PD1 therapy is thought to act on tumour-infiltrating effector $CD8^+$ T cells (Wei et al., 2017). If the drug is given systemically at low concentrations, there may not be sufficient penetration into the TME to act on the tumour-infiltrating effector cytotoxic T lymphocytes (CTLs, Kurino et al., 2020). Therefore, higher concentrations of anti-PD1 therapy may be necessary to promote a therapeutic response in the CT26 and P815 tumour models (Kurino et al., 2020). Alternatively, the drug may be more effective if it is given intratumourally rather than systemically. More testing is required to validate these theories.

Curiously, the P815 tumour model had isotype control-treated mice regress in our hands. As explained in the discussion section of our submitted manuscript (Chapter 3), our laboratory had treated 156 P815-challenged mice with intratumoural injections of either incomplete Freund's adjuvant (IFA) or saline (C. S. E. Carroll et al., 2015, 2021), yet treatments with systemic isotype control antibodies (given intravenously and

intraperitoneally) saw the first instances of control-treated animals regress by our laboratory (Chapter 3, Figure 1). Reviewing the literature, we learned that mast cells express Fcγ receptors (Malbec & Daeron, 2007) along with the well-known Fcϵ receptors. Indeed, when we tested for antibody binding using cultured cells with and without Fc-block (an anti-CD16/CD32 pre-treatment performed before flow cytometry staining to inhibit non-specific binding), we found that the isotype control and treatment antibodies bind with the Fcγ receptors on the surface of P815 cells (Chapter 3, Figure 2). These data led us to conclude that treatment and control IgG antibodies are binding with the Fcγ receptors on the P815 cell surface *in vivo*, thus leading to cell death and promoting tumour regression. This apparent reactivity to isotype control antibodies is essential to consider when using immune cell tumours for *in vivo* experiments. Additionally, this finding presents an intriguing avenue of investigation for treating immune cell cancers, i.e., using non-specific antibodies to engage Fc receptors and promote cancer cell regression.

We do not have a rational explanation for the regression of the sole control-treated CT26-challenged animal, nor for its sudden demise ten weeks after antibody injection (Figure 4.11). Though a necropsy did not reveal anything that may have contributed to its death, it is noteworthy that this mouse is the only observed instance of a spontaneous regression following control treatment among all the CT26 experiments performed in our laboratory.

7.4 Our First Antibiotics Experiment

Having identified that the CT26 and P815 models are most appropriate for our purposes, we asked if depleting the gut microbiota would impact anti-CTLA4 efficacy. Notably, the effect of antibiotics on anti-CTLA4 therapy has only been investigated in two published studies (Mager et al., 2020; Vetizou et al., 2015). Other research groups had focused on the gut microbiome's impact on PD1 blockade therapy, most likely because it is approved for use in a wider range of malignancies (Almonte et al., 2021).

Antibiotics are the most accessible means of modulating a mouse's gut microbiome (Almonte et al., 2022). Several antibiotic combinations have been used in the literature,

but a typical cocktail used in several papers published in high-impact journals contains ampicillin, colistin, and streptomycin (Mager et al., 2020; Routy et al., 2018; Vetizou et al., 2015; Viaud et al., 2013; Xu et al., 2020). Each antibiotic's mechanism of action is well defined: ampicillin is a semisynthetic penicillin compound that binds to and interrupts the function of proteins involved in bacterial cell-wall synthesis (Spratt, 1975); colistin disrupts the bacterial cytoplasmic membrane by binding to membrane phospholipids (Andrade et al., 2020); and streptomycin binds with a protein on the 30S subunit of the microbial ribosome and disrupts protein synthesis (Kogut & Prizant, 1975). Hence, this diverse spectrum of antimicrobial activity is enough to kill most of the commensal bacteria that inhabit the gut and is safe for consumption by the animal. We aimed to deplete the gut microbiota of CT26-challenged mice with this solution (fed *ad libitum* in their drinking water), treat their tumours with systemic anti-CTLA4 therapy, and observe what effects the resulting gut dysbiosis may have had both on treatment outcomes and TIL profiles.

We spent 16 months convincing the ANU AEEC to permit us to feed mice antibiotics, which appeared to have taken a stance against animal experimentation.

Unfortunately, we found that CT26-challenged BALB/c mice would not willingly drink the bitter-tasting broad-spectrum antibiotic solution, and the animals became severely dehydrated. We tried to mask the bitter taste by including a fruit drink concentrate at 1% and 5% concentrations, but both were unsuccessful (even the control animals would not drink the 5% solution). We successfully got the animals to consume some antibiotics and delayed the onset of severe dehydration by wetting food pellets with antibiotic water. Ultimately, we were obliged to end the antibiotic feeding period pre-maturely and modify our experiment timeline.

Regardless, we confirmed that the animals were consuming the antibiotics and that the commensals were depleted using culture methods. As shown in Figure 5.3, gut dysbiosis did not influence survival in CT26-challenged mice treated with anti-CTLA4. These results were surprising and contrary to what has been shown in the published literature. Vetizou *et al.* (2015) used the same antibiotics solution to show reduced responses in the MCA-205 OVA and MC38 tumour models (both syngeneic to C57BL/6 mice). Mager

et al. (2020) used chemically induced colon cancer and subcutaneous MC38 tumour models to show that depleted gut microbiota severely attenuates the efficacy of anti-CTLA4 therapy.

There are a few possible reasons for the differences in outcomes between our experiment and these published studies. First, our mice may not have been fed antibiotics long enough. As explained in Chapter 5, both Mager *et al.* (2020) and Vetizou *et al.* (2015) fed mice antibiotics for much longer time frames, 2 to 4 weeks, as opposed to our 6 days. Alternatively, the concentration of antibiotics consumed by BALB/c mice in our study may have been suboptimal. Ampicillin, for example, can be bacteriostatic (preventing bacterial growth) or bactericidal (killing bacteria), depending on both the concentration of the antibiotic and the bacterial species involved (Spratt, 1975). Given that we do not yet have a complete catalogue of all gut bacteria in mice or humans, it is impossible to say with certainty what effect the consumption of sub-optimal concentrations of antibiotics may have on gut commensals.

A second reason for the disparate findings may be that the genetics of the inbred mouse strains influence the effect of gut dysbiosis on immune responses and the tolerance for bitter taste. For example, C57BL/6 mice are a Th1-biased strain, while DBA/2 and BALB/c mice are Th2-biased strains (Mills et al., 2000; Ray et al., 2021; Watanabe et al., 2004). Additionally, Ray *et al.* (2021) suggest that feeding both BALB/c and C57BL/6 mice the same concentration of vancomycin (50 mg/kg body weight) produces different outcomes in cytokine profiles and microbial composition. Though this study made no *direct* comparison between the two mouse strains they evaluated, this is a possibility that cannot be discounted. Indeed, the aversion to the antibiotic's bitter taste results from genotypic differences between the mouse strains.

A final possible reason for the differences in experimental outcomes may be that our confirmation methods for antibiotic activity were inadequate, and we may have only partially depleted the gut microbiome. We used culture methods to determine the presence of bacteria before, during, and after antibiotic feeding (Figure 5.2). A shortcoming of this method is that not all bacteria in the gut are culturable, which means our calculations may be an underestimate of the actual bacterial load within the mouse gut. Notably, Vetizou

et al. (2015) also used culture methods to confirm antibiotic activity by cultivating the faecal pellets on blood agar plates in aerobic and anaerobic conditions. That said, 16S rRNA gene sequencing (for enumeration) or whole genome sequencing (for simple confirmation) should be considered for future experiments to obtain a more comprehensive assessment of antibiotic activity. For example, Mager *et al.* (2020) amplified and sequenced the V4 region of the 16S rRNA gene to confirm the bacterial presence in the colon in their studies. Whole gene amplification of the 16S rRNA gene (V1-V9 regions) with polymerase chain reaction (PCR) followed by sequencing with Oxford Nanopore™ sequencing technology could be a convenient means of confirming antibiotic activity and identifying genus-level bacteria taxonomy.

Despite the shortened time for antibiotic feeding and the lack of an effect on anti-CTLA4 efficacy, our preliminary results suggest that antibiotics consumption did appear to influence the proportions of tumour-infiltrating NK cells, T cells, and B cells in CT26 tumours. Our FNA results suggest that mice fed antibiotics had decreased intratumoural T cells on days 4 and 11 and significantly increased proportions of intratumoural B cells by day 11 (Figure 5.5). This finding contradicts data presented by Xu *et al.* (2020), who examined tumour-infiltrating T cells in CT26-challenged male BALB/c mice and found no differences in numbers between three antibiotic groups (including one fed the ampicillin/colistin/streptomycin cocktail) and a control group fed normal water. The reduced T cell infiltrate we observed could be a direct consequence of commensal depletion as antibiotics could induce an altered gut microbial state that impairs effector T cell responses (Pinato et al., 2019). Furthermore, the change in the microbial-associated molecular pattern (MAMP) repertoire that was typically provided by the commensal community before antibiotic-induce depletion could alter innate immune cell activation, especially among neutrophils (Pinato et al., 2019; Quail et al., 2022; C. K. Smith & Trinchieri, 2018). This change could consequently influence the anticancer T cell response as adaptive immunity is reliant on the activation of the innate immune response. In any case, a repeat of this experiment is required before any (strong) conclusions can be made.

7.5 Challenges to Progress

We have proposed a hypothesis explaining how gut microbiota affects immunotherapy outcomes and identified two tumour models for investigating our theory. Our initial attempts to explore the idea involved feeding CT26-challenged mice a solution of broad-spectrum antibiotics and treating them with systemic anti-CTLA4 therapy, but we faced significant challenges in making progress on this goal both from the ANU AEEC and the global COVID-19 pandemic.

The ANU AEEC has been a considerable obstacle to progressing our laboratory's projects. Requiring 18 months to obtain permission to feed mice common antibiotics that human patients routinely consume is dilatory and unacceptable. Moreover, the challenges we faced in this experiment led the AEEC to make the disheartening decision to stop all antibiotics-based experiments at the ANU. This decision, and others like it, hinders other researchers at the ANU from pursuing investigations that have a translatable impact on human patients. Such decisions also discourage researchers from taking risks to pursue new lines of inquiry, thus severely lessening ANU's competitiveness in these fields. Sadly, the actions of the AEEC were not limited to our antibiotics experiments and would continue to impact our laboratory's CFA studies (discussed in the next section). It is necessary and proper that animal experiments require ethical oversight, but when such oversight prevents progress, even when justifiable, non-invasive, and routinely published methods from high-impact journals are used, the AEEC's priorities must be re-evaluated.

The COVID-19 pandemic was the second significant challenge. The SARS-CoV-2 virus (the causative agent of COVID-19) spread globally from Wuhan, China, in late 2019. To limit the virus's spread, the Australian Government imposed strict travel restrictions and lockdown measures nationwide starting in March 2020, thus leading the ANU to halt all non-COVID-related research (Animal Ethics, personal communication, 25 March 2020). Although the Australian Capital Territory (ACT) was fortunate to experience little impact on daily life, research was still stalled as the required reagents, supplies, and mice were inaccessible. Consequently, progress in achieving PhD aims was effectively halted for approximately nine months, and accessibility to the DBA/2 mouse strain (required

for the P815 model) was impossible for at least two years. While experiments could resume after the lockdown policies were rescinded, the pandemic's effects continued to impact our research.

Despite these obstacles, we made significant progress in our first aim of investigating and validating our hypothesis. Our work identified the CT26 and P815 tumour models as the most appropriate for future experiments and demonstrated that antibiotics administration to BALB/c and DBA/2 mouse strains should be done through other means besides drinking water (e.g., oral or rectal gavage). Additionally, we showed how TIL profiles changed among various tumour models treated with immune checkpoint therapies, setting the foundation for future investigations. While we did not achieve our initial goals due to unavoidable external factors, we made significant strides toward answering our research question and laid the groundwork for future experiments.

7.6 Support for Our Hypothesis!

Since the publication of our literature review (Almonte et al., 2021) and during the writing of this dissertation, we were excited to find that an independent group has published strong and convincing evidence supporting our hypothesis. Using a B16 melanoma model, Choi *et al.* (2023) showed that gut bacteria translocate into tumours as a consequence of immune checkpoint therapy (i.e., anti-CTLA4 and anti-PD1 dual therapy).

There were several intriguing findings from this study. First, Choi *et al.* (2023) found pre-existing commensal gut bacteria levels present in mesenteric lymph node (mLN), spleens, and tumour-draining lymph node (TdLN) prior to injections with immune checkpoint therapy, thus challenging the notion that sites distant from mucosal barriers are inherently sterile. Second, immune checkpoint therapy induces the translocation of select gut microbes, and not just those that are most abundant in the gut lumen when the animals received treatment. Furthermore, different gut commensals may have unequal influences on the degree of immune activation. Third, the importance of the mLN for bacterial translocation in B16-challenged mice was demonstrated by surgically removing it, the TdLN, and the spleen (with sham surgeries used as controls) and subsequently treating

those mice with immune checkpoint therapy. Fourth, Choi *et al.* (2023) used a CD11c-diphteria toxin transgenic mouse model in which systemic injection of diphtheria toxin eliminates all CD11c$^+$ cells (e.g., dendritic cells, Jung et al., 2002). By using this model, they were able to show that treatment-induced bacterial translocation is severely reduced without dendritic cells. Finally, they found that inflammation caused by immune checkpoint therapy induces structural remodelling of the mLN, thus allowing the presence of GFP$^+$ *Escherichia coli* (which were injected directly into the mLN) to be significantly increased in the blood, TdLN, and (most importantly) the tumour after treatment with immune checkpoint therapy.

Hence, Choi *et al.* (2023) have proposed the following model: immune checkpoint therapy causes gut inflammation that induces the activation of gut-resident dendritic cells. Those dendritic cells then collect commensal gut bacteria from the gut lumen and traffic them to the mLN, which has been structurally modified to have increased blood vasculature due to immune checkpoint therapy. This modification offers bacteria in the mLN a means to disseminate into circulation (most likely via the haematological route) to various secondary lymphoid organs and the tumour. Bacteria within the TME then act in an adjuvant capacity, facilitating increased dendritic cell activation, TIL numbers, and effector T cell activation, all of which promote immune-mediated rejection of the tumour.

The findings of this study are compelling. They provide evidence directly supporting our gut translocation hypothesis (Almonte et al., 2021), and a means to explain why immune checkpoint therapies rely on gut bacteria; the authors also showed that depleting the gut microbiota attenuates immune checkpoint therapy effectiveness and gut translocation. Other studies have shown that tumours contain microbiomes but do not how they got there (Kalaora et al., 2021; Nejman et al., 2020). Aside from possibly arising from the microbes in the tumour's location (e.g., skin microbiome for melanoma, oral microbiome for lung cancer, gut microbiome for colorectal cancer), the findings of Choi *et al.* (2023) imply that a low-grade subclinical gut bacteria translocation into systemic circulation could be an additional mechanism by which tumour microbiomes develop in extraintestinal tumours. Furthermore, the authors also note that sepsis and bacteraemia have been associated with improved cancer outcomes in both preclinical models (Danahy

et al., 2019) and human patients (Adashek et al., 2018; Roelofsen et al., 2018), but that this correlation had yet to be shown with immune checkpoint therapy; their study may be the first to show direct evidence for this assertion.

However, several questions still remain. Firstly, if the model proposed by Choi *et al.* (2023) is found in the clinic, it may not necessarily be the exclusive means by which gut commensals can translocate out of the gut and colonise distant tumours. No appreciable deficit in gut barrier activity has been observed in mice treated with immune checkpoint therapy in this study or others (Vetizou et al., 2015). However, human patients treated with immune checkpoint therapies can experience severe colitis following treatment (Postow et al., 2018). This immune-related adverse event, which has been associated with improved immune checkpoint therapy responses (Soularue et al., 2018), may offer another way bacteria can translocate into systemic circulation. Additional questions include why select gut commensal species preferentially translocate out of the gut over others and why gut bacteria appear to have uneven influences on immune cell activation. There is also the question of whether the findings presented by Choi *et al.* (2023) are generalisable to other tumour models. Finally, now that the presence of translocated gut bacteria into solid tumours has been confirmed, could intratumoural injections of these bacteria be combined with systemic immune checkpoint therapy to improve immunotherapeutic responses? This last point may have direct implications for our laboratory's CFA therapy.

7.7 Conclusion

This PhD project had two main goals. First, we aimed to investigate the impact gut microbes had on immunotherapy treatment outcomes and attempt to validate our published gut translocation hypothesis. Second, we wanted to improve our intratumoural CFA treatment, either by combining it with immune checkpoint therapies or by increasing the concentration of heat-killed *M. butyricum* in the emulsion ten-fold. Although the AEEC and COVID-19 were significant impediments towards attaining these aims, I still made significant progress across two research institutions and with several mouse models.

Collectively, the experiments presented in this dissertation have laid the groundwork for us to further investigate these exciting topics.

Appendices

A
Supplementary Figures

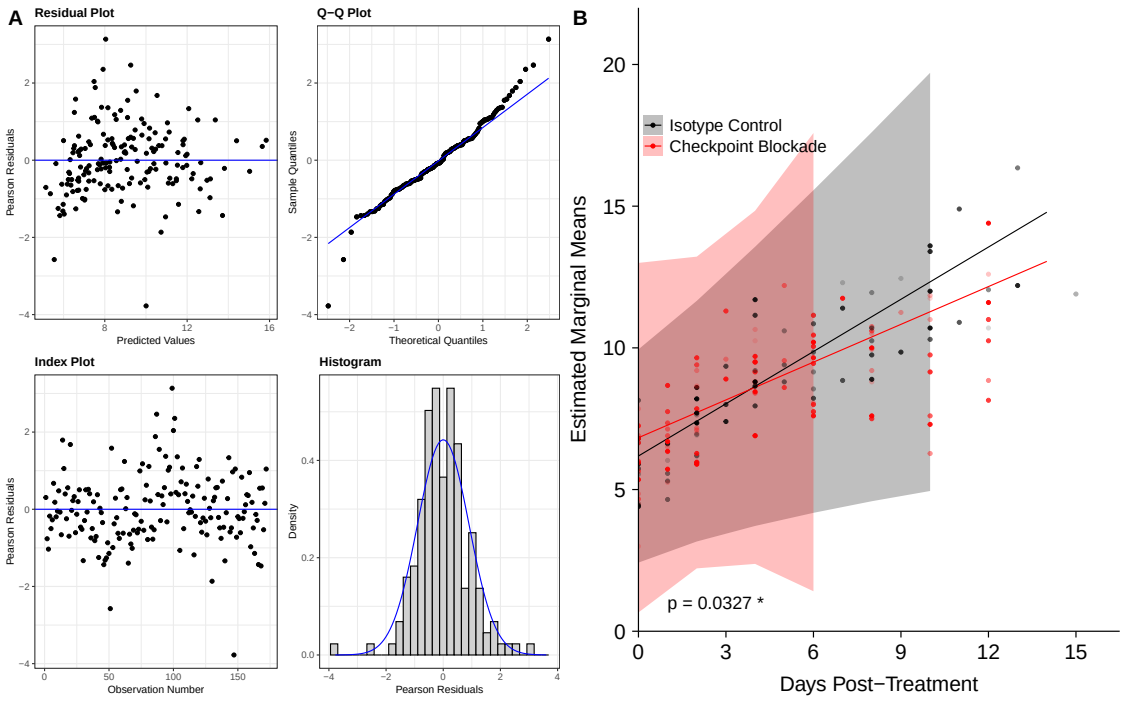


Figure A.1: The performance of the model used to analyse the MCA-205 tumour growth data presented in Figure 4.1B. **(A)** The residual panel and **(B)** plot of the estimated marginal means among the different treatment groups. Data from two experiments are shown. Each dot in (B) represents the average tumour diameter of a single mouse on any given day. Coloured ribbons correspond with treatment and indicate the 95% confidence intervals among the different treatment groups.

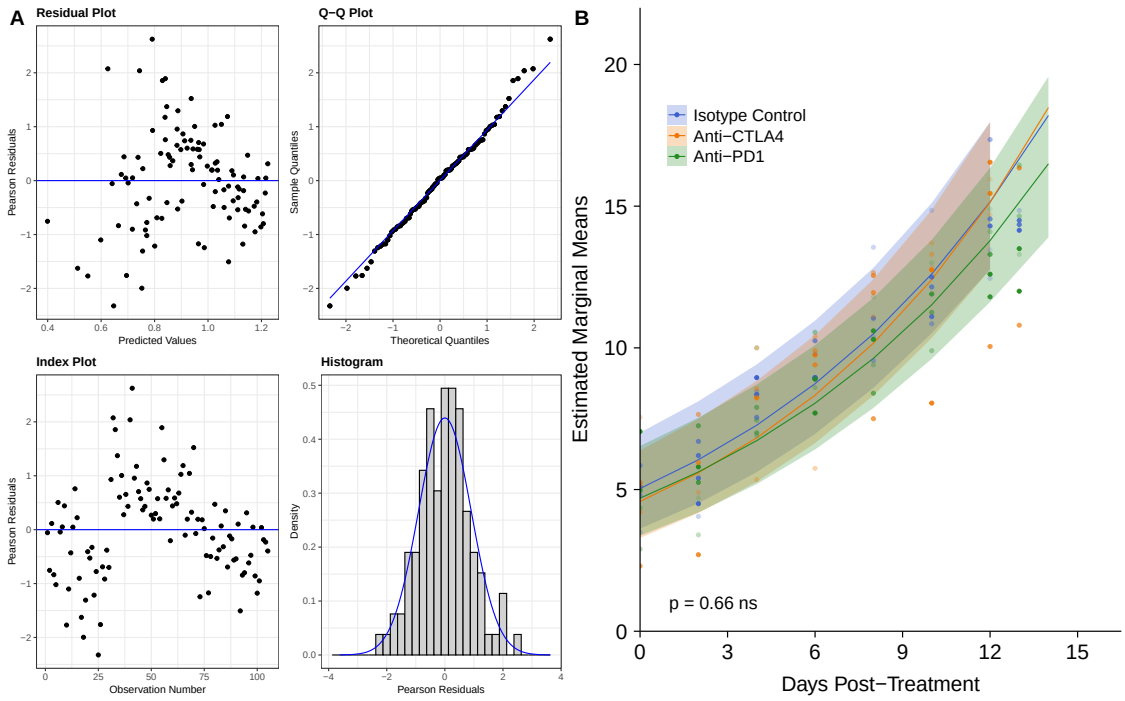


Figure A.2: The performance of the model used to analyse the MCA-205 tumour growth data presented in Figure 4.1B. **(A)** The residual panel and **(B)** plot of the estimated marginal means among the different treatment groups. Data from two experiments are shown. Each dot in (B) represents the average tumour diameter of a single mouse on any given day. Coloured ribbons correspond with treatment and indicate the 95% confidence intervals among the different treatment groups.

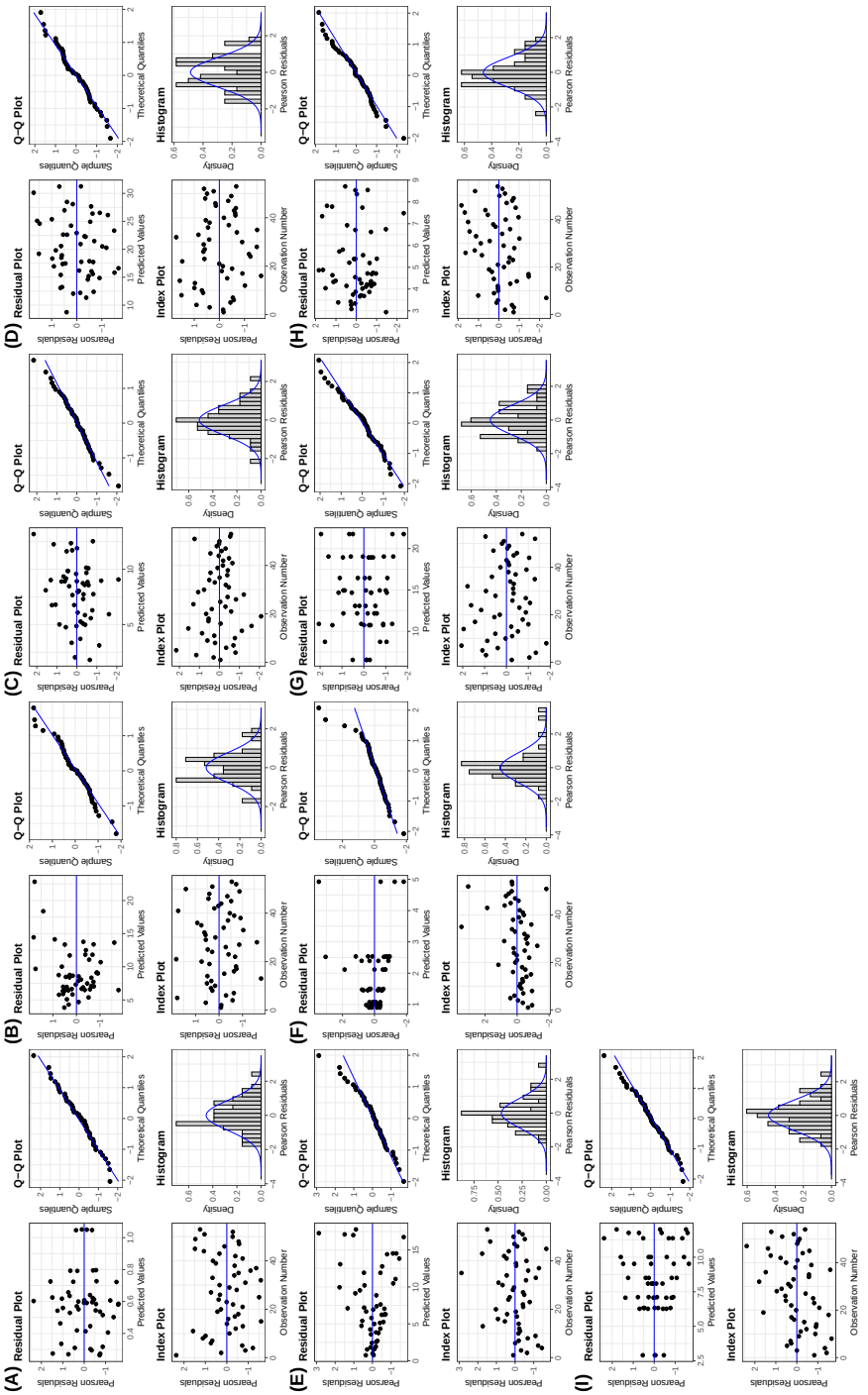


Figure A.3: Performances of linear mix-effects regression models of each TIL population identified in the B16.F10 model analysed for Figure 4.5. The residual plot, Q-Q plot, Index plot, and distribution of the Pearson Residuals are shown for each cell type analysed and presented in Figure 4.5. **(A)** $\gamma\delta$ T cells, **(B)** CD8$^+$ T cells, **(C)** CD4$^+$ T cells, **(D)** NK cells, **(E)** B cells, **(F)** Neutrophils, **(G)** Mϕ/Mo, **(H)** CD11b$^-$ Dendritic cells, and **(I)** CD11b$^+$ Dendritice cells. Mϕ, Macrophage; Mo, Monocyte

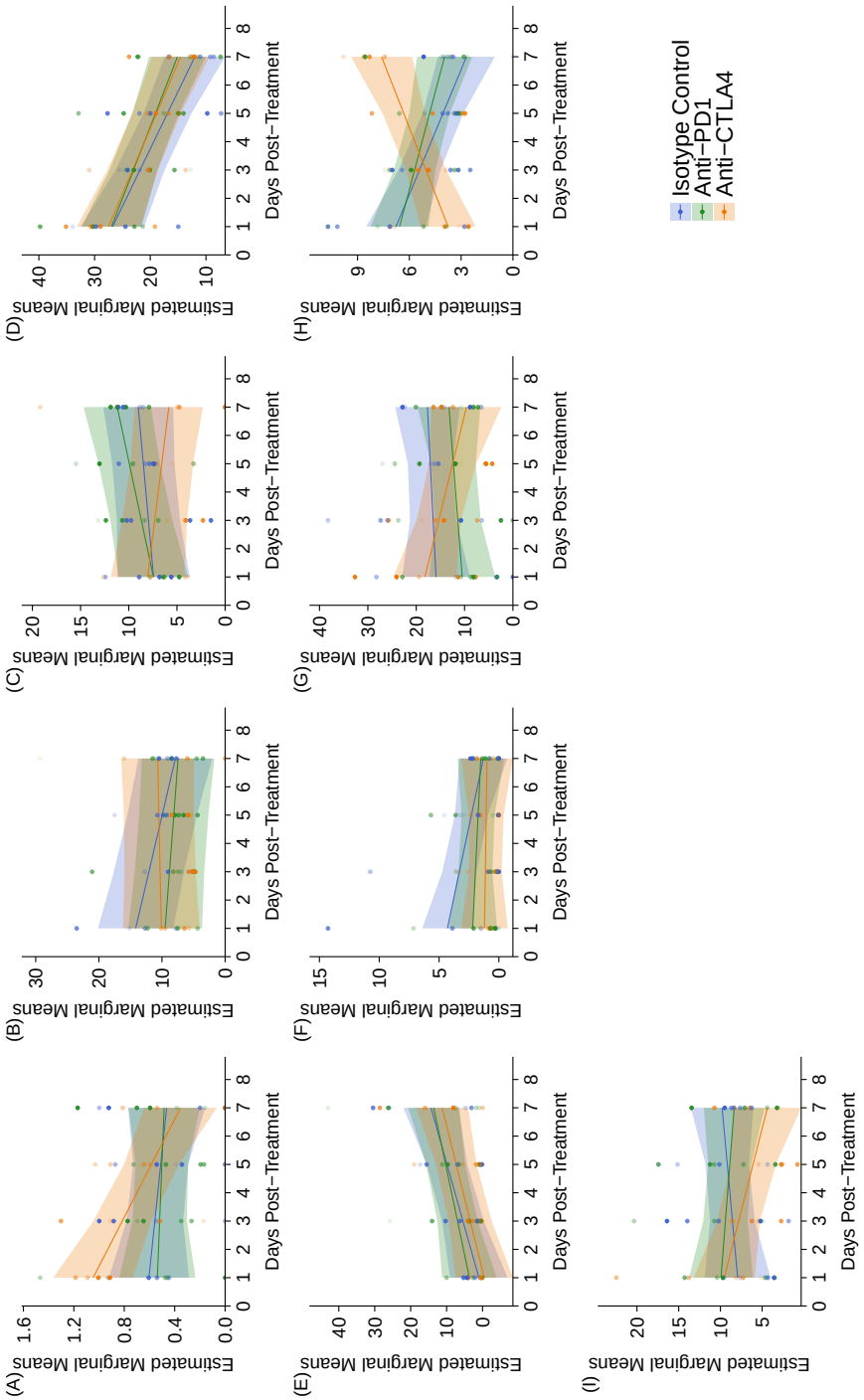


Figure A.4: The estimated marginal means among the different treatment groups for each cell type identified in the B16.F10 model in Figure 4.5. Each dot represents the proportions of the relavent cell type for a single mouse. The coloured ribbons correspond with treatment and indicate the 95% confidence intervals among the different treatment groups. **(A)** $\gamma\delta$ T cells, **(B)** CD8$^+$ T cells, **(C)** CD4$^+$ T cells, **(D)** NK cells, **(E)** B cells, **(F)** Neutrophils, **(G)** Mϕ/Mo, **(H)** CD11b$^-$ Dendritic cells, and **(I)** CD11b$^+$ Dendritice cells. Mϕ, Macrophage; Mo, Monocyte

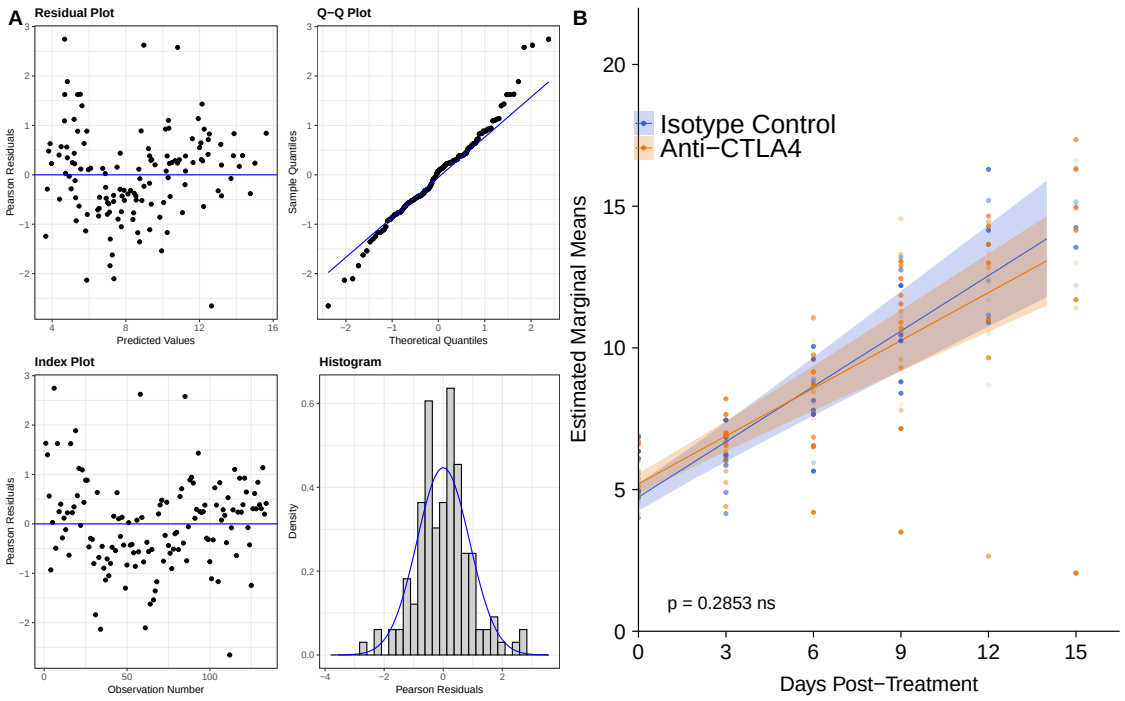


Figure A.5: The performance of the model used to analyse the MC38 tumour growth data presented in Figure 4.6B. **(A)** The residual panel and **(B)** plot of the estimated marginal means among the different treatment groups. Data from one experiment is shown. Each dot in (B) represents the average tumour diameter of a single mouse on any given day. Coloured ribbons correspond with treatment and indicate the 95% confidence intervals among the different treatment groups.

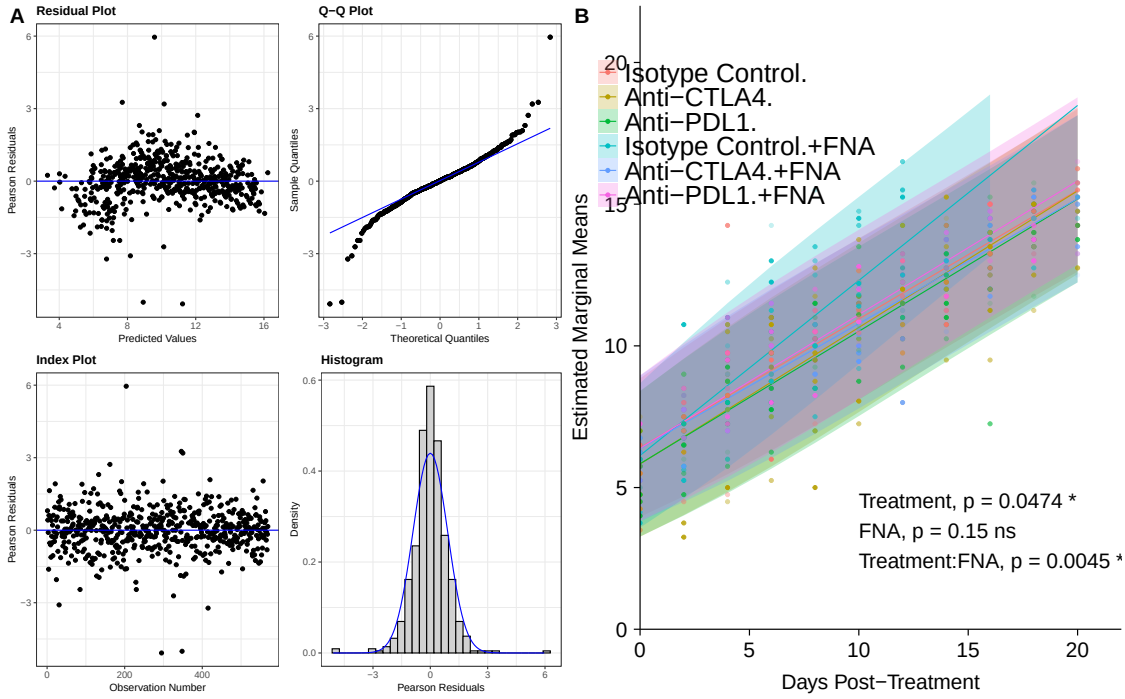


Figure A.6: The performance of the model used to analyse the 4T1 tumour growth data presented in Figure 4.7B. **(A)** The residual panel and **(B)** plot of the estimated marginal means among the different treatment groups and stratified by whether the animals were FNA-sampled. Data from two experiments are shown. Each dot in (B) represents the average tumour diameter of a single mouse on any given day. Coloured ribbons correspond with treatment and indicate the 95% confidence intervals among the different treatment groups.

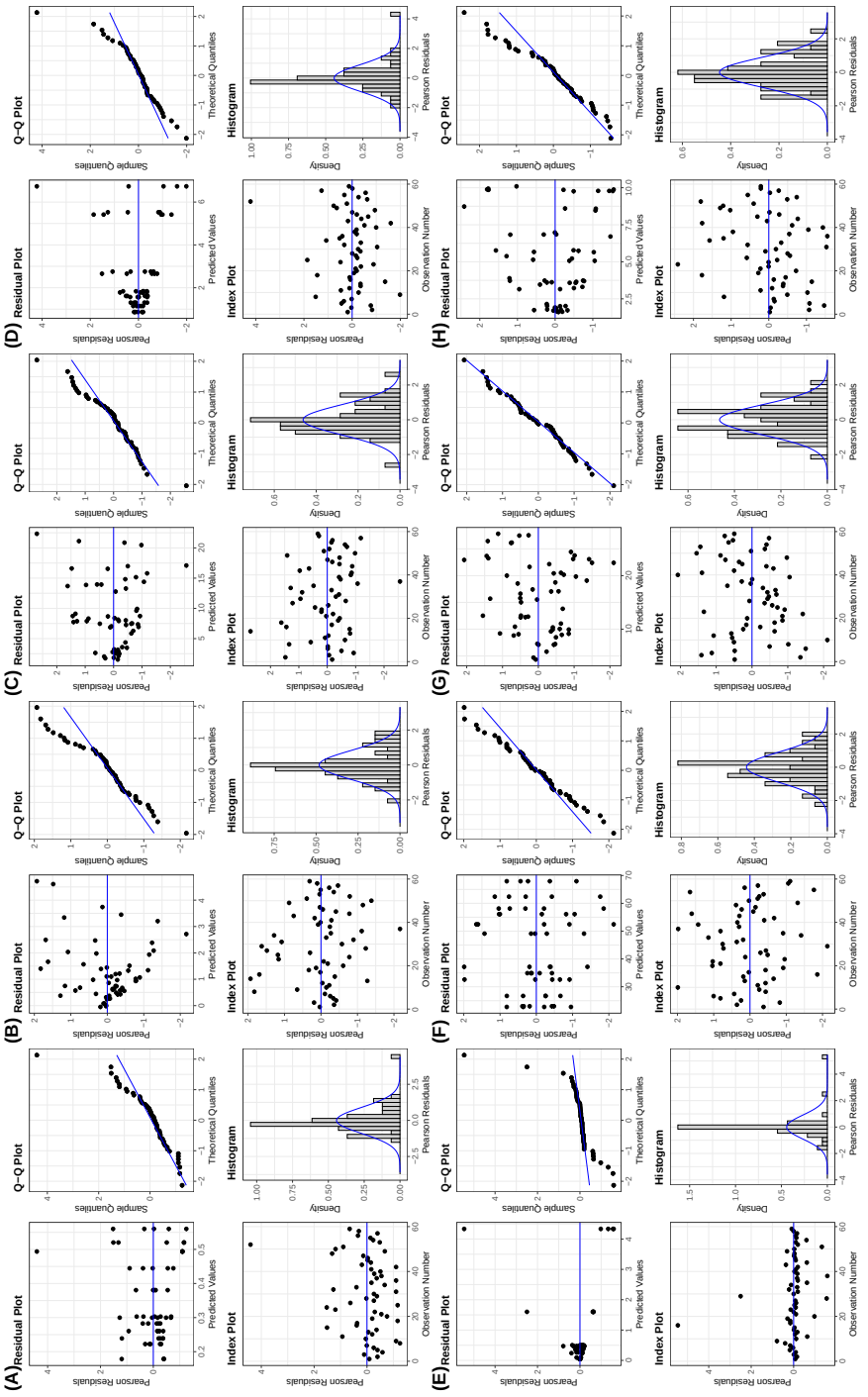


Figure A.7: Performances of linear mix-effects regression models of each TIL population identified in the 4T1 model analysed for Figure 4.10. The residual plot, Q-Q plot, Index plot, and distribution of the Pearson Residuals are shown for each cell type analysed and presented in Figure 4.10. **(A)** $\gamma\delta$ T cells, **(B)** CD8$^+$ T cells, **(C)** CD4$^+$ T cells, **(D)** NK cells, **(E)** B cells, **(F)** Neutrophils, **(G)** Mϕ/Mo, and **(H)** CD11b$^+$ Dendritice cells. Mϕ, Macrophage; Mo, Monocyte

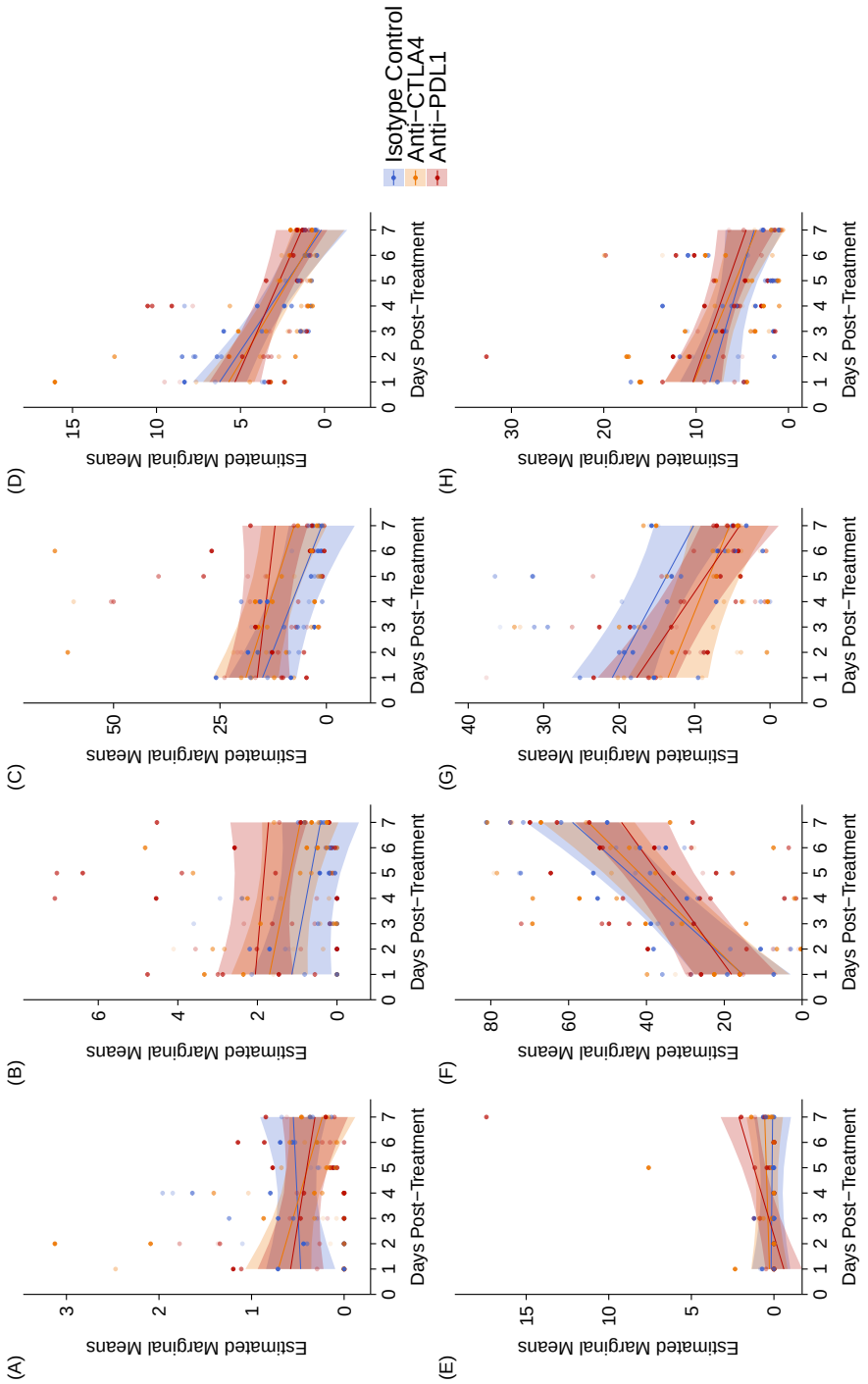


Figure A.8: The estimated marginal means among the different treatment groups for each cell type identified in the 4T1 model in Figure 4.10. Each dot represents the proportions of the relavent cell type for a single mouse. The coloured ribbons correspond with treatment and indicate the 95% confidence intervals among the different treatment groups. **(A)** $\gamma\delta$ T cells, **(B)** CD8$^+$ T cells, **(C)** CD4$^+$ T cells, **(D)** NK cells, **(E)** B cells, **(F)** Neutrophils, **(G)** Mϕ/Mo, and **(H)** Dendritice cells. Mϕ, Macrophage; Mo, Monocyte

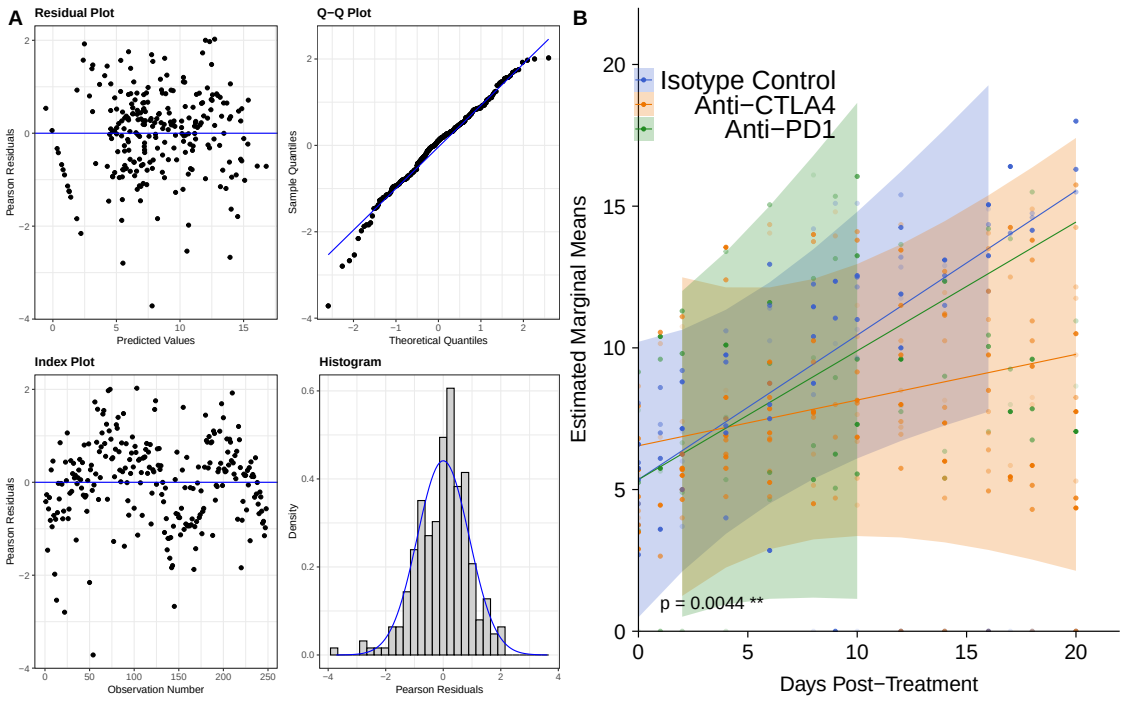


Figure A.9: The performance of the model used to analyse the CT26 tumour growth data presented in Figure 4.11B. **(A)** The residual panel and **(B)** plot of the estimated marginal means among the different treatment groups and stratified by whether the animals were FNA-sampled. Data from two experiments are shown. Each dot in (B) represents the average tumour diameter of a single mouse on any given day. Coloured ribbons correspond with treatment and indicate the 95% confidence intervals among the different treatment groups.

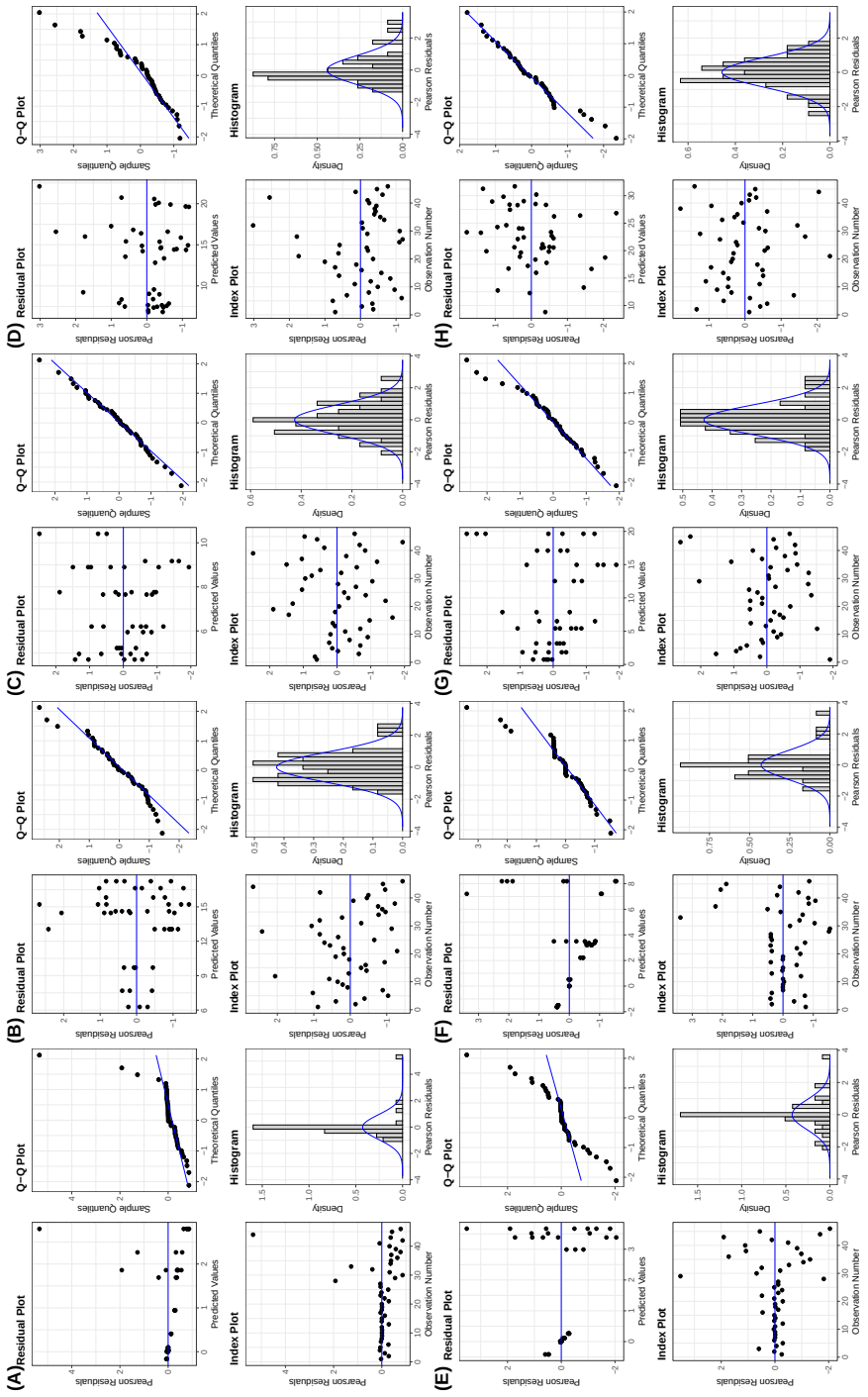


Figure A.10: Performances of linear mix-effects regression models of each TIL population identified in the CT26 model analysed for Figure 4.14. The residual plot, Q-Q plot, Index plot, and distribution of the Pearson Residuals are shown for each cell type analysed and presented in Figure 4.14. **(A)** $\gamma\delta$ T cells, **(B)** CD8$^+$ T cells, **(C)** CD4$^+$ T cells, **(D)** NK cells, **(E)** B cells, **(F)** Neutrophils, **(G)** Mϕ/Mo, and **(H)** CD11b$^+$ Dendritice cells. Mϕ, Macrophage; Mo, Monocyte

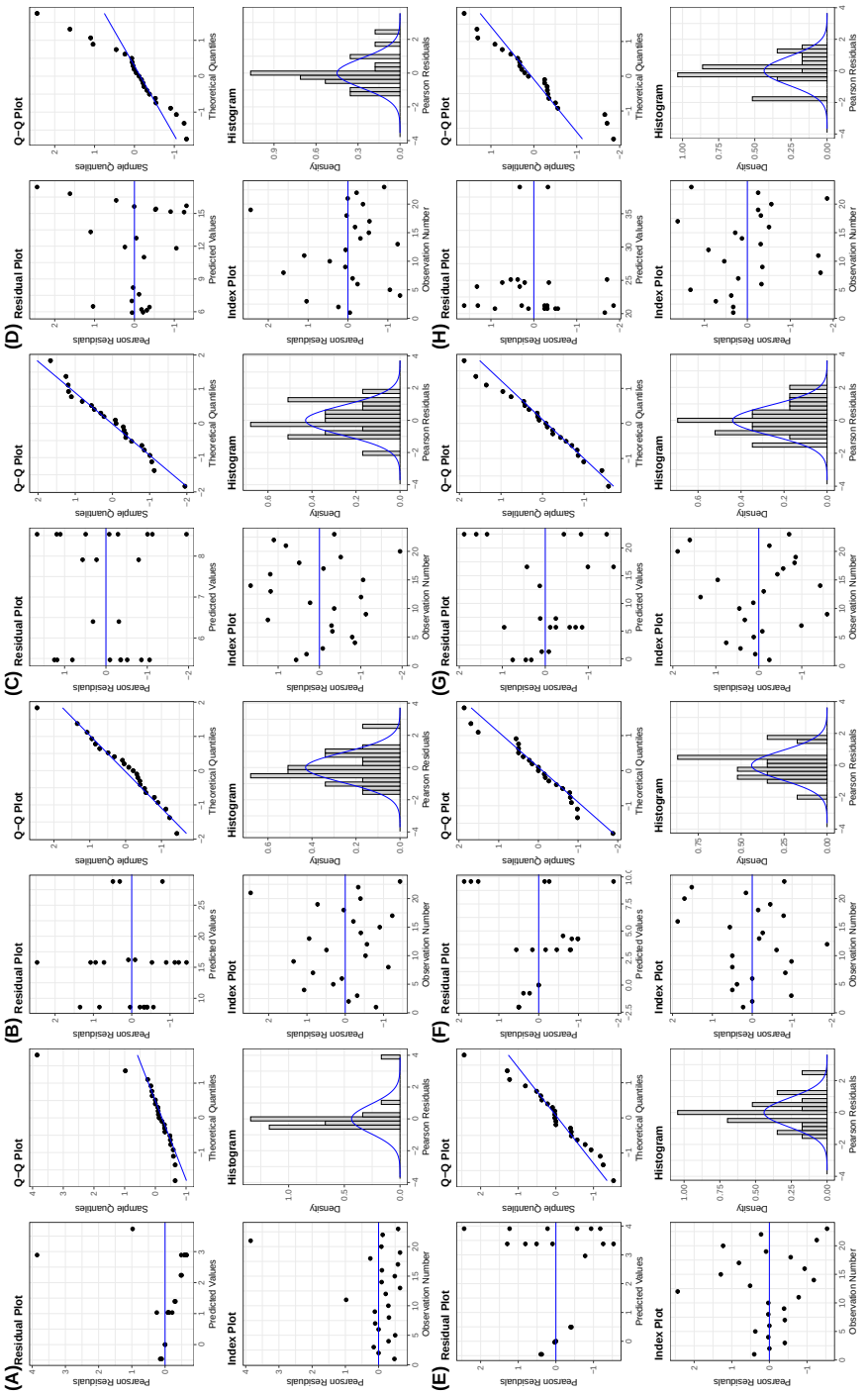


Figure A.11: Performances of linear mix-effects regression models of each TIL population identified in anti-CTLA4 - treated CT26 tumours analysed for Figure 4.15. The residual plot, Q-Q plot, Index plot, and distribution of the Pearson Residuals are shown for each cell type analysed and presented in Figure 4.15. **(A)** $\gamma\delta$ T cells, **(B)** CD8$^+$ T cells, **(C)** CD4$^+$ T cells, **(D)** NK cells, **(E)** B cells, **(F)** Neutrophils, **(G)** Mϕ/Mo, and **(H)** CD11b$^+$ Dendritice cells. Mϕ, Macrophage; Mo, Monocyte

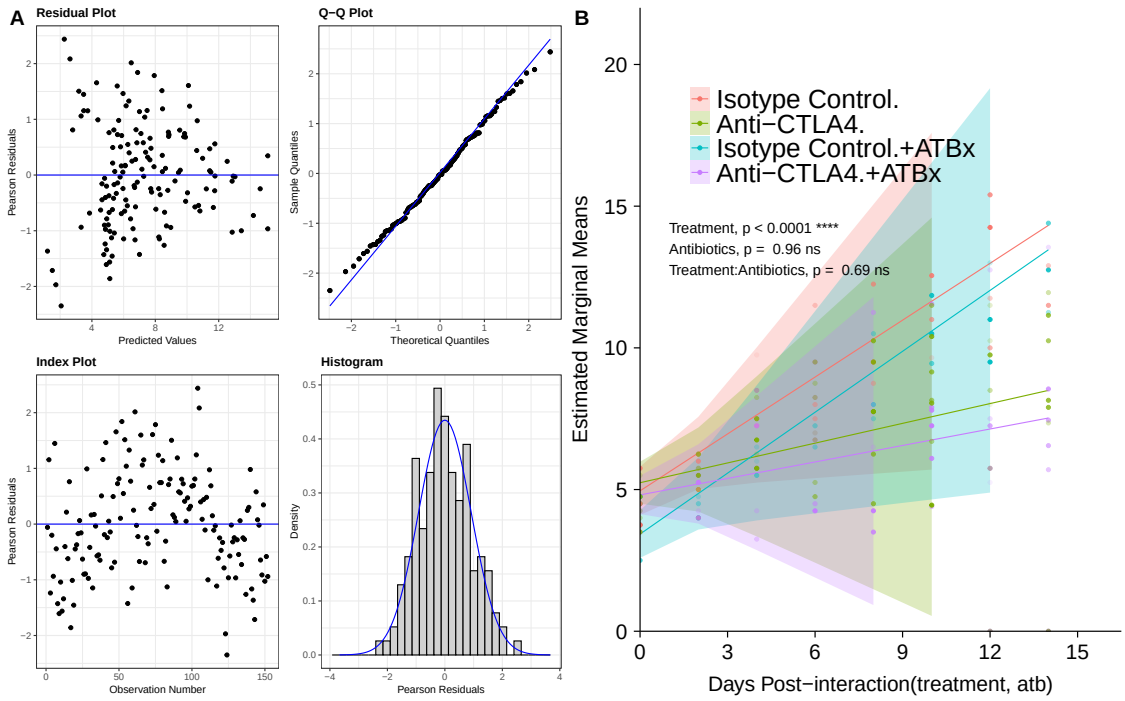


Figure A.12: The performance of the model used to analyse the CT26 tumour growth data presented in Figure 5.3B. **(A)** The residual panel and **(B)** plot of the estimated marginal means among the different treatment groups. Data from one experiment is shown. Each dot in (B) represents the average tumour diameter of a single mouse on any given day. Coloured ribbons correspond with treatment and indicate the 95% confidence intervals among the different treatment groups.

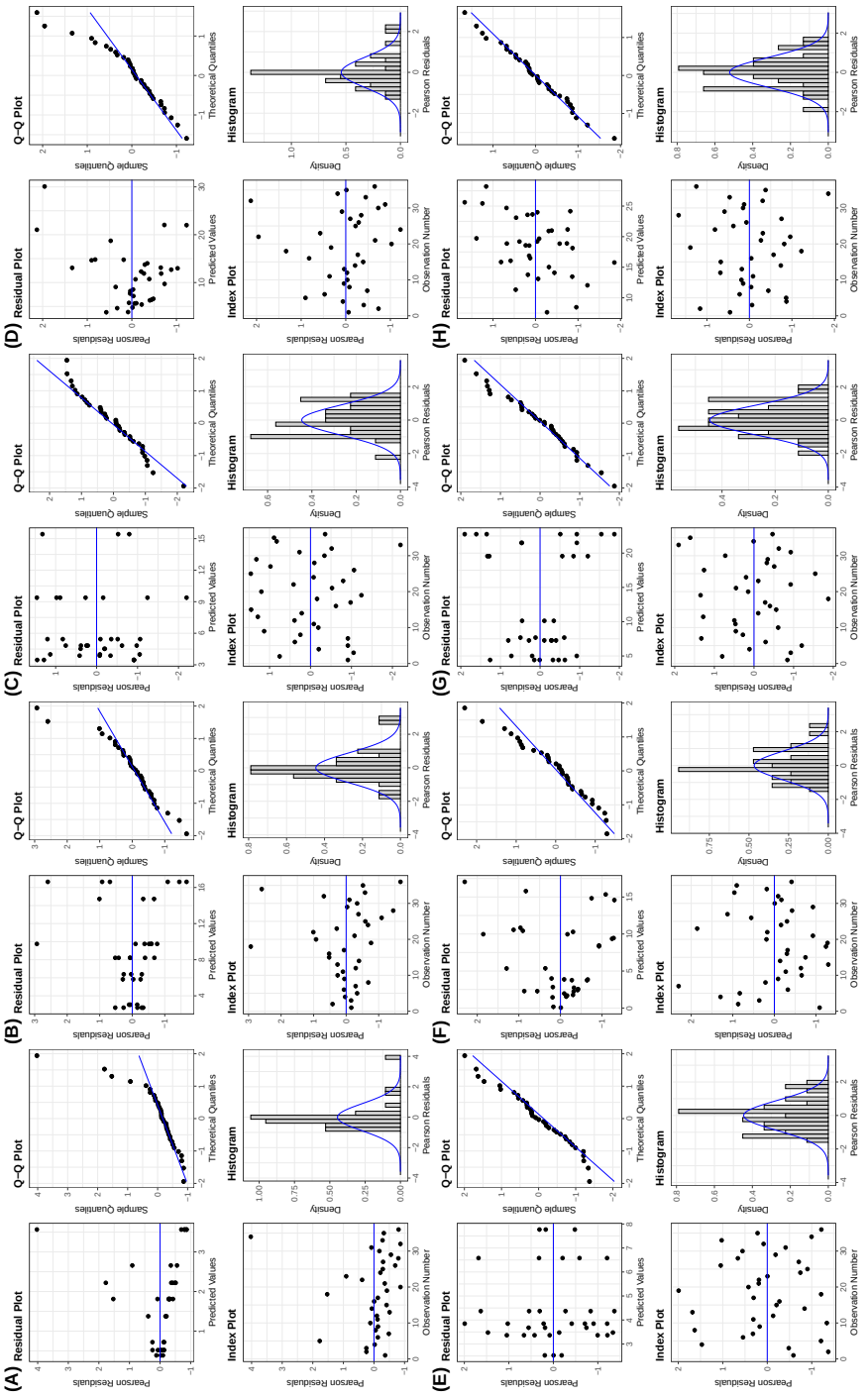


Figure A.13: Performances of linear mix-effects regression models of each TIL population identified in the CT26 model analysed for Figure 5.5. The residual plot, Q-Q plot, Index plot, and distribution of the Pearson Residuals are shown for each cell type analysed and presented in Figure 5.5. **(A)** $\gamma\delta$ T cells, **(B)** CD8$^+$ T cells, **(C)** CD4$^+$ T cells, **(D)** NK cells, **(E)** B cells, **(F)** Neutrophils, **(G)** Mϕ/Mo, and **(H)** CD11b$^+$ Dendritice cells. Mϕ, Macrophage; Mo, Monocyte

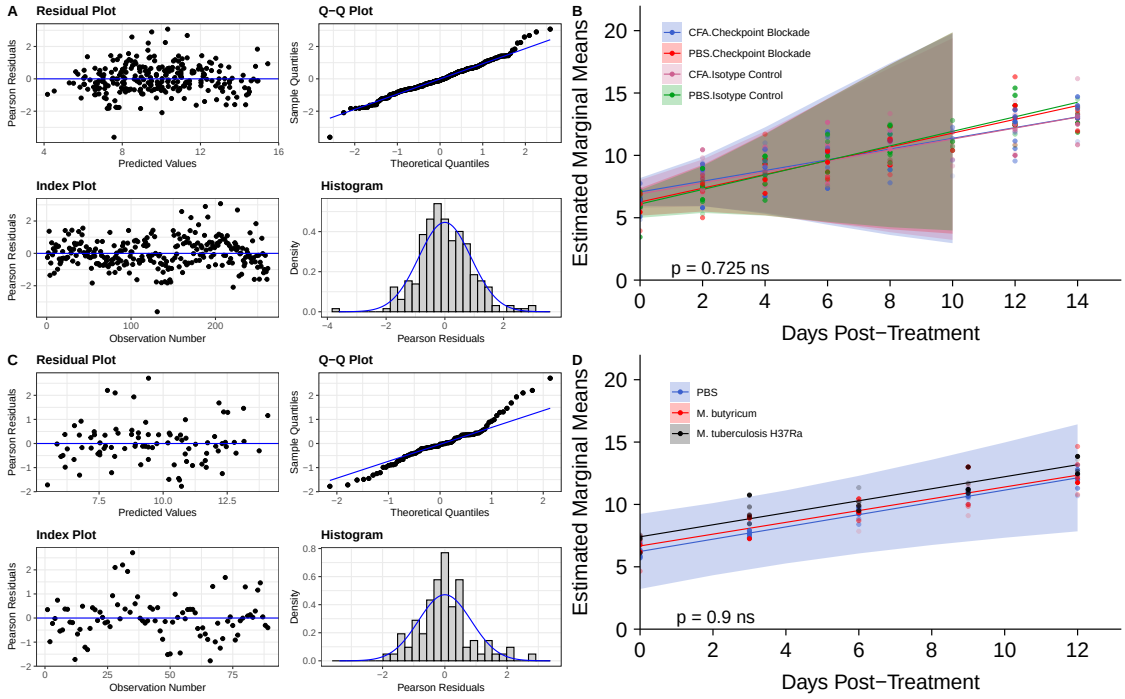


Figure A.14: The performance of the model used to analyse the 4T1 tumour growth data presented in Figure 6.2. **(A)** The residual panels and **(B)** plot of the estimated marginal means for the LMER model used in Figure 6.2B. **(C)** The residual panels and **(D)** plot of the estimated marginal means for the LMER model used in Figure 6.2D. Data from two experiments are shown. Each dot in (B) and (D) represents the average tumour diameter of a single mouse on any given day. The coloured bars show the 95% confidence intervals among the different treatment groups.

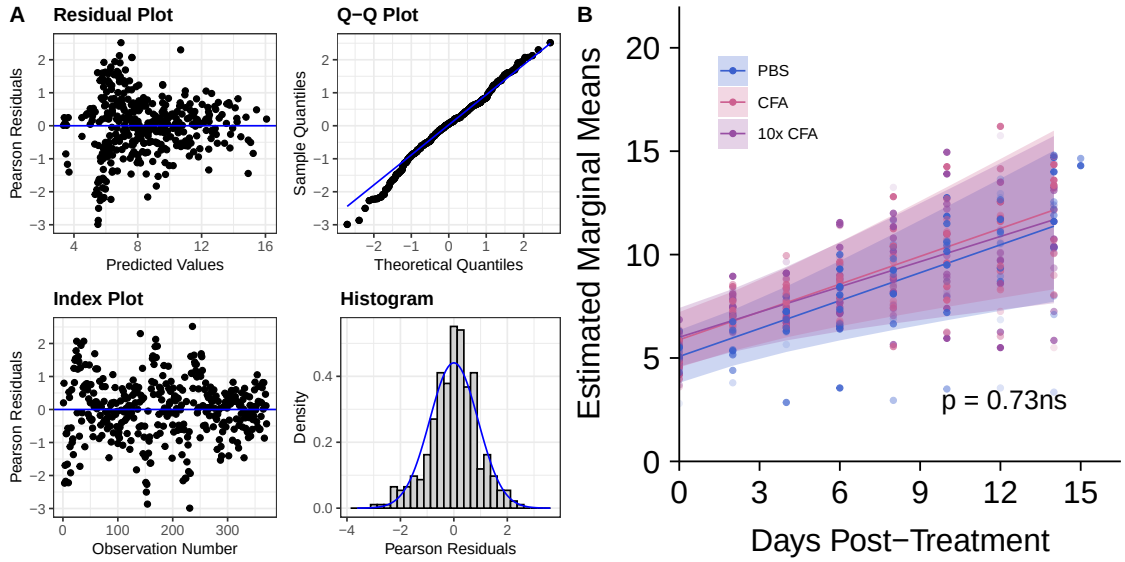


Figure A.15: The performance of the model used to analyse the 4T1 tumour growth data presented in Figure 6.5. **(A)** The residual panel and **(B)** plot of the estimated marginal means among the different treatment groups. Data from two experiments are shown. Each dot in (B) represents the average tumour diameter of a single mouse on any given day. The coloured bars show the 95% confidence intervals among the different treatment groups.

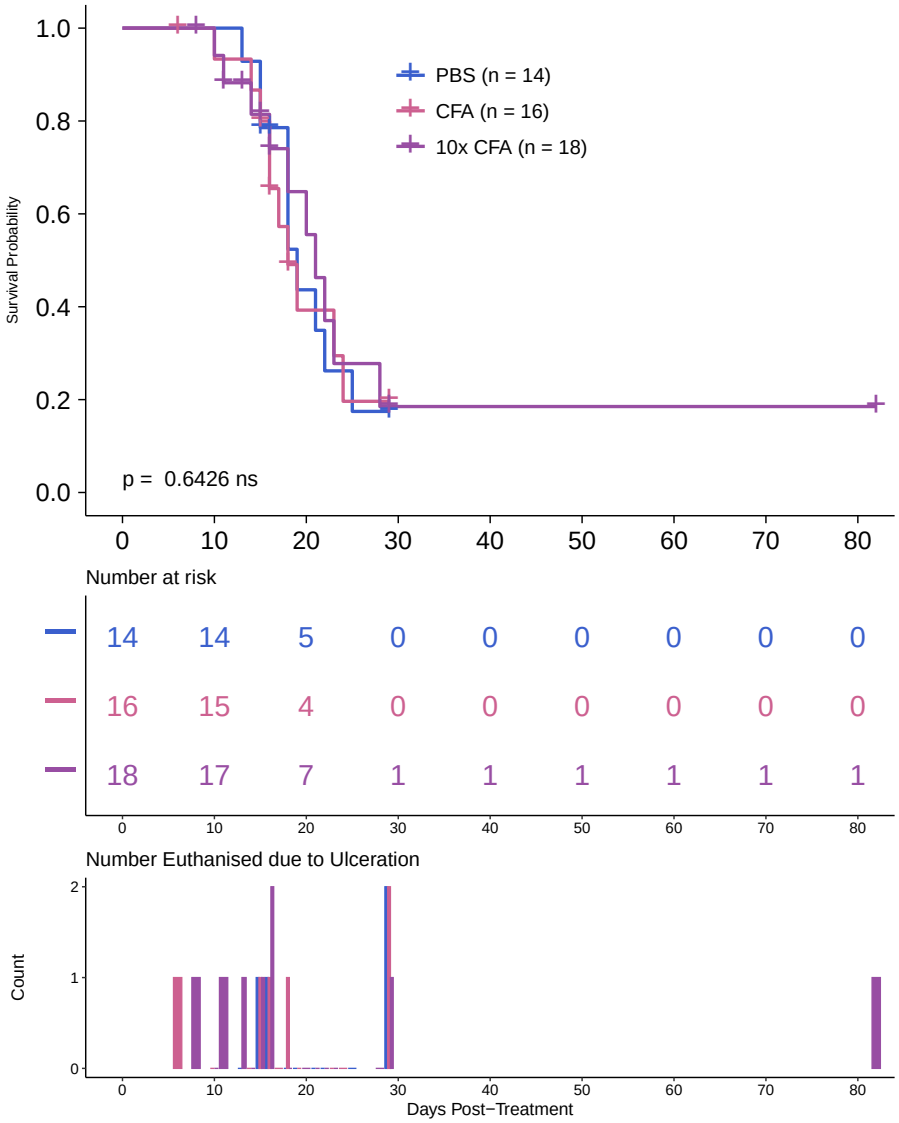


Figure A.16: Supplemental survival data for Figure 6.5. The same survival data shown in Figure 6.5C with addtitional information, specifically the number of animals at risk on any given day (middle) and the number of animals euthanised due to ulceration (bottom).

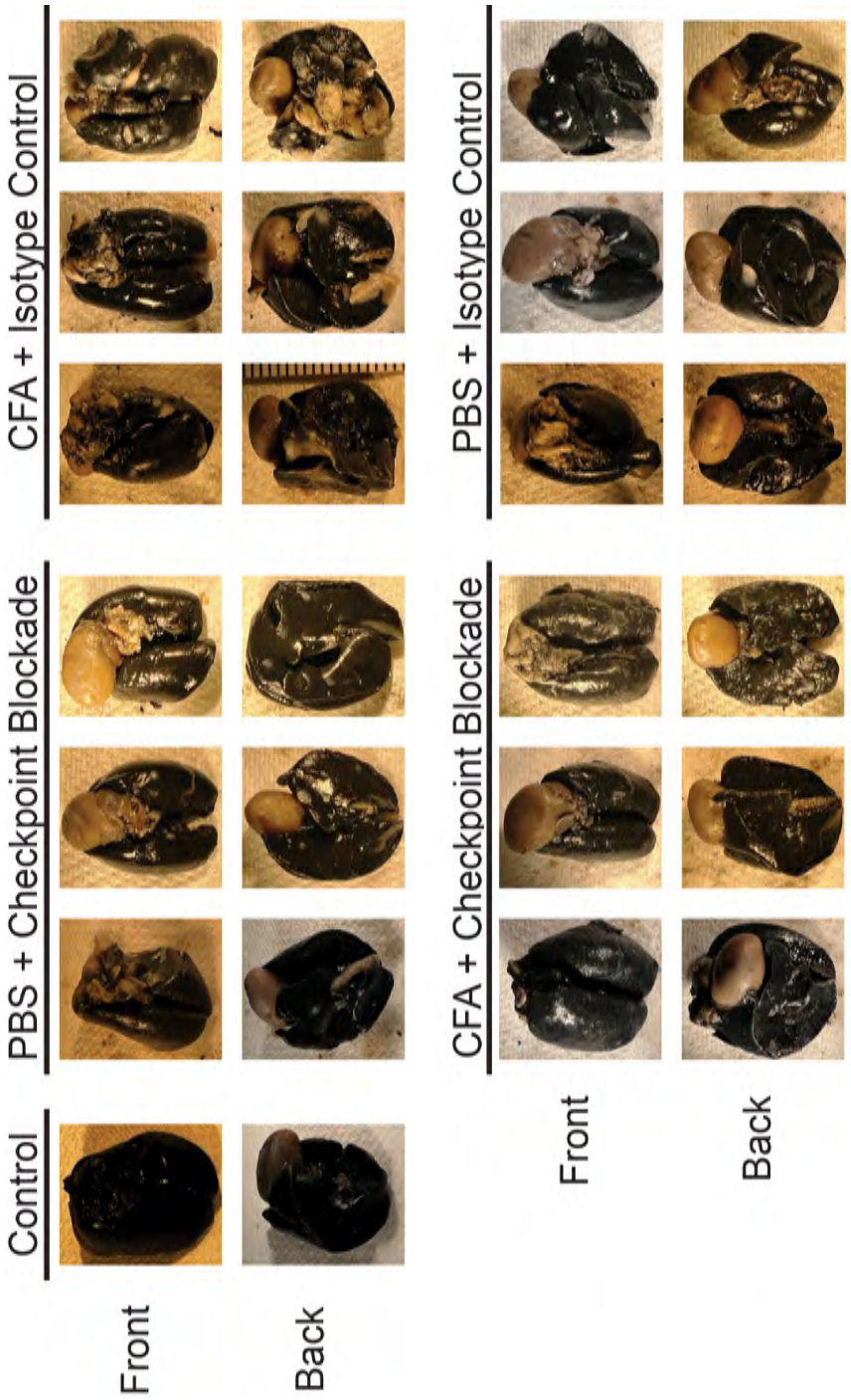


Figure A.17: Photos of all lungs evaluated with India ink and Fekete's solution. Female BALB/c mice were injected orthotopically with 0.5 x 10^6 4T1 cells into the mammary fat pad. They were treated seven days later with intratumoural injections of CFA or PBS and intraperitoneal injections of both anti-CTLA4 (0.1 mg, 9D9) and anti-PD1 (0.2 mg, RMP1-14), or relevant isotype control antibodies. The intratumoural injections were administered once, while antibody injections were given every three days for three injections. The mice were sacrificed on Days 11, 12, and 13, and their lungs were collected and examined for metastasis.

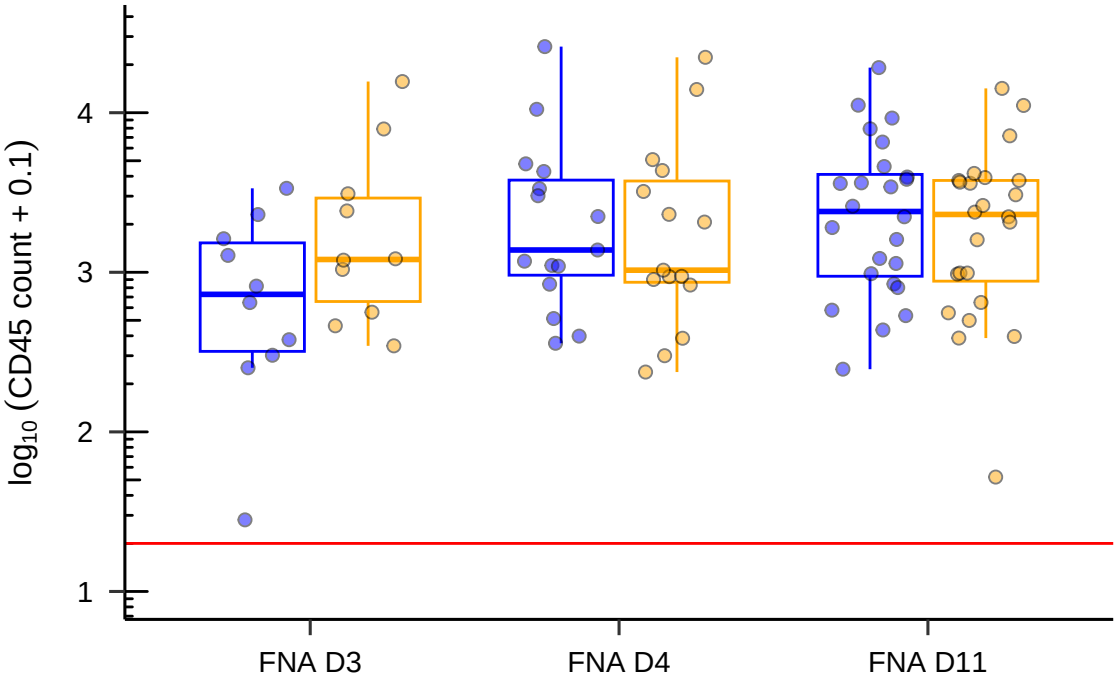


Figure A.18: Quality control assessment for FNA data presented in Figure 6.8. Only FNA samples with greater than 20 events in the live CD45.2+ gate were retained to minimise potential misrepresentation in the final analysis. Above the horizontal red threshold line, blue box plots and dots show sample counts from the Innate stain, while the orange box plots and dots show sample counts from the Adaptive stain. Of the 98 samples collected, 98 (100%) were retained for the final analysis. Each dot indicates the cell count in the relevant stain from a unique FNA sample.

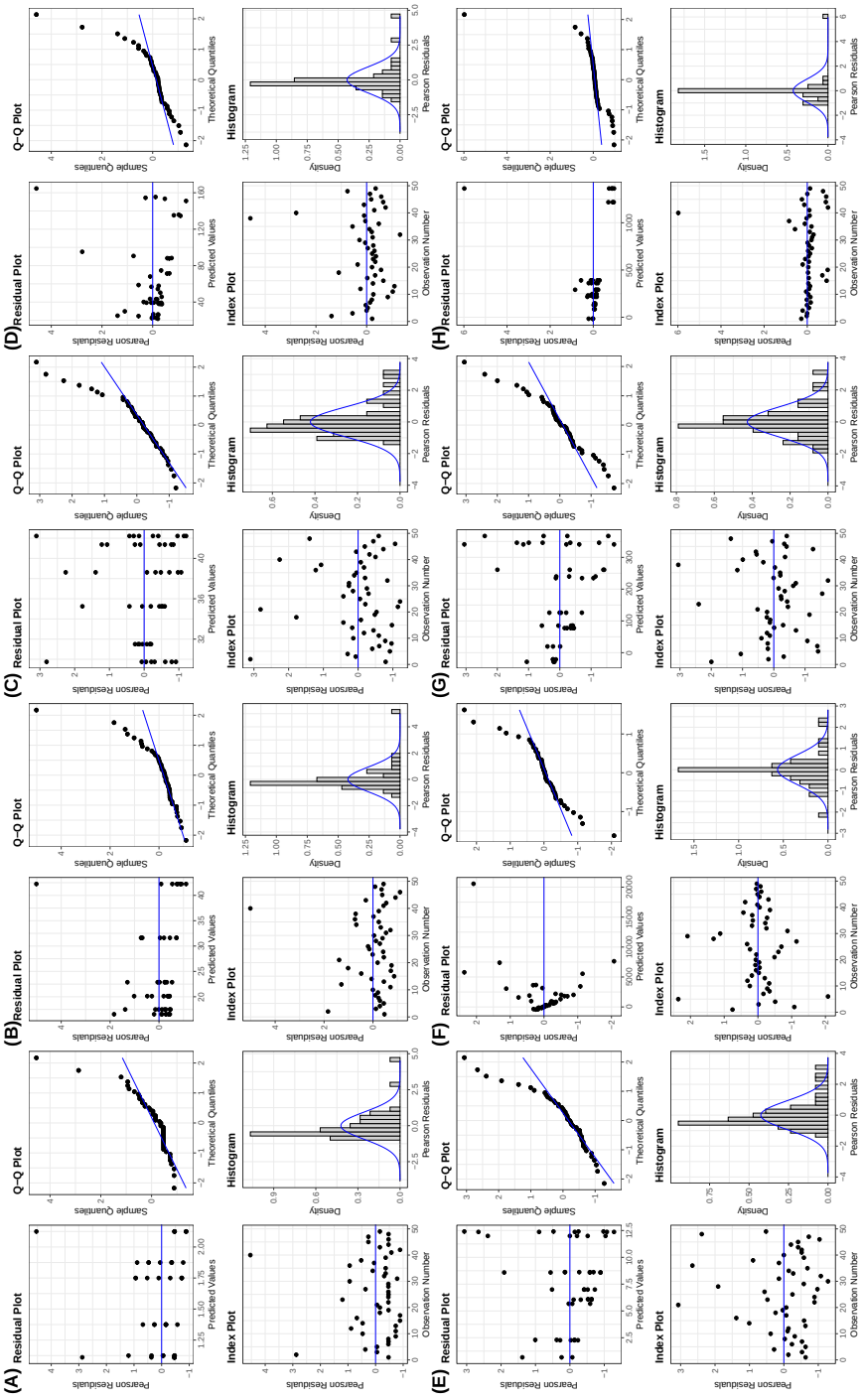


Figure A.19: Performances of linear mix-effects regression models of each TIL population identified in the CT26 model analysed for Figure 6.8. The residual plot, Q-Q plot, Index plot, and distribution of the Pearson Residuals are shown for each cell type analysed and presented in Figure 6.8. **(A)** $\gamma\delta$ T cells, **(B)** CD8$^+$ T cells, **(C)** CD4$^+$ T cells, **(D)** NK cells, **(E)** B cells, **(F)** Neutrophils, **(G)** Mϕ/Mo, and **(H)** CD11b$^+$ Dendritice cells. Mϕ, Macrophage; Mo, Monocyte

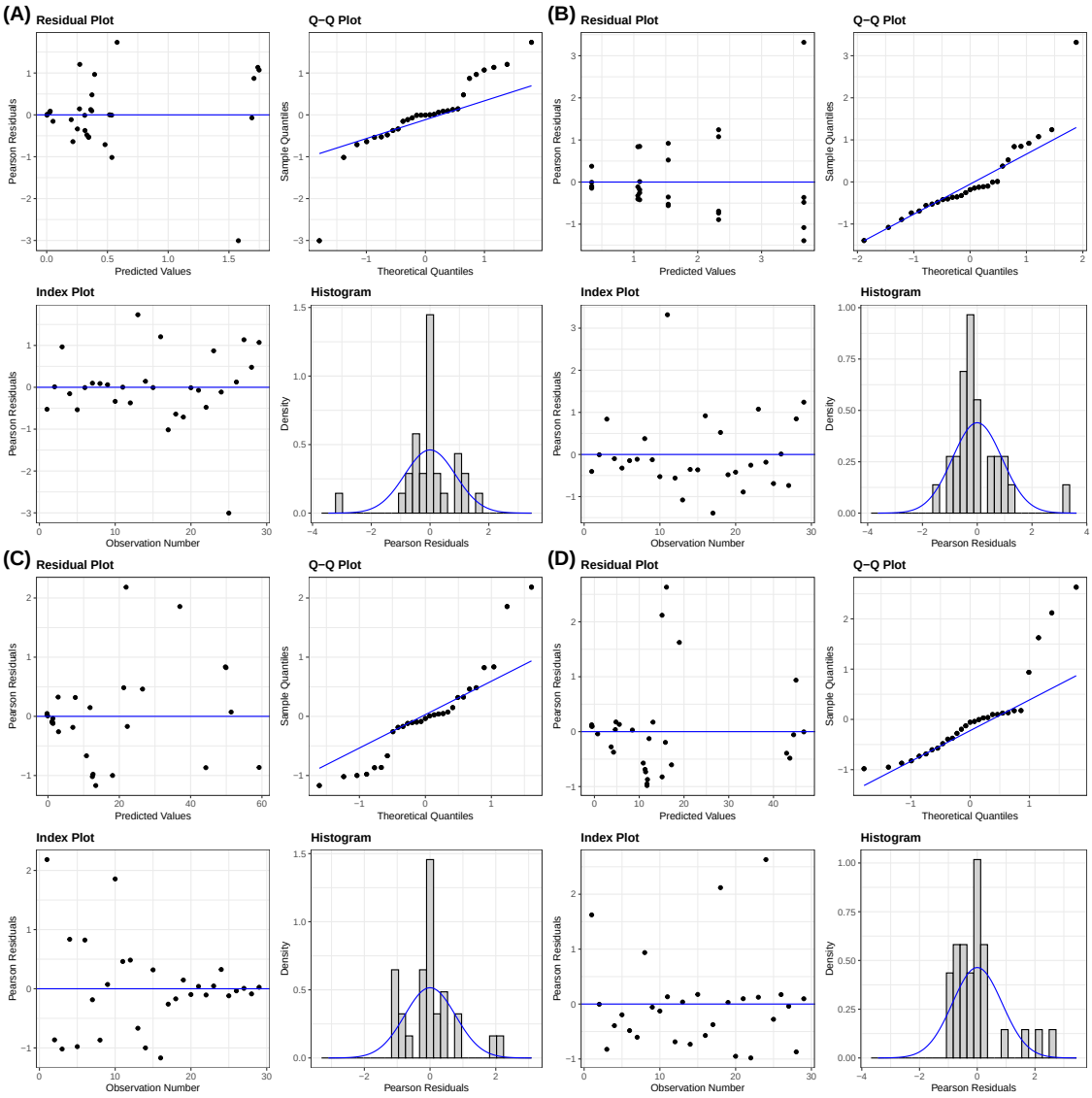


Figure A.20: LMER model performances of the neutrophil and CD4⁺ T cell populations analysed for Figure 6.10. The residual plot, Q-Q plot, Index plot, and distribution of the Pearson Residuals are shown for each cell type analysed and presented in Figure 6.10.**(A)** CD101⁻ Neutrophils, **(B)** CD101⁺ Neutrophils, **(C)** CD15⁻ CD4⁺ T cells, **(D)** CD15⁺ CD4⁺ T cells

B

Supplementary Tables

Table B.1: Hazard Ratios of covariates used in Cox-Proportional Hazards Model in Figure 4.1D

Characteristic	N	HR	95% CI	p-value
Treatment				>0.9
Isotype Control	8	—	—	
Checkpoint Blockade	14	0.85	0.00, Inf	
Experiment				>0.9
2021-1	5	—	—	
2021-2	17	0.00	0.00, Inf	
Cause of Death				0.13
sick	1	—	—	
size	2	0.00	0.00, Inf	
ulcer	19	0.00	0.00, Inf	

[1] HR = Hazard Ratio, CI = Confidence Interval

[2] *p<0.05;* ***p<0.01;*** p<0.001

Table B.2: Hazard Ratios of covariates used in Cox-Proportional Hazards Model in Figure 4.2C

Characteristic	N	HR	95% CI	p-value
Treatment				0.057
Isotype Control	5	—	—	
Anti-CTLA4	5	2.23	0.42, 12.0	
Anti-PD1	5	0.27	0.05, 1.59	
Cage				0.056
1	3	—	—	
2	4	30.6	1.78, 526	
3	4	5.95	0.79, 44.8	
4	4	4.57	0.40, 51.6	
Tumour Size when Treated	15	2.00	1.08, 3.72	0.028*

[1] HR = Hazard Ratio, CI = Confidence Interval

[2] *p<0.05;* ***p<0.01;*** p<0.001

Table B.3: Hazard Ratios of covariates used in Cox-Proportional Hazards Model in Figure 4.6C

Characteristic	N	HR	95% CI	p-value
Treatment				>0.9
Isotype Control	10	—	—	
Anti-CTLA4	17	1.02	0.43, 2.42	
Tumour Size when Treated	27	1.82	1.07, 3.09	0.026*

[1] HR = Hazard Ratio, CI = Confidence Interval

[2] *p<0.05;* ***p<0.01;*** p<0.001

Table B.4: Hazard Ratios of covariates used in Cox-Proportional Hazards Model in Figure 4.7C

Characteristic	N	HR	95% CI	p-value
Treatment				0.7
Isotype Control	19	—	—	
Anti-CTLA4	20	0.68	0.26, 1.82	
Anti-PDL1	20	0.77	0.30, 2.01	
FNA Sampling				0.8
Not performed	29	—	—	
Performed	30	0.91	0.35, 2.34	
Tumour Size when Treated	59	1.29	0.96, 1.73	0.090
Treatment * FNA Sampling	59			>0.9
Anti-CTLA4 * Performed	10	1.13	0.30, 4.29	
Anti-PDL1 * Performed	10	1.03	0.27, 3.90	

[1] HR = Hazard Ratio, CI = Confidence Interval

[2] *p<0.05;* ***p<0.01;*** p<0.001

Table B.5: Hazard Ratios of covariates used in Cox-Proportional Hazards Model in Figure 4.11C

Characteristic	N	HR	95% CI	p-value
Treatment				
Isotype Control	8	—	—	
Anti-CTLA4	12	0.27	0.10, 0.72	0.009**
Anti-PD1	5	0.62	0.19, 1.98	0.4

[1] HR = Hazard Ratio, CI = Confidence Interval

[2] *p<0.05;* ***p<0.01;*** p<0.001

Table B.6: Hazard Ratios of covariates used in Cox-Proportional Hazards Model in Figure 5.3A

Characteristic	N	HR	95% CI	p-value
Treatment				0.008**
Isotype Control	6	—	—	
Anti-CTLA4	13	0.07	0.01, 0.50	
Antibiotics				0.8
No Antibiotics	10	—	—	
With Antibiotics	9	0.82	0.16, 4.26	
Treatment * Antibiotics	19			0.8
Anti-CTLA4 * With Antibiotics	6	0.81	0.10, 6.60	

[1] HR = Hazard Ratio, CI = Confidence Interval

[2] *p<0.05;* ***p<0.01;*** p<0.001

Table B.7: Hazard Ratios of covariates used in Cox-Proportional Hazards Model in Figure 6.1B

Characteristic	N	HR	95% CI	p-value
Treatment				0.089
CFA	5	—	—	
CFA + Anti-CTLA4	5	0.26	0.06, 1.07	
CFA + Anti-PD1	5	0.59	0.16, 2.17	
Tri-therapy	5	0.16	0.04, 0.75	
Anti-CTLA4 + Anti-PD1	5	0.15	0.03, 0.72	
Anti-CTLA4	5	0.14	0.03, 0.65	
Age	30	0.31	0.12, 0.81	0.013*
Tumour Size when Treated	30	2.20	1.28, 3.77	0.002**

[1] HR = Hazard Ratio, CI = Confidence Interval

[2] *p<0.05;* ***p<0.01;*** p<0.001

Table B.8: Hazard Ratios of covariates used in Cox-Proportional Hazards Model in Figure 6.2A

Characteristic	N	HR	95% CI	p-value
Intraperitoneal Treatment				0.5
Checkpoint Blockade	19	—	—	
Isotype Control	18	0.69	0.25, 1.90	
Intratumoural Treatment				0.6
CFA	19	—	—	
PBS	18	1.30	0.47, 3.57	
Experiment				0.033*
2022-1	17	—	—	
2022-2	20	2.30	1.05, 5.04	
Cage				0.014*
1	7	—	—	
2	10	4.84	1.57, 15.0	
3	10	0.93	0.29, 2.93	
4	10	2.04	0.72, 5.78	
Intraperitoneal Treatment * Intratumoural Treatment	37			0.5
Isotype Control * PBS	9	1.69	0.37, 7.71	

[1] HR = Hazard Ratio, CI = Confidence Interval

[2] *p<0.05;* ***p<0.01;*** p<0.001

Table B.9: Hazard Ratios of covariates used in Cox-Proportional Hazards Model in Figure 6.2C

Characteristic	N	HR	95% CI	p-value
Treatment				0.059
PBS	8	—	—	
M. butyricum	5	4.02	1.10, 14.7	
M. tuberculosis H37Ra	5	3.35	0.95, 11.9	

[1] HR = Hazard Ratio, CI = Confidence Interval

[2] *p<0.05;* ***p<0.01;*** p<0.001

Table B.10: Hazard Ratios of covariates used in Cox-Proportional Hazards Model in Figure 6.5C

Characteristic	N	HR	95% CI	p-value
Treatment				0.6
PBS	14	—	—	
CFA	16	1.58	0.59, 4.21	
10x CFA	18	1.15	0.46, 2.91	
Tumour Size when Treated	48	1.76	1.11, 2.80	0.012*

[1] HR = Hazard Ratio, CI = Confidence Interval

[2] *p<0.05;* ***p<0.01;*** p<0.001

C

Simple and effective bacterial-based intratumoral cancer immunotherapy

Open access Original research

Journal for ImmunoTherapy of Cancer

Simple and effective bacterial-based intratumoral cancer immunotherapy

Christina S E Carroll,[1] Erin R Andrew,[1] Laeeq Malik,[2,3] Kathryn F Elliott,[4] Moira Brennan,[4] James Meyer,[5] Alexander Hintze,[6] Andrew A Almonte,[1] Cassandra Lappin,[4] Philip MacPherson,[4] Klaus-Martin Schulte,[3] Jane E Dahlstrom,[3,7] Rohit Tamhane,[8] Teresa Neeman,[9] Elizabeth W Herbert,[5] Maurice Orange,[6] Desmond Yip,[2,3] Rachel Allavena,[4] Aude M Fahrer [1]

To cite: Carroll CSE, Andrew ER, Malik L, *et al*. Simple and effective bacterial-based intratumoral cancer immunotherapy. *Journal for ImmunoTherapy of Cancer* 2021;**9**:e002688. doi:10.1136/jitc-2021-002688

► Additional supplemental material is published online only. To view, please visit the journal online (http://dx.doi.org/10.1136/jitc-2021-002688).

CSEC, ERA, LM and KFE contributed equally.
MO, DY, RA and AMF contributed equally.

Accepted 14 July 2021

Check for updates

© Author(s) (or their employer(s)) 2021. Re-use permitted under CC BY-NC. No commercial re-use. See rights and permissions. Published by BMJ.

For numbered affiliations see end of article.

Correspondence to
Dr Aude M Fahrer;
aude.fahrer@anu.edu.au

ABSTRACT

Background We describe intratumoral injection of a slow-release emulsion of killed mycobacteria (complete Freund's adjuvant (CFA)) in three preclinical species and in human cancer patients.

Methods Efficacy and safety were tested in mammary tumors in mice, in mastocytomas in mice and dogs, and in equine melanomas. In mice, survival, tumor growth, and tumor infiltration by six immune cell subsets (by flow cytometry) were investigated and analyzed using Cox proportional hazards, a random slopes model, and a full factorial model, respectively. Tumor growth and histology were investigated in dogs and horses, as well as survival and tumor immunohistochemistry in dogs. Tumor biopsies were taken from human cancer patients on day 5 (all patients) and day 28 (some patients) of treatment and analyzed by histology. CT scans are provided from one patient.

Results Significantly extended survival was observed in mouse P815 and 4T1 tumor models. Complete tumor regressions were observed in all three non-human species (6/186 (3%) of mouse mastocytomas; 3/14 (21%) of canine mastocytomas and 2/11 (18%) of equine melanomas). Evidence of systemic immune responses (regression of non-injected metastases) was also observed. Analysis of immune cells infiltrating mastocytoma tumors in mice showed that early neutrophil infiltration was predictive of treatment benefit. Analysis of the site of mastocytoma regression in dogs weeks or months after treatment demonstrated increased B and T cell infiltrates. Thus, activation of the innate immune system alone may be sufficient for regression of some injected tumors, followed by activation of the acquired immune system which can mediate regression of non-injected metastases. Finally, we report on the use of CFA in 12 human cancer patients. Treatment was well tolerated. CT scans showing tumor regression in a patient with late-stage renal cancer are provided.

Conclusion Our data demonstrate that intratumoral injection of CFA has major antitumor effects in a proportion of treated animals and is safe for use in human cancer patients. Further trials in human cancer patients are therefore warranted. Our novel treatment provides a simple and inexpensive cancer immunotherapy, immediately applicable to a wide range of solid tumors, and is suitable to patients in developing countries and advanced care settings.

INTRODUCTION

Induction of a systemic anti-cancer immune response by intratumoral injection of bacterial products has been previously proposed by our group[1] and has been recently confirmed in a seminal paper.[2] The rationale is that the immune system has evolved to recognize conserved pathogen-associated molecular patterns (PAMPs). Such recognition is the key to initiating a systemic immune response. Thus, injection of PAMPs directly into tumors has the potential to induce or restore the host immune response against the cancer.

Enlisting bacteria to treat cancers has a long history, dating back well over a century. Best known, historically, is the successful work of William Coley who repeatedly injected (every 2 to 3 days for several months) preparations of dead bacteria into hundreds of patients with inoperable cancers. For the first several years, he injected these 'Coley's toxins' into and around tumors. He later switched to intravenous injections. While both approaches resulted in durable cancer remissions in many patients (eg, of 312 inoperable sarcoma cases, 190 patients experienced complete tumor regressions[3]), it appears that he ultimately considered intratumoral injections most effective.[4]

More recently, interest has been revived in using bacteria and viruses to treat cancer.[5 6] Several therapies are based on live, often 'oncolytic' bacteria or viruses.[7 8] Others are based on dead bacteria or bacterial products.[2 9] Regardless of the published rationale, in all these cases, modulation of the immune response is a likely mechanism of action.[1 10]

Unexpectedly, bacteria have also been implicated in the mechanism of action of chemotherapies[11–13] and of checkpoint inhibitor cancer therapies.[14–16] We have recently proposed possible mechanisms for the latter.[17]

It has been known for several years that bacteria can colonize intestinal tumors.[18 19] Very recently, bacteria have been identified in human cancers previously assumed to be sterile,[20] and bacterial peptides have been identified on the major histocompatibility complex (MHC) molecules of melanomas,[21] thereby providing an extra target for lysis of melanomas by bacteria-specific cytotoxic T cells. Thus, harnessing bacteria in anticancer therapies is a promising and rapidly evolving field of research.

Here, we describe in vivo trials of a novel form of intratumoral immunotherapy, injection of emulsified complete Freund's adjuvant (CFA). CFA is an extremely potent immune stimulant, developed in the 1950s.[22] It is made up of three components: mineral oil and surfactant (together making up incomplete Freund's adjuvant (IFA), or Montanide ISA-51, which is already licensed for use in humans) and heat-killed *Mycobacteria*. Thus, both chemical components of CFA have previously been licensed for human use, and dead *Mycobacteria* are inherently safer than the live *Mycobacteria* used both in the widely administered childhood intradermal BCG vaccine against tuberculosis and as an intravesical treatment for superficial bladder cancer. If correctly emulsified, CFA forms a slow-release depot at the injection site, meaning that one injection provides continuous immunostimulation over a period of weeks. CFA therefore has the potential to be a simple and inexpensive form of cancer immunotherapy, accessible for use in both developed and emerging economies.

In this study, we describe the use of CFA in three preclinical species and in human cancer patients. We show that intratumoral injection of CFA induces anticancer responses in a significant proportion of treated animals, and is safe to use in human cancer patients.

MATERIALS AND METHODS

Complete freund's adjuvant

CFA for mouse, dog, and horse experiments, and for the Canberra patient trial, was from Becton Dickinson (New Jersey, USA, catalog number: 263810) containing 0.5 mg/mL *Mycobacterium butyricum*. CFA was emulsified 1:1 with sterile saline using two 5 mL Luer lock glass syringes or plastic syringes connected via an 18G microemulsifying needle (Cadence Science, Virginia, USA) to obtain a water-in-oil emulsion.

CFA used in Swiss patients 1 and 2 was from Sigma (Michigan, USA, catalog number: F5881). CFA used in patients 3 and 4 was AdjuLite from Pacific Immunology Corp (California, USA, catalog number: A5001). Both contain 1 mg/mL *Mycobacterium tuberculosis* strain H37Ra. CFA used in the Swiss patients was emusified with Abnova Viscum (Pforzheim, Germany) or other non-fermented extracts of Viscum Album (Hiscia, Arlesheim, Switzerland).

Mice and cell lines

P815 (ATCC TIB-64) mastocytoma cells, 4T1 (ATCC CRL-2539) mammary adenocarcinoma and CT26.wt (ATCC CRL-2638) colorectal carcinoma (American Tissue Culture Collection, Virginia, USA) were cultured in medium supplemented with 10% fetal calf serum (FCS), 1 mM sodium pyruvate, 0.1 M HEPES, 100 IU/mL penicillin, and 100 µg/mL streptomycin (Gibco). P815 cells were cultured in Dulbecco's Modified Eagle Medium (DMEM) containing 4.5 g/L D-glucose, and Glutamax (Gibco), 4T1 and CT26 cells in RPMI-1640 containing Glutamax (Gibco). Adherent cells were recovered using 0.25% trypsin (Gibco), and counted by hemocytometer, using Trypan Blue (Sigma-Aldrich) to exclude dead cells. Cells were re-suspended in 50% medium without supplements, 50% phosphate-buffered saline prior to injection.

Prior to P815 cell injection, female DBA/2 J mice between 6 and 12 weeks of age (Animal Resource Centre, Perth, Australia) were shaved at the injection site and anesthetized (2% isoflurane). Tumors were then induced by subcutaneous (orthotopic) injection of 3×10^5 P815 cells in a volume of 0.1 mL. 4T1 cells (1×10^5 cells in 15 µl)were injected orthotopically into the mammary fat pad or CT26 cells (5×10^5 in 0.1 mL) were injected subcutaneously into the shaved injection site (non-orthotopic) of anesthetized female 6-week-old to 10-week-old Balb/c mice (bred at the ANU).

Tumors typically reached 4–7 mm (average of two perpendicular measurements measured using electronic calipers) 7–14 days after injection. As tumor size was slightly variable, prior to treatment, mice were divided into groups based on tumor size (to the nearest 0.5 mm) and then mice in each size group were randomly assigned as treatment (0.05 mL intratumoral CFA) or control animals (0.05 mL intratumoral saline), to ensure groups had similar numbers of mice of each tumor size. Each cage contained both treatment and control animals to avoid cage-to-cage variation. For many experiments, treatment was semiblinded, recorded separately (not on the cages), and sealed until the completion of the experiment, so as to prevent bias in tumor measurements. Tumors were measured using digital calipers every 1–2 days. Mice were euthanized when tumors reached 15 mm in diameter or showed signs of illness (hunched posture, inactivity).

Analysis of tumor-infiltrating cells

Fine-needle aspirates (FNAs) were taken with a 25G needle from anesthetized P815 tumor-bearing mice on days 1, 3, 5, 8, 11, 14, and 16 post-treatment, with individual mice receiving between two and five FNAs.[23] Briefly, aspirates were digested at 37°C for 20 min using 5 mg/mL Collagenase type I (Worthington Biochemical, UK), 1.5 mg/mL Hyaluronidase (Sigma-Aldrich), and 0.01 mg/mL DNAse I (Worthington Biochemical) in DMEM supplemented with 1% FCS. Samples were then stained and analyzed by flow cytometry (LSRII, Becton Dickinson, USA; FlowJo, Treestar, USA). Two stains were used to identify immune cell types. Both stains contained a P815 tumor marker anti-CD63 (NVG-2) PE, pan-immune cell marker anti-CD45.2 (104) Alexa Fluor 488, and 7-aminoactinomycin-D (Life Technologies) for live/dead cell discrimination, as well as: Stain

A—anti-CD8α (53.6.7) APC Cy7 (BD Biosciences), anti-CD4 (GK1.5) PE-Cy7, anti-CD25 (PC61) Brilliant Violet 421, anti-CD19 (6D5) Brilliant Violet 510, and anti-Pan-NK (CD49b) (Dx5) APC. Stain B—anti-CD11b (M1/70) Brilliant Violet 510, anti-CD11c (N418) PE Cy7, anti-F4/80 (BM8) Brilliant Violet 421, anti-Ly6G/Ly6C (GR1) (RB6-8C5) APC Cy7, and anti-Siglec-F (E50-2440) Alexa Fluor 647 (BD Biosciences, USA). All antibodies were from Biolegend (California, USA) unless otherwise specified.

Dogs

Dog experiments were approved by the University of Queensland institutional animal ethics committee (AEC approval numbers SVS/45/12; SVS/328/14/JMKT; ANRFA/SVS/039/14). Dogs naturally suffering from mastocytoma (mast cell tumor), previously diagnosed by either biopsy or cytologic examination by their referring veterinarian or a commercial diagnostic company, were recruited after owner briefing and completion of consent forms. Medical records, pathology reports, and recuts of paraffin-embedded sections from pretrial biopsies were obtained from referring veterinarians and commercial diagnostic companies with owners' consent.

Dogs underwent a full clinical examination by a registered veterinary surgeon with hematology and clinical chemistry profiles taken if required, to ascertain their clinical status and ability to tolerate anesthesia and treatment. At least 30 min prior to CFA treatment, fine-needle aspiration or surgical biopsy, dogs were premedicated with 1–2 mL of Histamil (chlorpheniramine maleate 10 mg/mL; Ilium Troy laboratories Pty, Glendenning, NSW) to reduce the risk of mast cell degranulation anaphylactoid reactions caused by tumor handling. For biopsies, animals were anesthetized. Sedation was with acepromazine (0.05 mg/mL) and preoperative and postoperative pain relief was with methadone (0.5 mg/kg). Induction of anesthesia was with Alfaxan (10 mg/mL alfaxalone; Jurox Pty, Rutherford, NSW) and maintenance with gaseous anesthesia, isoflurane (100%).

Pretreatment incisional biopsy (8 mm punch or wedge as clinically indicated) or FNA sample was taken where confirmatory diagnosis from a pathologist had not been previously achieved. Tumor biopsies were fixed in 10% neutral buffered formalin before routine paraffin embedding and staining with either H&E or toluidine blue stain by routine methods. For lymphocyte identification, de-paraffinized formalin-fixed tumor sections were stained by routine immunohistochemical methods using Dako, clone F7.2.38 (Dako, Hamburg, Germany) for $CD3^+$ T cells at 1:600 and AbD Serotec clone HM57 (Serotec, Oxford, UK) at 1:1800 for CD79a B cells as primary antibodies. Normal canine lymph node was used as a positive control and omission of primary was used as a negative control for each run. Canine mastocytomas were graded based on the schemes proposed by Kiipel *et al*.[24]

Clinical assessments were performed at 1, 3, 6, and 12 weeks post-treatment as owner schedules allowed or on an ad hoc basis at owners' requests to address concerns or evaluate changes in clinical status. Dog well-being was further monitored with a questionnaire at 0 (pretreatment), 1, 3, 6, 12 weeks post-treatment, and as an ad hoc basis at later time points (The University of Queensland Institutional Human Research Ethics Approval 2014001294).

Horses

Gray horses diagnosed with melanoma were treated at the Adelaide Plains Equine Clinic (Gawler, South Australia). Informed consent was obtained from each owner and the veterinarian (author EWH) had general ethical research approval from the Department of Primary Industries and Regions, South Australia. Progression was followed by ultrasound measurements.

Equine melanoma biopsy material was fixed in 10% neutral buffered formalin before paraffin embedding, sectioning at 4 microns, and staining with either H&E by routine methods. Serial sections of tumors were subjected to melanin bleach.

Patients

Swiss patients were treated at the Ita Wegman Klinik and Lukas Klinik, now merged into Klinik Arlesheim, Arlesheim, Switzerland. Patients volunteering for treatment signed informed consent forms, as required under Swiss law.

Australian trial: Australian New Zealand Clinical Trials Registry: ACTRN12616001637437. Due to administrative oversight, the trial was (retrospectively) registered after recruitment of the first patient, but before any further patients were recruited. The trial was approved by the ACT Health Human Research Ethics Committee (ETH.11.15.234) and by the Australian National University Human Research Ethics Committee (Protocol 2016/395), and all patients volunteering for treatment signed informed consent forms. In this ongoing dose-escalation study, two cohorts of patients with advanced cancer (squamous cell carcinoma of the skin, clear cell renal cell carcinoma, adenocarcinoma of the prostate, transitional cell carcinoma of bladder, and cervical carcinoma) after exhausting standard of care therapies were treated with either 0.5 mL or 1 mL of CFA. CFA was administered into primary or metastatic cancer site either in clinic or under imaging guidance depending on tumor location. All patients underwent tumor biopsy 4 days after CFA administration. Clinical examination and laboratory assessments were performed every 6 weeks and CT scan repeated every 12 weeks. Patient history of BCG vaccination was not available. Tuberculin skin testing (TST) was not performed.

Histology

Four micrometer thick sections were made from formalin-fixed paraffin-embedded tissue. Sections were stained with H&E (Sigma-Aldrich, St Louis, Missouri, USA), and all specimens were examined by an experienced pathologist (JED).

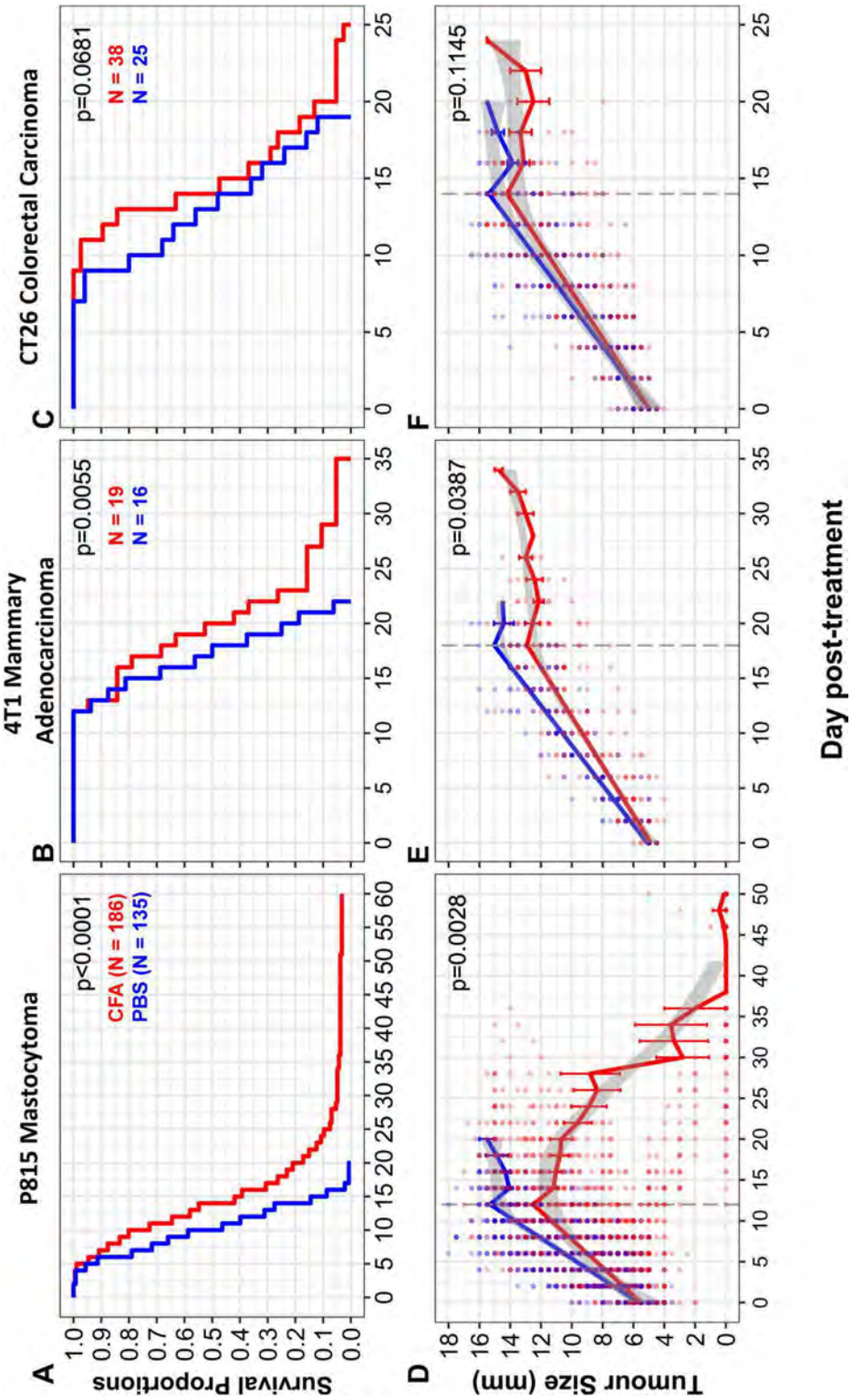


Figure 1 (Continued)

Figure 1 Treatment of solid tumors in mice with intratumoral CFA. Solid tumors were induced in 8-week-old to 12-week-old DBA/2J (P815) or BALB/c (4T1 or CT26) mice by subcutaneous injection of 3×10^5 (P815) or 5×10^5 (CT26) cells into the animals' flank or 1×10^5 cells into the mammary fat pad (4T1). Tumors were measured several times per week with digital calipers and the tumor size (mm) was determined as the average of two perpendicular measurements. Mice were treated with intratumoral CFA (red) or phosphate-buffered saline (PBS) (blue) when tumors reached 4–7 mm in average diameter. (A–C) Survival curves of CFA-treated and PBS-control mice were analyzed using a Cox proportional hazards model. (A) CFA increases survival in P815 tumor-bearing mice. CFA-treated mice had a statistically significant increase in survival compared with PBS-control mice (p<0.0001, HR: CFA:PBS=0.34, 95% CI (0.257 to 0.438)). The median survival of CFA-treated mice was higher (14 days post-treatment) than PBS-control mice (10 days post-treatment). CFA n=186, PBS n=135. Data pooled from 31 separate experiments. Six complete tumor regressions were observed in CFA-treated mice. (B) CFA increases survival in 4T1 tumor-bearing mice. A statistically significant increase in survival was observed in CFA-treated mice compared with PBS controls (p=0.0055, HR: CFA:PBS=0.32, 95% CI (0.145 to 0.717)). The median survival of CFA-treated mice was 20 days compared with 17.5 days for PBS controls. CFA n=19, PBS n=16. Data pooled from three separate experiments. (C) CFA does not significantly increase survival in CT26 tumor-bearing mice. Statistical analysis did not show a significant effect of intratumoral CFA treatment on survival compared with PBS-control mice (p=0.0681, HR: CFA:PBS=0.61, 95% CI (0.360 to 1.037)). The median survival of CFA-treated mice was 14 days compared with 13 days for PBS controls. CFA n=38, PBS n=25. Data pooled from three separate experiments. (D–F) Tumor growth rates. To determine if the rate of growth differed between CFA-treated (red) and PBS-control treated (blue) mice, a random slopes model was developed using R software to analyze the interaction between treatment and tumor growth over time. Tumor growth slopes were compared up to the point at which approximately 50% of mice were euthanized (as the attrition of mice confounds the analysis beyond this point: P815=day 12, 4T1=day 18, CT26=day 14; represented by the dashed line), after which the raw means are shown. Error bars represent the SE. Tumor sizes for individual mice are shown by dots, with opacity set to 50% to visualize overlapping points. The gray shaded area indicates 95% CI, determined by the locally estimated scatterplot smoothing (LOESS) method. (D) CFA decreases growth of P815 tumors. ANOVA p=0.0028, CFA n=32, PBS n=29. Data pooled from five separate experiments. (E) CFA reduces growth of 4T1 tumors. ANOVA p=0.148, CFA n=19, PBS n=16. Data pooled from three separate experiments. (F) CFA does not reduce tumor growth of CT26 tumors. ANOVA p=0.1145, CFA n=38, PBS n=25. Data pooled from three separate experiments. Mice that received fine-needle aspirates were included in part A but not in parts B–F. ANOVA, analysis of variance; CFA, complete Freund's adjuvant.

RESULTS

Mouse studies

Efficacy of intratumoral CFA injection was tested in three mouse models of cancer: P815 mastocytoma, 4T1 metastatic breast cancer, and CT26 colorectal cancer. Efficacy was observed in P815 and 4T1 (figure 1A,B). In both cases, tumor cell lines were injected orthotopically (subcutaneously or in the mammary fat pad, respectively). Statistically significant efficacy was not observed in the non-orthotopically injected CT26 colorectal cancer model (figure 1C). The tumors were allowed to grow to an average of 5 mm in diameter. They were then injected once with 0.05 mL of CFA emulsified in saline or with saline alone as a control. Mice were euthanized when they became ill or if the cancer reached 15 mm in diameter. As shown in figure 1A,B, mice treated with CFA survived longer than control mice (p<0.00001 for P815, p=0.0055 for 4T1). Tumor growth was significantly slowed in the P815 model and 4T1 models (figure 1D,E) but not in the CT26 model (figure 1F). Illness is almost always due to metastatic burden, and CFA was shown to slow the progression of liver metastases in the P815 model (online supplemental figure 1A). Six mice treated for mastocytoma showed complete regression of their tumor (figure 1A and online supplemental figure 1B) and survived for up to 2 years without tumor recurrence.

IFA was injected intratumorally as an extra control in some experiments. It was found that IFA was no better than saline, thus the mycobacteria rather than the mineral oil emulsion is key to success of the treatment (online supplemental figure 1C).

Canine studies

Given our success in treating mastocytoma in the mouse model, and the high incidence and associated morbidity and mortality of mastocytoma in the pet dog population, a pilot clinical trial using intratumoral CFA was conducted on pet dogs suffering from spontaneous mastocytoma. Dogs suffering from spontaneous cancers are increasingly being recognized as an excellent comparative oncology model in which to study cancer therapies.[25–27] Unlike mouse models seeded with rapidly dividing cell lines already selected for immune escape, canine cancers, like human cancers, will have developed over a long time frame and in the presence of the host immune response. Mastocytoma is common in dogs accounting for 7%–21% of canine cutaneous neoplasms.[24] High-grade mastocytoma has a median survival time of less than 4 months and is associated with paraneoplastic syndromes causing high morbidity.[24]

As shown in table 1, of 14 dogs treated with one injection of 0.05–0.2 mL of emulsified CFA, 3 dogs showed complete regression of their tumor, in 2 cases leading to substantially extended survival. The first in a Rottweiler whose nasal/lip mass returned following cessation of chemotherapy (predicted survival 8 weeks, actual 12 months), the second in a German short-haired pointer whose leg tumor recurred despite radical surgical resection (predicted survival 8–12 weeks, actual 16 months). Histology of pretreatment and post-treatment biopsies is shown in figure 2A, with few immune cells seen in the tumors before treatment, but residual immune cell infiltrates present following complete tumor regression. In

Table 1 Companion dogs with naturally occurring mastocytoma treated with CFA

Dog	MCT grade (Kiupel/ Patnaik)	Dose CFA	Clinical notes, response to therapy, side effects	Disease-free interval	Survival expected vs actual (weeks) PI	Response
Rottweiler 7 y MN	High/3	0.05	Permanent remission in injected unresectable tumor 5 weeks PI. Multiple de novo tumors from 4 months PI treated with surgery. Euthanased due to unrelated osteosarcoma. Side effects: local swelling, lethargy at 3 weeks post injection preceding mass regression.	4 months	8*/51	Remission. Extended survival
Maltese X Shih Tzu 8 y FN	Low/1	0.05	Gradual reduction in size PI. Tumor surgically resected 9 months post-treatment. Side effects: Nil reported	–	+104†/alive	Size reduction.
Maltese 13 y FN	High/3	0.05	Advanced disease on presentation. Rapidly progressive disease PI. Side effects: swelling and limping.	–	2*/2	–
German shorthaired pointer 6 y MN	Low/2	0.05	Permanent remission of injected tumor and distant untreated MCT 3 weeks PI. Euthanased after hemoptysis cause unknown. Side effects: nil reported within 12 months. Pruritus and coughing prior to euthanasia.	16.75 months	8–12*/67	Remission. Extended survival
Staffordshire bull terrier 9 y MN	Low/2	0.1	Static disease of injected tumor for 3 months. Euthanased for welfare reasons 6 months PI. Side effects: nil reported	–	ND/29	Static disease 3 months.
Golden retriever 9 y FN	High/2	0.1	Advanced disease on presentation. Rapidly progressive disease PI. Side effects: nil reported .	–	2*/2	–
Shar pei 6 y FN	High/3	0.1	Advanced disease on presentation. Rapidly progressive disease PI. Side effects: local ulceration at injection site.	–	12*/13	–
Belgian Shepherd 12 y FN	Ungraded	0.1	Gradual progressive disease. Side effects: nil reported	–	+104†/alive	–
Staffordshire bull terrier 7 y FN	Low/1	0.2	Gradual progressive disease. Side effects: nil reported	–	+104†/alive	–
Staffordshire bull terrier 12 y FN	Low/1	0.2	Static disease. Side effects: central scab, pruritus.	–	+104†/alive	Static disease.
Jack Russell 7 y FN	Low/1	0.2	Gradual progressive disease. Surgical removal 16 months post Tx. Local reoccurrence 6.5 months post-surgery. Side effects: pruritus	–	+104†/alive	–

Continued

Table 1 Continued

Dog	MCT grade (Kiupel/ Patnaik)	Dose CFA	Clinical notes, response to therapy, side effects	Disease-free interval	Survival expected vs actual (weeks) PI	Response
Staffordshire bull terrier 6 y FN	Low/2	0.2	Rapid progressive disease PI. Surgical removal of masses 19/8/14 Side effects: nil reported	–	ND/alive	–
Staffordshire bull terrier 8 y FN	Ungraded	0.2	Gradual reduction in size PI. Side effects: nil reported	–	ND/alive	Size reduction
Miniature poodle 9 y FN	Low/2	0.1	Permanent remission of injected MCT. Euthanased unrelated nasal adenocarcinoma. Side effects: ulceration.	+3 months	+104†/26	Remission

*Survival predicted by oncologist or veterinarian.
†Survival predicted from literature; alive=as at census date, March 1, 2016.
CFA, complete Freund's adjuvant; FN, female neuter; MN, male neuter; ND, not determined; PI, postinjection.

the German short-haired pointer, another unsampled secondary mass previously diagnosed as a mast cell tumor regressed in addition to the injected tumor. Figure 2B shows immunohistochemistry on the injected tumor mass and on a de novo high-grade mastocytoma arising in the neck of the Rottweiler 17 weeks after treatment of his nasal/lip mass. B and T cells can be seen to clearly increase at the site of tumor regression and are also seen in a de novo neck tumor (not injected with CFA), which notably did not recur despite incomplete surgical regression. Further, the treatment was well tolerated (table 1). A subset of dogs which previously had ulceration of skin or mucous membrane prior to treatment exhibited some ulceration after CFA injection. In the Rottweiler on the days preceding lip mass regression, there was a 24-hour period of malaise and reduced activity reported by the owner. Thus, the side effect profile was favorable and could be classified as grade 1 on the veterinary cooperative oncology group-common terminology criteria for adverse events.[28]

These results show that treatment with CFA can result in complete regression of naturally occurring tumors and importantly, suggest that the treatment can have a systemic immune-mediated effect.

Equine studies

As well as treating dogs, the treatment was trialed in horses suffering from naturally occurring melanoma. Melanoma is a common problem in gray horses (affecting >70%), as the mutation causing the gray colouration also predisposes to melanoma.[29] Tumors often occur around the tail, peri-anal area, lips and eyelids.[30] While the disease progression is not as aggressive as human melanoma, it is a substantial cause of morbidity and mortality in gray horses due to space occupying effects in the perineum and throat and the presence of tumors within the viscera and thoracic organs.[30] Few treatment options are available other than surgical resection, which is often impractical as the disease is multicentric.

Eleven horses were treated with intratumoral injections of 0.1–0.3 mL of CFA emulsified with saline into their melanomas. Details are given in online supplemental table 1. Representative histology is shown in online supplemental figure 2. Tumors were imaged by ultrasonography to follow progression of tumors after treatment. Three horses (27%) showed evidence of clinical response. This included mass remissions and reductions in mass size.

Correlation of immune infiltrate with survival

To investigate the timing of immune infiltration into the tumor following CFA injection, we again made use of the mouse mastocytoma model. We have previously published a novel technique that allows serial quantitation of immune infiltrates without altering survival in mice injected with P815 tumors.[23] As can be seen in figure 3, CFA treatment induced extensive infiltration of immune cells into the tumor compared with injection

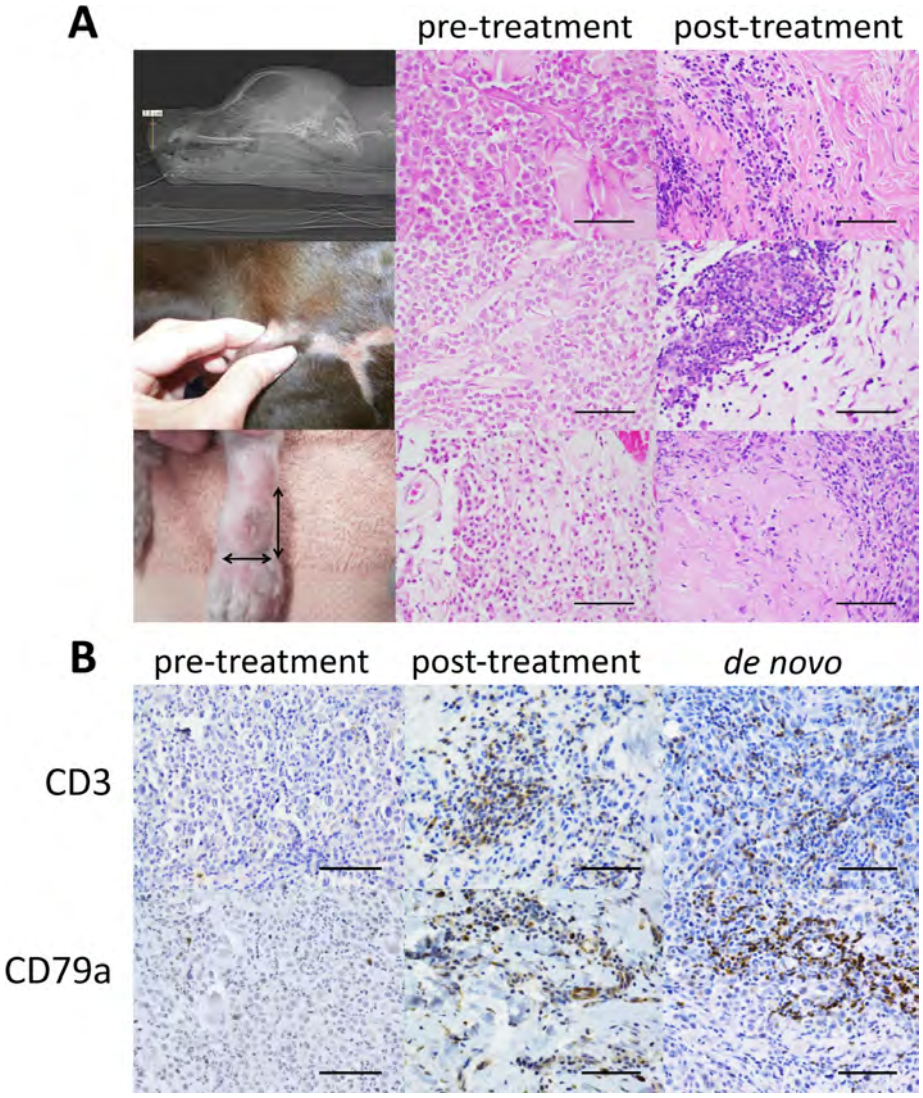


Figure 2 Histologic features of dogs showing regression. (A) Left column: macroscopic images, middle column: histology of pretreatment biopsies, right column: histology of post-treatment biopsies; in all three cases, the tumor has completely regressed and residual lymphocyte, plasma cell, and macrophage infiltrates are present in the dermal connective tissue. H&E stains magnification 400x, scale bar 50 microns. Top row: pretreatment medical imaging of 'Rottweiler' taken on October 9, 2012, showing a 3H×2.5Wx1.8D cm tumor within the nasal philtrum and lip (lateral view shown); pretreatment biopsy (September 27, 2012) showing a high-grade mast cell tumour; post-treatment biopsy of the site of tumor regression (October 23, 2013) approximately 4.5 months postinjection. Middle row: pretreatment morphology of the lateral thigh tumor in 'German short-haired pointer' on October 22, 2013, large surgical scars from the previous radical surgical resection are visible; pretreatment biopsy (July 11, 2013) showing a low-grade MCT; post-treatment biopsy at the site of tumor regression (November 29, 2013) approximately 22 days post-injection. Bottom row: pretreatment morphology of limb MCT in 'miniature poodle' on February 25, 2015; initial pretreatment biopsy (February 25, 2015) low-grade MCT; post-treatment autopsy tissue (November 13, 2015) at the site of tumor regression, approximately 8.5 months after injection. (B) Immunohistochemistry for T (CD3) top row and B (CD79a) bottom row lymphocytes on paraffin-embedded formalin-fixed tissue of high-grade MCTs from 'Rottweiler'. Left: pretreatment biopsy taken of the nasal/lip tumor (September 27, 2012) shows very rare T cells and rare plasma cells, clusters of lymphocytes and immune cells were absent. Middle: post-treatment biopsy of the site of lip/nasal tumor regression (October 23, 2013) shows clusters of co-associated T and B lymphocytes (serial sections). Right: representative de novo high-grade mastocytoma arising on the neck 17 weeks post-complete Freund's adjuvant treatment for the initial nasal/lip mass. Clusters of T and B lymphocytes were prominent throughout the tumor, which did not reoccur despite incomplete surgical resection. All panels magnification 400x; scale bar 50 microns. Note: vascular wall staining is a feature of the CD79a antibody.

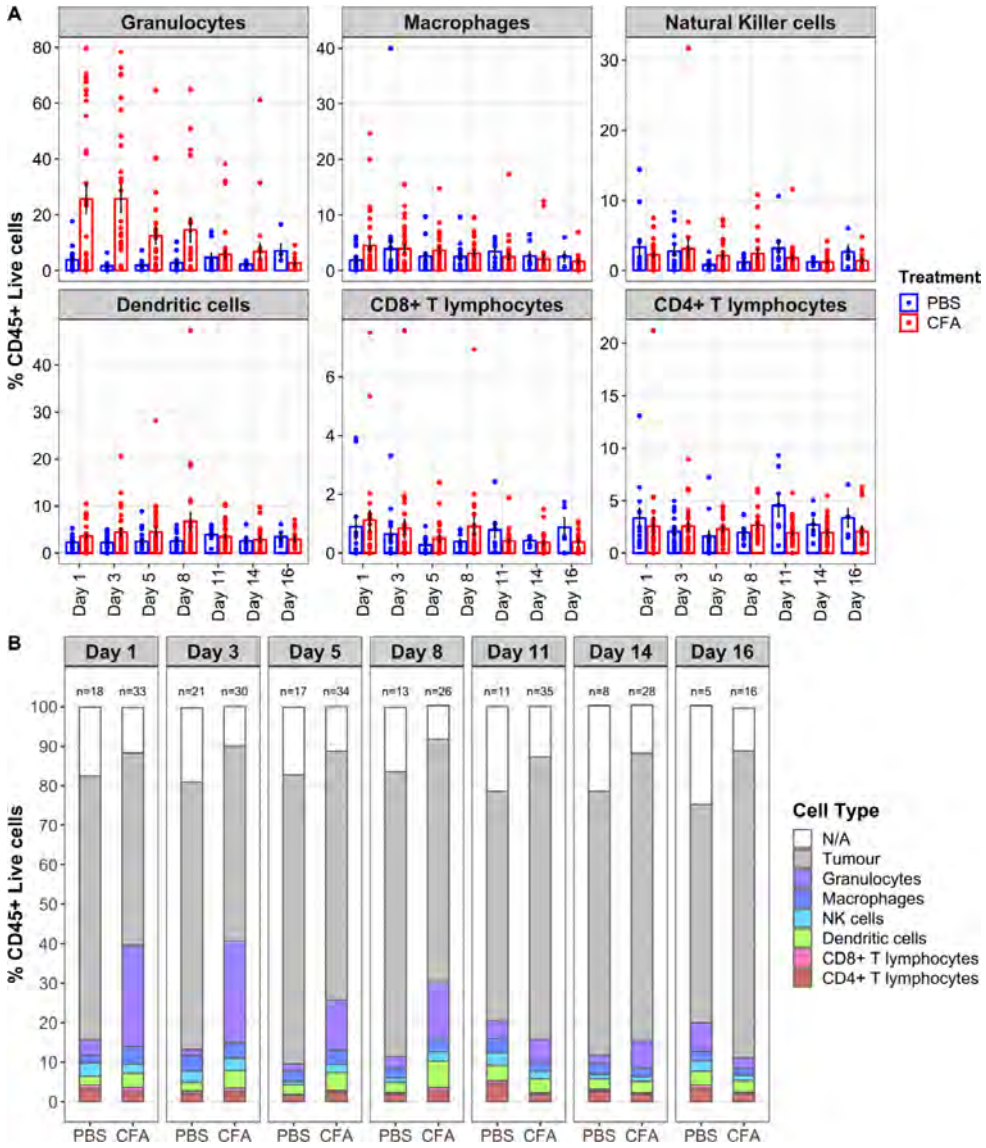


Figure 3 Enumeration of tumor-infiltrating immune cells in P815 tumors following treatment. Tumor-infiltrating immune cells identified by fine-needle aspirates (FNAs) of P815 tumors in mice. Tumor samples were collected by FNA on days 1, 3, 5, 8, 11, 14, and 16 following CFA/PBS treatment and analyzed by flow cytometry to identify tumor cells and tumor-infiltrating immune cells using the gating strategy previously described (Carroll *et al*, 2015). (A) The percentage of tumor-infiltrating immune cells are shown for individual CFA-treated mice (red dots) and PBS-control treated mice (blue dots). To avoid fluctuations in percentages due to low numbers of cells, any percentages from populations with less than 15 cells in the previous gate were excluded. The raw means and SEs are shown. A linear mixed effects model (to determine which cell types changed significantly in response to treatment, when considering overall data from all seven sampling days) revealed a significant effect of CFA treatment on the infiltration of granulocytes (p=0.0025) and dendritic cells (p=0.038). However, no significant increases in any of the other cell types were observed: $CD4^+$ T cells (p=0.8691), $CD8^+$ T cells (p=0.2232), NK cells (p=0.468), and macrophages (p=0.6494). Contrast analyses were also performed for each FNA day (not corrected for multiple comparisons). CFA-treated mice had significantly increased granulocytes on days 1 (p<0.0001), 3 (p<0.0001), and 5 (p=0.0438) post-treatment and significantly increased dendritic cells on day 8 post-treatment (p=0.0037). In addition, macrophages were increased on day 1 (p=0.0385) and CD4 cells decreased on day 11 (p=0.0137). Data pooled from six separate experiments. These data were used to generate (B). (B) The relative percentages of tumor-infiltrating immune cells and tumor cells for CFA-treated and PBS-control mice are shown, and the number of mice analyzed at each time point is shown above each bar. CFA, complete Freund's adjuvant; PBS, phosphate-buffered saline.

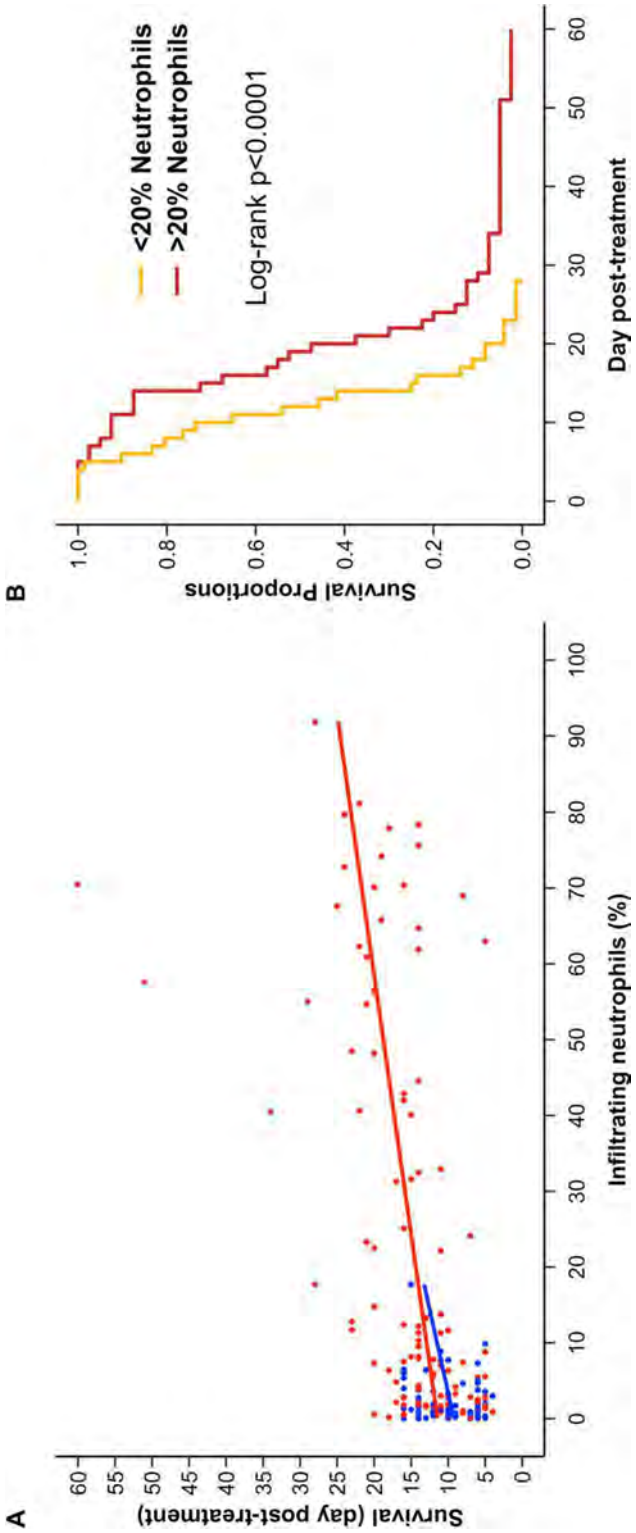


Figure 4 (Continued)

Figure 4 Early granulocyte infiltrate is the key to treatment success of P815 tumors. (A) The highest percentage of neutrophils identified on days 1–5 for each mouse is plotted against survival time. PBS-treated mice are shown in blue, CFA-treated mice are shown in red. Lines were fitted using a linear model with R software. Analysis of variance showed that infiltration of neutrophils by day 5 is highly associated with survival (p<0.0001) and that this association is independent of treatment (p=0.679). PBS n=69, CFA n=112. (B) CFA-treated mice (from A) were stratified based on the highest percentage of tumor-infiltrating neutrophils identified by FNA on days 1 to 5 post-treatment (mice with <20% neutrophils (n=72, orange) and >20% (n=40, red)). Survival analyses showed a statistically significant difference in survival between groups (log RANK p<0.0001). The 20% cut-off was chosen based on the maximum neutrophil infiltrate in PBS-treated mice, as seen in figure 4A. Data pooled from 18 separate experiments, in which FNA analysis was performed at least once on, or before, day 5. CFA, complete Freund's adjuvant; FNA, fine-needle aspirate; PBS, phosphate-buffered saline.

with saline (control). Even in this highly controlled cancer model, there was substantial variation in the proportion of immune infiltrates induced by intratumoral CFA injection (figure 3A). Importantly, mice with the highest levels of granulocytes at days 1–5 post intratumoral CFA injection lived significantly longer than mice with low granulocyte infiltrates (figure 4). Thus, in this model, early immune cell infiltration into the tumor was predictive of treatment benefit. The granulocyte infiltrate was shown to be composed almost entirely of neutrophils. Depletion of neutrophils in the P815 model led to shorter survival and abrogated the efficiency of CFA treatment (figure 5).

Human trials

Following evidence of benefit of CFA treatment in natural and induced animal models of mastocytoma, breast cancer, and melanoma, the question obviously arises: can this treatment be of benefit to human cancer patients? We provide preliminary reports from two human studies of CFA injected intratumorally in human cancer patients.

Four patients were treated at the Arlesheim Klinik in Switzerland; a 77-year-old man with incurable non-small cell lung cancer (NSCLC), a 17-year-old girl with metastatic osteosarcoma, and two 54-year-old women with invasive ductal breast cancer (one lost to follow-up). These patients received between one and four injections of CFA (in this series of patients, emulsified with Viscum). Details are given in online supplemental table 2A. One breast cancer patient exhibited local control for 2 years, confirmed by repeated ultrasound and MRI scans, but ultimately progressed.

Eight patients were treated as part of an ongoing phase I clinical trial being performed at The Canberra Hospital, Australia (Australian New Zealand Clinical Trials Registry: ACTRN12616001637437). In this ongoing dose-escalation study, two cohorts of previously treated patients with advanced cancer received either 0.5 mL or 1 mL of CFA on day 1 (online supplemental table 2B). CFA was administered into primary or metastatic cancer sites either in clinic or under imaging guidance, depending on tumor location. All patients had a mandatory tumor biopsy on day 5 (4 days after CFA injection) and were allowed to undergo optional tumor biopsy on day 28 to gauge the level of immune infiltrates.

Five of the first eight patients treated showed evidence of substantial immune infiltrate into the tumor, accompanied by extensive tumor necrosis 4 days after treatment (figure 6A and online supplemental figure 3). Clinical assessments and tumor biopsies did not show significant differences between patients who received 0.5 mL or 1 mL CFA. Patients are currently being enrolled into a 2 mL CFA cohort. Treatment was well tolerated in all patients from both centers. Side effects attributed to the therapy were limited to temporary pain at the injection site, inflammation around the injected tumor, and overnight fever; each seen in some patients. Thus, side effects compare very favorably to standard cancer therapies.

One 69-year-old man with metastatic renal cell cancer was treated with CFA after progressing on multiple lines of standard treatments including tyrosine kinase inhibitors. He underwent three doses of 1 mL CFA (6 weeks interval between treatments) that was directly administered into a neck tumor deposit. His serial imaging and histology from tumor biopsy are shown in figure 6 and online supplemental figure 4. Extensive immune infiltrate and tumor necrosis are shown in figure 6A. Figure 6B–D shows CT scans performed before treatment and 6 weeks after the second injection of CFA. In figure 6B, the injected neck tumor deposit can be seen to decrease in size and exhibit radiological changes. Furthermore, a distant lung metastasis was also shown to shrink substantially, accompanied by a decrease in plural effusion (figure 6C). Other metastases, however, were stable or increased in size (figure 6D and online supplemental figure 4).

DISCUSSION

In this paper, we provide proof of concept that intratumoral injection of CFA emulsified with saline can act as an effective cancer immunotherapy in a proportion of animal models with cancer (both experimentally induced and naturally occurring). We also show that this therapy is safe for use in human cancer patients and may provide benefit to a proportion of patients, thus warranting further clinical trials. Further, we have demonstrated through the use of traditional laboratory animal models, and naturally occurring cancers in two companion animal species (dogs and horses), an alternative comparative oncology methodology for defining proof of concept, efficacy and safety in novel cancer therapies.

Mouse models are excellent for studying the early phases of the antitumor immune response. CFA prolonged life in two mouse cancer models: P815 mastocytoma and 4T1 mammary cancer (figure 1), with complete regressions seen in the former. In the P815 model, improved

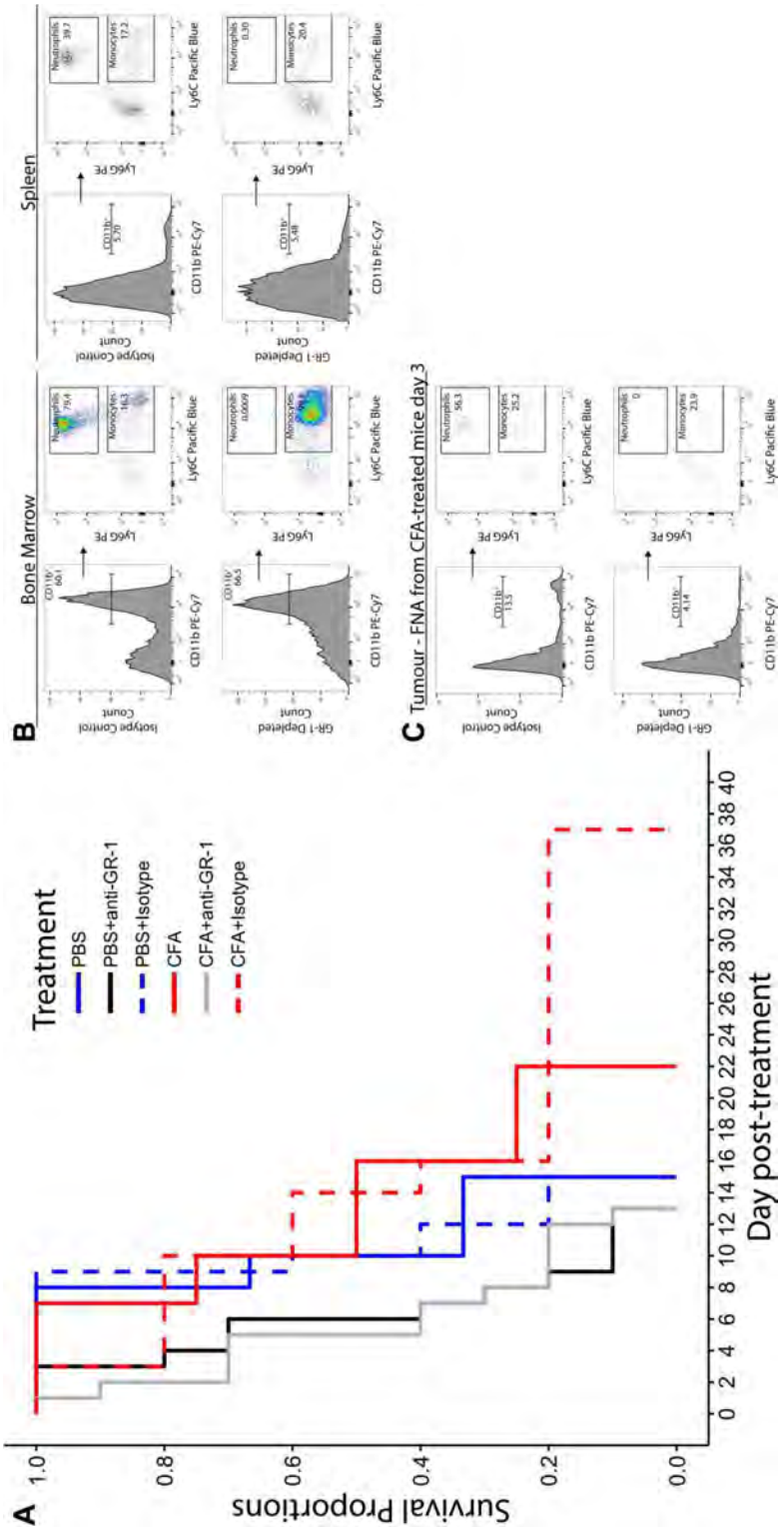


Figure 5 (Continued)

Figure 5 Neutrophil depletion abrogates the survival advantage of CFA treatment. (A) Mice bearing P815 tumors were treated with intratumoral CFA or PBS for controls. Mice additionally received either 0.2 mg anti-GR-1(RB6-8C5) or anti-isotype control antibody (LTF-2) by intraperitoneal injection every 2–3 days, beginning 3 days prior to CFA /PBS treatment. For statistical analysis, mice were stratified by treatment and by neutrophil status (neutrophil depleted or non-depleted). No interaction between neutrophil depletion and treatment was observed (p=0.230), indicating that treatment had no effect on the survival of neutrophil-depleted mice, and neutrophil depletion was found to significantly reduce survival (p=0.00016, HRs: non-depleted=1, GR-1-depleted=4.28). The median survival of CFA+anti-GR-1 mice was 5 days post-treatment compared with 13 days and 14 days for CFA and CFA+isotype control mice, respectively. The median survival of PBS+anti-GR-1 mice was 6 days post-treatment compared with 10 days for both PBS and PBS+isotype control mice. CFA n=4, PBS n=3, CFA+anti-isotype n=5, PBS+anti-isotype n=5, CFA+anti-GR-1 n=10, PBS+anti-GR-1 n=10. Data pooled from two separate experiments. (B) Assessment of neutrophil depletion in the spleen and bone marrow. Bone marrow cells from a non-depleted control mouse and a GR-1-depleted mouse were processed and stained with 7-AAD, anti-CD45.2-Alexa fluor 488, anti-CD11b-PE-Cy7, anti-Ly6G-PE, and anti-Ly6C-Brilliant violet 421 (BV421). Cells have been gated for CD45.2 positive, live (7-AAD negative) singlet cells. The histograms show that the proportion of myeloid cells (CD11b+) were similar in both non-depleted control mice (top panels) and GR-1-depleted mice (bottom panels). From the myeloid population, distinct populations of both neutrophils (Ly6G+Ly6C+) and monocytes (Ly6G- Ly6C+) could be identified in the non-depleted control mice. However, the neutrophil population is absent from the GR-1-depleted mouse, indicating that neutrophils had been successfully depleted using the anti-GR-1 antibody (RB6-8C5) (C). Assessment of neutrophil depletion in mice with P815 tumors. neutrophils were depleted from mice bearing P815 tumors starting 3 days prior to CFA treatment using 0.2 mg anti-GR-1 antibody (RB6-8C5), which was re-administered every 2–3 days. FNAs were taken from P815 tumors 3 days post-CFA treatment to ensure successful depletion of neutrophils by flow cytometry. FNA samples were pooled into groups from GR-1-depleted and isotype control mice. The neutrophil population (CD11b+Ly6G+Ly6C+) is present in the isotype control mice. CFA, complete Freund's adjuvant; FNA, fine-needle aspirate; PBS, phosphate-buffered saline; 7-AAD, 7-aminoactinomycin-D.

survival was dependent on early neutrophil infiltration into the tumor. Dogs allow longer term investigation in naturally occurring cancers, which are genetically and behaviourally similar to human cancers, and have developed in co-evolution with the immune system.[31] Our canine studies demonstrate the effectiveness of intratumoral CFA treatment in naturally occurring canine mastocytomas of both high and low grade, with a 21% complete response rate and a 35% overall response rate. It should be noted that we are targeting dogs with advanced terminal malignancies in our trial, and some animals have succumbed to their cancer in less than 2–4 weeks we predict it takes to mount a significant antitumor immune response. Histology of dog tissues after tumor regression (figure 2) showed B and T cell infiltration at the site of tumor regression, and in a de novo (not injected) cancer, providing evidence of a systemic immune response to the treatment in addition to regression of the injected tumor. In the dog trial, regressions were demonstrated after failure of chemotherapy and radical surgery, as well as in an untreated lesion, thus intratumoral CFA can be considered both as a first-line treatment, or after failure of other therapies.

Together, our data suggest that early stimulation of an innate immune response is the key to treatment success, sufficient for the resolution of some injected tumors. The ensuing adaptive (T and B cell) immune response (seen in late dog histology) is likely to be the key to the control of any metastases. This is very much in agreement with a similar hypothesis put forward by Colombo and colleagues.[32]

In our human patients, we show that intratumoral injection of CFA is safe and well-tolerated. Histology from tumor biopsies taken 4 days after CFA injection is consistent with our mouse flow cytometry data, with inflammatory immune cells seen in 5/8 patients, in each case accompanied by extensive tumor necrosis. We cannot expect small phase I trials in mostly end-stage cancer patients to conclusively demonstrate treatment efficacy. Nonetheless, at least one patient (patient 4 in the Canberra trial, figure 4) is likely to have derived benefit from the therapy.

The use of bacteria in cancer treatment has a long history,[33] but also a far more recent one. Live BCG is the current standard treatment for superficial bladder cancer[34] (note that CFA, used in our study, contains a closely related dead mycobacterium). Two seminal papers in 2012 showed that common chemotherapies also act through bacteria: pretreatment with antibiotics in mouse models abrogated the effectiveness of chemotherapy.[11 12] Chemotherapy was shown to damage the intestinal lining, allowing translocation of bacteria across the gut wall with bacteria found in the mesenteric lymph nodes and spleen.[11] Three classes of cancer therapeutic checkpoint inhibitors, anti-PDL-1, anti-CTLA4, and anti-PD-1, have shown similar dependence on gut bacteria,[14 35 36] with the effectiveness of the latter two also impaired by antibiotics. Routy *et al*[14] note the presence of bacterial-induced granulomas in the cancer after treatment of mice with anti PD-1. All three checkpoint inhibitors are known to cause gastrointestinal toxicities in patients and so impair the integrity of the intestinal lining. Associations between enterocolitis or immune-related adverse events after checkpoint inhibitor therapy and improved patient outcomes have been noted (reviewed by Soularue *et al*[37]). Importantly, retrospective studies of patients taking checkpoint inhibitors have shown that co-prescription of antibiotics leads to significantly shorter survival.[14 38] Taken together, these data support the thesis that the success of many cancer therapies relies on escape of bacteria from the gut; these bacteria can end up in tumors and in tumor-draining lymph nodes where they are able to activate first the

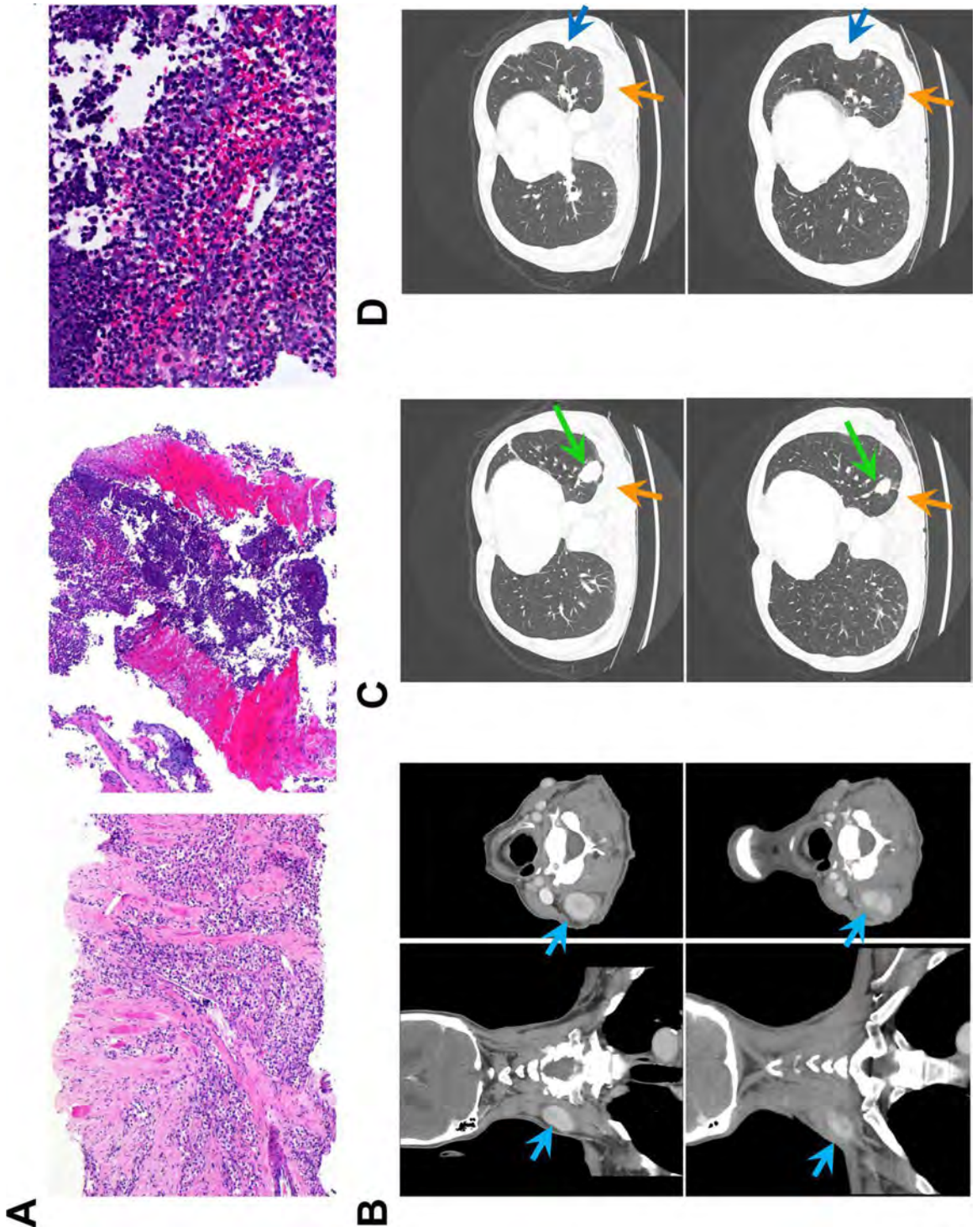


Figure 6 Histology and CT scans of treated patient. Patient 4 received three injections at 6-week intervals of 1 mL of CFA into a neck deposit of clear cell carcinoma of the kidney. (A) H&E sections of tumor on initial biopsy taken 1 year before CFA

Figure 6 (Continued)

treatment (left x100) and on biopsy taken 4 days after the first injection of CFA (middle x100, right x400). The post-treatment biopsy shows extensive immune infiltrate (predominantly neutrophils and macrophages) and no viable tumor. (B–D) CT scans taken 8 days before the first injection (top row) and 5 weeks after the second injection (bottom row). An earlier scan is shown in online supplemental figure 5. (B) Scans of the neck showing the injected lesion (light blue arrow; 40×27 mm before treatment, 28×18 mm after two injections). (C) Scans of lung showing tumor shrinkage (green arrow; 33 mm before treatment, 21 mm after) and substantially reduced pleural effusion (orange arrows). (D) Scans of lung showing a tumor that continued to grow despite treatment (dark blue arrow; 9 mm before treatment, 33 mm after). CFA, complete Freund's adjuvant.

innate immune response and then to activate or re-activate the anticancer acquired immune response.[17]

Evidently, if this is correct, a bacterial-based intratumoral cancer treatment could synergize with many current cancer treatment options or be used alone with dramatically fewer side effects. In support of this is (1) the original work of Coley,[33] (2) our current study, and (3) the recent paper by Sagiv-Barfi *et al*, which uses intratumoral injection of TLR9 or of TLR7/8 agonists (mimicking bacterial or viral PAMPs, respectively)[2]; these are effective at eliminating tumors into which they have been injected, and when combined with an immune-stimulating antibody against OX-40, produce a spectacular, systemic curative immune response in mice.

The question of which bacteria are most effective in cancer therapy has been addressed recently by a series of studies looking at gut bacteria in patients and animals who do or do not respond to chemotherapy or checkpoint inhibitor therapy. Different papers reach largely different conclusions. This suggests that many different bacterial genera may be able to effectively stimulate the anticancer immune response. Anticancer effects of different viral and bacterial vectors being trialed for oncolytic therapy are also likely to be based, at least in part, on the same mechanism, further increasing the range of potentially effective microbiological agents.

Our study investigated injection of emulsified CFA (a slow-release preparation of killed mycobacteria) directly into tumors. Experiments are underway to further elucidate the mechanism of action and to see if the efficacy can be improved. Given the low side effects, potentially wide applicability, and low cost of use (making this therapy applicable even in underdeveloped countries), our therapy warrants larger-scale investigation.

Author affiliations
[1]Research School of Biology, Australian National University, Canberra, Australian Capital Territory, Australia
[2]Department of Medical Oncology, Canberra Hospital, Canberra, Australian Capital Territory, Australia
[3]Medical School, Australian National University, Canberra, Australian Capital Territory, Australia
[4]School of Veterinary Science, The University of Queensland, Gatton, Queensland, Australia
[5]Adelaide Plains Equine Clinic, Gawler, South Australia, Australia
[6]Klinik Arlesheim, Haus Wegman, Arlseheim, Switzerland
[7]ACT Pathology, Canberra Hospital, Canberra, Australian Capital Territory, Australia
[8]Canberra Imaging Group, Canberra, Australian Capital Territory, Australia
[9]Biological Data Science Institute, Australian National University, Canberra, Australian Capital Territory, Australia

Twitter Andrew A Almonte @andrew_almo

Acknowledgements We would especially like to thank all patients with cancer who volunteered for treatment and their families. Thank you to Olive Doig, Clinical Trials Manager, and to Drs Robert Allen and Sayed Ali. AF would like to thank Claude Fahrer for helpful discussions, Roger Kelly and Hannah Clarke for facilitating this study. RA would like to thank Chiara Palmieri, Greg Simmons, Hanna Long, Andrea Schaffer-White. Thank you to the owners and referring veterinarians of the pet dogs.

Contributors CSEC and ERA performed mouse experiments, analyzed data, and edited manuscript. AAA analyzed mouse experiments and edited manuscript. LM organized Canberra clinical trial, drafted human ethics, and recruited patients. KFE, MB, and CL are veterinarians who designed and executed the canine clinical trial including patient treatment, data, sample collection, and analysis. PMP assisted with the research trial and conducted the histology and immunohistochemistry on the dog and horse samples. JM and EWH are veterinarians who performed equine trial, including provision and analysis of equine ultrasounds. K-MS treated patients in Canberra trial and provided input into experimental planning and analysis. RT treated patients in Canberra trial who required injection under ultrasound or CT; assessed and analyzed radiology. JED organised and interpreted Canberra patient histology samples. TN provided expert statistical advice for design and interpretation of mouse experiments. AH and MO treated Swiss patients. DY was in charge of Canberra Hospital clinical trial and edited manuscript. RA was in charge of the dog clinical trial, interpretation of samples collected for histology and immunohistochemistry for dogs and horses, manuscript drafting, and editing. AF oversaw study; was in charge of mouse experiments and analysis of data; prepared CFA and helped draft human ethics for Canberra clinical trial; helped prepare figures and tables; and wrote manuscript.

Funding Canberra trial: Canberra Hospital Private Practice Fund, Janice and Ron Parker Fund. Mouse preclinical studies: Lea Chapuis Memorial Fund. Canine preclinical studies: The John and Mary Kibble Trust (grants CT22492, CT21335) and the William Peter Richards Bequest for research into veterinary pathology. CSEC, ERA, and AAA was supported by Australian Government Research Training Program Stipend Scholarships. CSEC and K-MS were supported by Max Lindemann Memorial Foundation, Miami.

Competing interests None declared.

Patient consent for publication Not required.

Ethics approval Mouse experiments were approved by the Australian National University (ANU) animal experimentation ethics committee; approval numbers A2011/020, A2014/03, A2017_46.

Provenance and peer review Not commissioned; externally peer reviewed.

Data availability statement Data are available upon reasonable request. All data relevant to the study are included in the article or uploaded as supplementary information. We are happy to provide any further information. Please contact senior authors DY, MO, RA or AMF.

Supplemental material This content has been supplied by the author(s). It has not been vetted by BMJ Publishing Group Limited (BMJ) and may not have been peer-reviewed. Any opinions or recommendations discussed are solely those of the author(s) and are not endorsed by BMJ. BMJ disclaims all liability and responsibility arising from any reliance placed on the content. Where the content includes any translated material, BMJ does not warrant the accuracy and reliability of the translations (including but not limited to local regulations, clinical guidelines, terminology, drug names and drug dosages), and is not responsible for any error and/or omissions arising from translation and adaptation or otherwise.

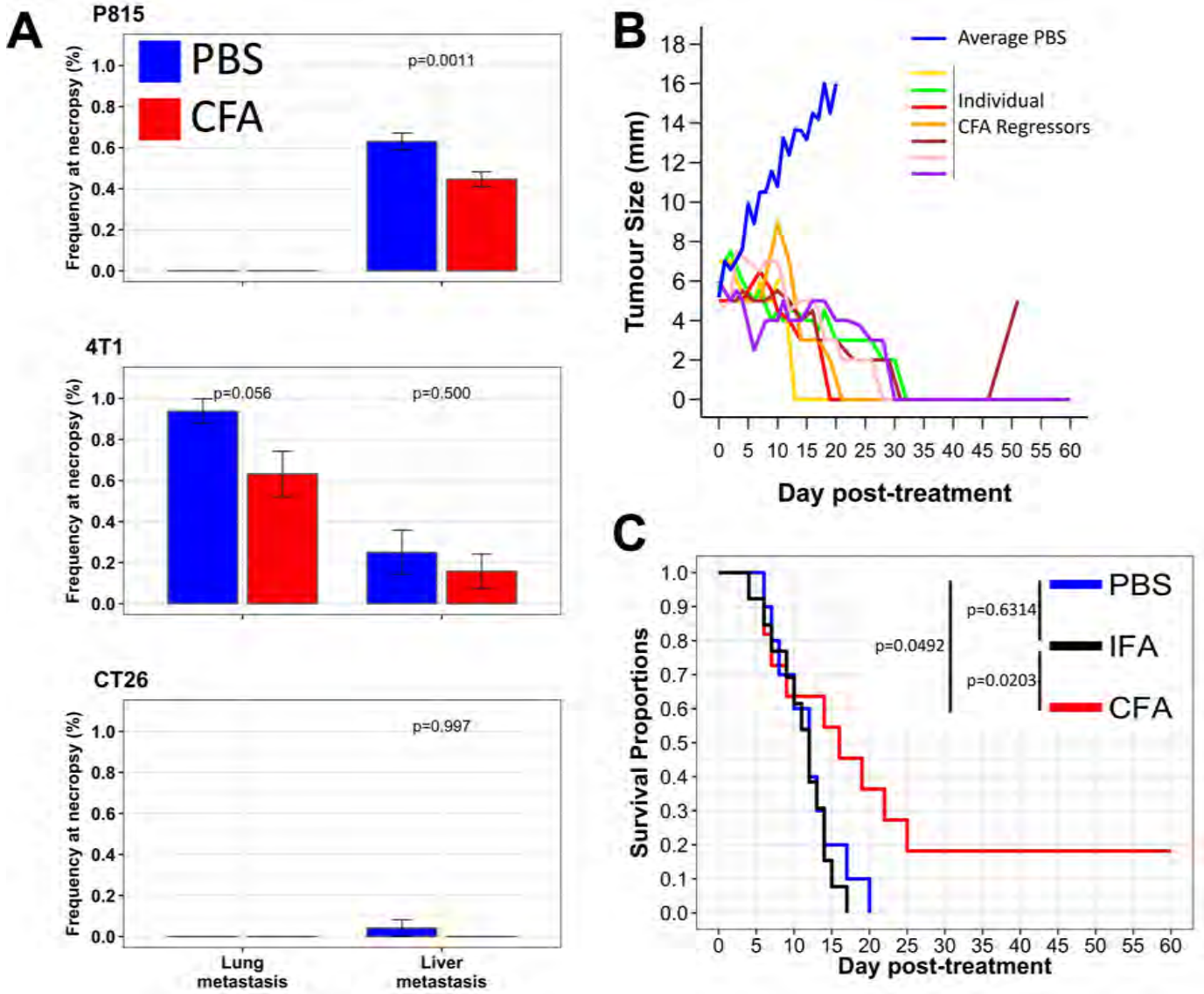
Open access This is an open access article distributed in accordance with the Creative Commons Attribution Non Commercial (CC BY-NC 4.0) license, which permits others to distribute, remix, adapt, build upon this work non-commercially, and license their derivative works on different terms, provided the original work is properly cited, appropriate credit is given, any changes made indicated, and the use is non-commercial. See http://creativecommons.org/licenses/by-nc/4.0/.

Open access

ORCID iD
Aude M Fahrer http://orcid.org/0000-0001-8556-0223

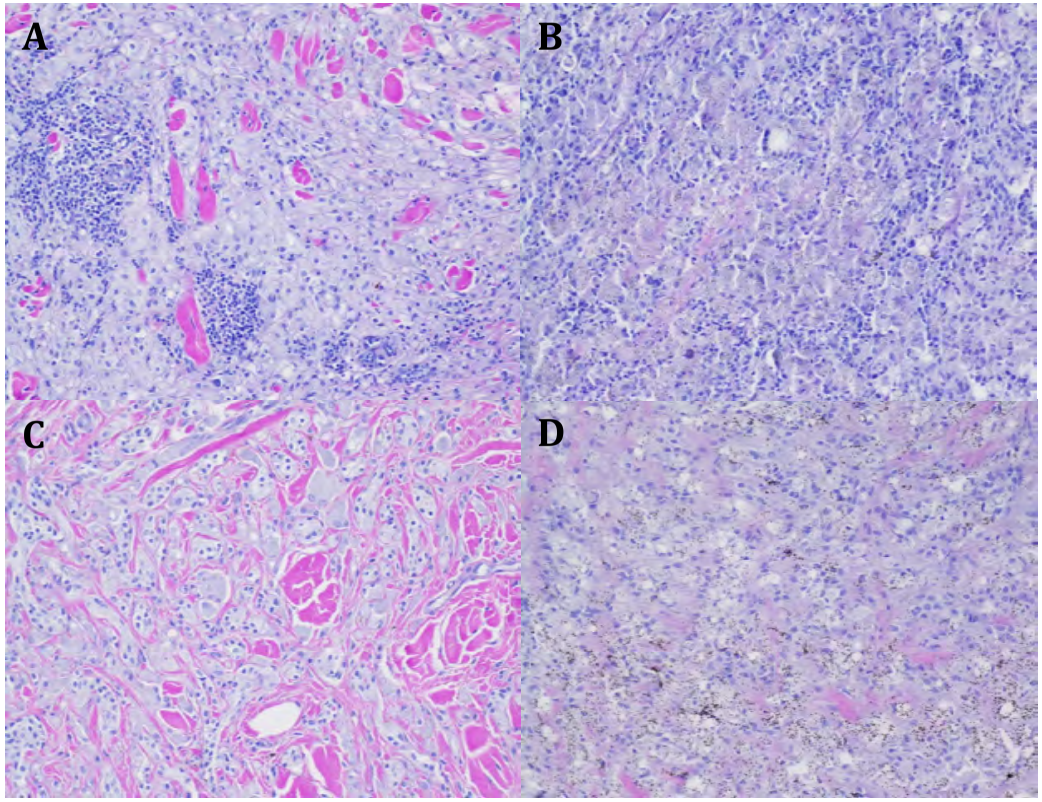
REFERENCES

1 Fahrer AM. A proposal for a simple and inexpensive therapeutic cancer vaccine. *Immunol Cell Biol* 2012;90:310–3.
2 Sagiv-Barfi I, Czerwinski DK, Levy S, *et al*. Eradication of spontaneous malignancy by local immunotherapy. *Sci Transl Med* 2018;10. doi:10.1126/scitranslmed.aan4488. [Epub ahead of print: 31 01 2018].
3 Nauts HC, Swift WE, Coley BL. The treatment of malignant tumors by bacterial toxins as developed by the late William B. Coley, M.D., reviewed in the light of modern research. *Cancer Res* 1946;6:205–16.
4 Nauts HC, McLaren JR. Coley toxins-the first century. *Adv Exp Med Biol* 1990;267:483–500.
5 Sedighi M, Zahedi Bialvaei A, Hamblin MR, *et al*. Therapeutic bacteria to combat cancer; current advances, challenges, and opportunities. *Cancer Med* 2019;8:3167–81.
6 Zhou S, Gravekamp C, Bermudes D, *et al*. Tumour-targeting bacteria engineered to fight cancer. *Nat Rev Cancer* 2018;18:727–43.
7 Twumasi-Boateng K, Pettigrew JL, Kwok YYE, *et al*. Oncolytic viruses as engineering platforms for combination immunotherapy. *Nat Rev Cancer* 2018;18:419–32.
8 Hernández-Luna MA, Luria-Pérez R. Cancer Immunotherapy: priming the Host Immune Response with Live Attenuated *Salmonella enterica*. *J Immunol Res* 2018;2018:1–15.
9 Lee S-Y, Yang S-B, Choi Y-M, *et al*. Heat-Killed Mycobacterium paragordonae therapy exerts an anti-cancer immune response via enhanced immune cell mediated oncolytic activity in xenograft mice model. *Cancer Lett* 2020;472:142–50.
10 Mathé G, Florentin I, Bruley-Rosset M, *et al*. Heat-Killed Pseudomonas aeruginosa as a systemic adjuvant in cancer immunotherapy. *Biomedicine* 1977;27:368–73.
11 Viaud S, Saccheri F, Mignot G, *et al*. The intestinal microbiota modulates the anticancer immune effects of cyclophosphamide. *Science* 2013;342:971–6.
12 Iida N, Dzutsev A, Stewart CA, *et al*. Commensal bacteria control cancer response to therapy by modulating the tumor microenvironment. *Science* 2013;342:967–70.
13 Yu T, Guo F, Yu Y, *et al*. Fusobacterium nucleatum promotes chemoresistance to colorectal cancer by modulating autophagy. *Cell* 2017;170:548–63.
14 Routy B, Le Chatelier E, Derosa L, *et al*. Gut microbiome influences efficacy of PD-1-based immunotherapy against epithelial tumors. *Science* 2018;359:91–7.
15 Baruch EN, Youngster I, Ben-Betzalel G, *et al*. Fecal microbiota transplant promotes response in immunotherapy-refractory melanoma patients. *Science* 2021;371:602–9.
16 Matson V, Fessler J, Bao R, *et al*. The commensal microbiome is associated with anti-PD-1 efficacy in metastatic melanoma patients. *Science* 2018;359:104–8.
17 Almonte AA, Rangarajan H, Yip D, *et al*. How does the gut microbiome influence immune checkpoint blockade therapy? *Immunol Cell Biol* 2021;99:361–72.
18 Marchesi JR, Dutilh BE, Hall N, *et al*. Towards the human colorectal cancer microbiome. *PLoS One* 2011;6:e20447.
19 Geller LT, Barzily-Rokni M, Danino T, *et al*. Potential role of intratumor bacteria in mediating tumor resistance to the chemotherapeutic drug gemcitabine. *Science* 2017;357:1156–60.
20 Nejman D, Livyatan I, Fuks G, *et al*. The human tumor microbiome is composed of tumor type-specific intracellular bacteria. *Science* 2020;368:973–80.
21 Kalaora S, Nagler A, Nejman D, *et al*. Identification of bacteria-derived HLA-bound peptides in melanoma. *Nature* 2021;592:138–43.
22 Freund J. The mode of action of immunologic adjuvants. *Bibl Tuberc* 1956;7:130–48.
23 Carroll CSE, Altin JG, Neeman T, *et al*. Repeated fine-needle aspiration of solid tumours in mice allows the identification of multiple infiltrating immune cell types. *J Immunol Methods* 2015;425:102–7.
24 Kiupel M, Webster JD, Bailey KL, *et al*. Proposal of a 2-tier histologic grading system for canine cutaneous mast cell tumors to more accurately predict biological behavior. *Vet Pathol* 2011;48:147–55.
25 Gordon I, Paoloni M, Mazcko C, *et al*. The comparative oncology trials Consortium: using spontaneously occurring cancers in dogs to inform the cancer drug development pathway. *PLoS Med* 2009;6:e1000161.
26 Paoloni M, Khanna C. Translation of new cancer treatments from PET dogs to humans. *Nat Rev Cancer* 2008;8:147–56.
27 Roberts NJ, Zhang L, Janku F, *et al*. Intratumoral injection of Clostridium novyi-NT spores induces antitumor responses. *Sci Transl Med* 2014;6:249ra111.
28 Veterinary cooperative oncology group. Common terminology criteria for adverse events (VCOG-CTCAE) following chemotherapy or biological antineoplastic therapy in dogs and cats v1.1. *Vet Comp Oncol* 2011;14:417–46.
29 Rosengren Pielberg G, Golovko A, Sundström E, *et al*. A cis-acting regulatory mutation causes premature hair graying and susceptibility to melanoma in the horse. *Nat Genet* 2008;40:1004–9.
30 Curik I, Druml T, Seltenhammer M, *et al*. Complex inheritance of melanoma and pigmentation of coat and skin in grey horses. *PLoS Genet* 2013;9:e1003248.
31 Park JS, Withers SS, Modiano JF, *et al*. Canine cancer immunotherapy studies: linking mouse and human. *J Immunother Cancer* 2016;4:97.
32 Guiducci C, Vicari AP, Sangaletti S, *et al*. Redirecting in vivo elicited tumor infiltrating macrophages and dendritic cells towards tumor rejection. *Cancer Res* 2005;65:3437–46.
33 Coley WB. The treatment of inoperable sarcoma by bacterial toxins (the mixed toxins of the Streptococcus erysipelas and the Bacillus prodigiosus). *Proc R Soc Med* 1910;3:1–48.
34 Redelman-Sidi G, Glickman MS, Bochner BH. The mechanism of action of BCG therapy for bladder cancer--a current perspective. *Nat Rev Urol* 2014;11:153–62.
35 Sivan A, Corrales L, Hubert N, *et al*. Commensal Bifidobacterium promotes antitumor immunity and facilitates anti-PD-L1 efficacy. *Science* 2015;350:1084–9.
36 Vétizou M, Pitt JM, Daillère R, *et al*. Anticancer immunotherapy by CTLA-4 blockade relies on the gut microbiota. *Science* 2015;350:1079–84.
37 Soularue E, Lepage P, Colombel JF, *et al*. Enterocolitis due to immune checkpoint inhibitors: a systematic review. *Gut* 2018;67:2056–67.
38 Derosa L, Hellmann MD, Spaziano M, *et al*. Negative association of antibiotics on clinical activity of immune checkpoint inhibitors in patients with advanced renal cell and non-small-cell lung cancer. *Ann Oncol* 2018;29:1437–44.

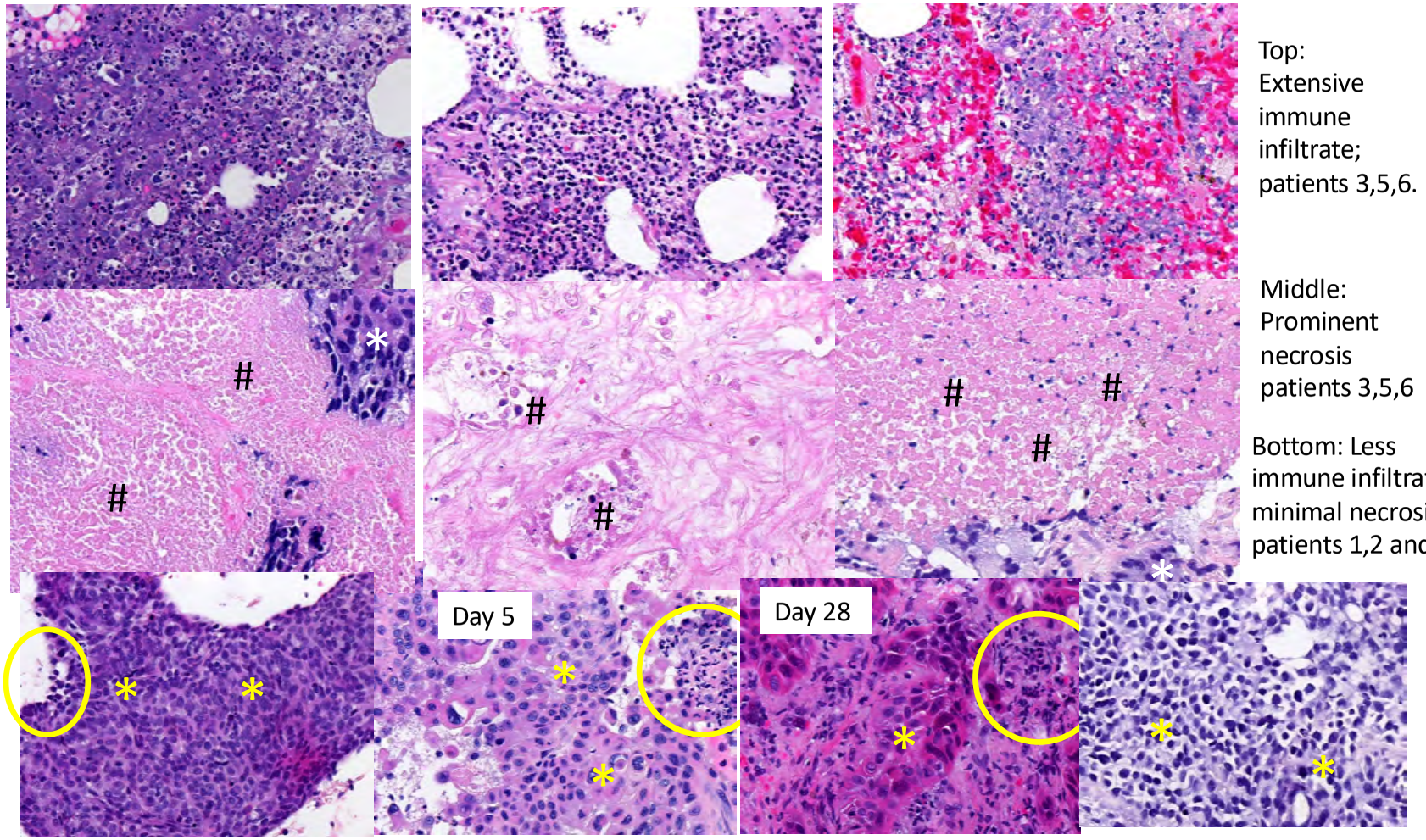


Supplementary figure 1

Supplementary figure 1. These data correspond to figure 1. **A. metastasis in tumour-bearing mice at necropsy.** P815, 4T1, and CT26 tumours were induced as described in figure 1 and treated with 50µl PBS (blue) or CFA (red). At the time of euthanasia (due to tumour size or illness) mice were analysed for the prevalence of metastasis to the lungs or liver. (Note that in the P815 and 4T1 tumour models, CFA treated mice live longer, on average than PBS-treated mice, so would have had more time, on average, to develop metastases). A generalized linear regression model was applied to binomial data for statistical analysis. Error bars represent the binomial uncertainty of the data. P-values are displayed above the bar plots. A trend of reduced lung metastases with CFA treatment was observed in the 4T1 model (p=0.056). P815 (exp. N=5); PBS (n=29), CFA (n=32). 4T1 (exp. N=3); PBS (n=16), CFA (n=19). CT26 (exp. N=3); PBS (n=25), CFA (n=38). **B. Tumour growth of regressing mice in the P815 model treated with CFA.** These data correspond to Figure 1A. Six complete tumour regressions were observed in CFA-treated mice and one mouse initially regressed but relapsed approximately 50 days post-treatment. Some mice received FNAs at 6-7 day intervals (up to three analyses) or 2-3 day intervals (up to seven analyses), and some mice did not receive FNAs. The mean tumour growth of PBS treated mice in the corresponding experiments (n=18) is shown for comparison. **C. IFA (incomplete Freund's adjuvant) is not an effective treatment for P815 mastocytoma.** P815 mastocytoma murine tumours were induced as previously described and treated intratumourally with 50µl PBS (blue), incomplete Freund's adjuvant (IFA ,black), or CFA (red). Data were analysed using Tukey adjustments for multiple comparisons. CFA-treated mice had significantly increased survival compared to IFA-treated mice (coxph p=0.0203, HR: CFA:IFA=0.3101, 95%CI[0.115, 0.834]). There was no significant survival difference between PBS-control and IFA-treated mice (coxph p=0.6314, HR: PBS:IFA=0.8145, 95%CI[0.352, 1.883]). The significant survival difference between CFA-treated and PBS-control mice was maintained (coxph p=0.0492, HR: CFA:PBS=0.3656, 95%CI[0.134, 0.996]).

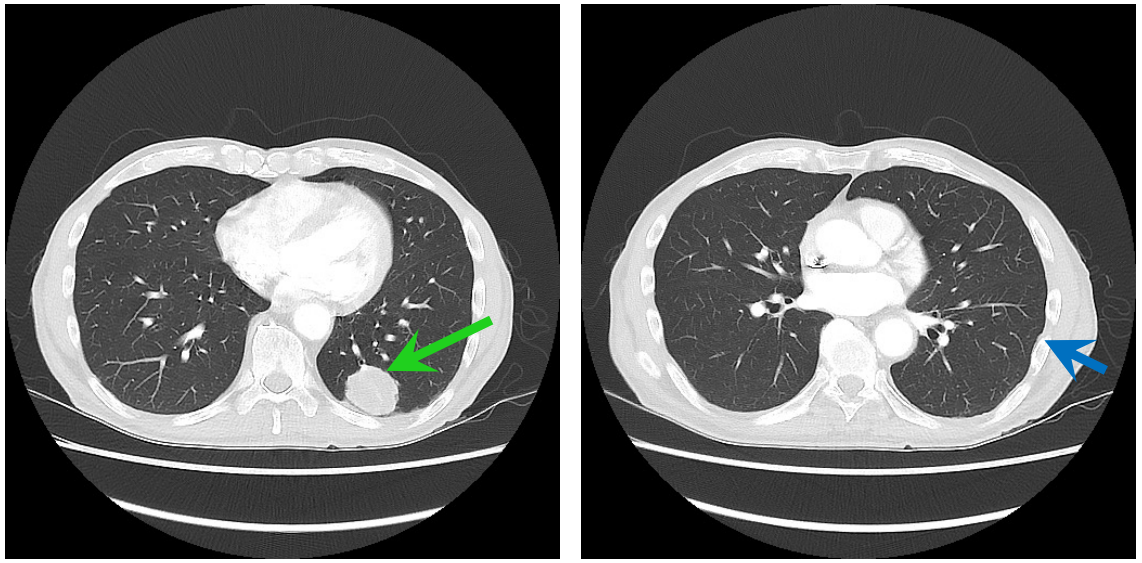


Supplementary figure 2. Histopathology post-CFA of grey horse melanoma. Panels A and B show intratumoral lymphocytic infiltrates in clusters (A: #003: 11 weeks after treatment) or more evenly dispersed (B: #008; 8 weeks after treatment) in horses which showed tumour regressions post treatment. Animals which showed no tumour regression typically had no (C: #009; 6 weeks after treatment) or sparse lymphocytic infiltrates (D: #001; 18 weeks after treatment). Paraffin-embedded formalin-fixed tissue stained with HE after melanin bleaching procedure; magnification 200x. # refers to numbering of horses in supplementary table 1.



Supplementary fig 3

Supplementary figure 3. Histology of patients after CFA injection. Biopsies were taken from patients on day 5 (compulsory) and day 28 (optional) after CFA injection (day 1). Biopsies were stained with H&E. All images x400. The **top row** shows biopsies with extensive immune infiltrate at day 5, the **middle row** shows biopsies from the same patients, all with prominent necrosis (patients 3, 5, and 6 shown left, middle and right, respectively in both the top and middle rows). **The bottom row** biopsies (left =patient 1 on day 5 ; middle two panels= patient 2 on days 5 and 28; right = patient 7 on day 5) have less immune infiltrate and minimal necrosis (all x400). Patient samples are numbered according to supplementary table 2, which contains details of each patient, and the type of cancer from which they are suffering. Histology from patient #4 is presented in figure 4, so is not included here. * indicates viable tumour; # indicates necrotic tumour; circles show focal inflammation.



Supplementary figure 4. CT scans of chest of patient #4, 3 months before CFA treatment. These images correspond to figures 6 C and D, and show that the lung metastatic deposit that reduced in size after CFA treatment, had also decreased after previous treatment with everolimus, the last dose of which was administered 6 weeks before the first CFA injection. However as the half-life of everolimus is only 30 hours, it was considered very unlikely that the shrinkage shown in Fig 6C could be attributed to this previous treatment. Tumour measurements: 39mm (left, green arrow), and 5mm (right, dark blue arrow).

#	Age	Sex	Breed	Mass location	Inj. (Y/N)	Vol. CFA (mL)	responder	comments
001	24	Mare	Thoroughbred x	Left thorax Right thorax Left thorax	Y N Y	0.3 0 0.2	no	Two approximately equal sized contralateral tumours; one injected, other "control" Third tumour injected 3 months after initial injections.
002	13	Mare	Warmblood	Tail Vulva	Y Y	0.2 0.1	YES	Complete regression of injected tumour in the tail six weeks after injection. Vulval tumour still present. (other small tumours in the tail are still present)
003	4	Gelding	Welsh x	Anus Tail	Y Y	0.1 0.2	YES	Young horse with melanomas. Complete regression of injected tail tumour at 10 weeks, and injected anal tumour at 4 months. However growth of new anal tumours.
004	14	Mare	Warmblood	Anus (super) Anus (deep)	Y N	0.3 0	no	Anal tumour removed by surgery 4 months after treatment.
005	16	Mare	Welsh	Anus	Y	0.3	no	Injected a small nodule, part of a very large anal tumour >10 x 15cm. Euthanased due to suspected melanoma associated impaction.
006	10	Mare	Quarter Horse	Anus Tail Salivary gland	N Y N	0 0.2 0	no	One tumour injected.
007	20	Gelding	Aust Riding Pony	Tail (prox) Tail (dist)	Y N	0.2 0	maybe	Reduction in size of un-injected tumour 3 months after treatment.
008	10	Gelding	Thoroughbred	Anus	Y	0.2	YES	Injected tumour did not regress, however subjective major reduction in size and number of melanomas at commissures of lips and on head. Reduction in size of neck melanoma (too big to fit on ultrasound screen on first visit, so not measured; fitted easily on screen at 3 months review.)
009	22	Mare	Andalusian	Anus	Y	0.25	no	Very large >25cm mass around anus and base of tail. Small tip of mass was measured, injected, and got smaller. Injected a second area on tail 3 months after first injection.
010	10	Gelding	Warmblood	Tail (prox)	Y	0.1	n.d.	
011	15	Mare	Welsh Pony	Tail Vuvla	Y Y	0.2 0.2	n.d.	

Supplementary Table 1. Grey horses with melanoma treated with Complete Freunds' Adjuvant.

Patient gender, age	Cancer type	Site of injection	Doses of CFA (emulsified with viscum)	Adverse events	Comments
M, 77	Non small cell lung carcinoma	Right thoracic tumour	4 doses 2x 1ml (75%CFA) at one month interval then 1x 2ml (50%CFA) at, two month interval, then 1x 1ml (50%CFA) at 6 week interval.	Fever following 3rd dose	Tumour changes on ultrasound, but tumour slowly progressed. Patient died of cancer 5 months after first CFA injection.
F, 54	Invasive grade 3 ductal breast cancer (ER/PgR+ve; HER2/neu –ve; Ki 40-40%).	Right breast	3x 2ml (50%CFA) at two month then three month intervals.	1st injection: Inflammation of breast, fever (39.6-40) requiring 24 hour hospitalisation. Abscess developed after viscum i.t. (no CFA) injection, resolved, but left scar. 2nd and 3rd injections: fever.	Tumour changes and gradual shrinkage on ultrasound. Local control for two years, after which progressed; underwent mastectomy/ chemotherapy/radiation. Patient well 5 years after initial CFA treatment.
F, 54	Invasive grade 2 ductal breast carcinoma (ER+/PgR-ve; Ki-67 45%; Her-2/neu –ve)	breast	1x 1.5ml CFA (33% CFA)	Inflammation of breast, lasting > 1 month, sterile pus discharge	Patient lost to follow up.
F, 18	Metastatic osteoblastc osteosarcoma	Pulmonary metastatic lesion, adhering to pleura	2 x 2ml (50%CFA), 7 weeks apart		Patient died of widespread metastatic disease 4 months after first CFA injection.

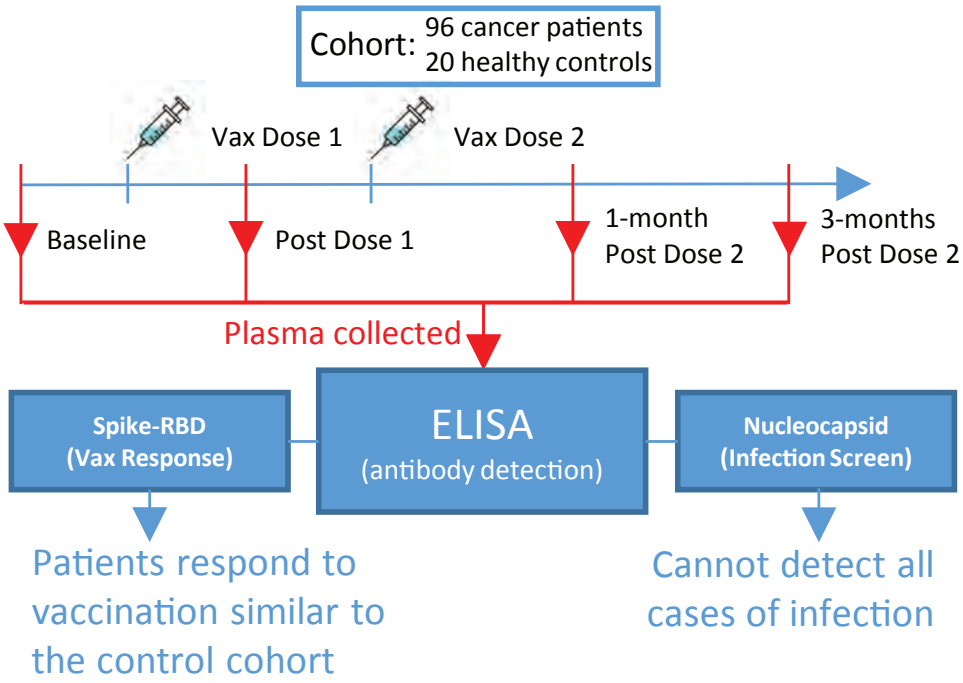
Supplementary Table 2A. Patients treated in Arlesheim, Switzerland. Note: patients were additionally treated with intravenous and intratumoural doses of viscum without CFA which also caused inflammation and fever.

Patient Initials, gender, age	Cancer type	Site of injection	Doses of CFA (emulsified in saline)	Adverse events	Comments
1. WR F, 79	Squamous cell cervical carcinoma	Supra-clavicular mass	1 x 0.5ml		Cancer progressed. Died 9 months after treatment
2. RPS M, 67	Squamous cell head and neck cancer	2cm deposit on neck	1 x 0.5ml		Withdrew from trial. Injected metastasis stable. Other metastases on face progressed. Treated with palliative chemotherapy, further radiation. Alive 4.25 years after CFA treatment.
3.AH M, 72	Prostate cancer, poorly differentiated	Metastasis on neck	2 x 0.5*ml	Inflammation at site of injection	Metastasis kept growing, PSA increasing. Withdrew from trial. Neck metastasis regressed following radiation. Received further antiandrogen therapy, chemotherapy and radiation to pelvis/prostate. Alive 4 years after last CFA treatment.
4. GC M, 69	Metastatic renal cancer	Deposit on neck	3x 1ml*	1st injection: 'flu like symptoms for 2-3 days. 3rd injection Grade 2 adverse event. Fever, worsening dementia	Lung effusion and shortness of breath disappeared after first treatment. Able to resume daily activities. Withdrew from trial after third injection. Died of cancer 7 months after first treatment.
5. IF F, 57	Metastatic renal cell carcinoma	Deposits on groin, neck scalp	1x treatment of 1ml in each deposit		Died of cancer 48 days after treatment.
6. MW M, 61	Lung cancer. Additional pancreatic cancer confirmed at time of first treatment.	Lung (CT guided injection)	1x 1ml		Died of cancer 20 days after treatment.
7.RM M, 71	Recurrent neuro-endocrine tumour of lung.	Deposit on neck	1x 1ml	Hospitalised 21 days after treatment; extremely short of breath.	Died of cancer 22 days after treatment.
8. DL M, 67	Urothelial cancer. Extensive lung metastases, brain metastases.	Deposit on left chest.	2x 1†ml in two different chest deposits.	Suspected seizure 7 days after injection, hospitalised for 2 days.	Died of cancer three months after first treatment.

Supplementary Table 2B. Patients treated at The Canberra Hospital, as part of clinical trial ACTRN12616001637437. * doses given at 6 week intervals. † doses given at 8 week interval.

D

Response to COVID-19 vaccination in patients on cancer therapy: analysis in a SARS-CoV-2-naïve population



COVID naïve population of Canberra was ideal for testing vaccine efficacy

Graphical Abstract. This study prospectively compared the antibody response to COVID-19 vaccination between cancer patients and healthy controls in a population with very low COVID prevalence. Serology was not effective at detecting all cases of infection, underlining the value of measuring immune responses in a COVID-naïve cohort. The majority of cancer patient and all controls were seropositive after two vaccinations.

D. Response to COVID-19 vaccination in patients on cancer therapy: analysis in a SARS-CoV-2-naïve population

TITLE

Response to COVID-19 vaccination in patients on cancer therapy: analysis in a SARS-CoV-2-naïve population

AUTHORS

George Cavic[1]*, BSc(Hons), 0000-0003-2657-8129

Andrew A. Almonte[1]*, M. Biol(Advanced), 0000-0002-8131-7805

Sarah M. Hicks[2]*, M. Biol(Advanced), 0000-0001-5712-124X

Teresa Neeman[4], PhD, 0000-0002-7315-3695

Jo-Wai Wang[1], MChD

Sue Brew[7]

Philip Y Choi[2,6], MBBS, PhD, 0000-0001-9340-8125

Ian Cockburn[2], PhD, 0000-0001-8220-9294

Elizabeth E. Gardiner[2]^, PhD, 0000-0001-9453-9688

Desmond Yip[3,6]^, MBBS, 0000-0002-2806-2401

Aude M. Fahrer[1,8]^, PhD, 0000-0001-8556-0223

Yada Kanjanapan^[3,6], MBBS, 0000-0002-9807-8695

*GC, AA and SH contributed equally to the manuscript

^EG, DY, AF and YK contributed equally to the manuscript

Affiliations:

[1]Research School of Biology, Australian National University, Canberra, Australia

[2]John Curtin School of Medical Research, Australian National University, Canberra, Australia

[3]ANU Medical School, Australian National University, Canberra, Australia

[4]Biological Data Science Institute, Australian National University, Canberra, Australia

[5]Department of Haematology, The Canberra Hospital, Canberra, Australia

[6]Department of Medical Oncology, The Canberra Hospital, Canberra, Australia

[7]Medical Oncology Clinical Trials Unit, The Canberra Hospital, Canberra, Australia

[8]Faculty of Science and Technology, University of Canberra, Canberra, Australia

Corresponding author:

Dr Yada Kanjanapan

The Canberra Hospital

Yamba Drive, Garran ACT 2605

Ph: +612 5124 8444 | Fax: 02 6244 4266

Yada.kanjanapan@act.gov.au

ACKNOWLEDGEMENTS

We wish to acknowledge funding support from The Canberra Hospital Private Practice Fund, Canberra Hospital Radiation Oncology Private Practice Fund and John James Foundation which made the study possible. We thank the patients and volunteers who participated in the study. We also wish to thank the medical and professional staff of The Canberra Hospital whose dedication and effort made this possible. G.C., A.A.A. and S.H. were supported by the Australian Government Research Training Program (AGRTP) Scholarship.

CONFLICTS OF INTEREST

Authors declare no conflicts of interest.

DATA AVAILABILITY

Data are available upon reasonable request from the corresponding author.

ETHICS APPROVAL

Ethics approval for this study was provided by ACT Health Human Research Ethics Committee (2021.ETH.00062). This applies to all data shown, unless explicitly stated otherwise in the text.

PARTICIPANT CONSENT

Informed consent was obtained from study participants in line with the approved ethics protocol by staff of The Canberra Hospital.

FUNDING

See ACKNOWLEGEMENTS.

D. Response to COVID-19 vaccination in patients on cancer therapy: analysis in a SARS-CoV-2-naïve population

ABSTRACT

Introduction: Cancer patients have increased morbidity and mortality from COVID-19, but may respond poorly to vaccination. The Evaluation of COVID-19 Vaccination Efficacy and Rare Events in Solid Tumors (EVEREST) study, comparing seropositivity between cancer patients and healthy controls in a low SARS-CoV-2 community-transmission setting, allows determination of vaccine response with minimal interference from infection.

Methods: Solid tumor patients from The Canberra Hospital, Canberra, Australia, and healthy controls who received COVID-19 vaccination between 3/2021–1/2022 were included. Blood samples were collected at baseline, pre-2nd vaccine dose and at one, three (primary endpoint) and six months post-2nd dose. SARS-CoV-2 anti-spike-RBD and anti-nucleocapsid IgG antibodies were measured.

Results: Ninety-six solid tumor patients and 20 healthy controls were enrolled, median age 62 years; 60% female. Participants received either AZD1222 (65%) or BNT162b2 (35%) COVID-19 vaccines. Seropositivity three months post-vaccination was 87% (76/87) in patients and 100% (20/20) in controls (p=0.12). Seropositivity was observed in 84% of patients on chemotherapy, 80% on immunotherapy and 96% on targeted therapy (differences not significant). Seropositivity in cancer patients increased from 40% (6/15) after first dose, to 95% (35/37) one month after second dose, then dropped to 87% three months after second dose.

Conclusions: Most patients and all controls became seropositive after two vaccine doses. Antibody concentrations and seropositivity showed a decrease between one- and three-months post vaccination, highlighting need for booster vaccinations. SARS-CoV-2 infection amplifies S-RBD antibody responses, however, cannot be adequately identified using nucleocapsid serology. This underlines the value of our COVID-naïve population in studying vaccine immunogenicity.

KEY WORDS: Solid tumor, COVID-19 vaccine, Seroconversion, SARS-CoV-2, serology

INTRODUCTION

Cancer patients have increased risk of morbidity and mortality from COVID-19(1). The extent to which COVID-19 vaccination protects cancer patients, especially those receiving immunosuppressive anti-neoplastic therapy, is important knowledge in protecting this vulnerable population. While numerous studies have examined the efficacy of COVID-19 vaccination in cancer patients, the majority have been conducted in settings of prevalent community transmission of SARS-CoV2, where immunity generated from recovery from COVID-19 can confound assessment of vaccine efficacy.

Canberra, Australia, had only 398 reported cases of COVID-19 in a population of approximately 460,000 up to August 2021(2). SARS-CoV-2 vaccination in Australia commenced in February 2021, initially in high-risk groups, with eligibility expanded to include all adults by August 2021. This study prospectively assessed the immunogenic response to COVID-19 vaccination in cancer patients receiving active systemic therapy, compared to a control cohort of healthy volunteers, in a high vaccination and low community transmission setting.

MATERIALS AND METHODS

The Evaluation of COVID-19 Vaccination Efficacy and Rare Events in Solid Tumors (EVEREST) study is a single-center, prospective study conducted through The Canberra Hospital and Australian National University (ANU), Canberra, Australia. The study was approved by the ACT Health Human Research Ethics Committee (HREC) (2021.ETH.00062). Study participants in the patient cohort had solid tumors and were receiving systemic anti-cancer treatment within two weeks of their first or second COVID-19 vaccination doses. The healthy control cohort had no history of malignancy within the past five years. Participants were recruited before, or within 90 days of receiving two doses of BNT162b2 (Pfizer) or AZD1222 (AstraZeneca) COVID-19 vaccines. Those with a past laboratory-confirmed diagnosis of COVID-19 were excluded.

Blood collection at up to five separate timepoints (Supplementary Figure 1) was undertaken. Timepoint (TP) 1 was the baseline sample prior to any COVID-19 vaccination. TP2 was collected after the first vaccine, up to two weeks before the second vaccine dose. TP3 was

collected 30 days after the second vaccine; TP4, 90 days after the second vaccine dose. During the study, an amendment was made to collect TP4 up to two weeks before the administration of a third vaccine dose, in response to changing public health guidelines by the Australian Technical Advisory Group on Immunisation (ATAGI), which allowed immunocompromised individuals (including cancer patients) to receive a third primary dose of vaccination from two months after their second dose. TP5 was 180 days post second vaccine dose. As booster vaccination were available to the general population at 3 – 6 months following the primary vaccination course, TP5 was amended to allow collection up to two weeks prior to the booster dose (3rd dose for the healthy cohort and 4th dose for the patient cohort). A two-week window before and after the participant's estimated date for sample collection was allowed for TP3-5.

Enzyme-linked immunosorbent assays (ELISA) for SARS-CoV-2 spike receptor binding domain (S-RBD) and nucleocapsid were conducted as described by Hicks et.al. (3). In brief, white 96-well Maxisorp microtiter plates (Nunc, 436110) were coated overnight at 4°C with 100 µL of 500 ng/mL recombinant S-RBD (GenScript Biotech, Z03483) or Nucleocapsid (GenScript Biotech, Z03480) protein – both derived from the Wuhan strain of the virus. Serial dilutions of the National Institute of Health (NIH) standard plasma (Frederick National Laboratory, MD, USA) were included on each plate to allow conversion of relative fluorescence units (RFU) to binding antibody units (BAU)/mL. In a departure from normal handling of this standard for other studies, Australian quarantine regulations required that the NIH standard was heat-inactivated (56^{o}C for 30 min) and refrozen prior to shipment. Extended transport times resulted in the standard being thawed prior to receipt. Participant plasma from EDTA collection tubes were heat inactivated at 56^{o}C for one hour. Plasma was diluted at 1/100 (for all samples on both S-RBD and nucleocapsid ELISAs) and 1/1000 (for some S-RBD samples only).

A 4-parameter logistic regression model was used to construct standard curves for each ELISA plate using the RFU values obtained from serially diluted NIH standard controls. These curves were used to estimate a subject's anti-RBD and anti-Nucleocapsid antibody concentration in BAU/mL. All subject samples were run in duplicate and the resulting RFU values were averaged before being evaluated with their respective curves. BAU/mL values of samples

tested in more than one assay were averaged. Twenty-five samples from healthy donors collected before December 2019 (pre-2020 controls) under protocols approved by the ANU HREC(2016/317) were included in the assay to determine the seropositive threshold. The threshold used to establish seropositivity was defined as three standard deviations above the geometric mean of the BAU/mL values obtained from these samples. The threshold values, represented by horizontal lines in Figure 1, were 17.25 BAU/mL for S-RBD and 45.36 BAU/mL for nucleocapsid (used to screen for patients with exposure to SARS-CoV-2).

Statistical analyses

Demographic data for participants were summarized by cohort. Baseline disease characteristics were summarized for the patient cohort. Differences in seroconversion rates between groups were evaluated using a two-sided Fisher's exact test. Differences in mean RBD antibody concentration (BAU/mL) between groups at TP3 and TP4 were assessed using a linear mixed model with timepoint and cohort as fixed effects and participant ID as a random effect. Statistical analyses were performed with RStudio (v. 4.1.2). A p-value less than 0.05 was considered statistically significant.

RESULTS

Participant demographics

A total of 102 patients and 22 controls were enrolled. Of these, 96 cancer patients and 20 control participants were included in our analyses, with data cut-off at 2 March 2022 (Supplementary Figure 2). Participants had a median age of 62 years, with 60% being female, and received AZD1222 (AstraZeneca; 65%) or BNT162b2 (Pfizer; 35%) COVID-19 vaccines as first dose (Supplementary Table 1). Demographic summary statistics were similar between cohorts. The cancer patient cohort received chemotherapy (60%), immunotherapy (15%) and targeted therapy (40%), with treatment categories being non-mutually exclusive (Supplementary Table 2).

Seroconversion three months post two vaccine doses

Eighty-seven patients and 20 control participants were eligible for the primary analysis of seroconversion at three months following two vaccine doses (TP4). The anti-S RBD antibody

seropositivity rate was 87% (76/87, 95% CI:79-94%) in cancer patients and 100% (20/20, 95% CI:83-100%) in the control cohort (p=0.12; Table 1).

Within the patient cohort, the anti-S-RBD antibody seropositivity rate at TP4 was 84% (43/51) for patients on any chemotherapy, 80% (8/10) for patients primarily on immunotherapy and 96% (25/26) for patients on targeted therapy (Table 1). Differences were not statistically significant compared to the controls.

Change in antibody response over time

Anti S-RBD concentrations at the defined study timepoints are shown in Table 2 and Figure 1A. Mean anti-S-RBD concentrations were numerically higher in healthy controls compared to cancer patients at both TP3 (410.2 vs 206.1 BAU/mL) and TP4 (169.6 vs 94.4 BAU/mL; Table 2), however, the differences were not significant. The seropositivity rate in cancer patients was 40% (6/15) after one vaccine dose and 95% (35/37) one month after the second vaccine dose, compared to the 87% at the 3-month primary endpoint (Figure 1A). Thus, we see a general trend of a rise in antibody concentrations between TP2 and TP3, and a fall between TP3 and TP4 (Figure 1A).

Anti-nucleocapsid antibody

Anti-nucleocapsid antibody concentrations remained below the seropositive threshold for all except one participant. Only two patients reported RT-PCR-confirmed infection with COVID-19, both 15 days before the primary endpoint sample was taken. Both patients showed a rise in anti-S-RBD (red dots in Figure 1 A & open circles C), however, only one patient was found to be seropositive for anti-N antibodies (red dot in Figure 1B and open circle in Supplementary Figure 3C).

Responses to different vaccines

We provide data delineated by primary vaccine course (AZD12221 or BNT162b2; Figure 1C & D). However, as the Australian immunization guidelines initially reserved Pfizer vaccination for people under 60 years of age, any analysis of differences in vaccine response would be inherently confounded by age.

DISCUSSION

A lower seropositivity rate of 87% in cancer patients, compared to 100% among controls, was observed three-months following two doses of SARS-CoV-2 vaccine, although the difference did not reach statistical significance in this study. Anti-S RBD concentrations were also numerically lower at 94.4 BAU/mL in cancer patients compared to 169.6 BAU/mL with controls. Importantly, our observations were made in a predominantly COVID-19-naïve population.

A number of studies observed lower antibody response following COVID-19 vaccination among solid organ cancer patients receiving chemotherapy(4-7). Thakkar et al., reported that among 242 solid tumor patients, those who received chemotherapy had significantly lower spike-IgG seropositivity of 92% compared to 99% in patients who did not receive chemotherapy(5). In the same series, patients on immunotherapy and hormonal therapy achieved 97% and 100% seropositivity rates respectively(5). The impact from combination therapy remains unclear. Massarweh et al., reported the RBD-IgG seropositivity to be lowest with combination of chemotherapy and immunotherapy at 14%, compared with chemotherapy alone at 29%, immunotherapy 22% and biologics at 11%, although differences were non- significant on multivariate analysis(8). Similarly, a meta-analysis of COVID-19 vaccination in cancer patients receiving immune checkpoint inhibitors found they had superior seroconversion compared with patients treated with chemotherapy, and no significant difference in seroconversion rate compared with healthy controls(9). We observed seroconversion to be highest patients on targeted therapy alone (96%), compared with chemotherapy (84%) or immunotherapy (80%). Our sample size may have limited the ability to detect any statistically significant difference. However, a large series of 503 solid tumor patients found comparable anti-S1 IgG response among immunotherapy (99.2%), chemotherapy (97.4%) and chemo-immunotherapy (100%) treated patients at 28 days after the second vaccination(10). Different timing of antibody measurement in relation to vaccine dosing may also partly account for the discordant findings.

The majority of analyses on early timepoints (within one month post vaccination) found comparable antibody responses among cancer patients and controls(10-12). One of the larger series of 503 solid tumor patients reported from the Netherlands found the 28-day anti-S antibody response in each of patient cohort (immunotherapy, chemotherapy or chemoimmunotherapy) to be non-inferior to the control cohort of individuals without cancer(10). Another study similarly found 95% and 100% seropositivity among solid cancer patients and controls respectively, at two weeks post two-dose BNT162b2 vaccination(11). These observations suggest most cancer patients, even those on active anticancer therapy, are capable of mounting an initial antibody response to vaccination.

When considering later timepoints, however, an inferior humoral response to COVID-19 vaccination among solid tumor patients compared with the general population can be more clearly appreciated. Similar to our findings, Grinshpun et al., reported seroconversion of 87.2% among 172 cancer patients with no history of COVID-19, compared with 100% among controls, at a median of 77 days from two-dose vaccination ($p < 0.001$)(13). The CANVAX cohort also found significantly lower antibody tires among cancer patients compared with healthy controls, at a median of 79 days following the first vaccine dose(4).

Decline in SARS-CoV-2 antibody level over time (without interval booster vaccination) has been a consistent finding across studies(14-18)including ours. Ehmsen et al., reported a drop in anti-S IgG seropositivity rate from 93% at 36 days after vaccination to 86% at three months, among 201 patients with solid cancers(15). The peak anti S-RBD level occurred at a median of 42 days post second vaccine dose, with antibody levels significantly decreased at four to six months (median 145.5 days) among 291 cancer patients(14). Solid tumor patients had higher peak and sustained antibody levels compared with hematological cancer patients(14, 15). Observations in our cancer patient cohort were similar, with a 95% seroconversion rate at one month and 88% at three months post two-dose COVID-19 vaccination contrasted with 100% seroconversion at one-and three-months post two-dose COVID-19 vaccination in controls (Figure 1A and 1C). These observations highlight need for additional protective measures in this vulnerable population(17, 18).

While it is useful to account for possible background COVID-19 infection using an anti-nucleocapsid ELISA, this will not capture all cases of previous infection. Several studies used anti-nucleocapsid antibody assessment as an indicator of past infection with SARS-CoV-2(4, 14, 19), given that the nucleocapsid protein is present on the viral particle but is not a component of most COVID-19 vaccines. While anti-N is a useful surrogate for previous COVID-19 infection, it is notable that only one of two patients with PCR-confirmed positive COVID-19 in our cohort was seropositive for nucleocapsid. We hypothesize that this is due to the short timeframe between SARS-CoV2 infection and sample collection for anti-nucleocapsid antibody. When the first COVID infection occurs after vaccination anti-nucleocapsid antibody concentration is expected to rise more slowly than anti-S-RBD antibody concentrations. This is due to generation of anti-nucleocapsid antibodies by a primary immune response while the anti-S-RBD response is a tertiary immune response (as vaccines targeting S-protein previously primed this response). This is important a the undetected COVID infections will result in substantially higher apparent antibody responses to COVID vaccines.

The major limitation of our study was the sample size, which may have restricted the ability to demonstrate statistical significance. However, our use of the NIH standard in calculation of the anti-S RBD levels allows for incorporation of our data in future metanalyses. We were also unable to differentiate results by COVID-19 vaccine type, however, BNT162b2 (Pfizer) was initially reserved for people under 60 years of age in Australia, any analysis of differences in vaccine response would be inherently confounded by age.

CONCLUSIONS

Two doses of AZD1222 (AstraZeneca) or BNT162b2 (Pfizer) COVID-19 vaccine achieved seroconversion in 87% of cancer patients compared with 100% of control participants, at three months post vaccination. Both seroconversion rate and mean anti-S-RBD antibody concentrations were numerically lower among cancer patients compared with controls, although the difference did not reach statistical significance in our cohort. Antibody concentrations and seroconversion rates showed a decrease between one- and three-months post vaccination, highlighting the role for subsequent booster vaccinations to maintain antibody response. Our data indicate that reliance on anti-nucleocapsid antibody assays is

not sufficient to exclude participants with previous COVID infection. Our study, conducted at a time of limited SARS-CoV-2 community transmission, provides a robust assessment of the humoral response from vaccination without the confounding impact of natural immunity due to infection.

REFERENCES

1. Khoury E, Nevitt S, Madsen WR, Turtle L, Davies G, Palmieri C. Differences in Outcomes and Factors Associated With Mortality Among Patients With SARS-CoV-2 Infection and Cancer Compared With Those Without Cancer: A Systematic Review and Meta-analysis. JAMA Netw Open. 2022;5(5):e2210880.
2. Hannah Ritchie EM, Lucas Rodés-Guirao, Cameron Appel, Charlie Giattino, Esteban Ortiz-Ospina, Joe Hasell, Bobbie Macdonald, Diana Beltekian and Max Roser. Our World in Data OurWorldinData.org2022 [updated 07/02/2022. Available from: https://ourworldindata.org/covid-vaccinations.
3. Hicks SM, Pohl K, Neeman T, McNamara HA, Parsons KM, He JS, et al. A Dual-Antigen Enzyme-Linked Immunosorbent Assay Allows the Assessment of Severe Acute Respiratory Syndrome Coronavirus 2 Antibody Seroprevalence in a Low-Transmission Setting. J Infect Dis. 2021;223(1):10-4.
4. Naranbhai V, Pernat CA, Gavralidis A, St Denis KJ, Lam EC, Spring LM, et al. Immunogenicity and Reactogenicity of SARS-CoV-2 Vaccines in Patients With Cancer: The CANVAX Cohort Study. J Clin Oncol. 2022;40(1):12-23.
5. Thakkar A, Gonzalez-Lugo JD, Goradia N, Gali R, Shapiro LC, Pradhan K, et al. Seroconversion rates following COVID-19 vaccination among patients with cancer. Cancer Cell. 2021;39(8):1081-90 e2.
6. Goshen-Lago T, Waldhorn I, Holland R, Szwarcwort-Cohen M, Reiner-Benaim A, Shachor-Meyouhas Y, et al. Serologic Status and Toxic Effects of the SARS-CoV-2 BNT162b2 Vaccine in Patients Undergoing Treatment for Cancer. JAMA Oncol. 2021;7(10):1507-13.
7. Palich R, Veyri M, Marot S, Vozy A, Gligorov J, Maingon P, et al. Weak immunogenicity after a single dose of SARS-CoV-2 mRNA vaccine in treated cancer patients. Ann Oncol. 2021;32(8):1051-3.
8. Massarweh A, Eliakim-Raz N, Stemmer A, Levy-Barda A, Yust-Katz S, Zer A, et al. Evaluation of Seropositivity Following BNT162b2 Messenger RNA Vaccination for SARS-CoV-2 in Patients Undergoing Treatment for Cancer. JAMA Oncol. 2021;7(8):1133-40.
9. Ruiz JI, Lopez-Olivo MA, Geng Y, Suarez-Almazor ME. COVID-19 vaccination in patients with cancer receiving immune checkpoint inhibitors: a systematic review and meta-analysis. J Immunother Cancer. 2023;11(2).
10. Oosting SF, van der Veldt AAM, GeurtsvanKessel CH, Fehrmann RSN, van Binnendijk RS, Dingemans A-MC, et al. mRNA-1273 COVID-19 vaccination in patients receiving chemotherapy, immunotherapy, or chemoimmunotherapy for solid tumours: a prospective, multicentre, non-inferiority trial. The Lancet Oncology. 2021;22(12):1681-91.
11. Monin L, Laing AG, Munoz-Ruiz M, McKenzie DR, Del Molino Del Barrio I, Alaguthurai T, et al. Safety and immunogenicity of one versus two doses of the COVID-19 vaccine BNT162b2 for patients with cancer: interim analysis of a prospective observational study. Lancet Oncol. 2021;22(6):765-78.

12. Fendler A, Shepherd STC, Au L, Wilkinson KA, Wu M, Byrne F, et al. Adaptive immunity and neutralizing antibodies against SARS-CoV-2 variants of concern following vaccination in patients with cancer: the CAPTURE study. Nature Cancer. 2021;2(12):1305-20.
13. Grinshpun A, Rottenberg Y, Ben-Dov IZ, Djian E, Wolf DG, Kadouri L. Serologic response to COVID-19 infection and/or vaccine in cancer patients on active treatment. ESMO Open. 2021;6(6):100283.
14. Figueiredo JC, Merin NM, Hamid O, Choi SY, Lemos T, Cozen W, et al. Longitudinal SARS-CoV-2 mRNA Vaccine-Induced Humoral Immune Responses in Patients with Cancer. Cancer Res. 2021;81(24):6273-80.
15. Ehmsen S, Asmussen A, Jeppesen SS, Nilsson AC, Osterlev S, Vestergaard H, et al. Antibody and T cell immune responses following mRNA COVID-19 vaccination in patients with cancer. Cancer Cell. 2021;39(8):1034-6.
16. Trontzas IP, Vathiotis I, Economidou C, Petridou I, Gomatou G, Grammoustianou M, et al. Assessment of Seroconversion after SARS-CoV-2 Vaccination in Patients with Lung Cancer. Vaccines (Basel). 2022;10(4).
17. Nelli F, Fabbri A, Onorato A, Giannarelli D, Silvestri MA, Pessina G, et al. Six month immunogenicity of COVID-19 mRNA-BNT162b2 vaccine in actively treated cancer patients: updated results of the Vax-On study. Ann Oncol. 2022;33(3):352-4.
18. Eliakim-Raz N, Massarweh A, Stemmer A, Stemmer SM. Durability of Response to SARS-CoV-2 BNT162b2 Vaccination in Patients on Active Anticancer Treatment. JAMA Oncol. 2021;7(11):1716-8.
19. Addeo A, Shah PK, Bordry N, Hudson RD, Albracht B, Di Marco M, et al. Immunogenicity of SARS-CoV-2 messenger RNA vaccines in patients with cancer. Cancer Cell. 2021;39(8):1091-8 e2.

D. Response to COVID-19 vaccination in patients on cancer therapy: analysis in a SARS-CoV-2-naïve population

Tables and Figures

Table 1. Comparison of Seropositivity between controls, patients and divisions of patients based on treatment type.

	Total	Seropositive			
	N	n	%	95% CI	p-value*
Controls	20	20	100	(83, 100)	
Patients	87	76	87	(79, 94)	0.121
Patients by therapy					
Chemotherapy	51	43	84	(71, 93)	0.095
Immunotherapy	10	8	80	(44, 97)	0.103
Targeted therapy	26	25	96	(80, 100)	1.000

*2-sided Fisher's Exact Test, all comparisons made to control cohort.

Table 2. Comparison of anti-S-RBD antibody concentration between patients and controls at TP3 and TP4

Timepoint	Participant	n	Antibody (BAU/mL)†	(95% CI)	Ratio	(95% CI)
TP3	cancer patient	37	206.1	(135.9, 312.7)	0.503	(0.139, 1.82)
	healthy control	3	410.2	(121.4, 1386.3)		
TP4	cancer patient	87	94.4	(67, 133.2)	0.557	(0.247, 1.254)
	healthy control	20	169.6	(81.3, 354.1)		

† Geometric mean

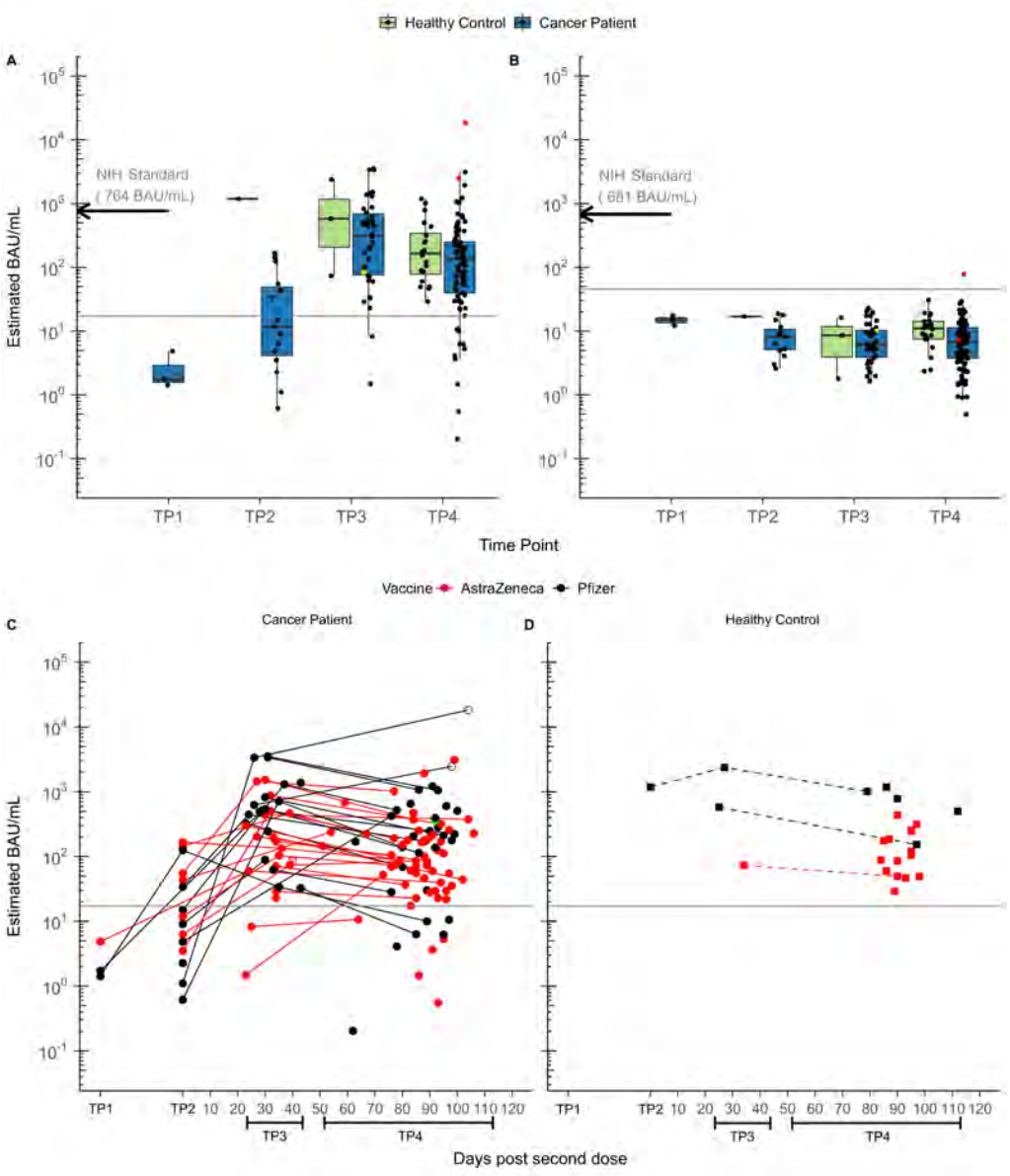
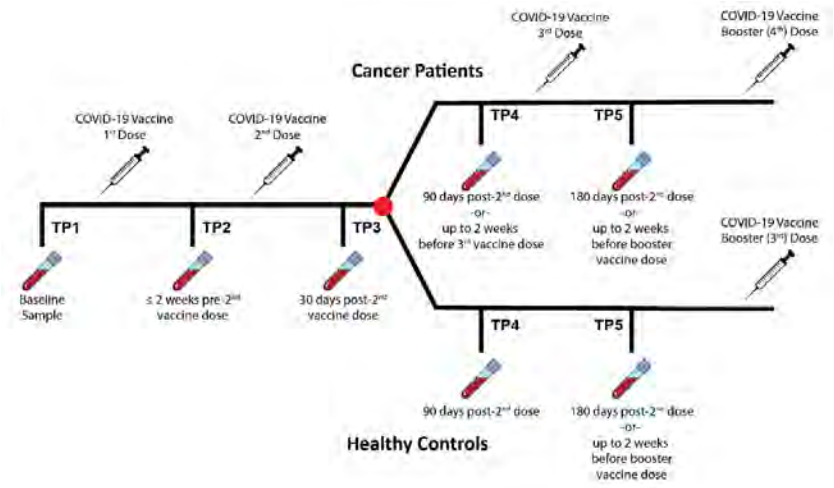
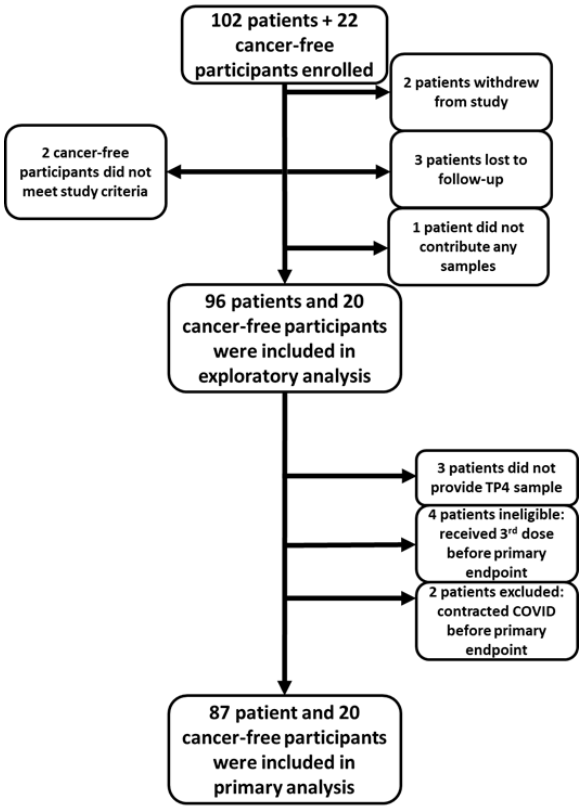

Healthy Control
Cancer Patient
A
B
NIH Standard
(764 BAU/mL)
NIH Standard
(681 BAU/mL)
Estimated BAU/mL
TP1
TP2
TP3
TP4
Time Point
Vaccine
AstraZeneca
Pfizer
C
Cancer Patient
D
Healthy Control
Days post second dose

Figure 1 (previous page). Anti-S-RBD and anti-Nucleocapsid antibody responses in cancer patients and healthy controls. (A) and **(B)** Responses of cancer patients vs. controls against **(A)** S-RBD (induced by vaccination) or **(B)** Nucleocapsid (induced by infection). Median and interquartile range (IQR) are shown for healthy controls (green) and cancer patients (blue). Black dots represent patients included in the median and IQR calculations. **(C)** and **(D)** Responses against S-RBD resolved by time after second vaccine dose, by vaccine type, and linking samples taken from the same individual, for **(C)** cancer patients and **(D)** healthy controls. Points and lines coloured according to vaccine type received; AstraZeneca (AZD1222) shown in red, Pfizer (BNT162b2) in black, one patient who received one of each vaccine in green – first dose AZD1222, second dose BNT162b2. Antibody response was measured by ELISA and converted to Binding Antibody Units per mL (BAU/mL) using the NIH standard. The threshold for seropositivity (shown by horizontal black lines in each graph) was calculated as three standard deviations above the geometric mean of 25 pre-2020 (negative control) sera; 17.25BAU/mL for S-RBD **(A, C, D)** and 45.36BAU/mL for Nucleocapsid **(B)**. Two patients who were infected with SARS-CoV-2 before TP4 are shown as red dots in **(A)** and **(B)** and as open circles in **(C)**. One patient who received three doses of vaccine before TP3 is shown as a yellow dot in **(A)** and **(B)**, and as an open square in **(C)**. TPs analysed include: before first dose (TP1), between first and second dose (TP2), approximately one month after second dose (23-43 days, median 31 days; TP3), approximately three months after second dose (51-112 days, median 89 days; TP4). Cancer patients (n=96), healthy controls (n=20).

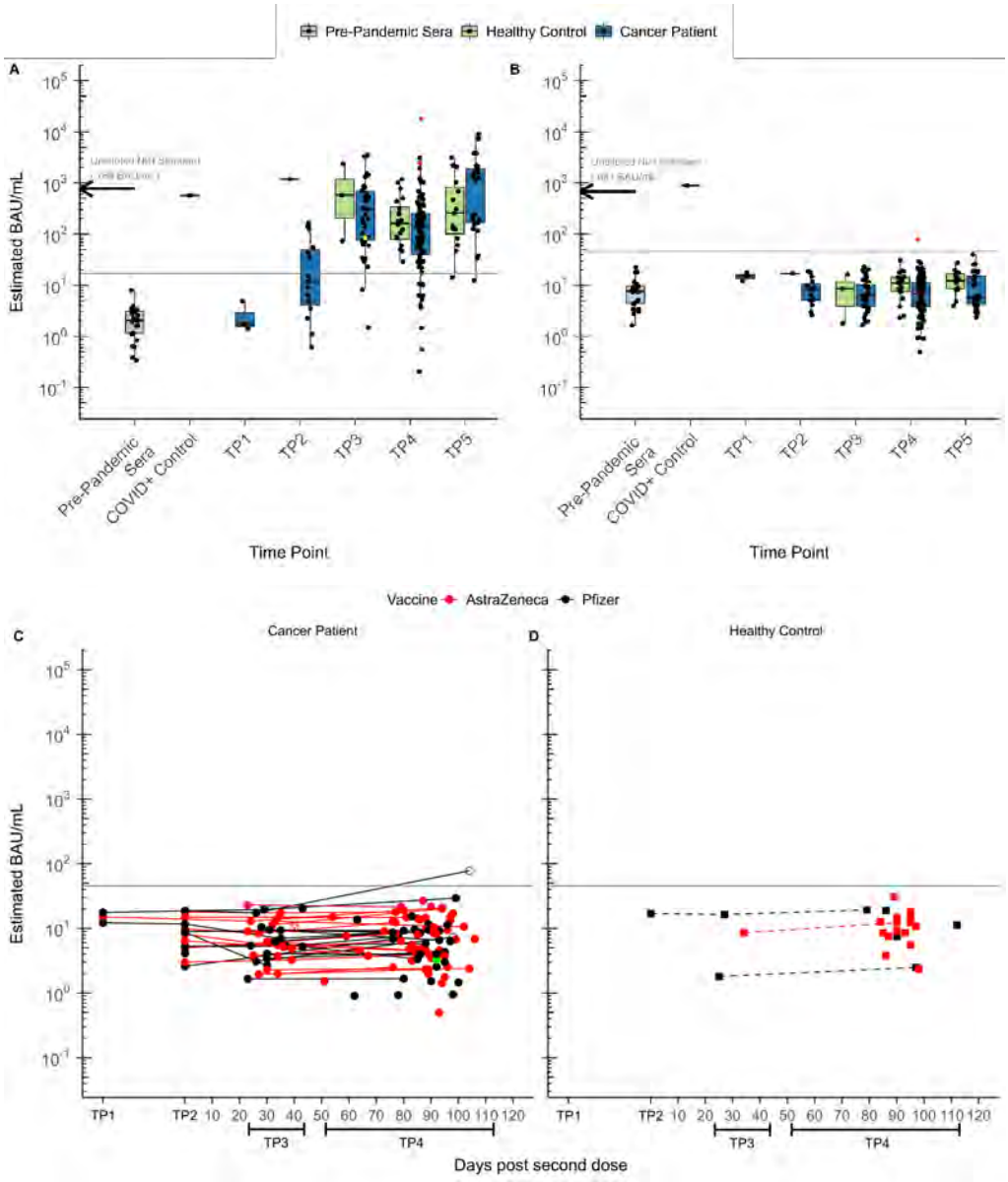
Supplementary



Supplementary Figure 1. Sample collection schedule. Plasma samples were collected from patients and healthy controls at five distinct time-points (TPs) during the SARS-CoV-2 vaccination course. TP1, 2, 3 and 5 were collected if possible, with TP4 utilized as the endpoint for primary analysis. TP1 (baseline) was collected before vaccination. TP2 samples were collected up to 14 days before the second vaccine dose. TP3 samples were collected 30 days after the second vaccine dose ± 14 days. TP4 samples were taken 90 days after the 2nd vaccine dose ± 14 days, or, for the patient cohort only, up to 14 days before a third dose was administered (the latter was introduced due to a change in public health advice during the course of the study which recommended a third primary dose for cancer patients, available two months after the second dose).TP5 samples were collected 180 days post 2nd vaccine dose ±14 days. Due to changes in the public health advice over the course of the study, the TP5 samples may include control participants who have or have not received a third (booster) dose and patients that have had either two doses, three doses or a fourth (booster) dose of vaccine.



Supplementary Figure 2. Subject disposition chart. Occurrences of participant withdrawal from the study or exclusion from primary analysis for both the cancer-free cohort (left) and the patient cohort (right) are shown. Participants were included in exploratory analyses contingent on having provided consent to participate in the study and a sample at any timepoint (TP). The primary analysis was conducted using TP4 samples.


Pre-Pandemic Sera
Healthy Control
Cancer Patient
A
B
Estimated BAU/mL
Pre-Pandemic Sera
COVID+ Control
TP1
TP2
TP3
TP4
TP5
Time Point
Vaccine
AstraZeneca
Pfizer
C
Cancer Patient
D
Healthy Control
Days post second dose

Supplementary Figure 3 (previous page). Anti-S-RBD and Anti-N Antibody Responses in Patients and Healthy Controls. Responses of cancer patients vs. controls against **(A)** S-RBD (induced by vaccination) or **(B)** Nucleocapsid (induced by infection). Median and interquartile range (IQR) are shown for pre-pandemic controls (n=25; light blue), healthy controls (green) and cancer patients (dark blue). Black dots represent patients included in the median and IQR calculations. Refer to legend of Figure 1 **(A)** and **(B)** for details. Shown in addition, are pre-pandemic sera used for the calculation of the seropositivity threshold, serum from a known COVID infected patient, and TP5 samples collected up to the 2nd of March 2022. Number of samples represented in each respective column are as follows: TP1 - three patients, TP2 - 15 patients and one control, TP3 - 38 patients (one of whom had a third vaccine dose prior to TP3 sample collection – outside of normal vaccine scheduling – point shown in yellow) and three controls, TP4 - 89 patients (two of whom were COVID positive before TP4 sample collection, points shown in red) and 20 controls and TP5 – 29 patients and 15 controls. Coloured points representing participant samples that were collected but did not meet the study criteria were excluded from the primary analysis, and not considered in the medians and IQR's shown in the graphs above. **(C)** and **(D)** Responses against Nucleocapsid resolved by time after second vaccine dose, by vaccine type, and linking samples taken from the same individual, for **(C)** cancer patients and **(D)** healthy controls. Refer to legend of Figure 1 **(C)** and **(D)** for details.

Supplementary Table 1. Participant Demographic Data

Characteristic	Cancer patient N = 96[1]	Health control, N = 20[1]	Total, N = 116[1]
Gender			
Female	60 (62%)	10 (50%)	70 (60%)
Male	36 (38%)	10 (50%)	46 (40%)
Age			
Mean (SD)	61 (13)	59 (18)	61 (14)
Median (Range)	61 (23, 87)	62 (24, 86)	62 (23, 87)
Vaccine Dose 1			
AZD1222	60 (62%)	15 (75%)	75 (65%)
BNT162b2	36 (38%)	5 (25%)	41 (35%)
Vaccine Dose 2			
AZD1222	59 (61%)	15 (75%)	74 (64%)
BNT162b2	37 (39%)	5 (25%)	42 (36%)

[1]n (%)

D. Response to COVID-19 vaccination in patients on cancer therapy: analysis in a SARS-CoV-2-naïve population

Supplementary Table 2. Baseline Characteristics – Patients

Characteristic	N = 96
Tumour type	
Breast	26 (27%)
Gastrointestinal	30 (31%)
Genitourinary	12 (12%)
Gynaecological	15 (16%)
Lung	5 (5.2%)
Melanoma/Skin	5 (5.2%)
Other	3 (3.1%)
Treatment intent	
Curative	32 (33%)
Palliative	64 (67%)
Extent of disease	
Local	30 (31%)
Metastatic	66 (69%)
ECOG	
0	48 (50%)
1	41 (43%)
2	7 (7.3%)
Chemotherapy	58 (60%)
Immunotherapy	14 (15%)
Targeted Therapy	38 (40%)
Corticosteroids	5 (5.2%)
Lymphocyte count (x10^9/L)	
N	95
Mean (SD)	1.38 (0.73)
Median (Range)	1.30 (0.07, 3.60)
Unknown	1
Charlson comorbidity index	
N	96
Mean (SD)	6.92 (2.52)
Median (Range)	7.00 (2.00, 12.00)

E

A cost-effective detection method for SARS-CoV-2 and other RNA viruses in wastewater

A cost-effective detection method for SARS-CoV-2 and other RNA viruses in wastewater

Ruth A. Purcell [a, b, 1], Pey-Tsyr Chiou [b], Pawan Parajuli [a, b, 2], Andrew A. Almonte [a], Graham J. Mann [b], Peter Collignon [c, d], Kathryn Glass [e], Danswell Starrs [f], Darren Gray [e], Rippei Hayashi [b], Dominik Spensberger [b, *], Anselm Enders [b, *, ✉], Aude M. Fahrer [a, *, ✉], & Aparna Lal [e, *, ✉]

* These authors contributed equally to this work.

✉ Corresponding author. Email address: aparna.lal@anu.edu.au (A.L); aude.fahrer@anu.edu.au (A.M.F); anselm.enders@anu.edu.au (A.E.)

[a] Division of Biomedical Science and Biochemistry, Research School of Biology, The Australian National University, ACT 2601, Australia

[b] John Curtin School of Medical Research, Australian National University, ACT 2601, Australia

[c] Medical School, The Australian National University, ACT 2601, Australia

[d] Canberra Hospital, Garran, ACT 2605, Australia

[e] National Centre for Epidemiology and Population Health, Australian National University, ACT 2601, Australia

[f] Environment Planning and Sustainable Development Directorate, ACT Government, Canberra, Australia

[1] Present address: Department of Microbiology and Immunology, University of Melbourne, at the Peter Doherty Institute for Infection and Immunity, VIC 3000, Australia

[2] Present address: Australian Centre for Disease Preparedness (ACDP), Commonwealth Scientific and Industrial Research Organisation, VIC 3220, Australia

Abstract

Surveillance for RNA viruses in wastewater samples is of intense interest due to the severe acute respiratory syndrome coronavirus 2 (SARS-CoV-2) pandemic. In this study, we used readily available reagents and laboratory consumables to optimise viral purification and SARS-CoV-2 and rotavirus detection in targeted hotel quarantine facility and daily wastewater treatment plant samples. Standard practice sees the well-described problem of PCR inhibitor co-concentration from wastewater during pathogen isolation overcome with expensive inhibitor removal kits. We developed a modified silica column-based RNA purification method with an alcohol wash that removes PCR inhibitors, thus allowing efficient viral detection and quantification. Our use of ethanol, rather than commercial kits, is a cost-effective alternative with

broad applicability during supply chain disruptions and in resource-limited settings. This method enabled detection of SARS-CoV-2 in samples collected when five individuals out of the ~400,000 serviced by the water treatment plant were infected, as well as from samples stored for four months at 4°C, a key finding that has important practical applications for surveillance and retrospective analysis of stored samples. Our methodology uses the readily available and safe Rotarix vaccine for verification and quantitation of viral purification efficacy for every sample and can reliably detect ~1 $CCID_{50}$ copy of virus/mL of wastewater. This fully-controlled, cost-effective method is a highly-sensitive tool for laboratories around the world needing to validate and optimise wastewater detection protocols for specific variants including Omicron, with a focus on detecting intact virus, as well as screening biobanked samples. Our method highlights the usefulness of wastewater testing for both active community surveillance, and also retrospective surveillance.

Keywords

SARS-CoV-2; Wastewater surveillance; RNA virus detection; PCR inhibitor; environmental epidemiology

1. Introduction

Widespread use of wastewater surveillance to track the spread of disease began with poliovirus and is now frequently employed to track the use of commonly prescribed drugs and illicit substances (Böttiger et al., 1992; Castiglioni et al., 2006; Östman et al., 2014; Thomas et al., 2012). It is also routinely used as a cost-effective environmental surveillance method for several enteric viruses such as astrovirus, hepatitis A virus, norovirus, enterovirus and rotavirus (Arraj et al., 2008; Shieh et al., 1997; Strubbia et al., 2019; Tsai et al., 1994). The utility of wastewater screening further extends to the many respiratory viruses that are primarily transmitted person-to-person through respiratory droplets but have also been detected in stool and sewage samples such as rhinoviruses (Harvala et al., 2012; Savolainen-Kopra et al., 2013) and human coronaviruses (HCoV) (Jevšnik et al., 2013; Risku et al., 2010; Vabret et al., 2006; Vabret et al., 2005).

Wastewater testing has proved useful to complement other surveillance methods for detecting community transmission of severe acute respiratory syndrome coronavirus 2 (SARS-CoV-2). In the early phase of the pandemic, before wide-spread infections, the detection of viral fragments in some areas of the Netherlands and the United States of America preceded many clinical cases being identified as well as the peak in reported and hospitalised cases, validating the use of wastewater monitoring as an early warning system (Medema et al., 2020; Wu et al., 2020). Environmental surveillance using wastewater to detect SARS-CoV-2 has already been demonstrated in several other parts of the world including Australia (Ahmed et al., 2020a), France (Wurtzer et al., 2020) and Italy (La Rosa et al., 2020). Wastewater screening has been most useful as an early detection tool for viruses. However, compatibility of isolated viral genetic material with a variety of nucleic acid sequencing methods further enables identification of new SARS-CoV-2 variants of that can be detected by specific PCRs, for example the recent Omicron variant (Smyth et al., 2022). This early detection of viruses or emerging variants through environmental surveillance using wastewater has demonstrated potential to strengthen timely detection of clusters and supplement public health response measures, particularly when case numbers are low, either through strict quarantine and lock-down or with targeted vaccination campaigns (Sharara et al., 2021). Importantly, the availability of cheap and simple methods of viral detection in wastewater allows the surveillance of smaller areas or even individual buildings like aged-care facilities or other high-risk environments.

One of the biggest challenges with wastewater testing during the pandemic has been the lack of a publicly available, standardised method for detection. The methodological approach for viral concentration, RNA extraction, and viral detection varies, and the literature remains conflicted as to the most effective method. There are also concerns about the global competition for consumables (e.g. specialised filters and reagents) and the availability of specialised equipment in laboratories in resource-limited settings (e.g. ultracentrifuges) as well as problems associated with the global supply chain. Therefore, there is an urgent need for a cost-effective, optimised and validated protocol for viral detection in wastewater using readily available reagents (Michael-Kordatou et al., 2020).

The main aim of this study was to develop a cost-effective method for detection of viruses from wastewater. In contrast to many other methods, our method aimed to concentrate SARS-CoV-2 virions endogenous to the sampled wastewater, rather than a surrogate virus or irradiated SARS-CoV-2, and is selective for viral particles over nucleic acids. A novel contribution of this study is the use of Rotarix, a live attenuated oral rotavirus vaccine from GlaxoSmithKline to provide a positive process control for each extraction, as well as a way of testing each purified sample for the presence of PCR inhibitors. This method has the advantage of safety, and of wide availability. Our method is based on polyethylene glycol (PEG) precipitation that has previously been used for the detection of SARS-CoV-2 (Wu et al., 2020) and other pathogenic viruses (Hjelmsø et al., 2017; Monpoeho et al., 2001). We have optimized the RNA purification protocol for overcoming RT-qPCR inhibitors which are ubiquitous in wastewater samples (Gibson et al., 2012) by the use of column purification with additional ethanol washes. We provide a cost-effective workflow for viral concentration and RNA purification for wastewater surveillance for use in the current COVID-19 pandemic and beyond, Further, we demonstrate the use of easily available human Rotarix vaccine as a positive control, with the novel finding that this method can detect the virus in stored samples that are four months old without notable signal degradation.

2. Material and methods

2.1. Wastewater samples

Raw wastewater samples were collected from the Lower Molonglo Water Quality Control Centre (LMWQCC) of Icon Water Limited, Canberra, Australia. The LMWQCC serves ~400,000 residents of the Australian Capital Territory (Canberra, ACT) region. The samples were collected daily using

the flow-weighted composite method over 24 hours and transported to the laboratory on ice. The wastewater samples were stored at 4°C until further processing.

2.2. Rotavirus control

A live attenuated oral rotavirus vaccine (Rotarix, GlaxoSmithKline, Belgium) was used to optimise and control the protocol. Each 1.5 mL dose of the vaccine contains no fewer than 10^6 cell culture infectious dose 50% ($CCID_{50}$) of human rotavirus (RIX4414 strain) of the G1(P8) type (O'Ryan 2007).

2.3. Viral concentration

The viral concentration method was based on PEG precipitation described by Wu et al. (2020) with some modifications. The wastewater samples were first heated to 60°C for 90 minutes to inactivate any SARS-CoV-2 that might be present. 5 mL of glycine buffer (0.25 M glycine, 15% beef extract, pH 9.6) was added to 200 ml of wastewater sample to help detach viruses bound to organic material (Hjelmsø et al. 2017). The samples were then centrifuged at 4,700 x g for 30 minutes at 4°C to remove the larger debris. Rotavirus vaccine was spiked into the sample at this point. The collected supernatant was filtered through a 0.45 µM nitrocellulose filter (Millipore, Sydney, Australia) to remove any bacterial and eukaryotic cells. The pH of the filtrate was adjusted to 7.0 – 7.3 by adding hydrochloric acid. PEG 8000 (10% w/v) (Millipore, Sydney, Australia) and NaCl (2% w/v) (Thermo Fisher Scientific, Scoresby, Australia) were added to the samples which were then agitated overnight in a shaker at 4°C, 100 rpm. Virus was pelleted by centrifugation at 12,500 x g for 2 hours at 4°C. The pellet was used for immediate RNA extraction.

2.4. RNA extraction

200 µL nuclease-free water was directly applied to the viral pellet on the side of the centrifuge bottle obtained via PEG precipitation. Viral particles were then lysed by vigorous resuspension in 500 µL lysis buffer from the FastPure Viral DNA/RNA Mini Kit (Vazyme, Nanjing, China). RNA was isolated using the silica column-based method according to the manufacturer's instructions (Vazyme, Nanjing, China), or modified to include additional ethanol washes. To reduce levels of RT-qPCR inhibitors, the column was washed three times with 600 µL of 80% ethanol after the last application of the supplied kit wash buffer, prior to elution. To confirm that inhibitory effects observed were not specific to the Vazyme columns, RNA extraction was also performed using

the RNeasy Mini Kit (Qiagen) according to the manufacturer's instructions with and without three additional ethanol washes. The RNA was then eluted in 50 µL nuclease-free water heated to 70°C.

Column isolations of other samples (e.g., Rotarix vaccine control) were performed by adding 500 µL of Vazyme lysis buffer to samples made up to 200 µL in phosphate-buffered saline, followed by standard column extraction protocol as per manufacturer's instructions.

2.5. RT-qPCR analysis

The detection of rotavirus was performed using the Power *SYBR*® Green RNA-to-CT one-step kit (Applied Biosystems, California, USA). We amplified an 87 bp fragment from a highly conserved region of the non-structural protein 3 (NSP3) gene of the rotavirus genome using the primer pairs- Rota NSP3-F (5'-3'): accatctacacatgaccctc and Rota NSP3-R (5'-3'): ggtcacataacgcccc (Pang et al. 2004). The RT-qPCR reaction was performed in a 10 µL reaction volume containing 1 µL of RNA template (except where otherwise stated), 5 µL of green RT-PCR mix (2x), 0.08 µL RT enzyme mix (125x) and 150 nM of each primer. The RT-qPCR was performed using a QuantStudio 12K Flex Real-Time PCR system (Thermo Fisher Scientific, Carlsbad, USA) with 30 min reverse transcription at 48°C followed by initial denaturation at 95°C for 10 mins and subsequent 45 amplification cycles with denaturation at 95°C for 15 secs and with primer annealing/extension at 60°C for 1 min. Data collection was enabled at the extension step. All the samples were run in duplicates at a minimum. RT-qPCR was performed in a separate laboratory from the RNA extraction to avoid contamination of samples with amplified PCR products during RNA extraction and RT-qPCR preparation.

The detection of SARS-CoV-2 was performed using the Triplex RT-qPCR detection kit (Cat #: CD302, Vazyme); using Taqman® probe detection. The kit amplified the SARS-CoV-2 ORF1ab gene (RdRP region) and N gene, avoiding non-specific interference from SARS-CoV-1 and Bat SARS-like virus strains. An internal control targeting the human RNAse P (RNP) gene was also included in the kit but was not relevant to our experiments as human cells were largely filtered out of the wastewater by the 0.45 µM nitrocellulose filters. Synthetic SARS-CoV-2 RNA (Twist Biosciences, CA, USA) was run as a control to confirm the RT-qPCR had proceeded successfully. The reaction was carried out in 10 µL total volume, using 6 µL of master mix (Detection buffer 5.2 µL and Enymer mix 0.8 µL). The method was optimised for 1 µL of template (+3 µL water, to maintain volume), but where stated, 4 µL of template was used. The RT-qPCR was performed

using a QuantStudio 12K Flex Real-Time PCR system (Thermo Fisher Scientific, Carlsbad, USA) with 15 min reverse transcription at 50°C followed by initial denaturation at 95°C for 30 sec and subsequent 45 amplification cycles with denaturation at 95°C for 10 sec and with primer annealing/extension at 58°C for 30 sec. Data collection was enabled at the extension step. Manuscript figures were prepared using R version 4.1.2

3. Results and discussion

Using cost-effective, standard molecular biology lab materials, we modified and optimised previously published protocols (Hjelmsø et al., 2017; Wu et al., 2020) to monitor wastewater daily for SARS-CoV-2. The Rotarix vaccine—a safe, readily available source of live RNA virus—was used to control for virus recovery. The rapid development of this method under the restrictive setting of a pandemic, which led to supply chain interruptions, and difficulty obtaining specialised laboratory reagents, demonstrates its suitability for emergency surveillance. The validation of this optimised method: in a setting where precise numbers of infected individuals were known; using upstream and downstream samples from a hotel quarantine facility; and the (re)detection of SARS-CoV-2 in positive samples after four months of storage are novel and important additions to our rapidly emerging understanding of the utility of wastewater-based epidemiology during outbreaks.

3.1. Rotavirus detection

Our first attempt to detect Rotavirus from spiked wastewater samples failed. Following removal of debris from the wastewater by centrifugation, 15 µL of Rotarix vaccine containing ~10^4 $CCID_{50}$ copies of rotavirus, was added to 200 mL of wastewater. Rotavirus NSP3 gene could not be detected via RT-qPCR in these samples subjected to standard PEG-precipitation and column-based nucleic acid extraction methods. However, in tap water samples spiked with ~10^4 $CCID_{50}$ copies of rotavirus, the NSP3 gene was readily detectable with Ct scores (number of RT-qPCR cycles to positive signal) comparable to those obtained for RNA isolated directly from the Rotarix vaccine (mean Ct of 29.3 and 28.7, respectively) (Fig. 1).

To determine whether our inability to detect virus in wastewater was due to a failure of virus purification, or due to inhibition of the PCR reaction, 3 µL of RNA extracted from wastewater (dark green lines in Fig. 2A) was added to 1 µL of RNA purified directed from Rotarix vaccine. As shown in Fig. 2A, complete inhibition was observed. Even 1 µL of RNA from wastewater (pale green lines in Fig. 2B) produced substantial inhibition. In addition, multiple peaks are

generated during qPCR melt curve analysis for wastewater RNA samples subject to the simple dilution strategy commonly used to overcome PCR inhibitors (representative melt curves shown in Supp. Fig. 1), indicating substantial sample contamination. We concluded that components of the wastewater co-extracted with the viral RNA were inhibiting the RT-qPCR reaction. Wastewater is well-documented to contain a variety of PCR inhibitors (reviewed by Schrader et al. 2012).

3.2. SARS-CoV-2 detection

Inhibition by wastewater of the TaqMan COVID-19 PCR was present but less severe than that of the SYBR Green Rotavirus PCR. This may reflect the different chemistries of the reaction mixes or the sensitivity of the polymerases in the different kits to inhibitors. Furthermore, even using the same chemistry, the use of different primers showed different levels of inhibition. Inhibition assays showed that when 3 µL of RNA extracted from wastewater was added to 1 µL of SARS-CoV-2 control RNA (maximum of 200 copies RNA), the N gene, and less often, the ORF1ab gene, remained detectable, allowing presence or absence of SARS-CoV-2 to be confirmed (Fig. 3). In agreement, previous studies (Zhang et al., 2020; Zhou et al., 2020) have also identified limitations in ORF1ab amplification, implicating this gene as a less reliable marker for SARS-CoV-2 detection in wastewater. This suggests optimisation of the individual primers may be helpful when required to detect viruses and viral variants in wastewater.

3.3. Inhibitor removal

Gold standard practice for inhibitor removal requires expensive proprietary kits which may be inaccessible to under-resourced labs or any lab facing supply chain issues. Jue et al. (2020) proposed a two-phase wash to solve the issue of contaminant-carryover of inhibitors from wash buffers in commercial nucleic acid extraction kits into samples. The long-chain alcohols, such as 1-undecanol, highlighted as optimal for this purpose are not readily available in molecular biology labs. Nevertheless, ethanol was suggested to potentially reduce PCR inhibition but not explored in depth. Based on this study, we trialed additional washes with 80% ethanol (readily available in any molecular biology lab) as a cheap and accessible alternative to inhibitor removal kits. Manufacturers' instructions were followed for silica-based column purification, however, thee additional ethanol washes were applied immediately before RNA elution.

The effect of the additional ethanol washes was striking. When using 1 µL of RNA template (rather than the 4 µL suggested by the RT-qPCR kit manufacturers), three washes with 80%

ethanol completely restored amplification of the rotavirus NSP3 gene in all samples tested covering the variable range of wastewater conditions present from December 2020 to April 2021 (summer through spring). In addition, clean melt curves with a single peak at the ~73.5 °C expected for the rotavirus NSP3 gene were obtained for all samples subjected to the 80% ethanol wash step (Fig. 4). Additionally, inhibition of the SARS-CoV-2 N gene was reversed and inhibition of the ORF1ab gene was lessened but not fully restored.

Similar results were observed when RNA was extracted using an alternative brand of RNA spin column—RNeasy Mini Kit (Qiagen). Following the manufacturer's instructions resulted in substantial to complete inhibition of amplification which was recovered upon washing with 80% ethanol (Supp. Fig. 2). This suggests that our technique to reduce RT-qPCR inhibitors from wastewater is generalisable to silica-based spin columns, regardless of manufacturer.

We confirmed the sensitivity of our method by spiking wastewater samples from both the treatment plant and hotel quarantine facility with a 50-fold lower concentration of rotavirus, ~200 virions in 200 ml of wastewater, and detected the rotavirus NSP3 gene in all samples (Supp. Fig. 3).

3.4. Wastewater surveillance

Canberra's experience of COVID-19 was unique in that between September 2020 and August 2021, no cases of community transmission were identified—all cases in that time were imported by travellers into Canberra who were isolated in hotel or household quarantine. We conducted daily wastewater testing for SARS-CoV-2 in Canberra between May 2020 and May 2021 in samples from the Lower Molonglo Water Quality Control Centre (LMWQCC) which services ~400,000 residents. Using our protocol prior to optimisation (i.e. following the manufacturer's instructions for nucleic acid extraction), we were able to detect SARS-CoV-2 in wastewater samples collected on the 8th, 9th and 10th of March 2021 (Fig. 5A-C).

On 11 March 2021, a total of five COVID-19 cases were quarantined in a single hotel. We used this as an opportunity to further validate our method for building-level surveillance. In a city with no confirmed community transmission and at a time when local transmission had not occurred in almost a year, it was reasonable to assume that no SARS-CoV-2 would be detected upstream of the hotel, allowing wastewater samples collected upstream to serve as negative controls. We collected two wastewater samples upstream of the quarantine hotel and two samples downstream of the hotel. We detected SARS-CoV-2 in both samples collected

284 downstream of the hotel but not in any upstream samples, validating our method as a reliable
285 and specific detection tool (Figure 5D).

286 **3.5. Long-term SARS-CoV-2 stability**

287 Following optimisation and validation of our method, the samples collected upstream and
288 downstream of the hotel quarantine facility were retested to determine the stability of SARS-
289 CoV-2 in wastewater after storage at 4°C for four months. SARS-CoV-2 was successfully
290 detected in the hotel downstream samples (Fig. 6).

291 That SARS-CoV-2 can be detected in wastewater stored at 4°C for at least four months is
292 hugely significant to researchers relying on biobanked samples.

293 To our knowledge, this is the first evidence for SARS-CoV-2 detection in wastewater after
294 storage for more than 100 days. Ahmed et al. (2020b) detected SARS-CoV-2 RNA in untreated
295 wastewater after 33 days at 4°C using high concentrations of intact, gamma irradiated SARS-
296 CoV-2 spiked into low volumes of wastewater without the need for virus concentration.
297 Hokajärvi et al. (2021) detected SARS-CoV-2 RNA in wastewater influent stored at 4°C for 84
298 days, but further modelling based on wastewater spiked with SARS-CoV-2 collected from
299 nasopharageal swabs suggested the T_{99} (time to 99% reduction) to be 73 or 105 days,
300 depending on detection method.

301 PEG precipitation has been shown to be biased towards virion, rather than RNA, concentration
302 (Amdiouni et al., 2012). As free RNA degrades rapidly degraded in wastewater (Wurtzer et al.,
303 2021), we hypothesise that our method, which was designed to concentrate viral particles (in
304 which the RNA is protected from degradation in wastewater), makes extended virus detection
305 possible.

306 Indeed, it is possible that much of the variation in efficacy observed between different viral
307 concentration methods is owed to a poor understanding of the ratio of free viral genome to intact
308 or partially degraded virion contributing to RT-qPCR signal.

309 We expect our method will be useful for the validation and optimisation of virus recovery from
310 wastewater in laboratories around the world, including in resource-limited settings. This
311 technique could also be used to identify the early spread of new SARS-CoV-2 variants through
312 communities. Any virus or novel viral variant for which a specific PCR amplicon and probe can

be designed could be monitored using this technique. Furthermore, stored wastewater samples can be retrospectively interrogated for the presence of novel viral strains.

4. Conclusion

- We describe a cost-effective wastewater surveillance method for SARS-CoV-2 that can be readily adopted on short notice by any laboratory with basic molecular biology capabilities.
- Our method is sensitive enough to detect 5 positive cases in a population of ~400,000, and its specificity is applicable to building-level surveillance, such as that of hotel quarantine facilities.
- Removal of PCR inhibitors in wastewater can be achieved with an 80% ethanol wash step in lieu of expensive inhibitor removal kits.
- SARS-CoV-2 is detectable in raw wastewater samples stored at 4°C for at least four months.

Acknowledgments

We thank Prof David Tscharke, ANU, Dr Mathis Hjort Hjelmsø,Technical University of Denmark and Prof. Peter White, UNSW for helpful personal communications. We are grateful to Dr. Rita da Costa Goncalves Ferreira and to the staff of the Australian Cancer Research Foundation Biomolecular Resource Facility at the Australian National University for their resources and the instruments. We acknowledge BioRender for the graphical abstract template. We thank the Australian Capital Territory Health Directorate for project funding.

Declaration of Competing Interest

The authors declare that they have no known competing financial interests or personal relationships that could have appeared to influence the work reported in this paper.

References

Ahmed, W., Angel, N., Edson, J., Bibby, K., Bivins, A., O'Brien, J.W., Choi, P.M., Kitajima, M., Simpson, S.L. and Li, J. (2020a) First confirmed detection of SARS-CoV-2 in untreated wastewater in Australia: A proof of concept for the wastewater surveillance of COVID-19 in the community. Science of The Total Environment, 138764.

Ahmed, W., Bertsch, P.M., Bibby, K., Haramoto, E., Hewitt, J., Huygens, F., Gyawali, P., Korajkic, A., Riddell, S., Sherchan, S .P., Simpson, S .L., Sirikanchana, K., Symonds, E .M., Verhagen, R., Vasan, S.S., Kitajima, M., Bivins, A. (2020b) Decay of SARS-CoV-2 and surrogate murine hepatitis virus RNA in untreated wastewater to inform application in wastewater-based epidemiology. Environmental Research 191, 110092

Amdiouni, H., Maunula, L., Hajjami, K. *et al.* Recovery Comparison of Two Virus Concentration Methods from Wastewater Using Cell Culture and Real-Time PCR. *Curr Microbiol* **65,** 432–437 (2012). https://doi.org/10.1007/s00284-012-0174-8

Arraj, A., Bohatier, J., Aumeran, C., Bailly, J.-L., Laveran, H. and Traore, O. (2008) An epidemiological study of enteric viruses in sewage with molecular characterization by RT-PCR and sequence analysis. Journal of water and health 6(3), 351-358.

Böttiger M. and Herrström, E. (1992) Isolation of Polioviruses from Sewage and their Characteristics: Experience over Two Decades in Sweden. Scandinavian Journal of Infectious Diseases, 24:2, 151-155.

Castiglioni, S., Zuccato, E., Crisci, E., Chiabrando, C., Fanelli, R. and Bagnati, R. (2006) Identification and measurement of illicit drugs and their metabolites in urban wastewater by liquid chromatography−tandem mass spectrometry. Analytical Chemistry 78(24), 8421-8429.

Gibson, K.E., Schwab, K.J., Spencer, S.K. and Borchardt, M.A. (2012) Measuring and mitigating inhibition during quantitative real time PCR analysis of viral nucleic acid extracts from large-volume environmental water samples. Water Research 46(13), 4281-4291.

Harvala, H., McIntyre, C., McLeish, N., Kondracka, J., Palmer, J., Molyneaux, P., Gunson, R., Bennett, S., Templeton, K. and Simmonds, P. (2012) High detection frequency and viral loads of human rhinovirus species A to C in fecal samples; diagnostic and clinical implications. Journal of medical virology 84(3), 536-542.

Hjelmsø, M.H., Hellmér, M., Fernandez-Cassi, X., Timoneda, N., Lukjancenko, O., Seidel, M., Elsässer, D., Aarestrup, F.M., Löfström, C., Bofill-Mas, S., Abril, J.F., Girones, R. and Schultz, A.C. (2017) Evaluation of Methods for the Concentration and Extraction of Viruses from Sewage in the Context of Metagenomic Sequencing. PloS one 12(1), e0170199-e0170199.

Hokajärvi, A.-M., Rytkönen, A., Tiwari, A., Kauppinen, A., Oikarinen, S., Lehto, .-M., Kankaanpää, A., Gunnar, T., Al-Hello, H., Blomqvist, S., Miettinen, I.T., Savolainen-Kopra, C., Pitkänen. T. (2021) The detection and stability of the SARS-CoV-2 RNA biomarkers in wastewater influent in Helsinki, Finland. Science of the Total Environment 770, 145274

Jevšnik, M., Steyer, A., Zrim, T., Pokorn, M., Mrvič, T., Grosek, Š., Strle, F., Lusa, L. and Petrovec, M. (2013) Detection of human coronaviruses in simultaneously collected stool samples and nasopharyngeal swabs from hospitalized children with acute gastroenteritis. Virology journal 10(1), 46.

Jue, E., Witters, D., Ismagilov (2020) Two-phase wash to solve the ubiquitous contaminant-carryover problem in commercial nucleic-acid extraction kits. Scientific Reports 10, 1940

La Rosa, G., Iaconelli, M., Mancini, P., Ferraro, G.B., Veneri, C., Bonadonna, L. and Lucentini, L. Suffredini E. (2020) First detection of SARS-CoV-2 in untreated wastewaters in Italy. Science of the Total Environment 736: 139652.

Medema, G., Heijnen, L., Elsinga, G., Italiaander, R. and Brouwer, A. (2020) Presence of SARS-Coronavirus-2 RNA in Sewage and Correlation with Reported COVID-19 Prevalence in the Early Stage of the Epidemic in The Netherlands. Environmental Science & Technology Letters 7, 7, 511–516.

Michael-Kordatou, I., Karaolia, P. and Fatta-Kassinos, D. (2020) Sewage analysis as a tool for the COVID-19 pandemic response and management: the urgent need for optimised protocols for SARS-CoV-2 detection and quantification. Journal of Environmental Chemical Engineering 8(5), 104306.

Monpoeho, S., Maul, A., Mignotte-Cadiergues, B., Schwartzbrod, L., Billaudel, S. and Ferré, V. (2001) Best Viral Elution Method Available for Quantification of Enteroviruses in Sludge by Both Cell Culture and Reverse Transcription-PCR. Applied and environmental microbiology 67(6), 2484.

O'Ryan, M. (2007) Rotarix™ (RIX4414): an oral human rotavirus vaccine. Expert Review of Vaccines 6(1), 11-19.

Östman, M., Fick, J., Näsström, E. and Lindberg, R.H. (2014) A snapshot of illicit drug use in Sweden acquired through sewage water analysis. Science of The Total Environment 472, 862-871.

Pang, X.L., Lee, B., Boroumand, N., Leblanc, B., Preiksaitis, J.K. and Yu Ip, C.C. (2004) Increased detection of rotavirus using a real time reverse transcription-polymerase chain reaction (RT-PCR) assay in stool specimens from children with diarrhea. Journal of medical virology 72(3), 496-501.

Risku, M., Lappalainen, S., Räsänen, S. and Vesikari, T. (2010) Detection of human coronaviruses in children with acute gastroenteritis. Journal of Clinical Virology 48(1), 27-30.

Savolainen-Kopra, C., Simonen-Tikka, M.L., Klemola, P., Blomqvist, S., Suomenrinne, S., Näntö-Salonen, K., Simell, O. and Roivainen, M. (2013) Human rhinoviruses in INDIS-study material—evidence for recovery of viable rhinovirus from fecal specimens. Journal of medical virology 85(8), 1466-1472.

Schrader, C., Schielke, A., Ellerbroek, L., Johne, R. (2012) PCR inhibitors – occurrence, properties and removal. Journal of Applied microbiology 113(5), 1014-1026 https://doi.org/10.1111/j.1365-2672.2012.05384.x

Sharara N, Endo N, Duvallet C, Ghaeli N, Matus M, et al. (2021) Wastewater network infrastructure in public health: Applications and learnings from the COVID-19 pandemic. PLOS Global Public Health 1(12): e0000061.

Shieh, Y., Baric, R.S. and Sobsey, M.D. (1997) Detection of low levels of enteric viruses in metropolitan and airplane sewage. Applied and environmental microbiology 63(11), 4401-4407.

Smyth, D.S., Trujillo, M., Gregory, D.A. et al. (2022) Tracking cryptic SARS-CoV-2 lineages detected in NYC wastewater. Nature Communications 13, 635 (2022). https://doi.org/10.1038/s41467-022-28246-3

Strubbia, S., Phan, M.V., Schaeffer, J., Koopmans, M., Cotten, M. and Le Guyader, F.S. (2019) Characterization of norovirus and other human enteric viruses in sewage and stool samples through next-generation sequencing. Food and environmental virology 11(4), 400-409.

Thomas, K.V., Bijlsma, L., Castiglioni, S., Covaci, A., Emke, E., Grabic, R., Hernández, F., Karolak, S., Kasprzyk-Hordern, B. and Lindberg, R.H. (2012) Comparing illicit drug use in 19 European cities through sewage analysis. Science of the Total Environment 432, 432-439.

Tsai, Y.-L., Tran, B., Sangermano, L.R. and Palmer, C.J. (1994) Detection of poliovirus, hepatitis A virus, and rotavirus from sewage and ocean water by triplex reverse transcriptase PCR. Applied and environmental microbiology 60(7), 2400-2407.

Vabret, A., Dina, J., Gouarin, S., Petitjean, J., Corbet, S. and Freymuth, F. (2006) Detection of the new human coronavirus HKU1: a report of 6 cases. Clinical infectious diseases 42(5), 634-639.

Vabret, A., Mourez, T., Dina, J., Van Der Hoek, L., Gouarin, S., Petitjean, J., Brouard, J. and Freymuth, F. (2005) Human coronavirus NL63, France. Emerging infectious diseases 11(8), 1225.

Wu, F., Zhang, J., Xiao, A., Gu, X., Lee, W.L., Armas, F., Kauffman, K., Hanage, W., Matus, M. and Ghaeli, N. (2020) SARS-CoV-2 titers in wastewater are higher than expected from clinically confirmed cases. mSystems 5(4). https://doi.org/10.1128/mSystems.00614-20

Wurtzer, S., Marechal, V., Mouchel, J.M., Maday, Y., Teyssou, R., Richard, E., Almayrac, J.L., Moulin L. (2020) Evaluation of lockdown effect on SARS-CoV-2 dynamics through viral genome quantification in waste water, Greater Paris, France, 5 March to 23 April 2020. Eurosurveillance 25(50): 2000776. 10.2807/1560-7917.ES.2020.25.50.2000776

Wurtzer, S., Waldman, P., Ferrier-Rembert, A., Frenois-Veyrat, G., Mouchel, J.M., Boni, M., Maday, Y., OBEPINE consortium, Marechal, V., Moulin, L. (2021) Several forms of SARS-CoV-2 RNA can be detected in wastewaters: Implication for wastewater-based epidemiology and risk assessment. Water Research, 198, 117183. https://doi.org/10.1016/j.watres.2021.117183

Zhang, X., Li, M., Zhang, B., Chen, T., Lv, D., Xia, P., Sun, Z., Shentu, X., Chen, H., Li, L., Qian, W. (2020) The N gene of SARS-CoV-2 was the main positive component in repositive samples from a cohort of COVID-19 patients in Wuhan, China. Clinica Chimica Acta, 511, 291-297. https://doi.org/10.1016/j.cca.2020.10.019.

Zhou, Y., Pei, F., Ji, M., Wang, L., Zhao, H., Li, H., Yang, W., Wang, Q., Zhao, Q., & Wang, Y. (2020). Sensitivity evaluation of 2019 novel coronavirus (SARS-CoV-2) RT-PCR detection kits

451 and strategy to reduce false negative. *PloS one*, *15*(11), e0241469.
452 https://doi.org/10.1371/journal.pone.0241469

MAIN

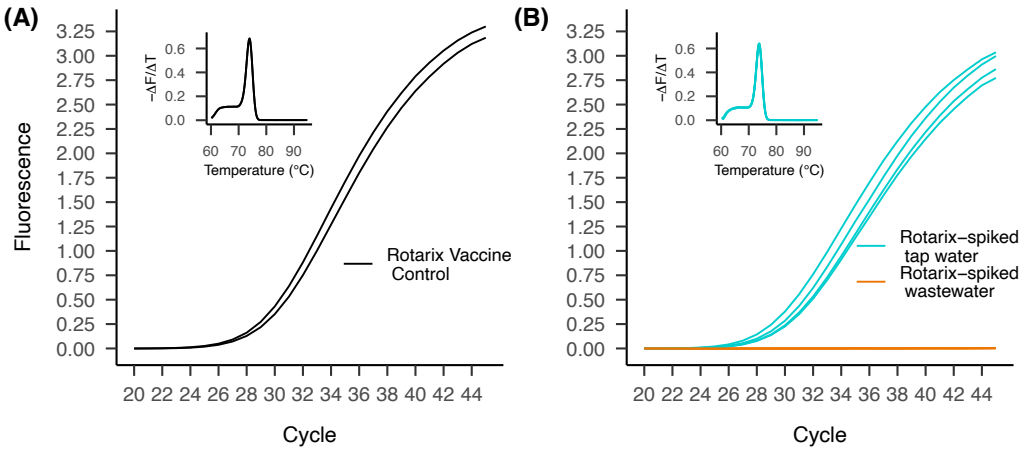


Figure 1. Rotarix vaccine can be detected in tap water but not in wastewater.
A. Amplification of the NSP3 gene from rotavirus RNA extracted from 15 µL of Rotarix vaccine (~10^4 $CCID_{50}$). **B.** Amplification of the NSP3 gene from rotavirus RNA extracted from viral pellets purified from 200ml of tap water (aqua blue) or 200 mL of wastewater (orange) spiked with 15 µL Rotarix vaccine. RNA extraction was performed using Vazyme silica columns according to manufacturer's instructions (with no additional ethanol washes) and eluted in 50 µL. 4 µL of RNA template (equivalent to ~800 $CCID_{50}$) was used in each PCR reaction. Insets show melt curves. 2 samples of tap water and 2 samples of wastewater each with two technical replicates are shown. Representative of at least 3 independent experiments.

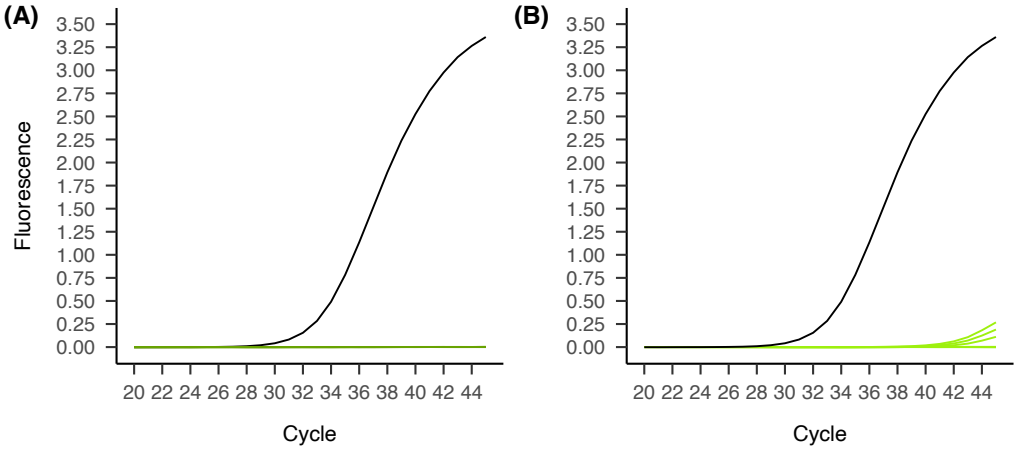


Figure 2. RNA purified from sewage contains SYBR Green qPCR inhibitors. Amplification of rotavirus NSP3 gene from RNA purified directly from Rotarix vaccine mixed with RNA extracted from viral pellets purified from wastewater. 1 µL of Rotarix RNA purified directly from 15 µL of Rotarix (~200 $CCID_{50}$) was added to 3 µL water (black) or **A**. 3µl wastewater RNA (dark green) or **B**. 1 µl wastewater RNA + 2 µL water (pale green) and analysed by qPCR. 3 wastewater samples, each assayed in duplicate (6 samples in total) are shown in the dark green and pale green lines. Representative of 5 independent experiments.

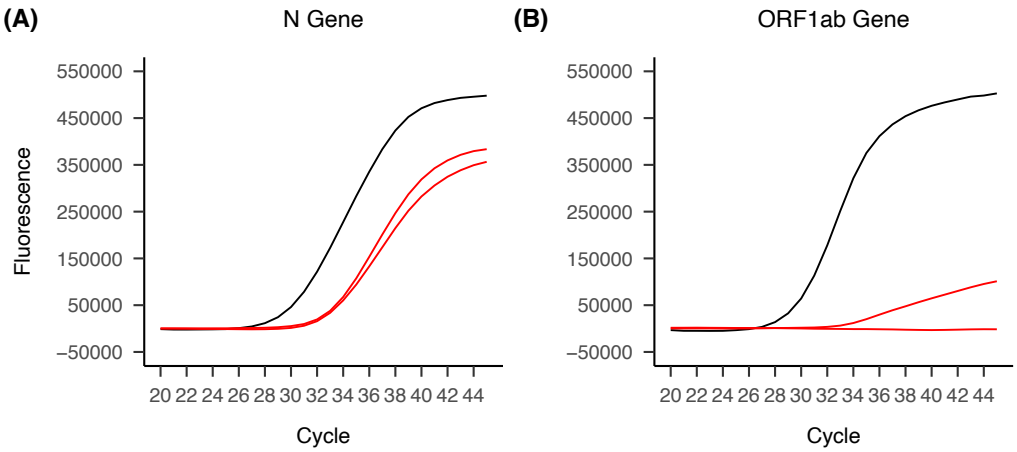


Figure 3. Inhibition of Covid TaqMan qPCR reactions is also apparent, but less severe.
RNA was extracted from viral pellets purified from 200 mL of wastewater. 3 µL of water (black) or 3 µL of wastewater RNA (red) was added to 1 µL containing 10^4 copies Twist SARS-CoV-2 RNA. **A.** Amplification of the SARS-CoV-2 N gene. **B.** Amplification of the SARS-CoV-2 ORF1ab gene from the multiplex Vazyme qPCR assay. 2 biological replicates were each assayed in duplicate, but a single technical replicate is shown for clarity. Representative of 3 independent experiments.

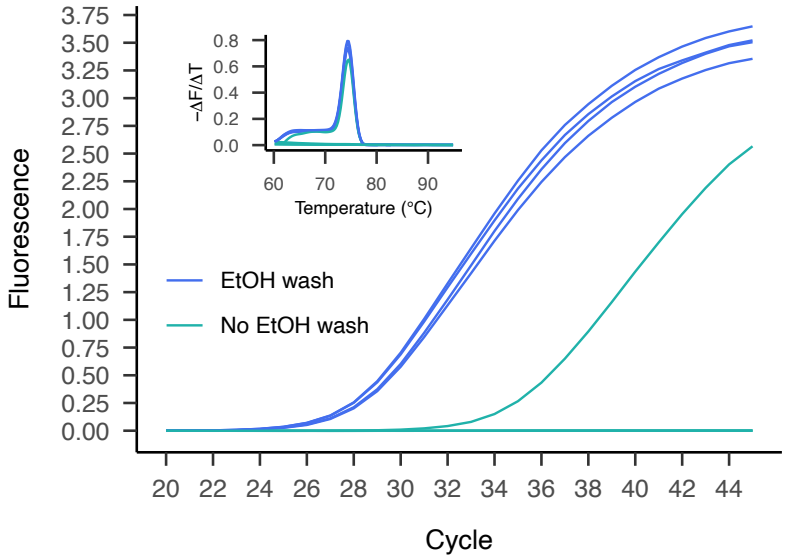


Figure 4. Washing columns with 80% ethanol removes qPCR inhibitors in sewage and allows amplification of the rotavirus NSP3 gene.
Amplification of rotavirus NSP3 gene on RNA isolated from 200 mL wastewater samples spiked with 15 µL of Rotarix and isolated using RNA column-extraction with (dark blue) or without (teal blue) three additional 80% ethanol washes. 1 µL of RNA was used in the RT-qPCR reaction. Inset shows melt curves. Without ethanol washes, amplification was completely inhibited in all but one technical replicate (teal blue). The figure shows 2 biological replicates, each with 2 technical replicates, and is representative of 7 independent experiments.

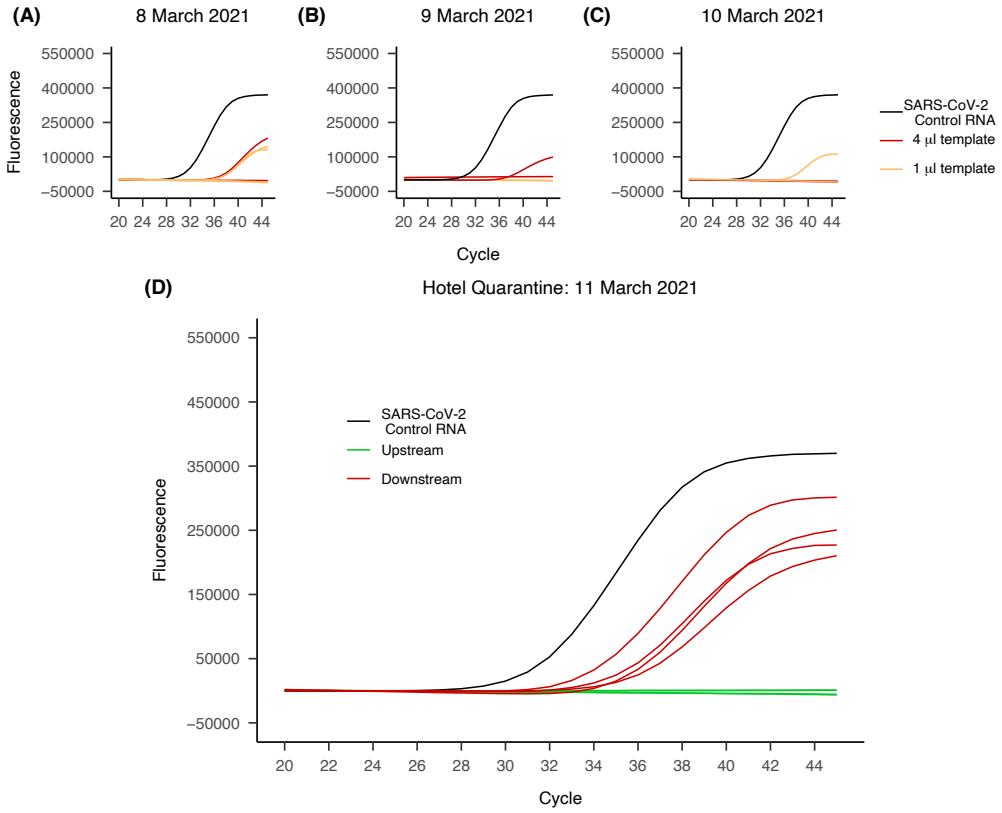


Figure 5. SARS-CoV-2 N gene was detected in sewage prior to protocol optimisation.
A-C. Detection of SARS-CoV-2 N gene is wastewater samples from the Molonglo sewage treatment plant (which services a population of ~400,000) on **A.** 8 March 2021 **B.** 9 March 2021 **C.** 10 March 2021. Different volumes of template RNA used are indicated red (4 µL) or mustard (1 µL). The SARS-CoV-2 N gene was detected in 3 out of 6 **(A)**, 1 out of 4 **(B)** and 1 out of 4 **(C)** technical replicates. **D.** Sewage collected upstream and downstream of the hotel quarantine facility on 11 March 2021 was screened as validation of the positive result. SARS-CoV-2 (N and ORF1ab genes) was detected only in sewage collected downstream of the hotel (red); upstream samples (green) were negative for both genes. For clarity, only the N gene is shown. Black curves indicate N gene amplified from 4 x 10^4 copies Twist SARS-CoV-2 RNA control.

E. A cost-effective detection method for SARS-CoV-2 and other RNA viruses in wastewater

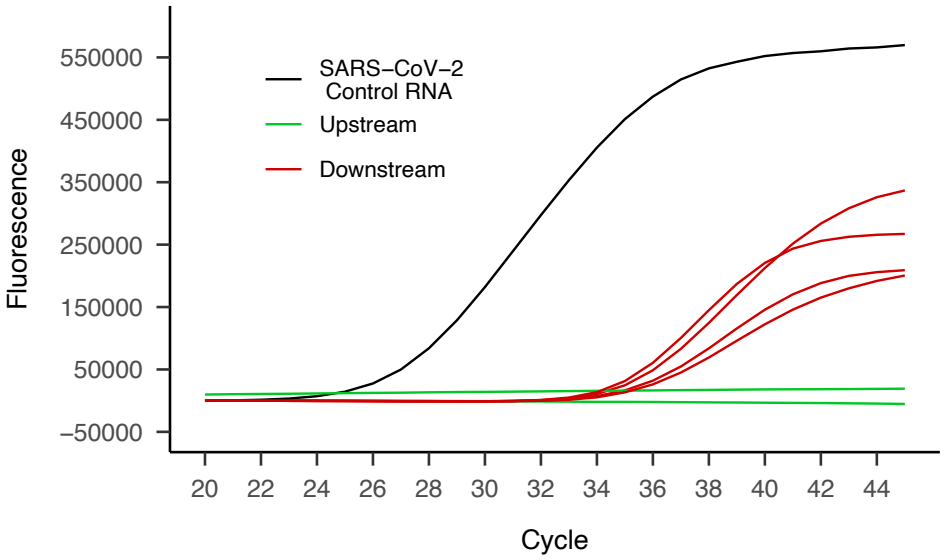
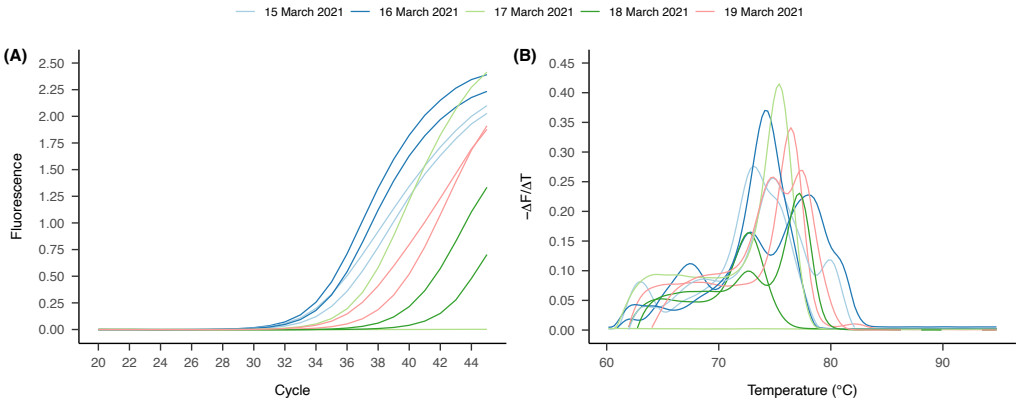
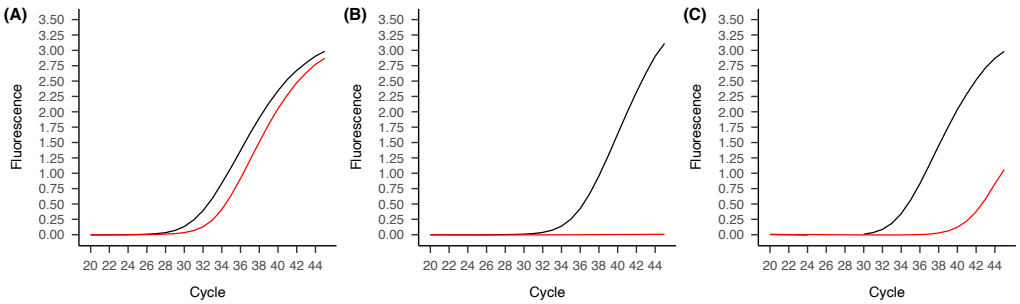


Figure 6. SARS-CoV-2 N gene can be detected in wastewater from previously positive hotel quarantine samples stored at 4°C for 4 months.
RNA was extracted using the optimised method in which Vazyme RNA isolation columns were washed three times with 80% ethanol before elution and 1 µL sample RNA per RT-qPCR reaction was used as template. Amplification of the SARS-CoV-2 N gene was detected in samples collected on 11 March downstream (red), but not upstream (green), of the Canberra hotel quarantine facility where five COVID-19 cases were isolated. The figure shows 2 biological replicates, each with 2 technical replicates. Black curve indicates 10^4 copies Twist SARS-CoV-2 RNA control.

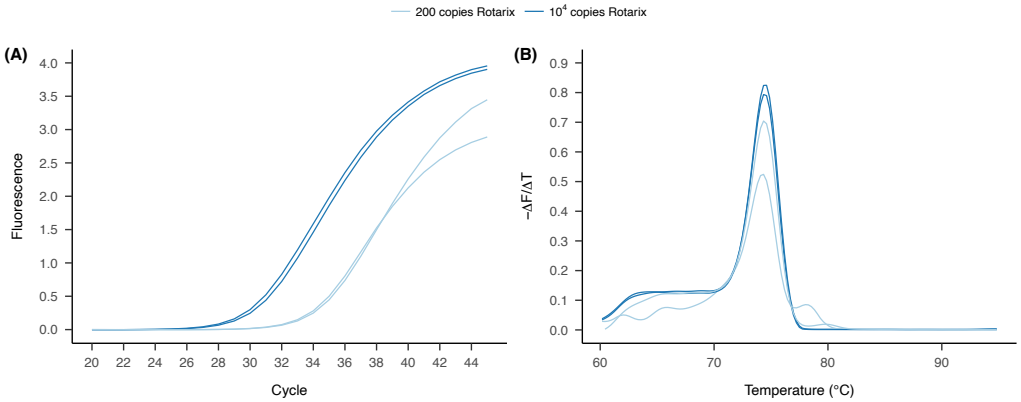
SUPPLEMENTARY



Supp. Fig. 1. Sample dilution enables modest amplification of some Rotarix-spiked wastewater samples. **A.** Rotavirus NSP3 gene can be detected in a limited number of samples spiked with 15 µL of Rotarix vaccine (~10^4 $CCID_{50}$) but sensitivity is reduced, as indicated by the variation in Ct scores between technical replicates (lines of the same colour) and high Ct scores >36. **B.** Dilution of template without washing columns with 80% ethanol gives low quality melt curves with multiple peaks. Representative samples from 15-19 March 2021, in which template dilution reversed RT-qPCR inhibition to some extent, are shown. Technical replicates are displayed in the same colour; each colour represents a different daily sample. Representative of at least 10 independent experiments.



Supp. Fig. 2. Ethanol washes improve viral detection sensitivity regardless of RNA extraction kit brand. Washing columns with 80% ethanol improves sensitivity of rotavirus NSP3 gene detection when 1 µL, rather than 4 µL, template RNA is used (i.e. the template is diluted). RNA was extracted either according to the manufacturer's instructions (red) or with additional 80% ethanol washes applied (black). The effect was sustained across samples collected on different dates: **A.** 29 November 2020**; B.** 6 December 2020**; C.** 13 December 2020. Representative of at least 3 independent experiments.



Supp. Fig. 3. Wastewater containing ~1 $CCID_{50}$ copy of virus/mL is reliably detected.
A. The rotavirus NSP3 gene was detected in wastewater spiked with ~200 $CCID_{50}$ Rotarix (pale blue). Wastewater spiked with ~10^4 $CCID_{50}$ Rotarix (dark blue) is shown for reference. The 50-fold decrease in Rotarix concentration yielded Ct scores the expected ~6 cycles lower. **B.** Melt curves for wastewater spiked with ~200 $CCID_{50}$ (pale blue) or ~10^4 $CCID_{50}$ Rotarix (dark blue) show single peaks at the ~73.5°C expected for the rotavirus NSP3 gene. Representative of at least 3 independent experiments.

References

Adashek, M., Chan, A., & Medina, A. (2018). Gastrointestinal perforation after rituximab therapy in mantle cell lymphoma: A case report [Journal Article]. *Case Rep Oncol*, *11*(3), 784–790. https://doi.org/10.1159/000494828

Agata, Y., Kawasaki, A., Nishimura, H., Ishida, Y., Tsubata, T., Yagita, H., & Honjo, T. (1996). Expression of the PD-1 antigen on the surface of stimulated mouse t and b lymphocytes [Journal Article]. *Int Immunol*, *8*(5), 765–772.

Agdashian, D., ElGindi, M., Xie, C., Sandhu, M., Pratt, D., Kleiner, D. E., Figg, W. D., Rytlewski, J. A., Sanders, C., Yusko, E. C., Wood, B., Venzon, D., Brar, G., Duffy, A. G., Greten, T. F., & Korangy, F. (2019). The effect of anti-CTLA4 treatment on peripheral and intra-tumoral t cells in patients with hepatocellular carcinoma [Journal Article]. *Cancer Immunol Immunother*, *68*(4), 599–608. https://doi.org/10.1007/s00262-019-02299-8

Allison, A. G., & Gregoriadis, G. (1974). Liposomes as immunological adjuvants [Journal Article]. *Nature*, *252*(5480), 252.

Almonte, A. A., Cavic, G., Neeman, T., Enders, A., & Fahrer, A. M. (2022). Gut microbiome-depleting antibiotic regimens are not tolerated by all mouse strains: Learn from (our) bitter experience [Journal Article]. *J Immunother Cancer*, *10*(11). https://doi.org/10.1136/jitc-2022-005575

Almonte, A. A., Rangarajan, H., Yip, D., & Fahrer, A. M. (2021). How does the gut microbiome influence immune checkpoint blockade therapy? [Journal Article]. *Immunol Cell Biol*, *99*(4), 361–372.

Amar-Costesec, A., Godelaine, D., Van den Eynde, B., & Beaufay, H. (1994). Identification and characterization of the tumor-specific P1A gene product [Journal Article]. *Biol Cell*, *81*(3), 195–203. https://doi.org/10.1016/0248-4900(94)90001-9

Andrade, F. F., Silva, D., Rodrigues, A., & Pina-Vaz, C. (2020). Colistin update on its mechanism of action and resistance, present and future challenges [Journal Article]. *Microorganisms*, *8*(11). https://doi.org/10.3390/microorganisms8111716

Andrew, E. (2020). *Analysis of tumour infiltrating leukocytes in murine models of cancer* [Thesis].

Andrews, M. C., Duong, C. P. M., Gopalakrishnan, V., Iebba, V., Chen, W. S., Derosa, L.,

Khan, M. A. W., Cogdill, A. P., White, M. G., Wong, M. C., Ferrere, G., Fluckiger, A., Roberti, M. P., Opolon, P., Alou, M. T., Yonekura, S., Roh, W., Spencer, C. N., Curbelo, I. F., … Wargo, J. A. (2021). Gut microbiota signatures are associated with toxicity to combined CTLA-4 and PD-1 blockade [Journal Article]. *Nat Med*, *27*(8), 1432–1441. https://doi.org/10.1038/s41591-021-01406-6

Andzinski, L., Kasnitz, N., Stahnke, S., Wu, C. F., Gereke, M., Kockritz-Blickwede, M. von, Schilling, B., Brandau, S., Weiss, S., & Jablonska, J. (2016). Type i IFNs induce anti-tumor polarization of tumor associated neutrophils in mice and human [Journal Article]. *Int J Cancer*, *138*(8), 1982–1993. https://doi.org/10.1002/ijc.29945

Animal research advisory committee (ARAC) guidelines | OACU. (2023). [Pamphlet]. National Institutes of Health. https://oacu.oir.nih.gov/animal-research-advisory-committee-arac-guidelines

Arai, T., Kokubo, T., Tang, R., Abo, H., Terui, A., Hirakawa, J., Akita, H., Kawashima, H., Hisaka, A., & Hatakeyama, H. (2022). Tumor-associated neutrophils and macrophages exacerbate antidrug IgG-mediated anaphylactic reaction against an immune checkpoint inhibitor [Journal Article]. *J Immunother Cancer*, *10*(12). https://doi.org/10.1136/jitc-2022-005657

Arce Vargas, F., Furness, A. J. S., Litchfield, K., Joshi, K., Rosenthal, R., Ghorani, E., Solomon, I., Lesko, M. H., Ruef, N., Roddie, C., Henry, J. Y., Spain, L., Ben Aissa, A., Georgiou, A., Wong, Y. N. S., Smith, M., Strauss, D., Hayes, A., Nicol, D., … Quezada, S. A. (2018). Fc effector function contributes to the activity of human anti-CTLA-4 antibodies [Journal Article]. *Cancer Cell*, *33*(4), 649–663 e4. https://doi.org/10.1016/j.ccell.2018.02.010

Auguie, B. (2017). *gridExtra: Miscellaneous functions for "grid" graphics*. https://CRAN.R-project.org/package=gridExtra

Aust, F., & Barth, M. (2022). *Papaja: Prepare american psychological association journal articles with r markdown*. https://github.com/crsh/papaja

AUSTRALIA IS CLOSED: PM. (2020). In *7NEWS*. https://7news.com.au/lifestyle/health-wellbeing/australia-closes-borders-to-stop-coronavirus-c-752927.

Azuma, M., Ito, D., Yagita, H., Okumura, K., Phillips, J. H., Lanier, L. L., & Somoza, C. (1993). B70 antigen is a second ligand for CTLA-4 and CD28 [Journal Article]. *Nature*, *366*(6450), 76–79.

Barrett, T., Wilhite, S. E., Ledoux, P., Evangelista, C., Kim, I. F., Tomashevsky, M., Marshall, K. A., Phillippy, K. H., Sherman, P. M., Holko, M., Yefanov, A., Lee, H., Zhang, N., Robertson, C. L., Serova, N., Davis, S., & Soboleva, A. (2013). NCBI GEO: Archive for functional genomics data sets–update [Journal Article]. *Nucleic*

Acids Res, *41*(Database issue), D991–5.

Barth, Jr., R. J., Bock, S. N., Mule, J. J., & Rosenberg, S. A. (1990). Unique murine tumor-associated antigens identified by tumor infiltrating lymphocytes [Journal Article]. *J Immunol*, *144*(4), 1531–1537.

Basu, S., Pathak, S. K., Banerjee, A., Pathak, S., Bhattacharyya, A., Yang, Z., Talarico, S., Kundu, M., & Basu, J. (2007). Execution of macrophage apoptosis by PE_PGRS33 of mycobacterium tuberculosis is mediated by toll-like receptor 2-dependent release of tumor necrosis factor-alpha [Journal Article]. *J Biol Chem*, *282*(2), 1039–1050.

Bates, D., Maechler, M., Bolker, B., & Walker, S. (2022). *lme4: Linear mixed-effects models using eigen and S4*. https://github.com/lme4/lme4/

Belnap, L. P., Cleveland, P. H., Colmerauer, M. E., Barone, R. M., & Pilch, Y. H. (1979). Immunogenicity of chemically induced murine colon cancers [Journal Article]. *Cancer Res*, *39*(4), 1174–1179.

Ben-David, U., Siranosian, B., Ha, G., Tang, H., Oren, Y., Hinohara, K., Strathdee, C. A., Dempster, J., Lyons, N. J., Burns, R., Nag, A., Kugener, G., Cimini, B., Tsvetkov, P., Maruvka, Y. E., O'Rourke, R., Garrity, A., Tubelli, A. A., Bandopadhayay, P., … Golub, T. R. (2018). Genetic and transcriptional evolution alters cancer cell line drug response [Journal Article]. *Nature*, *560*(7718), 325–330.

Bianchini, M., Duchene, J., Santovito, D., Schloss, M. J., Evrard, M., Winkels, H., Aslani, M., Mohanta, S. K., Horckmans, M., Blanchet, X., Lacy, M., Hundelshausen, P. von, Atzler, D., Habenicht, A., Gerdes, N., Pelisek, J., Ng, L. G., Steffens, S., Weber, C., & Megens, R. T. A. (2019). PD-L1 expression on nonclassical monocytes reveals their origin and immunoregulatory function [Journal Article]. *Sci Immunol*, *4*(36). https://doi.org/ARTN eaar3054 10.1126/sciimmunol.aar3054

Billiau, A., & Matthys, P. (2001). Modes of action of freund's adjuvants in experimental models of autoimmune diseases [Journal Article]. *J Leukoc Biol*, *70*(6), 849–860.

Blischak, J. D., Tailleux, L., Mitrano, A., Barreiro, L. B., & Gilad, Y. (2015). Mycobacterial infection induces a specific human innate immune response [Journal Article]. *Sci Rep*, *5*, 16882.

Blizard, D. A. (2007). Sweet and bitter taste of ethanol in C57BL/6J and DBA2/j mouse strains [Journal Article]. *Behav Genet*, *37*(1), 146–159. https://doi.org/10.1007/s10519-006-9121-4

Borriello, F., Sethna, M. P., Boyd, S. D., Schweitzer, A. N., Tivol, E. A., Jacoby, D., Strom, T. B., Simpson, E. M., Freeman, G. J., & Sharpe, A. H. (1997). B7-1 and B7-2 have overlapping, critical roles in immunoglobulin class switching and germinal center formation [Journal Article]. *Immunity*, *6*(3), 303–313. https://doi.org/Doi 10.1016/S1074-7613(00)80333-7

Boughter, Jr., J. D., & Bachmanov, A. A. (2007). Behavioral genetics and taste [Journal Article]. *BMC Neurosci*, *8 Suppl 3*, S3. https://doi.org/10.1186/1471-2202-8-S3-S3

Boussiotis, V. A., Freeman, G. J., Gribben, J. G., Daley, J., Gray, G., & Nadler, L. M. (1993). Activated human b lymphocytes express three CTLA-4 counterreceptors that costimulate t-cell activation [Journal Article]. *Proc Natl Acad Sci USA*, *90*(23), 11059–11063.

Brunet, J. F., Denizot, F., Luciani, M. F., Roux-Dosseto, M., Suzan, M., Mattei, M. G., & Golstein, P. (1987). A new member of the immunoglobulin superfamily–CTLA-4 [Journal Article]. *Nature*, *328*(6127), 267–270.

Bulut, Y., Michelsen, K. S., Hayrapetian, L., Naiki, Y., Spallek, R., Singh, M., & Arditi, M. (2005). Mycobacterium tuberculosis heat shock proteins use diverse toll-like receptor pathways to activate pro-inflammatory signals [Journal Article]. *J Biol Chem*, *280*(22), 20961–20967.

Cabrita, R., Lauss, M., Sanna, A., Donia, M., Skaarup Larsen, M., Mitra, S., Johansson, I., Phung, B., Harbst, K., Vallon-Christersson, J., Schoiack, A. van, Lovgren, K., Warren, S., Jirstrom, K., Olsson, H., Pietras, K., Ingvar, C., Isaksson, K., Schadendorf, D., … Jonsson, G. (2020). Tertiary lymphoid structures improve immunotherapy and survival in melanoma [Journal Article]. *Nature*, *577*(7791), 561–565.

Candon, S., Perez-Arroyo, A., Marquet, C., Valette, F., Foray, A. P., Pelletier, B., Milani, C., Ventura, M., Bach, J. F., & Chatenoud, L. (2015). Antibiotics in early life alter the gut microbiome and increase disease incidence in a spontaneous mouse model of autoimmune insulin-dependent diabetes [Journal Article]. *PLoS One*, *10*(5), e0125448.

Cao, J., Wu, X., Qin, X., & Li, Z. (2021). Uncovering the effect of passage number on HT29 cell line based on the cell metabolomic approach [Journal Article]. *J Proteome Res*, *20*(3), 1582–1590.

Carmona, J., Cruz, A., Moreira-Teixeira, L., Sousa, C., Sousa, J., Osorio, N. S., Saraiva, A. L., Svenson, S., Kallenius, G., Pedrosa, J., Rodrigues, F., Castro, A. G., & Saraiva, M. (2013). Mycobacterium tuberculosis strains are differentially recognized by TLRs with an impact on the immune response [Journal Article]. *PLoS One*, *8*(6), e67277.

Carroll, C. (2016). *The treatment of solid tumours with complete freund's adjuvant* [Thesis].

Carroll, C. S. E., Altin, J. G., Neeman, T., & Fahrer, A. M. (2015). Repeated fine-needle aspiration of solid tumours in mice allows the identification of multiple infiltrating immune cell types [Journal Article]. *J Immunol Methods*, *425*, 102–107.

Carroll, C. S. E., Andrew, E. R., Malik, L., Elliott, K. F., Brennan, M., Meyer, J., Hintze, A., Almonte, A. A., Lappin, C., MacPherson, P., Schulte, K. M., Dahlstrom, J. E.,

Tamhane, R., Neeman, T., Herbert, E. W., Orange, M., Yip, D., Allavena, R., & Fahrer, A. M. (2021). Simple and effective bacterial-based intratumoral cancer immunotherapy [Journal Article]. *J Immunother Cancer*, *9*(9).

Cehovin, A., Coates, A. R., Hu, Y., Riffo-Vasquez, Y., Tormay, P., Botanch, C., Altare, F., & Henderson, B. (2010). Comparison of the moonlighting actions of the two highly homologous chaperonin 60 proteins of mycobacterium tuberculosis [Journal Article]. *Infect Immun*, *78*(7), 3196–3206.

Chatterjee, S., Dwivedi, V. P., Singh, Y., Siddiqui, I., Sharma, P., Van Kaer, L., Chattopadhyay, D., & Das, G. (2011). Early secreted antigen ESAT-6 of mycobacterium tuberculosis promotes protective t helper 17 cell responses in a toll-like receptor-2-dependent manner [Journal Article]. *PLoS Pathog*, *7*(11), e1002378.

Chebib, J., Jackson, B. C., Lopez-Cortegano, E., Tautz, D., & Keightley, P. D. (2021). Inbred lab mice are not isogenic: Genetic variation within inbred strains used to infer the mutation rate per nucleotide site [Journal Article]. *Heredity (Edinb)*, *126*(1), 107–116.

Chen, P. L., Roh, W., Reuben, A., Cooper, Z. A., Spencer, C. N., Prieto, P. A., Miller, J. P., Bassett, R. L., Gopalakrishnan, V., Wani, K., De Macedo, M. P., Austin-Breneman, J. L., Jiang, H., Chang, Q., Reddy, S. M., Chen, W. S., Tetzlaff, M. T., Broaddus, R. J., Davies, M. A., … Wargo, J. A. (2016). Analysis of immune signatures in longitudinal tumor samples yields insight into biomarkers of response and mechanisms of resistance to immune checkpoint blockade [Journal Article]. *Cancer Discov*, *6*(8), 827–837.

Choi, Y., Lichterman, J. N., Coughlin, L. A., Poulides, N., Li, W., Del Valle, P., Palmer, S. N., Gan, S., Kim, J., Zhan, X., Gao, Y., Evers, B. M., Hooper, L. V., Pasare, C., & Koh, A. Y. (2023). Immune checkpoint blockade induces gut microbiota translocation that augments extraintestinal antitumor immunity [Journal Article]. *Sci Immunol*, *8*(81), eabo2003.

Chu, R. S., Targoni, O. S., Krieg, A. M., Lehmann, P. V., & Harding, C. V. (1997). CpG oligodeoxynucleotides act as adjuvants that switch on t helper 1 (Th1) immunity [Journal Article]. *J Exp Med*, *186*(10), 1623–1631.

Coley, W. B. (1909). The treatment of inoperable sarcoma by bacterial toxins (the mixed toxins of the streptococcus erysipelas and the bacillus prodigiosus) [Journal Article]. *Proc R Soc Med*, *3*(Surg Sect), 1–48.

Coley, W. B. (1991). The treatment of malignant tumors by repeated inoculations of erysipelas. With a report of ten original cases. 1893 [Journal Article]. *Clin Orthop Relat Res*, *262*, 3–11.

Colmerauer, M. E., Koziol, J. A., & Pilch, Y. H. (1980). Enhancement of metastasis de-

velopment by BCG immunotherapy [Journal Article]. *J Surg Oncol*, *15*(3), 235–241.

Contarini, G., Giusti, P., & Skaper, S. D. (2018). Active induction of experimental autoimmune encephalomyelitis in C57BL/6 mice [Journal Article]. *Methods Mol Biol*, *1727*, 353–360.

Corbett, T. H., Griswold, Jr., D. P., Roberts, B. J., Peckham, J. C., & Schabel, Jr., F. M. (1975). Tumor induction relationships in development of transplantable cancers of the colon in mice for chemotherapy assays, with a note on carcinogen structure [Journal Article]. *Cancer Res*, *35*(9), 2434–2439.

Curran, M. A., & Allison, J. P. (2009). Tumor vaccines expressing flt3 ligand synergize with ctla-4 blockade to reject preimplanted tumors [Journal Article]. *Cancer Res*, *69*(19), 7747–7755.

Curran, M. A., Montalvo, W., Yagita, H., & Allison, J. P. (2010). PD-1 and CTLA-4 combination blockade expands infiltrating t cells and reduces regulatory t and myeloid cells within B16 melanoma tumors [Journal Article]. *Proc Natl Acad Sci USA*, *107*(9), 4275–4280.

Dahan, R., Sega, E., Engelhardt, J., Selby, M., Korman, A. J., & Ravetch, J. V. (2015). FcγRs modulate the anti-tumor activity of antibodies targeting the PD-1/PD-L1 axis [Journal Article]. *Cancer Cell*, *28*(3), 285–295.

Daillere, R., Vetizou, M., Waldschmitt, N., Yamazaki, T., Isnard, C., Poirier-Colame, V., Duong, C. P. M., Flament, C., Lepage, P., Roberti, M. P., Routy, B., Jacquelot, N., Apetoh, L., Becharef, S., Rusakiewicz, S., Langella, P., Sokol, H., Kroemer, G., Enot, D., … Zitvogel, L. (2016). Enterococcus hirae and barnesiella intestinihominis facilitate cyclophosphamide-induced therapeutic immunomodulatory effects [Journal Article]. *Immunity*, *45*(4), 931–943. https://doi.org/10.1016/j.immuni.2016.09.009

Danahy, D. B., Jensen, I. J., Griffith, T. S., & Badovinac, V. P. (2019). Cutting edge: Polymicrobial sepsis has the capacity to reinvigorate tumor-infiltrating CD8 t cells and prolong host survival [Journal Article]. *J Immunol*, *202*(10), 2843–2848.

Dariavach, P., Mattei, M. G., Golstein, P., & Lefranc, M. P. (1988). Human ig superfamily CTLA-4 gene: Chromosomal localization and identity of protein sequence between murine and human CTLA-4 cytoplasmic domains [Journal Article]. *Eur J Immunol*, *18*(12), 1901–1905.

Davar, D., Dzutsev, A. K., McCulloch, J. A., Rodrigues, R. R., Chauvin, J. M., Morrison, R. M., Deblasio, R. N., Menna, C., Ding, Q., Pagliano, O., Zidi, B., Zhang, S., Badger, J. H., Vetizou, M., Cole, A. M., Fernandes, M. R., Prescott, S., Costa, R. G. F., Balaji, A. K., … Zarour, H. M. (2021). Fecal microbiota transplant overcomes resistance to anti-PD-1 therapy in melanoma patients [Journal Article]. *Sci-*

ence, *371*(6529), 595–602.

Davis, A. A., & Patel, V. G. (2019). The role of PD-L1 expression as a predictive biomarker: An analysis of all US food and drug administration (FDA) approvals of immune checkpoint inhibitors [Journal Article]. *J Immunother Cancer*, *7*(1), 278.

Demaria, S., Kawashima, N., Yang, A. M., Devitt, M. L., Babb, J. S., Allison, J. P., & Formenti, S. C. (2005). Immune-mediated inhibition of metastases after treatment with local radiation and CTLA-4 blockade in a mouse model of breast cancer [Journal Article]. *Clin Cancer Res*, *11*(2 Pt 1), 728–734.

Derosa, L., Hellmann, M. D., Spaziano, M., Halpenny, D., Fidelle, M., Rizvi, H., Long, N., Plodkowski, A. J., Arbour, K. C., Chaft, J. E., Rouche, J. A., Zitvogel, L., Zalcman, G., Albiges, L., Escudier, B., & Routy, B. (2018). Negative association of antibiotics on clinical activity of immune checkpoint inhibitors in patients with advanced renal cell and non-small-cell lung cancer [Journal Article]. *Ann Oncol*, *29*(6), 1437–1444.

Dexter, D. L., Kowalski, H. M., Blazar, B. A., Fligiel, Z., Vogel, R., & Heppner, G. H. (1978). Heterogeneity of tumor cells from a single mouse mammary tumor [Journal Article]. *Cancer Res*, *38*(10), 3174–3181.

Dienes, L. (1928). Further observations concerning the sensitization of tuberculous guinea pigs [Journal Article]. *J Immunol*, *15*(2), 153–174.

Dienes, L., & Schoenheit, E. W. (1929). The reproduction of tuberculin hypersensitiveness in guinea pigs with various protein substances [Journal Article]. *Am Rev Tuberc*, *20*(1), 92–105.

Dong, H., Zhu, G., Tamada, K., & Chen, L. (1999). B7-H1, a third member of the B7 family, co-stimulates t-cell proliferation and interleukin-10 secretion [Journal Article]. *Nat Med*, *5*(12), 1365–1369.

Dranoff, G., Jaffee, E., Lazenby, A., Golumbek, P., Levitsky, H., Brose, K., Jackson, V., Hamada, H., Pardoll, D., & Mulligan, R. C. (1993). Vaccination with irradiated tumor cells engineered to secrete murine granulocyte-macrophage colony-stimulating factor stimulates potent, specific, and long-lasting anti-tumor immunity [Journal Article]. *Proc Natl Acad Sci USA*, *90*(8), 3539–3543.

Draube, A., Klein-Gonzalez, N., Mattheus, S., Brillant, C., Hellmich, M., Engert, A., & Bergwelt-Baildon, M. von. (2011). Dendritic cell based tumor vaccination in prostate and renal cell cancer: A systematic review and meta-analysis [Journal Article]. *PLoS One*, *6*(4), e18801.

Du, X., Tang, F., Liu, M., Su, J., Zhang, Y., Wu, W., Devenport, M., Lazarski, C. A., Zhang, P., Wang, X., Ye, P., Wang, C., Hwang, E., Zhu, T., Xu, T., Zheng, P., & Liu, Y. (2018). A reappraisal of CTLA-4 checkpoint blockade in cancer immunotherapy [Journal Article]. *Cell Res*, *28*(4), 416–432.

Dunn, G. P., Bruce, A. T., Ikeda, H., Old, L. J., & Schreiber, R. D. (2002). Cancer immunoediting: From immunosurveillance to tumor escape [Journal Article]. *Nat Immunol*, *3*(11), 991–998.

Dunn, T. B., & Potter, M. (1957). A transplantable mast-cell neoplasm in the mouse [Journal Article]. *J Natl Cancer Inst*, *18*(4), 587–601.

DuPre, S. A., & Hunter, Jr., K. W. (2007). Murine mammary carcinoma 4T1 induces a leukemoid reaction with splenomegaly: Association with tumor-derived growth factors [Journal Article]. *Exp Mol Pathol*, *82*(1), 12–24.

DuPre, S. A., Redelman, D., & Hunter, Jr., K. W. (2007). The mouse mammary carcinoma 4T1: Characterization of the cellular landscape of primary tumours and metastatic tumour foci [Journal Article]. *Int J Exp Pathol*, *88*(5), 351–360.

DuPre, S. A., Redelman, D., & Hunter, Jr., K. W. (2008). Microenvironment of the murine mammary carcinoma 4T1: Endogenous IFN-gamma affects tumor phenotype, growth, and metastasis [Journal Article]. *Exp Mol Pathol*, *85*(3), 174–188.

Dyck, L., Wilk, M. M., Raverdeau, M., Misiak, A., Boon, L., & Mills, K. H. (2016). Anti-PD-1 inhibits Foxp3(+) treg cell conversion and unleashes intratumoural effector t cells thereby enhancing the efficacy of a cancer vaccine in a mouse model [Journal Article]. *Cancer Immunol Immunother*, *65*(12), 1491–1498.

Einhorn, J. (1985). Nitrogen mustard: The origin of chemotherapy for cancer [Journal Article]. *Int J Radiat Oncol Biol Phys*, *11*(7), 1375–1378.

Elsas, A. van, Hurwitz, A. A., & Allison, J. P. (1999). Combination immunotherapy of B16 melanoma using anti-cytotoxic t lymphocyte-associated antigen 4 (CTLA-4) and granulocyte/macrophage colony-stimulating factor (GM-CSF)-producing vaccines induces rejection of subcutaneous and metastatic tumors accompanied by autoimmune depigmentation [Journal Article]. *J Exp Med*, *190*(3), 355–366. https://doi.org/10.1084/jem.190.3.355

Evrard, M., Kwok, I. W. H., Chong, S. Z., Teng, K. W. W., Becht, E., Chen, J., Sieow, J. L., Penny, H. L., Ching, G. C., Devi, S., Adrover, J. M., Li, J. L. Y., Liong, K. H., Tan, L., Poon, Z., Foo, S., Chua, J. W., Su, I. H., Balabanian, K., … Ng, L. G. (2018). Developmental analysis of bone marrow neutrophils reveals populations specialized in expansion, trafficking, and effector functions [Journal Article]. *Immunity*, *48*(2), 364–379 e8.

Fahrer, A. M. (2012). A proposal for a simple and inexpensive therapeutic cancer vaccine [Journal Article]. *Immunol Cell Biol*, *90*(3), 310–313.

Farias, A., Soto, A., Puttur, F., Goldin, C. J., Sosa, S., Gil, C., Goldbaum, F. A., & Berguer, P. M. (2021). A TLR4 agonist improves immune checkpoint blockade treatment by increasing the ratio of effector to regulatory cells within the tumor mi-

croenvironment [Journal Article]. *Sci Rep*, *11*(1), 15406. https://doi.org/10.1038/s41598-021-94837-7

Fehleisen, F. (1882). Ueber die züchtung der erysipelkokken auf künstlichem nährboden und ihre übertragbarkeit auf den menschen [Journal Article]. *Dtsch Med Wochenschr*, *8*, 552–554.

Fenwick, C., Loredo-Varela, J. L., Joo, V., Pellaton, C., Farina, A., Rajah, N., Esteves-Leuenberger, L., Decaillon, T., Suffiotti, M., Noto, A., Ohmiti, K., Gottardo, R., Weissenhorn, W., & Pantaleo, G. (2019). Tumor suppression of novel anti-PD-1 antibodies mediated through CD28 costimulatory pathway [Journal Article]. *J Exp Med*, *216*(7), 1525–1541.

Fluckiger, A., Daillere, R., Sassi, M., Sixt, B. S., Liu, P., Loos, F., Richard, C., Rabu, C., Alou, M. T., Goubet, A. G., Lemaitre, F., Ferrere, G., Derosa, L., Duong, C. P. M., Messaoudene, M., Gagne, A., Joubert, P., De Sordi, L., Debarbieux, L., … Zitvogel, L. (2020). Cross-reactivity between tumor MHC class i-restricted antigens and an enterococcal bacteriophage [Journal Article]. *Science*, *369*(6506), 936–942. https://doi.org/10.1126/science.aax0701

Fox, J., & Weisberg, S. (2019). *An R companion to applied regression* (Third). Sage. https://socialsciences.mcmaster.ca/jfox/Books/Companion/

Freeman, G. J., Borriello, F., Hodes, R. J., Reiser, H., Hathcock, K. S., Laszlo, G., McKnight, A. J., Kim, J., Du, L. N., Lombard, D. B., Gray, G. S., Nadler, L. M., & Sharpe, A. H. (1993). Uncovering of functional alternative ctla-4 counter-receptor in B7-deficient mice [Journal Article]. *Science*, *262*(5135), 907–909.

Freeman, G. J., Long, A. J., Iwai, Y., Bourque, K., Chernova, T., Nishimura, H., Fitz, L. J., Malenkovich, N., Okazaki, T., Byrne, M. C., Horton, H. F., Fouser, L., Carter, L., Ling, V., Bowman, M. R., Carreno, B. M., Collins, M., Wood, C. R., & Honjo, T. (2000). Engagement of the PD-1 immunoinhibitory receptor by a novel B7 family member leads to negative regulation of lymphocyte activation [Journal Article]. *J Exp Med*, *192*(7), 1027–1034.

Freund, J. (1947). Some aspects of active immunization [Journal Article]. *Annu Rev Microbiol*, *1*, 291–308. https://doi.org/https //doi.org/10.1146/annurev.mi.01.100147.001451

Freund, J. (1951). The effect of paraffin oil and myco-bacteria on antibody formation and sensitlzation. A review. [Journal Article]. *Am J Clin Pathol*, *21*(7), 645–656.

Freund, J. (1956). The mode of action of immunologic adjuvants [Journal Article]. *Bibl Tuberc*, *10*, 130–148.

Freund, J., & Bonanto, M. V. (1944). The effect of paraffin oil, lanolin-like substances and killed tubercle bacilli on immunization with diphtheric toxoid and bact. typhosum [Journal Article]. *J Immunol*, *48*, 325–334.

Freund, J., Casals, J., & Hosmer, E. P. (1937). Sensitisation and antibody formation after injection of tubercle bacilli and paraffin oil [Journal Article]. *Proc Soc Exp Biol Med*, *37*, 509–513.

Freund, J., Casals-Ariet, J., & Genghof, D. S. (1940). The synergistic effect of paraffin-oil combined with heat-killed tubercle-bacilli [Journal Article]. *J Immunol*, *38*(1), 67–79.

Freund, J., & Lipton, M. M. (1955). Experimental allergic encephalomyelitis after teh excision of the injection site of antigen-adjuvant emulsion [Journal Article]. *J Immunol*, *75*, 454–459.

Freund, J., & McDermott, K. (1942). Sensitization to horse serum by means of adjuvants [Journal Article]. *Prec See Exper Biol & Med*, *49*, 548–553.

Freund, J., Sommer, H. E., & Annabel, W. W. (1945). Immunization against malaria: Vaccination of ducks with killed parasites incorporated with adjuvants [Journal Article]. *Science*, *102*(2643), 200–202.

Freund, J., Thomson, K. J., Sommer, H. E., Annabel, W. W., & Schenkein, E. L. (1945). Immunization of rhesus monkeys against malarial infection (p. Knowlesi) with killed parasites and adjuvants [Journal Article]. *Science*, *102*(2643), 202–204.

Fridlender, Z. G., Sun, J., Kim, S., Kapoor, V., Cheng, G., Ling, L., Worthen, G. S., & Albelda, S. M. (2009). Polarization of tumor-associated neutrophil phenotype by TGF-β: N1 versus N2 TAN [Journal Article]. *Cancer Cell*, *16*(3), 183–194.

Gehring, A. J., Dobos, K. M., Belisle, J. T., Harding, C. V., & Boom, W. H. (2004). Mycobacterium tuberculosis LprG (Rv1411c): A novel TLR-2 ligand that inhibits human macrophage class II MHC antigen processing [Journal Article]. *J Immunol*, *173*(4), 2660–2668.

Gilleron, M., Himoudi, N., Adam, O., Constant, P., Venisse, A., Riviere, M., & Puzo, G. (1997). Mycobacterium smegmatis phosphoinositols-glyceroarabinomannans. Structure and localization of alkali-labile and alkali-stable phosphoinositides [Journal Article]. *J Biol Chem*, *272*(1), 117–124.

Goode, K., & Rey, K. (2019). *ggResidpanel: Panels and interactive versions of diagnostic plots using ggplot2*. https://goodekat.github.io/ggResidpanel/

Gopalakrishnan, V., Spencer, C. N., Nezi, L., Reuben, A., Andrews, M. C., Karpinets, T. V., Prieto, P. A., Vicente, D., Hoffman, K., Wei, S. C., Cogdill, A. P., Zhao, L., Hudgens, C. W., Hutchinson, D. S., Manzo, T., Petaccia de Macedo, M., Cotechini, T., Kumar, T., Chen, W. S., … Wargo, J. A. (2018). Gut microbiome modulates response to anti-PD-1 immunotherapy in melanoma patients [Journal Article]. *Science*, *359*(6371), 97–103.

Grasselly, C., Denis, M., Bourguignon, A., Talhi, N., Mathe, D., Tourette, A., Serre,

L., Jordheim, L. P., Matera, E. L., & Dumontet, C. (2018). The antitumor activity of combinations of cytotoxic chemotherapy and immune checkpoint inhibitors is model-dependent [Journal Article]. *Front Immunol*, *9*, 2100. https://doi.org/10.3389/fimmu.2018.02100

Griffin, M. E., Espinosa, J., Becker, J. L., Luo, J. D., Carroll, T. S., Jha, J. K., Fanger, G. R., & Hang, H. C. (2021). Enterococcus peptidoglycan remodeling promotes checkpoint inhibitor cancer immunotherapy [Journal Article]. *Science*, *373*(6558), 1040–1046. https://doi.org/10.1126/science.abc9113

Gunderson, C. G., & Martinello, R. A. (2012). A systematic review of bacteremias in cellulitis and erysipelas [Journal Article]. *J Infect*, *64*(2), 148–155.

Hakozaki, T., Richard, C., Elkrief, A., Hosomi, Y., Benlaifaoui, M., Mimpen, I., Terrisse, S., Derosa, L., Zitvogel, L., Routy, B., & Okuma, Y. (2020). The gut microbiome associates with immune checkpoint inhibition outcomes in patients with advanced non-small cell lung cancer [Journal Article]. *Cancer Immunol Res*, *8*(10), 1243–1250.

Halbert, S. P., Mudd, S., & Smolen, J. (1946). The increased antigenicity of shigella paradysenteriae (flexneri) in saline-in-mineral oil emulsion [Journal Article]. *J Immunol*, *53*, 291–301.

Hannani, D., Vetizou, M., Enot, D., Rusakiewicz, S., Chaput, N., Klatzmann, D., Desbois, M., Jacquelot, N., Vimond, N., Chouaib, S., Mateus, C., Allison, J. P., Ribas, A., Wolchok, J. D., Yuan, J., Wong, P., Postow, M., Mackiewicz, A., Mackiewicz, J., … Zitvogel, L. (2015). Anticancer immunotherapy by CTLA-4 blockade: Obligatory contribution of IL-2 receptors and negative prognostic impact of soluble CD25 [Journal Article]. *Cell Res*, *25*(2), 208–224.

Harper, K., Balzano, C., Rouvier, E., Mattei, M. G., Luciani, M. F., & Golstein, P. (1991). CTLA-4 and CD28 activated lymphocyte molecules are closely related in both mouse and human as to sequence, message expression, gene structure, and chromosomal location [Journal Article]. *J Immunol*, *147*(3), 1037–1044.

Havel, J. J., Chowell, D., & Chan, T. A. (2019). The evolving landscape of biomarkers for checkpoint inhibitor immunotherapy [Journal Article]. *Nat Rev Cancer*, *19*(3), 133–150.

Hellmann, M. D., Paz-Ares, L., Bernabe Caro, R., Zurawski, B., Kim, S. W., Carcereny Costa, E., Park, K., Alexandru, A., Lupinacci, L., Mora Jimenez, E. de la, Sakai, H., Albert, I., Vergnenegre, A., Peters, S., Syrigos, K., Barlesi, F., Reck, M., Borghaei, H., Brahmer, J. R., … Ramalingam, S. S. (2019). Nivolumab plus ipilimumab in advanced non-small-cell lung cancer [Journal Article]. *N Engl J Med*, *381*(21), 2020–2031.

Hemmi, H., Takeuchi, O., Kawai, T., Kaisho, T., Sato, S., Sanjo, H., Matsumoto, M.,

Hoshino, K., Wagner, H., Takeda, K., & Akira, S. (2000). A toll-like receptor recognizes bacterial DNA [Journal Article]. *Nature*, *408*(6813), 740–745.

Hills, Jr., R. D., Pontefract, B. A., Mishcon, H. R., Black, C. A., Sutton, S. C., & Theberge, C. R. (2019). Gut microbiome: Profound implications for diet and disease [Journal Article]. *Nutrients*, *11*(7).

Hollinshead, A. (1991). Active specific immunotherapy and immunochemotherapy in the treatment of lung and colon cancer [Journal Article]. *Semin Surg Oncol*, *7*(4), 199–210.

Holmgaard, R. B., Zamarin, D., Munn, D. H., Wolchok, J. D., & Allison, J. P. (2013). Indoleamine 2,3-dioxygenase is a critical resistance mechanism in antitumor t cell immunotherapy targeting CTLA-4 [Journal Article]. *J Exp Med*, *210*(7), 1389–1402. https://doi.org/10.1084/jem.20130066

Hoption Cann, S. A., Netten, J. P. van, & Netten, C. van. (2003). Dr william coley and tumour regression: A place in history or in the future [Journal Article]. *Postgrad Med J*, *79*(938), 672–680.

Hsu, B. E., Tabaries, S., Johnson, R. M., Andrzejewski, S., Senecal, J., Lehuede, C., Annis, M. G., Ma, E. H., Vols, S., Ramsay, L., Froment, R., Monast, A., Watson, I. R., Granot, Z., Jones, R. G., St-Pierre, J., & Siegel, P. M. (2019). Immature low-density neutrophils exhibit metabolic flexibility that facilitates breast cancer liver metastasis [Journal Article]. *Cell Rep*, *27*(13), 3902–3915 e6.

Hsu, J., Hodgins, J. J., Marathe, M., Nicolai, C. J., Bourgeois-Daigneault, M. C., Trevino, T. N., Azimi, C. S., Scheer, A. K., Randolph, H. E., Thompson, T. W., Zhang, L., Iannello, A., Mathur, N., Jardine, K. E., Kirn, G. A., Bell, J. C., McBurney, M. W., Raulet, D. H., & Ardolino, M. (2018). Contribution of NK cells to immunotherapy mediated by PD-1/PD-L1 blockade [Journal Article]. *J Clin Invest*, *128*(10), 4654–4668.

Hufeldt, M. R., Nielsen, D. S., Vogensen, F. K., Midtvedt, T., & Hansen, A. K. (2010). Variation in the gut microbiota of laboratory mice is related to both genetic and environmental factors [Journal Article]. *Comp Med*, *60*(5), 336–347.

Huggins, C., & Hodges, C. V. (2002). Studies on prostatic cancer. I. The effect of castration, of estrogen and of androgen injection on serum phosphatases in metastatic carcinoma of the prostate. 1941 [Journal Article]. *J Urol*, *167*(2 Pt 2), 948–51; discussion 952.

Hughes, L. E., Kearney, R., & Tully, M. (1970). A study in clinical cancer immunotherapy [Journal Article]. *Cancer*, *26*(2), 269–278.

Iannone, R., Cheng, J., Schloerke, B., Hughes, E., & Seo, J. (2022). *Gt: Easily create presentation-ready display tables*. https://CRAN.R-project.org/package=gt

Iida, N., Dzutsev, A., Stewart, C. A., Smith, L., Bouladoux, N., Weingarten, R. A., Molina, D. A., Salcedo, R., Back, T., Cramer, S., Dai, R. M., Kiu, H., Cardone, M., Naik, S., Patri, A. K., Wang, E., Marincola, F. M., Frank, K. M., Belkaid, Y., … Goldszmid, R. S. (2013). Commensal bacteria control cancer response to therapy by modulating the tumor microenvironment [Journal Article]. *Science*, *342*(6161), 967–970.

Ishida, M., Iwai, Y., Tanaka, Y., Okazaki, T., Freeman, G. J., Minato, N., & Honjo, T. (2002). Differential expression of PD-L1 and PD-L2, ligands for an inhibitory receptor PD-1, in the cells of lymphohematopoietic tissues [Journal Article]. *Immunol Lett*, *84*(1), 57–62.

Ishida, Y., Agata, Y., Shibahara, K., & Honjo, T. (1992). Induced expression of PD-1, a novel member of the immunoglobulin gene superfamily, upon programmed cell death [Journal Article]. *Embo J*, *11*(11), 3887–3895.

Ishikawa, E., Ishikawa, T., Morita, Y. S., Toyonaga, K., Yamada, H., Takeuchi, O., Kinoshita, T., Akira, S., Yoshikai, Y., & Yamasaki, S. (2009). Direct recognition of the mycobacterial glycolipid, trehalose dimycolate, by c-type lectin mincle [Journal Article]. *J Exp Med*, *206*(13), 2879–2888.

Ivanov, I., Atarashi, K., Manel, N., Brodie, E. L., Shima, T., Karaoz, U., Wei, D., Goldfarb, K. C., Santee, C. A., Lynch, S. V., Tanoue, T., Imaoka, A., Itoh, K., Takeda, K., Umesaki, Y., Honda, K., & Littman, D. R. (2009). Induction of intestinal Th17 cells by segmented filamentous bacteria [Journal Article]. *Cell*, *139*(3), 485–498.

Iwai, Y., Ishida, M., Tanaka, Y., Okazaki, T., Honjo, T., & Minato, N. (2002). Involvement of PD-L1 on tumor cells in the escape from host immune system and tumor immunotherapy by PD-L1 blockade [Journal Article]. *Proc Natl Acad Sci USA*, *99*(19), 12293–12297.

Jeong, Y., Kim, G. B., Ji, Y., Kwak, G. J., Nam, G. H., Hong, Y., Kim, S., An, J., Kim, S. H., Yang, Y., Chung, H. S., & Kim, I. S. (2020). Dendritic cell activation by an e. Coli-derived monophosphoryl lipid a enhances the efficacy of PD-1 blockade [Journal Article]. *Cancer Lett*, *472*, 19–28.

Johnston, B. (2022). *Figpatch: Easily arrange external figures with patchwork alongside ggplot2 figures*. https://github.com/BradyAJohnston/figpatch

Jones, B. W., Means, T. K., Heldwein, K. A., Keen, M. A., Hill, P. J., Belisle, J. T., & Fenton, M. J. (2001). Different toll-like receptor agonists induce distinct macrophage responses [Journal Article]. *J Leukoc Biol*, *69*(6), 1036–1044.

Jung, S., Unutmaz, D., Wong, P., Sano, G., De los Santos, K., Sparwasser, T., Wu, S., Vuthoori, S., Ko, K., Zavala, F., Pamer, E. G., Littman, D. R., & Lang, R. A. (2002). In vivo depletion of CD11c+ dendritic cells abrogates priming of CD8+ t cells by exogenous cell-associated antigens [Journal Article]. *Immunity*, *17*(2), 211–220.

Kalaora, S., Nagler, A., Nejman, D., Alon, M., Barbolin, C., Barnea, E., Ketelaars, S. L. C., Cheng, K., Vervier, K., Shental, N., Bussi, Y., Rotkopf, R., Levy, R., Benedek, G., Trabish, S., Dadosh, T., Levin-Zaidman, S., Geller, L. T., Wang, K., … Samuels, Y. (2021). Identification of bacteria-derived HLA-bound peptides in melanoma [Journal Article]. *Nature*, *592*(7852), 138–143.

Kassambara, A. (2023). *Ggpubr: ggplot2 based publication ready plots*. https://rpkgs.datanovia.com/ggpubr/

Kassambara, A., Kosinski, M., & Biecek, P. (2021). *Survminer: Drawing survival curves using ggplot2*. https://rpkgs.datanovia.com/survminer/index.html

Kim, K., Skora, A. D., Li, Z., Liu, Q., Tam, A. J., Blosser, R. L., Diaz, Jr., L. A., Papadopoulos, N., Kinzler, K. W., Vogelstein, B., & Zhou, S. (2014). Eradication of metastatic mouse cancers resistant to immune checkpoint blockade by suppression of myeloid-derived cells [Journal Article]. *Proc Natl Acad Sci USA*, *111*(32), 11774–11779.

Kim, K., Sohn, H., Kim, J. S., Choi, H. G., Byun, E. H., Lee, K. I., Shin, S. J., Song, C. H., Park, J. K., & Kim, H. J. (2012). Mycobacterium tuberculosis Rv0652 stimulates production of tumour necrosis factor and monocytes chemoattractant protein-1 in macrophages through the toll-like receptor 4 pathway [Journal Article]. *Immunology*, *136*(2), 231–240.

Kline, J., Zhang, L., Battaglia, L., Cohen, K. S., & Gajewski, T. F. (2012). Cellular and molecular requirements for rejection of B16 melanoma in the setting of regulatory t cell depletion and homeostatic proliferation [Journal Article]. *J Immunol*, *188*(6), 2630–2642.

Koenig, S., & Elicker, J. (2011). *FDA approves YERVOY™ (ipilimumab) for the treatment of patients with newly diagnosed or previously-treated unresectable or metastatic melanoma, the deadliest form of skin cancer* [Press Release]. BRISTOL-MYERS SQUIBB COMPANY. https://news.bms.com/news/details/2011/FDA-Approves-YERVOY-ipilimumab-for-the-Treatment-of-Patients-with-Newly-Diagnosed-or-Previously-Treated-Unresectable-or-Metastatic-Melanoma-the-Deadliest-Form-of-Skin-Cancer/default.aspx

Kogut, M., & Prizant, E. (1975). Effects of dihydrostreptomycin on ribosome function in vivo: Lack of correlation between changes in ribosome patterns and growth [Journal Article]. *Antimicrob Agents Chemother*, *7*(3), 341–348.

Kraal, G., Laan, L. J. van der, Elomaa, O., & Tryggvason, K. (2000). The macrophage receptor MARCO [Journal Article]. *Microbes Infect*, *2*(3), 313–316.

Krummel, M. F., & Allison, J. P. (1995). CD28 and CTLA-4 have opposing effects on the response of t cells to stimulation [Journal Article]. *J Exp Med*, *182*(2), 459–465.

Kurino, T., Matsuda, R., Terui, A., Suzuki, H., Kokubo, T., Uehara, T., Arano, Y., Hisaka, A., & Hatakeyama, H. (2020). Poor outcome with anti-programmed death-ligand 1 (PD-L1) antibody due to poor pharmacokinetic properties in PD-1/PD-L1 blockade-sensitive mouse models [Journal Article]. *J Immunother Cancer*, *8*(1).

Larkin, J., Chiarion-Sileni, V., Gonzalez, R., Grob, J. J., Cowey, C. L., Lao, C. D., Schadendorf, D., Dummer, R., Smylie, M., Rutkowski, P., Ferrucci, P. F., Hill, A., Wagstaff, J., Carlino, M. S., Haanen, J. B., Maio, M., Marquez-Rodas, I., McArthur, G. A., Ascierto, P. A., … Wolchok, J. D. (2015). Combined nivolumab and ipilimumab or monotherapy in untreated melanoma [Journal Article]. *N Engl J Med*, *373*(1), 23–34.

Latchman, Y. E., Liang, S. C., Wu, Y., Chernova, T., Sobel, R. A., Klemm, M., Kuchroo, V. K., Freeman, G. J., & Sharpe, A. H. (2004). PD-L1-deficient mice show that PD-L1 on t cells, antigen-presenting cells, and host tissues negatively regulates t cells [Journal Article]. *Proc Natl Acad Sci USA*, *101*(29), 10691–10696. https://doi.org/10.1073/pnas.0307252101

Latchman, Y., Wood, C. R., Chernova, T., Chaudhary, D., Borde, M., Chernova, I., Iwai, Y., Long, A. J., Brown, J. A., Nunes, R., Greenfield, E. A., Bourque, K., Boussiotis, V. A., Carter, L. L., Carreno, B. M., Malenkovich, N., Nishimura, H., Okazaki, T., Honjo, T., … Freeman, G. J. (2001). PD-L2 is a second ligand for PD-1 and inhibits t cell activation [Journal Article]. *Nat Immunol*, *2*(3), 261–268.

Leach, D. R., Krummel, M. F., & Allison, J. P. (1996). Enhancement of antitumor immunity by CTLA-4 blockade [Journal Article]. *Science*, *271*(5256), 1734–1736.

Lechner, M. G., Karimi, S. S., Barry-Holson, K., Angell, T. E., Murphy, K. A., Church, C. H., Ohlfest, J. R., Hu, P., & Epstein, A. L. (2013). Immunogenicity of murine solid tumor models as a defining feature of in vivo behavior and response to immunotherapy [Journal Article]. *J Immunother*, *36*(9), 477–489.

Lee, H. M., Yuk, J. M., Shin, D. M., & Jo, E. K. (2009). Dectin-1 is inducible and plays an essential role for mycobacteria-induced innate immune responses in airway epithelial cells [Journal Article]. *J Clin Immunol*, *29*(6), 795–805.

Lei, Q., Wang, D., Sun, K., Wang, L., & Zhang, Y. (2020). Resistance mechanisms of anti-PD1/PDL1 therapy in solid tumors [Journal Article]. *Front Cell Dev Biol*, *8*, 672.

Lenth, R. V. (2023). *Emmeans: Estimated marginal means, aka least-squares means*. https://github.com/rvlenth/emmeans

Leonard, W. J., Kronke, M., Peffer, N. J., Depper, J. M., & Greene, W. C. (1985). Interleukin 2 receptor gene expression in normal human t lymphocytes [Journal Article]. *Proc Natl Acad Sci USA*, *82*(18), 6281–6285. https://doi.org/10.1073/pnas.82.18.6281

Linsley, P. S., Brady, W., Urnes, M., Grosmaire, L. S., Damle, N. K., & Ledbetter, J. A. (1991). CTLA-4 is a second receptor for the b cell activation antigen B7 [Journal Article]. *J Exp Med*, *174*(3), 561–569.

Linsley, P. S., Clark, E. A., & Ledbetter, J. A. (1990). T-cell antigen CD28 mediates adhesion with b cells by interacting with activation antigen B7/BB-1 [Journal Article]. *Proc Natl Acad Sci USA*, *87*(13), 5031–5035.

Linsley, P. S., Greene, J. L., Brady, W., Bajorath, J., Ledbetter, J. A., & Peach, R. (1994). Human B7-1 (CD80) and B7-2 (CD86) bind with similar avidities but distinct kinetics to CD28 and CTLA-4 receptors [Journal Article]. *Immunity*, *1*(9), 793–801.

Linsley, P. S., Greene, J. L., Tan, P., Bradshaw, J., Ledbetter, J. A., Anasetti, C., & Damle, N. K. (1992). Coexpression and functional cooperation of CTLA-4 and CD28 on activated t lymphocytes [Journal Article]. *J Exp Med*, *176*(6), 1595–1604.

Linsley, P. S., & Ledbetter, J. A. (1993). The role of the CD28 receptor during t cell responses to antigen [Journal Article]. *Annu Rev Immunol*, *11*, 191–212.

Linsley, P. S., Wallace, P. M., Johnson, J., Gibson, M. G., Greene, J. L., Ledbetter, J. A., Singh, C., & Tepper, M. A. (1992). Immunosuppression in vivo by a soluble form of the CTLA-4 t cell activation molecule [Journal Article]. *Science*, *257*(5071), 792–795.

Liu, S., Jia, H., Hou, S., Zhang, G., Xin, T., Li, H., Yuan, W., Guo, X., Gao, X., Li, M., Wu, J., & Zhu, H. (2014). Recombinant TB10.4 of mycobacterium bovis induces cytokine production in RAW264.7 macrophages through activation of the MAPK and NF-kappaB pathways via TLR2 [Journal Article]. *Mol Immunol*, *62*(1), 227–234.

Lobo, N., Brooks, N. A., Zlotta, A. R., Cirillo, J. D., Boorjian, S., Black, P. C., Meeks, J. J., Bivalacqua, T. J., Gontero, P., Steinberg, G. D., McConkey, D., Babjuk, M., Alfred Witjes, J., & Kamat, A. M. (2021). 100 years of bacillus calmette-guerin immunotherapy: From cattle to COVID-19 [Journal Article]. *Nat Rev Urol*, *18*(10), 611–622. https://doi.org/10.1038/s41585-021-00481-1

Lochner, M., Berard, M., Sawa, S., Hauer, S., Gaboriau-Routhiau, V., Fernandez, T. D., Snel, J., Bousso, P., Cerf-Bensussan, N., & Eberl, G. (2011). Restricted microbiota and absence of cognate TCR antigen leads to an unbalanced generation of Th17 cells [Journal Article]. *J Immunol*, *186*(3), 1531–1537.

Loke, P., & Allison, J. P. (2003). PD-L1 and PD-L2 are differentially regulated by Th1 and Th2 cells [Journal Article]. *Proc Natl Acad Sci USA*, *100*(9), 5336–5341. https://doi.org/10.1073/pnas.0931259100

Luca, S., & Mihaescu, T. (2013). History of BCG vaccine [Journal Article]. *Maedica (Bucur)*, *8*(1), 53–58.

Lyngs, U. (2019). Oxforddown: An oxford university thesis template for r markdown.

In *GitHub repository*. https://github.com/ulyngs/oxforddown; GitHub. https://doi.org/10.5281/zenodo.3484681

Mackey, J. B. G., Coffelt, S. B., & Carlin, L. M. (2019). Neutrophil maturity in cancer [Journal Article]. *Front Immunol*, *10*, 1912.

Mager, L. F., Burkhard, R., Pett, N., Cooke, N. C. A., Brown, K., Ramay, H., Paik, S., Stagg, J., Groves, R. A., Gallo, M., Lewis, I. A., Geuking, M. B., & McCoy, K. D. (2020). Microbiome-derived inosine modulates response to checkpoint inhibitor immunotherapy [Journal Article]. *Science*, *369*(6510), 1481–1489.

Malbec, O., & Daeron, M. (2007). The mast cell IgG receptors and their roles in tissue inflammation [Journal Article]. *Immunol Rev*, *217*, 206–221.

Mall, C., Sckisel, G. D., Proia, D. A., Mirsoian, A., Grossenbacher, S. K., Pai, C. S., Chen, M., Monjazeb, A. M., Kelly, K., Blazar, B. R., & Murphy, W. J. (2016). Repeated PD-1/PD-L1 monoclonal antibody administration induces fatal xenogeneic hypersensitivity reactions in a murine model of breast cancer [Journal Article]. *OncoImmunology*, *5*(2), e1075114.

Manz, M. G., & Boettcher, S. (2014). Emergency granulopoiesis [Journal Article]. *Nat Rev Immunol*, *14*(5), 302–314.

Marabelle, A., Kohrt, H., Sagiv-Barfi, I., Ajami, B., Axtell, R. C., Zhou, G., Rajapaksa, R., Green, M. R., Torchia, J., Brody, J., Luong, R., Rosenblum, M. D., Steinman, L., Levitsky, H. I., Tse, V., & Levy, R. (2013). Depleting tumor-specific tregs at a single site eradicates disseminated tumors [Journal Article]. *J Clin Invest*, *123*(6), 2447–2463.

Martinez-Pomares, L. (2012). The mannose receptor [Journal Article]. *J Leukoc Biol*, *92*(6), 1177–1186.

Matson, V., Fessler, J., Bao, R., Chongsuwat, T., Zha, Y., Alegre, M. L., Luke, J. J., & Gajewski, T. F. (2018). The commensal microbiome is associated with anti-PD-1 efficacy in metastatic melanoma patients [Journal Article]. *Science*, *359*(6371), 104–108.

Mills, C. D., Kincaid, K., Alt, J. M., Heilman, M. J., & Hill, A. M. (2000). M-1/m-2 macrophages and the Th1/Th2 paradigm [Journal Article]. *J Immunol*, *164*(12), 6166–6173.

Monticelli, L. A., Sonnenberg, G. F., Abt, M. C., Alenghat, T., Ziegler, C. G., Doering, T. A., Angelosanto, J. M., Laidlaw, B. J., Yang, C. Y., Sathaliyawala, T., Kubota, M., Turner, D., Diamond, J. M., Goldrath, A. W., Farber, D. L., Collman, R. G., Wherry, E. J., & Artis, D. (2011). Innate lymphoid cells promote lung-tissue homeostasis after infection with influenza virus [Journal Article]. *Nat Immunol*, *12*(11), 1045–1054. https://doi.org/10.1031/ni.2131

Motoshima, T., Komohara, Y., Horlad, H., Takeuchi, A., Maeda, Y., Tanoue, K., Kawano, Y., Harada, M., Takeya, M., & Eto, M. (2015). Sorafenib enhances the antitumor effects of anti-CTLA-4 antibody in a murine cancer model by inhibiting myeloid-derived suppressor cells [Journal Article]. *Oncol Rep*, *33*(6), 2947–2953.

Nauts, H. C., & McLaren, J. R. (1990). Coley toxins–the first century [Journal Article]. *Adv Exp Med Biol*, *267*, 483–500.

Nauts, H. C., Swift, W. E., & Coley, B. L. (1946). The treatment of malignant tumors by bacterial toxins as developed by the late william b. Coley, m.d., reviewed in the light of modern research [Journal Article]. *Cancer Res*, *6*, 205–216.

Nejman, D., Livyatan, I., Fuks, G., Gavert, N., Zwang, Y., Geller, L. T., Rotter-Maskowitz, A., Weiser, R., Mallel, G., Gigi, E., Meltser, A., Douglas, G. M., Kamer, I., Gopalakrishnan, V., Dadosh, T., Levin-Zaidman, S., Avnet, S., Atlan, T., Cooper, Z. A., … Straussman, R. (2020). The human tumor microbiome is composed of tumor type-specific intracellular bacteria [Journal Article]. *Science*, *368*(6494), 973–980.

News of science. (1957). [Journal Article]. *Science*, *125*(3236), 18–22.

Ngiow, S. F., Young, A., Jacquelot, N., Yamazaki, T., Enot, D., Zitvogel, L., & Smyth, M. J. (2015). A threshold level of intratumor CD8+ t-cell PD1 expression dictates therapeutic response to anti-PD1 [Journal Article]. *Cancer Res*, *75*(18), 3800–3811. https://doi.org/10.1158/0008-5472.CAN-15-1082

Nishimura, H., Agata, Y., Kawasaki, A., Sato, M., Imamura, S., Minato, N., Yagita, H., Nakano, T., & Honjo, T. (1996). Developmentally regulated expression of the PD-1 protein on the surface of double-negative (CD4-CD8-) thymocytes [Journal Article]. *Int Immunol*, *8*(5), 773–780.

Nishimura, H., Minato, N., Nakano, T., & Honjo, T. (1998). Immunological studies on PD-1 deficient mice: Implication of PD-1 as a negative regulator for b cell responses [Journal Article]. *Int Immunol*, *10*(10), 1563–1572.

Nishimura, H., Nose, M., Hiai, H., Minato, N., & Honjo, T. (1999). Development of lupus-like autoimmune diseases by disruption of the PD-1 gene encoding an ITIM motif-carrying immunoreceptor [Journal Article]. *Immunity*, *11*(2), 141–151.

Osebold, J. W. (1982). Mechanisms of action by immunologic adjuvants [Journal Article]. *J Am Vet Med Assoc*, *181*, 983–987.

Pauken, K. E., Sammons, M. A., Odorizzi, P. M., Manne, S., Godec, J., Khan, O., Drake, A. M., Chen, Z., Sen, D. R., Kurachi, M., Barnitz, R. A., Bartman, C., Bengsch, B., Huang, A. C., Schenkel, J. M., Vahedi, G., Haining, W. N., Berger, S. L., & Wherry, E. J. (2016). Epigenetic stability of exhausted t cells limits durability of reinvigoration by PD-1 blockade [Journal Article]. *Science*, *354*(6316), 1160–1165.

Pecora, N. D., Gehring, A. J., Canaday, D. H., Boom, W. H., & Harding, C. V. (2006).

Mycobacterium tuberculosis LprA is a lipoprotein agonist of TLR2 that regulates innate immunity and APC function [Journal Article]. *J Immunol*, *177*(1), 422–429.

Pedersen, T. L. (2022). *Patchwork: The composer of plots*. https://CRAN.R-project.org/package=patchwork

Perry, J. L., Reuter, K. G., Luft, J. C., Pecot, C. V., Zamboni, W., & DeSimone, J. M. (2017). Mediating passive tumor accumulation through particle size, tumor type, and location [Journal Article]. *Nano Lett*, *17*(5), 2879–2886.

Perry, L. M., Cruz, S. M., Kleber, K. T., Judge, S. J., Darrow, M. A., Jones, L. B., Basmaci, U. N., Joshi, N., Settles, M. L., Durbin-Johnson, B. P., Gingrich, A. A., Monjazeb, A. M., Carr-Ascher, J., Thorpe, S. W., Murphy, W. J., Eisen, J. A., & Canter, R. J. (2023). Human soft tissue sarcomas harbor an intratumoral viral microbiome which is linked with natural killer cell infiltrate and prognosis [Journal Article]. *J Immunother Cancer*, *11*(1).

Pinato, D. J., Gramenitskaya, D., Altmann, D. M., Boyton, R. J., Mullish, B. H., Marchesi, J. R., & Bower, M. (2019). Antibiotic therapy and outcome from immune-checkpoint inhibitors [Journal Article]. *J Immunother Cancer*, *7*(1), 287.

Pirlog, C. F., Parosanu, A. I., Slavu, C. O., Olaru, M., Popa, A. M., Iaciu, C., Nita, I., Motatu, P., Horia, C., Manolescu, L. S. C., & Nitipir, C. (2022). Nivolumab hypersensitivity reactions a myth or reality in solid tumors-a systematic review of the literature [Journal Article]. *Curr Oncol*, *29*(12), 9428–9436. https://doi.org/10.3390/curroncol29120741

Postow, M. A., Sidlow, R., & Hellmann, M. D. (2018). Immune-related adverse events associated with immune checkpoint blockade [Journal Article]. *N Engl J Med*, *378*(2), 158–168.

Prados-Rosales, R., Baena, A., Martinez, L. R., Luque-Garcia, J., Kalscheuer, R., Veeraraghavan, U., Camara, C., Nosanchuk, J. D., Besra, G. S., Chen, B., Jimenez, J., Glatman-Freedman, A., Jacobs, Jr., W. R., Porcelli, S. A., & Casadevall, A. (2011). Mycobacteria release active membrane vesicles that modulate immune responses in a TLR2-dependent manner in mice [Journal Article]. *J Clin Invest*, *121*(4), 1471–1483.

Principe, N., Kidman, J., Goh, S., Tilsed, C. M., Fisher, S. A., Fear, V. S., Forbes, C. A., Zemek, R. M., Chopra, A., Watson, M., Dick, I. M., Boon, L., Holt, R. A., Lake, R. A., Nowak, A. K., Lesterhuis, W. J., McDonnell, A. M., & Chee, J. (2020). Tumor infiltrating effector memory antigen-specific CD8(+) t cells predict response to immune checkpoint therapy [Journal Article]. *Front Immunol*, *11*, 584423.

Pulaski, B. A., & Ostrand-Rosenberg, S. (1998). Reduction of established spontaneous mammary carcinoma metastases following immunotherapy with major histocompatibility complex class II and B7.1 cell-based tumor vaccines [Journal Article]. *Cancer*

Res, *58*(7), 1486–1493.

Pulaski, B. A., & Ostrand-Rosenberg, S. (2001). Mouse 4T1 breast tumor model [Journal Article]. *Curr Protoc Immunol*, *Chapter 20*, Unit 20 2.

Quail, D. F., Amulic, B., Aziz, M., Barnes, B. J., Eruslanov, E., Fridlender, Z. G., Goodridge, H. S., Granot, Z., Hidalgo, A., Huttenlocher, A., Kaplan, M. J., Malanchi, I., Merghoub, T., Meylan, E., Mittal, V., Pittet, M. J., Rubio-Ponce, A., Udalova, I. A., Berg, T. K. van den, … Kubes, P. (2022). Neutrophil phenotypes and functions in cancer: A consensus statement [Journal Article]. *J Exp Med*, *219*(6).

Quesniaux, V. J., Nicolle, D. M., Torres, D., Kremer, L., Guerardel, Y., Nigou, J., Puzo, G., Erard, F., & Ryffel, B. (2004). Toll-like receptor 2 (TLR2)-dependent-positive and TLR2-independent-negative regulation of proinflammatory cytokines by mycobacterial lipomannans [Journal Article]. *J Immunol*, *172*(7), 4425–4434.

Quezada, S. A., & Peggs, K. S. (2019). Lost in translation: Deciphering the mechanism of action of anti-human CTLA-4 [Journal Article]. *Clin Cancer Res*, *25*(4), 1130–1132.

Quezada, S. A., Peggs, K. S., Curran, M. A., & Allison, J. P. (2006). CTLA4 blockade and GM-CSF combination immunotherapy alters the intratumor balance of effector and regulatory t cells [Journal Article]. *J Clin Invest*, *116*(7), 1935–1945.

R Core Team. (2021). *R: A language and environment for statistical computing*. R Foundation for Statistical Computing. https://www.R-project.org/

Raffel, S. (1948). The components of the tubercle bacillus responsible for the delayed type of "infectious" allergy [Journal Article]. *J Infect Dis*, *82*, 267–293.

Rashidian, M., Ingram, J. R., Dougan, M., Dongre, A., Whang, K. A., LeGall, C., Cragnolini, J. J., Bierie, B., Gostissa, M., Gorman, J., Grotenbreg, G. M., Bhan, A., Weinberg, R. A., & Ploegh, H. L. (2017). Predicting the response to CTLA-4 blockade by longitudinal noninvasive monitoring of CD8 t cells [Journal Article]. *J Exp Med*, *214*(8), 2243–2255.

Rasmussen, T. S., Vries, L. de, Kot, W., Hansen, L. H., Castro-Mejia, J. L., Vogensen, F. K., Hansen, A. K., & Nielsen, D. S. (2019). Mouse vendor influence on the bacterial and viral gut composition exceeds the effect of diet [Journal Article]. *Viruses*, *11*(5).

Ray, P., Pandey, U., & Aich, P. (2021). Comparative analysis of beneficial effects of vancomycin treatment on Th1- and Th2-biased mice and the role of gut microbiota [Journal Article]. *J Appl Microbiol*, *130*(4), 1337–1356.

Redmond, W. L., Linch, S. N., & Kasiewicz, M. J. (2014). Combined targeting of costimulatory (OX40) and coinhibitory (CTLA-4) pathways elicits potent effector t cells capable of driving robust antitumor immunity [Journal Article]. *Cancer Immunol Res*, *2*(2), 142–153.

Rice, C. M., Davies, L. C., Subleski, J. J., Maio, N., Gonzalez-Cotto, M., Andrews, C.,

Patel, N. L., Palmieri, E. M., Weiss, J. M., Lee, J. M., Annunziata, C. M., Rouault, T. A., Durum, S. K., & McVicar, D. W. (2018). Tumour-elicited neutrophils engage mitochondrial metabolism to circumvent nutrient limitations and maintain immune suppression [Journal Article]. *Nat Commun*, *9*(1), 5099.

Rizvi, Z. A., Dalal, R., Sadhu, S., Kumar, Y., Kumar, S., Gupta, S. K., Tripathy, M. R., Rathore, D. K., & Awasthi, A. (2021). High-salt diet mediates interplay between NK cells and gut microbiota to induce potent tumor immunity [Journal Article]. *Sci Adv*, *7*(37), eabg5016.

Robert, C., Thomas, L., Bondarenko, I., O'Day, S., Weber, J., Garbe, C., Lebbe, C., Baurain, J. F., Testori, A., Grob, J. J., Davidson, N., Richards, J., Maio, M., Hauschild, A., Miller, Jr., W. H., Gascon, P., Lotem, M., Harmankaya, K., Ibrahim, R., … Wolchok, J. D. (2011). Ipilimumab plus dacarbazine for previously untreated metastatic melanoma [Journal Article]. *N Engl J Med*, *364*(26), 2517–2526.

Robinson, D., Hayes, A., & Couch, S. (2023). *Broom: Convert statistical objects into tidy tibbles*. https://CRAN.R-project.org/package=broom

Roelofsen, T., Wefers, C., Gorris, M. A. J., Textor, J. C., Massuger, L., Vries, I. J. M. de, & Altena, A. M. van. (2018). Spontaneous regression of ovarian carcinoma after septic peritonitis; a unique case report [Journal Article]. *Front Oncol*, *8*, 562.

Routy, B., Le Chatelier, E., Derosa, L., Duong, C. P. M., Alou, M. T., Daillere, R., Fluckiger, A., Messaoudene, M., Rauber, C., Roberti, M. P., Fidelle, M., Flament, C., Poirier-Colame, V., Opolon, P., Klein, C., Iribarren, K., Mondragon, L., Jacquelot, N., Qu, B., … Zitvogel, L. (2018). Gut microbiome influences efficacy of PD-1-based immunotherapy against epithelial tumors [Journal Article]. *Science*, *359*(6371), 91–97.

Sade-Feldman, M., Yizhak, K., Bjorgaard, S. L., Ray, J. P., Boer, C. G. de, Jenkins, R. W., Lieb, D. J., Chen, J. H., Frederick, D. T., Barzily-Rokni, M., Freeman, S. S., Reuben, A., Hoover, P. J., Villani, A. C., Ivanova, E., Portell, A., Lizotte, P. H., Aref, A. R., Eliane, J. P., … Hacohen, N. (2018). Defining t cell states associated with response to checkpoint immunotherapy in melanoma [Journal Article]. *Cell*, *175*(4), 998–1013 e20.

Sagiv, J. Y., Michaeli, J., Assi, S., Mishalian, I., Kisos, H., Levy, L., Damti, P., Lumbroso, D., Polyansky, L., Sionov, R. V., Ariel, A., Hovav, A. H., Henke, E., Fridlender, Z. G., & Granot, Z. (2015). Phenotypic diversity and plasticity in circulating neutrophil subpopulations in cancer [Journal Article]. *Cell Rep*, *10*(4), 562–573.

Sagiv-Barfi, I., Czerwinski, D. K., Levy, S., Alam, I. S., Mayer, A. T., Gambhir, S. S., & Levy, R. (2018). Eradication of spontaneous malignancy by local immunotherapy [Journal Article]. *Sci Transl Med*, *10*(426).

Sakaguchi, S., Sakaguchi, N., Asano, M., Itoh, M., & Toda, M. (1995). Immunologic self-tolerance maintained by activated t cells expressing IL-2 receptor alpha-chains (CD25). Breakdown of a single mechanism of self-tolerance causes various autoimmune diseases [Journal Article]. *J Immunol*, *155*(3), 1151–1164.

Sawa, S., Lochner, M., Satoh-Takayama, N., Dulauroy, S., Berard, M., Kleinschek, M., Cua, D., Di Santo, J. P., & Eberl, G. (2011). RORgammat+ innate lymphoid cells regulate intestinal homeostasis by integrating negative signals from the symbiotic microbiota [Journal Article]. *Nat Immunol*, *12*(4), 320–326.

Scheetz, L., Kadiyala, P., Sun, X., Son, S., Hassani Najafabadi, A., Aikins, M., Lowenstein, P. R., Schwendeman, A., Castro, M. G., & Moon, J. J. (2020). Synthetic high-density lipoprotein nanodiscs for personalized immunotherapy against gliomas [Journal Article]. *Clin Cancer Res*, *26*(16), 4369–4380. https://doi.org/10.1158/1078-0432.CCR-20-0341

Schrors, B., Hos, B. J., Yildiz, I. G., Lower, M., Lang, F., Holtstrater, C., Becker, J., Vormehr, M., Sahin, U., Ossendorp, F., & Diken, M. (2023). MC38 colorectal tumor cell lines from two different sources display substantial differences in transcriptome, mutanome and neoantigen expression [Journal Article]. *Front Immunol*, *14*, 1102282. https://doi.org/10.3389/fimmu.2023.1102282

Seidel, J. A., Otsuka, A., & Kabashima, K. (2018). Anti-PD-1 and anti-CTLA-4 therapies in cancer: Mechanisms of action, efficacy, and limitations [Journal Article]. *Front Oncol*, *8*, 86.

Selby, M. J., Engelhardt, J. J., Quigley, M., Henning, K. A., Chen, T., Srinivasan, M., & Korman, A. J. (2013). Anti-CTLA-4 antibodies of IgG2a isotype enhance antitumor activity through reduction of intratumoral regulatory t cells [Journal Article]. *Cancer Immunol Res*, *1*(1), 32–42.

Shah, S., Bohsali, A., Ahlbrand, S. E., Srinivasan, L., Rathinam, V. A., Vogel, S. N., Fitzgerald, K. A., Sutterwala, F. S., & Briken, V. (2013). Cutting edge: Mycobacterium tuberculosis but not nonvirulent mycobacteria inhibits IFN-beta and AIM2 inflammasome-dependent IL-1beta production via its ESX-1 secretion system [Journal Article]. *J Immunol*, *191*(7), 3514–3518.

Shahinian, A., Pfeffer, K., Lee, K. P., Kundig, T. M., Kishihara, K., Wakeham, A., Kawai, K., Ohashi, P. S., Thompson, C. B., & Mak, T. W. (1993). Differential t-cell costimulatory requirements in Cd28-deficient mice [Journal Article]. *Science*, *261*(5121), 609–612. https://doi.org/DOI 10.1126/science.7688139

Sharma, N., Vacher, J., & Allison, J. P. (2019). TLR1/2 ligand enhances antitumor efficacy of CTLA-4 blockade by increasing intratumoral treg depletion [Journal Article]. *Proc Natl Acad Sci USA*, *116*(21), 10453–10462.

Shaul, M. E., & Fridlender, Z. G. (2019). Tumour-associated neutrophils in patients with cancer [Journal Article]. *Nat Rev Clin Oncol*, *16*(10), 601–620.

Shin, T., Yoshimura, K., Shin, T., Crafton, E. B., Tsuchiya, H., Housseau, F., Koseki, H., Schulick, R. D., Chen, L. P., & Pardoll, D. M. (2005). In vivo costimulatory role of B7-DC in tuning t helper cell 1 and cytotoxic t lymphocyte responses [Journal Article]. *J Exp Med*, *201*(10), 1531–1541. https://doi.org/10.1084/jem.20050072

Shinohara, T., Taniwaki, M., Ishida, Y., Kawaichi, M., & Honjo, T. (1994). Structure and chromosomal localization of the human PD-1 gene (PDCD1) [Journal Article]. *Genomics*, *23*(3), 704–706.

Shurin, M. R., Esche, C., & Lotze, M. T. (1998). FLT3: Receptor and ligand. Biology and potential clinical application [Journal Article]. *Cytokine Growth Factor Rev*, *9*(1), 37–48.

Simpson, T. R., Li, F., Montalvo-Ortiz, W., Sepulveda, M. A., Bergerhoff, K., Arce, F., Roddie, C., Henry, J. Y., Yagita, H., Wolchok, J. D., Peggs, K. S., Ravetch, J. V., Allison, J. P., & Quezada, S. A. (2013). Fc-dependent depletion of tumor-infiltrating regulatory t cells co-defines the efficacy of anti-CTLA-4 therapy against melanoma [Journal Article]. *J Exp Med*, *210*(9), 1695–1710.

Sitnikova, S. I., Munnings-Tomes, S., Galvani, E., Kentner, S., Mulgrew, K., Rands, C., Espana Agusti, J., Zhang, T., Ilieva, K. M., Rosignoli, G., Ghadially, H., Robinson, M. J., Slidel, T., Wilkinson, R. W., & Dovedi, S. J. (2021). Novel non-terminal tumor sampling procedure using fine needle aspiration supports immuno-oncology biomarker discovery in preclinical mouse models [Journal Article]. *J Immunother Cancer*, *9*(6).

Sivan, A., Corrales, L., Hubert, N., Williams, J. B., Aquino-Michaels, K., Earley, Z. M., Benyamin, F. W., Lei, Y. M., Jabri, B., Alegre, M. L., Chang, E. B., & Gajewski, T. F. (2015). Commensal bifidobacterium promotes antitumor immunity and facilitates anti-PD-L1 efficacy [Journal Article]. *Science*, *350*(6264), 1084–1089.

Sjoberg, D. D., Whiting, K., Curry, M., Lavery, J. A., & Larmarange, J. (2021). Reproducible summary tables with the gtsummary package. *The R Journal*, *13*, 570–580. https://doi.org/10.32614/RJ-2021-053

Smith, C. K., & Trinchieri, G. (2018). The interplay between neutrophils and microbiota in cancer [Journal Article]. *J Leukoc Biol*, *104*(4), 701–715.

Smith, S. L. (2017). War! What is it good for? Mustard gas medicine [Journal Article]. *Cmaj*, *189*(8), E321–E322.

Soularue, E., Lepage, P., Colombel, J. F., Coutzac, C., Faleck, D., Marthey, L., Collins, M., Chaput, N., Robert, C., & Carbonnel, F. (2018). Enterocolitis due to immune checkpoint inhibitors: A systematic review [Journal Article]. *Gut*, *67*(11), 2056–

2067.

Spiess, P. J., Yang, J. C., & Rosenberg, S. A. (1987). In vivo antitumor activity of tumor-infiltrating lymphocytes expanded in recombinant interleukin-2 [Journal Article]. *J Natl Cancer Inst*, *79*(5), 1067–1075.

Spinu, V., Grolemund, G., & Wickham, H. (2023). *Lubridate: Make dealing with dates a little easier*. https://CRAN.R-project.org/package=lubridate

Spolski, R., Li, P., & Leonard, W. J. (2018). Biology and regulation of IL-2: From molecular mechanisms to human therapy [Journal Article]. *Nat Rev Immunol*, *18*(10), 648–659.

Spratt, B. G. (1975). Distinct penicillin binding proteins involved in the division, elongation, and shape of escherichia coli K12 [Journal Article]. *Proc Natl Acad Sci USA*, *72*(8), 2999–3003.

Srivastava, S., & Riddell, S. R. (2015). Engineering CAR-t cells: Design concepts [Journal Article]. *Trends Immunol*, *36*(8), 494–502.

Stamm, C. E., Collins, A. C., & Shiloh, M. U. (2015). Sensing of mycobacterium tuberculosis and consequences to both host and bacillus [Journal Article]. *Immunol Rev*, *264*(1), 204–219.

Stewart, T. H., Hollinshead, A. C., Harris, J. E., Belanger, R., Crepeau, A., Hooper, G. D., Sachs, H. J., Klaassen, D. J., Hirte, W., Rapp, E., Crook, A. F., Orizaga, M., Sengar, D. P., & Raman, S. (1976). Immunochemotherapy of lung cancer [Journal Article]. *Ann N Y Acad Sci*, *277*(00), 436–466.

Stills, Jr., H. F. (2005). Adjuvants and antibody production: Dispelling the myths associated with freund's complete and other adjuvants [Journal Article]. *Ilar J*, *46*(3), 280–293.

Stromnes, I. M., & Goverman, J. M. (2006a). Active induction of experimental allergic encephalomyelitis [Journal Article]. *Nat Protoc*, *1*(4), 1810–1819.

Stromnes, I. M., & Goverman, J. M. (2006b). Passive induction of experimental allergic encephalomyelitis [Journal Article]. *Nat Protoc*, *1*(4), 1952–1960.

Tailleux, L., Schwartz, O., Herrmann, J. L., Pivert, E., Jackson, M., Amara, A., Legres, L., Dreher, D., Nicod, L. P., Gluckman, J. C., Lagrange, P. H., Gicquel, B., & Neyrolles, O. (2003). DC-SIGN is the major mycobacterium tuberculosis receptor on human dendritic cells [Journal Article]. *J Exp Med*, *197*(1), 121–127.

Takeshita, T., Asao, H., Ohtani, K., Ishii, N., Kumaki, S., Tanaka, N., Munakata, H., Nakamura, M., & Sugamura, K. (1992). Cloning of the gamma chain of the human IL-2 receptor [Journal Article]. *Science*, *257*(5068), 379–382. https://doi.org/10.1126/science.1631559

Takita, H., Hollinshead, A. C., Adler, R. H., Bhayana, J., Ramundo, M., Moskowitz, R., Rao, U. N., & Raman, S. (1991). Adjuvant, specific, active immunotherapy for resectable squamous cell lung carcinoma: A 5-year survival analysis [Journal Article]. *J Surg Oncol*, *46*(1), 9–14.

Tanoue, T., Morita, S., Plichta, D. R., Skelly, A. N., Suda, W., Sugiura, Y., Narushima, S., Vlamakis, H., Motoo, I., Sugita, K., Shiota, A., Takeshita, K., Yasuma-Mitobe, K., Riethmacher, D., Kaisho, T., Norman, J. M., Mucida, D., Suematsu, M., Yaguchi, T., … Honda, K. (2019). A defined commensal consortium elicits CD8 t cells and anti-cancer immunity [Journal Article]. *Nature*, *565*(7741), 600–605.

Terry M. Therneau, & Patricia M. Grambsch. (2000). *Modeling survival data: Extending the Cox model*. Springer.

Therneau, T. M. (2023). *Survival: Survival analysis*. https://github.com/therneau/survival

Thoma-Uszynski, S., Stenger, S., Takeuchi, O., Ochoa, M. T., Engele, M., Sieling, P. A., Barnes, P. F., Rollinghoff, M., Bolcskei, P. L., Wagner, M., Akira, S., Norgard, M. V., Belisle, J. T., Godowski, P. J., Bloom, B. R., & Modlin, R. L. (2001). Induction of direct antimicrobial activity through mammalian toll-like receptors [Journal Article]. *Science*, *291*(5508), 1544–1547.

Tivol, E. A., Borriello, F., Schweitzer, A. N., Lynch, W. P., Bluestone, J. A., & Sharpe, A. H. (1995). Loss of CTLA-4 leads to massive lymphoproliferation and fatal multiorgan tissue destruction, revealing a critical negative regulatory role of CTLA-4 [Journal Article]. *Immunity*, *3*(5), 541–547.

Triplett, T. A., Garrison, K. C., Marshall, N., Donkor, M., Blazeck, J., Lamb, C., Qerqez, A., Dekker, J. D., Tanno, Y., Lu, W. C., Karamitros, C. S., Ford, K., Tan, B., Zhang, X. M., McGovern, K., Coma, S., Kumada, Y., Yamany, M. S., Sentandreu, E., … Georgiou, G. (2018). Reversal of indoleamine 2,3-dioxygenase-mediated cancer immune suppression by systemic kynurenine depletion with a therapeutic enzyme [Journal Article]. *Nat Biotechnol*, *36*(8), 758–764. https://doi.org/10.1038/nbt.4180

Tseng, S. Y., Otsuji, M., Gorski, K., Huang, X., Slansky, J. E., Pai, S. I., Shalabi, A., Shin, T., Pardoll, D. M., & Tsuchiya, H. (2001). B7-DC, a new dendritic cell molecule with potent costimulatory properties for t cells [Journal Article]. *J Exp Med*, *193*(7), 839–846.

Tsukamoto, H., Kubota, K., Shichiku, A., Maekawa, M., Mano, N., Yagita, H., Ohta, S., & Tomioka, Y. (2019). An agonistic anti-toll-like receptor 4 monoclonal antibody as an effective adjuvant for cancer immunotherapy [Journal Article]. *Immunology*, *158*(2), 136–149.

Tumeh, P. C., Harview, C. L., Yearley, J. H., Shintaku, I. P., Taylor, E. J., Robert, L.,

Chmielowski, B., Spasic, M., Henry, G., Ciobanu, V., West, A. N., Carmona, M., Kivork, C., Seja, E., Cherry, G., Gutierrez, A. J., Grogan, T. R., Mateus, C., Tomasic, G., … Ribas, A. (2014). PD-1 blockade induces responses by inhibiting adaptive immune resistance [Journal Article]. *Nature*, *515*(7528), 568–571.

Uruga, H., & Mino-Kenudson, M. (2021). Predictive biomarkers for response to immune checkpoint inhibitors in lung cancer: PD-L1 and beyond [Journal Article]. *Virchows Arch*, *478*(1), 31–44.

Ustyanovska Avtenyuk, N., Visser, N., Bremer, E., & Wiersma, V. R. (2020). The neutrophil: The underdog that packs a punch in the fight against cancer [Journal Article]. *Int J Mol Sci*, *21*(21).

Vetizou, M., Pitt, J. M., Daillere, R., Lepage, P., Waldschmitt, N., Flament, C., Rusakiewicz, S., Routy, B., Roberti, M. P., Duong, C. P., Poirier-Colame, V., Roux, A., Becharef, S., Formenti, S., Golden, E., Cording, S., Eberl, G., Schlitzer, A., Ginhoux, F., … Zitvogel, L. (2015). Anticancer immunotherapy by CTLA-4 blockade relies on the gut microbiota [Journal Article]. *Science*, *350*(6264), 1079–1084.

Viaud, S., Daillere, R., Boneca, I. G., Lepage, P., Langella, P., Chamaillard, M., Pittet, M. J., Ghiringhelli, F., Trinchieri, G., Goldszmid, R., & Zitvogel, L. (2015). Gut microbiome and anticancer immune response: Really hot sh*t! [Journal Article]. *Cell Death Differ*, *22*(2), 199–214.

Viaud, S., Saccheri, F., Mignot, G., Yamazaki, T., Daillere, R., Hannani, D., Enot, D. P., Pfirschke, C., Engblom, C., Pittet, M. J., Schlitzer, A., Ginhoux, F., Apetoh, L., Chachaty, E., Woerther, P. L., Eberl, G., Berard, M., Ecobichon, C., Clermont, D., … Zitvogel, L. (2013). The intestinal microbiota modulates the anticancer immune effects of cyclophosphamide [Journal Article]. *Science*, *342*(6161), 971–976.

Waksman, B. H. (1979). Adjuvants and immune regulation by lymphoid cells [Journal Article]. *Springer Semin Immunopathol*, *2*, 5–9.

Walker, L. S., & Sansom, D. M. (2011). The emerging role of CTLA4 as a cell-extrinsic regulator of t cell responses [Journal Article]. *Nat Rev Immunol*, *11*(12), 852–863.

Walunas, T. L., Lenschow, D. J., Bakker, C. Y., Linsley, P. S., Freeman, G. J., Green, J. M., Thompson, C. B., & Bluestone, J. A. (1994). CTLA-4 can function as a negative regulator of t cell activation [Journal Article]. *Immunity*, *1*(5), 405–413.

Wang, M., Bronte, V., Chen, P. W., Gritz, L., Panicali, D., Rosenberg, S. A., & Restifo, N. P. (1995). Active immunotherapy of cancer with a nonreplicating recombinant fowlpox virus encoding a model tumor-associated antigen [Journal Article]. *J Immunol*, *154*(9), 4685–4692.

Wang, S., Campos, J., Gallotta, M., Gong, M., Crain, C., Naik, E., Coffman, R. L., & Guiducci, C. (2016). Intratumoral injection of a CpG oligonucleotide reverts resis-

tance to PD-1 blockade by expanding multifunctional CD8+ t cells [Journal Article]. *Proc Natl Acad Sci USA*, *113*(46), E7240–E7249.

Wang, X., Lupardus, P., Laporte, S. L., & Garcia, K. C. (2009). Structural biology of shared cytokine receptors [Journal Article]. *Annu Rev Immunol*, *27*, 29–60. https://doi.org/10.1146/annurev.immunol.24.021605.090616

Watanabe, H., Numata, K., Ito, T., Takagi, K., & Matsukawa, A. (2004). Innate immune response in Th1- and Th2-dominant mouse strains [Journal Article]. *Shock*, *22*(5), 460–466.

Waterhouse, P., Penninger, J. M., Timms, E., Wakeham, A., Shahinian, A., Lee, K. P., Thompson, C. B., Griesser, H., & Mak, T. W. (1995). Lymphoproliferative disorders with early lethality in mice deficient in ctla-4 [Journal Article]. *Science*, *270*(5238), 985–988.

Wei, S. C., Anang, N. A. S., Sharma, R., Andrews, M. C., Reuben, A., Levine, J. H., Cogdill, A. P., Mancuso, J. J., Wargo, J. A., Pe'er, D., & Allison, J. P. (2019). Combination anti-CTLA-4 plus anti-PD-1 checkpoint blockade utilizes cellular mechanisms partially distinct from monotherapies [Journal Article]. *Proc Natl Acad Sci USA*, *116*(45), 22699–22709.

Wei, S. C., Levine, J. H., Cogdill, A. P., Zhao, Y., Anang, N. A. S., Andrews, M. C., Sharma, P., Wang, J., Wargo, J. A., Pe'er, D., & Allison, J. P. (2017). Distinct cellular mechanisms underlie anti-CTLA-4 and anti-PD-1 checkpoint blockade [Journal Article]. *Cell*, *170*(6), 1120–1133 e17.

Wickham, H., Averick, M., Bryan, J., Chang, W., McGowan, L. D., François, R., Grolemund, G., Hayes, A., Henry, L., Hester, J., Kuhn, M., Pedersen, T. L., Miller, E., Bache, S. M., Müller, K., Ooms, J., Robinson, D., Seidel, D. P., Spinu, V., … Yutani, H. (2019). Welcome to the tidyverse. *Journal of Open Source Software*, *4*(43), 1686. https://doi.org/10.21105/joss.01686

Wickham, H., & Bryan, J. (2023). *Readxl: Read excel files*. https://CRAN.R-project.org/package=readxl

Wickham, H., Chang, W., Henry, L., Pedersen, T. L., Takahashi, K., Wilke, C., Woo, K., Yutani, H., & Dunnington, D. (2023). *ggplot2: Create elegant data visualisations using the grammar of graphics*. https://CRAN.R-project.org/package=ggplot2

Wickham, H., & Seidel, D. (2022). *Scales: Scale functions for visualization*. https://CRAN.R-project.org/package=scales

Winkelhake, J. L., & Nicolson, G. L. (1976). Determination of adhesive properties of variant metastatic melanoma cells to BALB/3T3 cells and their virus-transformed derivatives by a monolayer attachment assay [Journal Article]. *J Natl Cancer Inst*, *56*(2), 285–291. https://doi.org/10.1093/jnci/56.2.285

Xu, X., Lv, J., Guo, F., Li, J., Jia, Y., Jiang, D., Wang, N., Zhang, C., Kong, L., Liu, Y., Zhang, Y., Lv, J., & Li, Z. (2020). Gut microbiome influences the efficacy of PD-1 antibody immunotherapy on MSS-type colorectal cancer via metabolic pathway [Journal Article]. *Front Microbiol*, *11*, 814.

Ye, W., Olsson-Brown, A., Watson, R. A., Cheung, V. T. F., Morgan, R. D., Nassiri, I., Cooper, R., Taylor, C. A., Akbani, U., Brain, O., Matin, R. N., Coupe, N., Middleton, M. R., Coles, M., Sacco, J. J., Payne, M. J., & Fairfax, B. P. (2021). Checkpoint-blocker-induced autoimmunity is associated with favourable outcome in metastatic melanoma and distinct t-cell expression profiles [Journal Article]. *Br J Cancer*, *124*(10), 1661–1669.

Yee, C., Thompson, J. A., Byrd, D., Riddell, S. R., Roche, P., Celis, E., & Greenberg, P. D. (2002). Adoptive t cell therapy using antigen-specific CD8+ t cell clones for the treatment of patients with metastatic melanoma: In vivo persistence, migration, and antitumor effect of transferred t cells [Journal Article]. *Proc Natl Acad Sci USA*, *99*(25), 16168–16173.

Yost, K. E., Satpathy, A. T., Wells, D. K., Qi, Y., Wang, C., Kageyama, R., McNamara, K. L., Granja, J. M., Sarin, K. Y., Brown, R. A., Gupta, R. K., Curtis, C., Bucktrout, S. L., Davis, M. M., Chang, A. L. S., & Chang, H. Y. (2019). Clonal replacement of tumor-specific t cells following PD-1 blockade [Journal Article]. *Nat Med*, *25*(8), 1251–1259.

Yu, X., Long, Y., Chen, B., Tong, Y., Shan, M., Jia, X., Hu, C., Liu, M., Zhou, J., Tang, F., Lu, H., Chen, R., Xu, P., Huang, W., Ren, J., Wan, Y., Sun, J., Li, J., Jin, G., & Gong, L. (2022). PD-L1/TLR7 dual-targeting nanobody-drug conjugate mediates potent tumor regression via elevating tumor immunogenicity in a host-expressed PD-L1 bias-dependent way [Journal Article]. *J Immunother Cancer*, *10*(10). https://doi.org/10.1136/jitc-2022-004590

Zemek, R. M., Fear, V. S., Forbes, C., Jong, E. de, Casey, T. H., Boon, L., Lassmann, T., Bosco, A., Millward, M. J., Nowak, A. K., Lake, R. A., & Lesterhuis, W. J. (2020). Bilateral murine tumor models for characterizing the response to immune checkpoint blockade [Journal Article]. *Nat Protoc*, *15*(5), 1628–1648.

Zhang, Y., Chung, Y., Bishop, C., Daugherty, B., Chute, H., Hoist, P., Kurahara, C., Lott, F., Sun, N., Welcher, A. A., & Dong, C. (2006). Regulation of t cell activation and tolerance by PDL2 [Journal Article]. *Proc Natl Acad Sci USA*, *103*(31), 11695–11700. https://doi.org/10.1073/pnas.0601347103

Zhang, Y., & Zhang, Z. (2020). The history and advances in cancer immunotherapy: Understanding the characteristics of tumor-infiltrating immune cells and their therapeutic implications [Journal Article]. *Cell Mol Immunol*, *17*(8), 807–821.

Zhao, Y., Lee, C. K., Lin, C. H., Gassen, R. B., Xu, X., Huang, Z., Xiao, C., Bonorino, C., Lu, L. F., Bui, J. D., & Hui, E. (2019). PD-L1:CD80 cis-heterodimer triggers the co-stimulatory receptor CD28 while repressing the inhibitory PD-1 and CTLA-4 pathways [Journal Article]. *Immunity*, *51*(6), 1059–1073 e9. https://doi.org/10.1016/j.immuni.2019.11.003

Zhou, B., Yan, J., Guo, L., Zhang, B., Liu, S., Yu, M., Chen, Z., Zhang, K., Zhang, W., Li, X., Xu, Y., Xiao, Y., Zhou, J., Fan, J., Hung, M. C., Li, H., & Ye, Q. (2020). Hepatoma cell-intrinsic TLR9 activation induces immune escape through PD-L1 upregulation in hepatocellular carcinoma [Journal Article]. *Theranostics*, *10*(14), 6530–6543. https://doi.org/10.7150/thno.44417

Zilionis, R., Engblom, C., Pfirschke, C., Savova, V., Zemmour, D., Saatcioglu, H. D., Krishnan, I., Maroni, G., Meyerovitz, C. V., Kerwin, C. M., Choi, S., Richards, W. G., De Rienzo, A., Tenen, D. G., Bueno, R., Levantini, E., Pittet, M. J., & Klein, A. M. (2019). Single-cell transcriptomics of human and mouse lung cancers reveals conserved myeloid populations across individuals and species [Journal Article]. *Immunity*, *50*(5), 1317–1334 e10.

Zimmerman, M., Hu, X., & Liu, K. (2010). Experimental metastasis and CTL adoptive transfer immunotherapy mouse model [Journal Article]. *J Vis Exp*, *45*.